Estimation and Compensation of High-Order Disturbance for Motion Control Systems

March 2017

A thesis submitted in partial fulfillment of the requirements for the degree of
Doctor of Philosophy in Engineering

Keio University

Graduate School of Science and Technology
School of Integrated Design Engineering

NAGATSU, Yuki

Acknowledgements

This dissertation is summary of my research from April 2011 to March 2017 as the member of Katsura Laboratory, in Keio University. In the six years since I entered the laboratory, I have had many valuable experiences and I was supported by a lot of people. Here, I would like to express my gratitude to all people who have given me the supports and advices.

Firstly, I would like to express my sincere gratitude to my supervisor Associate Professor Dr. Seiichiro Katsura, Department of System Design Engineering, Keio University. I am always surprised by his foresight. His fruitful advice forms the basis of this dissertation. He is my destination as a researcher who explores knowledge with sincerity and an educator who lead students with passions. Additionally, he provided a lot of opportunities such as participating in exhibitions, making the presentation of my research at domestic and international conference, and being published in academic journals. It is really fortunate for me to learn and to research under him.

I would like to offer my special thanks to the members of my Ph. D. dissertation committee, Professor Dr. Hiromitsu Ohmori, Department of System Design Engineering, Keio University, Professor Dr. Toshiyuki Murakami, Department of System Design Engineering, Keio University, Professor Dr. Masayuki Kohiyama Department of System Design Engineering, Keio University.

I would like to show my appreciation to Professors who gave precious comments at the research meetings. I would like to thank Professor Dr. Kouhei Ohnishi in Keio University, Associate Professor Dr. Takahiro Yakoh in Keio University, Professor Dr. Hiroaki Nishi in Keio University, and Assistant Professor Dr. Takahiro Nozaki in Keio University.

I also want to convey my gratitude to Professor Dr. Hideki Hashimoto in Chuo University, Department of Electrical, Electronic, and Communication Engineering. He gave me a lot of advices as a researcher and an educator.

Many thanks go to members of Katsura laboratory. I deeply thank Mr. Noboru Tsunashima and Dr. Hidetaka Morimitsu and Dr. Eiichi Saito who are my seniors in Katsura laboratory. I have a lot of respect for their orientations to research.

The Fujiwara scholarship fund, Keio University Doctorate Student Grant-in-Aid Program and Keio Leading-edge Laboratory of Science and Technology (KLL) Ph.D. Program Research Grant have pro-

vided me the financial support. I would like to thank the organizations. By the support, I could get various opportunities to conduct my research and to make the presentation at the domestic and international conferences.

Let me appreciate everyone who collaborated with and help me in Katsura Laboratory. The things which I obtained at this laboratory are precious for me. Especially, I want to express my deep gratitude to Mr. Hiroki Nagashima and Mr. Kazumasa Miura who joined the laboratory in the same year and are working toward Ph. D. degree. I want to show my thankfulness also to Mr. Issei Takeuchi who are a mature age Ph. D. student. Discussions with them are very stimulative for my research.

Finally, I would like to express my deep gratitude to my parents and grandparents who have brought me. Your kind and warm-hearted assistance have enabled me to study without any inconvenience.

I would like to express my appreciation from my heart for everyone who supported me in student life in Keio University.

March, 2017
Yuki Nagatsu

Table of Contents

List of Figures

List of Tables

Nomenclature

Abbreviation

DOF	degree-of-freedom
DOB	disturbance observer
RTOB	reaction torque observer
RFOB	reaction force observer
MDOF	multi-degree-of-freedom
RDOF	redundant degree of freedom
MCS	motion-copying system
WDOB	work space disturbance observer
MDOB	mode space disturbance observer
KFSO	Kalman filter based state observer
SSKF	steady state Kalman filter
HDOB	high-order disturbance observer
EnvD	environmental disturbance
MR	motion reproducibility
LPF	low-pass filter
HPF	high-pass filter
PD	proportional-derivative (controller)
DARE	discrete time algebraic Riccati equation
TraD	trainee disturbance

$\boldsymbol{bold\ type}$	vector and matrix
t	time
k	sampling instant
s	Laplace operator
z	time shift operator
g	poles of filters
T_s	sampling time
X	position
Y	position out put
F	force
$\boldsymbol{x}$	position vector
$\boldsymbol{f}$	force vector
$\boldsymbol{X}$	transformed position vector
$\boldsymbol{F}$	transformed force vector
$\boldsymbol{T}$	transformation matrix
$d_\bullet$	constant
$\dot{\bullet}$, $\ddot{\bullet}$, $\dddot{\bullet}$	time derivative
$\hat{\bullet}$	estimated value
K_f	force control gain
K_τ	external torque control gain
$K_{\bullet d}$	differential gain
$K_{\bullet p}$	proportional gain
$K_{\bullet v}$	velocity feedback gain
$C_f = K_f$	force controller
$C_p(s) = K_p + K_v s$	position PD controller
$C_f(s) = K_{fp} + K_{fd} s$	force PD controller
$C_\tau(s) = K_{\tau p} + K_{\tau d} s$	torque PD controller
$\boldsymbol{C}_f$	diagonal matrix with force controller in diagonal elements
$\boldsymbol{C}_p(s)$	diagonal matrix with position controller in diagonal elements
$g^\bullet(\cdot)$, $G^\bullet(\cdot)$	transfer function
$\boldsymbol{g}^\bullet(\cdot)$, $\boldsymbol{G}^\bullet(\cdot)$	matrix with transfer functions
$N_{\mathrm{um}}(\bullet)$, $\boldsymbol{N}_{\mathrm{um}}(\bullet)$	denominator of transfer function
$D_{\mathrm{en}}(\bullet)$, $\boldsymbol{D}_{\mathrm{en}}(\bullet)$	numerator of transfer function

$n_{\mathrm{um}}(\bullet)$, $\boldsymbol{n}_{\mathrm{um}}(\bullet)$	denominator of transfer function in joint space
$d_{\mathrm{en}}(\bullet)$, $\boldsymbol{d}_{\mathrm{en}}(\bullet)$	numerator of transfer function in joint space
$\boldsymbol{I}$	identity matrix
$\boldsymbol{S}$	selection matrix for position control system
J, $\boldsymbol{J}$	inertia (mass) matrix in joint space
M	mass
$\boldsymbol{M}$	mass (inertia) matrix in work space or modal space
$\boldsymbol{C}^r\left(\boldsymbol{q}, \dot{\boldsymbol{q}}\right)$	Coriolis term
K_t, $\boldsymbol{K}_t$	torque (force) coefficient
$\Delta\bullet$	parameter variation
$P(\bullet)$	transfer function of plant
$Z_e(\bullet)$, $\boldsymbol{Z}_e(\bullet)$	environmental impedance
M_e, $\boldsymbol{M}_e$	environmental mass
D_e, $\boldsymbol{D}_e$	environmental viscosity
K_e, $\boldsymbol{K}_e$	environmental stiffness
M_f	virtual mass of force control (reciprocal force control gain)
D_f	virtual damping of force control (reciprocal force control gain)
X_f	virtual position response of admittance control
K_r	torsional force feedback gain
K_l	load side spring coefficient
F_l^{dis}	load side disturbance
ω_a	actuator side resonance frequency
ω_e	environmental side resonance frequency
r_e	resonance ratio for the force tracking control
ω_m	motor side resonance frequency
ω_l	load side resonance frequency
r_l	resonance ratio of the two-mass resonance system
$\boldsymbol{q}$	joint angle (position) vector
$\boldsymbol{\tau}$	joint torque (force) vector
$\boldsymbol{G}(\boldsymbol{q})$	direct kinematics, Jacobian matrix
$\boldsymbol{J}_{\mathrm{aco}}$	Jacobian matrix
$\boldsymbol{X}_W = \boldsymbol{G}_W(\boldsymbol{q})$	work space position vector
$\dot{\boldsymbol{X}}_W = \boldsymbol{J}_{\mathrm{aco}}\dot{\boldsymbol{q}}$	work space velocity vector

$\ddot{\boldsymbol{X}}_W = \boldsymbol{J}_{\mathrm{aco}}\ddot{\boldsymbol{q}} + \dot{\boldsymbol{J}}_{\mathrm{aco}}\dot{\boldsymbol{q}}$	work space acceleration vector
$\boldsymbol{F}_W = \boldsymbol{J}_{\mathrm{aco}}^{-T}\boldsymbol{\tau}$	work space force vector
$\boldsymbol{G}_{\mathrm{ra}}$	grasping matrix
$\boldsymbol{Q}$	generalized position vector
$\boldsymbol{N}$	generalized force vector
$\boldsymbol{\Xi}$	transformation matrix to extended object space (extended Jacobian matrix)
$\boldsymbol{p}^{\mathrm{dis}}$, $\boldsymbol{P}^{\mathrm{dis}}$	disturbances through high-pass filter
$\boldsymbol{p}^{\mathrm{ext}}$, $\boldsymbol{P}^{\mathrm{ext}}$	external force (torque) through high-pass filter
$\boldsymbol{Z}(\bullet)$	state variable
$\boldsymbol{Y}(\bullet)$	measured variable
$\boldsymbol{u}(\bullet)$, $\boldsymbol{U}(\bullet)$	control input in continuous time domain
$\mathbf{A}$	system matrix in continuous time domain
$\mathbf{B}$	input vector
$\mathbf{e}^{\bullet}$	state transition matrix
$\mathbf{A}_d$	system matrix in discrete time domain
$\mathbf{B}_d$	input vector in discrete time domain
$\boldsymbol{c}$	observation matrix
$w(\bullet)$, $\boldsymbol{W}(\bullet)$	observation noise
$v(\bullet)$, $\boldsymbol{V}(\bullet)$	process noise
$\mathrm{E}[\bullet]$	expectation operator
σ^2	variance
$\mathbf{\Sigma}^2$	covariance matrices
$\mathbf{R}$	covariance matrices with respect to observation noise
$\mathbf{Q}$	covariance matrices with respect to process noise
$\boldsymbol{e}$	estimation error vector
$\mathbf{P}(k)$	error covariance matrix
$\mathbf{G}_{\mathrm{kf}}(k)$	Kalman gain
$\boldsymbol{\mathcal{P}}$	solution of discrete time algebraic Riccati equation (DARE)
$\boldsymbol{\mathcal{G}}$	steady state Kalman gain
$\bullet^{-}$	prior estimated value
$\bar{\bullet}$	mean value

Superscripts

res	response value
dis	disturbance force (torque)
ext	external force (torque)
fric	friction force (torque)
load	load force (torque) except for external force (torque)
cmd	command value
ref	reference value
pd	pseudo differentiation
inv	inverse system
fdd	frequency domain damping
P	Position estimation
v	velocity estimation
f	reproduction with respect to force
p	reproduction with respect to position
n	parameter corresponding to n-th order time derivative of force
h	parameter related to high-order disturbance
T	transpose matrix
$+$	pseudo inverse matrix

Subscripts

n	nominal value
W	work space
m	master system
s	slave system
v	element of process noise
$\mathrm{dif^n}$	system noise with n-th order time derivative of force/torque
kf	Kalman filter
skf	steady state Kalman filter
hkf	Kalman filter with high-order disturbance estimation
hskf	steady state Kalman filter with high-order disturbance estimation
$\mathrm{2nd}$	second order low-pass filter
Int	integrated information
e	environment
a	actuator
t	torsion
l	low-pass filter in joint space
h	high-pass filter in joint space
L	low-pass filter in work space or modal space
H	high-pass filter in work space or modal space
N	noise sensitivity
F	element of force control system
X	element of force control system
phl	phase lead compensation
cmp	parameter with respect to compensation value
sub	subtasks
S	parameter of motion saving system
R	parameter of motion reproduction system
ad	additional disturbance/external force in motion reproduction
r	response characteristics
d	disturbance response (suppression) characteristics
E	elemental motion components
O	coordinate for grasped object and robot

O_b	grasped object
i	parameter of i-th joint
t	parameter with respect to trainee
T	parameter with respect to temporal compensation

Chapter 1

Introduction

1.1 Background of This Dissertation

1.1.1 Motion Control Systems in Open Environment

In the future, it is predicted that some developed countries will face problems with an aged society because of decreasing birth rates [1]. Concerns associated with an aged society include the decreased number of workers and the shortage of technical skills of skilled workers. In addition, the number of elderly people who require nursing care will increase. In such a society, motion control technologies will become important for robots, which will substitute human workers and support human beings [2, 3]. Acquiring and analyzing human motions by using robot techniques is important issue. Thus, motion control systems will be widely used not only in industrial applications but also in cooperative systems with human beings in open environments.

In order to realize robot systems realizing desired tasks in open environments with human being and/or unknown environment, precise and flexible motion control systems should be required. Especially, the precise trajectory and force control for contact motions are required to preserve and reproduce the techniques of skilled workers . In order to realize the motion control systems in the open environments, information of disturbance and external force should be obtained.

A two-degree-of-freedom (DOF) control system [4] based on a disturbance observer (DOB) [5–8] is one of the most effective methods for realizing robust motion control systems. The control system using the DOB is easy to implement and understand compared to other robust control methods (e.g., H_∞ control [9] and/or sliding mode control [10]). Several studies are reported in which robust and precise

positioning control is realized by DOB-Based methods [11–15]. On the contrary, reaction torque/force control is required for precise control needed for making contact with delicate objects and for interacting wit, unknown objects and/or human beings [16, 17]. Especially, robust reaction torque/force control systems based on DOBs without force sensors based on reaction torque/force observers (RTOBs/RFOBs) [6, 18, 19] have been developed as the effective controllers. Advantages of the observer based approach have been confirmed in literatures (e.g. [20]). The four-channel bilateral controller based on an acceleration controller is a kind of DOB-based 2-DOF control structure, and many DOBs have been developed for other applications such as multi-DOF (MDOF) systems [21], two-mass resonant systems [22–24], and time-delay systems [25].

The acceleration-based reaction torque control technique can be applied also to as bilateral teleoperation systems [26–28]. The bilateral control systems are the subject of many research efforts with the ultimate goal of realizing teleoperation [29–33]. The bilateral control system is also being actively researched to realize many other advanced applications [34–39]. A bilateral control system consists of a pair of robots (i.e., a master robot and a slave robot). The goal is usually to achieve position tracking and haptic feedback (artificial reconstruction of "law of action and reaction") between the master and slave systems. Therefore, operators can manipulate objects with precise kinesthetic feedback as if the objects were in their own hands. Transparency [29] is introduced as a performance index for bilateral control. The index represents the degree of coincidence between an impedance that an operator recognizes and an environmental impedance. A four-channel bilateral controller [26] based on an acceleration controller can realize the high transparency. The transparency can be analyzed in detail by being divided into operationality and reproducibility [26]. Bilateral control systems are expected to become a key technology for remote medical care, remote communications, and for taking the part of human operatives in hazardous environments. Additionally, bilateral control systems can also be utilized to obtain and analyze an operative's motions including force information [40, 41].

Not only analysing human motions, but also storing and reproducing (inherit) human motions such as skilled techniques will also be important in order to deal with the loss of them. Motion capture [42] is often used to analyze human motions. Much research and development has also gone into demonstrating human motions with robots [43–45]. However, most studies have mainly utilized motion trajectory information; analyzing or imitating contact motions conducted by human operators is difficult.

For storing and reproducing human motions including contact motions, bilateral control is also utilized in motion-copying system (MCS) [46]. The MCS was developed as a method for storing and

reproducing human motions, including kinesthetic senses, to realize contact motions with the environment or humans using robots. The MCS has two phases: motion saving and motion reproduction. In the motion-saving phase, the motions of human operators are recorded with a bilateral control system. In the motion-reproduction phase, the motions of the operator are reproduced through pseudo-bilateral control between the database (virtual master system) and the slave system using both the position and force information. The motion saving phase corresponds to a robot programing method by human demonstration [43, 47–50]. On the other hand, MCS can obtain more vivid and accurate haptic information than the conventional programing by the demonstration because the MCS utilizes the acceleration based bilateral control system. The MCS has the potential to realize complicated tasks like repeating free and contact motions. Besides reproduction, the MCS is also anticipated to be applied to training and power assist systems [51,52] to pass techniques down to younger generations and for rehabilitation with robots [53, 54].

A lot of useful applications have been developed based on DOB/RFOB based motion-control systems which are not able to be mentioned above.

However, motion control systems do not necessarily demonstrate desired performance depending on the conditions of devices and environments such as appearances of unknown disturbances which DOBs cannot suppress and effects of noises from sensors.

1.1.2 Effect of Noise in Disturbance/External Force Estimation

If the signals observed for estimating disturbance/external torque (i.e., velocity or position information), however, includes observation noise or quantization error, the effect of the noises is enhanced [8, 15, 55]. This is because the two times time derivative of the position information from sensors is required to estimate the disturbance information. As a result, estimation and control system performances based on DOB/RFOB are adversely affected. Therefore, there is a trade-off between a performance and noise sensitivity in the determination of the bandwidth of the disturbance estimation. Noise or quantization errors adversely affect control performances in many cases [56]. Not only the estimated disturbance/external torque but also the position or velocity signals that include noisy signals are fed back to the system, adversely affecting the control system performance.

Kalman filter technologies have been actively researched for reducing the effects of noise in control systems. Kalman filters have been applied for reducing noise effects in the estimation of system state variables [57–63]. Several studies in which DOBs and RTOBs are combined with Kalman filter tech-

niques have been reported [64–67]. Mitsantisuk $et\ al.$ proposed a Kalman filter-based state observer (KFSO) with disturbance torque as a state variable and a method for sensor fusion of position and acceleration sensors by using a Kalman filter for realizing wide-band DOBs [65]. The methods discussed above have been applied for acceleration-based bilateral control systems By using the Kalman filter, the noise effect can be suppressed effectively in motion control systems based on DOBs and RTOBs.

It is known that the performance of the Kalman filter depends on the determination of the covariance matrix with respect to system noise [68]. If the state estimation including disturbance torque is considered, the number of the elements in the matrix is nine [65] However, many researches determine the parameters by tests and simulations and the parameter determination process is not clear [65, 67, 69]. The relationship between the parameters is also not clear. Furthermore, it is difficult to perform torque estimation for obtaining the actual value of the variances of system noise, though a conventional method for estimating velocity information [67] obtains the values through experiments and tests.

1.1.3 Contact Motion with Unknown Environment

It is known that the performance characteristics of conventional force control based on the DOB/RFOB depends on environmental characteristics [8, 18, 19]. Therefore, depending on environment, the response of the force tracking control system becomes oscillatory and in the worst case becomes unstable.

If the velocity damping is utilized for stabilization, however, this reads the deterioration from the view point of control stiffness [7, 70]. In the ideal force control system, the control stiffness should be zero. However, the control stiffness with velocity damping becomes larger because the velocity feedback term behaves as artificial viscous friction. Therefore, simultaneous realization of stabilization and ideal control stiffness is difficult.

There are several researches regarding achieving stable and improved performance of the force tracking control system [71, 72]. However, the design methods for the force tracking control of the conventional methods are not clear.

In addition, second order time derivative of the estimated disturbance force is required if the variation of the environmental parameters are tried to be compensated for fixing environmental characteristics [23, 73, 74]. The second order time derivative of the estimated disturbance corresponds to fourth order time derivative position information form sensors. Therefore, the compensation results in further enlargement of the noise effect.

1.1.4 Position/Force Hybrid Control for Human Motion Extraction

In motion control systems, hybrid control systems in which position/force control systems are constructed in different axes [75] will be important for the interaction with human beings and outer environments. The bilateral control system is a kind of the hybrid control system.

To determine the general versatility of the MCS, precise bilateral control should be realized even if the master and slave systems are configured differently (having different masses, for example). To achieve the appropriate bilateral control, decoupling control of the position and force control systems should be realized. Decoupling control is particularly important for motion control systems [76, 77]. Shimono *et al.* proposed a bilateral control system with master and slave systems having different masses by using a standardization matrix [78]. However, this method has to include mass elements in the control goals and they mentioned only a single DOF master and slave system. Sakaino *et al.* described the bilateral control system as a hybrid controller [79] of the position and force control systems, and identified the points at which the force and position control systems interfere with each other in a conventional hybrid control scheme [75]. By introducing an equivalent mass matrix [21, 75], in the modal spaces (e.g., the common and differential modal spaces [78]), the problems associated with bilateral control using a conventional hybrid controller can be clarified. To eliminate the interferences, a precise hybrid controller with a hybrid matrix [79, 80] was proposed and realized improvements over a conventional hybrid controller [75]. However, the dynamics in the modal space after the implementation of the methods are still not clear. On the other hand, a hybrid controller based on an MDOB was proposed [81] to realize decoupling control in the modal space by extending the workspace observer [21]. In the study, the MDOB realized a higher level of performances than was possible with the hybrid matrix based method under certain conditions. As indicated in [21], decoupling control based on a force controller using WDOB offers the possibility of becoming unstable when the system configuration is subject to substantial fluctuations. Therefore, the variation in the equivalent mass matrix should be considered in order to realize stable and desired responses [21].

If a robot manipulator has a redundant degree of freedom (RDOF), it will be possible for the robot to not only execute primary tasks with subtasks in a null space, but also to perform obstacle avoidance, singularity avoidance, and adaptation to the environment [82, 83]. Therefore, hybrid control systems with RDOF will be necessary for motion control systems to perform future applications for human support systems and robots in unknown and open environments. However, in the case of the redundant manipu-

lator, the effect of manipulator variation may become significant. Furthermore, not only the decoupling of the position and force control systems but also the decoupling of a task space (a mode space) should be considered. If inverse kinematics of a manipulator are conducted, the null space response interferes with work space motions [84].

Several methods have been developed to cancel the inertial force, as presented in [85, 86]. The method using a force-based DOB [85] constructs DOBs in the modal spaces, rather than in the joint space, for hybrid control. A hybrid controller using a force-based DOB, however, has the same structure as an MDOB in a position-control system. Therefore, this method will present the same problems as an MDOB-based method regarding the variation in the stability with the manipulator configuration. A compensation method based on an acceleration observer relies on information related to the estimated acceleration in the actuator spaces (in both the master and slave systems). Therefore, the total dynamics in the modal space are not adequately reflected on the compensation.

In addition, scaled bilateral [34, 35] control systems also have a problem with respect to enlargement of noise effect. Macro-micro bilateral control with scaling factor enables operators to manipulate small objects with feeling scaled tactile and kinesthetic sense feedback as if they are large at hand. However, a higher scaling factor leads the relative enlargement of noise from slave system. The noise effect results in the deterioration of the performance of the scaled bilateral control system.

1.1.5 Human Motion Reproduction with Variation of Environments

One problem with the MCS is a lack of flexibility with regard to variances in the environments between the saving and reproduction phases [87–90]. Here, a variance means a difference in distances between the actuators (slave side) and environment or differences in environmental impedances. External forces that are not added to the slave system in the saving phase are also included in the differences in impedances. When variances in the environment occur, both the trajectories and contact motions are not reproduced, and the stored motions lack general versatility. In order to actually utilize the MCS in industrial applications or operations in an open environment, where robots interact with humans, the stored motions need to show flexibility and general versatility despite environmental variances. In [87], motion-reproduction system with coordinate modification was proposed, but the design methodology is ambiguous. Furthermore, the method addressed only force reproduction. Therefore, the effect of the environmental variance on the position reproduction is neglected. In order to deal with differences in distances, a velocity-based motion reproduction method was developed [88]. To realize flexible robot

tasks, force-based impedance control systems have been developed for motion control, such as in [91]. However, using the velocity-based method or force-based impedance control system in the reproduction phase requires altering the controllers of the bilateral control system in the saving phase. These alterations mean that the transparency from using the four-channel bilateral controller is lost. Thus, the above approaches degrade the motion reproduction performance. In addition, the velocity-based method is difficult to apply in the presence of unknown disturbances because the trajectory reproduction is neglected, so the system cannot return to the original trajectory once it has been deorbited by the additional disturbance.

1.2 Motivation of This Dissertation

As described above, even though the DOB/RFOB based robust control systems are implemented in the each application, there are a lot of situations where the control system cannot achieve their original and/or desired performances. Dealing with unknown parameter variations or disturbances with unknown and open environments or sensing noises are important issues for the engineering and industrial applications.

This dissertation focuses on the disturbance and noise attenuation to realize precise and flexible motion control systems including position/force hybrid control for the bilateral control systems and motion-reproduction systems. The purpose of this dissertation is to establish strategies for the estimation and compensation of high-order disturbance in motion control systems for solving the problems described above. Not only the disturbance suppression in an actuator, but also disturbances in multi-degree-of-freedom (MDOF) systems and environmental variations are included in category of aims in this dissertation.

Usually, the model of disturbance in conventional disturbance estimation is regarded as a step signal [7, 92] and its time derivative is regarded as zero. Therefore, the conventional DOBs are called "zero-order DOB". On the other hand, this dissertation addresses on higher order disturbance [93–95] estimation with considering stochastic behavior for noise suppression based on Kalman filters. Additionally, higher order time derivatives of the disturbances are actively utilized for the performance improvement of the control systems.

This dissertation also focuses on the similarity between two mass resonant system and force control system in order to realize a flexible and stable force control system. To construct the force control system, parameter variations of environment are defined as environmental disturbance (EnvD) [73, 74].

The higher order disturbance and its time derivatives are utilized also for suppressing the EnvDs. Furthermore, the difference of environment between motion saving phase and reproduction phase is also regarded as EnvD.The general framework for the motion reproduction based on compensation of EnvD [96] is established in this dissertation.

In order to improve performance of the position/force hybrid control systems including bilateral control, a novel disturbance observer is proposed in this dissertation [97]. By using the proposed approach, the decoupling control, performance improvement of hybrid control and the simplification of controller design are achieved. The novel DOB is extended also to the redundant system and combined with KFSO based on the proposed design methodology.

Moreover, the proposed high-order disturbance estimation in actuators and environments is integrated for the motion-reproduction system for flexible adapting the difference with respect to not only environment but also reproduction device itself.

The framework derived in this dissertation for the estimation and compensation of high-order disturbance will play an important role for further improvement of performance of industrial applications. The conceptual figure of this dissertation is shown in Fig. 1-1. The proposed method for the estimation and compensation of high-order disturbances will contribute to expand the versatility of the motion control systems.

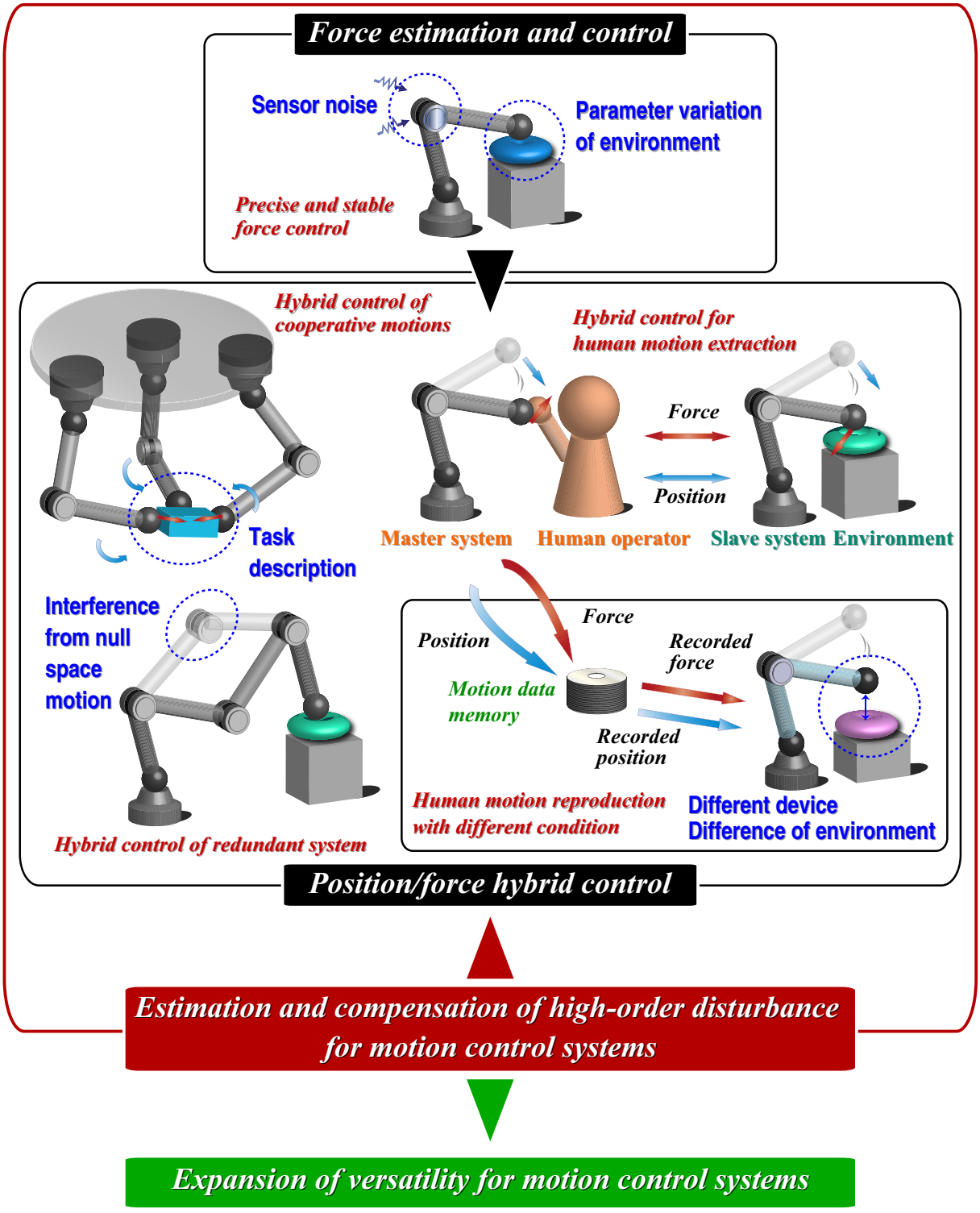

Fig. 1-1: Conceptual figure of this dissertation.

1.3 Chapter Organization of This Dissertation

Fig. 1-2 shows the chapter organization of this dissertation.

In chapter 2, models of the high-order disturbances with considering stochastic behavior in actuators and environments are defined to clarify effects of noises in the estimation. A fundamental approach of designing KFSO for the disturbance estimation based on the proposed modeling are shown in this chapter. This chapter also shows that a high-order disturbance observer based on a Kalman filter [98] becomes easy to design by including a process noise in highest order of the time derivative of the disturbance as a model. Additionally, the proposed observers are applied to force control systems and the performance is investigated.

Chapter 3 shows that the resonance ratio control [22] for a vibration control can be applied to the force control systems by considering the similarity between a two mass resonant system and a force control system [74]. Additionally, Kalman filter based high-order environmental disturbance compensation is realized by considering the correspondence of load side disturbances and parameter variations of an environment. The proposed method achieves the simultaneous realization of maintaining an ideal characteristic of force control and stable contact motions.

Chapter 4 shows that a decoupling control of a hybrid control for the human motion extraction can be realized by extending an acceleration controller in a work space of a robot to hybrid control system [97]. Furthermore, the method for suppressing a particular disturbance in hybrid controller is proposed. The performance enhancement of the proposal is confirmed. Moreover, the proposed method is extended for the redundant systems and integration of the Kalman filter based disturbance estimation [99] is also proposed.

Chapter 5 shows that an adaptation method for environmental variation between the motion extraction phase and motion-reproduction phase. By formulating the characteristics of tracking performance with respect to the motion-reproduction control, the performance deterioration of the conventional motion-reproduction controllers are clarified. Furthermore, by regarding the environmental variation as the environmental disturbance in the motion reproduction, motion-reproduction compensators are proposed to suppress the environmental disturbance. The proposed method achieves the simultaneous realization of the precise motion reproduction and flexible adaptation to environmental variation which are difficult for the conventional method. The fundamental principle and design framework for the motion-reproduction system is established in this chapter [96].

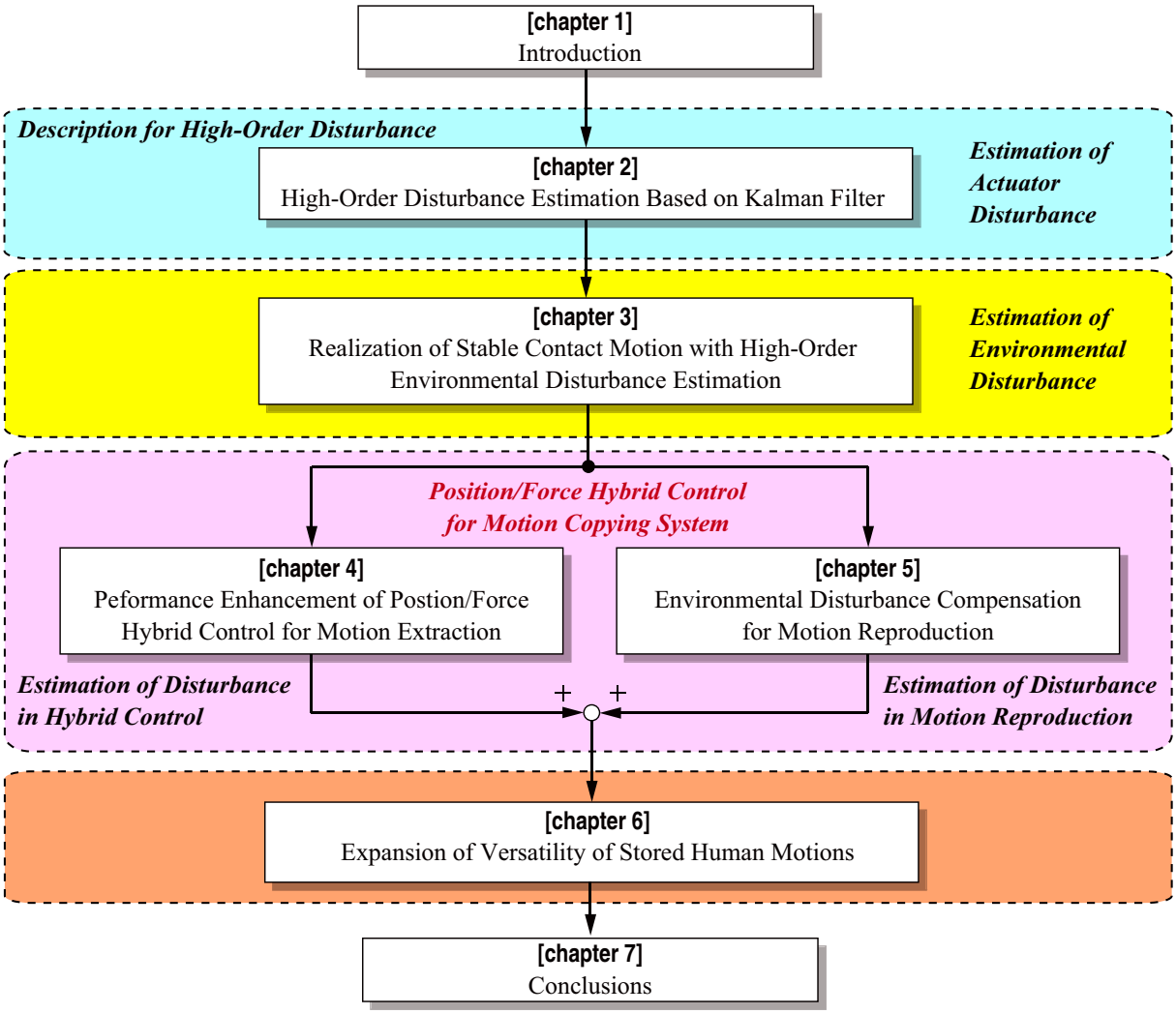

Fig. 1-2: Chapter Organization of this dissertation.

Chapter 6 describes the proposed method for extending the general versatility of the saved human motion information. By integrating and applying the methods shown in the former chapters to a motion-reproduction system, the flexible and robust motion reproduction is realized against the environmental variations and effect of noises. Finally, this dissertation is concluded in chapter 7.

Chapter 2

High-Order Disturbance Estimation Based on Kalman Filter

2.1 Introduction of Chapter 2

In this chapter, high-order disturbances with considering stochastic behavior are described. The high-order disturbances in an actuator, a multi-degree-of-freedom (MDOF) system and an environment are explained.

Based on the modeling of the higher order disturbance with considering stochastic behavior, this chapter shows a design of the Kalman filter based state observer (KFSO) [65] for high-order disturbance estimation. This chapter focuses on the tuning of the covariance matrix with respect to process noise. As for the most simple case, the tuning of the KFSO for zero-order disturbance estimation is described for the confirmation.

By the proposed tuning structure, the number of parameters to be determined is reduced from nine to two compared with the conventional researches without considering the stochastic behavior of the disturbances [65, 67]. The structure of Kalman filter-based external torque estimation without using a nonlinear Kalman filter [63, 100] is also proposed. The characteristics of the Kalman filter designed by the proposed structure are analyzed using the steady-state Kalman filter (SSKF). The analysis reveals that the relationship between the two parameters for realizing appropriate tuning of disturbance and external torques estimation.

Experimental results validated the tuning method and analytical results.

Additionally, this chapter also shows a high-order disturbance estimation using Kalman filter for pre-

cise reaction-torque control [98]. The disturbance/external torque is modeled as ramp signal of a time function [93, 95] although the disturbances are usually modeled as step signals in conventional DOBs or KFSOs [65]. Here, the disturbance observer structure is included in a different form of the KFSO [67]. By using the proposed high-order disturbance/external torque estimation method, a reaction torque control system with a PD controller is constructed by using the estimated external torque and the estimated time derivative of the external torque with compensating disturbance term. Usually, reaction torque control systems based on a DOB or RTOB have used a proportional (P) controller for the feedback loop. A performance improvement of the reaction torque control can be expected by using the proportional derivative controller (PD) as an alternative to the P controller. However, the PD controller is difficult to use because the differentiation of the estimated external torque by the RTOB often enlarges the effect of the noise or the quantization error. If the noise or the quantization error is included in the observed signals, the estimated disturbance and reaction torque are affected by the observation noises. On the other hand, the proposed method realizes the suppression of noise effect not only in the disturbance estimation but also in estimation of its time derivative for D controller. In addition, frequency characteristics of the proposed KFSO are approximately analyzed by deriving a steady-state Kalman filter (SSKF). The validity of the proposed method is confirmed through an experiment of the reaction torque control that makes contact with an environment by using a single degree-of-freedom rotary motor.

2.2 Description of High-Order Disturbances

2.2.1 Motion Equation of An Actuator with Disturbance

This part describes a high-order disturbance in an actuator is described. A motion equation of an actuator with parameter variation is expressed as

$$M\ddot{X}^{\mathrm{res}} = K_t I^{\mathrm{ref}} - F^{\mathrm{ext}} - F^{\mathrm{fric}} \tag{2.1}$$

$$(M_n + \Delta M)\,\ddot{X}^{\mathrm{res}} = (K_{tn} + \Delta K_t)\, I^{\mathrm{ref}} - F^{\mathrm{ext}} - F^{\mathrm{fric}} \tag{2.2}$$

$$= F^{\mathrm{ref}} - F^{\mathrm{ext}} - F^{\mathrm{fric}} + \Delta K_t I^{\mathrm{ref}} \tag{2.3}$$

where X, I, F^{ext}, F^{fric}, F^{ref} M, K_t and $\Delta\bullet$ represent a position, a current, an external force, a friction force, a reference force, a mass, a thrust force coefficient, and a parameter variation, respectively. In addition, a subscript n represent a nominal value. In the motion equation (2.2), a disturbance force F^{dis}

is defined as follows:

$$F^{\mathrm{dis}} = F^{\mathrm{ext}} + F^{\mathrm{fric}} + \Delta M \ddot{X}^{\mathrm{res}} - \Delta K_t I^{\mathrm{ref}} \tag{2.4}$$

$$F^{\mathrm{load}} = F^{\mathrm{fric}} + \Delta M \ddot{X}^{\mathrm{res}} - \Delta K_t I^{\mathrm{ref}}. \tag{2.5}$$

The disturbance term can be estimated by using a DOB as follows [5–7]:

$$\hat{F}^{\mathrm{dis}} = g_l^{\mathrm{dis}}(s)\left[F^{\mathrm{ref}} - M_n s^2 X^{\mathrm{res}}\right] \tag{2.6}$$

$$= g_l^{\mathrm{dis}}(s) F^{\mathrm{dis}} \tag{2.7}$$

where $g_l^{\mathrm{dis}}(s)$ is a low-pass filter in disturbance estimation for suppressing noise effect. By feeding back the estimated disturbance, a robust acceleration control can be realized if the bandwidth of $g_l^{\mathrm{dis}}(s)$ is sufficiently high, as follows:

$$M_n \ddot{X}^{\mathrm{res}} = F^{\mathrm{ref}} + \hat{F}^{\mathrm{dis}} - F^{\mathrm{dis}} \tag{2.8}$$

$$= M_n \ddot{X}^{\mathrm{ref}} - g_h^{\mathrm{dis}}(s) F^{\mathrm{dis}} = M_n \ddot{X}^{\mathrm{ref}} - P^{\mathrm{dis}} \tag{2.9}$$

$$\approx M_n \ddot{X}^{\mathrm{ref}} \tag{2.10}$$

$$\ddot{X}^{\mathrm{res}} = \ddot{X}^{\mathrm{ref}} \tag{2.11}$$

where M_n and P^{dis} represent a nominal value and an equivalent disturbance through a high-pass filter, respectively. In actual cases, however, a position response from a sensing device includes a observation noise. An estimated disturbance considering the observation noise w is described as follows:

$$\hat{F}^{\mathrm{dis}} = g_l^{\mathrm{dis}}(s)\left[F^{\mathrm{ref}} - M_n s^2 Y^{\mathrm{res}}\right] \tag{2.12}$$

$$= g_l^{\mathrm{dis}}(s)\left[F^{\mathrm{ref}} - M_n s^2 X^{\mathrm{res}}\right] + M_n g_l^{\mathrm{dis}}(s) s^2 w \tag{2.13}$$

$$= g_l^{\mathrm{dis}}(s) F^{\mathrm{dis}} + g_N^{\mathrm{dis}}(s) w \tag{2.14}$$

where output signal $Y(t)$ includes an observation noise $w(t)$ as

$$Y^{\mathrm{res}}(t) = X^{\mathrm{res}}(t) + w(t). \tag{2.15}$$

In this dissertation, the observation noise is assumed to be a normal white noise. In (2.13), $g_N^{\mathrm{dis}}(s)$ represents a noise sensitivity function. Because the noise effect is enlarged if the bandwidth of the low-pass filter is set to higher value, the bandwidth of the DOB have a constraint in actual case.

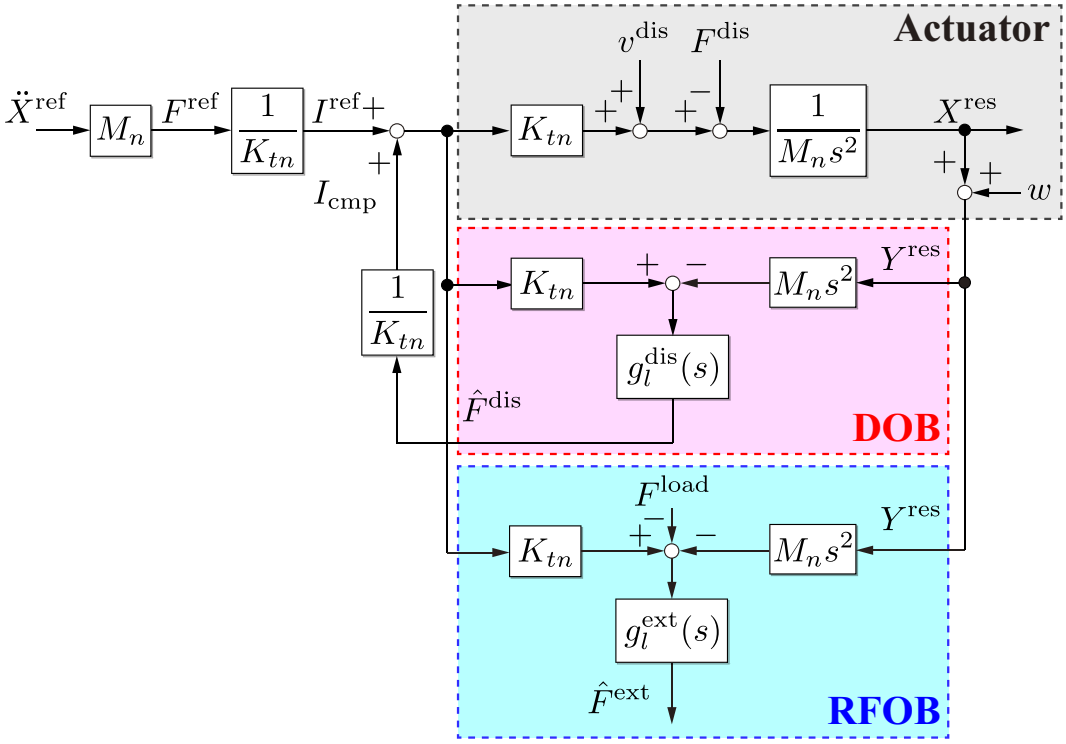

Fig. 2-1: Block diagram of DOB and RFOB.

A DOB based on the velocity information [5, 6, 8, 18] estimates the disturbance by using estimated velocity signal form pseudo differentiator as

$$\hat{F}^{\mathrm{dis}} = g_l^{\mathrm{dis}}(s)\left[F^{\mathrm{ref}} - M_n s\hat{X}^{\mathrm{res}}\right] + M_n g_l^{\mathrm{dis}}(s) g_l^{\mathrm{pd}}(s) s^2 w \tag{2.16}$$

$$\hat{\dot{X}}^{\mathrm{res}} = g_l^{\mathrm{pd}}(s) s X^{\mathrm{res}}. \tag{2.17}$$

Similarly, the external force can be estimated by using RFOB [6, 19] as follows:

$$\hat{F}^{\mathrm{ext}} = g_l^{\mathrm{ext}}(s)\left[F^{\mathrm{ref}} - F^{\mathrm{load}} - M_n s^2 X^{\mathrm{res}}\right] + M_n g_l^{\mathrm{ext}}(s) s^2 w \tag{2.18}$$

$$= g_l^{\mathrm{ext}}(s) F^{\mathrm{ext}} + g_N^{\mathrm{ext}}(s) w. \tag{2.19}$$

For the estimation of the external force, the load force except for the external force F^{load} should be identified.

The motion equation of the actuator is rewritten with considering noise effect from a motion controller

$C(s)w$ in F^{ref} as follows:

$$M_n\ddot{X}^{\mathrm{res}} = F^{\mathrm{ref}} + \hat{F}^{\mathrm{dis}} - F^{\mathrm{dis}} \tag{2.20}$$

$$= F^{\mathrm{ref}} + g_l^{\mathrm{dis}}(s)F^{\mathrm{dis}} - F^{\mathrm{dis}} + C(s)w + g_N^{\mathrm{dis}}(s)w \tag{2.21}$$

$$= F_n^{\mathrm{ref}} - F^{\mathrm{dis}} + C(s)w + g_N^{\mathrm{dis}}(s)w. \tag{2.22}$$

A motion equation is rewritten with the noises expressed as a process noise v^{dis} as follows:

$$M_n\ddot{X}^{\mathrm{res}} = F_n^{\mathrm{ref}} - F^{\mathrm{dis}} + v^{\mathrm{dis}} \tag{2.23}$$

$$v^{\mathrm{dis}} = C_N(s)w + g_N^{\mathrm{dis}}(s)w. \tag{2.24}$$

where v^{dis} is a process noise in the dimension of the disturbance. The process noise is also assumed to be a normal white noise in this dissertation. In this dissertation, the process noise v^{dis} is assumed not to have correlation with $w(t)$.

Fig. 2-1 shows a block diagram of the disturbance/external force estimation based on a DOB and a RFOB.

2.2.2 Model for High Order Disturbance with Stochastic Behavior

In order to estimate the disturbance term, a model of the disturbance should be defined. In this dissertation, the model of the disturbance with considering a stochastic behavior is defined as follows:

$$\frac{d^{n+1}}{dt^{n+1}}F^{\mathrm{dis}}(t) = v_{\mathrm{dif}^n}^{\mathrm{dis}}(t) \tag{2.25}$$

where $v_{\mathrm{dif}^n}^{\mathrm{dis}}(t)$ is a process noise which drives the n-th-order time derivative of the disturbance $\frac{d^{n+1}}{dt^{n+1}}F^{\mathrm{dis}}(t)$. The process noise is also assumed to be a normal white noise in this dissertation. The integrals of the (2.26) is described as follows:

$$\frac{d^n}{dt^n}F^{\mathrm{dis}}(t) = D_n + \int_0^t v_{\mathrm{dif}^n}^{\mathrm{dis}}(T)dT \tag{2.26}$$

$$\vdots$$

$$\frac{d}{dt}F^{\mathrm{dis}}(t) = D_1 + \cdots \frac{1}{(n-1)!}D_n t^{n-1} + \int_0^t \cdots \int_0^t v_{\mathrm{dif}^n}^{\mathrm{dis}}(T)dT^n \tag{2.27}$$

$$F^{\mathrm{dis}}(t) = D_0 + D_1 t + \cdots + \frac{1}{n!}D_n t^n + \int_0^t \cdots \int_0^t v_{\mathrm{dif}^n}^{\mathrm{dis}}(T)dT^{n+1} \tag{2.28}$$

The above equations are rewritten as follows:

$$F^{\mathrm{dis}}(t) = d_0 + d_1 t + \cdots + d_n t^n + \int_0^t \cdots \int_0^t v_{\mathrm{dif}^n}^{\mathrm{dis}}(T) dT^{n+1} \tag{2.29}$$

$$\frac{d}{dt}F^{\mathrm{dis}}(t) = \dot{F}^{\mathrm{dis}}(t) \tag{2.30}$$

$$= d_1 + \cdots + n d_n t^{n-1} + \int_0^t \cdots \int_0^t v_{\mathrm{dif}^n}^{\mathrm{dis}}(T) dT^n \tag{2.31}$$

$$\vdots$$

$$\frac{d^n}{dt^n}F^{\mathrm{dis}}(t) = n! d_n + \int_0^t v_{\mathrm{dif}^n}^{\mathrm{dis}}(T) dT \tag{2.32}$$

$$\frac{d^{n+1}}{dt^{n+1}}F^{\mathrm{dis}}(t) = v_{\mathrm{dif}^n}^{\mathrm{dis}}(t) \tag{2.33}$$

where

$$d_k = \frac{1}{k!} D_k \ (k = 0,\ 1,\ \cdots\ n-1,\ n). \tag{2.34}$$

In this dissertation, the process noise $v_{\mathrm{dif}^n}^{\mathrm{dis}}(t)$ is also assumed not to have correlation with $w(t)$ and v^{dis}.

In usual zeroth-order DOBs, the model of the disturbance is set as follows: [5, 92]

$$\dot{F}^{\mathrm{dis}}(t) = 0. \tag{2.35}$$

This equation represents that the disturbance is modeled as step signal. Even though the higher-order DOBs, the highest-order time derivative of disturbance is also set to zero [93–95], because they are approximated by polynomials of n-th-order of the time t. However, these neglect cause difficulty in constructing and designing Kalman filter based state observer (KFSO) for the disturbance estimation [65].

On the other hand, this dissertation considers the presence of the process noise in the highest-order time derivative of the process noise as shown in (2.33). This makes it possible to construct and design KFSOs for disturbance estimation. The details of the design are described in the following parts.

2.2.3 High-Order Disturbance in MDOF Hybrid Control System

It is known that an acceleration controller based on joint space DOBs realizes a decoupling control in MDOF systems [21]. However, a disturbance caused by simplification of inverse kinematics is remained even though the DOBs work ideally. The disturbance is expressed as follows:

$$\ddot{\boldsymbol{X}}^{\mathrm{dis}} = -\dot{\boldsymbol{T}}\dot{\boldsymbol{x}}^{\mathrm{res}} \tag{2.36}$$

$$= \ddot{\boldsymbol{X}}^{\mathrm{ref}} - \ddot{\boldsymbol{X}}^{\mathrm{res}} \tag{2.37}$$

where $\boldsymbol{X}$ and $\boldsymbol{T}$ represent a position vector and a transformation matrix, respectively. In addition, if the local system has a redundancy, interference from the null space $\boldsymbol{T}\ddot{\boldsymbol{x}}^{\mathrm{ref}}_{\mathrm{null}}$ is added to the disturbance as follows [82, 84, 101]:

$$\begin{aligned} \ddot{\boldsymbol{X}}^{\mathrm{dis}} &= -\dot{\boldsymbol{T}}\dot{\boldsymbol{x}}^{\mathrm{res}} - \boldsymbol{T}\ddot{\boldsymbol{x}}^{\mathrm{ref}}_{\mathrm{null}} && (2.38)\\ &= \ddot{\boldsymbol{X}}^{\mathrm{ref}} - \ddot{\boldsymbol{X}}^{\mathrm{res}}. && (2.39) \end{aligned}$$

Furthermore, if a force control system in a hybrid controller is focused on, a inertia force term behaves as a disturbance term [85, 97] as follows:

$$\begin{aligned} \boldsymbol{A}^{\mathrm{dis}} &= (\boldsymbol{I}-\boldsymbol{S})\,\ddot{\boldsymbol{X}}^{\mathrm{res}} - \boldsymbol{T}\ddot{\boldsymbol{x}}^{\mathrm{ref}}_{\mathrm{null}} - \dot{\boldsymbol{T}}\dot{\boldsymbol{x}}^{\mathrm{res}} \\ &\quad + \left[\boldsymbol{M}^{-1} - (\boldsymbol{I}-\boldsymbol{S})\,\mathrm{diag}\left[\boldsymbol{M}^{-1}\right]\right]\boldsymbol{P}^{\mathrm{dis}} + (\boldsymbol{I}-\boldsymbol{S})\,\mathrm{diag}\left[\boldsymbol{M}^{-1}\right]\boldsymbol{P}^{\mathrm{load}} && (2.40)\\ &= \ddot{\boldsymbol{X}}^{\mathrm{ref}}_{n} - \boldsymbol{S}\ddot{\boldsymbol{X}}^{\mathrm{res}} - (\boldsymbol{I}-\boldsymbol{S})\,\mathrm{diag}\left[\boldsymbol{M}^{-1}\right]\boldsymbol{P}^{\mathrm{ext}}. && (2.41) \end{aligned}$$

where $\boldsymbol{A}^{\mathrm{dis}}$, $\boldsymbol{S}$ and $\boldsymbol{I}$ represent an acceleration disturbance in a hybrid controller, a selection matrix for position control and identity matrix, respectively. The disturbance vector in MDOF systems are also modeled with the time derivative of the process noise as follows:

$$\begin{aligned} \boldsymbol{A}^{\mathrm{dis}}(t) &= \boldsymbol{d}_0 + \boldsymbol{d}_1 t + \cdots + \boldsymbol{d}_n t^n + \int_0^t \cdots \int_0^t \boldsymbol{v}^{\mathrm{dis}}_{\mathrm{dif}^n}(T)dT^{n+1} && (2.42)\\ \frac{d}{dt}\boldsymbol{A}^{\mathrm{dis}}(t) &= \dot{\boldsymbol{A}}^{\mathrm{dis}}(t) = \boldsymbol{d}_1 + \cdots n\boldsymbol{d}_n t^{n-1} + \int_0^t \cdots \int_0^t \boldsymbol{v}^{\mathrm{dis}}_{\mathrm{dif}^n}(T)dT^{n} && (2.43)\\ &\vdots \\ \frac{d^n}{dt^n}\boldsymbol{A}^{\mathrm{dis}}(t) &= n!\boldsymbol{d}_n + \int_0^t \boldsymbol{v}^{\mathrm{dis}}_{\mathrm{dif}^n}(T)dT && (2.44)\\ \frac{d^{n+1}}{dt^{n+1}}\boldsymbol{A}^{\mathrm{dis}}(t) &= \boldsymbol{v}^{\mathrm{dis}}_{\mathrm{dif}^n}(t). && (2.45) \end{aligned}$$

Details of the decoupling process and the suppression of disturbance in the hybrid controller is explained in chapter 5.

2.2.4 High-Order Environmental Disturbance [73, 74, 96]

Environmental Disturbance as Impedance Variation [73, 74]

Parameter variations in environmental characteristics can also be regarded as disturbances. A relationship between the external force and an environmental impedance with a parameter variation from

nominal model is described as follows:

$$F^{\mathrm{ext}} = Z_e(s)X^{\mathrm{res}} = \left(Z_{en}(s) + \Delta Z_e(s)\right) X^{\mathrm{res}} \tag{2.46}$$

where $Z_e(s)$ represent an environmental impedance. An environmental disturbance (EnvD) is defined as below

$$F_e^{\mathrm{dis}} = -\Delta Z_e(s)X^{\mathrm{res}} = Z_{en}(s)X^{\mathrm{res}} - F^{\mathrm{ext}}. \tag{2.47}$$

Environmental Disturbance in Motion Reproduction System [96]

A variation of an environment between motion-saving phase and reproduction phase can also be regarded as an EnvD [96]. If an environmental impedance in motion-saving phase is regarded as a nominal environmental impedance, a relationship between the external force and an environmental impedance in motion reproduction system is described as follows:

$$\begin{aligned} F^{R,\mathrm{ext}} &= Z_e^R(s)X^{R,\mathrm{res}} = \left(Z_{en}^R(s) + \Delta Z_e^R(s)\right) X^{R,\mathrm{res}} && (2.48)\\ &= Z_e^S(s))X^{R,\mathrm{res}} + \Delta Z_e^R(s)X^{R,\mathrm{res}} && (2.49)\\ Z_e^R(s) &= Z_e^S(s). && (2.50) \end{aligned}$$

where superscripts S and R represent a saved value and reproduced value, respectively. From above equations, an EnvD in motion reproduction system is defined as

$$F_e^{R,\mathrm{dis}} = Z_e^S(s)X^{R,\mathrm{res}} - F^{R,\mathrm{ext}}. \tag{2.51}$$

The EnvDs are also modeled with the time derivative of the process noise as follows:

$$\begin{aligned} F_e^{\mathrm{dis}}(t) &= d_{e0} + d_{e1}t + \cdots + d_{en}t^n + \int_0^t \cdots \int_0^t v_{\mathrm{edif^n}}^{\mathrm{dis}}(T)dT^{n+1} && (2.52)\\ \frac{d}{dt}F^{\mathrm{dis}}(t) &= \dot{F}_e^{\mathrm{dis}}(t) = d_{e1} + \int_0^t \cdots \int_0^t v_{\mathrm{edif^n}}^{\mathrm{dis}}(T)dT^n && (2.53)\\ &\vdots \\ \frac{d^n}{dt^n}F_e^{\mathrm{dis}}(t) &= n!d_{en} + \int_0^t v_{\mathrm{edif^n}}^{\mathrm{dis}}(T)dT && (2.54)\\ \frac{d^{n+1}}{dt^{n+1}}F_e^{\mathrm{dis}}(t) &= v_{\mathrm{edif^n}}^{\mathrm{dis}}(t). && (2.55) \end{aligned}$$

Details of suppressing the EnvD in a force control system and motion reproduction system is proposed in chapter 3 and chapter 5, respectively.

2.3 Indices for Setting the Order of Disturbances

This part describes indices for setting the order of disturbances n. Generally, the n-th-order disturbance $F^{\mathrm{dis,n}}$ is estimated by a DOB through $n+1$-th-order low-pass filter as follows [93–95]:

$$\hat{F}^{\mathrm{dis,n}} = \frac{a_n s^n + a_{n-1}s^{n-1} + \cdots a_0}{b_{n+1}s^{n+1} + b_n s^n + \cdots b_0} F^{\mathrm{dis,n}} \tag{2.56}$$

where a, b represents positive constants. A motion equation with compensation by the estimated disturbance, $\hat{F}^{\mathrm{dis,n}}$ is expressed as follows:

$$\begin{aligned} M_n \ddot{X}^{\mathrm{res}} &= F^{\mathrm{ref}} - \left(1 - \frac{a_n s^n + a_{n-1}s^{n-1} + \cdots a_0}{b_{n+1}s^{n+1} + b_n s^n + \cdots b_0}\right) F^{\mathrm{dis,n}} && (2.57) \\ &= F^{\mathrm{ref}} - G^{\mathrm{dis,n}}_{\mathrm{sen}}(s) F^{\mathrm{dis,n}} && (2.58) \end{aligned}$$

where $G^{\mathrm{dis}}_{\mathrm{sen}}(s)$ is a sensitivity to the disturbance. $G^{\mathrm{dis}}_{\mathrm{sen}}(s)$ has a high-pass filter structure. If the filter is set to have a double root $g^{\mathrm{dis,1}}$ in the case of $n = 1$, the 1st-order (ramp signal) disturbance is estimated as

$$\hat{F}^{\mathrm{dis,1}} = \frac{2g^{\mathrm{dis,1}} s + {g^{\mathrm{dis,1}}}^2}{(s + g^{\mathrm{dis,1}})^2} F^{\mathrm{dis,1}}. \tag{2.59}$$

Similarly, the 0th-order (step signal) disturbance is estimated as

$$\hat{F}^{\mathrm{dis,0}} = \frac{g^{\mathrm{dis,0}}}{s + g^{\mathrm{dis,0}}} F^{\mathrm{dis,0}}. \tag{2.60}$$

The sensitivities to the disturbances are expressed as below:

$$\begin{aligned} G^{\mathrm{dis,1}}_{\mathrm{sen}}(s) &= 1 - \frac{2g^{\mathrm{dis,1}} s + {g^{\mathrm{dis,1}}}^2}{(s + g^{\mathrm{dis,1}})^2} = \frac{s^2}{(s + g^{\mathrm{dis,1}})^2} && (2.61) \\ G^{\mathrm{dis,0}}_{\mathrm{sen}}(s) &= 1 - \frac{g^{\mathrm{dis,0}}}{s + g^{\mathrm{dis,0}}} = \frac{s}{s + g^{\mathrm{dis,1}}}. && (2.62) \end{aligned}$$

If a ramp disturbance D^{dis}/s^2 is applied to the system, the disturbance can be eliminated by a 1st-order DOB by considering the final value theorem, as follows:

$$\lim_{s\to 0} s \cdot G^{\mathrm{dis,1}}_{\mathrm{sen}}(s) = \lim_{s\to 0} s \cdot \frac{s^2}{(s + g^{\mathrm{dis,1}})^2} \frac{D^{\mathrm{dis}}}{s^2} = 0. \tag{2.63}$$

0th-order DOB can also suppress the disturbance if the bandwidth of the DOB $g^{\mathrm{dis,0}}$ is set to sufficiently high as follows:

$$\lim_{s\to 0} s \cdot G^{\mathrm{dis,0}}_{\mathrm{sen}}(s) = \lim_{s\to 0} s \cdot \frac{s}{s + g^{\mathrm{dis,0}}} \frac{D^{\mathrm{dis}}}{s^2} = \frac{D^{\mathrm{dis}}}{g^{\mathrm{dis,0}}} \to 0 \ (g^{\mathrm{dis,0}} \to \infty). \tag{2.64}$$

Fig. 2-3 shows response against ramp disturbance D^{dis}/s^2 with respect to 0th-order and 1st-order DOBs. The figure also confirms that the disturbance can be eliminated by the 1st-order DOB and the 0th-order DOB can be suppress the disturbance if the bandwidth of the disturbance estimation is sufficiently high.

On the other hand, if the step disturbance D^{dis}/s is added, the sensitivities to the disturbances are expressed as follows:

$$\lim_{s\to 0} s \cdot G_{\mathrm{sen}}^{\mathrm{dis},1}(s) = \lim_{s\to 0} s \cdot \frac{s^2}{(s+g^{\mathrm{dis},1})^2}\frac{D^{\mathrm{dis}}}{s} = 0 \tag{2.65}$$

$$\lim_{s\to 0} s \cdot G_{\mathrm{sen}}^{\mathrm{dis},0}(s) = \lim_{s\to 0} s \cdot \frac{s}{s+g^{\mathrm{dis},0}}\frac{D^{\mathrm{dis}}}{s} = 0. \tag{2.66}$$

As shown in the above equations, the step disturbance can be suppressed in the both cases. However, the disturbance response of the 1st-order DOB against the step disturbance tend to oscillate as shown in Fig. 2-2. This is because a zero in the numerator of $G_{\mathrm{sen}}^{\mathrm{dis},1}(s)$ is remained in the case of the 1st-order DOB as shown in (2.65). In actual case, the feedback of the estimated value by the 1st-order DOB has a potential to read instability. This is because the number of the resulting integrators from the estimated value of 1st-order DOB is larger than that of the 0th-order DOB. This phenomenon indicates that increasing the order of the disturbance model have a possibility to cause instability, though the disturbance suppression performance is improved. Therefore, the order should set to the same value as the order of disturbance if the characteristics of the disturbance can be identified. (e. g. in the case of a step disturbance, n should be set to 0. In the case of a ramp disturbance, n should be set to 1.

Additionally, if the time derivatives of the disturbance are need, the order of the disturbance model should be set to the order of the time derivatives. (e. g. in the case that a force proportional-derivative (PD) controller is needed, the order of the disturbance model should be set to 1. In the case that a second-order time derivative is needed, the disturbance model should be set to 2.)

2.4 Disturbances Estimation Based on Kalman Filter

This section describes disturbance estimation based on the KFSO [65] to suppress noise effects.

2.4.1 Augmented State Space Model for Disturbances Estimation

An augmented state variables with disturbance and n-th higher-order time derivatives of the disturbance can be described as follows:

$$\boldsymbol{Z}^n(t) = \left[X^{\mathrm{res}}(t) \;\; \dot{X}^{\mathrm{res}}(t) \;\; F^{\mathrm{dis}}(t) \;\; \dot{F}^{\mathrm{dis}}(t) \;\; \cdots \;\; \frac{d^{n-1}}{dt^{n-1}}F^{\mathrm{dis}}(t) \;\; \frac{d^n}{dt^n}F^{\mathrm{dis}}(t)\right]^T. \tag{2.67}$$

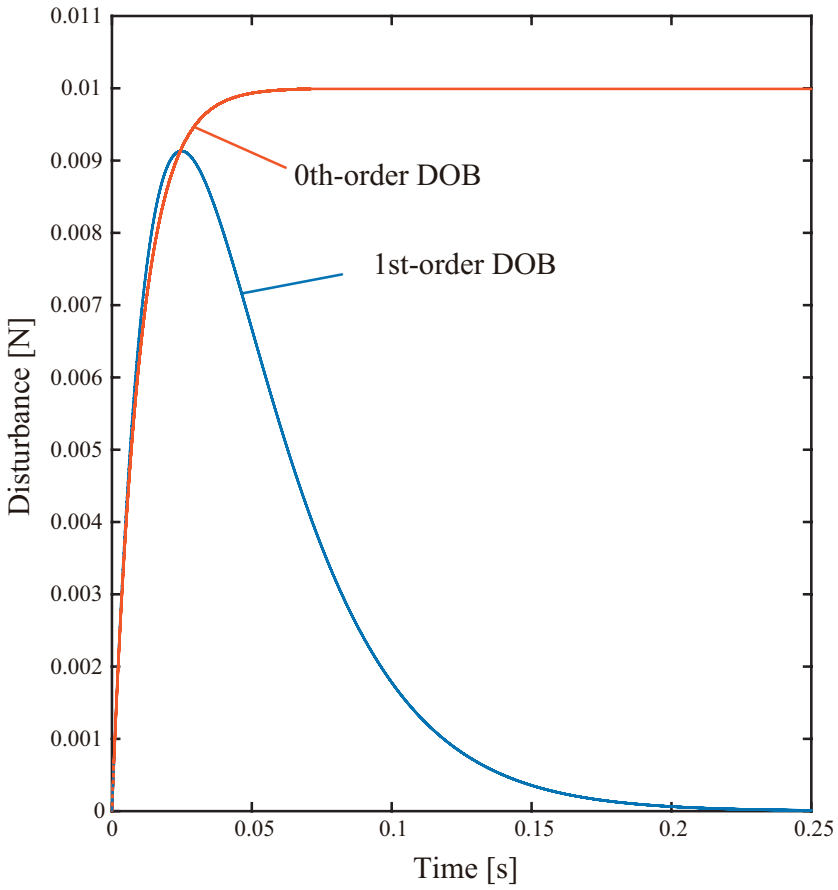

Fig. 2-2: Response against ramp disturbance D^{dis}/s^2 with respect to 0th-order and 1st-order DOBs.

In general case, an augmented state space model for disturbance estimation with higher-order time derivatives of the disturbance can be derived as follows:

$$\dot{\boldsymbol{Z}}^n(t) = \mathbf{A}^n \boldsymbol{Z}^n(t) + \mathbf{B}^n \boldsymbol{U}(t) + \mathbf{B}_v^n \boldsymbol{V}^n(t) \tag{2.68}$$

$$\boldsymbol{Y}(t) = \boldsymbol{c}\boldsymbol{Z}^n(t) + \boldsymbol{W}(t) \tag{2.69}$$

$$= X^{\mathrm{res}}(t) + w(t) \tag{2.70}$$

$$\boldsymbol{U}(t) = F^{\mathrm{ref}}(t) \tag{2.71}$$

$$\boldsymbol{V}^n(t) = \left[v^{\mathrm{dis}}(t) \;\; v_{\mathrm{dif}^n}^{\mathrm{dis}}(t) \right]^T \tag{2.72}$$

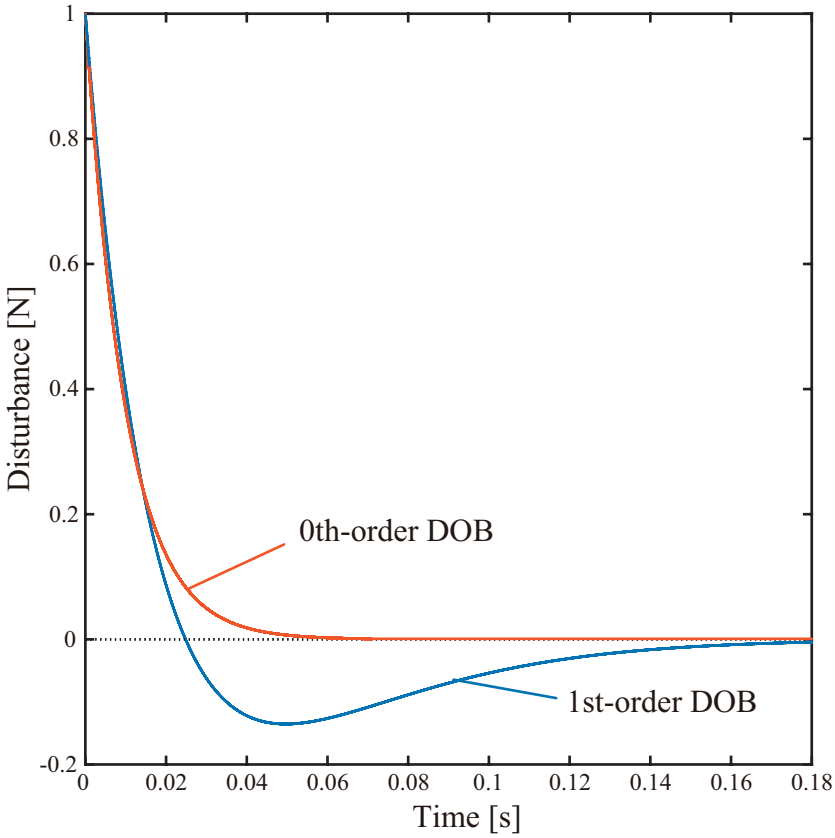

Fig. 2-3: Response against step disturbance D^{dis}/s with respect to 0th-order and 1st-order DOBs.

where

$$\mathbf{A}^n = \begin{bmatrix} 0 & 1 & 0 & 0 & 0 & \cdots & 0 \\ 0 & 0 & -\frac{1}{M_n} & 0 & 0 & \cdots & 0 \\ 0 & 0 & 0 & 1 & 0 & \cdots & 0 \\ 0 & 0 & 0 & 0 & 0 & \ddots & \vdots \\ 0 & 0 & 0 & 0 & 0 & \cdots & 0 \end{bmatrix}, \ \mathbf{B}^n = \begin{bmatrix} 0 \\ \frac{1}{M_n} \\ 0 \\ \vdots \\ 0 \end{bmatrix}, \ \boldsymbol{c}^n = \begin{bmatrix} 1 & 0 & 0 & \cdots & 0 \end{bmatrix} \tag{2.73}$$

$$\mathbf{B}_v^n = \begin{bmatrix} 0 & 0 \\ \frac{1}{M_n} & 0 \\ 0 & 0 \\ \vdots & \vdots \\ 0 & 1 \end{bmatrix}. \tag{2.74}$$

In the state space model, the process noises only in dimensions of the disturbance and highest-order time derivative of the disturbance should be considered. A discrete-time state space model on a sampling

point with a zero order holder and a simpler is described as follows:

$$\boldsymbol{Z}^n(k+1) = \mathbf{A}_d^n \boldsymbol{Z}(k) + \mathbf{B}_d^n \boldsymbol{U}(k) + \mathbf{B}_{vd}^n \boldsymbol{V}^n(k) \tag{2.75}$$

$$\boldsymbol{Z}^n(k) = \left[X^{\mathrm{res}}(k) \;\; \dot{X}^{\mathrm{res}}(k) \;\; F^{\mathrm{dis}}(k) \;\; \dot{F}^{\mathrm{dis}}(k) \;\; \cdots \;\; \frac{d^{n-1}}{dt^{n-1}} F^{\mathrm{dis}}(k) \;\; \frac{d^n}{dt^n} F^{\mathrm{dis}}(k) \right]^T \tag{2.76}$$

$$\boldsymbol{Y}(k) = \boldsymbol{c}^n \boldsymbol{Z}^n(k) + \boldsymbol{W}(k) \tag{2.77}$$

$$= X^{\mathrm{res}}(k) + w(k) \tag{2.78}$$

$$\mathbf{A}_d^n = \mathbf{e}^{\mathbf{A}^n T_s} \tag{2.79}$$

$$\mathbf{B}_d^n = \int_0^{T_s} \mathbf{e}^{\mathbf{A}^n t} \mathbf{B}^n dt \tag{2.80}$$

where k, T_s and $\mathbf{e}^{\bullet}$ represent a sampling instant, a sampling time and a state transition matrix, respectively. By using the above state space model in the discrete-time domain, a KFSO for disturbance estimation can be constructed.

2.4.2 Kalman Filtering

Kalman filter is known as an optimal filter to minimize the following evaluation function $J(k)$ [102]

$$J^n(k) = \mathrm{E}\left[\boldsymbol{e}^{n2}(k) \right] \tag{2.81}$$

$$\boldsymbol{e}^n(k) = \boldsymbol{Z}^n(k) - \hat{\boldsymbol{Z}}^n(k) \tag{2.82}$$

where $\mathrm{E}[\bullet]$, $\hat{\boldsymbol{Z}}^n(k)$ and $\boldsymbol{e}^n(k)$ represent an expectation operator, an estimated state vector and estimation error vector, respectively. The right hand side of (2.81) represents a mean square error. An estimated variables with minimum mean square error can be obtained through the Kalman filtering process.

An observer gain of Kalman filter which is called "Kalman gain" $\mathbf{G}_{\mathrm{kf}}^n(k)$ is expressed as follows:

$$\mathbf{G}_{\mathrm{kf}}^n(k) = \mathbf{P}^{n-}(k) \boldsymbol{c}^{nT} \left(\boldsymbol{c}^n \mathbf{P}^{n-}(k) \boldsymbol{c}^n + \mathbf{R} \right)^{-1} \tag{2.83}$$

where $\mathbf{P}^-(k)$ and $\mathbf{R}$ represent an prior error covariance matrix and a covariance matrix of the observation noise. The prior error covariance matrix satisfies the following equation

$$\mathbf{P}^{n-}(k) = \mathbf{A}_d^n \left[\mathbf{P}^{n-}(k-1) - \boldsymbol{c}^{nT} \left(\boldsymbol{c}^n \mathbf{P}^{\boldsymbol{n}-}(k-1) \boldsymbol{c}^n + \mathbf{R} \right)^{-1} \boldsymbol{c}^n \mathbf{P}^{n-}(k-1) \right] \mathbf{A}_d^n + \boldsymbol{Q}^n \tag{2.84}$$

where $\boldsymbol{Q}^n$ represents a covariance matrix of the process noise. Eq. (2.84) represents a discrete time Riccati equation. In the estimation process of Kalman filter, the initial values of the estimated variables

$\hat{\boldsymbol{Z}}^n(0)$ and the error covariance matrix $\mathbf{P}^n(0)$ are given as follows [102]:

$$\hat{\boldsymbol{Z}}^n(0) = \mathrm{E}\left[\boldsymbol{Z}^n(0)\right] = \boldsymbol{Z}^n(0) \tag{2.85}$$

$$\mathbf{P}^n(0) = \mathrm{E}\left[\left(\boldsymbol{Z}^n(0) - \mathrm{E}\left[\boldsymbol{Z}^n(0)\right]\right)\left(\boldsymbol{Z}^n(0) - \mathrm{E}\left[\boldsymbol{Z}^n(0)\right]\right)^T\right] = \boldsymbol{\Sigma}(0) = \mathbf{0} \tag{2.86}$$

The Kalman filtering process is divided into the following two steps: the prediction step and updating step. The Kalman filtering process is summarized in the next page.

Kalman filtering process

Prediction Step

The predicted (a priori) state estimate $\hat{\boldsymbol{Z}}^{n-}(k)$ and predicted (a priori) estimate error covariance matrix $\mathbf{P}^{n-}(k)$ are estimated.

- Predicted (a priori) state estimate

$$\hat{\boldsymbol{Z}}^{n-}(k) = \mathbf{A}_d^n \hat{\boldsymbol{Z}}^n(k-1) + \mathbf{B}_d^n \boldsymbol{U}(k-1) \tag{2.87}$$

$$= \left[\hat{X}^{-\mathrm{res}}(t) \;\; \dot{\hat{X}}^{-\mathrm{res}}(t) \;\; \hat{F}^{-\mathrm{dis}}(t) \;\; \dot{\hat{F}}^{-\mathrm{dis}}(t) \;\; \cdots \;\; \frac{d^{n-1}}{dt^{n-1}}\hat{F^{-\mathrm{dis}}}(t) \;\; \frac{d^n}{dt^n}\hat{F}^{-\mathrm{dis}}(t)\right]^T \tag{2.88}$$

- Predicted (a priori) estimate error covariance matrix

$$\mathbf{P}^{n-}(k) = \mathbf{A}_d^n \mathbf{P}^n(k-1)\mathbf{A}_d^{nT} + \mathbf{Q}^n \tag{2.89}$$

Updating Step

The Kalman filter gain matrix $\mathbf{G}_{\mathrm{kf}}^n(k)$ is calculated. The estimated (a posteriori) state vector $\hat{\boldsymbol{Z}}^n(k)$ and the (a posteriori) error matrix covariance matrix $\mathbf{P}^n(k)$are updated using the Kalman gain and an actual measurement $\boldsymbol{Y}(k)$ at every sampling instant.

- Kalman gain

$$\mathbf{G}_{\mathrm{kf}}^n(k) = \mathbf{P}^{n-}(k)\boldsymbol{c}^{nT}\left(\boldsymbol{c}^n\mathbf{P}^{n-}(k)\boldsymbol{c}^n + \mathbf{R}\right)^{-1} \tag{2.90}$$

- The estimated (a posteriori) state vector

$$\hat{\boldsymbol{Z}}^n(k) = \hat{\boldsymbol{Z}^{n-}}(k) + \mathbf{G}_{\mathrm{kf}}^n(k)\left(\boldsymbol{Y}(k) - \boldsymbol{c}^n\hat{\boldsymbol{Z}^{n-}}(k)\right) \tag{2.91}$$

$$= \left[\hat{X}^{\mathrm{res}}(t) \;\; \dot{\hat{X}}^{\mathrm{res}}(t) \;\; \hat{F}^{\mathrm{dis}}(t) \;\; \dot{\hat{F}}^{\mathrm{dis}}(t) \;\; \cdots \;\; \frac{d^{n-1}}{dt^{n-1}}\hat{F^{\mathrm{dis}}}(t) \;\; \frac{d^n}{dt^n}\hat{F}^{\mathrm{dis}}(t)\right]^T \tag{2.92}$$

- The estimated (a posteriori) state vector

$$\mathbf{P}^n(k) = \left(\boldsymbol{I} - \mathbf{G}_{\mathrm{kf}}^n(k)\boldsymbol{c}^n\right)\mathbf{P}^{n-}(k) \tag{2.93}$$

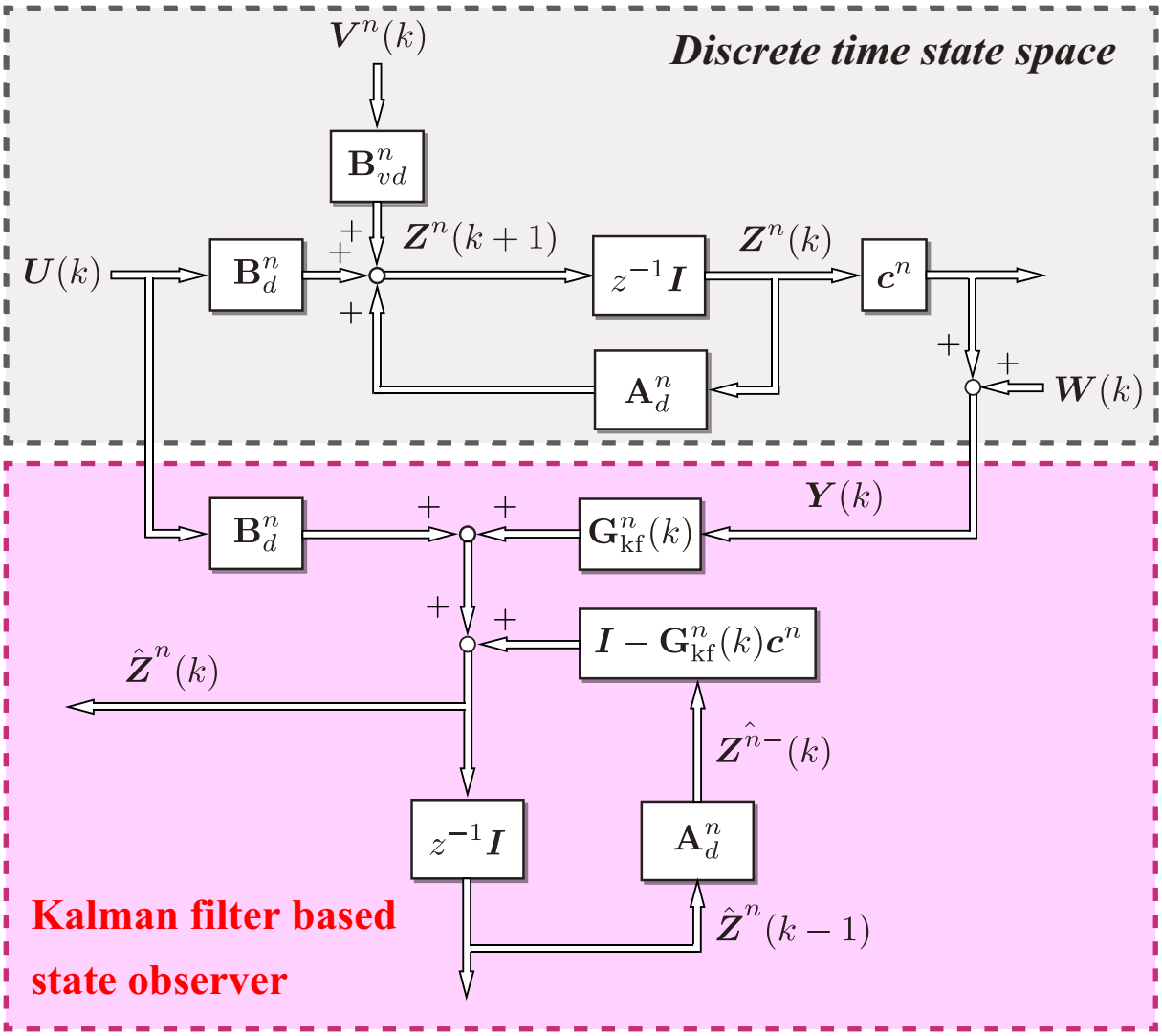

Fig. 2-4: Block diagram of the Kalman filtering process.

Through the above process, the estimated state vector with the estimated state variables $\hat{\boldsymbol{Z}}^n(k)$ is obtained with the minimum mean square error. Fig. 2-4 shows a block diagram of the Kalman filtering process.

2.4.3 Derivation for Structure of Covariance Matrix for Kalman Filter

In the Kalman filtering process, the covariance matrices $\mathbf{R}$ and $\mathbf{Q}^n$ have free parameters. The covariance matrix of the observation noise $\mathbf{R}$ can be determined by considering sensor resolution [66]. Therefore, the elements of $\mathbf{Q}^n$ are design parameters.

However, the determination process of the elements of $\mathbf{Q}^n$ in conventional researches are not clear [65, 67, 69]. The conventional researches [65, 69] rely on tests and simulations for determining elements of $\mathbf{Q}^n$. Or, the conventional research [67] utilizes the calculated values by using the sensor value.

In contrast, this dissertation shows a clear process for determining the structure of $\mathbf{Q}^n$ for the disturbance estimation.

In order to determine the structure of $\mathbf{Q}^n$, the derivation of a prior error covariance matrix is considered [102]. To derive the prior error covariance matrix, a prior state estimation error is utilized. The prior state estimation error $\boldsymbol{e}^{n-}(k)$ is described as

$$\begin{aligned} \boldsymbol{e}^{n-}(k) &= \boldsymbol{Z}^n(k) - \hat{\boldsymbol{Z}}^{n-}(k) && (2.94)\\ &= \mathbf{A}_d^n \boldsymbol{e}^n(k-1) + \mathbf{B}_{vd}^n \boldsymbol{V}^n(k-1). && (2.95) \end{aligned}$$

To obtain (2.95) the following assumption in Kalman filtering is utilized:

$$\mathrm{E}\left[\boldsymbol{V}^n(k-1)\right] = \bar{\boldsymbol{V}}^n = \mathbf{0} \tag{2.96}$$

where $\mathrm{E}[\bullet]$ is a expectation value. This equation represents that the mean values of the process noises are equal to zero. By using (2.95), the prior error covariance matrix is derived as follows:

$$\begin{aligned} \mathbf{P}^{n-}(k) &= \mathrm{E}\left[\boldsymbol{e}^{n-}(k)\boldsymbol{e}^{n-}(k)^T\right] + \mathbf{A}_d^n \mathrm{E}\left[\boldsymbol{e}^n(k-1)\boldsymbol{e}^n(k-1)^T\right] \mathbf{A}_d^{nT} \\ &\quad + \mathbf{B}_{vd}^n \mathrm{E}\left[\boldsymbol{V}^n(k-1)\boldsymbol{V}^n(k-1)^T\right] {\mathbf{B}_{vd}^n}^T && (2.97)\\ &= \mathbf{A}_d^n \mathbf{P}^n(k-1)\mathbf{A}_d^{nT} + \mathbf{B}_{vd}^n \boldsymbol{\Sigma}_v^{n2} {\mathbf{B}_{vd}^n}^T && (2.98)\\ \boldsymbol{\Sigma}_v^{n2} &= \mathrm{E}\left[\left\{\boldsymbol{V}^n(k-1) - \bar{\boldsymbol{V}}^n\right\}\left\{\boldsymbol{V}^n(k-1)^T - \bar{\boldsymbol{V}}^n\right\}\right] && (2.99) \end{aligned}$$

where $\boldsymbol{\Sigma}_v^2$ represents the covariance matrix of process noise. In the derivation of the prior error covariance matrix, the following assumption of Kalman filtering is utilized:

$$\mathrm{E}\left[\boldsymbol{e}^{n-}(k)\boldsymbol{V}^n(k-1)^T\right] = \mathbf{0}. \tag{2.100}$$

If v^{dis} and $v_{\mathrm{dif^n}}^{\mathrm{dis}}$ are assumed to be independent, the covariance of these process noises is equal to zero as given below:

$$\begin{aligned}
\sigma^2_{v^{\mathrm{dis}}v_{\mathrm{dif^n}}^{\mathrm{dis}}} &= \mathrm{E}\left[\{v^{\mathrm{dis}}(k)-\bar{v}^{\mathrm{dis}}\}\{v_{\mathrm{dif^n}}^{\mathrm{dis}}(k)-\bar{v}^{\mathrm{dis}}\}\right] && (2.101)\\
&= \mathrm{E}\left[v^{\mathrm{dis}}(k)v_{\mathrm{dif^n}}^{\mathrm{dis}}(k)\right]-\bar{v}^{\mathrm{dis}}\bar{v}_{\mathrm{dif^n}}^{\mathrm{dis}} && (2.102)\\
&= \mathrm{E}\left[v^{\mathrm{dis}}(k)\right]\mathrm{E}\left[v_{\mathrm{dif^n}}^{\mathrm{dis}}(k)\right]-\bar{v}^{\mathrm{dis}}\bar{v}_{\mathrm{dif^n}}^{\mathrm{dis}} && (2.103)\\
&= 0. && (2.104)
\end{aligned}$$

According to (2.96), (2.99), and (2.104), the covariance matrix of process noise is derived as follows:

$$\mathbf{\Sigma}_v^{n2}=\begin{bmatrix}\sigma^2_{v^{\mathrm{dis}}} & 0\\ 0 & \sigma^2_{v_{\mathrm{dif^n}}^{\mathrm{dis}}}\end{bmatrix}. \tag{2.105}$$

Finally, according to (2.98) and (2.105), the resulting covariance matrix $\mathbf{Q}^n$ is obtained as

$$\begin{aligned}
\mathbf{Q}^n &= \mathbf{B}_{vd}^n\mathbf{\Sigma}_v^{n2}{\mathbf{B}_{vd}^n}^T && (2.106)\\
&= \left[\int_0^{T_s}\mathbf{e}^{\mathbf{A}^n t}dt\mathbf{B}_v^n\right]\begin{bmatrix}\sigma^2_{v^{\mathrm{dis}}} & 0\\ 0 & \sigma^2_{v_{\mathrm{dif^n}}^{\mathrm{dis}}}\end{bmatrix}\left[\mathbf{B}_v^{nT}\int_0^{T_s}\mathbf{e}^{\mathbf{A}^{nT}t}dt\right]. && (2.107)
\end{aligned}$$

Although the conventional research requires three variances of the process noise [67], only two variances should be considered for the disturbance estimation according to the derived process by this dissertation as shown by (2.107).

2.5 Example for Second Order Disturbance Estimation

This part shows an example for second order disturbance estimation based on a Kalman filter based state observer. In this case, the model of disturbance is described as

$$\frac{d^3}{dt^3}F^{\mathrm{dis}}=v_{\mathrm{dif^3}}^{\mathrm{dis}}. \tag{2.108}$$

If the model of the third order time derivative is set to zero, the covariance matrix for the Kalman filtering [65, 68] cannot be appropriately determined.

Fig. 2-5 (a) shows a gain diagrams for estimation of disturbance with respect to the conventional velocity based DOBs and the derived Kalman filter based disturbance estimation. In this dissertation, a steady state Kalman filter is utilized for obtaining the frequency characteristics [98]. As shown in the figure, 2nd-order DOB without considering time derivative of process noise cannot achieve the estimation

with the same level of the other method. This is because the element in the covariance matrix is regarded as a kind of gain for Kalman filter as shown in [68]. Even though the gain is increased, the estimation is difficult in the case of disturbance estimation. On the other hand, the designed KFSO realize the estimation with the same bandwidth of the conventional DOBs. Fig. 2-5 (b) shows a gain diagrams for noise sensitivity in disturbance estimation. The transfer function is obtained based on (2.13). As shown in the figure, the gradient of the gain diagram of the conventional DOBs in higher frequency domain is almost 0 dB/dec. Therefore, it is difficult to reduce noise effect. However, the proposed Kalman filter based disturbance estimation has a gradient with -20 dB/dec. Therefore, the proposed method shows a better noise suppression performance compared to the conventional method.

From the next part, the details for designing KFSOs are described. First, a state estimation by the Kalman filter for a 0th-order disturbance is derived in order to confirm the validities of the proposed modeling.

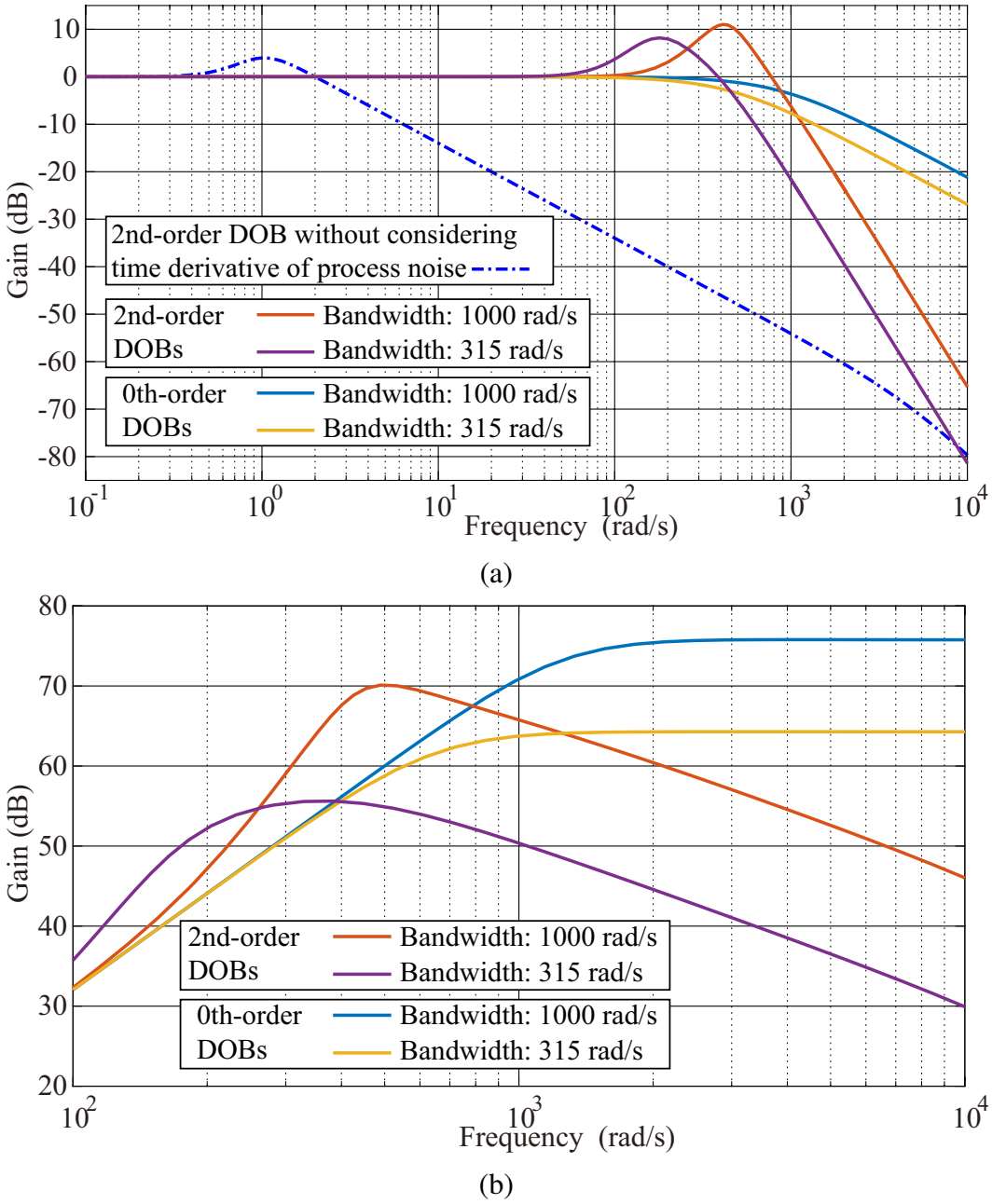

Fig. 2-5: Gain diagrams. (a) Disturbance estimation. (b) Noise sensitivity in disturbance estimation.

2.6 Kalman Filter Based State Observer

This part describes a design of a KFSO for estimating state variables including the 0th-order disturbance/external torque. A state-space equation of an actuator in which the state variable includes a disturbance term can be described as follows [7]:

$$\dot{\boldsymbol{Z}}(t) = \mathbf{A}\boldsymbol{Z}(t) + \mathbf{B}\boldsymbol{u}(t) + \mathbf{B}_v\boldsymbol{V}(t) \tag{2.109}$$

$$\boldsymbol{Z}(t) = \left[q^{\mathrm{res}}(t) \;\; \dot{q}^{\mathrm{res}}(t) \;\; \tau^{\mathrm{dis}}(t)\right]^T \tag{2.110}$$

$$\boldsymbol{Y}(t) = \boldsymbol{c}\boldsymbol{Z}(t) + \boldsymbol{W}(t) = q^{\mathrm{res}}(t) + w(t) \tag{2.111}$$

where

$$\mathbf{A} = \begin{bmatrix} 0 & 1 & 0 \\ 0 & 0 & -\frac{1}{J_n} \\ 0 & 0 & 0 \end{bmatrix}, \; \mathbf{B} = \begin{bmatrix} 0 \\ \frac{1}{J_n} \\ 0 \end{bmatrix}, \; \boldsymbol{c}^T = \begin{bmatrix} 1 \\ 0 \\ 0 \end{bmatrix}. \tag{2.112}$$

Here, $q^{\mathrm{res}}(t)$, $\tau^{\mathrm{dis}}(t)$ and J_n represent a joint angle, a joint torque and a nominal inertia, respectively. An actuator dynamics model in the discrete-time domain can be formulated as

$$\boldsymbol{Z}(k+1) = \mathbf{A}_d\boldsymbol{Z}(k) + \mathbf{B}_d u(k) + \mathbf{B}_{vd}\boldsymbol{V}(k) \tag{2.113}$$

$$\boldsymbol{Z}(k) = \left[q^{\mathrm{res}}(k) \;\; \dot{q}^{\mathrm{res}}(k) \;\; \tau^{\mathrm{dis}}(k)\right]^T \tag{2.114}$$

$$\boldsymbol{Y}(k) = \boldsymbol{c}\boldsymbol{Z}(k) + \boldsymbol{W}(k) = q^{\mathrm{res}}(k) + w(k) \tag{2.115}$$

$$\mathbf{A}_d = \mathbf{e}^{\mathbf{A}T_s} \tag{2.116}$$

$$\mathbf{B}_d = \int_0^{T_s} \mathbf{e}^{\mathbf{A}T_s}\mathbf{B}dt \tag{2.117}$$

where T_s is a sampling time. The Kalman filtering process is executed based on (2.113). The filtering process can be divided into the prediction and updating phases. In the prediction phase, predicted (a priori) state estimate $\hat{\boldsymbol{Z}}^-(k)$ and predicted (a priori) estimate error covariance matrix $\mathbf{P}^-(k)$ are estimated as follows:

$$\hat{\boldsymbol{Z}}^-(k) = \mathbf{A}_d\hat{\boldsymbol{Z}}(k-1) + \mathbf{B}_d u(k-1) \tag{2.118}$$

$$= \left[\hat{q}_{\mathrm{kf}}^{-\mathrm{res}}(k) \;\; \hat{\dot{q}}_{\mathrm{kf}}^{-\mathrm{res}}(k) \;\; \hat{\tau}_{\mathrm{kf}}^{-\mathrm{dis}}(k)\right]^T \tag{2.119}$$

$$\mathbf{P}^-(k) = \mathbf{A}_d\mathbf{P}(k-1)\mathbf{A}_d^T + \mathbf{Q}. \tag{2.120}$$

where k, q and τ represent a sampling instant, a joint angel and joint torque, respectively. In addition, $\bullet^-$, subscript kf represent a prior estimated value and estimated variable by a Kalman filter, respectively. In the updating phase, the Kalman filter gain matrix $\mathbf{G}_{\rm kf}(k)$ is calculated as

$$\mathbf{G}_{\rm kf}(k) = \mathbf{P}^-(k)\boldsymbol{c}^T\left(\boldsymbol{c}\mathbf{P}^-(k)\boldsymbol{c} + \mathbf{R}\right)^{-1} \tag{2.121}$$

where $\mathbf{R}$ is a covariance matrix of the observation noise. The estimated (a posteriori) state vector and the (a posteriori) error matrix covariance matrix are updated using an actual measurement $\boldsymbol{Y}(k)$ at every sampling instant as follows:

$$\hat{\boldsymbol{Z}}(k) = \hat{\boldsymbol{Z}}^-(k) + \mathbf{G}_{\rm kf}(k)\left(\boldsymbol{Y}(k) - \boldsymbol{c}\hat{\boldsymbol{Z}}^-(k)\right) \tag{2.122}$$

$$= \left[\hat{q}^{\rm res}_{\rm kf}(k) \;\; \hat{q}^{\rm res}_{\rm kf}(k) \;\; \hat{\tau}^{\rm dis}_{\rm kf}(k)\right]^T \tag{2.123}$$

$$\mathbf{P}(k) = \left(\boldsymbol{I} - \mathbf{G}_{\rm kf}(k)\boldsymbol{c}\right)\mathbf{P}^-(k). \tag{2.124}$$

The estimated variables $\hat{\boldsymbol{Z}}(k)$ are used for control systems. In (2.120), $\mathbf{Q}$ represents a covariance matrix with respect to system noise. The elements of this matrix are the design parameters of the Kalman filter. $\mathbf{R}$ can be determined by considering the resolution of sensors as follows [66]:

$$\mathbf{R} = \sigma_w^2 = \frac{\Delta q^2}{12} \tag{2.125}$$

where Δq is a sensor resolution. It is known that the performance of estimation by the Kalman filter highly depends on the determination of $\mathbf{Q}$ [68]. In this case, $\mathbf{Q}$ has nine elements as follows:

$$\begin{aligned}
\mathbf{Q} &= \mathbf{B}_{vd}\boldsymbol{\Sigma}_v^2\mathbf{B}_{vd}^T \\
&= \left[\int_0^{T_s} \mathbf{e}^{\mathbf{A}t}dt\mathbf{B}_v\right]\boldsymbol{\Sigma}_v^2\left[\mathbf{B}_v^T\int_0^{T_s}\mathbf{e}^{\mathbf{A}^T t}dt\right] \\
&= \begin{bmatrix} Q_{11} & Q_{12} & Q_{13} \\ Q_{21} & Q_{22} & Q_{23} \\ Q_{31} & Q_{32} & Q_{33} \end{bmatrix}.
\end{aligned} \tag{2.126}$$

As shown in (2.126), the number of design parameters in the KFSO is larger than that in normal DOBs, though the design parameters of the DOBs are usually one or two poles [8, 103], which are related to the bandwidth of disturbance estimation. In conventional research, however, the elements of $\mathbf{Q}$ are determined by trial and error through simulations or experiments [65, 67, 68]. However, it is difficult to measure the actual variance in the dimension of disturbance/external torque. In the next section, the structure of $\mathbf{Q}$ is determined in order to reduce the number of design parameters.

2.7 Determination of Covariance Matrix Q for Disturbance/External Torque Estimation

2.7.1 Motion Equation and State-Space Equation Considering System Noise

If the presence of process noise is explicitly considered, the motion equation of an actuator is described as

$$J_n \ddot{q}^{\mathrm{res}}(t) = \tau^{\mathrm{ref}}(t) - \tau^{\mathrm{dis}}(t) + v^{\mathrm{dis}}(t) \tag{2.127}$$

$$\tau^{\mathrm{dis}}(t) = \tau^{\mathrm{ext}}(t) + \tau^{\mathrm{load}}(t) \tag{2.128}$$

where $\tau^{\mathrm{load}}(t)$ represents the disturbance torque that includes parameter variation and friction terms except that for the external torque. Additionally, the model of disturbance is assumed as shown in the following equation:

$$\dot{\tau}^{\mathrm{dis}}(t) = v^{\mathrm{dis}}_{\mathrm{dif}^0}(t). \tag{2.129}$$

Usually, the time derivative of disturbance is set to zero [92, 103] as the model of disturbance. However, this dissertation assumes the presence of the process noise in the model for the time derivative of disturbance to determine the appropriate covariance matrix. According to (2.127) and (2.129), the state vector and the input vector in (2.109) can be determined as follows:

$$\boldsymbol{V}(t) = \begin{bmatrix} v^{\mathrm{dis}}(t) & v^{\mathrm{dis}}_{\mathrm{dif}^0}(t) \end{bmatrix}^T \tag{2.130}$$

$$\mathbf{B}_v = \begin{bmatrix} 0 & \frac{1}{J_n} & 0 \\ 0 & 0 & 1 \end{bmatrix}^T. \tag{2.131}$$

2.7.2 Derivation of Covariance-Matrix Structure

In order to determine the structure of $\mathbf{Q}$, the derivation of a prior error covariance matrix is considered. To derive the prior error covariance matrix, a prior state estimation error is utilized. The prior state estimation error $\boldsymbol{e}^-(k)$ is described as

$$\boldsymbol{e}^-(k) = \boldsymbol{Z}(k) - \hat{\boldsymbol{Z}}^-(k) \tag{2.132}$$

$$= \mathbf{A}_d \boldsymbol{e}(k-1) + \mathbf{B}_{vd} \boldsymbol{V}(k-1). \tag{2.133}$$

To obtain (2.133) the following assumption in Kalman filtering is utilized:

$$\mathrm{E}\left[\boldsymbol{V}(k-1)\right] = \bar{\boldsymbol{V}} = \mathbf{0} \tag{2.134}$$

where $\mathrm{E}[\bullet]$ is a expectation value. This equation represents that the mean values of the process noises are equal to zero. By using (2.133), the prior error covariance matrix is derived as follows:

$$\begin{aligned}\mathbf{P}^{-}(k) &= \mathrm{E}\left[\boldsymbol{e}^{-}(k)\boldsymbol{e}^{-}(k)^{T}\right] + \mathbf{A}_d \mathrm{E}\left[\boldsymbol{e}(k-1)\boldsymbol{e}(k-1)^{T}\right]\mathbf{A}_d^{T} \\ &\quad + \mathbf{B}_{vd}\mathrm{E}\left[\boldsymbol{V}(k-1)\boldsymbol{V}(k-1)^{T}\right]\mathbf{B}_{vd}^{T} \qquad (2.135)\\ &= \mathbf{A}_d\mathbf{P}(k-1)\mathbf{A}_d^{T} + \mathbf{B}_{vd}\boldsymbol{\Sigma}_v^2\mathbf{B}_{vd}^{T} \qquad (2.136)\\ \boldsymbol{\Sigma}_v^2 &= \mathrm{E}\left[\left\{\boldsymbol{V}(k-1) - \bar{\boldsymbol{V}}\right\}\left\{\boldsymbol{V}(k-1)^{T} - \bar{\boldsymbol{V}}\right\}\right] \qquad (2.137)\end{aligned}$$

where $\boldsymbol{\Sigma}_v^2$ represents the covariance matrix of process noise. In the derivation of the prior error covariance matrix, the following assumption of Kalman filtering is utilized:

$$\mathrm{E}\left[\boldsymbol{e}^{-}(k)\boldsymbol{V}(k-1)^{T}\right] = \mathbf{0}. \qquad (2.138)$$

If it is assumed that v^{dis} and $v_{\mathrm{dif}^0}^{\mathrm{dis}}$ are independent, the covariance of these process noises is equal to zero as given below:

$$\begin{aligned}\sigma^2_{v^{\mathrm{dis}}v_{\mathrm{dif}^0}^{\mathrm{dis}}} &= \mathrm{E}\left[\{v^{\mathrm{dis}}(k) - \bar{v}^{\mathrm{dis}}\}\{v_{\mathrm{dif}^0}^{\mathrm{dis}}(k) - \bar{v}^{\mathrm{dis}}\}\right] \qquad (2.139)\\ &= \mathrm{E}\left[v^{\mathrm{dis}}(k)v_{\mathrm{dif}^0}^{\mathrm{dis}}(k)\right] - \bar{v}^{\mathrm{dis}}\bar{v}^{\mathrm{dis}} \qquad (2.140)\\ &= \mathrm{E}\left[v^{\mathrm{dis}}(k)\right]\mathrm{E}\left[v_{\mathrm{dif}^0}^{\mathrm{dis}}(k)\right] - \bar{v}^{\mathrm{dis}}\bar{v}^{\mathrm{dis}} \qquad (2.141)\\ &= 0. \qquad (2.142)\end{aligned}$$

According to (2.134), (2.137), and (2.142), the covariance matrix of process noise is derived as follows:

$$\boldsymbol{\Sigma}_v^2 = \begin{bmatrix}\sigma^2_{v^{\mathrm{dis}}} & 0\\ 0 & \sigma^2_{v_{\mathrm{dif}^0}^{\mathrm{dis}}}\end{bmatrix}. \qquad (2.143)$$

Finally, according to (2.136) and (2.143), the resulting covariance matrix $\mathbf{Q}$ is obtained as

$$\begin{aligned}\mathbf{Q} &= \mathbf{B}_{vd}\boldsymbol{\Sigma}_v^2\mathbf{B}_{vd}^{T} \qquad (2.144)\\ &= \left[\int_0^{T_s}\mathbf{e}^{\boldsymbol{A}t}dt\mathbf{B}_v\right]\boldsymbol{\Sigma}_v^2\left[\mathbf{B}_v^{T}\int_0^{T_s}\mathbf{e}^{\boldsymbol{A}^{T}t}dt\right]. \qquad (2.145)\end{aligned}$$

Though the number of elements in $\mathbf{Q}$ is nine as shown in (2.126), only two parameters $\sigma^2_{v^{\mathrm{dis}}}$ and $\sigma^2_{v_{\mathrm{dif}^0}^{\mathrm{dis}}}$ should be determined by considering the existences of two process noises v^{dis} and $v_{\mathrm{dif}^0}^{\mathrm{dis}}$.

2.7.3 Kalman Filter-Based Reaction Torque Estimation for Multi-DOF Manipulator

In this subsection, the Kalman filter-based RTOB for a multi-DOF manipulator is proposed. Based on the last subsection, the design of the resulting covariance matrix $\mathbf{Q}$ is also applicable to external torque estimation.

The state variables of the i-th joint for external (reaction) torque estimation are given as follows:

$$\boldsymbol{Z}_i^r(t) = \left[q_i^{\mathrm{res}}(t) \;\; \dot{q}_i^{\mathrm{res}}(t) \;\; \tau_i^{\mathrm{ext}}(t) \;\; \tau_i^{\mathrm{load}}(t)\right]^T \tag{2.146}$$

$$\boldsymbol{V}_i^r(t) = \left[v_i^{\mathrm{dis}}(t) \;\; v_{i\mathrm{dif}^0}^{\mathrm{ext}}(t) \;\; v_{\mathrm{dif}^0}^{\mathrm{load}}(t)\right]^T \tag{2.147}$$

$$v_i^{\mathrm{dis}}(t) = v_i^{\mathrm{ext}}(t) + v_i^{\mathrm{load}}(t) \tag{2.148}$$

where τ_i^{load} represents the disturbance excluding external torque as follows:

$$\begin{aligned}\boldsymbol{\tau}^{\mathrm{load}}(t) = {} & \Delta\boldsymbol{J}\ddot{\boldsymbol{q}}^{\mathrm{res}} - \Delta\boldsymbol{K}_t\boldsymbol{I}^{ref} + \boldsymbol{\tau}^c + \boldsymbol{D}\dot{\boldsymbol{q}}^{\mathrm{res}} \\ & + \boldsymbol{C}^r\left(\boldsymbol{q}^{\mathrm{res}}, \dot{\boldsymbol{q}}^{\mathrm{res}}\right) + \boldsymbol{g}(\boldsymbol{q}^{\mathrm{res}}).\end{aligned} \tag{2.149}$$

The terms in $\boldsymbol{\tau}^{\mathrm{load}}(t)$ cannot be directly measured, but they can be calculated using measurable variables $\boldsymbol{q}^{\mathrm{res}}$ and its time derivative and by identifying parameter variations and friction elements. Here, $\Delta\boldsymbol{J}$ includes not only parameter (inertia) variations but also non-diagonal elements of the inertia matrix of the manipulator. The state-space equation is described as follows:

$$\dot{\boldsymbol{Z}}_i^r(t) = \boldsymbol{A}_i^r\boldsymbol{Z}_i^r(t) + \mathbf{B}_i^r u_i(t) + \mathbf{B}_{vi}^r\boldsymbol{V}_i^r(t) \tag{2.150}$$

$$\boldsymbol{Y}_i^r(t) = \boldsymbol{c}\boldsymbol{Z}_i^r(t) + \boldsymbol{W}_i^r(t) \tag{2.151}$$

$$= \left[q_i^{\mathrm{res}}(t) \;\; \tau_i^{\mathrm{load}}(t)\right] + \boldsymbol{W}_i^r(t) \tag{2.152}$$

$$\boldsymbol{A}_i^r = \begin{bmatrix} 0 & 1 & 0 & 0 \\ 0 & 0 & -\frac{1}{J_{in}} & -\frac{1}{J_{in}} \\ 0 & 0 & 0 & 0 \\ 0 & 0 & 0 & 0 \end{bmatrix},\; \mathbf{B}_i^r = \begin{bmatrix} 0 \\ \frac{1}{J_{in}} \\ 0 \\ 0 \end{bmatrix},$$

$$\mathbf{B}_{iv}^r = \begin{bmatrix} 0 & 0 & 0 \\ \frac{1}{J_{in}} & 0 & 0 \\ 0 & 1 & 0 \\ 0 & 0 & 1 \end{bmatrix},\; \boldsymbol{c}^r = \begin{bmatrix} 1 & 0 & 0 & 0 \\ 0 & 0 & 0 & 1 \end{bmatrix}. \tag{2.153}$$

Based on the above equations, the Kalman filter for external torque estimation is constructed in the discrete-time domain. Similar to disturbance torque estimation discussed in the last subsection, only the

following three variances need to be considered:

$$\boldsymbol{\Sigma}_v^{r\,2} = \begin{bmatrix} \sigma^2_{v^{\mathrm{dis}}} & 0 & 0 \\ 0 & \sigma^2_{v^{\mathrm{ext}}_{\mathrm{dif}^0}} & 0 \\ 0 & 0 & \sigma^2_{v^{\mathrm{load}}_{\mathrm{dif}^0}} \end{bmatrix}. \tag{2.154}$$

The resulting covariance matrix is obtained as

$$\mathbf{Q}_i^r = \mathbf{B}_{vid}\boldsymbol{\Sigma}_v^{r\,2}\mathbf{B}_{vid}^T \tag{2.155}$$

$$= \left[\int_0^{T_s} \mathbf{e}^{\boldsymbol{A}_i^r t} dt \mathbf{B}_{vi}^r\right] \boldsymbol{\Sigma}_{\boldsymbol{v}}^{\boldsymbol{r}\,2} \left[\mathbf{B}_{vi}^{r\;T} \int_0^{T_s} \mathbf{e}^{\boldsymbol{A}_i^{r\,T} t} dt\right]. \tag{2.156}$$

In conventional state estimation of manipulators, nonlinear Kalman filters (e.g., extended Kalman filter) are usually used [63,100]. However, some linear approximations by using Jacobian matrices are required in nonlinear Kalman filter algorithms and the processes become complex. Including the nonlinear terms in the measured variable, on the other hand, the proposed Kalman filter-based RTOB can estimate the external torque through a Kalman filter algorithm without using the approximations. Here, the model of $\boldsymbol{\tau}^{\mathrm{load}}(t)$ in 2.149 basically can be derived from Lagrange equation. The detailed models for the torques (e.g. Coulomb frictions, viscose frictions) can be obtained through identification methods (e.g. [6,19,104]). The identified value of $\boldsymbol{\tau}^{\mathrm{load}}(t)$ can be combined in the proposed Kalman filter-based RTOB in (2.152).

2.7.4 Derivation of Steady-State Kalman Filter for Tuning Q

This chapter utilizes the steady-state Kalman filter (SSKF) as a substation for the LPF and HPF of the KFSO for tuning and analyzing the KFSO. In order to obtain the steady-state Kalman gain, the following discrete-time algebraic Riccati equation (DARE) [105] should be solved:

$$\mathbf{P} = \mathbf{A}_d \left[\mathbf{P} - \mathbf{P}\boldsymbol{c}^T \left(\boldsymbol{c}\mathbf{P}\boldsymbol{c}^T + \mathbf{R}\right)^{-1} \boldsymbol{c}\mathbf{P}\right] \mathbf{A}_d^T + \mathbf{Q}. \tag{2.157}$$

To obtain the solution, the eigen values of the following matrix are utilized:

$$\boldsymbol{H}_{\mathrm{skf}} = \begin{bmatrix} \mathbf{A}_d^T + \boldsymbol{c}^T\mathbf{R}^{-1}\boldsymbol{c}\mathbf{A}_d^{-1}\mathbf{Q} & -\boldsymbol{c}^T\mathbf{R}^{-1}\boldsymbol{c}\mathbf{A}_d^{-1} \\ -\mathbf{A}_d^{-1}\mathbf{Q} & \mathbf{A}_d^{-1} \end{bmatrix}. \tag{2.158}$$

The eigen values with absolute values less than one are described as follows:

$$\boldsymbol{\epsilon}_{\mathrm{skf,i}} = \begin{bmatrix} \boldsymbol{\eta}_i & \boldsymbol{\xi}_i \end{bmatrix}^T \; (i = 1, \cdots \mathrm{n}). \tag{2.159}$$

By using $\boldsymbol{\epsilon}_{\mathrm{skf}}$, the solution of DARE $\boldsymbol{\mathcal{P}}$ is obtained as

$$\boldsymbol{\mathcal{P}} = \left[\boldsymbol{\xi}_1 \cdots \boldsymbol{\xi}_{\mathrm{n}}\right] \left[\boldsymbol{\eta}_i \cdots \boldsymbol{\eta}_{\mathrm{n}}\right]^{-1}. \tag{2.160}$$

By using the solution of DARE $\boldsymbol{\mathcal{P}}$, the steady-state Kalman gain $\boldsymbol{\mathcal{G}}_{\mathrm{skf}}$ is obtained as follows:

$$\boldsymbol{\mathcal{G}}_{\mathrm{skf}} = \boldsymbol{\mathcal{P}}\boldsymbol{c}^T \left(\boldsymbol{c}\boldsymbol{\mathcal{P}}\boldsymbol{c}^T + \mathbf{R}\right). \tag{2.161}$$

By using $\boldsymbol{\mathcal{G}}_{\mathrm{skf}}$, the state estimated by the steady-state Kalman filter is derived from (2.118) and (2.122) as follows:

$$\hat{\boldsymbol{Z}}_{\mathrm{skf}}(z) = \left[\boldsymbol{I} - \left(\boldsymbol{I} - \boldsymbol{\mathcal{G}}_{\mathrm{skf}}\boldsymbol{c}\right)\mathbf{A}_d z^{-1}\right]^{-1} \left[\boldsymbol{\mathcal{G}}_{\mathrm{skf}}\boldsymbol{Y}(z) + \left(\boldsymbol{I} - \boldsymbol{\mathcal{G}}_{\mathrm{skf}}\boldsymbol{c}\right)\boldsymbol{b}_d z^{-1}\boldsymbol{u}(z)\right] \tag{2.162}$$

where subscript skf represents a variable of steady state Kalman filter. From (2.162), a steady-state Kalman filter for disturbance estimation $G^f_{L\mathrm{skf}}(z)$ is derived as

$$\hat{\tau}^{\mathrm{dis}}_{\mathrm{skf}} = g^{\mathrm{dis}}_{l\mathrm{skf}}(z)\tau^{\mathrm{dis}} + g^{\mathrm{dis}}_{N\mathrm{skf}}(z)w \tag{2.163}$$

$$\hat{\tau}^{\mathrm{ext}}_{\mathrm{skf}} = g^{\mathrm{ext}}_{l\mathrm{skf}}(z)\tau^{\mathrm{ext}} + g^{\mathrm{load}}_{h\mathrm{skf}}(z)\tau^{\mathrm{load}} + g^{\mathrm{ext}}_{N\mathrm{skf}}(z)w \tag{2.164}$$

where $g^{\mathrm{load}}_{h\mathrm{skf}}(z)$ represents the sensitivity to τ^{load}. In addition, w is a observation noise included in the position response as shown in (2.13). The observation noise included also in the case of Kalman filter based disturbance estimation. The HPF in disturbance compensation $g^{\mathrm{dis}}_{h\mathrm{skf}}(z)$ are expressed as

$$g^{\mathrm{dis}}_{l\mathrm{skf}}(z) = 1 - g^{\mathrm{dis}}_{h\mathrm{skf}}(z). \tag{2.165}$$

Additionally, the estimated states of the angular velocity and the angle in (2.114) are described as follows:

$$\hat{\dot{q}}^{\mathrm{res}}_{\mathrm{skf}} = g^{v}_{\mathrm{skf}}(z)\dot{q}^{\mathrm{res}} + g^{v}_{N\mathrm{skf}}(z)w + g^{v}_{\mathrm{skf}\delta}(z)\delta^{v} \tag{2.166}$$

$$\hat{q}^{\mathrm{res}}_{\mathrm{skf}} = q^{\mathrm{res}} + g^{P}_{N\mathrm{skf}}(z)w + g^{P}_{\mathrm{skf}\delta}(z)\delta^{p} \tag{2.167}$$

where superscripts v and p represent a parameters of velocity estimation and position estimation, respectively. Here, the effect of $\delta^{\bullet}$ is assumed to be negligibly small.

Table 2.1: Parameters for analysis of Kalman filter based disturbance/external torque estimation

Parameter	Description	Value
T_s	Sampling time	0.2 ms
$J_{n1} = J_1$	inertia of actuator	0.004 kgm^2
$J_{n2} = J_2$	inertia of actuator	0.0548 kgm^2
g^{dis}, g^{ext}	cut-off frequency of DOB and RTOB	364 rad/s
g^v	cut-off frequency of velocity est.	1820 rad/s
g^p_{skf}	bandwidth of noise sensitivity (position)	1617 rad/s
g^v_{skf}	bandwidth of noise sensitivity (velocity)	1095 rad/s

2.8 Analysis Based on Steady-State Kalman Filter

In this section, the approximated performance of the KFSO is analyzed using the SSKF. Parameters used in the analysis are shown in Table 2.1.

2.8.1 Relationship between Bandwidth and Parameters

Here, the relationship between the bandwidth of the SSKF $g^{\bullet}_{l\mathrm{skf}}(z)$ and parameters of the KFSO is analyzed.

Fig. 2-6 shows the relationship between the bandwidth and variance $\sigma^2_{v^{\mathrm{dis}}_{\mathrm{dif}0}}$. As shown in Fig. 2-6, the bandwidth increases with an increase in the variance of process noise with respect to the time derivative of torque $\sigma^2_{v^{\mathrm{dis}}_{\mathrm{dif}0}}$. On the other hand, the bandwidth is inversely proportional to the inertia J_n as shown in Fig. 2-6 (a). The increase in the variance of observation noise also tends to reduce the bandwidth as indicated in Fig. 2-6 (b). These figures show that the Kalman filter tends to reduce the effect of observation noise automatically because the larger variance of process noise and inertia result in a higher level of noise effect and a greater noise sensitivity, respectively. If a desired estimation performance is not able to be obtained, the bandwidth should be adjusted by tuning the value of $\sigma^2_{v^{\mathrm{dis}}_{\mathrm{dif}0}}$. Fig. 2-7 represents the relationship between the bandwidth and variances with J_n=0.004 kgm^2 and J_n=0.0548 kgm^2, respectively. It is observed that the bandwidth is inversely proportional to the variance of process noise in torque dimension v^{dis}, though the bandwidth is proportional to the variance $\sigma^2_{v^{\mathrm{dis}}_{\mathrm{dif}0}}$. This indicates that just increasing both variances will lead to estimation failure, though $\mathbf{Q}$ can be regarded as a gain of the Kalman filter [68]. Fig. 2-7 (b) shows the relationship between the bandwidth and variances with J_n=0.0548 kgm^2. The tendency of the graph is similar to that in Fig. 2-7 (a). However, Fig. 2-7 (b)

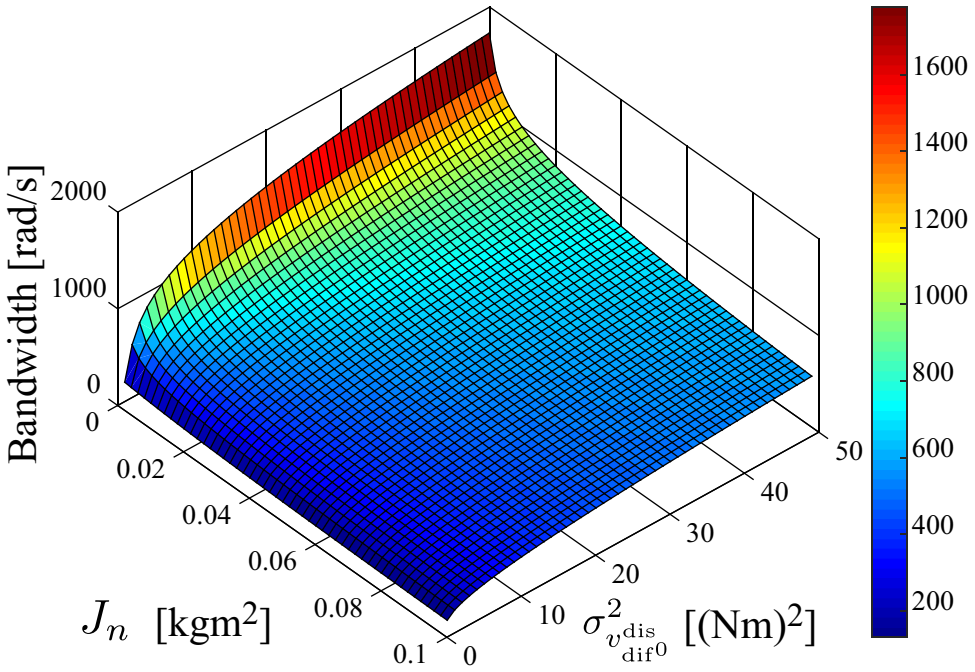

(a)

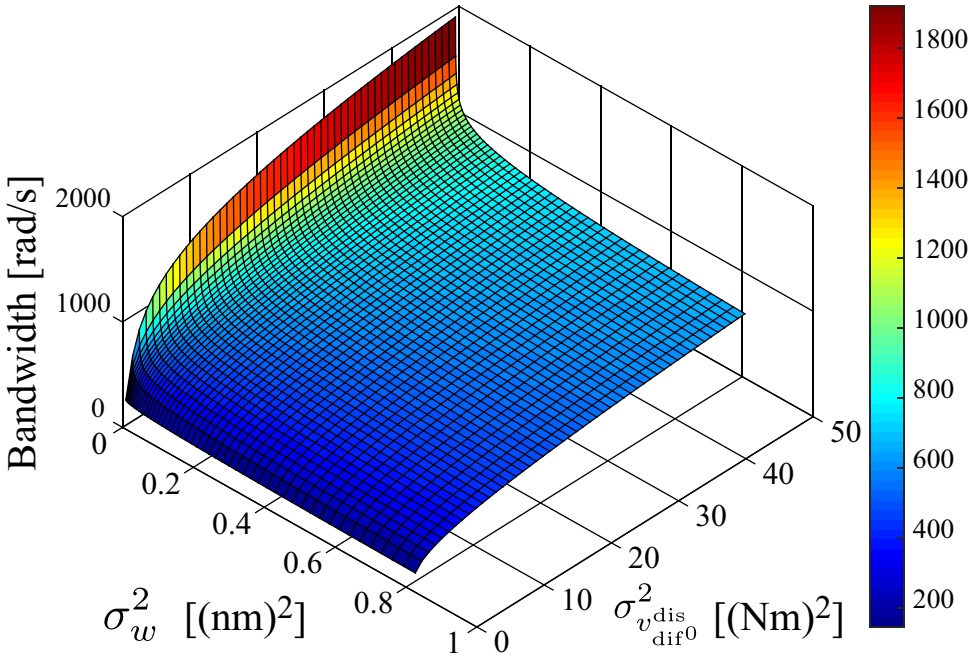

(b)

Fig. 2-6: Relationship between bandwidth and variances (a) With J_n=0.004 kgm^2. (b) With J_n=0.0548 kgm^2.

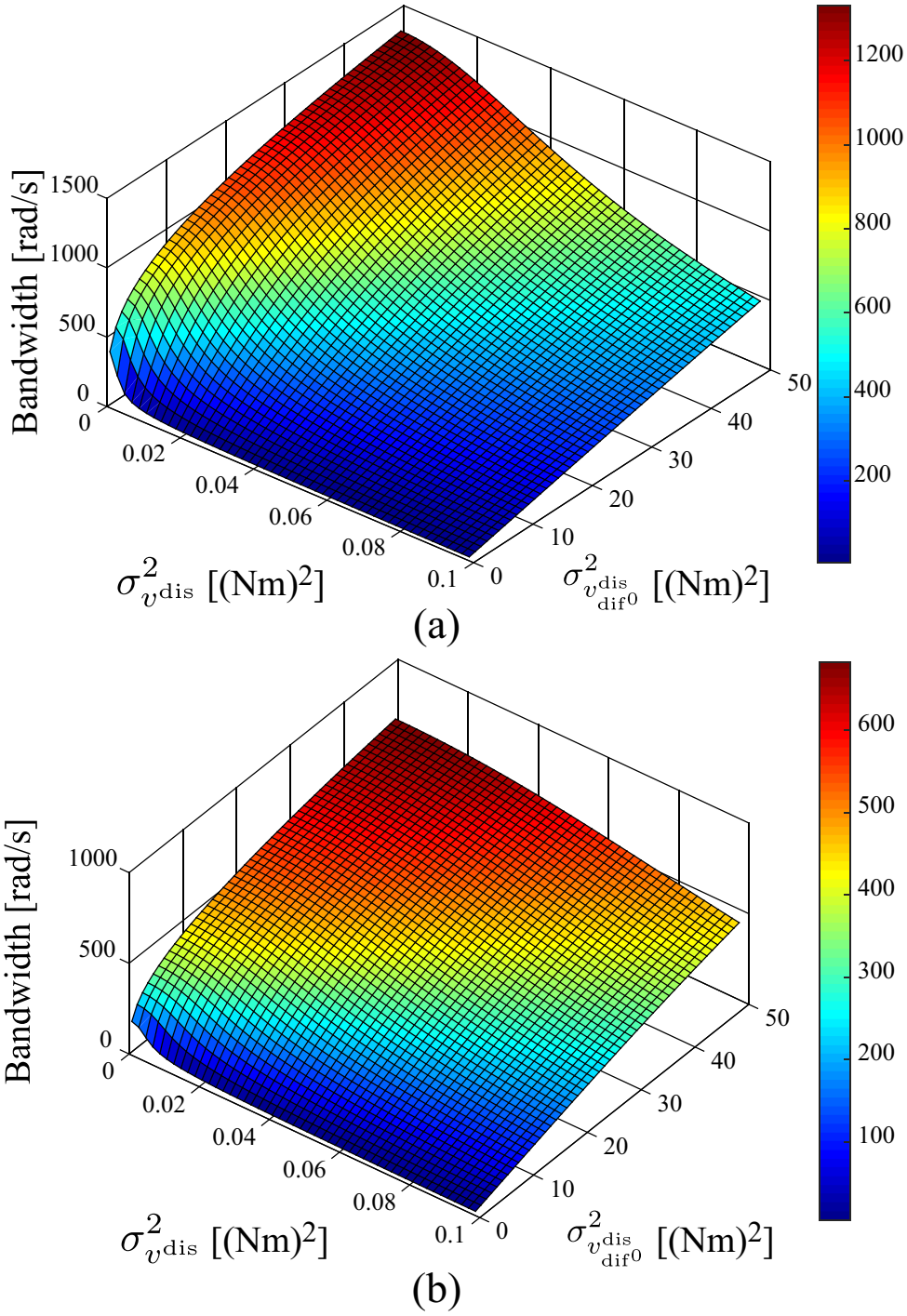

Fig. 2-7: Relationship between bandwidth and variances (a) With J_n=0.004 kgm^2. (b) With J_n=0.0548 kgm^2.

reflects the effect of the value of inertia as shown in Fig. 2-6 (a). Fig. 2-8 (a) shows the relationship between the bandwidth and variances in Kalman filter-based reaction torque estimation with J_n=0.004 kgm^2. From the figure, a similar tendency to the KFSO with respect to the relationship between the variance $\sigma^2_{v^{\mathrm{ext}}_{\mathrm{dif}^0}}$ and the bandwidth can be observed in Kalman filter-based external torque estimation. Fig. 2-8 (b) shows the relationship between the bandwidth and two variances $\sigma^2_{v_{\mathrm{dif}^0}}$ and $\sigma^2_{v^{\mathrm{ext}}_{\mathrm{dif}^0}}$ with J_n=0.004 kgm^2. It is found that the variance of $\sigma^2_{v_{\mathrm{dif}^0}}$ does not interfere with the estimation bandwidth of the external torque.

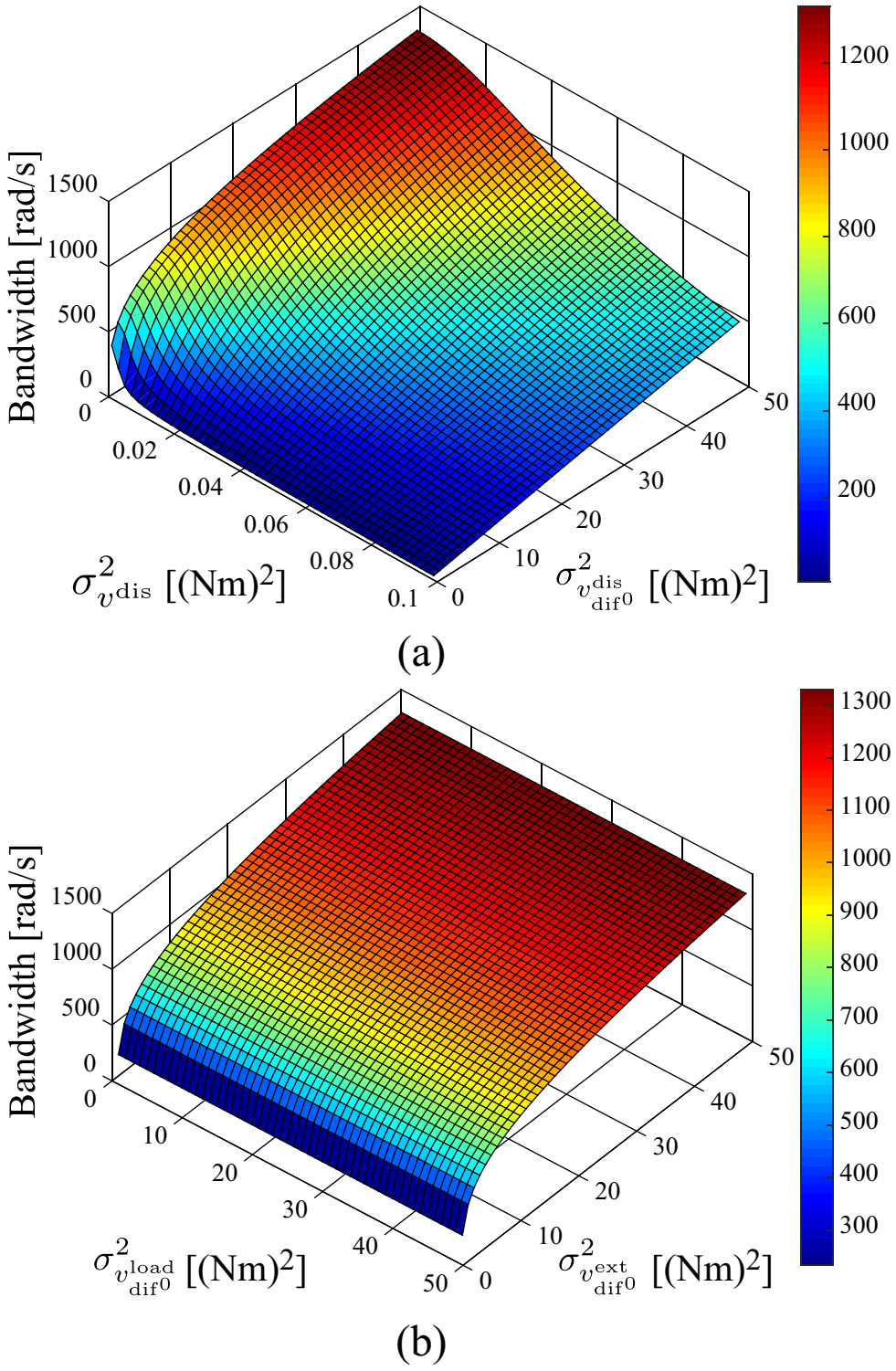

Fig. 2-8: Relationship between bandwidth and variances. (a) External torque estimation with J_n=0.004 kgm^2. (b) External torque estimation with the variation of $\sigma^2_{v^{\mathrm{load}}_{\mathrm{dif}0}}$ and $\sigma^2_{v^{\mathrm{ext}}_{\mathrm{dif}0}}$ (J_n=0.004 kgm^2).

2.8.2 Frequency Characteristics of Disturbance Estimation

Fig. 2-9 shows the bode diagrams in disturbance torque estimation and the resulting HPF in disturbance compensation with the variation of the variance $\sigma^2_{v^{\bullet}_{\mathrm{dif}}}$. From Fig. 2-9 (a) and (b), it is found that the performance of disturbance estimation and suppression are improved by increasing the variance with respect to the time derivative of process noise. In addition, as indicated in the last subsection , it is confirmed that the estimation just regarding both the variances as gains [68] and increasing the two variances without considering the relationship will be broken down as shown by the dash-dotted line in the figure. The figure also shows the disturbance model with neglecting the of process noise in the time derivative of disturbance Fig. 2.129 will broke down the estimation. Fig. 2-10 shows the bode diagram of $g^{\mathrm{ext}}_{l\mathrm{skf}}(z)$ and $g^{\mathrm{load}}_{h\mathrm{skf}}(z)$. It is confirmed that the sensitivity to τ^{load} can be independently changed from external torque estimation by including τ^{load} to the state variables, though the same filter as the external torque is inserted in the case of normal DOBs. As a result, the equivalent cut-off frequency with respect to τ^{load} can be reduced without affecting estimation of τ^{ext} in the lower frequency domain if the noise included in τ^{load} is serious. Fig. 2-11 shows bode diagrams in disturbance estimation with the comparison between the KFSO and normal DOBs. Fig. 2-12 shows bode diagrams of the noise sensitivity in disturbance estimation. In this figure, the normal velocity-based (with first-order LPF) and position-based (with second-order LPF and third-order) DOBs have the same bandwidth as the SSKF. It is found that noise reduction performance is improved by the KFSO in disturbance estimation as indicated by Figs. 2-11 (a) and 2-12, though the robustness against disturbance is less compared to that of normal DOBs as shown in Fig. 2-11 (b). Fig. 2-13 shows the bode diagrams of the angle and the angular velocity estimation. It is confirmed that the Kalman filter can estimate the state variables without phase lag and with higher noise suppression performance compared to the normal LPF with the same bandwidth as the SSKF.

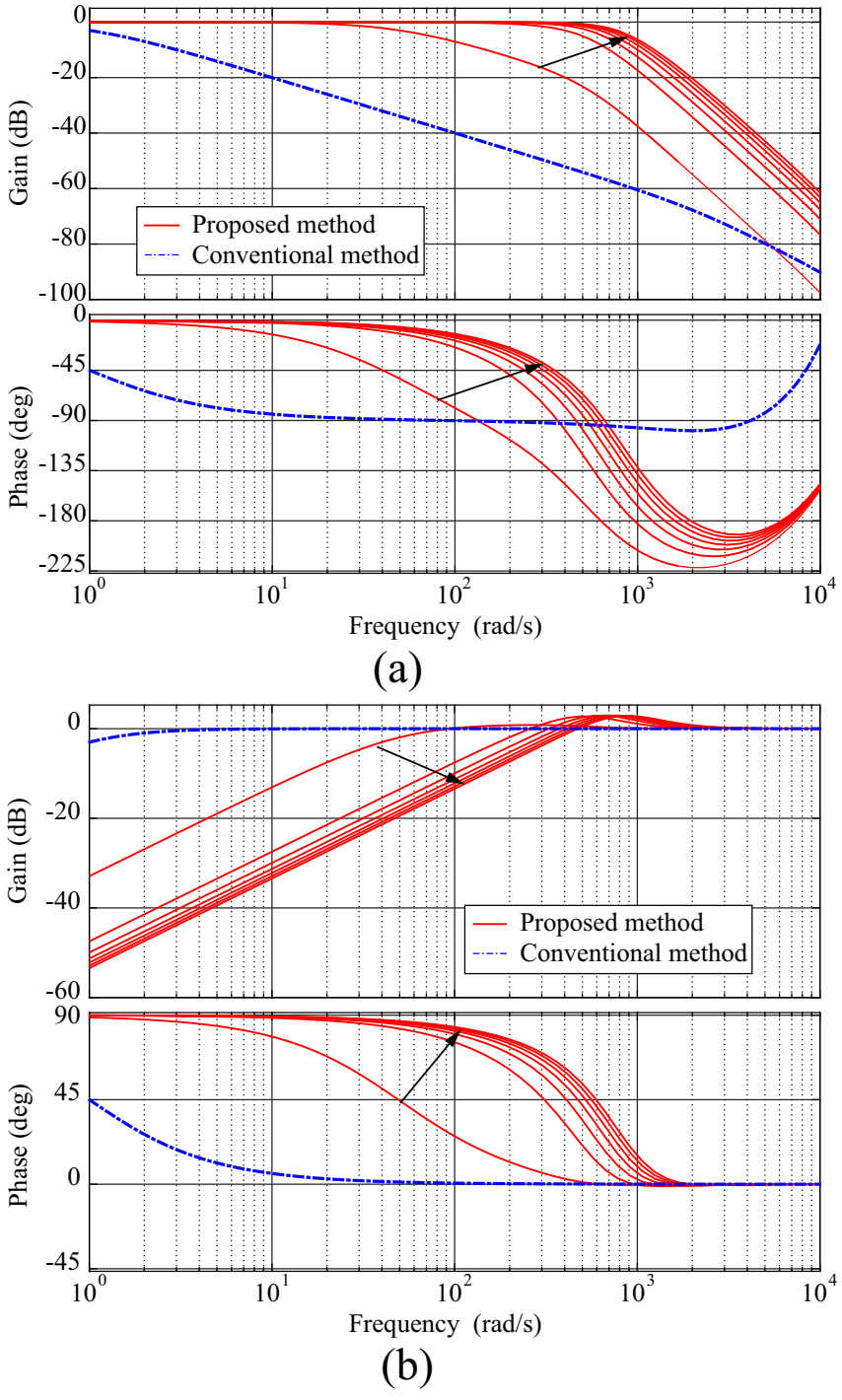

Fig. 2-9: Bode diagram of disturbance torque estimation with the variation of variance in respect to process noise $\sigma^2_{v^{\mathrm{dis}}_{\mathrm{dif}^0}}$ from 0.1 to 6.1. (a) Characteristics of disturbance estimation. (b) Resulting HPF in disturbance compensation.

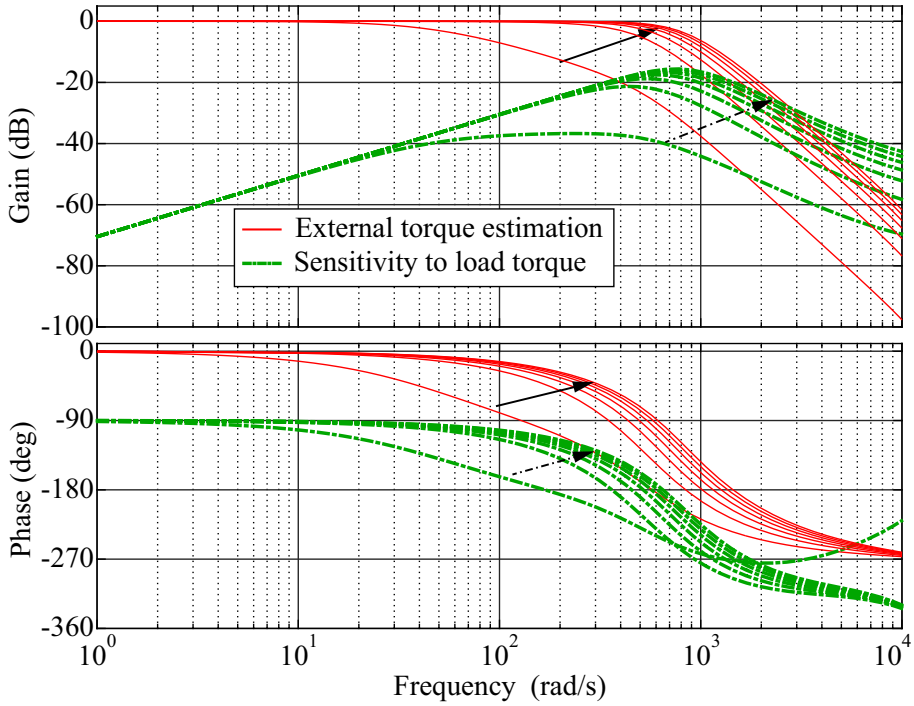

Fig. 2-10: Bode diagram of external torque estimation and sensitivity to load torque with the variation of variance in respect to process noise $\sigma^2_{v^{\text{ext}}_{\text{dif}0}}$ from 0.1 to 6.1.

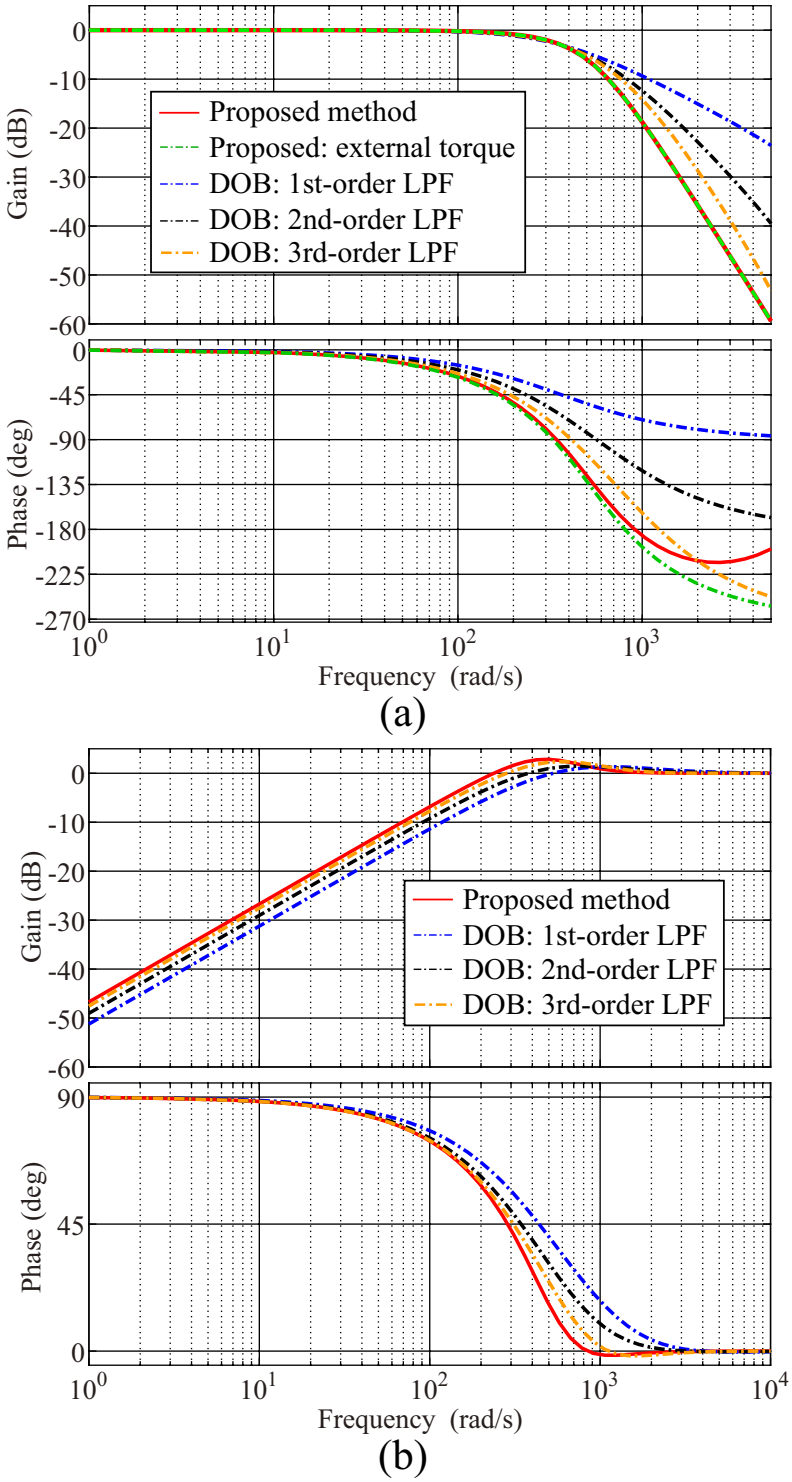

Fig. 2-11: Bode diagram with the comparison between KFSO and normal DOBs. (a) LPF in estimation. (b) Resulting HPF.

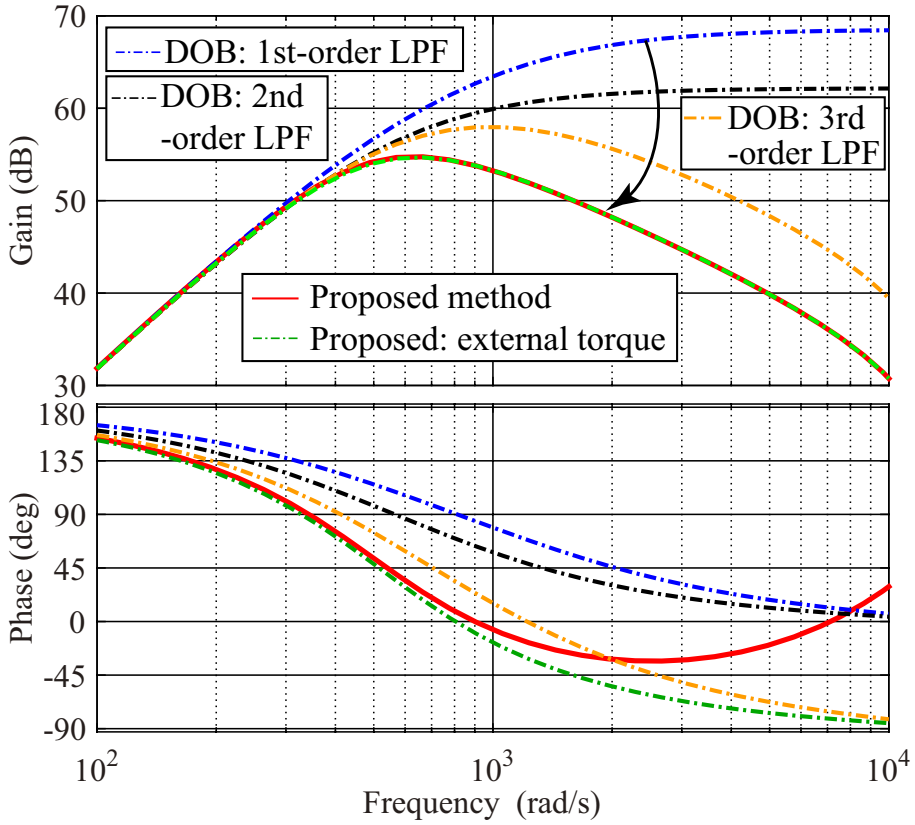

Fig. 2-12: Bode diagram with the comparison between KFSO and normal DOBs with respect to the noise sensitivity in estimation.

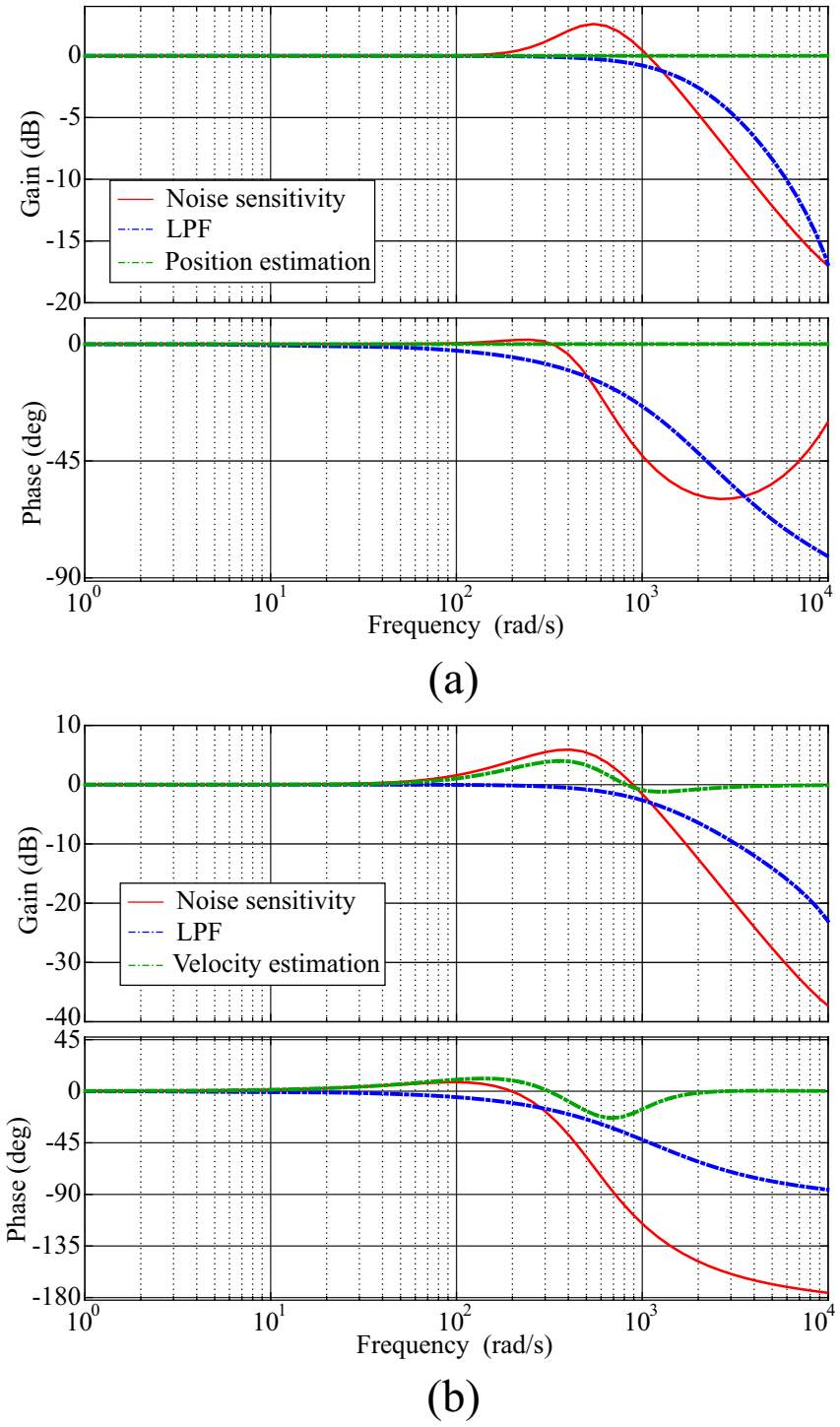

Fig. 2-13: Bode diagram of state estimation. (a) Angle. (b) Velocity.

2.8.3 Design and Tuning for Q

The proposed design and the tuning method for determining $\mathbf{Q}$ are summarized as follows:

1. Derive the vectors with respect to the process noise $\boldsymbol{V}(k)$ and $\boldsymbol{B}_{vd}$
2. Determine the structure of $\mathbf{Q}$ by deriving $\mathbf{P}^{-}(k)$
3. Derive the SSFK to check the approximate frequency characteristics
4. Determine $\sigma^2_{v^{\mathrm{dis}}}$ and $\sigma^2_{v^{\mathrm{dis}}_{\mathrm{dif}^0}}$ to obtain desired frequency characteristics.

Here, we have to take account of the fact that the bandwidth is inversely proportional to σ_v^2, though the higher σ_v^2 increases the bandwidth as discussed earlier.

Additionally, the bandwidth also varies with depending on the variance in respect to observation noise σ_w^2 and inertia J_n as shown in Fig. 2-6. If the proposed method is applied for another actuator or sensor, σ_v^2 and $\sigma^2_{v^{\mathrm{dis}}_{\mathrm{dif}^0}}$ should be readjusted.

Here, if it is possible to obtain the actual values of the variances of process noises in some way and to set the variances to the actual values, the estimation with minimum mean square error as shown in (2.81) is guaranteed. However, it is difficult to obtain the actual values of the variances of process noises in the dimensions of the disturbance and the time derivative of disturbance. Therefore, this dissertation uses the above tuning process.

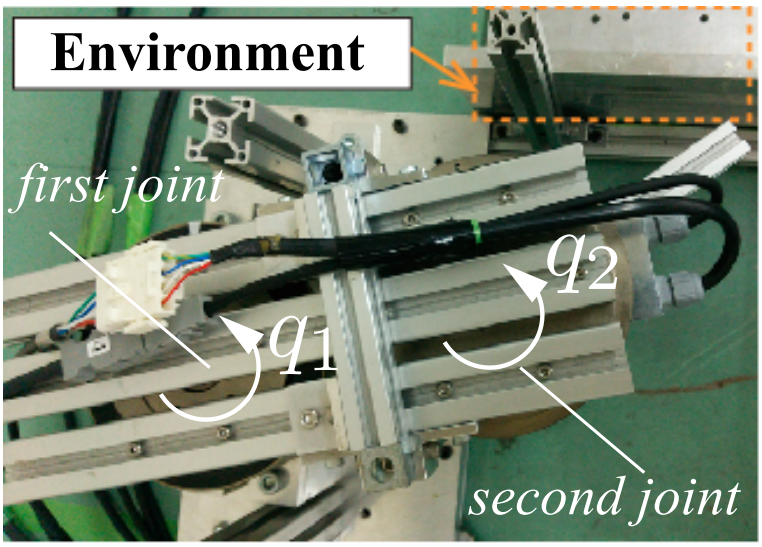

Fig. 2-14: Experimental setup.

2.9 Experiments for Verification of Designed KFSO

2.9.1 Experimental Setup for 2-DOF Serial-link Manipulator

To confirm the validity of the proposal, experiments of position control and reaction torque control in joint spaces were conducted. Fig. 2-14 shows the experimental set up of a 2-DOF serial-link manipulator constructed by direct drive motors. Fig. 2-15 shows the block diagram of the position control and reaction torque control with KFSOs. Two cases of experiments are conducted for both position and reaction torque control. In case 1, artificial noise generated by random numbers is given to the actual sensor value (rotary encoder) in order to confirm the performance of the KFSO. This additional noise has another role which imitates the lower-performance sensor device. The obtained value from the sensor including the artificial noise is regarded as the output signal and is used for the control system. In case 2, artificial noise is not given in the measured signal from the sensor.

In the first experiment with case 1, the reaction torque control $\tau^{\mathrm{cmd}} = 0$ is conducted and a human operator manipulates the manipulator freely to validate the Kalman filter performance as an estimator. In this experiment, the cut-off frequencies of the DOB and RFOB are set to 100 rad/s. On the other hand, the cut-off frequency of the DOB/RFOB used only for estimation is set as 364 rad/s. In the second and third experiments, position and reaction torque controls are tested with the condition of case 1, respectively. In the fourth experiment, the reaction torque control of the aluminum plate and block as shown in Fig. 2-14

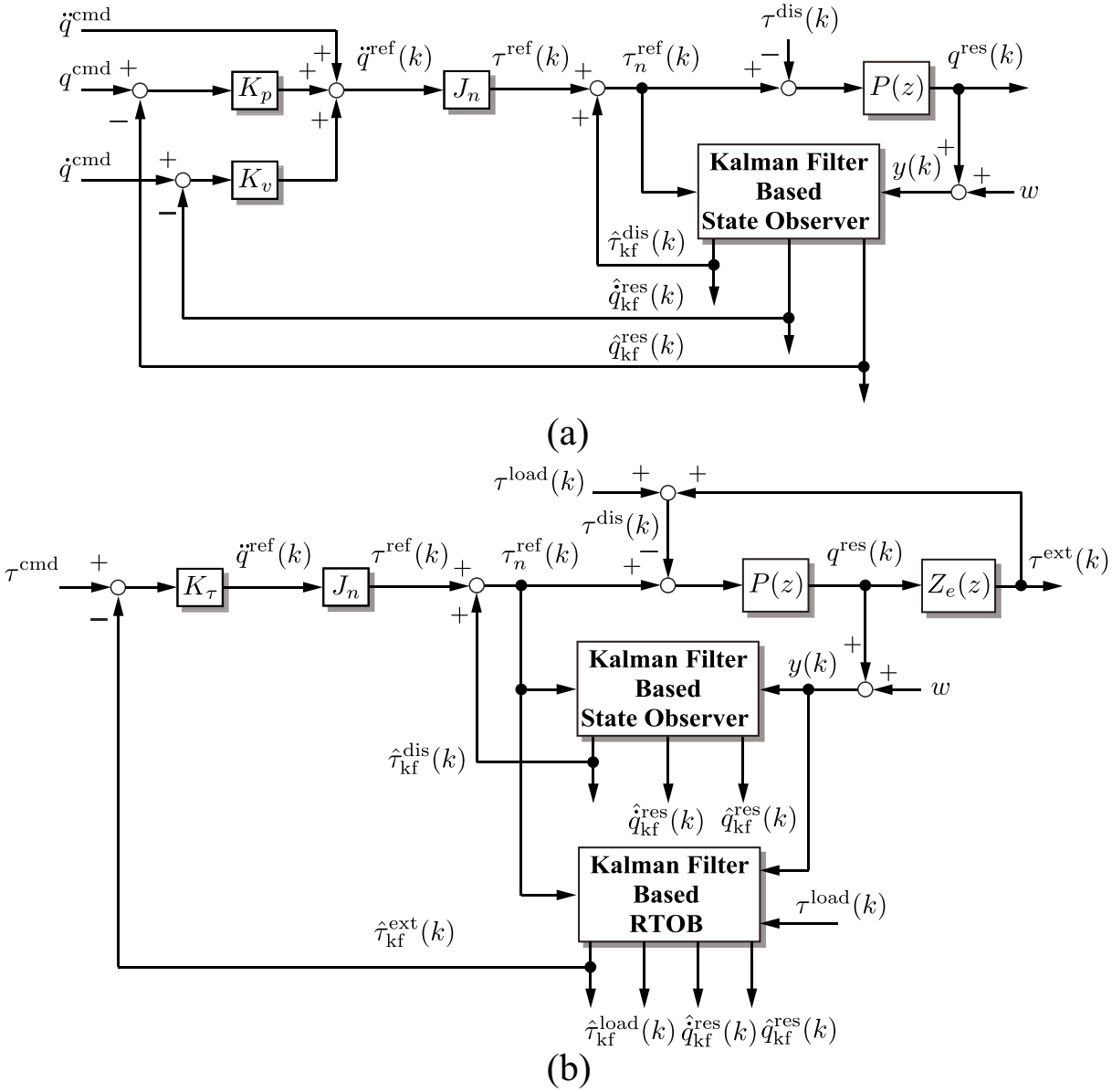

Fig. 2-15: Block diagrams. (a) Position control. (b) Reaction torque control.

is conducted with the condition of case 2. From the second to fourth experiments, Kalman filter -based control systems with the proposed method are compared with the control system that uses conventional

Table 2.2: Experimental parameters for position and reaction torque control with Kalman filters

Parameter	Description	Value
K_t	torque coefficient	1.18
$K_{\tau 1}$	torque control gain	10
$K_{\tau 2}$	torque control gain	150
K_p	position gain	1100
K_v	velocity gain	66.3
δq	resolution of encoder	1.0 $\times 10^6$ pulses/rev
σ_{v1}^2	variance in prop. method	1.0 $\times 10^{-4}$ $\mathrm{N^2m^2}$
σ_{v2}^2	variance in prop. method	2.0 $\times 10^{-3}$ $\mathrm{N^2m^2}$
$\sigma_{\dot{v}1}^2$	variance in prop. method	5.9 $\mathrm{N^2m^2/s^2}$
$\sigma_{\dot{v}2}^2$	variance in prop. method	0.93 $\mathrm{N^2m^2/s^2}$
σ_{v2}^2	variance in conv. method	2.0 $\mathrm{N^2m^{2\ 2}}$
$\sigma_{\dot{v}2}^2$	variance in conv. method	2.0 $\mathrm{N^2m^2/s^2}$

velocity-based DOB/RTOB. In these experiments, the angle and torque commands are given as follows:

$$q^{\mathrm{cmd}} = \begin{cases} 0.1 \text{ deg}, & 0 \leq t < 5 \\ 0.1 + 0.1 \sin 3(t-5) \text{ deg}, & 5 \leq t < 10. \end{cases} \tag{2.168}$$

$$\tau^{\mathrm{cmd}} = \begin{cases} 0.05 \text{ Nm}, & 0 \leq t < 5 \\ 0.05 + 0.05 \sin^2(3(t-5)) \text{ Nm}, & 5 \leq t < 10. \end{cases} \tag{2.169}$$

Table 2.2 lists the experimental parameters. This chapter assumes that parameter variation and the friction effect of actuators are negligible. The other parameters are same as those used in the analysis, which are given in Table 2.1.

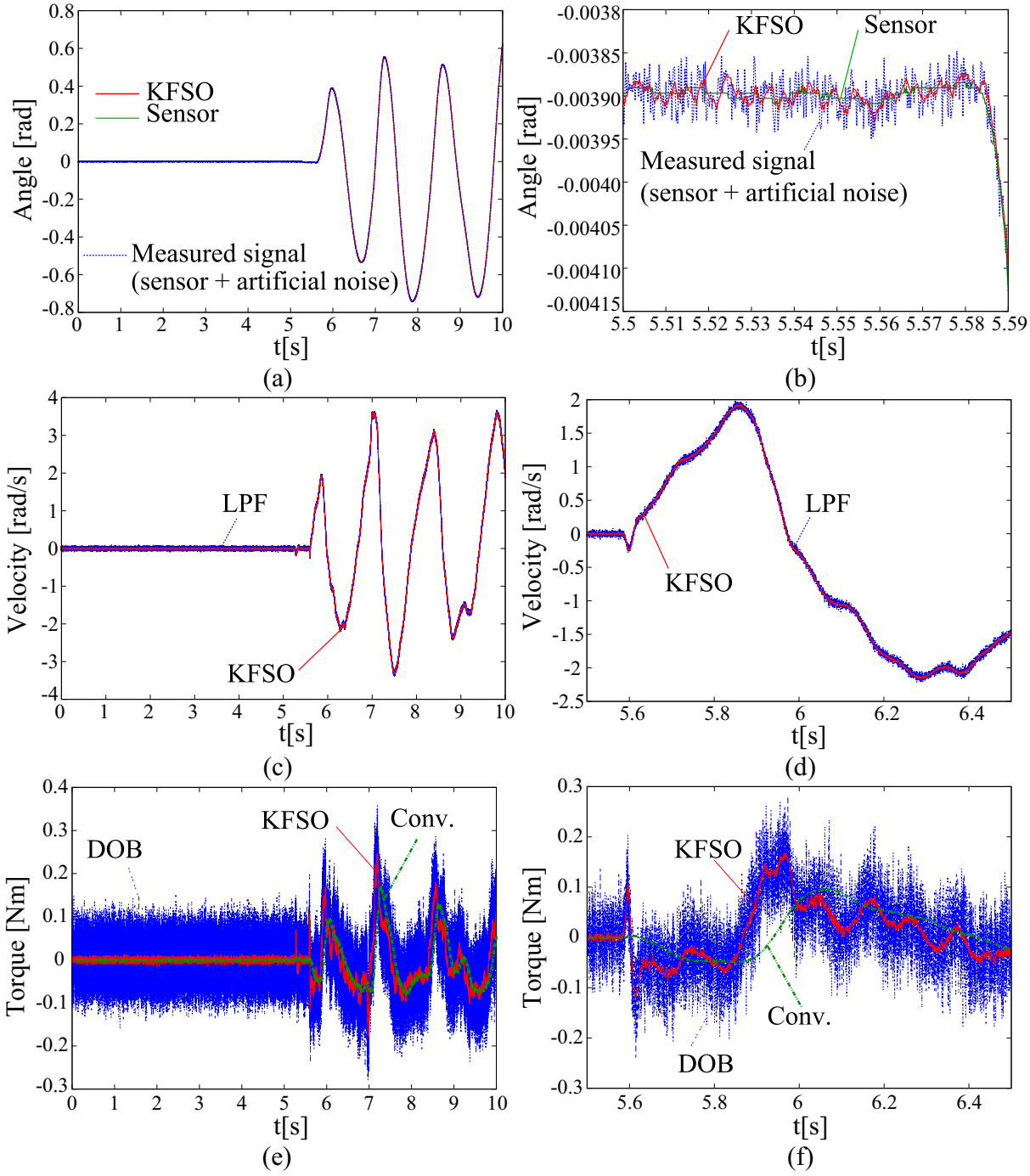

Fig. 2-16: Experimental results for state estimation. (a) Angle. (b) Enlarged view of (a). (c) Velocity. (d) Enlarged view of (c). (e) Disturbance torque. (f) Enlarged view of (e).

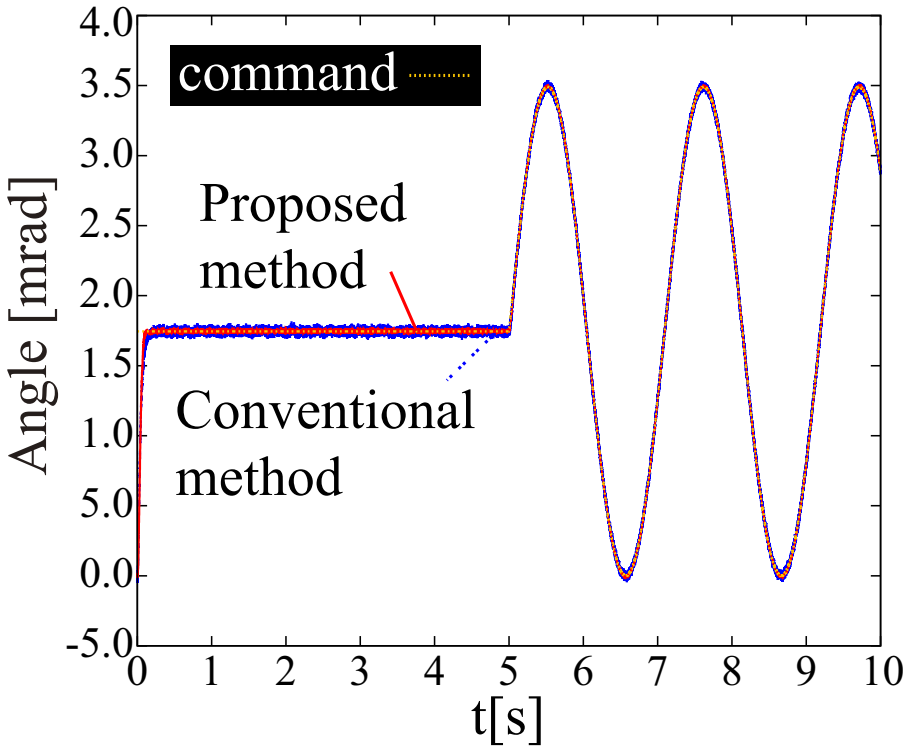

Fig. 2-17: Experimental result of position control in case 1.

2.9.2 Experimental Results for Verification of Designed KFSO

Fig. 2-16 shows the experimental results of the first experiment (1st link responses) and its enlarged views, respectively. As shown in Figs 2-16 (a) and (b), the KFSO successfully estimates the angle response without estimation delay and with reduced noise effect. Figs. 2-16 (c) and (d) show that velocity information is also effectively estimated by the KFSO. Although, the cut-off frequency of the SSKF for noise suppression is smaller than that of the pseudo-differentiation in Figs. 2-16 (c) and (d), the Kalman filter can estimate the angular velocity without estimation delay and with lower noise level compared to the pseudo-differentiation. Figs. 2-16 (e) and (f) represent experimental results of disturbance torque estimation. As shown in the figure, the proposed tuning method can estimate the disturbance torque with a low noise level and almost no phase lags compared to the normal DOB. On the other hand, the conventional tuning concept in which the elements in $\boldsymbol{Q}$ are regarded as gains of the Kalman filter fails to estimate the disturbance torque. This is because the elements are just increased and the relationships between the elements are not considered. These experimental results show that the proposed design and tuning method for the Kalman filter are effective not only for disturbance/external torque estimation but

also for angle and the velocity estimation.

Figs. 2-17 and 2-18 show the results of position control in the second experiment (2nd link responses). From the figures, it is clear that the noise effects are suppressed by the Kalman filter based control system with the proposed method. As a result, the perturbation in angle responses are suppressed by the proposed system compared to the DOB-based system as shown in Fig. 2-18.

Fig. 2-19 shows the experimental results of reaction torque control in the third experiment (2nd link responses). As shown in Fig. 2-19 (a), external torque information cannot be estimated appropriately by using the conventional RTOB in the reaction torque control system. On the contrary, the proposed method can reduce the effect of noise compared to the normal RTOB-based method and track the torque command without a notable phase delay as shown in Fig. 2-19 (c). Fig. 2-19 (c) shows the resulting angle responses in the experiments of reaction torque control. It is found that the perturbation of angle is reduced because of the lower noise level in torque estimation, though the conventional method enhances the perturbation caused by the noise torque response. As a result, the proposed method realizes more stable contact motion than that realized in the conventional method.

Fig. 2-20 shows the results of the fourth experiment (2nd link responses). As shown in the figure, the noise and quantization error are enlarged in the external torque response of the conventional RTOB. In contrast, Kalman filter based control that uses the proposed design method can reduce the noise effects compared with the conventional method. Additionally, the external torque response shows good tracking performance. As a result, the perturbations in the angle response are suppressed in the proposed method and stable contact motions are realized as shown in Fig. 2-20 (b).

From these results, the validity of the proposal can be confirmed.

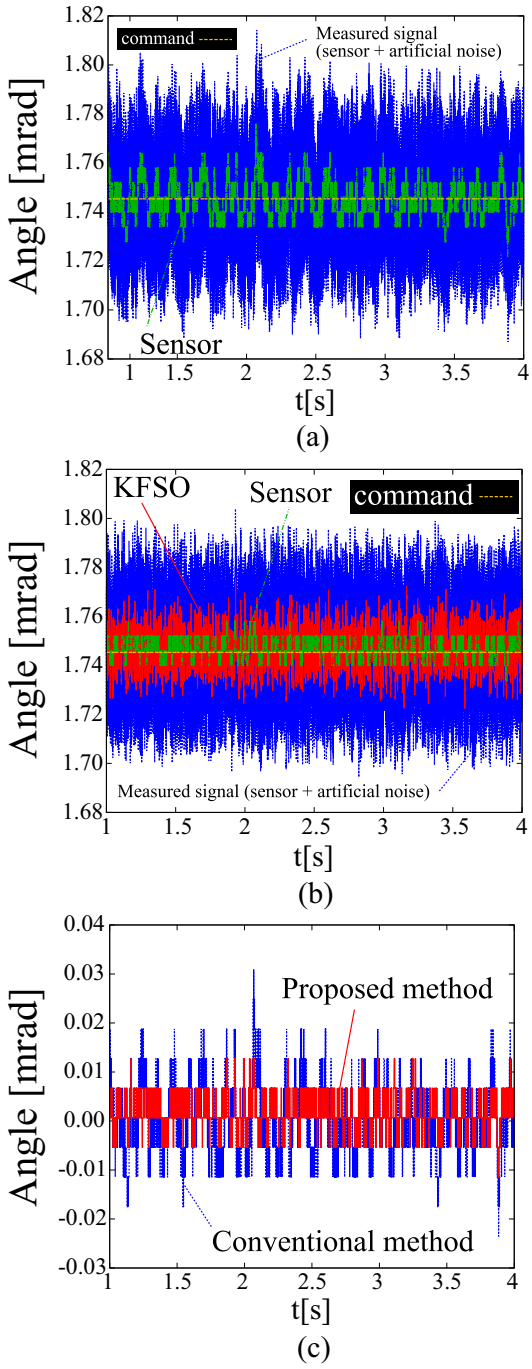

Fig. 2-18: Enlarged views of Fig. 2-17. (a) Result with DOB. (b) Result with the proposal. (c) Error responses.

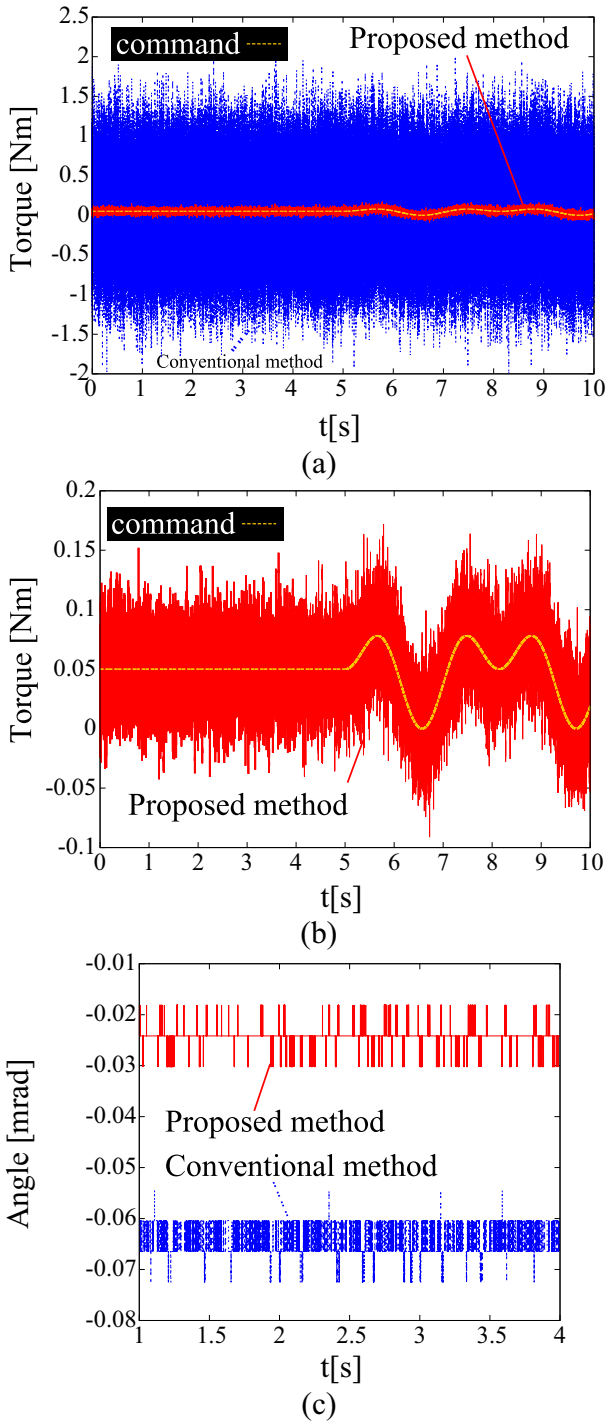

Fig. 2-19: Experimental results of reaction torque control in case 1. (a) Result with DOB. (b) Result with the proposal. (c) Resulting position responses.

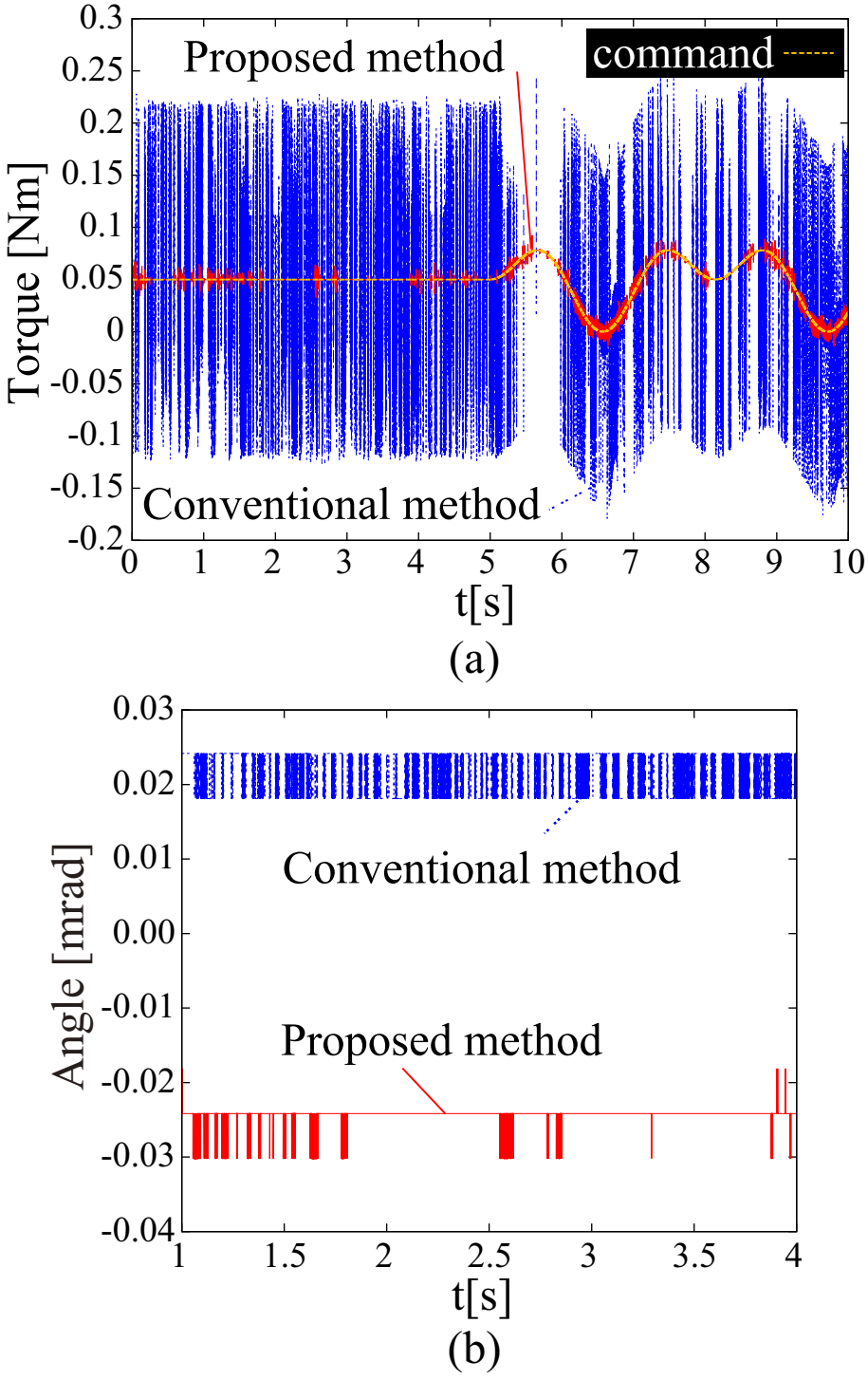

Fig. 2-20: Experimental results of reaction torque control in case 1. (a) External torque responses. (c) Resulting position responses.

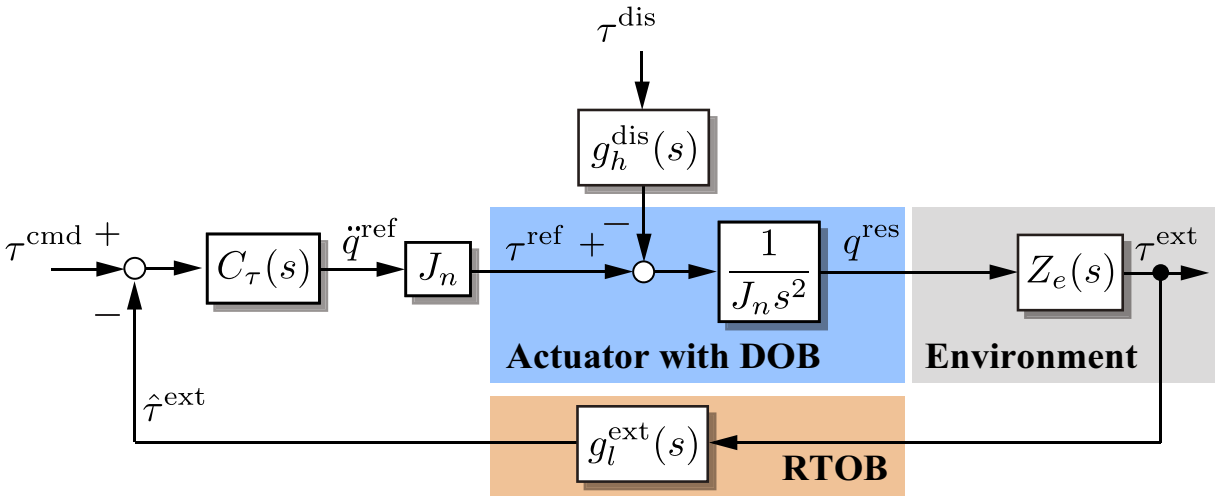

Fig. 2-21: Block diagram of reaction torque control with DOB and RTOB.

2.10 High-order Disturbance Estimation for Proportional-Derivative Force Control

This part describes a high-order disturbance estimation using a Kalman filter for precise reaction-torque control. The proposed method can realize a reaction torque control system by using a proportional derivative (PD) controller. It is confirmed that the proposed PD controller for the reaction torque can improve the control system performance without enhancing the noise effect. This is because the variables estimated using the proposed Kalman-filter-based high-order disturbance/reaction torque observer are utilized in the PD controller. The observer can estimate the disturbance/external torque and its time derivative with a lower noise level than with conventional disturbance observers (DOBs) or reaction torque observers (RTOBs).

2.11 Reaction Torque Control with DOB and RTOB

Fig. 2-21 shows a simplified block diagram of the reaction torque control system with DOB and RTOB. The disturbance torque and the external torque from an environment are estimated using a low-pass filter (LPF) in DOB and RTOB as follows:

$$\hat{\tau}^{\mathrm{dis}} = g_l^{\mathrm{dis}}(s)\tau^{\mathrm{dis}} \tag{2.170}$$

$$\tau^{\mathrm{dis}} = \tau^{\mathrm{ext}} + \tau^{\mathrm{load}}. \tag{2.171}$$

The LPF and the resulting high- pass filter (HPF) for disturbance compensation can be expressed as

$$g_l^{\rm dis}(s) = \frac{g^{\rm dis}}{s + g^{\rm dis}} \tag{2.172}$$

$$g_l^{\rm ext}(s) = \frac{g^{\rm ext}}{s + g^{\rm ext}} \tag{2.173}$$

$$g_h^{\rm dis}(s) = 1 - g_l^{\rm dis}(s) = \frac{s}{s + g^{\rm dis}} \tag{2.174}$$

where $g^{\bullet}$ represent a pole of the filter. For simplicity, the cutoff frequency of DOB and RTOB are assumed to be infinite. By considering this assumption, the transfer function from the torque command to the external torque response using a proportional controller can be expressed as follows:

$$\frac{\tau^{\rm ext}}{\tau^{\rm cmd}} = \frac{C_\tau Z_e(s)}{s^2 + C_\tau Z_e(s)} \tag{2.175}$$

$$C_\tau = K_{\tau p} \tag{2.176}$$

$$Z_e(s) = D_e s + K_e \tag{2.177}$$

where D_e, K_e and $C_\tau = K_{\tau p}$ represent an environmental damper and an environmental stiffness and a torque control gain, respectively. On the other hand, if the proportional-derivative controller is utilized, the transfer function is rewritten as follows:

$$\frac{\tau^{\rm ext}}{\tau^{\rm cmd}} = \frac{C_\tau(s) Z_e(s)}{s^2 + C_\tau(s) Z_e(s)} \tag{2.178}$$

$$= \frac{a_2 s^2 + a_1 s + a_0}{(1 + a_2) s^2 + a_1 s + a_0} \tag{2.179}$$

$$a_2 = D_e K_{\tau d} G_\tau^{\rm pd}(s) \tag{2.180}$$

$$a_1 = K_e K_{\tau d} G_\tau^{\rm pd}(s) + D_e K_{\tau p} \tag{2.181}$$

$$a_0 = K_e K_{\tau p} \tag{2.182}$$

$$C_\tau(s) = K_{\tau p} + K_{\tau d} s G_{\tau \rm pd}(s) \tag{2.183}$$

$$G_\tau^{\rm pd}(s) = \frac{g_\tau^{\rm pd}}{s + g_\tau^{\rm pd}} \tag{2.184}$$

where $G_\tau^{\rm pd}(s)$ represents the LPF of pseudo differentiation. Fig. 2-22 shows a Bode diagram of the response characteristics as shown in (2.175) and (2.178). As shown in the figure, if a PD controller is utilized, the performance of the reaction torque control can be improved, even though the cutoff frequency of the pseudo differentiation is finite.

However, it is difficult to obtain the derivative of the external/disturbance torque because it often includes heavy noise if practical applications are taken into account.

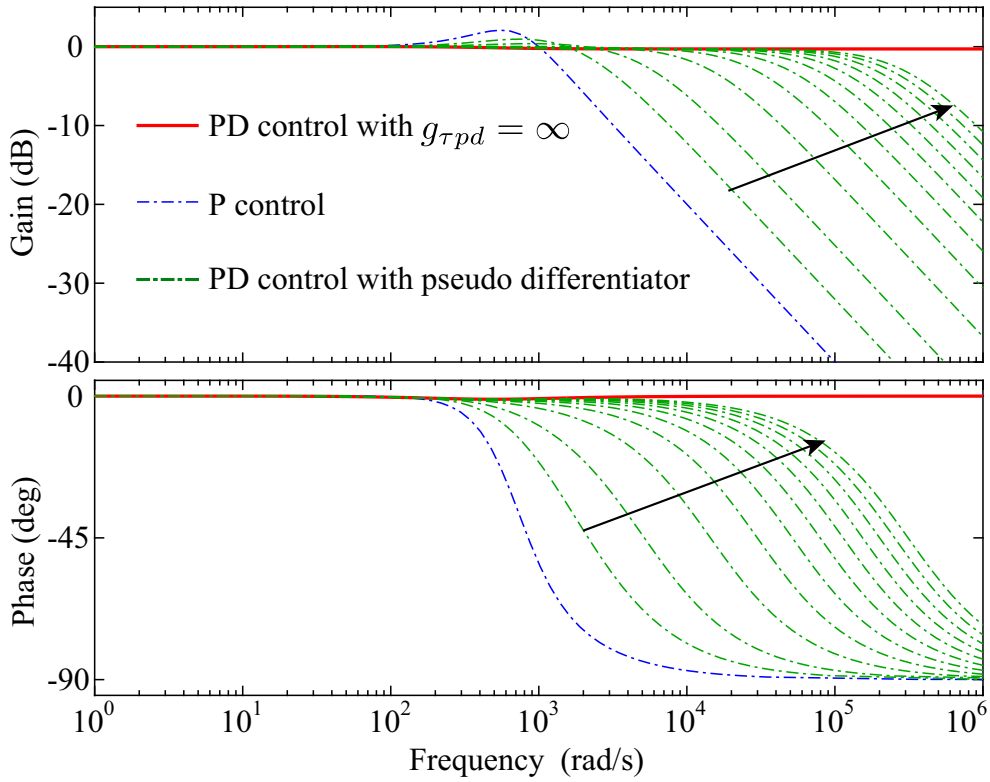

Fig. 2-22: Bode diagram of the reaction torque control system with the variation of $g_\tau^{\mathrm{pd}} = 50$ to 10000.

2.12 Kalman-Filter-Based State Observer With High-Order Disturbance Estimation

This chapter proposed a Kalman-filter-based state observer (KFSO) with a high-order disturbance/external torque estimation in order to suppress noise effects and to obtain the first-order time derivative of the disturbance/reaction torque.

2.12.1 Motion Equation and State-Space Equation Considering System Noise

If the presence of system noise is explicitly considered, the motion equation of an actuator is described as

$$J_n \ddot{q}^{\mathrm{res}}(t) = \tau^{\mathrm{ref}}(t) - \tau^{\mathrm{dis}}(t) + v^{\mathrm{dis}}(t) \tag{2.185}$$

$$\tau^{\mathrm{dis}}(t) = \tau^{\mathrm{ext}}(t) + \tau^{\mathrm{load}}(t) \tag{2.186}$$

where $\tau^{\mathrm{load}}(t)$ represents the disturbance torque that includes parameter variation and friction terms except that for the external torque.

2.12.2 Kalman Filtering Process

A state space equation of an actuator in which the sate variable includes disturbance terms can be described as follows:

$$\dot{\boldsymbol{Z}}^{h1}(t) = \mathbf{A}^h \boldsymbol{Z}^h(t) + \mathbf{B}^h \boldsymbol{u}(t) + \mathbf{B}_v^h \boldsymbol{V}^h(t) \tag{2.187}$$

$$\dot{\boldsymbol{Z}}^h(t) = \left[\dot{q}^{\mathrm{res}}(t) \;\; \ddot{q}^{\mathrm{res}}(t) \;\; \dot{\tau}^{\mathrm{dis}}(t) \;\; \ddot{\tau}^{\mathrm{dis}}(t)\right]^T \tag{2.188}$$

$$\boldsymbol{Y}(t) = \boldsymbol{c}\boldsymbol{Z}(t) + \boldsymbol{W}(t) = q^{\mathrm{res}}(t) + w(t) \tag{2.189}$$

where

$$\mathbf{A}^h = \begin{bmatrix} 0 & 1 & 0 & 0 \\ 0 & 0 & -\frac{1}{J_n} & 0 \\ 0 & 0 & 0 & 1 \\ 0 & 0 & 0 & 0 \end{bmatrix}, \; \mathbf{B}^h = \begin{bmatrix} 0 \\ \frac{1}{J_n} \\ 0 \\ 0 \end{bmatrix}, \; \left[\boldsymbol{c}^h\right]^T = \begin{bmatrix} 1 \\ 0 \\ 0 \\ 0 \end{bmatrix}. \tag{2.190}$$

The superscript h represent a parameter corresponding to the high order (1st-order) disturbance estimation. In the state space model, the model of disturbance is assumed as shown in the following equation:

$$\tau^{\mathrm{dis}}(t) = d_0 + d_1 t + \int_0^t \int_0^t v_{\mathrm{dif}^1}^{\mathrm{dis}}(T) dT^2 \tag{2.191}$$

$$\dot{\tau}^{\mathrm{dis}}(t) = d_0 + \int_0^t v_{\mathrm{dif}^1}^{\mathrm{dis}}(T) dT \tag{2.192}$$

$$\ddot{\tau}^{\mathrm{dis}}(t) = v_{\mathrm{dif}^1}^{\mathrm{dis}}(t). \tag{2.193}$$

In this model, the second-order derivative (higher-order differentiation) of the disturbance is considered to be a different form of the usual KFSO [65]. The disturbance is modeled as a ramp signal with the integral of the process noise $v_{\mathrm{dif}^1}^{\mathrm{dis}}(t)$ in a sampling period. Usually, the time derivative of disturbance is set to zero [92, 103] as the model of disturbance. However, this dissertation assumes the presence of the process noise in the model for the time derivative of the disturbance to determine the appropriate covariance matrix as described in the last part. According to (2.185) and (2.191) to (2.193), the state

vector and the input vector in (2.187) can be determined as follows:

$$\boldsymbol{V}^h(t) = \left[v^{\mathrm{dis}}(t) \;\; v^{\mathrm{dis}}_{\mathrm{dif}^1}(t) \right]^T \tag{2.194}$$

$$\mathbf{B}^h_v = \begin{bmatrix} 0 & 0 \\ \frac{1}{J_n} & 0 \\ 0 & 0 \\ 0 & 1 \end{bmatrix} \tag{2.195}$$

where superscript h represent a corresponding parameter to the high-order disturbance estimation. An actuator dynamics model in a discrete time domain can be formulated as follows:

$$\boldsymbol{Z}^h(k+1) = \mathbf{A}^h_d \boldsymbol{Z}^h(k) + \mathbf{B}^h_d u(k) + \mathbf{B}^h_{vd} \boldsymbol{V}^h(k) \tag{2.196}$$

$$\boldsymbol{Z}^h(k) = \left[q^{\mathrm{res}}(k) \;\; \dot{q}^{\mathrm{res}}(k) \;\; \tau^{\mathrm{dis}}(k) \;\; \dot{\tau}^{\mathrm{dis}}(k) \right]^T \tag{2.197}$$

$$\boldsymbol{Y}(k) = \boldsymbol{c}^h \boldsymbol{Z}^h(k) + \boldsymbol{W}(k) = q^{\mathrm{res}}(k) + w(k) \tag{2.198}$$

$$\mathbf{A}^h_d = \mathbf{e}^{\mathbf{A}^h T_s} \tag{2.199}$$

$$\mathbf{B}^h_d = \int_0^{T_s} \mathbf{e}^{\mathbf{A}^h t} \mathbf{B}^h dt. \tag{2.200}$$

The proposed Kalman filtering is executed based on (2.196) to (2.200). The filtering process can be divided into prediction and updating phases. In the prediction phase, the predicted (a priori) state estimate $\hat{\boldsymbol{Z}}^{h^-}(k)$ and predicted (a priori) estimate error covariance matrix $\mathbf{P}^{h-}(k)$ are estimated as follows:

$$\boldsymbol{Z}^{h^-}(k) = \mathbf{A}^h_d \hat{\boldsymbol{Z}}^h(k-1) + \mathbf{B}^h_d u(k-1) \tag{2.201}$$

$$= \left[\hat{q}^{\mathrm{res}}_{\mathrm{hkf}}(k) \;\; \hat{\dot{q}}^{-\mathrm{res}}_{\mathrm{hkf}}(k) \;\; \hat{\tau}^{-\mathrm{dis}}_{\mathrm{hkf}}(k) \;\; \hat{\dot{\tau}}^{-\mathrm{dis}}_{\mathrm{hkf}}(k) \right]^T \tag{2.202}$$

$$\mathbf{P}^{h-}(k) = \mathbf{A}^h_d \mathbf{P}(k-1) \mathbf{A}^{h^T}_d + \mathbf{Q}^h. \tag{2.203}$$

In the updating phase, the Kalman filter gain matrix $\boldsymbol{G}_{\mathrm{hkf}}(k)$ is calculated as

$$\mathbf{G}^h_{\mathrm{kf}}(k) = \mathbf{P}^{h-}(k) \boldsymbol{c}^{h^T} \left(\boldsymbol{c}^h \mathbf{P}^{h-}(k) \boldsymbol{c}^h + \mathbf{R} \right)^{-1}. \tag{2.204}$$

The estimated (a posteriori) state vector and the (a posteriori) error matrix covariance matrix are updated by using an actual measurement $\boldsymbol{Y}(k)$ at every sampling instant as follows:

$$\hat{\boldsymbol{Z}}^h(k) = \boldsymbol{Z}^{h^-}(k) + \mathbf{G}^h_{\mathrm{kf}}(k) \left(\boldsymbol{Y}(k) - \boldsymbol{c}^h \hat{\boldsymbol{Z}}^{h^-}(k) \right) \tag{2.205}$$

$$= \left[\hat{q}^{\mathrm{res}}_{\mathrm{hkf}}(k) \;\; \hat{\dot{q}}^{\mathrm{res}}_{\mathrm{hkf}}(k) \;\; \hat{\tau}^{\mathrm{dis}}_{\mathrm{hkf}}(k) \;\; \hat{\dot{\tau}}^{\mathrm{dis}}_{\mathrm{hkf}}(k) \right]^T \tag{2.206}$$

$$\mathbf{P}(k) = \left(\boldsymbol{I} - \mathbf{G}^h_{\mathrm{kf}}(k) \boldsymbol{c}^h \right) \mathbf{P}^{h-}(k). \tag{2.207}$$

The estimated variables $\hat{\boldsymbol{Z}}^h(k)$ are used for the control system. In the case of the external torque estimation, $\hat{\tau}^{\rm ext}_{\rm hkf}(k)$ and $\hat{\dot{\tau}}^{\rm ext}_{\rm hkf}(k)$ is estimated by removing $\tau^{\rm load}$ from a priori state estimate $\hat{\boldsymbol{Z}}^-(k)$ as follows:

$$\boldsymbol{Z}^{h-}(k) = \mathbf{A}_d^h \hat{\boldsymbol{Z}}^h(k-1) + \mathbf{B}_d^h \left[u(k-1) - \tau^{\rm load}(k-1) \right] \tag{2.208}$$

$$\hat{\boldsymbol{Z}}^h(k) = \left[\hat{q}^{\rm res}_{\rm hkf}(k) \;\; \hat{\dot{q}}^{\rm res}_{\rm hkf}(k) \;\; \hat{\tau}^{\rm ext}_{\rm hkf}(k) \;\; \hat{\dot{\tau}}^{\rm ext}_{\rm hkf}(k) \right]^T. \tag{2.209}$$

2.12.3 Derivation of Covariance-Matrix Structure

In order to determine the structure of $\mathbf{Q}^h$, the derivation of a prior error covariance matrix is considered in the same way as the case of the 0th-order disturbance estimation. To derive the prior error covariance matrix, a prior state estimation error is utilized. The prior state estimation error $\boldsymbol{e}^-(k)$ is described as

$$\boldsymbol{e}^-(k) = \boldsymbol{Z}^h(k) - \boldsymbol{Z}^{h-}(k) \tag{2.210}$$

$$= \mathbf{A}_d^h \boldsymbol{e}(k-1) + \mathbf{B}_{vd}^h \boldsymbol{V}^h(k-1). \tag{2.211}$$

To obtain (2.211) the following assumption in Kalman filtering is utilized:

$$\mathrm{E}\left[\boldsymbol{V}^h(k-1) \right] = \bar{\boldsymbol{V}}^h = \mathbf{0}. \tag{2.212}$$

This equation represents that the mean values of the system noises are equal to zero. By using (2.211), the prior error covariance matrix is derived as follows:

$$\begin{aligned} \mathbf{P}^{h-}(k) = {} & \mathrm{E}\left[\boldsymbol{e}^-(k) \boldsymbol{e}^-(k)^T \right] + \mathbf{A}_d^h \mathrm{E}\left[\boldsymbol{e}(k-1) \boldsymbol{e}(k-1)^T \right] \mathbf{A}_d^{h\,T} \\ & + \mathbf{B}_{vd}^h \mathrm{E}\left[\boldsymbol{V}^h(k-1) \boldsymbol{V}^h(k-1)^T \right] \mathbf{B}_{vd}^{h\,T} \end{aligned} \tag{2.213}$$

$$= \mathbf{A}_d^h \mathbf{P}(k-1) \mathbf{A}_d^{h\,T} + \mathbf{B}_{vd}^h \boldsymbol{\Sigma}_v^2 \mathbf{B}_{vd}^{h\,T} \tag{2.214}$$

$$\boldsymbol{\Sigma}_v^2 = \mathrm{E}\left[\left\{ \boldsymbol{V}^h(k-1) - \bar{\boldsymbol{V}}^h \right\} \left\{ \boldsymbol{V}^h(k-1)^T - \bar{\boldsymbol{V}}^h \right\} \right] \tag{2.215}$$

where $\boldsymbol{\Sigma}_v^2$ represents the covariance matrix of system noise. In the derivation of the prior error covariance matrix, the following assumption of Kalman filtering is utilized:

$$\mathrm{E}\left[\boldsymbol{e}^-(k) \boldsymbol{V}^h(k-1)^T \right] = \mathbf{0}. \tag{2.216}$$

If it is assumed that v^{dis} and $v^{\mathrm{dis}}_{\mathrm{dif}^1}$ are independent, the covariance of these system noises is equal to zero as given below:

$$\sigma^2_{v^{\mathrm{dis}}v^{\mathrm{dis}}_{\mathrm{dif}^1}} = \mathrm{E}\left[\{v^{\mathrm{dis}}(k) - \bar{v}^{\mathrm{dis}}\}\{v^{\mathrm{dis}}_{\mathrm{dif}^1}(k) - \bar{v}^{\mathrm{dis}}_{\mathrm{dif}^1}\}\right] \tag{2.217}$$

$$= \mathrm{E}\left[v^{\mathrm{dis}}(k)v^{\mathrm{dis}}_{\mathrm{dif}^1}(k)\right] - \bar{v}^{\mathrm{dis}}\bar{v}^{\mathrm{dis}}_{\mathrm{dif}^1} \tag{2.218}$$

$$= \mathrm{E}\left[v^{\mathrm{dis}}(k)\right]\mathrm{E}\left[v^{\mathrm{dis}}_{\mathrm{dif}^1}(k)\right] - \bar{v}^{\mathrm{dis}}\bar{v}^{\mathrm{dis}}_{\mathrm{dif}^1} \tag{2.219}$$

$$= 0. \tag{2.220}$$

According to (2.212), (2.215), and (2.220), the covariance matrix of system noise is derived as follows:

$$\boldsymbol{\Sigma}^{h\,2}_v = \begin{bmatrix} \sigma^2_{v^{\mathrm{dis}}} & 0 \\ 0 & \sigma^2_{v^{\mathrm{dis}}_{\mathrm{dif}^1}} \end{bmatrix}. \tag{2.221}$$

Finally, according to (2.214) and (2.221), the resulting covariance matrix $\mathbf{Q}^h$ is obtained as

$$\mathbf{Q}^h = \mathbf{B}^h_{vd}\boldsymbol{\Sigma}^{h\,2}_v{\mathbf{B}^h_{vd}}^T \tag{2.222}$$

$$= \left[\int_0^{T_s} \mathbf{e}^{{\mathbf{A}^h}^t} dt \mathbf{B}^h_v\right] \boldsymbol{\Sigma}^{h\,2}_v \left[\mathbf{B}^{h\,T}_v \int_0^{T_s} \mathbf{e}^{{\mathbf{A}^h}^{T} t} dt\right]. \tag{2.223}$$

Only two parameters $\sigma^2_{v^{\mathrm{dis}}}$ and $\sigma^2_{v^{\mathrm{dis}}_{\mathrm{dif}^1}}$ should be determined by considering the existences of two system noises v^{dis} and $v^{\mathrm{dis}}_{\mathrm{dif}^1}$.

2.12.4 Derivation of Steady-State Kalman Filter

This part also utilizes a steady-state Kalman filter (SSKF) as a substation for the LPF and HPF of KFSO for analyzing KFSO. In order to obtain the steady-state Kalman gain, the following discrete time algebraic Riccati equation (DARE) [105] should be solved:

$$\mathbf{P} = \mathbf{A}^h_d \left[\mathbf{P} - \mathbf{P}\boldsymbol{c}^{h\,T}\left(\boldsymbol{c}^h\mathbf{P}\boldsymbol{c}^{h\,T} + \mathbf{R}\right)^{-1}\boldsymbol{c}^h\mathbf{P}\right]\mathbf{A}^{h\,T}_d + \mathbf{Q}^h. \tag{2.224}$$

By using the solution of DARE $\boldsymbol{\mathcal{P}^h}$, the steady state Kalman gain $\boldsymbol{\mathcal{G}}^h_{\mathrm{skf}}$ is obtained as follows:

$$\boldsymbol{\mathcal{G}}^h_{\mathrm{skf}} = \boldsymbol{\mathcal{P}}^h\boldsymbol{c}^{h\,T}\left(\boldsymbol{c}^h\boldsymbol{\mathcal{P}}^h\boldsymbol{c}^{h\,T} + \mathbf{R}\right) \tag{2.225}$$

By using $\boldsymbol{\mathcal{G}}^h_{\mathrm{skf}}$, the estimated state by the steady-state Kalman filter is derived from (2.201) and (2.205) as follows:

$$\hat{\boldsymbol{Z}}^h_{\mathrm{skf}}(z) = \left[\boldsymbol{I} - \left(\boldsymbol{I} - \boldsymbol{\mathcal{G}}^h_{\mathrm{skf}}\boldsymbol{c}^h\right)\mathbf{A}^h_d z^{-1}\right]^{-1} \times \left[\boldsymbol{\mathcal{G}}^h_{\mathrm{skf}}\boldsymbol{Y}(z) + \left(\boldsymbol{I} - \boldsymbol{\mathcal{G}}^h\boldsymbol{c}^h\right)\boldsymbol{b}_d z^{-1}\boldsymbol{u}(z)\right]. \tag{2.226}$$

Table 2.3: Parameters for analysis of high-order disturbance/external torque estimation with Kalman filters

Parameter	Description	Value
T_s	sampling time	0.2 ms
$J_n = J$	inertia of actuator	0.004 kgm^2
$g^{\mathrm{dis}} = g^{\mathrm{dis}}_{\mathrm{skf}}$	cut-off frequency of DOBs and SSKF	365 rad/s
g^v	cut-off frequency of velocity est.	1775 rad/s

A steady-state Kalman filter for disturbance/external torque estimation $g^{\mathrm{dis}}_{l\mathrm{hskf}}(z)$, its noise sensitivity $g^{\mathrm{dis}}_{N\mathrm{hskf}}(z)$, A steady-state Kalman filter for the time derivative of disturbance/external torque estimation $g^{\mathrm{pd}}_{l\mathrm{hskf}}(z)$, its noise sensitivity $g^{\mathrm{pd}}_{N\mathrm{hskf}}(z)$ and the sensitivity to the disturbance $g^{\mathrm{dis}}_{h\mathrm{hskf}}(z)$ are derived as

$$\hat{\tau}^{\mathrm{dis}}_{\mathrm{hskf}} = g^{\mathrm{dis}}_{l\mathrm{hskf}}(z)\tau^{\mathrm{dis}} + g^{\mathrm{dis}}_{N\mathrm{hskf}}(z)w \tag{2.227}$$

$$\hat{\dot{\tau}}^{\mathrm{dis}}_{\mathrm{hskf}} = g^{\mathrm{pd}}_{l\mathrm{hskf}}(z)\dot{\tau}^{\mathrm{dis}} + g^{\mathrm{pd}}_{N\mathrm{hskf}}(z)w \tag{2.228}$$

$$g^{\mathrm{dis}}_{h\mathrm{hskf}}(z) = 1 - g^{\mathrm{dis}}_{l\mathrm{hskf}}(z) \tag{2.229}$$

where subscript hskf represents a corresponding parameter to the Kalman filter for high-order disturbance estimation. From the discrete time state space model, the time derivative of the disturbance torque $\dot{\tau}^{\mathrm{dis}}$ is described as follows:

$$\dot{\tau}^{\mathrm{dis}} = \frac{2}{T_s}\frac{z-1}{z+1}\tau^{\mathrm{dis}} \tag{2.230}$$

where w is a observation noise included in the position response as shown in (2.13). The observation noise included also in the case of Kalman filter based disturbance estimation.

2.13 Analysis

In this section, the approximated performance of the KFSO is analyzed using the SSKF. Parameters used in the analysis are shown in Table 2.3.

2.13.1 Relationship between Bandwidth and Parameters

Here, the relationship between the bandwidth of the SSKF $G^{\bullet}_{\mathrm{skf}L}(z)$ and parameters of the KFSO is analyzed.

Fig. 2-23 shows the relationship between the bandwidth and variance $\sigma^2_{v^{\mathrm{dis}}_{\mathrm{dif}^1}}$. As shown in Fig. 2-23, the bandwidth increases with an increase in the variance of system noise with respect to the time derivative of torque $\sigma^2_{v^{\mathrm{dis}}_{\mathrm{dif}^1}}$. On the other hand, the bandwidth is inversely proportional to the inertia J_n as shown in Fig. 2-23 (a). The increase in the variance of observation noise σ^2_w also tends to reduce the bandwidth as indicated in Fig. 2-23 (b). These figures show that the Kalman filter tends to reduce the effect of observation noise automatically because the larger variance of system noise and inertia result in a higher level of noise effect and a greater noise sensitivity, respectively. Because σ^2_w is determined by (2.125), the other parameters should be adjusted if the resulting estimation is not appropriate. Fig. 2-24 represents the relationship between the bandwidth and variances with J_n=0.004 kgm^2.It is observed that the bandwidth is inversely proportional to the variance of system noise in torque dimension v^{dis}, though the bandwidth is proportional to the variance $\sigma^2_{v^{\mathrm{dis}}_{\mathrm{dif}^1}}$. This indicates that just increasing both variances will lead to estimation failure, though $\mathbf{Q}$ can be regarded as a gain of the Kalman filter [68].

Fig. 2-25 shows the relationship between the bandwidth and variances in respect to estimation of time derivative of disturbance torque with J_n=0.004 kgm^2. The tendency of the graph is similar to that in Fig. 2-24.

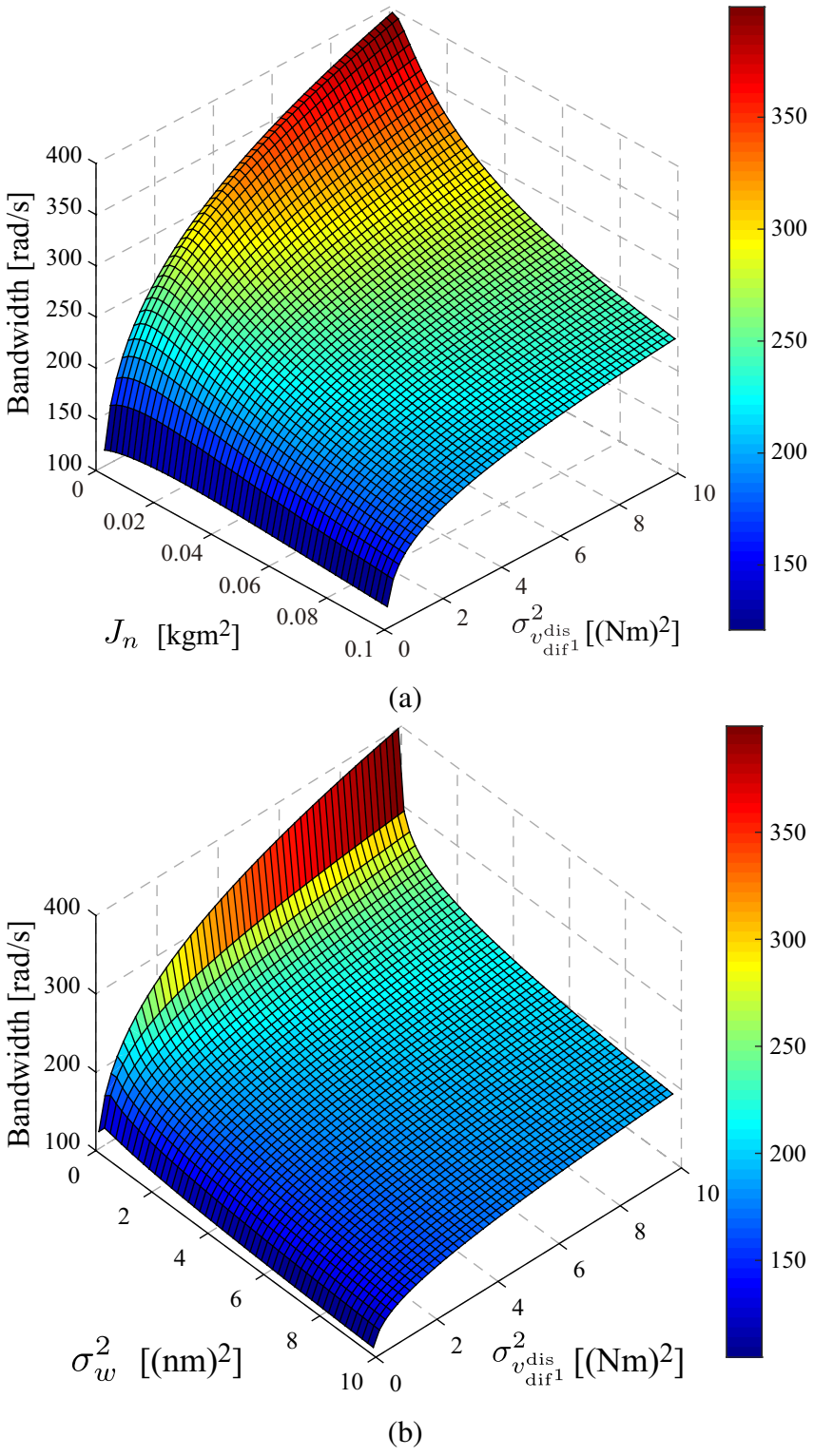

Fig. 2-23: Relationship between bandwidth and variance $\sigma^2_{v^{\mathrm{dis}}_{\mathrm{dif}1}}$ (a) with the variation of nominal inertia. (b) with the variation of variance in respect to observation noise σ^2_w.

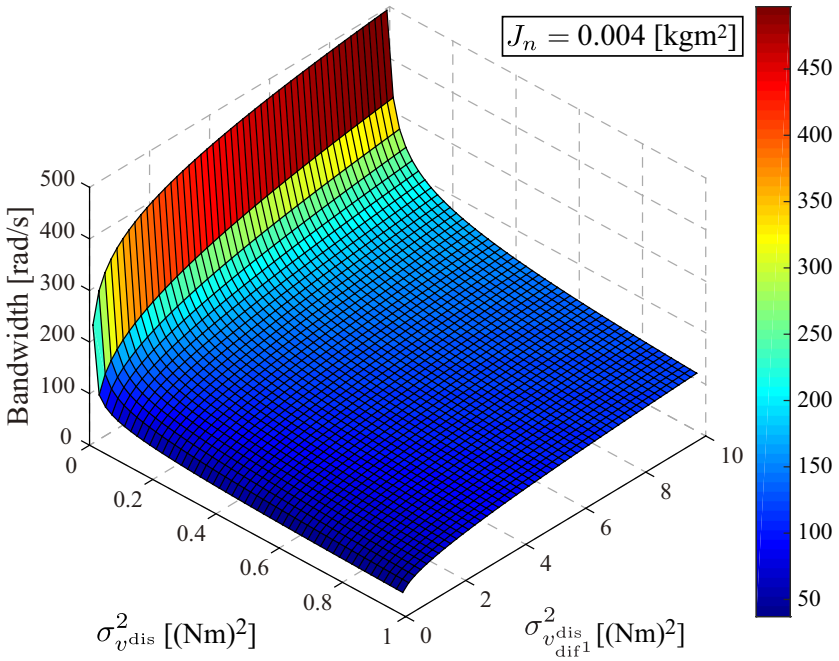

Fig. 2-24: Relationship between bandwidth and variances with J_n=0.004 kgm^2.

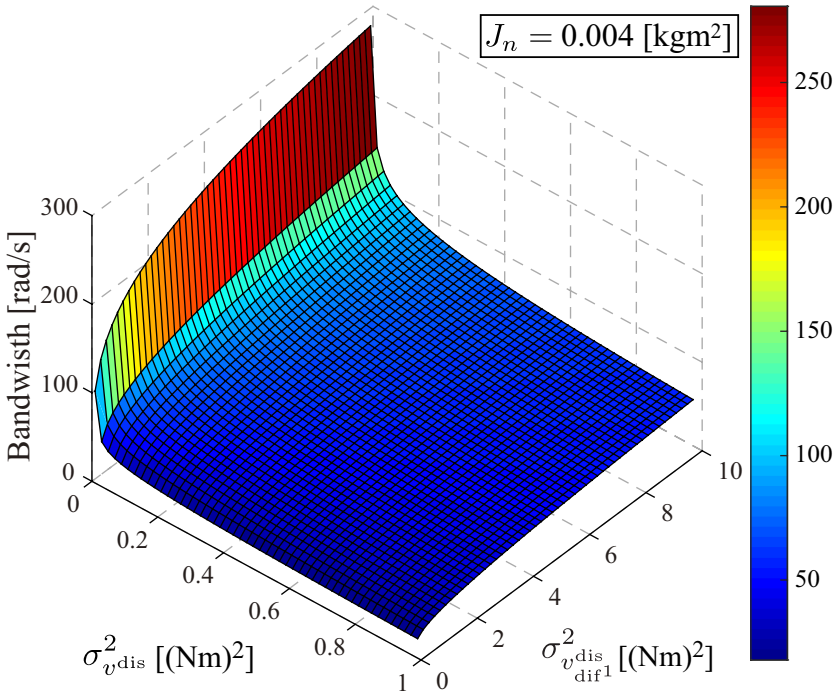

Fig. 2-25: Relationship between bandwidth and variances with respect to estimation of time derivative of disturbance torque with J_n=0.004 kgm^2.

2.13.2 Frequency Characteristics of Disturbance Estimation

Figs. 2-26, 2-27, and 2-28 represent bode diagram in respect to the disturbance estimation with the comparison between KFSO and normal DOBs, bode diagram of resulting HPF and gain diagram of noise sensitivity, respectively. In the figures, the bandwidth of conventional DOBs is set to the same values of the SSKF for the comparison. It is found that the disturbance suppression performance and noise reduction performance are improved by the proposed high-order disturbance estimation based on KF, as indicated by Figs. 2-27 and 2-28. Although the disturbance suppression performance of the high-order (ramp) DOB (HDOB) is almost same level as the proposed method, the noise suppression performance of the proposal is better than the HDOB. In addition, the noise sensitivity of the conventional KFSO is almost same level as the proposal, the disturbance suppression performance of the proposal is superior to the conventional KFSO.

Fig. 2-29 shows the LPF of SSKF and a normal first-order LPF in the estimation of the first derivative of the external/disturbance torque. As shown in the figure, the gain of the SSKF in a higher frequency domain is smaller than the usual first-order LPF with the same bandwidth.

From these results, an improvement in the noise suppression and the performance of the reaction torque control can be expected.

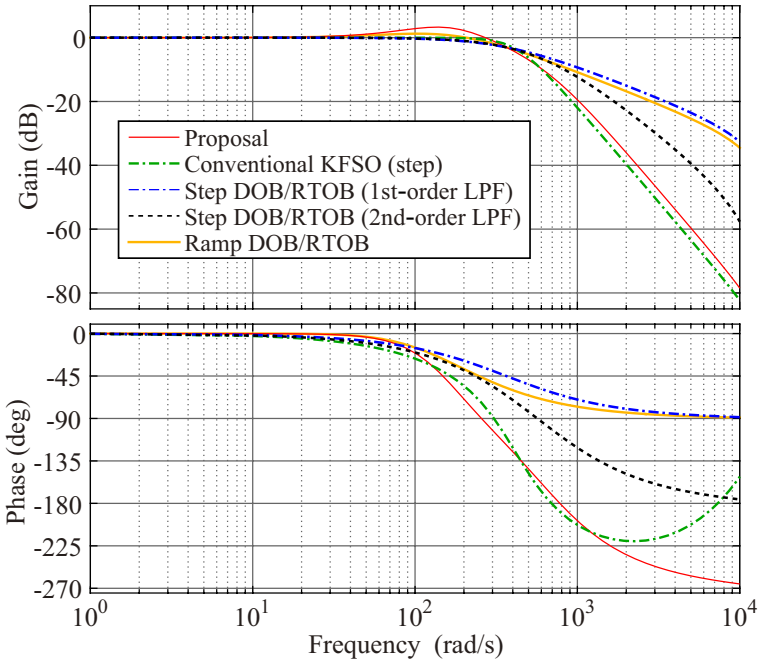

Fig. 2-26: Bode diagram of disturbance estimation with the comparison between the proposed KFSO and normal DOBs.

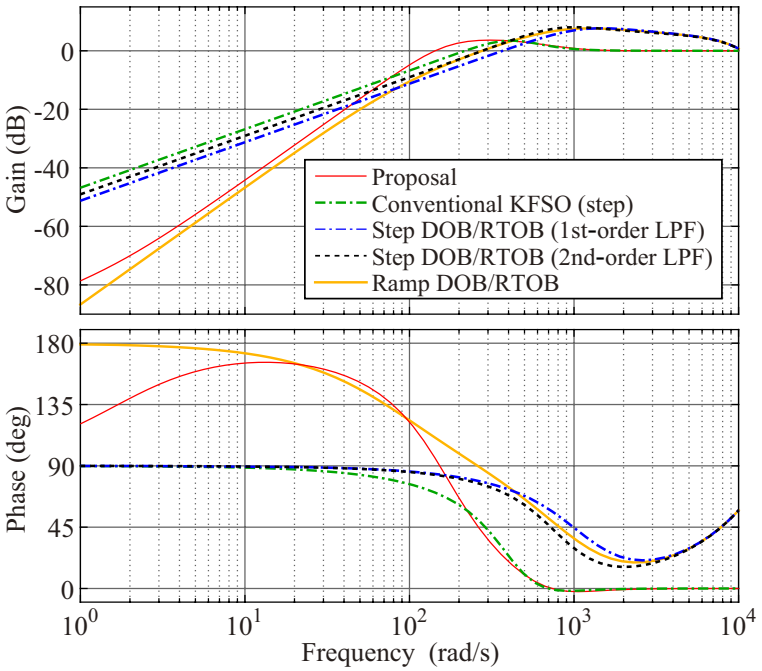

Fig. 2-27: Bode diagram of resulting HPF with the comparison between the proposed KFSO and normal DOBs.

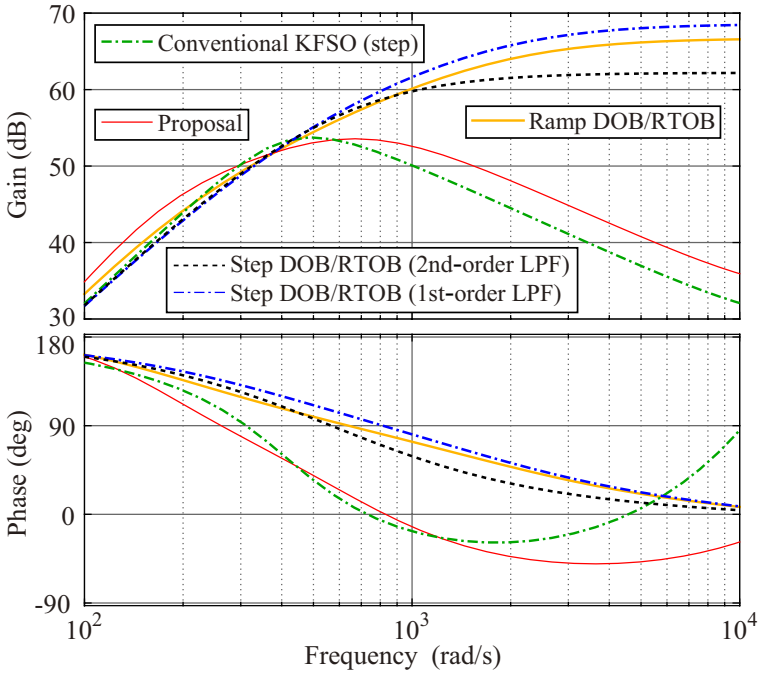

Fig. 2-28: Gain diagram of noise sensitivity with the comparison between the proposed KFSO and normal DOBs.

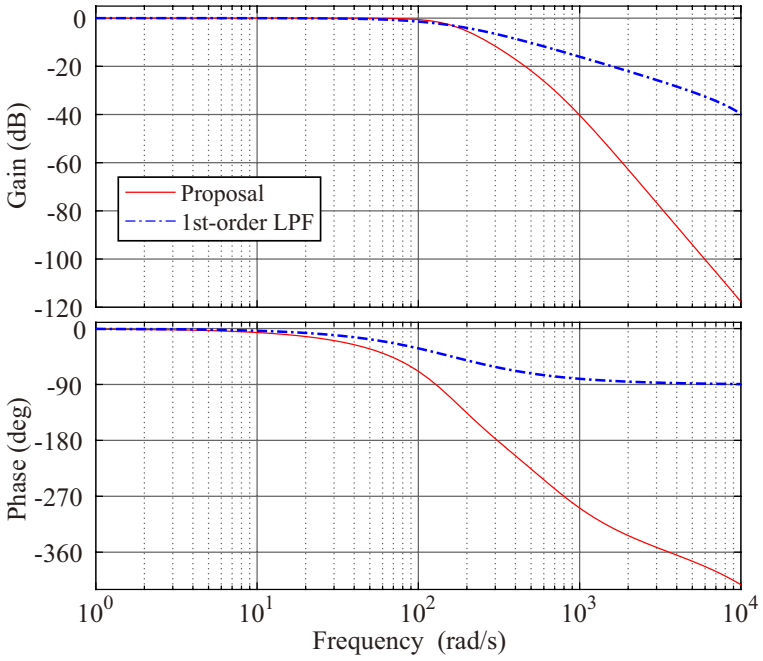

Fig. 2-29: Bode diagram of estimation for the time derivative of external torque with the comparison between the proposed KFSO and normal LPF.

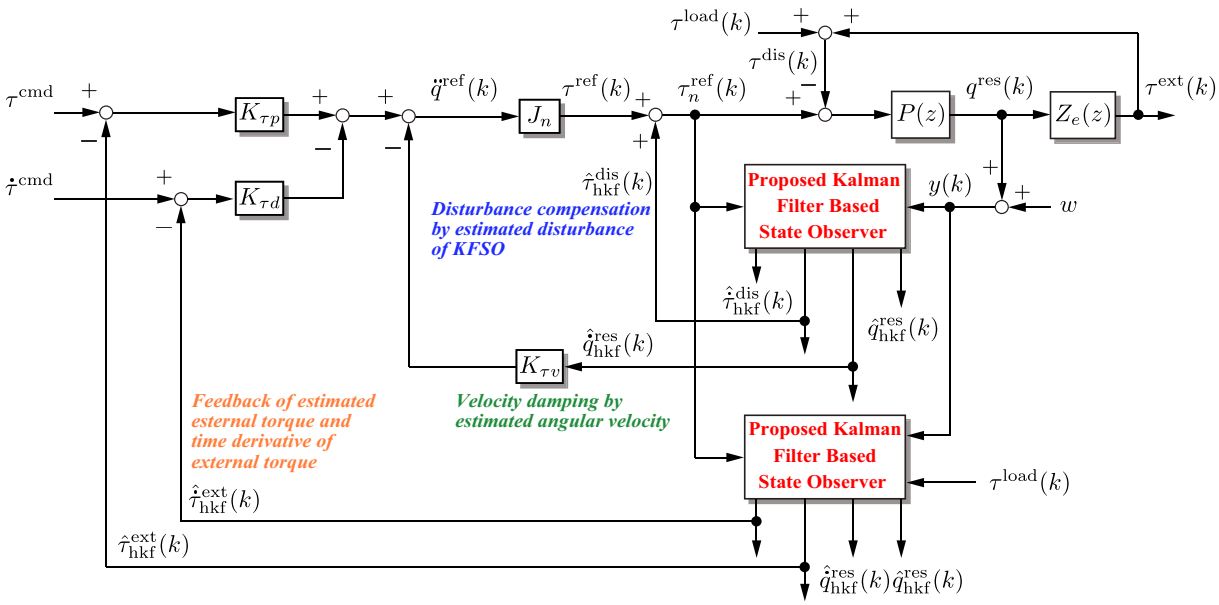

Fig. 2-30: Block diagram of the proposed reaction torque control system.

2.14 Proposed Reaction Torque Control System

By using the estimated variables $\hat{\tau}^{\mathrm{dis}}_{\mathrm{hkf}}(k)$ and $\hat{\dot{\tau}}^{\mathrm{dis}}_{\mathrm{hkf}}(k)$, the reaction torque control with proportional-derivative controller can be constructed with a lower noise level. An acceleration reference of the proposed reaction torque control is expressed as follows:

$$\ddot{q}^{\mathrm{ref}}(k) = K_{\tau p}\left(\tau^{\mathrm{cmd}} - \hat{\tau}^{\mathrm{ext}}_{\mathrm{hkf}}(k)\right) + K_{\tau d}\left(\dot{\tau}^{\mathrm{cmd}} - \hat{\dot{\tau}}^{\mathrm{dis}}_{\mathrm{hkf}}(k)\right). \tag{2.231}$$

As another structure that uses the estimated variable of the Kalman filter, a reaction torque controller with velocity damping can be realized as

$$\ddot{q}^{\mathrm{ref}}(k) = K_{\tau p}\left(\tau^{\mathrm{cmd}} - \hat{\tau}^{\mathrm{ext}}_{\mathrm{hkf}}(k)\right) + K_{\tau d}\left(\dot{\tau}^{\mathrm{cmd}} - \hat{\dot{\tau}}^{\mathrm{dis}}_{\mathrm{hkf}}(k)\right) - K_{\tau v}\hat{\dot{q}}^{\mathrm{res}}_{\mathrm{hkf}}(k). \tag{2.232}$$

The torque reference for the actuator is given by adding the estimated disturbance torque $\hat{\tau}^{\mathrm{dis}}_{\mathrm{hkf}}(k)$ as follows:

$$\tau_n^{\mathrm{ref}}(k) = J_n\ddot{q}^{\mathrm{ref}}(k) + \hat{\tau}^{\mathrm{dis}}_{\mathrm{hkf}}(k) = \tau^{\mathrm{ref}} + \hat{\tau}^{\mathrm{dis}}_{\mathrm{hkf}}(k). \tag{2.233}$$

The entire block diagram of the proposed method is shown in Fig. 2-30.

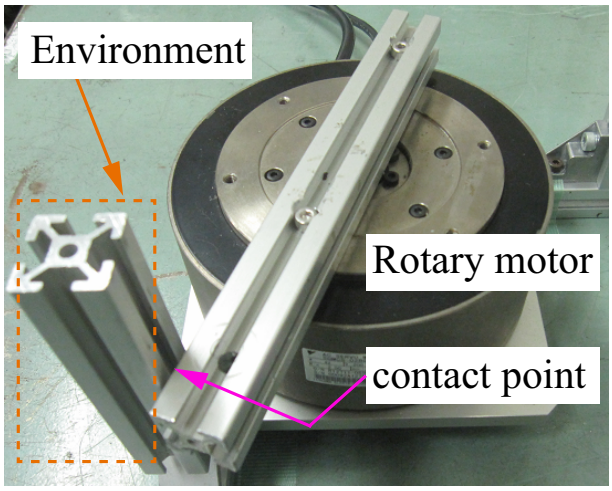

Fig. 2-31: Experimental setup for reaction torque control based on high-order disturbance/external torque estimation with Kalman filters.

Table 2.4: Experimental parameters for reaction torque control with PD controller.

Parameter	Description	Value
$K_{\tau p}$	proportional gain of torque control	50
$K_{\tau d}$	derivative gain of torque control	2
$K_{\tau v}$	damping coefficient	3
δq	resolution of rotary encoder	1.0×10^{6} puls/rev

2.15 Experiments for Reaction Torque with the Proposed KFSO

2.15.1 Experimental Setup for Reaction Torque by a Single DOF Direct-drive Motor

To confirm the validity of the proposal, experiments of the reaction torque control in joint spaces were conducted to test DOB/RFOB and KFSO. Fig. 2-31 shows the experimental set up of a single DOF direct-drive motor. This part assumes the parameter variation and friction effect of the actuators are negligible. Table 2.4 lists the experimental parameters. The other parameters are the same as those used in the analysis, and are listed in Table 2.3.

2.15.2 Experimental Results of Reaction Torque Control System with and without Proposed KFSO

Fig. 2-32 shows the experimental results of the reaction torque control by a conventional method and the proposed method. As shown in the figure, the noise-suppression performance of the proposed

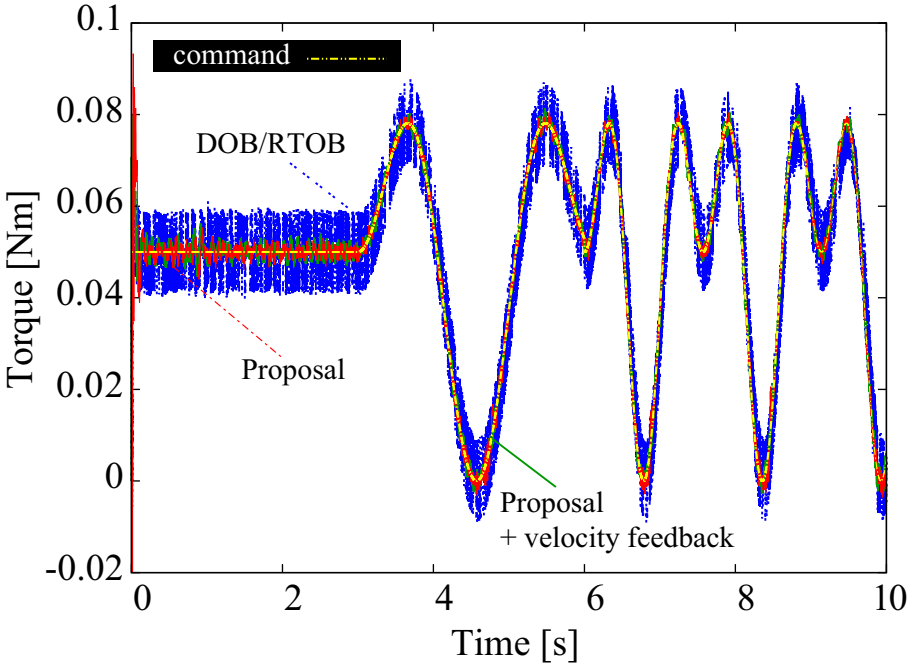

Fig. 2-32: Experimental results of reaction torque responses.

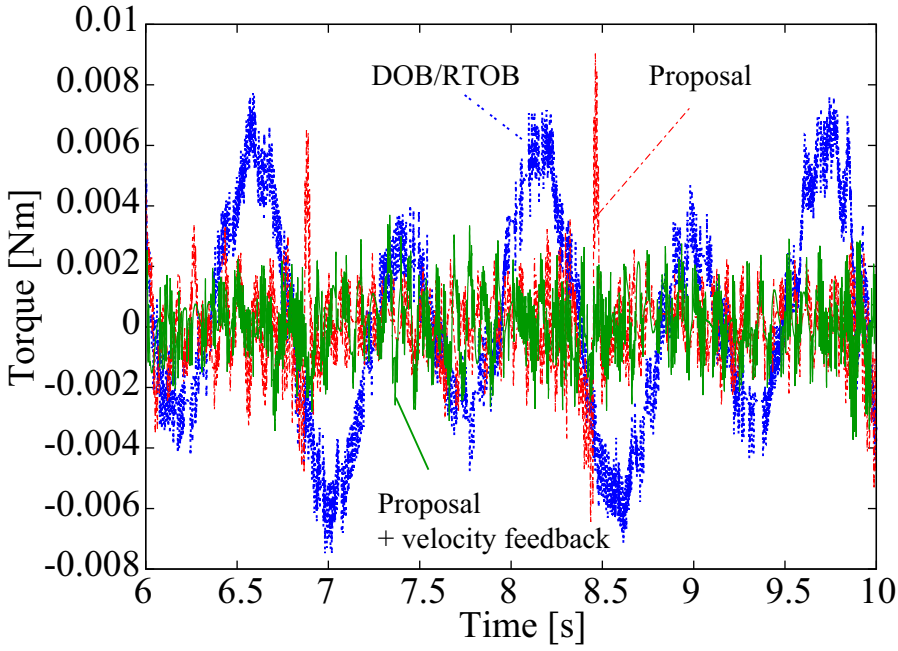

Fig. 2-33: Enlarged view of error responses from 6.0 s to 10.0 s.

methods are improved compared with those of the conventional DOB-based reaction torque control.

Fig. 2-33 shows the enlarged view of the error responses about the reaction torque when the actuator made contact with the environment. It can be confirmed that the proposed method shows better tracking performance than the conventional method.

From these results, the validity of the proposal is confirmed.

2.16 Summary of Chapter 2

In this chapter, high-order disturbances with considering stochastic behavior were described. The high-order disturbances in an actuator, a multi-degree-of-freedom (MDOF) system and an environment were explained.

This chapter also showed a design method of a KFSO for tuning the covariance matrix with respect to system noise. A high-order disturbance observer based on a Kalman filter for realization of the precise force control was also shown.

By the proposed tuning structure, the numbers of parameters that have to be determined were reduced from nine to two parameters because the time derivative of system noise in torque dimension is taken into consideration in the disturbance model. Furthermore, the structure of Kalman filter-based external torque estimation without using nonlinear Kalman filter was proposed. In addition, the relationships between the two parameters were confirmed by utilizing the steady-state Kalman filter. It is observed that the Kalman filter is not able to estimate the disturbance/external torque appropriately if the tuning of the covariance matrix is failed by regarding the parameters in $\boldsymbol{Q}$ as just the gains of the Kalman filter. Experimental results validated the tuning method and analytical results. Furthermore, this chapter also showed a method to improve the performance of a reaction torque control system by using a high-order disturbance/reaction torque estimation based on a Kalman filter. The proposed method can realize a reaction torque control system by using a proportional-derivative controller. It was confirmed that the proposed proportional derivative controller for the reaction torque can improve control system performance while suppressing the noise effect. This is because the estimated variables by the proposed Kalman-filter-based high-order disturbance/reaction torque observer are utilized in the PD controller. The observer can estimate the disturbance/external torque and its time derivative with lower noise levels than conventional DOBs or RTOBs.

The validity of the proposed method is confirmed through an experiment of the reaction torque control that makes contact with an environment by using a single degree-of-freedom rotary motor.

Chapter 3

Realization of Stable Contact Motion with High-Order Environmental Disturbance Estimation

---

3.1 Introduction of Chapter 3

This chapter shows a realization of stable contact motion with high-order environmental disturbance estimation.

There are two types of control systems for realizing contact motions. One is an impedance control (force-based compliance control)- based force control system [91]. This corresponds to the conventional force control system based on DOB and RFOB. The force control system based on the structure is combined with KFSOs in the last chapter.

The other type of force control system is an admittance control (position- based compliance control)-based force control system [91, 106].

As mentioned in chapter 1, it is known that the performance and stability of the contact motions for force tracking control are highly dependent on the environmental impedance [8,18,19]. If a velocity term is implemented in the force control system, a stabilization of the contact motion is achieved. However, the utilization of the velocity damping causes a deterioration of the force control from the view point of the control stiffness [7, 70].

In the case of the ideal position control systems, the control stiffness should be infinite. This means displacement against external force should not be generated (should be zero). On the other hand, the control stiffness should be zero in the case of the ideal force control systems. This represents the dis-

placement against external force should be generated without constraint.

However, the velocity feedback term for the damping behaves as artificial viscous friction as a constraint force. Therefore, simultaneous realization of stabilization and ideal control stiffness is difficult.

On the other hand, this chapter shows a method of stable contact motions for force tracking control based on the concept of resonance ratio control [74]. The similarity in the structure for admittance control for contact motions and two-mass resonance systems [22] is derived. From the similarity, it is found that the concept of the resonance ratio control can be applicable to the force tracking control.

Based on the concept of resonance ratio control, an admittance controller for contact motion with the environmental disturbance (EnvD) compensation is proposed. By using the proposed method, the vibration suppression in contact motion is realized even if the environment has no or insufficient viscosity. The response characteristics of contact motion for force control can be determined arbitrarily by the proposed method.

The proposed method realizes the simultaneous realization of stabilization and ideal control stiffness. In accordance with the derivation of similarity between the two mass resonance system and the force control system, EnvD is introduced which corresponds to a load side disturbance [23, 24, 107]. Similarly to the compensation of the load side disturbance [23, 24, 107], the compensation of the EnvD in admittance based force control system is also requires second and first order time derivatives of estimated EnvD [74]. DOB/RFOB based control structure neglects the higher order derivative terms in order to avoid enlarging the noise effect in the estimation [23, 24, 74, 107]

This chapter also proposes the higher order EnvD estimation based on Kalman filter including the time derivatives of EnvD for the compensation. A state observer with considering the model of high-order time derivatives of EnvD is introduced. The disturbance/external torque is modeled as a second-order signal of a time function though the disturbances are usually modeled as a step signal in conventional DOBs or KFSO [65]. The highest (third) order time derivative of environmental disturbance is modeled as behaving as random walk. The estimated variable of the proposed Kalman filter based high-order environmental disturbance observer can be utilized for the compensation without enlarging noise effect in time derivatives

Here, the target of this chapter is the realization of the contact motion for force tracking control by a rigid actuator and the environment. This differs from the force control system for the actual two- (or multi) mass resonant systems [108].

3.2 Two Types of Force Control Based on DOB and RFOB

3.2.1 Force Control Based on Impedance Control

Fig. 3-1 shows a simplified block diagram of the force control system with DOB and RFOB. This force control system can be regarded as a kind of impedance control with a virtual mass M_f which corresponds to the force control gain. In the figure, s, F, X Z_e and M represent the Laplace operator, force, position, environmental impedance and mass of the actuator, respectively. Superscripts $\bullet^{\mathrm{dis}}$, $\bullet^{\mathrm{ext}}$, $\bullet^{\mathrm{load}}$, $\bullet^{\mathrm{ref}}$, $\bullet^{\mathrm{cmd}}$ and a subscript $\bullet_n$ represent a disturbance force, external force, load force (with the exception of external force), reference value, and nominal value, respectively. $\hat{\bullet}$ represents an estimated value. The disturbance force and the external force from the environment are estimated using a low-pass filter (LPF) $g_l(s)$ in DOB and RFOB as follows:

$$\hat{F}^{\mathrm{dis}} = g_l^{\mathrm{dis}}(s)F^{\mathrm{dis}} = g_l^{\mathrm{dis}}(s)\left(F^{\mathrm{ext}} + F^{\mathrm{load}}\right) \tag{3.1}$$

$$\hat{F}^{\mathrm{ext}} = g_l^{\mathrm{ext}}(s)F^{\mathrm{ext}}. \tag{3.2}$$

The LPFs and the resulting high- pass filter (HPF) $g_h(s)$ for disturbance compensation can be expressed as

$$\left[g_l^{\mathrm{dis}}(s), g_l^{\mathrm{ext}}(s)\right] = \left[\frac{g^{\mathrm{dis}}}{s+g^{\mathrm{dis}}}, \frac{g^{\mathrm{ext}}}{s+g^{\mathrm{ext}}}\right] \tag{3.3}$$

$$g_h^{\mathrm{dis}}(s) = 1 - g_l^{\mathrm{dis}}(s) = \frac{s}{s+g^{\mathrm{dis}}} \tag{3.4}$$

where g represents the cut-off frequency. For simplicity, the cutoff frequency of DOB and RFOB are assumed to be infinite. By considering this assumption, the transfer function from the torque command to the external torque response using a proportional controller can be expressed as follows:

$$\frac{F^{\mathrm{ext}}}{F^{\mathrm{cmd}}} = \frac{\frac{Z_e(s)}{M_f}}{s^2 + \frac{Z_e(s)}{M_f}} \tag{3.5}$$

$$Z_e(s) = M_e s^2 + D_e s + K_e \tag{3.6}$$

where M_e, D_e and K_e represent the environmental mass, viscosity, and stiffness, respectively. As shown by (3.5), the performance and stability of the force control system is highly dependent on the environmental impedance. For example, the force response becomes oscillatory if the environment does not have sufficient viscosity.

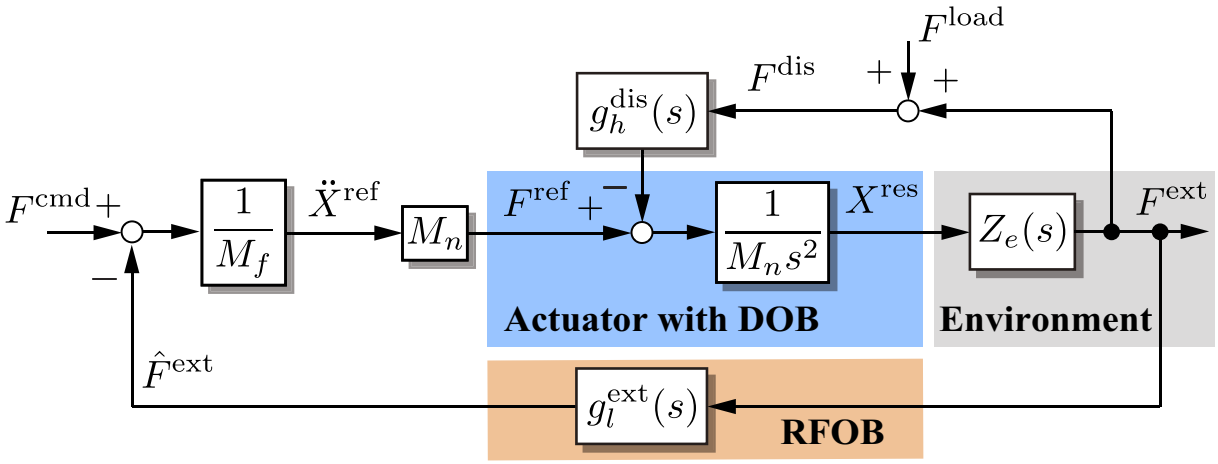

Fig. 3-1: Block diagram of force control based on impedance control with DOB and RFOB [8].

3.2.2 Realization of Contact Motion By Admittance Control

In contrast to the conventional force control system, the contact motion for the force tracking control can also be realized by an admittance control system. Fig. 3-2 shows the admittance control for the force tracking control, where $C_p(s)$=$K_v s + K_p$ represents the position controller. K_v and K_p are the velocity gain and position gain, respectively. The force command F^{cmd} is achieved through the position controller, as shown in Fig. 3-2 (a). The acceleration reference for the controller is given as follows:

$$\ddot{X}^{\mathrm{ref}} = K_p(X_f^{\mathrm{cmd}} - X_f^{\mathrm{res}} - X^{\mathrm{res}}) + K_v(\dot{X}_f^{\mathrm{cmd}} - \dot{X}_f^{\mathrm{res}} - \dot{X}^{\mathrm{res}}) + \ddot{X}_f^{\mathrm{cmd}} - \ddot{X}_f^{\mathrm{res}} \tag{3.7}$$

where $\ddot{X}_f^{\mathrm{cmd}}$, $\ddot{X}_f^{\mathrm{res}}$ and $\ddot{X}_f^{\mathrm{ref}}$ are defined as

$$\frac{1}{M_f}\left(F^{\mathrm{cmd}} - F^{\mathrm{ext}}\right) = \ddot{X}_f^{\mathrm{cmd}} - \ddot{X}_f^{\mathrm{res}} = \ddot{X}_f^{\mathrm{ref}}. \tag{3.8}$$

In the position control part, because $\ddot{X}_f^{\mathrm{ref}}$ behaves as a feedforward term of the acceleration, the transfer function of position control becomes as follows:

$$s^2 X^{\mathrm{res}} = (K_p + K_v s)(X_f^{\mathrm{ref}} - X^{\mathrm{res}}) + s^2 X_f^{\mathrm{ref}} \tag{3.9}$$

$$X^{\mathrm{res}} = X_f^{\mathrm{ref}} = \frac{1}{M_f s^2}\left(F^{\mathrm{cmd}} - F^{\mathrm{ext}}\right). \tag{3.10}$$

According to (3.10), the resulting force response is represented by:

$$F^{\mathrm{ext}} = F^{\mathrm{cmd}} - M_f s^2 X^{\mathrm{res}}. \tag{3.11}$$

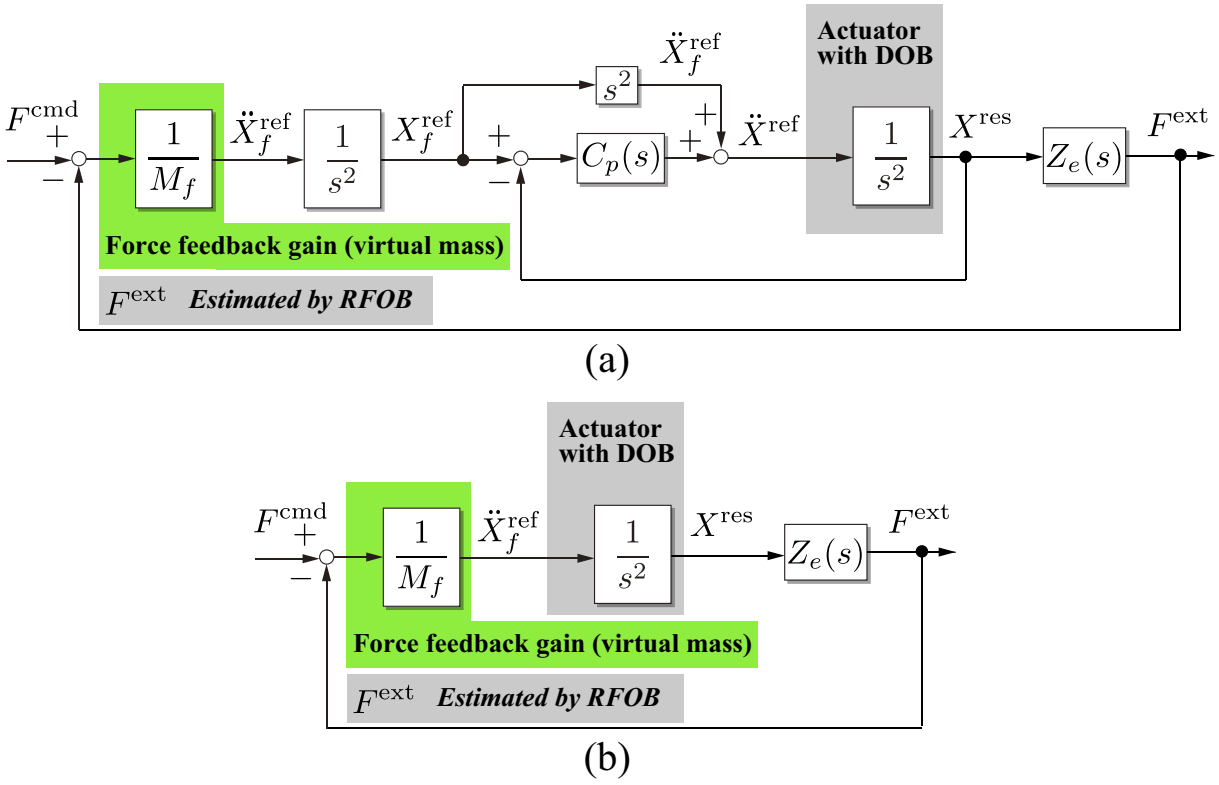

Fig. 3-2: Block diagram of admittance control for contact motions. (a) Admittance control through position control. (b) Equivalent transform.

From this discussion, it is found that the control structure of the admittance control for the contact motions corresponds to the force control system based on impedance control, as shown in Fig. 3-2 (b). This result implies that the performance and stability of the contact motions for the force tracking control have the possibility of improvement by not only adjusting the force control loop itself, but also the inner loop position control system.

3.3 Realization of Contact Motions Based on Concept of Resonance Ratio Control

3.3.1 Definition of Environmental Disturbance

In order to fix the environmental characteristics, an EnvD [96] is introduced. The EnvD $F_e^{\rm dis}$ is derived as follows:

$$F^{\rm ext} = Z_e(s)X^{\rm res} = Z_{en}(s)X^{\rm res} - F_e^{\rm dis} = F_e^{\rm ref} - F_e^{\rm dis} \tag{3.12}$$

$$F_e^{\rm dis} = -\Delta Z_e(s)X^{\rm res} = Z_{en}(s)X^{\rm res} - F^{\rm ext}. \tag{3.13}$$

The EnvD represents a disturbance force which is generated by variations of the environmental impedance $\Delta Z_e(s)$ from the nominal impedance $Z_{en}(s)$. There are some researches regarding the fixing of environments (e.g, reference [73]). In contrast to the conventional researches, however, the definition of EnvD in this research does not require the second-order time derivative of the force response, which would cause a high-level noise effect, and the nominal mass of the motor. This chapter assumes that the nominal environmental impedance consists of a stiffness of $Z_{en}(s) = K_{en}$.

3.3.2 Force Tracking Control Systems as Two-Mass Resonant System

The block diagrams of the force tracking control systems (Figs. 3-1 and 3-2) are transformed to those shown in Fig. 3-3 if the DOB and RFOB work ideally. Fig. 3-3 (a) represents an equivalent transformation of the force tracking control system based on impedance control. In Fig. 3-3 (a), $X_v^{\rm res}$ represents the virtual position response, which excludes $X_f^{\rm res}$ from the actual position response of $X^{\rm res}$. $\ddot{X}^{\rm ref}$ represents an acceleration reference. In the case of the typical (ideal) force tracking control system, an equivalent torsional force feedback gain (K_r in the figure) is set to zero. The transfer functions with regard to the position and force responses are described as follows:

$$X_v^{\rm res} = \frac{s^2 + \frac{K_{en}}{M_f}}{s^2 + \frac{K_{en}}{M_f}(1 + K_r M_f)} \frac{1}{s^2} \frac{1}{M_f} F^{\rm cmd} \tag{3.14}$$

$$X_f^{\rm res} = \frac{\frac{K_{en}}{M_f}}{s^2 + \frac{K_{en}}{M_f}} X_v^{\rm res} \tag{3.15}$$

$$F^{\rm ext} = \frac{\frac{K_{en}}{M_f}}{s^2 + \frac{K_{en}}{M_f}(1 + K_r M_f)} F^{\rm cmd}. \tag{3.16}$$

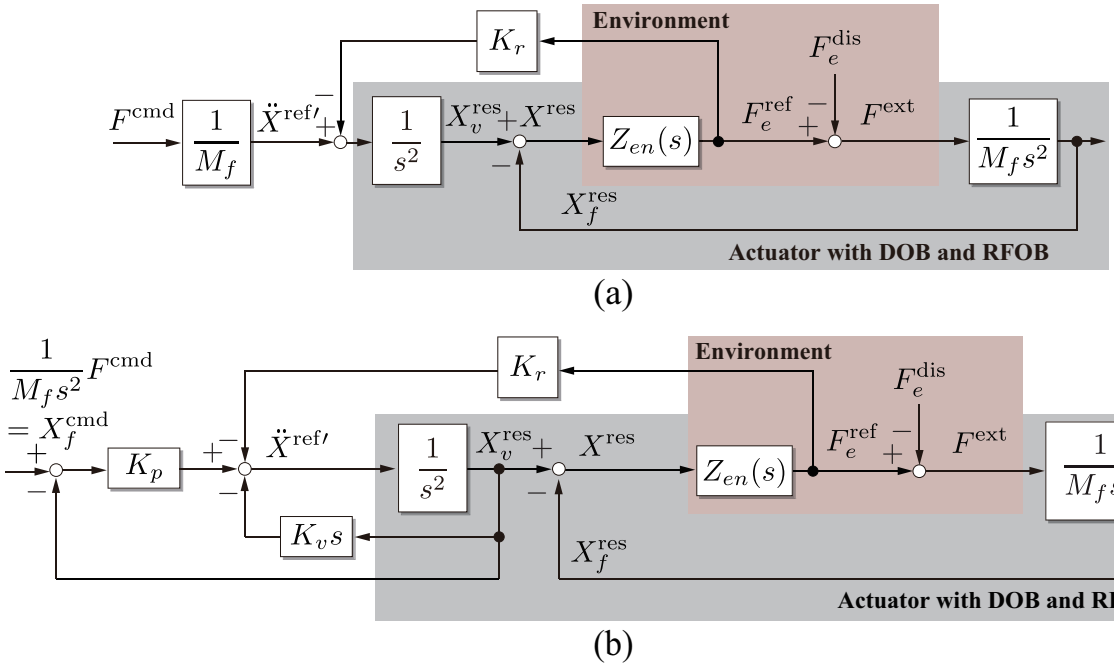

Fig. 3-3: Equivalent transform of force control systems. (a) Impedance control. (b) Admittance control.

On the other hand, the force tracking control based on the admittance control system is also transformed, as shown in Fig. 3-3 (b). The usual case for the force tracking control, K_r in Fig. 3-3 (b), is also set to zero. Here, in order to avoid zeros in the position control system, a velocity feedback is utilized in the minor loop. The transfer functions are derived as follows:

$$X_v^{\mathrm{res}} = \frac{(s^2 + \frac{K_{en}}{M_f})K_p}{\mathrm{Den}(s)} X_f^{\mathrm{cmd}} \tag{3.17}$$

$$X_f^{\mathrm{res}} = \frac{\frac{K_{en}}{M_f}K_p}{\mathrm{Den}(s)} X_f^{\mathrm{cmd}} \tag{3.18}$$

$$F^{\mathrm{ext}} = \frac{\frac{K_{en}}{M_f}K_p}{\mathrm{Den}(s)} F^{\mathrm{cmd}} \tag{3.19}$$

$$\mathrm{Den}(s) = s^4 + K_v s^3 + (\frac{K_{en}}{M_f} + K_r K_{en} + K_p)s^2 + \frac{K_{en}}{M_f}K_v s + \frac{K_{en}}{M_f}K_p. \tag{3.20}$$

These forms of the force tracking control systems correspond to the two-mass resonant system with an acceleration feedforward, and a position control system, in the presence of load side disturbance, as shown in Fig. 3-4 (a) and (b), respectively [22, 23]. In Fig. 3-4, K_l, X_t, F_t, and subscripts a and l represent the load side spring coefficient, torsional position, torsional force, actuator side, and load side, respectively. X_a^{res}, X_l^{res}, and F_l^{dis} correspond to X_v^{res}, X_f^{res}, and F_e^{dis}.

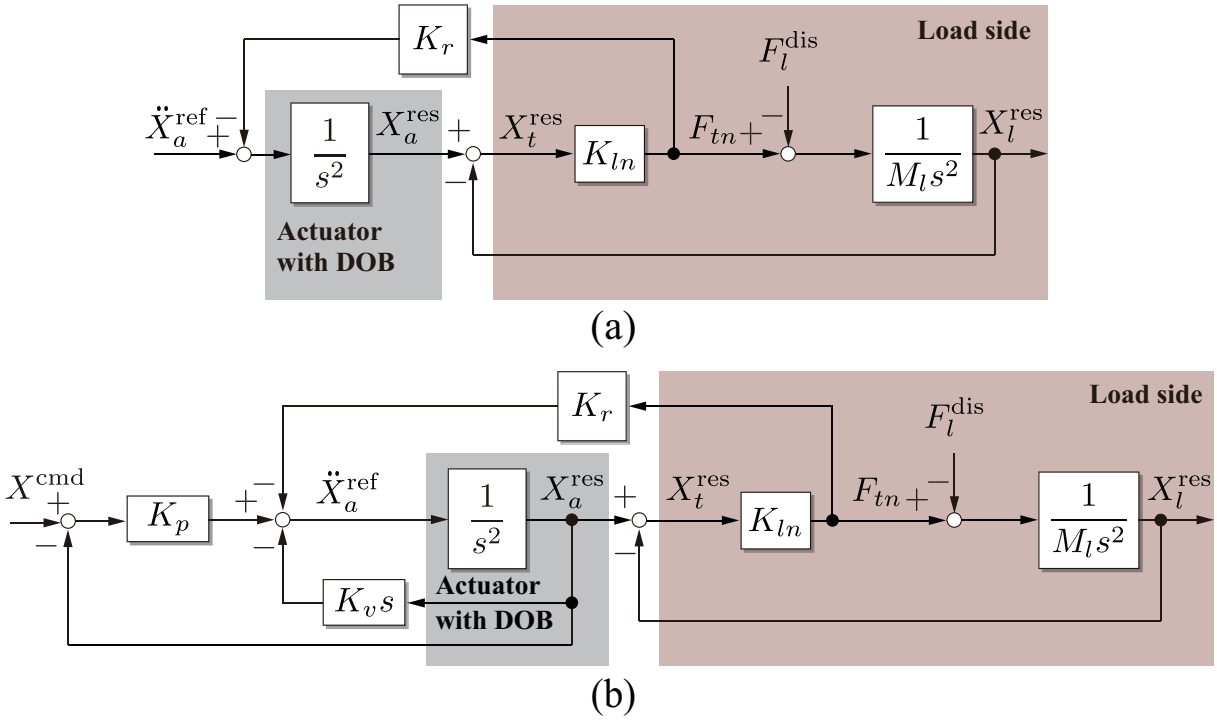

Fig. 3-4: Block diagram of two mass resonance systems. (a) Acceleration feedforward. (b) Position control.

The results of the transformation indicate that the control strategies for the two-mass resonant system are applicable to the contact motions for force tracking control.

3.3.3 Resonance Ratio Control for Contact Motion

Resonance ratio control was developed as an effective vibration suppression control method for the two-mass resonance system [22, 23]. According to the consideration regarding the similarity of the two-mass resonance and force tracking control systems, this chapter proposes a force tracking control system based on the concept of resonance ratio control. An actuator side resonance frequency ω_{an}, environmental resonance frequency ω_{en} and the resonance ratio for the force tracking control r_e are defined as follows:

$$\left[\omega_{an}, \omega_{en}, r_e\right] = \left[\sqrt{\frac{K_{en}}{M_f}(1 + K_r M_f)}, \sqrt{\frac{K_{en}}{M_f}}, \frac{\omega_{an}}{\omega_{en}}\right]. \tag{3.21}$$

The parameters of the force control system ω_{an}, ω_{en} and r_e correspond to ω_m: motor side resonance frequency, ω_l: load side resonance frequency and r_l: resonance ratio of the two-mass resonance system,

respectively. It is known that the parameter gains can be determined to improve control performance and to suppress the vibration of the position control of the two-mass resonance system. If the resonance ratio is set to $\sqrt{5}$ the control system has a quadruple root [22, 23]. In accordance with (3.18) and (3.19), the transfer function of the force command to the force response has the same characteristics as that of the position command to the position response. By considering these characteristics, if the resonance ratio of the contact motion is set as $r_e = \sqrt{5}$, the force tracking control system based on the admittance control has a quadruple root. With respect to the force control system of the two-mass resonance system, the resonance ratio should be set to the other value. If the similarity of the force control and position control of the two-mass resonance system described above is considered, however, the resonance ratio for the control system should be set to $r_e = \sqrt{5}$. In this case, the parameter gains of the admittance control for force tracking control are determined as follows:

$$\begin{bmatrix} K_r & K_v & K_p \end{bmatrix} = \begin{bmatrix} \frac{4}{M_f} & 4\omega_{en} & \omega_{en}^2 \end{bmatrix}. \tag{3.22}$$

3.3.4 EnvD Compensation for The Proposed System

In order to fix the environmental impedance as the nominal impedance $Z_{en}(s) = K_{en}$, the EnvD compensation for the contact motion based on admittance control is considered. The EnvD can be estimated by using the estimated value of the RFOB $\hat{F}^{\mathrm{ext}}$ as follows:

$$\hat{F}_e^{\mathrm{dis}} = g_l^{\mathrm{dis}}(s) F_e^{\mathrm{dis}} = g_l^{\mathrm{dis}}(s) \left(F_e^{\mathrm{ref}} - F^{\mathrm{ext}} \right) \tag{3.23}$$

$$= g_l^{\mathrm{dis}}(s) Z_{en}(s) X^{\mathrm{res}} - \hat{F}^{\mathrm{ext}}. \tag{3.24}$$

By considering the inverse system from the position command to the EnvD, the compensation value of the EnvD is derived as follows:

$$\begin{aligned} X_{\mathrm{cmp}}^p &= \frac{s^2 + K_v s + K_r Z_{en}(s) + K_p}{K_p Z_{en}(s)} \hat{F}_e^{\mathrm{dis}} \\ &\approx \frac{K_r K_{en} + K_p}{K_p K_{en}} \hat{F}_e^{\mathrm{dis}}. \end{aligned} \tag{3.25}$$

By compensating the EnvD through the position control system, the zero order term in (3.25) can be used for the compensation. By attempting to add the compensation value to the acceleration reference, the zero order term cannot be used, and the second order-derivative of EnvD directory must be used instead. This will result in higher level of noise.

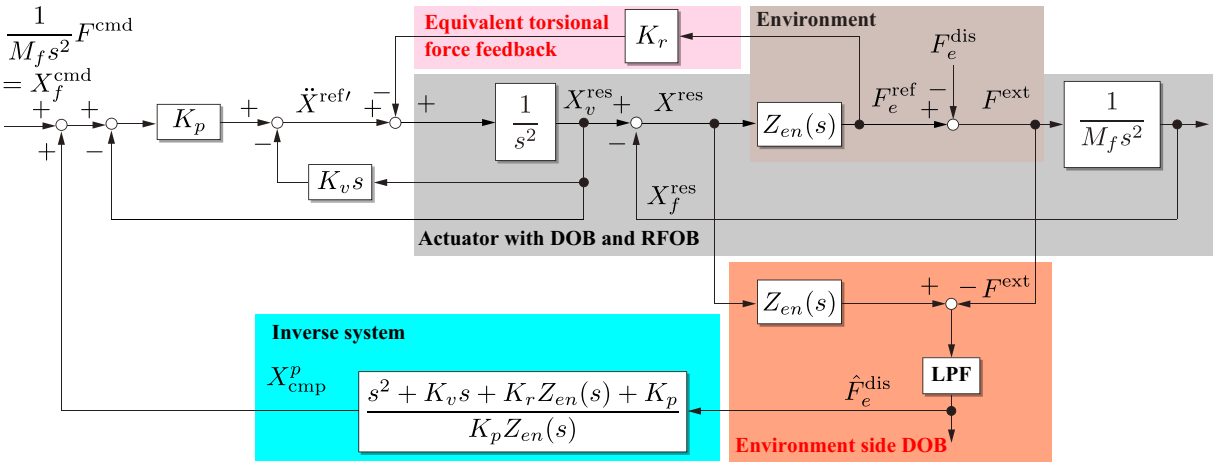

Fig. 3-5: Block diagram of admittance control for contact motion based on equivalent resonance ratio control and environmental disturbance compensation.

3.3.5 Whole Control System of the Proposed Method

The whole block diagram of the proposed method which shows a similarity to the two mass system is shown in Fig. 3-5. The actual control reference of the actuator is given as follows:

$$\begin{aligned}\ddot{X}^{\mathrm{ref}} = K_p(X_f^{\mathrm{cmd}} + X_{\mathrm{cmp}}^p - X_f^{\mathrm{res}} - X^{\mathrm{res}}) \\ +K_v(0 - \dot{X}_f^{\mathrm{res}} - \dot{X}^{\mathrm{res}}) - \ddot{X}_f^{\mathrm{res}} - K_r F_e^{\mathrm{ref}}.\end{aligned} \tag{3.26}$$

The last term on the right side of (3.26) corresponds to the equivalent torsional force feedback in Fig. 3-5. Additionally, a block diagram of the proposed method for actual implementation is shown in Fig. 3-6.

By using the proposed method, the vibration suppression in contact motion is realized even if the environment has no, or insufficient, damping (decay). The response characteristics of contact motion for force tracking control can be determined arbitrarily by the proposed method.

3.3.6 Analysis for Control Stiffness

This section analyzes the control stiffness with respect to both the conventional method and the proposed method. In this case, the effect of EnvD is neglected. The control stiffness is described as follows:

$$\kappa = \frac{\partial F}{\partial X}. \tag{3.27}$$

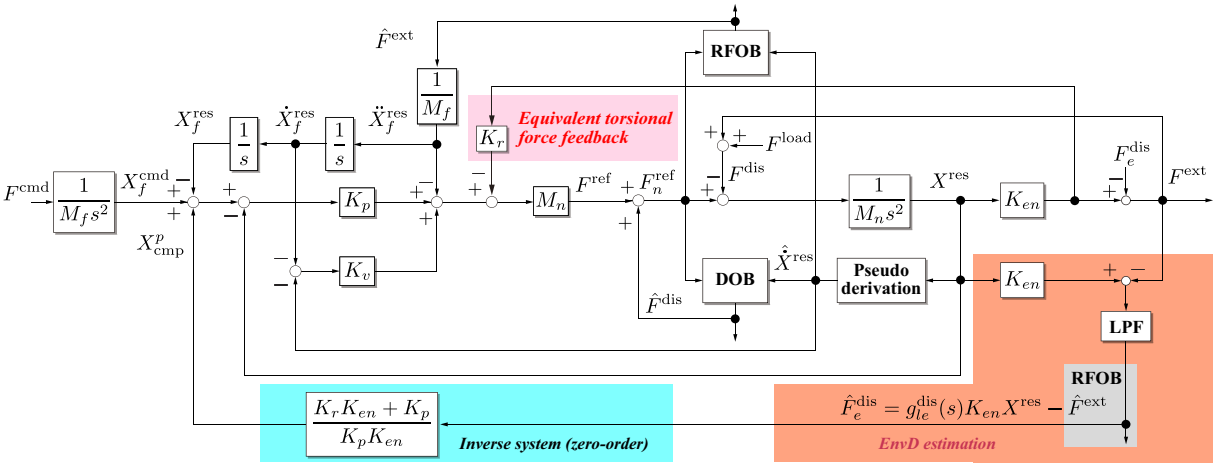

Fig. 3-6: Block diagram of the proposed method for actual implementation.

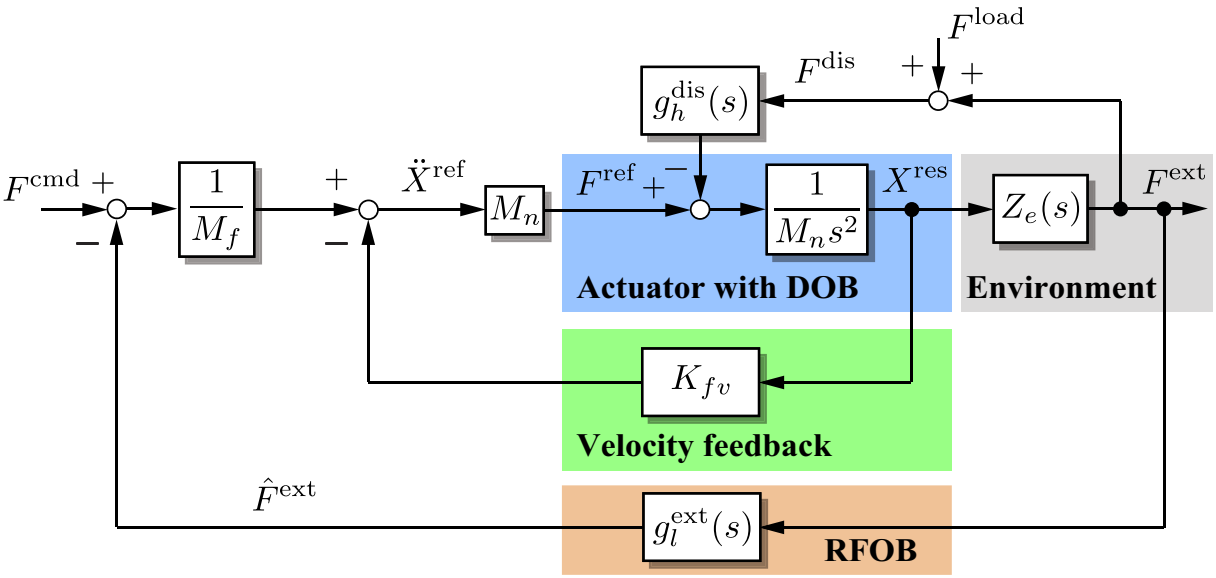

Fig. 3-7: Block diagram of the force control with a velocity damping.

In the case of ideal position control, the control stiffness is infinite. However, in the case of ideal force control, the control stiffness is zero.

As an alternative method to stabilize the force control system, an impedance controller with a velocity damping can be considered. A transfer function related to the control stiffness is derived as follows:

$$\frac{F^{\mathrm{ext}}}{X^{\mathrm{res}}} = -\frac{M_f s^2 + D_f s}{g_l^{\mathrm{ext}}(s) + \frac{M_f}{M_n} g_h^{\mathrm{dis}}(s)} \tag{3.28}$$

$$D_f = M_f K_{fv} \tag{3.29}$$

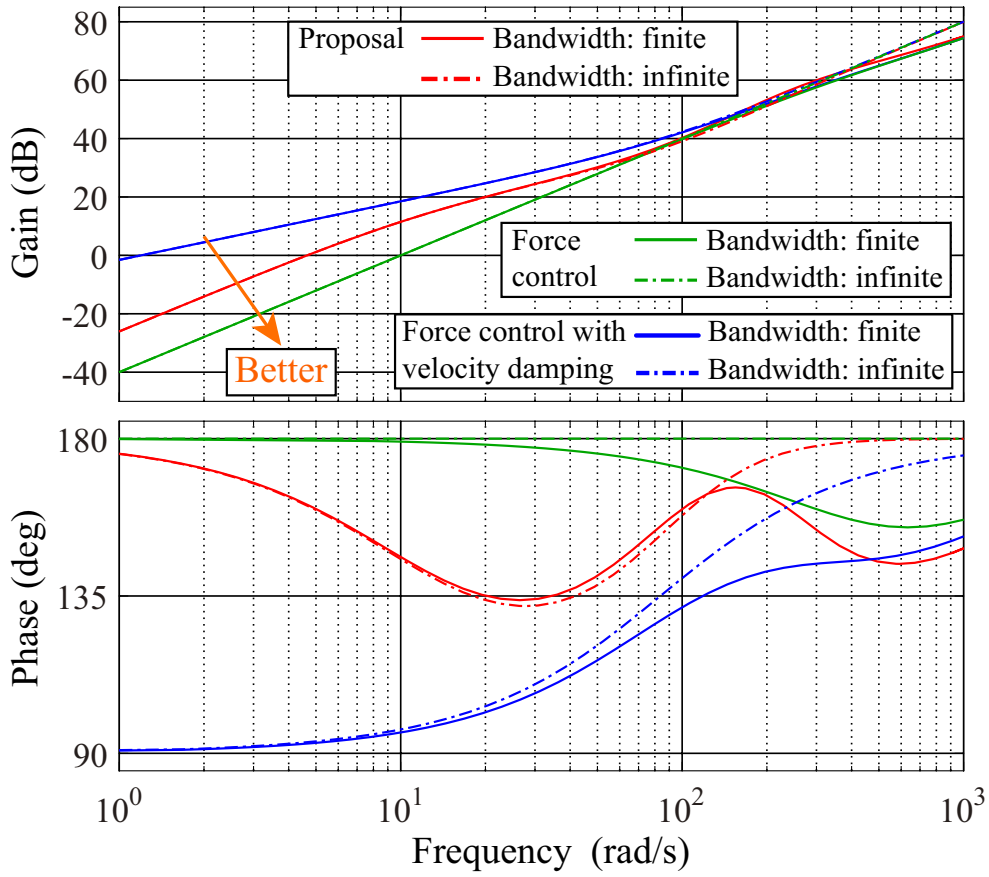

Fig. 3-8: Bode diagram with respect to control stiffness.

where $D_f = M_f K_{fv}$ represents the damping coefficient. The block diagram of the force control system with the velocity damping is shown in Fig. 3-7. If D_f is zero, the system becomes the typical (ideal) force control system.

On the other hand, the transfer function related to the control stiffness of the proposed method is derived as follows:

$$\frac{F^{\text{ext}}}{X^{\text{res}}} = -M_f s^2 \frac{s^2 + K_v s + K_p + K_r K_{en}}{(s^2 + K_v s + K_p) g_l^{\text{ext}}(s) + \frac{M_f}{M_n} g_h^{\text{dis}}(s)}. \tag{3.30}$$

If the bandwidth of the RFOB and DOB are infinite, the transfer function is expressed as

$$\frac{F^{\text{ext}}}{X^{\text{res}}} = -\left(M_f s^2 + \frac{K_r K_{en} M_f s^2}{s^2 + K_v s + K_p} \right). \tag{3.31}$$

The control stiffness of these methods is zero in the steady state in both cases. Fig. 3-8 shows a bode diagram corresponding to the control stiffness with and without considering the filters of DOB and

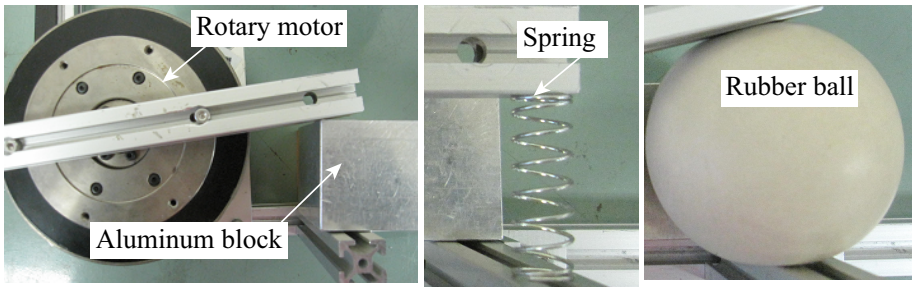

Fig. 3-9: Experimental setup for contact motions to a spring, a rubber ball and an aluminum block.

RFOBs (Bandwidth is 1000 rad/s). It is found that effect of the bandwidth of DOBs and RFOBs are small on the amplitude of the gains. As shown in Fig. 3-8, however, the frequency responses related to the control stiffness are not equal to zero in the higher frequency domain. It should be noted that the proposed method yields better characteristics with respect to the control stiffness than the force control with the velocity damping. This is because the gain of the proposed method is lower than that of the conventional force control with the velocity damping, as shown in Fig. 3-8.

3.4 Experiments for Force Control Systems

3.4.1 Experimental Setup for Contact Motions with Various Environments

To confirm the validity of the proposal, experiments of contact motions for force tracking control were conducted. Fig. 3-9 shows the experimental set up of a single DOF direct-drive rotary motor. As shown in Fig. 3-9, a spring, a rubber ball, and an aluminum block are used as experimental environment. Table 3.1 lists the experimental parameters. Table 3.1 lists the experimental parameters.

3.4.2 Experimental Results of Force Control Systems

Fig. 3-10 shows the experimental results of the spring environment. In the case of proposed (2), the force control gain (virtual inertia) M_f are reduce to half of the other case and nominal stiffness is set to five times larger than the other case As shown in Fig. 3-10 (a), the response of the conventional force control system based on impedance control is oscillatory. Although the oscillation is reduced by the velocity damping, an overshoot is seen. Additionally, the conventional force control with equivalent torsional force feedback (based on Fig. 3-3 (a)) cannot converge with the command torque. On the other hand, the proposed method shows a stable response and the external torque response converges with

Table 3.1: Experimental parameters for contact motions to a spring, a rubber ball and an aluminum block

Parameter	Description	Value
T_s	sampling time	0.1 ms
g^{dis}, g^{ext}	cut-off frequency of DOB and RFOB	1000 rad/s
g_e^{dis}	cut-off frequency of EnvD estimation	1000 rad/s
g_v^{pd}	cut-off frequency of velocity estimation	2500 rad/s
M_f	force control gain (virtual inertia)	0.01 kgm^2
J_n	nominal inertia of actuator	0.004 kgm^2
K_{tn}	nominal torque coefficient	1.18 Nm/A
K_r	equivalent torsional force feedback gain	400
K_e	stiffness of spring	7.15 Nm/rad
K_p	position control gain for spring	715
K_v	velocity feedback gain for spring	107
K_{en}	nominal stiffness of rubber ball	3 Nm/rad
K_p	position control gain for rubber ball	300
K_v	velocity feedback gain for rubber ball	69
K_{en}	nominal stiffness of aluminum block	130 Nm/rad
K_p	position control gain for aluminum block	13000
K_v	velocity feedback gain for aluminum block	456

the command torque. Even though the force control gain (virtual inertia) and nominal stiffness is set larger (proposed (2)), similar revel of the response as the conventional method with velocity damping is obtained Fig. 3-10 (b) shows the effect of the variation of the nominal stiffness from the actual stiffness, as well as the effect of the equivalent torsional force feedback and EnvD compensation. As shown in the figure, a higher nominal stiffness causes an overshoot, whereas a lower nominal stiffness results in a stable but slow response. Although there is an overshoot, the proposed method with the higher nominal stiffness can achieve a more stable response than the conventional method, as shown in the figure. If the force control gain (virtual mass) M_f of the conventional method is reduced, a more stable response than in the case of the higher gain can also be achieved. However, the control stiffness is degraded. On the other hand, it is found that the response becomes oscillatory and the convergence becomes slower if the equivalent torsional torque feedback and EnvD compensation are not implemented. Fig. 3-11 shows the experimental results with respect to rubber ball and aluminum block. In the case of proposed (2), the force control gain (virtual inertia) M_f is multiplied by 0.3. As shown in Fig. 3-11 (a), the

proposed method achieves a stable response in the case of the rubber ball, although the responses of the conventional methods vibrate in the transient phase. As indicated by Fig. 3-11 (b), the conventional method (impedance control based method) generates an overshoot, however the conventional method with velocity damping and the proposed method show similar stable responses.

As shown in Fig. 3-12, however, the proposed method achieves a lower level of operating force in the free motion compared to the conventional method with velocity damping. From the view point of force tracking control, Fig. 3-12 (a) represents the conventional method with velocity damping deteriorates the disturbance response. Additionally, the operating force of the proposed method is at the same level as the conventional (normal) force control system. This indicates that the control stiffness of the proposed method is close to the ideal case. From these results, the validity of the proposed method can be confirmed.

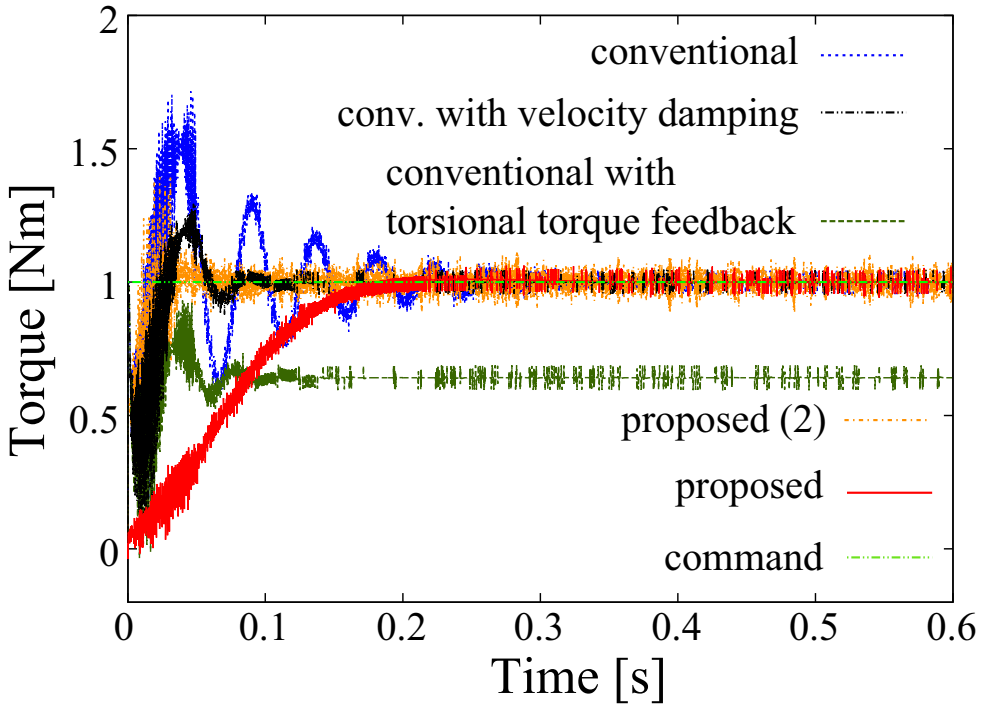

(a)

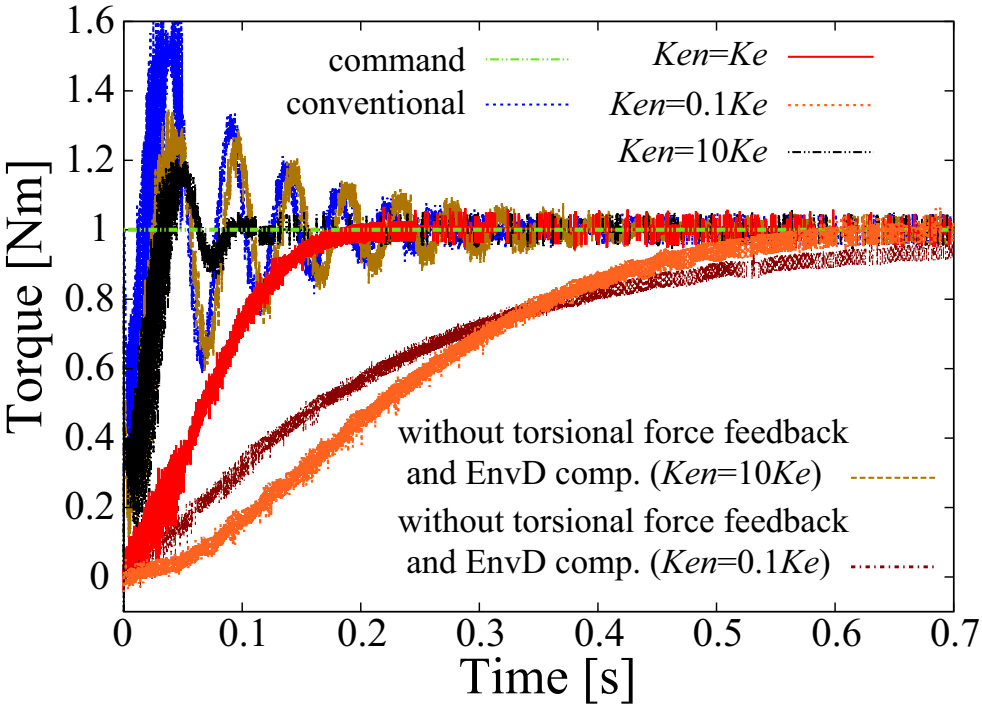

(b)

Fig. 3-10: Experimental results of the spring. (a) Comparison between the conventional methods and the proposed method. (b) Comparison of the variation of nominal stiffness.

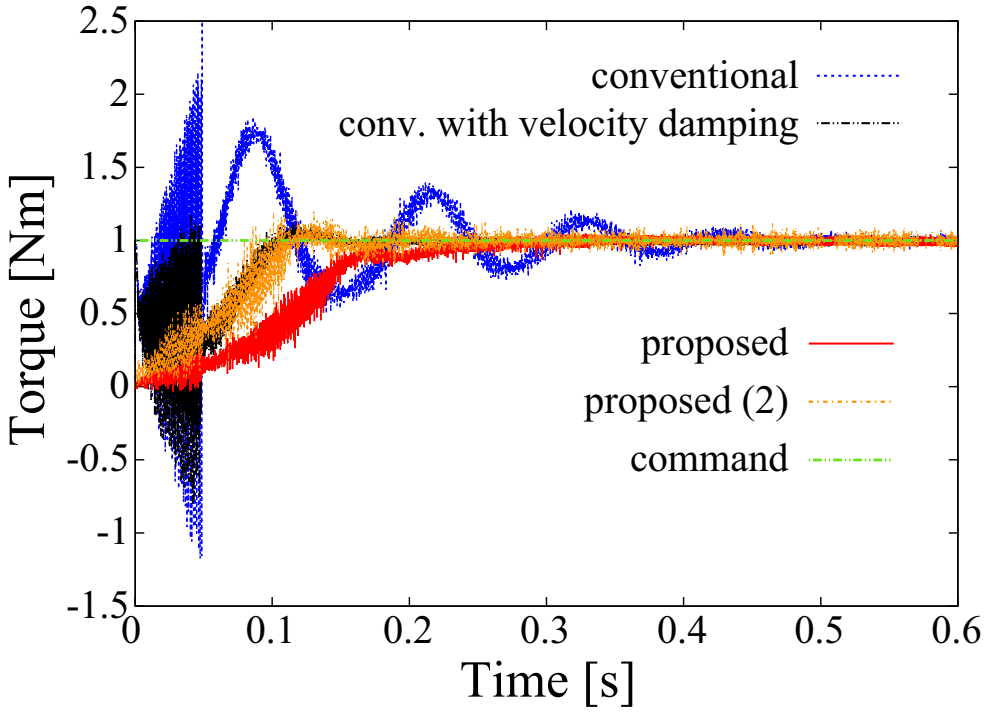

(a)

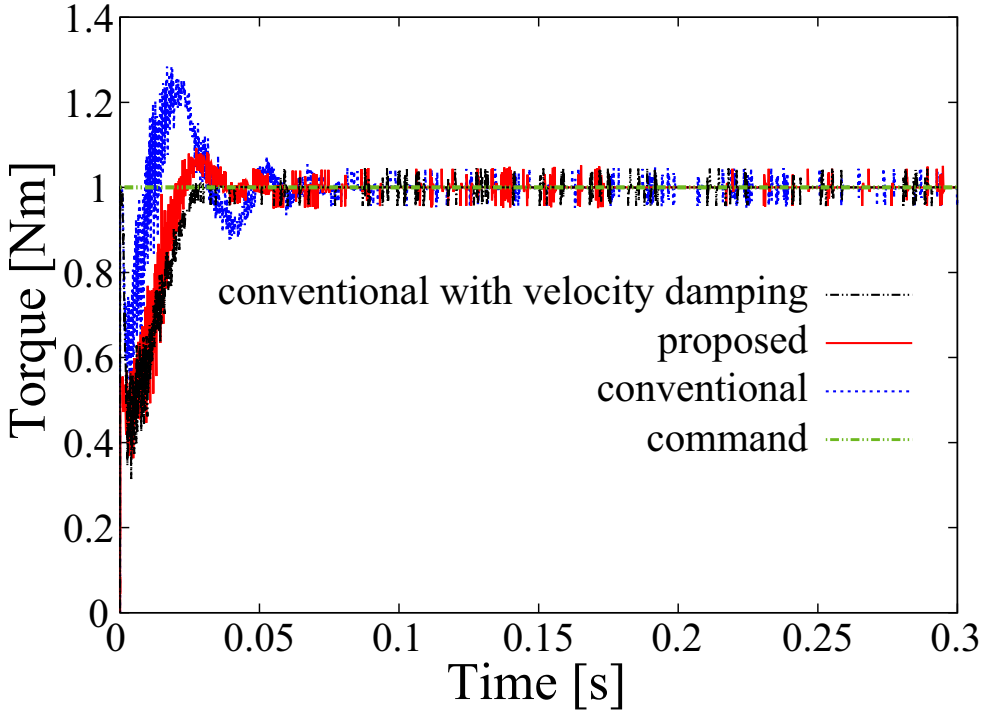

(b)

Fig. 3-11: Experimental results for a rubber ball and an aluminum block. (a) a rubber ball. (b) an aluminum block.

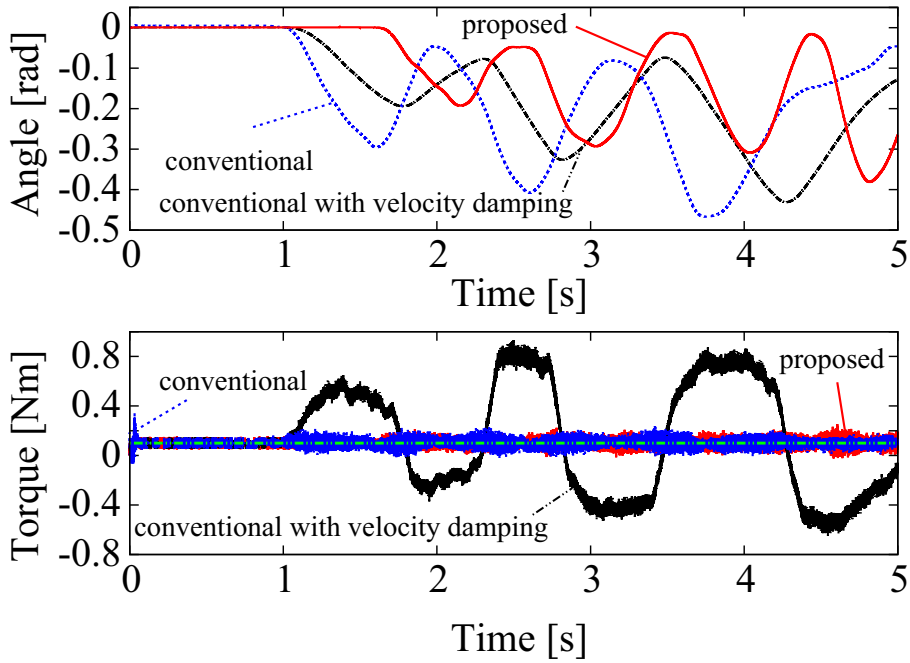

(a)

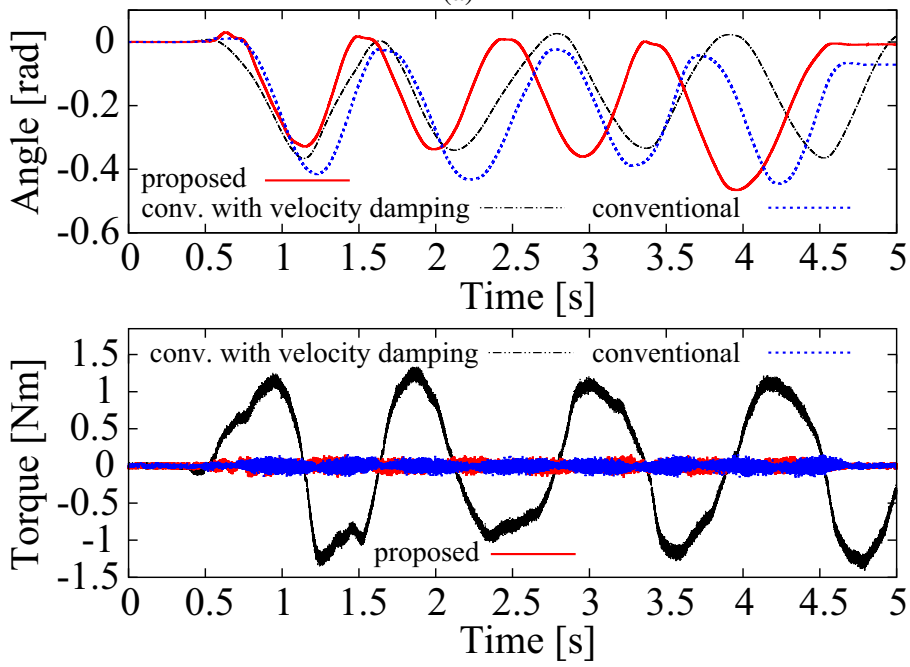

(b)

Fig. 3-12: Experimental results with pushing motions performed by a human operator to validate control stiffness (equivalent parameters to Fig. 3-11 (b)). (a) Torque command is set to 0.2 Nm. (b) Torque command is set to 0.0 Nm (free motions).

3.5 Estimation and Compensation for High-Order Environmental Disturbance and Its Time derivatives Based on Kalman Filter

In the last part, admittance control based force control with environmental disturbance compensation is introduced which corresponding to load disturbance in a two mass resonance system.

For the compensation of the environmental disturbance, only the zero order term inverse system is considered in order to avoid enlarging noise effect by implementing time derivatives of estimated environmental disturbance. The higher-order terms of timed derivatives are usually neglected also for the compensation of load disturbance in the two mass resonance system.

This chapter considers utilizing the higher-order time derivative terms in compensation for environmental disturbance. The high-order environmental disturbance is estimated by a Kalman filter including higher-order time derivative of environmental disturbance. The estimated variable of the proposed Kalman filter based high-order environmental disturbance observer can be utilized for the compensation without enlarging noise effect in time derivatives

3.6 Analysis for EnvD Compensation with Considering Higher-Order Derivative Term of EnvD

In the last part, the inverse system for constructing the EnvD compensator is approximated by a zero-order system in order to avoid enhancing noise effects as shown in (3.25). However, the actual system is a second order system. Therefore, this part realizes the inverse system by using pseudo differentiation for the time derivatives of the EnvD. Additionally, the effect of the inverse system and the EnvD Observer are analysed.

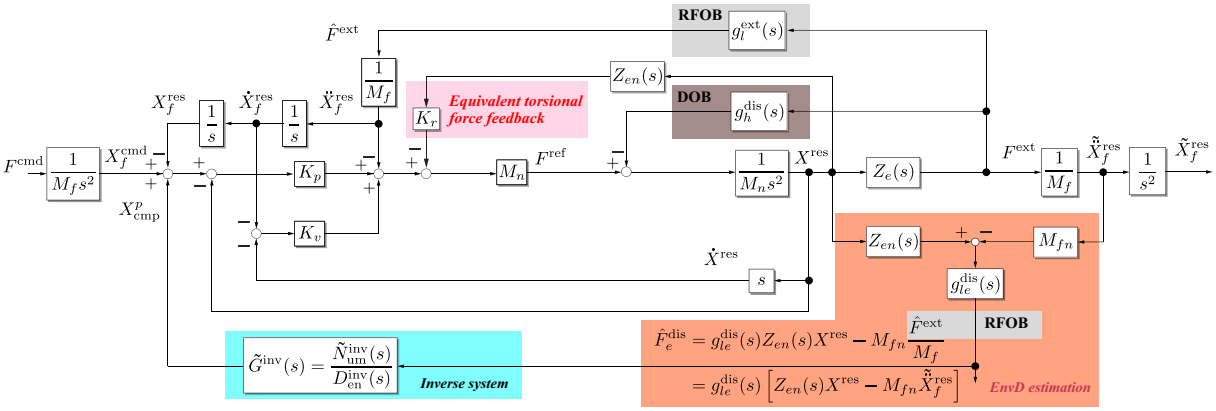

Fig. 3-13: Block diagram of the proposed method with EnvD compensation.

3.6.1 Modeling with Inverse System

The compensation value is obtained as follows:

$$X^{p}_{\mathrm{cmp}} = \frac{s^2 + K_v s + K_r Z_{en}(s) + K_p}{K_p Z_{en}(s)} \hat{F}^{\mathrm{dis}}_{e} = G^{\mathrm{inv}}(s)\hat{F}^{\mathrm{dis}}_{e} = \frac{N^{\mathrm{inv}}_{\mathrm{num}}(s)}{D^{\mathrm{inv}}_{\mathrm{en}}(s)} \hat{F}^{\mathrm{dis}}_{e} \tag{3.32}$$

$$\approx \frac{g^{\mathrm{pd}}_{l2\mathrm{nd}}(s)s^2 + K_v g^{\mathrm{pd}}_{l}(s)s + K_r Z_{en}(s) + K_p}{K_p Z_{en}(s)} \hat{F}^{\mathrm{dis}}_{e}$$

$$= \tilde{G}^{\mathrm{inv}}(s)\hat{F}^{\mathrm{dis}}_{e} = \frac{\tilde{N}^{\mathrm{inv}}_{\mathrm{num}}(s)}{\tilde{D}^{\mathrm{inv}}_{\mathrm{en}}(s)} \hat{F}^{\mathrm{dis}}_{e} \tag{3.33}$$

$$G^{\mathrm{inv}}(s) = \frac{N^{\mathrm{inv}}_{\mathrm{num}}(s)}{D^{\mathrm{inv}}_{\mathrm{en}}(s)} \tag{3.34}$$

$$\tilde{G}^{\mathrm{inv}}(s) = \frac{\tilde{N}^{\mathrm{inv}}_{\mathrm{num}}(s)}{\tilde{D}^{\mathrm{inv}}_{\mathrm{en}}(s)} \tag{3.35}$$

where $g^{\mathrm{pd}}_{l2\mathrm{nd}}(s)$, $g^{\mathrm{pd}}_{l}(s)$, $G^{\mathrm{inv}}(s)$, $N^{\mathrm{inv}}_{\mathrm{num}}(s)$, $D^{\mathrm{inv}}_{\mathrm{en}}(s)$ $\tilde{\bullet}$ represent a 2nd-order low-pass filter, a 1st-order low-pass filter, a transfer function of the inverse system, a numerator of the inverse system, denominator of the inverse system and transfer functions of the inverse system with pseudo-differentiation, respectively. The block diagram for the analytical model with the compensation value by (3.33) is shown in Fig. 3-13. The block diagram is equivalently transformed as shown in Fig. 3-14. As for the EnvD estimation in Fig. 3-14, the nominal force control gain $\frac{1}{M_{fn}}$ is inserted as a virtual nominal value. If the bandwidth of the pseudo differentiation in the inverse system is infinite, from Fig. 3-13, the transfer function from F^{cmd} to F^{ext} with the variation of the environmental impedance from the nominal value is described as

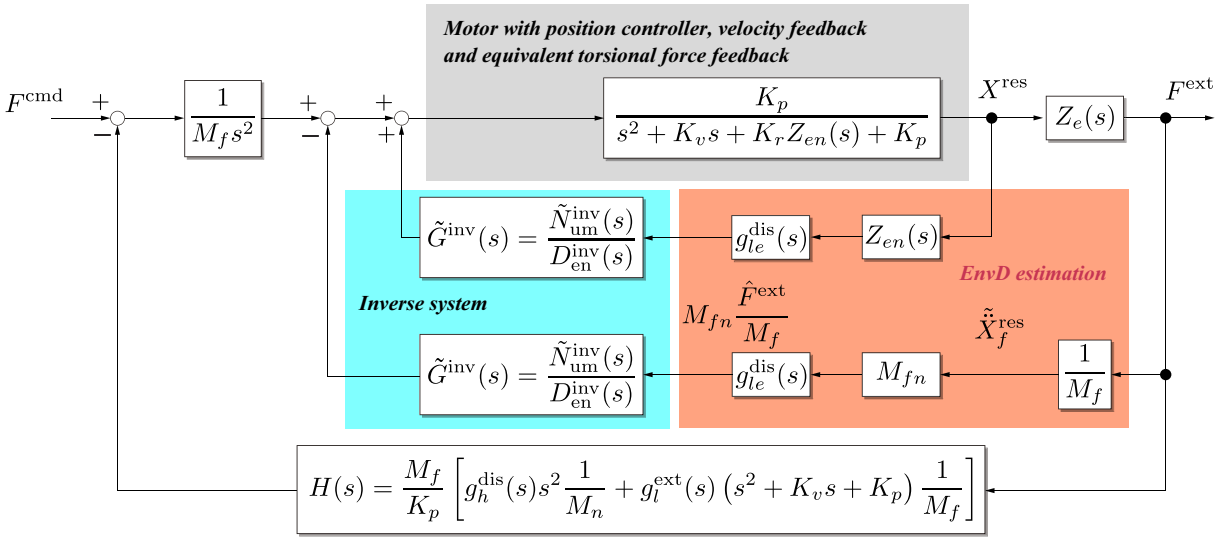

Fig. 3-14: Equivalent transform of Fig. 3-13.

follows:

$$\frac{F^{\mathrm{ext}}}{F^{\mathrm{cmd}}}=\frac{\frac{Z_e(s)}{M_f}K_p}{D_{\mathrm{en}}(s)+K_p\left(Z_e(s)-Z_{en}(s)\right)G^{\mathrm{inv}}(s)g^{\mathrm{dis}}_{le}(s)s^2} \tag{3.36}$$

$$=\frac{N_{\mathrm{um}}(s)}{D_{\mathrm{en}}(s)+K_pM_{fn}\left(\frac{Z_e(s)}{M_f}-\frac{Z_{en}(s)}{M_{fn}}\right)G^{\mathrm{inv}}(s)g^{\mathrm{dis}}_{le}(s)s^2} \tag{3.37}$$

$$\begin{aligned}D_{\mathrm{en}}(s)=&s^4+K_vs^3+\left(K_rZ_{en}(s)+K_p+\frac{Z_e(s)}{M_f}g^{\mathrm{ext}}_l(s)+\frac{Z_e(s)}{M}g^{\mathrm{dis}}_h(s)\right)s^2\\&+\frac{Z_e(s)}{M_f}K_vg^{\mathrm{ext}}_l(s)s+\frac{Z_e(s)}{M_f}K_pg^{\mathrm{ext}}_l(s)\end{aligned} \tag{3.38}$$

where $g^{\mathrm{dis}}_{le}(s)$ and $g^{\mathrm{dis}}_h(s)$ represent a low-pass filter for EnvD estimation and equivalent high pass filter for disturbance suppression, respectively. If the bandwidth of the EnvD estimation assumed to be infinite, ($g^{\mathrm{dis}}_{le}\to\infty$ ($g^{\mathrm{dis}}_{le}(s)\to 1$)), the transfer function is rewritten as

$$\frac{F^{\mathrm{ext}}}{F^{\mathrm{cmd}}}=\frac{\frac{Z_{en}(s)}{Z_e(s)}\frac{Z_e(s)}{M_f}K_p}{\frac{Z_{en}(s)}{Z_e(s)}\left[D_{\mathrm{en}}(s)+K_p\left(Z_e(s)-Z_{en}(s)\right)G^{\mathrm{inv}}(s)g^{\mathrm{dis}}_{le}(s)s^2\right]} \tag{3.39}$$

where

$$\begin{aligned}\frac{Z_{en}(s)}{Z_e(s)}D_{\mathrm{en}}(s)=&\frac{Z_{en}(s)}{Z_e(s)}\left[s^4+K_vs^3+\left(K_rZ_{en}(s)+K_p\right)s^2\right]+\left(\frac{Z_{en}(s)}{M_f}g^{\mathrm{ext}}_l(s)+\frac{Z_{en}(s)}{M}g^{\mathrm{dis}}_h(s)\right)s^2\\&+\frac{Z_{en}(s)}{M_f}K_vg^{\mathrm{ext}}_l(s)s+\frac{Z_{en}(s)}{M_f}K_pg^{\mathrm{ext}}_l(s).\end{aligned} \tag{3.40}$$

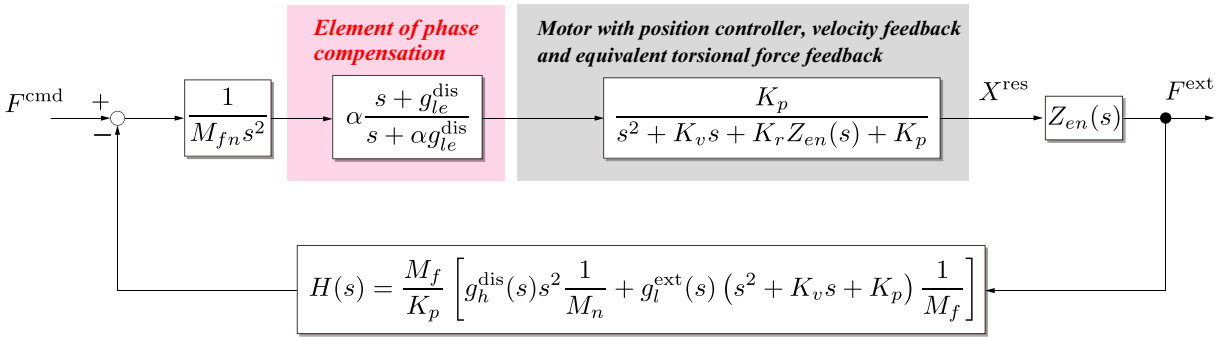

Fig. 3-15: Equivalent transform of Fig. 3-13.

The remained term in (3.39) is expressed as follows:

$$\begin{aligned}&\frac{Z_{en}(s)}{Z_e(s)}\left(K_p\left(Z_e(s)-Z_{en}(s)\right)G^{\mathrm{inv}}(s)g_{le}^{\mathrm{dis}}(s)s^2\right)\\&=\frac{Z_{en}(s)}{Z_e(s)}K_pZ_e(s)\frac{s^4+K_vs^3+\left(K_rZ_{en}(s)+K_p\right)s^2}{K_pZ_{en}(s)}\\&\quad-\frac{Z_{en}(s)}{Z_e(s)}\left[s^4+K_vs^3+\left(K_rZ_{en}(s)+K_p\right)s^2\right].\end{aligned}\tag{3.41}$$

As shown in (3.43), $Z_e(s)$ and M_f are replaced by $Z_{en}(s)$ and M_{fn} if the bandwidth of the EnvD compensation is sufficiently high.

$$\frac{F^{\mathrm{ext}}}{F^{\mathrm{cmd}}}=\frac{N_{\mathrm{umn}}(s)}{D_{\mathrm{enn}}(s)}\tag{3.42}$$

$$\begin{aligned}D_{\mathrm{enn}}(s)=s^4+K_vs^3+&\left(K_rZ_{en}(s)+K_p+\frac{Z_{en}(s)}{M_{fn}}g_l^{\mathrm{ext}}(s)+\frac{Z_{en}(s)}{M}g_h^{\mathrm{dis}}(s)\right)s^2\\&+\frac{Z_{en}(s)}{M_{fn}}K_vg_l^{\mathrm{ext}}(s)+\frac{Z_{en}(s)}{M_{fn}}K_pg_l^{\mathrm{ext}}(s)\end{aligned}\tag{3.43}$$

Therefore, the system becomes nominal system by using the EnvD compensation in the ideal case ($g_{le}^{\mathrm{dis}}(s)\to 1$) is confirmed.

3.6.2 Effect of Variations of Environmental Impedance from Nominal Values

In the Case That Bandwidth of Pseudo Differentiation in Inverse System Is Infinite

If the bandwidth of the pseudo differentiation in the inverse system is infinite, the block diagram shown in Fig. 3-14 is transformed to Fig. 3-15. In the figure, the variation of the environmental impedance (stiffness) and virtual mass from nominal values are expressed as follows:

$$\frac{M_{fn}}{Z_{en}(s)}\frac{K_e}{M_f}=\frac{M_{fn}}{K_{en}(s)}\frac{K_e}{M_f}=\alpha.\tag{3.44}$$

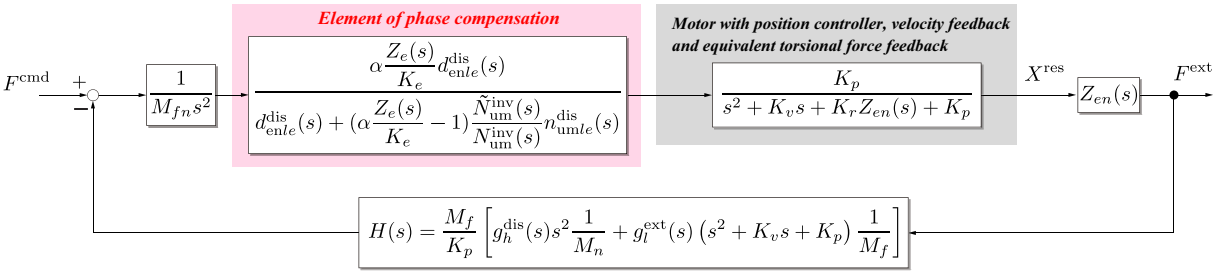

Fig. 3-16: Equivalent transform of Fig. 3-13 with the finite bandwidth of the pseudo differentiation in the inverse system.

In the figure, we considered stiffness only as a nominal environmental impedance. As shown in Fig. 3-15, a element of phase compensator $G^{\mathrm{ph}}(s)$ is appeared by considering α as follows:

$$G^{\mathrm{ph}}(s) = \alpha\frac{s+g^{\mathrm{dis}}_{le}}{s+\alpha g^{\mathrm{dis}}_{le}}. \tag{3.45}$$

If the nominal environmental impedance $Z_{en}(s) = K_{en}$ is smaller than the actual stiffness and nominal force control gain M_{fn} is larger than M_f, the element of phase compensator becomes a phase lead compensator. On the other hand, if the nominal environmental impedance $Z_{en}(s)$ is larger than the actual stiffness and nominal force control gain M_{fn} is smaller than M_f, the element of phase compensator becomes a phase lag compensator. This relationship is similar to the relationship between a nominal torque coefficient K_t and a nominal mass in a DOB [8].

In the Case That Bandwidth of Pseudo Differentiation in Inverse System Is Finite

If the bandwidth of the pseudo differentiation in the inverse system is finite, Fig. 3-14 is transformed to Fig. 3-16. In Fig. 3-16, not only the environmental stiffness but also environmental damper and mass are considered. In this case, the element of the phase compensator $\tilde{G}^{\mathrm{ph}}(s)$ is also appeared as follows:

$$\tilde{G}^{\mathrm{ph}}(s) = \frac{\alpha\frac{Z_e(s)}{K_e}d^{\mathrm{dis}}_{\mathrm{enle}}(s)}{d^{\mathrm{dis}}_{\mathrm{enle}}(s)+(\alpha\frac{Z_e(s)}{K_e}-1)\frac{\tilde{N}^{\mathrm{inv}}_{\mathrm{um}}(s)}{N^{\mathrm{inv}}_{\mathrm{um}}(s)}n^{\mathrm{dis}}_{\mathrm{umle}}(s)} \tag{3.46}$$

where $n^{\mathrm{dis}}_{\mathrm{umle}}(s)$ and $d^{\mathrm{dis}}_{\mathrm{enle}}(s)$ represent a numerator and a denominator of the estimation for EnvD. Fig. 3-17 shows a bode diagram of $\tilde{G}^{\mathrm{ph}}(s)$ with the variation of $g^{\mathrm{pd}}_{l2\mathrm{nd}}$ and g^{pd}_{l}. In this figure, the structure of

the EnvD is a 2nd-order disturbance observer. The estimated value is expressed as

$$\hat{F}_e^{\mathrm{dis}} = g_{le}^{\mathrm{dis}} F_e^{\mathrm{dis}} = \frac{3{g_{le}^{\mathrm{dis}}}s^2 + 3{g_{le}^{\mathrm{dis}}}^2 s + {g_{le}^{\mathrm{dis}}}^3}{s^3 + 3{g_{le}^{\mathrm{dis}}}s^2 + 3{g_{le}^{\mathrm{dis}}}^2 s + {g_{le}^{\mathrm{dis}}}^3} F_e^{\mathrm{dis}} \tag{3.47}$$

$$g_{le}^{\mathrm{dis}}(s) = \frac{n_{\mathrm{uml}e}^{\mathrm{dis}}(s)}{d_{\mathrm{en}le}^{\mathrm{dis}}(s)} = \frac{3{g_{le}^{\mathrm{dis}}}s^2 + 3{g_{le}^{\mathrm{dis}}}^2 s + {g_{le}^{\mathrm{dis}}}^3}{s^3 + 3{g_{le}^{\mathrm{dis}}}s^2 + 3{g_{le}^{\mathrm{dis}}}^2 s + {g_{le}^{\mathrm{dis}}}^3} \tag{3.48}$$

$$\tag{3.49}$$

where $n_{\mathrm{uml}e}^{\mathrm{dis}}(s)$ and $d_{\mathrm{en}le}^{\mathrm{dis}}(s)$ represent a numerator and denominate of $g_{le}^{\mathrm{dis}}(s)$, as follows:

$$n_{\mathrm{uml}e}^{\mathrm{dis}}(s) = 3{g_{le}^{\mathrm{dis}}}s^2 + 3{g_{le}^{\mathrm{dis}}}^2 s + {g_{le}^{\mathrm{dis}}}^3 \tag{3.50}$$

$$d_{\mathrm{en}le}^{\mathrm{dis}}(s) = s^3 + 3{g_{le}^{\mathrm{dis}}}s^2 + 3{g_{le}^{\mathrm{dis}}}^2 s + {g_{le}^{\mathrm{dis}}}^3. \tag{3.51}$$

The bandwidths of the 2nd-order DOBs for EnvD compensation are set to 876 rad/s. In Fig. 3-17, the bode diagram without higher-order term and bode diagram of following three cases are plotted. In this figure, α is varied from 0.4 to 2.0.

- case 1: $K_e = 10$, $g_{l2\mathrm{nd}}^{\mathrm{pd}} = 100$ rad/s and $g_l^{\mathrm{pd}} = 50$ rad/s.
- case 2: $K_e = 10$, $g_{l2\mathrm{nd}}^{\mathrm{pd}} = 409$ rad/s and $g_l^{\mathrm{pd}} = 199$ rad/s.
- case 2: $K_e = 10$, $g_{l2\mathrm{nd}}^{\mathrm{pd}} = 2000$ rad/s and $g_l^{\mathrm{pd}} = 1000$ rad/s.

As shown in the figure, the effect of phase lead/lag compensation can be confirmed. Additionally, in accordance with the increasing the bandwidth of the pseudo differentiation, the frequency domain for the phase compensation is also increased.

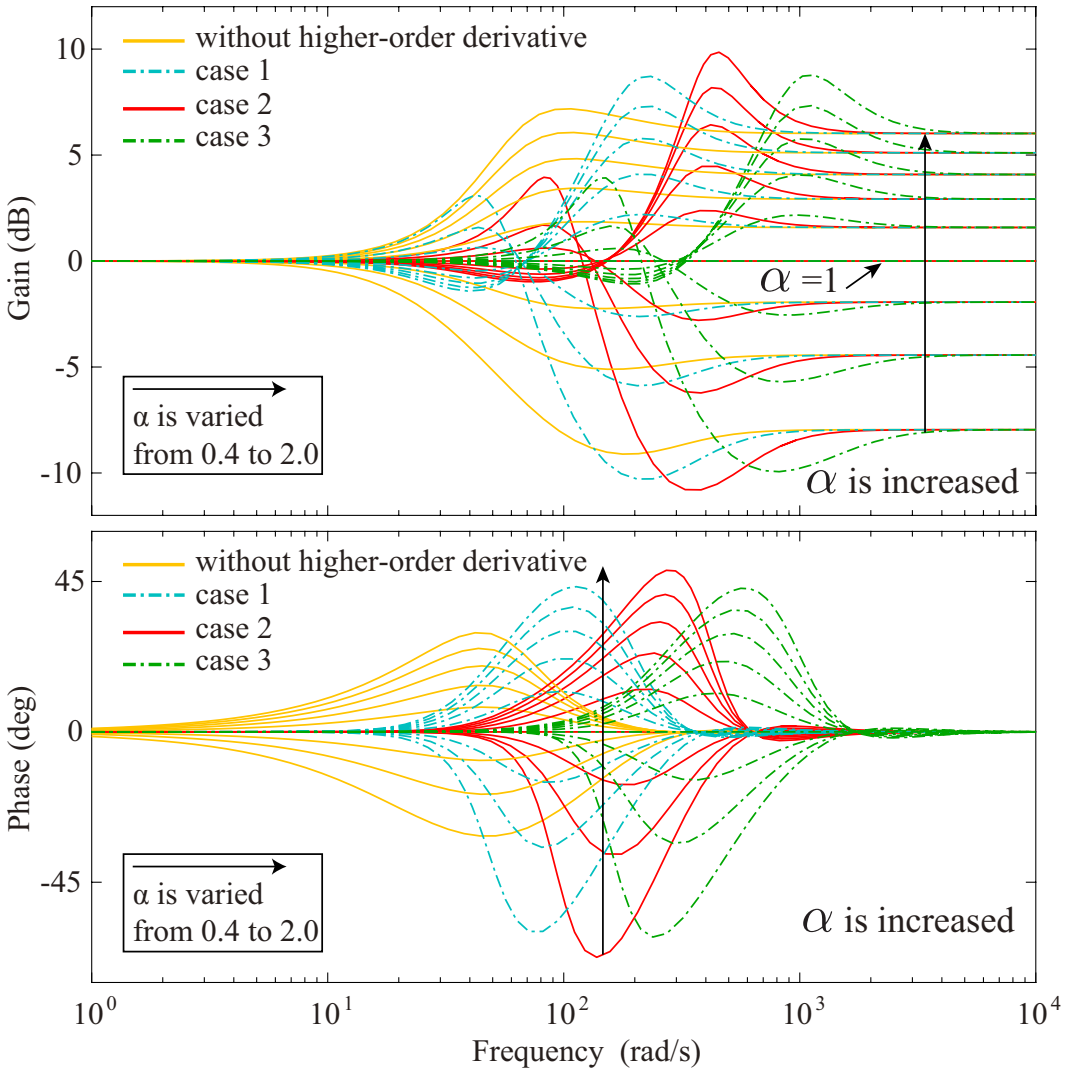

Fig. 3-17: Bode diagram of $\tilde{G}^{\mathrm{ph}}(s)$ with the variation of $g_{l2\mathrm{nd}}^{\mathrm{pd}}$ and g_{l}^{pd} with the variation of α from 0.4 to 2.0.

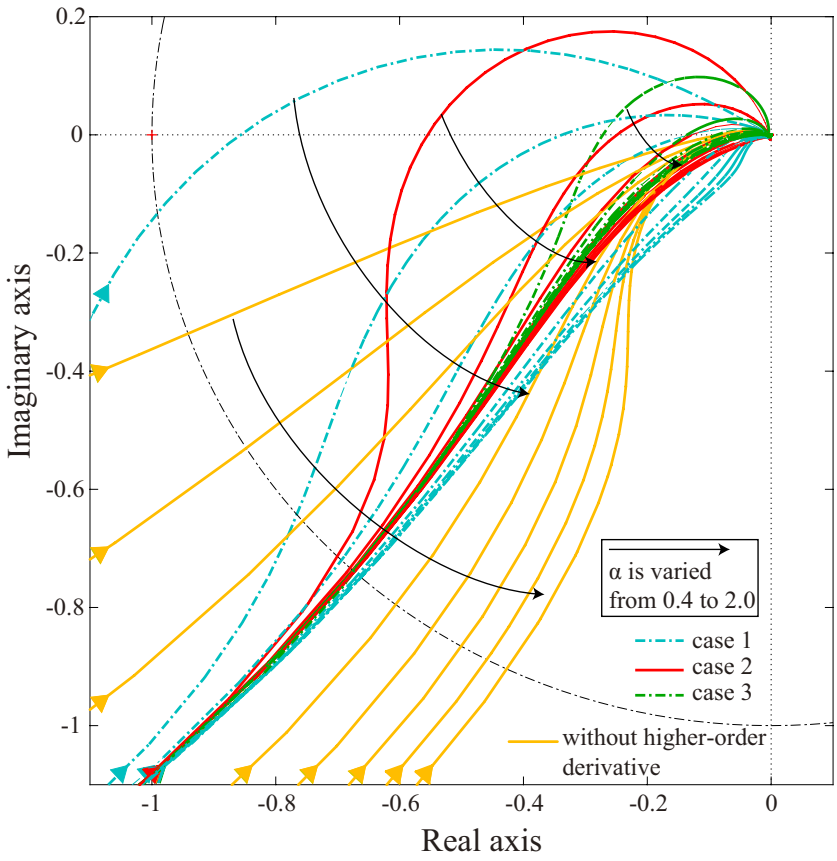

Fig. 3-18: Nyquist plot of open loop transfer functions for cases 1 to 3 and the case without higher-order term with the variation of α from 0.4 to 2.0.

3.6.3 Stability Analysis

This part analyzes the stability of the proposed system with the inverse system. The open loop and the closed loop transfer functions for the analysis are derived from Fig. 3-16. In the analysis, the system is assumed to be discretized by zero-order hold. The bandwidth of the DOBs and RFOBs are set to 1000 rad/s.

Effect of Parameter Variations

Fig. 3-18 shows the Nyquist plot for the open loop transfer function without higher-order term and cases 1, 2 and 3. As shown in the figure, the stability is improved in accordance with the α and bandwidth of the pseudo differentiation are increased. However, it should be noted that if the bandwidth of the pseudo differentiation is not sufficiently high, the stability of the higher-order differentiation inferior to

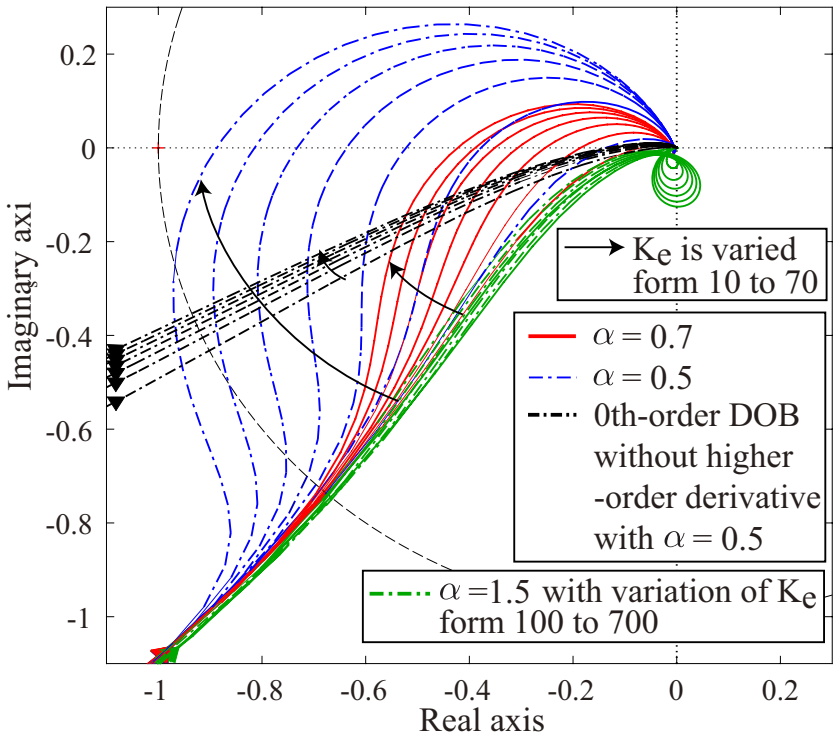

Fig. 3-19: Nyquist plot with the variation of environmental stiffness K_e from 10 to 70 and 100 to 700.

the system without the higher-order differentiation in the case with the phase lag element.

Therefore, in the case where the sufficient differentiation is not achieved, the inverse system should be set to the 0th-order. Fig. 3-19 shows the Nyquist plot with the variation of environmental stiffness K_e from 10 to 70 and 100 to 700 in case 2 with different α. The figure indicates that the stabilities of the all systems are deteriorated with increasing the environmental stiffness K_e. As shown in the figure, the stability is seriously affected compared to the 0th-order DOB when α is less than 1. On the other hand, if α is larger than 1, the effect of the stiffness variation on stability is smaller than that of case 2. In addition to Fig. 3-18, this figure indicates that the system with the large phase element and insufficient differentiator should employ the 0th-order DOB. Fig. 3-19 shows the Nyquist plot with the variation of environmental damper D_e from 5 to 70 in case 2 with different α. As shown by the figure, compared to the variation of the stiffness, the effect of the variation of damper is small. Fig. 3-19 shows the Nyquist plot with the variation of the environmental mass from 0.001 to 0.007 in case 2 with different α. The variation of environmental mass is most serious compared to the stiffness and damper.

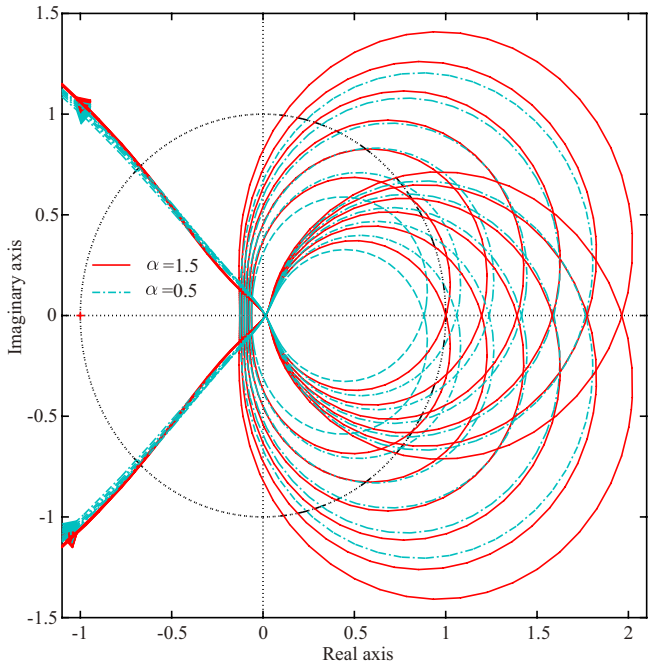

Fig. 3-20: Nyquist plot with the variation of the environmental damper D_e from 5 to 70 (with the condition of case 2).

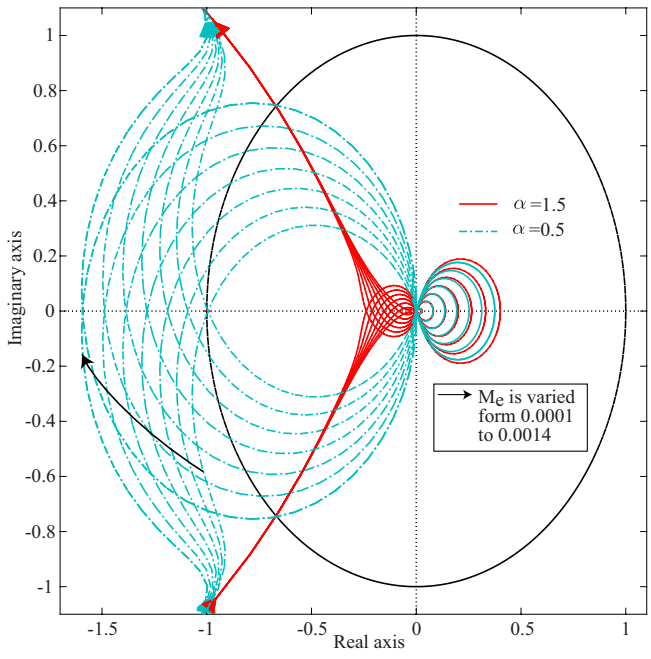

Fig. 3-21: Nyquist plot with the variation of environmental mass M_e from 0.001 to 0.007 (with the condition of case 2).

Effect of Discretization

Fig. 3-22 shows the Nyquist plot with the variation of sampling time in order to confirm the effect of discretization with case 2. The variation is from 0.0001s to 0.06 s. As shown in the figure, the stability is deteriorated in accordance with increasing the sampling time. However, the degree of deterioration with respect to Fig. 3-22 (b) is smaller than (a). Therefore, it is found that the effect on the discretization can be kept lower level if α is larger than 1.

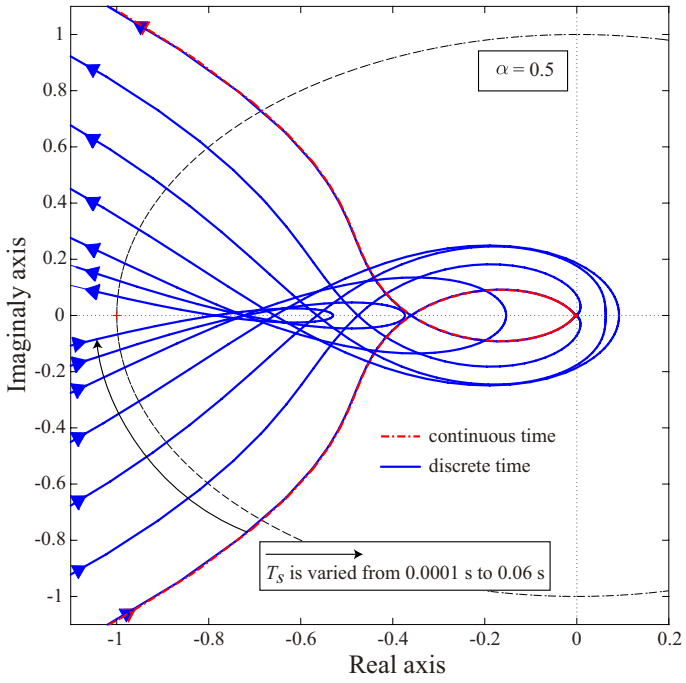

(a)

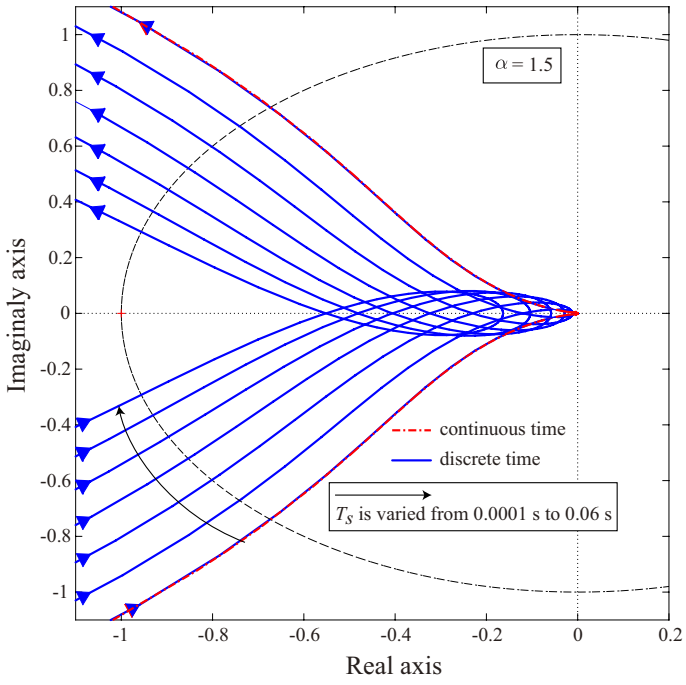

(b)

Fig. 3-22: Nyquist plot with the variation of sampling time T_s from 0.0001s to 0.06 (with the condition of case 2) (a) $\alpha = 0.5$. (b) $\alpha = 1.5$.

3.6.4 Step Responses of Closed Loop System

Fig. 3-23 shows step responses of the closed loop system with different α. The system with 0th order DOBs without higher-order time derivatives, the system with 2nd order DOBs without higher-order time derivatives, the system with 2nd order DOB without EnvD compensation, the system with 2nd order DOBs with higher-order time derivatives and nominal system with a quadruple root are compared. As shown in the figure, the system with 2nd order DOB without EnvD compensation becomes oscillating even if α is larger than 1. On the other hand the responses of the system with 2nd order DOBs with higher-order time derivatives is closest compared with the other system. These result shows that to obtain a nominal system (desired performance), the higher-order time derivative in the inverse system is needed.

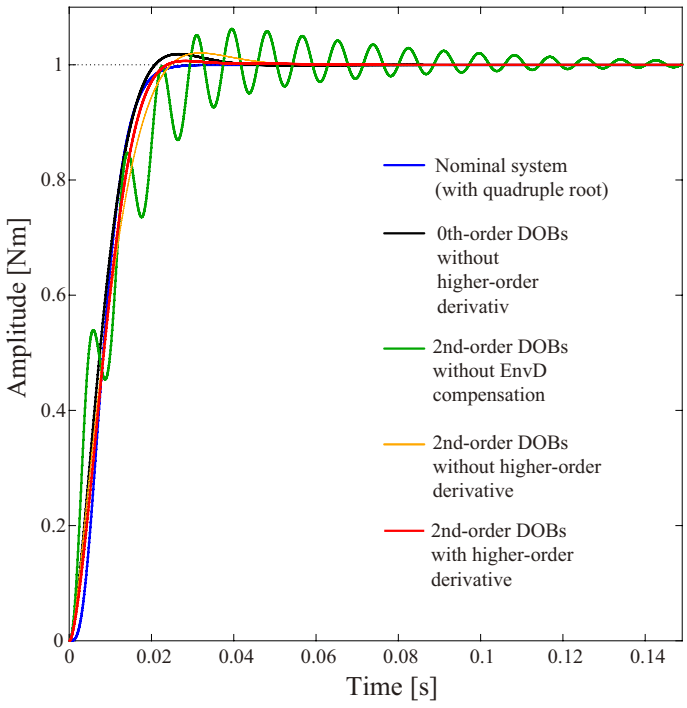

(a)

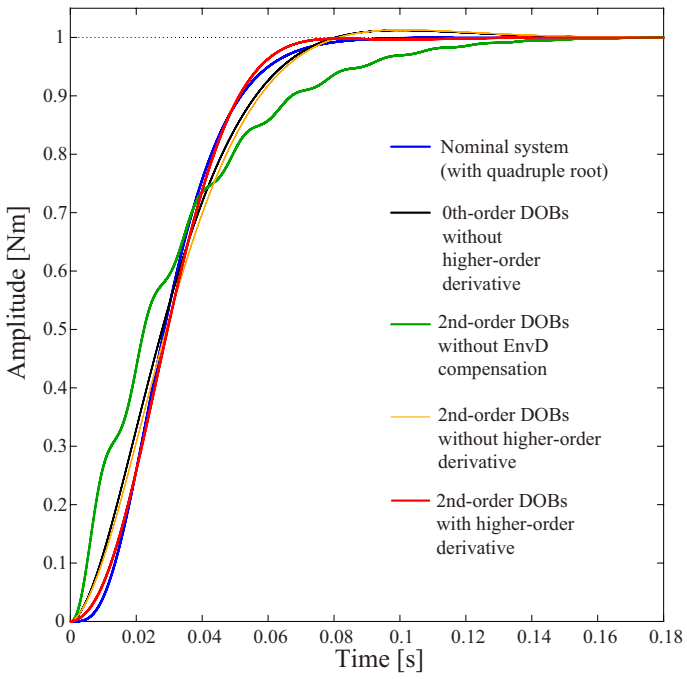

(b)

Fig. 3-23: Step responses of closed loop system with $Z_e(s) = 0.001s^2 + 50s + 1000$ (a) $\alpha = 0.5$. (b) $\alpha = 1.5$.

3.7 Summary of Analysis

From the above part, the results of the analysis are summarized as follows:

- The stability is improved if α is larger than 1.
- If the bandwidth of the pseudo differentiation for the inverse system is small and variation of environmental mass and stiffness is large, the stability is deteriorated even though α is larger than 1.
- The stability with insufficient differentiator and large phase lag the system is inferior to the system without the higher-order differentiation
- The system performance is improved by implementing the higher-order differentiation and increasing the bandwidth.

Therefore, this chapter derives Kalman filter for estimation of higher EnvD and its time derivatives without increasing noise effect. From next part, the derivation of the Kalman filter is described.

3.8 Derivation of Kalman Filter Based State Observer with High Order Environmental Disturbance Estimation

This chapter proposed a Kalman filter based state observer (KFSO) with the high-order environmental disturbance estimation in order to suppress noise effects and to obtain the first and second order time derivative of environmental disturbance.

3.8.1 Kalman Filtering Process

A motion equation including environmental disturbance can be obtained as follows:

$$M_n \ddot{X}^{\mathrm{res}}(t) = F^{\mathrm{ref}}(t) - F^{\mathrm{load}}(t) - F^{\mathrm{ext}}(t) + v^{\mathrm{dis}}(t) \tag{3.52}$$

$$F_e^{\mathrm{dis}} = K_{en} X^{\mathrm{res}} - F^{\mathrm{ext}} \tag{3.53}$$

$$M_n \ddot{X}^{\mathrm{res}}(t) = F^{\mathrm{ref}}(t) - F^{\mathrm{load}}(t) + F_e^{\mathrm{dis}}(t) - K_{en} X^{\mathrm{res}}(t) + v^{\mathrm{dis}}(t). \tag{3.54}$$

A state space equation of an actuator in which the sate vector includes EnvD and its time derivatives can be described as follows:

$$\dot{\boldsymbol{Z}}_e^h(t) = \mathbf{A}_e^h \boldsymbol{Z}_e^h(t) + \mathbf{B}_e^h \boldsymbol{u}(t) + \mathbf{B}_{ev}^h \boldsymbol{V}_e^h(t) \tag{3.55}$$

$$\boldsymbol{Z}_e^h(t) = \left[X^{\mathrm{res}} \quad \dot{X}^{\mathrm{res}} \quad F_e^{\mathrm{dis}} \quad \dot{F}_e^{\mathrm{dis}} \quad \ddot{F}_e^{\mathrm{dis}} \right]^T \tag{3.56}$$

$$\boldsymbol{Y}_e(t) = \boldsymbol{c}_e \boldsymbol{Z}_e(t) + \boldsymbol{W}(t) = X^{\mathrm{res}}(t) + w(t) \tag{3.57}$$

$$\boldsymbol{V}_e^h(t) = \left[v^{\mathrm{dis}}(t) \; v_{\mathrm{edif}^2}^{\mathrm{dis}}(t) \right]^T \tag{3.58}$$

$$u(t) = F^{\mathrm{ref}} + \hat{F}_{\mathrm{hkf}}^{\mathrm{dis}} - K_{en} X^{\mathrm{res}} - F^{\mathrm{load}} \tag{3.59}$$

where

$$\mathbf{A}_e^h = \begin{bmatrix} 0 & 1 & 0 & 0 & 0 \\ 0 & 0 & \frac{1}{M_n} & 0 & 0 \\ 0 & 0 & 0 & 1 & 0 \\ 0 & 0 & 0 & 0 & 1 \\ 0 & 0 & 0 & 0 & 0 \end{bmatrix}, \; \mathbf{B}_e^h = \begin{bmatrix} 0 \\ \frac{1}{M_n} \\ 0 \\ 0 \\ 0 \end{bmatrix}, \; \boldsymbol{c}_e^h = \begin{bmatrix} 1 & 0 & 0 & 0 & 0 \end{bmatrix} \tag{3.60}$$

$$\mathbf{B}_{ev}^h = \begin{bmatrix} 0 & 0 \\ \frac{1}{M_n} & 0 \\ 0 & 0 \\ 0 & 0 \\ 0 & 1 \end{bmatrix}. \tag{3.61}$$

In the state space model, the model of EnvD is expressed as

$$F_e^{\mathrm{dis}}(t) = d_{e0} + d_{e1} t + d_{e2} t^2 + \int_0^t \int_0^t \int_0^t v_{\mathrm{edif}^2}^{\mathrm{dis}}(T) dT^3 \tag{3.62}$$

$$\dot{F}_e^{\mathrm{dis}}(t) = d_{e1} + \frac{d_{e2}}{2} t + \int_0^t \int_0^t v_{\mathrm{edif}^2}^{\mathrm{dis}}(T) dT^2 \tag{3.63}$$

$$\ddot{F}_e^{\mathrm{dis}}(t) = \frac{d_{e2}}{2} + \int_0^t v_{\mathrm{edif}^2}^{\mathrm{dis}}(T) dT \tag{3.64}$$

$$\dddot{F}_e^{\mathrm{dis}}(t) = v_{\mathrm{edif}^2}^{\mathrm{dis}}(t). \tag{3.65}$$

In this model, the third order derivative (higher-order differentiation) of the disturbance is considered differently form the usual KFSO [65]. The disturbance/external torque is modeled as a second order signal of a time function though the disturbances are usually modeled as a step signal in conventional DOBs or KFSO [65]. The presence of third order time derivative of system noise should be assumed in order to construct Kalman filter based disturbance estimation. The highest (third) order time derivative of environmental disturbance is modeled as behaving random walk.

An actuator dynamics model in discrete time domain can be formulated as follows:

$$\begin{aligned}
\boldsymbol{Z}_e^h(k+1) &= \mathbf{A}_{ed}^h \boldsymbol{Z}_e^h(k) + \mathbf{B}_{ed}^h(k) + \mathbf{B}_{edv}^h \boldsymbol{V}(k) && (3.66)\\
\boldsymbol{Z}_e^h(k) &= \left[X^{\mathrm{res}}(k) \;\; \dot{X}^{\mathrm{res}}(k) \;\; F_e^{\mathrm{dis}}(k) \;\; \dot{F}_e^{\mathrm{dis}}(k) \;\; \ddot{F}_e^{\mathrm{dis}}(k) \right]^T && (3.67)\\
\boldsymbol{Y}(k) &= \boldsymbol{c}_e^h \boldsymbol{Z}_e^h(k) + \boldsymbol{W}(k) = X^{\mathrm{res}}(k) + w(k) && (3.68)\\
\mathbf{A}_{ed}^h &= \mathbf{e}^{\mathbf{A}_e^h T_s} && (3.69)\\
\mathbf{B}_{ed}^h &= \int_0^{T_s} \mathbf{e}^{\mathbf{A}_e^h t} \mathbf{B}_e^h dt. && (3.70)
\end{aligned}$$

A Kalman filtering proposes is executed based on (3.66). The filtering process can be divided into the prediction and updating phases. In the prediction phase, predicted (a priori) state estimate $\hat{\boldsymbol{Z}}^-(k)$ and predicted (a priori) estimate error covariance matrix $\mathbf{P}_e^{h-}(k)$ are estimated as follows:

$$\begin{aligned}
\boldsymbol{Z}_e^{h-}(k) &= \mathbf{A}_{ed}^h \hat{\boldsymbol{Z}}_e^h(k-1) + \mathbf{B}_{ed}^h u(k-1) && (3.71)\\
&= \left[\hat{X}_{\mathrm{hkf}}^{\mathrm{res}-} \;\; \hat{\dot{X}}_{\mathrm{hkf}}^{\mathrm{res}-} \;\; \hat{F}_{\mathrm{hkf}}^{\mathrm{dis}-} \;\; \hat{\dot{F}}_{\mathrm{hkf}}^{\mathrm{dis}-} \;\; \hat{\ddot{F}}_{\mathrm{hkf}}^{\mathrm{dis}-} \right]^T && (3.72)\\
\mathbf{P}_e^{h-}(k) &= \mathbf{A}_{ed}^h \mathbf{P}_e^h(k-1) \mathbf{A}_{ed}^{h\,T} + \mathbf{Q}_{ed}^h. && (3.73)
\end{aligned}$$

In the updating phase, the Kalman filter gain matrix $\mathbf{G}_{\mathrm{ekf}}^h(k)$ is calculated as

$$\mathbf{G}_{\mathrm{ekf}}^h(k) = \mathbf{P}_e^{h-}(k) \boldsymbol{c}_e^{h\,T} \left(\boldsymbol{c}_e^h \mathbf{P}_e^{h-}(k) \boldsymbol{c}_e^h + \mathbf{R}_e \right)^{-1}. \tag{3.74}$$

The estimated (a posteriori) state vector and the (a posteriori) error matrix covariance matrix are updated by using an actual measurement $\boldsymbol{Y}(k)$ at every sampling instant as follows:

$$\begin{aligned}
\hat{\boldsymbol{Z}}_e^h(k) &= \boldsymbol{Z}_e^{h-}(k) + \mathbf{G}_{\mathrm{ekf}}^h(k) \left(\boldsymbol{Y}(k) - \boldsymbol{c}_e^h \hat{\boldsymbol{Z}}_e^{h-}(k) \right) && (3.75)\\
&= \left[\hat{X}_{\mathrm{hkf}}^{\mathrm{res}} \;\; \hat{\dot{X}}_{\mathrm{hkf}}^{\mathrm{res}} \;\; \hat{F}_{e\mathrm{hkf}}^{\mathrm{dis}} \;\; \hat{\dot{F}}_{e\mathrm{hkf}}^{\mathrm{dis}} \;\; \hat{\ddot{F}}_{e\mathrm{hkf}}^{\mathrm{dis}} \right]^T && (3.76)\\
\mathbf{P}_e^h(k) &= \left(\boldsymbol{I} - \mathbf{G}_{\mathrm{ekf}}^h(k) \boldsymbol{c}_e^h \right) \mathbf{P}_e^{h-}(k). && (3.77)
\end{aligned}$$

The estimated variables $\hat{\boldsymbol{Z}}(k)$ are used for the control system. The estimated EnvD and its time derivatives are expressed as follows:

$$\begin{aligned}
\hat{F}_{e\mathrm{hkf}}^{\mathrm{dis}} &= g_{le\mathrm{hkf}}^{\mathrm{dis}}(z) F_e^{\mathrm{dis}} + g_{Ne\mathrm{hkf}}^{\mathrm{dis}}(z) w && (3.78)\\
\hat{\dot{F}}_{e\mathrm{hkf}}^{\mathrm{dis}} &= g_{le\mathrm{hkf}}^{\mathrm{pd}}(z) \dot{F}_e^{\mathrm{dis}} + g_{Ne\mathrm{hkf}}^{\mathrm{pd}}(z) w && (3.79)\\
\hat{\ddot{F}}_{e\mathrm{hkf}}^{\mathrm{dis}} &= g_{le\mathrm{hkf2nd}}^{\mathrm{pd}}(z) \ddot{F}_e^{\mathrm{dis}} + g_{Ne\mathrm{hkf2nd}}^{\mathrm{pd}}(z) w && (3.80)\\
g_{he\mathrm{hkf}}^{\mathrm{dis}}(z) &= 1 - g_{le\mathrm{hkf}}^{\mathrm{dis}}(z). && (3.81)
\end{aligned}$$

By considering state space equation, the time derivatives of EnvD can be expressed as follows:

$$\dot{F}_e^{\rm dis} = \frac{2}{T_s}\frac{z-1}{z+1}F_e^{\rm dis} \tag{3.82}$$

$$\ddot{F}_e^{\rm dis} = \frac{2}{T_s^2}\frac{(z-1)^2}{z+1}F_e^{\rm dis}. \tag{3.83}$$

Because $g_{le\rm hkf}^{\rm dis}(z)$, $g_{le\rm hkf}^{\rm pd}(z)$ and $g_{le\rm hkf2nd}^{\rm pd}(z)$ have a same denominator, the estimated values of the time derivatives of EnvD are rewritten as follows:

$$\hat{\dot{F}}_{e\rm hkf}^{\rm dis} = \frac{n_{le\rm hkf}^{\rm pd}(z)}{d_{le\rm hkf}^{\rm dis}(z)}\dot{F}_e^{\rm dis} + g_{Ne\rm hkf}^{\rm pd}(z)w \tag{3.84}$$

$$= \frac{n_{le\rm hkf}^{\rm pd}(z)}{n_{le\rm hkf}^{\rm dis}(z)}\frac{n_{le\rm hkf}^{\rm dis}(z)}{d_{le\rm hkf}^{\rm dis}(z)}\frac{2}{T_s}\frac{z-1}{z+1}F_e^{\rm dis} + g_{Ne\rm hkf}^{\rm pd}(z)w \tag{3.85}$$

$$= \frac{n_{le\rm hkf}^{\rm pd}(z)}{n_{le\rm hkf}^{\rm dis}(z)}g_{le\rm hkf}^{\rm dis}(z)\frac{2}{T_s}\frac{z-1}{z+1}F_e^{\rm dis} + g_{Ne\rm hkf}^{\rm pd}(z)w \tag{3.86}$$

$$= g_{le\rm hkf}^{\rm pd\prime}(z)g_{le\rm hkf}^{\rm dis}(z)\frac{2}{T_s}\frac{z-1}{z+1}F_e^{\rm dis} + g_{Ne\rm hkf}^{\rm pd}(z)w \tag{3.87}$$

$$\hat{\ddot{F}}_{e\rm hkf}^{\rm dis} = \frac{n_{le\rm hkf2nd}^{\rm pd}(z)}{d_{le\rm hkf2nd}^{\rm dis}(z)}\dot{F}_e^{\rm dis} + g_{Ne\rm hkf}^{\rm pd}(z)w \tag{3.88}$$

$$= \frac{n_{le\rm hkf2nd}^{\rm pd}(z)}{n_{le\rm hkf2nd}^{\rm dis}(z)}\frac{n_{le\rm hkf}^{\rm dis}(z)}{d_{le\rm hkf}^{\rm dis}(z)}\frac{2}{T_s^2}\frac{(z-1)^2}{z+1}F_e^{\rm dis} + g_{Ne\rm hkf2nd}^{\rm pd}(z)w \tag{3.89}$$

$$= \frac{n_{le\rm hkf2nd}^{\rm pd}(z)}{n_{le\rm hkf2nd}^{\rm dis}(z)}g_{le\rm hkf}^{\rm dis}(z)\frac{2}{T_s^2}\frac{(z-1)^2}{z+1}F_e^{\rm dis} + g_{Ne\rm hkf2nd}^{\rm pd}(z)w \tag{3.90}$$

$$= g_{le\rm hkf2nd}^{\rm pd\prime}(z)g_{le\rm hkf}^{\rm dis}(z)\frac{2}{T_s^2}\frac{(z-1)^2}{z+1}F_e^{\rm dis} + g_{Ne\rm hkf2nd}^{\rm pd}(z)w \tag{3.91}$$

where

$$g_{le\rm hkf}^{\rm pd\prime}(z) = \frac{n_{le\rm hkf}^{\rm pd}(z)}{n_{le\rm hkf}^{\rm dis}(z)} \tag{3.92}$$

$$g_{le\rm hkf2nd}^{\rm pd\prime}(z) = \frac{n_{le\rm hkf2nd}^{\rm pd}(z)}{n_{le\rm hkf2nd}^{\rm dis}(z)}. \tag{3.93}$$

Tuning method for $\mathbf{Q}_{ed}^h$ is conducted in the similar way as the case of the high-order disturbance estimation shown in chapter 2. Only the variances with respect to $v_e^{\rm dis}(t)$ and $v_{e\rm dif^2}^{\rm dis}(t)$ $\sigma_{v_e^{\rm dis}}^2$ and $\sigma_{v_{e\rm dif^2}^{\rm dis}}^2$ should be determined.

3.8.2 Proposed Method

The estimated variables by the designed Kalman filter are applied for admittance control based force control. In the discrete time domain, the ideal compensation value for the EnvD is expressed as follows:

$$X^p_{\rm cmp} = \frac{s^2 + K_v s + K_r K_{en} + K_p}{K_p K_{en}} F^{\rm dis}_{\rm ehkf} \tag{3.94}$$

$$= \frac{\dfrac{2}{T_s^2}\dfrac{(z-1)^2}{z+1} + K_v \dfrac{2}{T_s}\dfrac{z-1}{z+1} + K_r K_{en} + K_p}{K_p K_{en}} F^{\rm dis}_{\rm ehkf}. \tag{3.95}$$

The compensation value for the environmental disturbance compensation is derived by using the state variables estimated by the proposed Kalman filter as follows:

$$X^p_{\rm cmp} = \frac{\hat{\ddot{F}}^{\rm dis}_{\rm ehkf} + K_v \hat{\dot{F}}^{\rm dis}_{\rm ehkf} + (K_r K_{en} + K_p)\hat{F}^{\rm dis}_{\rm ehkf}}{K_p K_{en}}. \tag{3.96}$$

By considering (3.87) and (3.91), (3.96) is rewritten as follows:

$$X^p_{\rm cmp} = \frac{g^{\rm pd\prime}_{l\rm ehkf2nd}(z)\dfrac{2}{T_s^2}\dfrac{(z-1)^2}{z+1} + K_v g^{\rm pd\prime}_{l\rm ehkf}(z)\dfrac{2}{T_s}\dfrac{z-1}{z+1} + K_r K_{en} + K_p}{K_p K_{en}} \hat{F}^{\rm dis}_{\rm ehkf}. \tag{3.97}$$

As shown in (3.97), the compensation value is equivalently composed by the inverse system with the pseudo differentiators and estimated EnvD through the Kalman filter.

The acceleration reference and resulting reference force are obtained as follows:

$$\ddot{X}^{\rm ref} = K_p(X^{\rm cmd}_f + X^p_{\rm cmp} - X^{\rm res}_f - \hat{X}^{\rm res}_{\rm hkf}) + K_v(0 - \dot{X}^{\rm res}_f - \hat{\dot{X}}^{\rm res}_{\rm hkf}) - \ddot{X}^{\rm res}_f - K_r F^{\rm ref}_e \tag{3.98}$$

$$\ddot{X}^{\rm res}_f = \ddot{X}^{\rm cmd}_f - \ddot{X}^{\rm res}_f = \frac{1}{M_f}\left(F^{\rm cmd} - \hat{F}^{\rm ext}_{\rm hkf}\right) \tag{3.99}$$

$$F^{\rm ref}_n = M_n \ddot{X}^{\rm ref} + \hat{F}^{\rm dis}_{\rm hkf}. \tag{3.100}$$

In the same way as the proposed high-order environmental disturbance estimation by Kalman filter, the higher-order state observer for an actuator can be constructed. The state variables $\hat{X}^{\rm res}_{\rm hkf}$, $\dot{X}^{\rm res}_f$, $\hat{F}^{\rm ext}_{\rm hkf}$ and $\hat{F}^{\rm dis}_{\rm hkf}$ in (3.98) are estimated by the Kalman filter based state observer. A state space equation of an actuator in which the sate vector includes the 2nd-order disturbance and its time derivatives can be

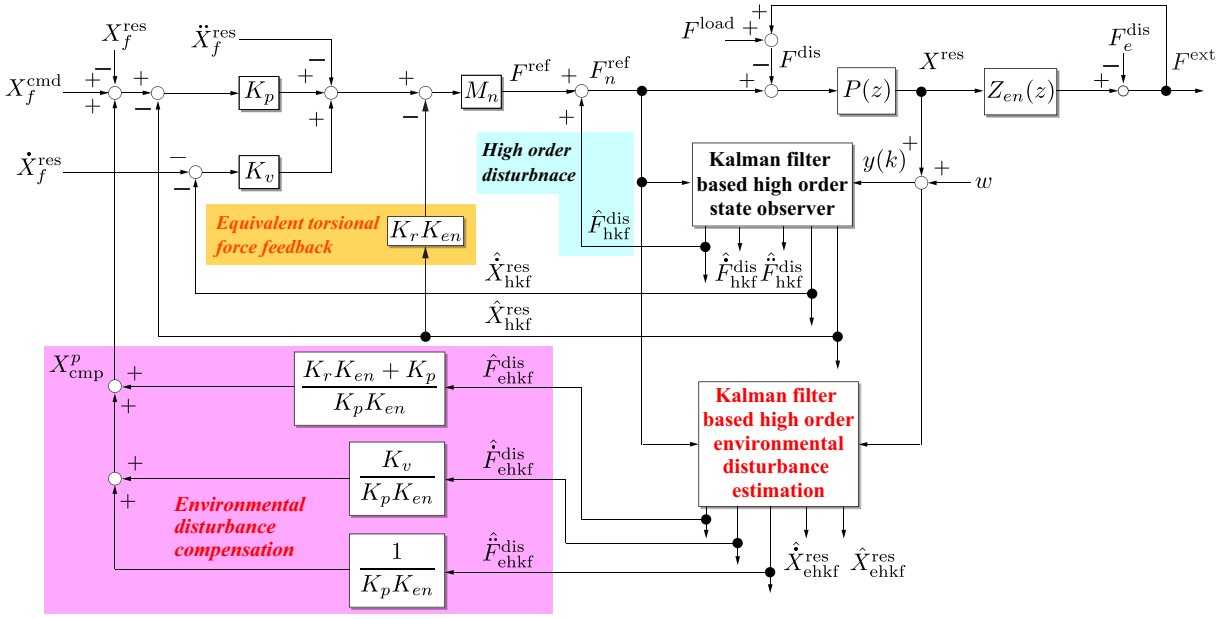

Fig. 3-24: Block diagram of the proposed reaction torque control system.

described as follows:

$$\dot{\boldsymbol{Z}}^{h2}(t) = \mathbf{A}^{h2}\boldsymbol{Z}^{h2}(t) + \mathbf{B}^{h2}\boldsymbol{u}(t) + \mathbf{B}_v^{h2}\boldsymbol{V}^{h2}(t) \tag{3.101}$$

$$\boldsymbol{Z}^{h2}(t) = \left[X^{\mathrm{res}} \;\; \dot{X}^{\mathrm{res}} \;\; F^{\mathrm{dis}} \;\; \dot{F}^{\mathrm{dis}} \;\; \ddot{F}^{\mathrm{dis}}\right]^T \tag{3.102}$$

$$\boldsymbol{Y}(t) = \boldsymbol{c}\boldsymbol{Z}(t) + \boldsymbol{W}(t) = X^{\mathrm{res}}(t) + w(t) \tag{3.103}$$

$$\boldsymbol{V}^{h2}(t) = \left[v^{\mathrm{dis}}(t) \;\; v_{\mathrm{dif}}^{\mathrm{dis}}(t)\right]^T \tag{3.104}$$

$$u(t) = F^{\mathrm{ref}} \tag{3.105}$$

where

$$\mathbf{A}^{h2} = \begin{bmatrix} 0 & 1 & 0 & 0 & 0 \\ 0 & 0 & -\frac{1}{M_n} & 0 & 0 \\ 0 & 0 & 0 & 1 & 0 \\ 0 & 0 & 0 & 0 & 1 \\ 0 & 0 & 0 & 0 & 0 \end{bmatrix}, \; \mathbf{B}^{h2} = \begin{bmatrix} 0 \\ \frac{1}{M_n} \\ 0 \\ 0 \\ 0 \end{bmatrix}, \; \boldsymbol{c}^{h2} = \begin{bmatrix} 1 & 0 & 0 & 0 & 0 \end{bmatrix} \tag{3.106}$$

$$\mathbf{B}_v^{h2} = \begin{bmatrix} 0 & 0 \\ \frac{1}{M_n} & 0 \\ 0 & 0 \\ 0 & 0 \\ 0 & 1 \end{bmatrix}. \tag{3.107}$$

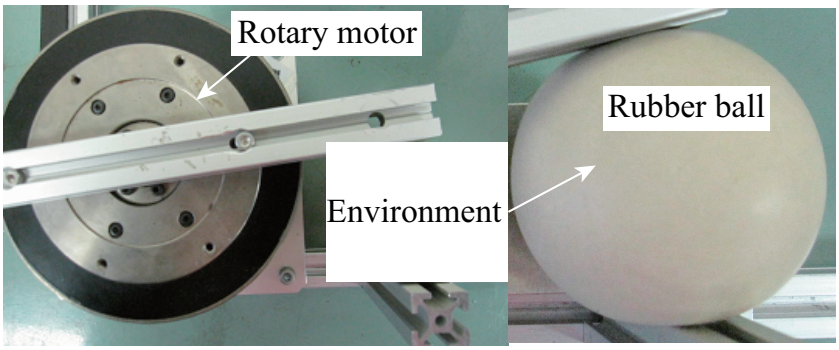

Fig. 3-25: Experimental setup for comparison of EnvD compensation.

The subscript $h2$ represents the variables corresponding to the 2nd-order disturbance estimation. In the state space model, the model of disturbance force is expressed as

$$F^{\mathrm{dis}}(t) = d_0 + d_1 t + d_2 t^2 + \int_0^t \int_0^t \int_0^t v_{\mathrm{dif}^2}^{\mathrm{dis}}(T) dT^3 \tag{3.108}$$

$$\dot{F}^{\mathrm{dis}}(t) = d_1 + \frac{d_2}{2} t + \int_0^t \int_0^t v_{\mathrm{dif}^2}^{\mathrm{dis}}(T) dT^2 \tag{3.109}$$

$$\ddot{F}^{\mathrm{dis}}(t) = \frac{d_2}{2} + \int_0^t v_{\mathrm{dif}^2}^{\mathrm{dis}}(T) dT \tag{3.110}$$

$$\dddot{F}^{\mathrm{dis}}(t) = v_{\mathrm{dif}^2}^{\mathrm{dis}}(t). \tag{3.111}$$

The whole block diagram of the proposed method is shown in Fig. 3-24. In this system is assumed to have an ideal sampler and a holder with sampling time T_s.

By using the proposed method, noise suppression and performance improvement are expected.

3.9 Experiments for Verification of EnvD Compensation

3.9.1 Experimental Setup for Contact Motion with EnvD

To confirm the validity of the proposal, experiments of contact motions for force tracking control were conducted. As shown in Fig. 3-25, a rubber ball is used as experimental environment. Table 3.2 lists the experimental parameters.

3.9.2 Experimental Results

Fig. 3-26 shows the experimental results of the conventional methods and the proposed method. Methods without considering high-order term in compensation become oscillating. Conventional method with considering high-order term in compensation enlarges effect of noise though the bandwidth of the pseudo differentiation of environmental disturbance is smaller than that of the proposed method.

Table 3.2: Experimental parameters for comparison of EnvD compensation

Parameter	Description	Value
T_s	sampling time	0.1 ms
g^{dis}	bandwidth of DOB	1000 rad/s
g^{ext}	bandwidth of RTOB	1000 rad/s
$g^{\mathrm{dis}}_{\mathrm{hkf}}$	bandwidth of KF based DOB	1000 rad/s
$g^{\mathrm{ext}}_{\mathrm{hkf}}$	bandwidth of KF based RTOB	1000 rad/s
g^{dis}_{e}	bandwidth of EnvD estimation	876 rad/s
$g^{\mathrm{dis}}_{e\mathrm{kf}}$	bandwidth of KF based EnvD estimation	876 rad/s
g^{pd}_{e1}	bandwidth of (1st) diff. of env. Dist.	408 rad/s
g^{pd}_{e2}	bandwidth of (2nd) diff. of env. Dist.	199 rad/s
$g^{\mathrm{pd}}_{e1\mathrm{hkf}}$	bandwidth of (1st) diff. of env. dist.	649 rad/s
$g^{\mathrm{pd}}_{e2\mathrm{hkf}}$	bandwidth of (2nd) diff. of env. dist.	438 rad/s
g^{pd}_{v}	cut-off frequency of velocity estimation	1173 rad/s
M_f	force control gain (virtual inertia)	0.01 kgm^2
J_n	nominal inertia of actuator	0.004 kgm^2
K_{tn}	nominal torque coefficient	1.18 Nm/A
K_r	equivalent torsional force feedback gain for spring	400
K_{en}	nominal stiffness of rubber ball	70 Nm/rad
K_p	position control gain for rubber ball	7000
K_v	velocity feedback gain for rubber ball	335

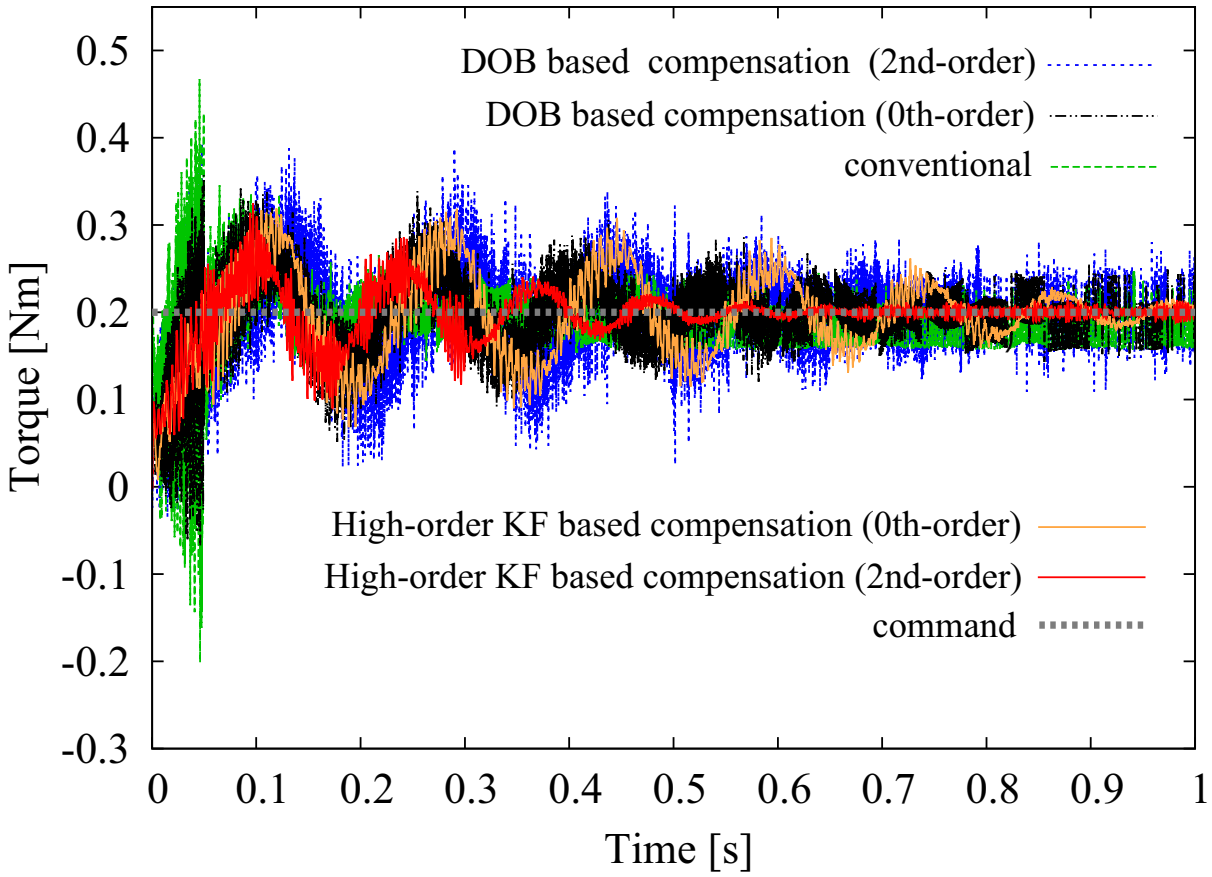

Fig. 3-26: External torque responses with EnvD compensation.

In a contrasting situation, the proposed method achieves lower level of oscillation than the conventional method and suppresses noise effect compared with DOB based methods.

Fig. 3-27 shows the comparison of the time derivatives of environmental disturbance between the conventional method and the proposed method. As shown by the figure, suppression of the noise effect can be confirmed also in the time derivatives of environmental disturbance. As for the case of the first-order time derivative, especially, the phase lag is found in the response of the DOB based method. This is because the time derivative is obtained from the estimated EnvD which get through a low-pass filter of a DOB.

On the other hand, the proposed method achieves the faster and clearer response than the conventional method.

From these result, the validities of the proposal can be confirmed.

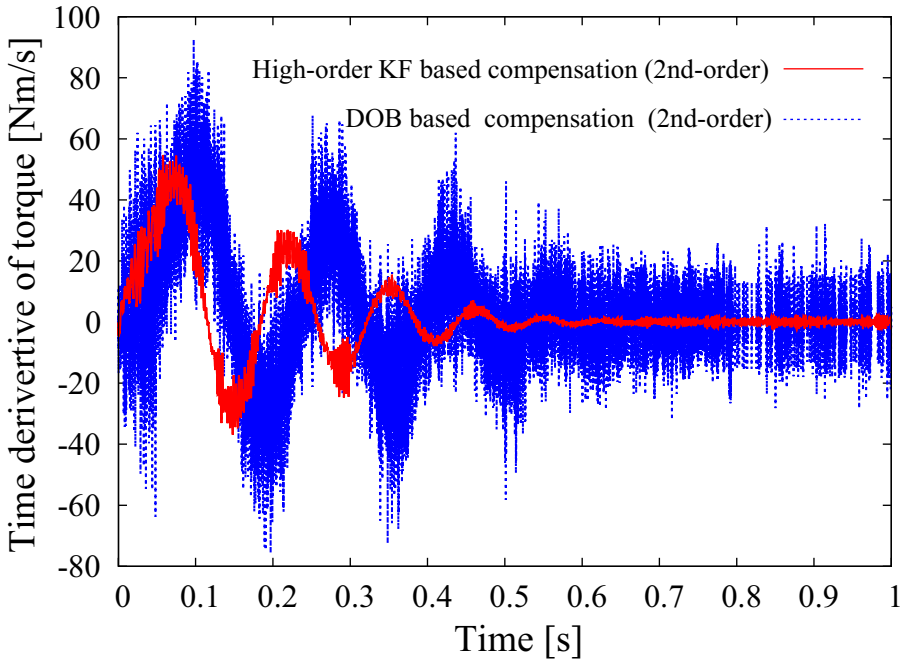

(a)

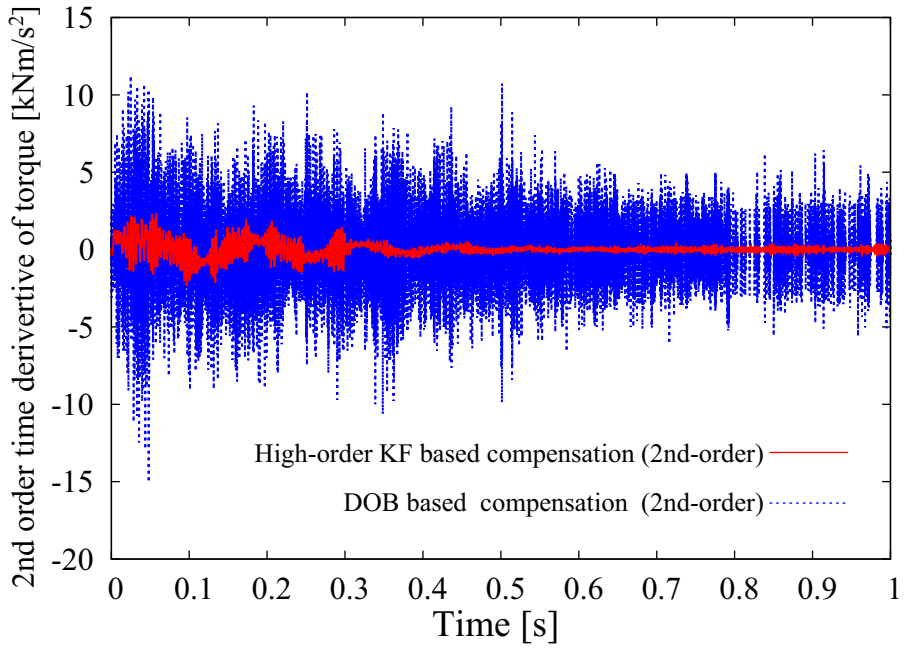

(b)

Fig. 3-27: Experimental results of time derivatives of environmental disturbance. (a) 1st-order derivative. (b) 2nd-order derivative.

3.10 Summary of Chapter 3

This chapter showed a method of stable contact motions for force tracking control based on the concept of resonance ratio control.

The similarity in the structure for admittance control for contact motions and two-mass resonance systems was derived. From the similarity, it was found that the concept of resonance ratio control is applicable to force tracking control. Based on the concept of resonance ratio control, an admittance controller for contact motion with the EnvD compensation was proposed. By using the proposed method, vibration suppression during contact motion was realized even if the environment had no, or insufficient, viscosity. The response characteristics of contact motion for force tracking control can be determined arbitrarily by the proposed method.

This part also considered utilizing the higher-order derivative terms in compensation for environmental disturbance.

For the compensation of the environmental disturbance, only the zero order term inverse system was considered in order to avoid enlarging noise effect by implementing time derivatives of estimated environmental disturbance. The higher-order terms of timed derivatives were neglected also for the compensation of load disturbance in the two mass resonance system.

In this chapter, the high-order EnvD was estimated by a Kalman filter including higher-order time derivatives of the EnvD. The estimated variable of the proposed Kalman filter based high-order environmental disturbance observer can be utilized for the compensation without enlarging noise effect in time derivatives

The experimental results validated the proposed method.

Chapter 4

Performance Enhancement of Position/Force Hybrid Control for Motion Extraction

---

4.1 Introduction of Chapter 4

This chapter introduces a hybrid control system based on an acceleration controller in the modal space, which is capable of realizing decoupling control and performance improvement of the bilateral control system [97]. In motion control systems, hybrid control systems in which position/force control systems are constructed in different axes [75] will be important for the interaction with human beings and outer environments. This chapter shows how an acceleration controller can realize decoupling control in the modal space. Furthermore, a novel disturbance observer for enhancing the performance of an acceleration controller is proposed. Differently from the conventional hybrid controllers [79–81], the proposed controller does not affected by the variation of manipulator configurations except for neighborhood of a singular point because he structure of the proposed method is based on the acceleration controller [21, 84]. Moreover, this chapter proposes a method for the simultaneous achievement of performance improvement, decoupling of null space and suppression of the noise effect for the hybrid control system with RDOF. The authors show that a hybrid controller based on an acceleration controller in the modal space performs decoupling control of the position and force control systems of the bilateral control [97]. In addition, the authors proposed a DOB with the aim of improving performance of the hybrid controller in the modal space [97]. This study suppresses the operating (inertia) force and the interference from null space with the simplification of inverse kinematics by extending the DOB for hybrid controllers to

the redundant systems. Furthermore, the reconstruction of the DOB by coupling with a Kalman filter is proposed to suppress the noise effect. The validities of the proposal are confirmed by analyses and experiments.

4.2 Kinematics and Dynamics of Hybrid Control

This part describes a kinematics and dynamics for hybrid controllers.

4.2.1 Kinematics of Bilateral Control as a Hybrid Control

The control goals of bilateral control are described in terms of the position and force responses of the master and slave systems, as follows:

$$\boldsymbol{F}_F^{\mathrm{ext}} = \boldsymbol{F}_m^{\mathrm{ext}} + \boldsymbol{F}_s^{\mathrm{ext}} = \boldsymbol{F}_F^{\mathrm{cmd}} = \boldsymbol{0} \tag{4.1}$$

$$\boldsymbol{X}_X^{\mathrm{res}} = \boldsymbol{X}_m^{\mathrm{res}} - \boldsymbol{X}_s^{\mathrm{res}} = \boldsymbol{X}_X^{\mathrm{cmd}} = \boldsymbol{0} \tag{4.2}$$

where $\boldsymbol{F}$ and $\boldsymbol{X}$ represent a force and position vector. In addition, subscripts m, s, F and X represent a master system, a slave system, a force control system and a position control system, respectively. Eq. (4.1) represents the realization of haptic feedback (law of action and reaction) between the master and slave systems. On the other hand, (4.2) represents the position tracking of the master and slave systems. These control goals are achieved by the application of force control and position control. Therefore, a bilateral control system can be regarded as being a force-position hybrid control system [79–81]. To describe and realize hybrid control, the force and position information of the master and slave systems is transformed to the modal space. Fig. 4-1 shows block diagrams of the conventional bilateral control systems based on force controllers. Fig. 4-1 (a) shows the block diagram of the bilateral controller using the hybrid matrix-based method [79, 80]. On the other hand, Fig. 4-1 (b) shows the hybrid controller based on MDOB [81]. In the right sides of Fig. 4-1, the workspace represents the Cartesian coordinate that corresponds to the hand coordinate of the master and slave manipulators. In the left sides of Fig. 4-1, on the other hand, the modal space is defined as a virtual coordinate space for describing the tasks to be executed.

If the position-control axis and the force-control axis have a geometric relationship (e. g. a hybrid controller in work space [75] or a grasping and manipulating control [109–113]), the direct kinematics (coordinate transformation) from the workspace to the modal space with respect to the position, velocity

and acceleration is given as

$$\boldsymbol{X}^{\mathrm{res}} = \begin{bmatrix} \boldsymbol{X}_F^{\mathrm{res}} \\ \boldsymbol{X}_X^{\mathrm{res}} \end{bmatrix} = \boldsymbol{G}(\boldsymbol{X}_W^{\mathrm{res}}) \tag{4.3}$$

$$\dot{\boldsymbol{X}}^{\mathrm{res}} = \begin{bmatrix} \dot{\boldsymbol{X}}_F^{\mathrm{res}} \\ \dot{\boldsymbol{X}}_X^{\mathrm{res}} \end{bmatrix} = \boldsymbol{\Gamma}\dot{\boldsymbol{X}}_W^{\mathrm{res}} \tag{4.4}$$

$$\ddot{\boldsymbol{X}}^{\mathrm{res}} = \begin{bmatrix} \ddot{\boldsymbol{X}}_F^{\mathrm{res}} \\ \ddot{\boldsymbol{X}}_X^{\mathrm{res}} \end{bmatrix} = \boldsymbol{\Gamma}\ddot{\boldsymbol{X}}_W^{\mathrm{res}} + \dot{\boldsymbol{\Gamma}}\dot{\boldsymbol{X}}_W^{\mathrm{res}} \tag{4.5}$$

where subscript W represent a work space. The workspace coordinate system is transformed to the modal space coordinate system using a modal transformation matrix $\boldsymbol{\Gamma}$. This is a type of Jacobian matrix. The coordinate transformation of the force information is defined by considering the principle of virtual work as follows:

$$\boldsymbol{F}^{\mathrm{ext}} = \begin{bmatrix} \boldsymbol{F}_F^{\mathrm{ext}} & \boldsymbol{F}_X^{\mathrm{ext}} \end{bmatrix}^T = \boldsymbol{\Gamma}^{-T}\boldsymbol{F}_W^{\mathrm{ext}}. \tag{4.6}$$

In this case, the task (coordinate system) of the force control system is constrained by the geometric relationship $\boldsymbol{G}(\bullet)$ or $\boldsymbol{\Gamma}$. Therefore the task (coordinate system) of the force control system itself cannot be determined by a designer.

On the other hand, in the case of hybrid controller without kinematic constraint between the force and position control system (e. g. bilateral control including scaled bilateral control [26, 78, 80]), the task (coordinate system) of the force control system can be determined. In the case of bilateral control, the position control task (coordinate transformation for position control task) is described as

$$\boldsymbol{X}_X^{\mathrm{res}} = \boldsymbol{G}_X(\boldsymbol{X}_W^{\mathrm{res}}) \tag{4.7}$$

where $\boldsymbol{G}_X(\bullet)$ represents a direct kinematics. If the coordinate transformation is linear, the coordinate transformation is rewritten as

$$\boldsymbol{X}_X^{\mathrm{res}} = \begin{bmatrix} \boldsymbol{0} & \boldsymbol{I} \end{bmatrix} \boldsymbol{\Gamma}_X \boldsymbol{X}_W^{\mathrm{res}} = \begin{bmatrix} \boldsymbol{0} & \boldsymbol{I} \end{bmatrix} \begin{bmatrix} \boldsymbol{X}_{\mathrm{XF}}^{\mathrm{res}} \\ \boldsymbol{X}_X^{\mathrm{res}} \end{bmatrix} \tag{4.8}$$

where $\boldsymbol{\Gamma}_X$ represent a transformation matrix for the position control system. Here, $\boldsymbol{X}_{\mathrm{XF}}^{\mathrm{res}}$ is not used for the controller. If the desired coordinate transformation for the force control system is also linear, the task for force control can be described as

$$\boldsymbol{F}_F^{\mathrm{ext}} = \boldsymbol{G}_F(\boldsymbol{F}_W^{\mathrm{ext}}) = \begin{bmatrix} \boldsymbol{I} & \boldsymbol{0} \end{bmatrix} \boldsymbol{\Gamma}_F \boldsymbol{F}_W^{\mathrm{ext}} = \begin{bmatrix} \boldsymbol{I} & \boldsymbol{0} \end{bmatrix} \begin{bmatrix} \boldsymbol{F}_F^{\mathrm{ext}} \\ \boldsymbol{F}_{\mathrm{FX}}^{\mathrm{ext}} \end{bmatrix} \tag{4.9}$$

where $\mathbf{\Gamma}_F$ represent a transformation matrix for the force control system. Here, $\boldsymbol{F}_{\mathrm{FX}}^{\mathrm{ext}}$ also is not used for the controller. The motion equations for the force control and position control are described as follows;

$$\begin{bmatrix}\boldsymbol{I} & \boldsymbol{0}\end{bmatrix}\mathbf{\Gamma}_F\boldsymbol{M}_W\ddot{\boldsymbol{X}}_W^{\mathrm{res}} = \begin{bmatrix}\boldsymbol{I} & \boldsymbol{0}\end{bmatrix}\mathbf{\Gamma}_F\boldsymbol{F}_W^{\mathrm{ref}} - \begin{bmatrix}\boldsymbol{I} & \boldsymbol{0}\end{bmatrix}\mathbf{\Gamma}_F\boldsymbol{F}_W^{\mathrm{ext}} + \begin{bmatrix}\boldsymbol{I} & \boldsymbol{0}\end{bmatrix}\mathbf{\Gamma}_F\boldsymbol{M}_W\dot{\boldsymbol{J}}_{\mathrm{aco}}\dot{\boldsymbol{X}}_W^{\mathrm{res}} \quad (4.10)$$

$$\begin{bmatrix}\boldsymbol{0} & \boldsymbol{I}\end{bmatrix}\mathbf{\Gamma}_X\boldsymbol{M}_W\ddot{\boldsymbol{X}}_W^{\mathrm{res}} = \begin{bmatrix}\boldsymbol{0} & \boldsymbol{I}\end{bmatrix}\mathbf{\Gamma}_X\boldsymbol{F}_W^{\mathrm{ref}} - \begin{bmatrix}\boldsymbol{0} & \boldsymbol{I}\end{bmatrix}\mathbf{\Gamma}_X\boldsymbol{F}_W^{\mathrm{ext}} + \begin{bmatrix}\boldsymbol{0} & \boldsymbol{I}\end{bmatrix}\mathbf{\Gamma}_X\boldsymbol{M}_W\dot{\boldsymbol{J}}_{\mathrm{aco}}\dot{\boldsymbol{X}}_W^{\mathrm{res}} \quad (4.11)$$

where $\boldsymbol{M}_W$ and $\boldsymbol{J}_{\mathrm{aco}}$ represent an equivalent mass matrix in the work space and a Jacobian matrix, respectively. By adding (4.10) and (4.11), a motion equation for hybrid controller is obtained as

$$\mathbf{\Gamma}\boldsymbol{M}_W\ddot{\boldsymbol{X}}_W^{\mathrm{res}} = \mathbf{\Gamma}\boldsymbol{F}_W^{\mathrm{ref}} - \mathbf{\Gamma}\boldsymbol{F}_W^{\mathrm{ext}} + \mathbf{\Gamma}\boldsymbol{M}_W\dot{\boldsymbol{J}}_{\mathrm{aco}}\dot{\boldsymbol{X}}_W^{\mathrm{res}} \quad (4.12)$$

$$\mathbf{\Gamma}\boldsymbol{M}_W\mathbf{\Gamma}^{-1}\ddot{\boldsymbol{X}}^{\mathrm{res}} = \boldsymbol{F}^{\mathrm{ref}} - \boldsymbol{F}^{\mathrm{ext}} + \mathbf{\Gamma}\boldsymbol{M}_W\dot{\boldsymbol{J}}_{\mathrm{aco}}\dot{\boldsymbol{X}}_W^{\mathrm{res}}. \quad (4.13)$$

According to (4.10), (4.11) and (4.13), the coordinate transformation for the hybrid control system is defined as

$$\boldsymbol{X}^{\mathrm{res}} = \mathbf{\Gamma}\boldsymbol{X}_W^{\mathrm{res}} \quad (4.14)$$

$$\boldsymbol{F} = \mathbf{\Gamma}\boldsymbol{F}_W \quad (4.15)$$

$$\mathbf{\Gamma} = (\boldsymbol{I}-\boldsymbol{S})\mathbf{\Gamma}_F + \boldsymbol{S}\mathbf{\Gamma}_X = \begin{bmatrix}\boldsymbol{I} & \boldsymbol{0}\\ \boldsymbol{0} & \boldsymbol{0}\end{bmatrix}\mathbf{\Gamma}_F + \begin{bmatrix}\boldsymbol{0} & \boldsymbol{0}\\ \boldsymbol{0} & \boldsymbol{I}\end{bmatrix}\mathbf{\Gamma}_X \quad (4.16)$$

where $\boldsymbol{S}$ is a selection matrix for the position control system. Differently form (4.6), the transformation of the force control system in (4.15) is described by using the same transformation matrix as the position control system. In other words, the designer should set the both transformation matrices as the same structure. By considering the motion equation, the relationship of coordinate transformation can be obtained. Additionally, an equivalent mass matrix for the hybrid control system in (4.13) is defined as follows:

$$\boldsymbol{M} = \mathbf{\Gamma}\boldsymbol{M}_W\mathbf{\Gamma}^{-1}. \quad (4.17)$$

In the case of the bilateral control system, the direct kinematics from the workspace to the modal space is represented as

$$\boldsymbol{X}^{\mathrm{res}} = \begin{bmatrix}\boldsymbol{X}_F^{\mathrm{res}}\\ \boldsymbol{X}_X^{\mathrm{res}}\end{bmatrix} = \boldsymbol{G}(\boldsymbol{X}_W^{\mathrm{res}}) = \mathbf{\Gamma}\boldsymbol{X}_W^{\mathrm{res}} = \begin{bmatrix}\boldsymbol{I} & \boldsymbol{I}\\ \boldsymbol{I} & -\boldsymbol{I}\end{bmatrix}\begin{bmatrix}\boldsymbol{X}_m^{\mathrm{res}}\\ \boldsymbol{X}_s^{\mathrm{res}}\end{bmatrix}. \quad (4.18)$$

The coordinate transformation of the force information is also defined by using the same matrix as below

$$\boldsymbol{F}^{\mathrm{ext}} = \begin{bmatrix}\boldsymbol{F}_F^{\mathrm{ext}}\\ \boldsymbol{F}_X^{\mathrm{ext}}\end{bmatrix}^T = \mathbf{\Gamma}\boldsymbol{F}_W^{\mathrm{ext}} = \begin{bmatrix}\boldsymbol{I} & \boldsymbol{I}\\ \boldsymbol{I} & -\boldsymbol{I}\end{bmatrix}\begin{bmatrix}\boldsymbol{F}_m^{\mathrm{ext}}\\ \boldsymbol{F}_s^{\mathrm{ext}}\end{bmatrix}^T. \quad (4.19)$$

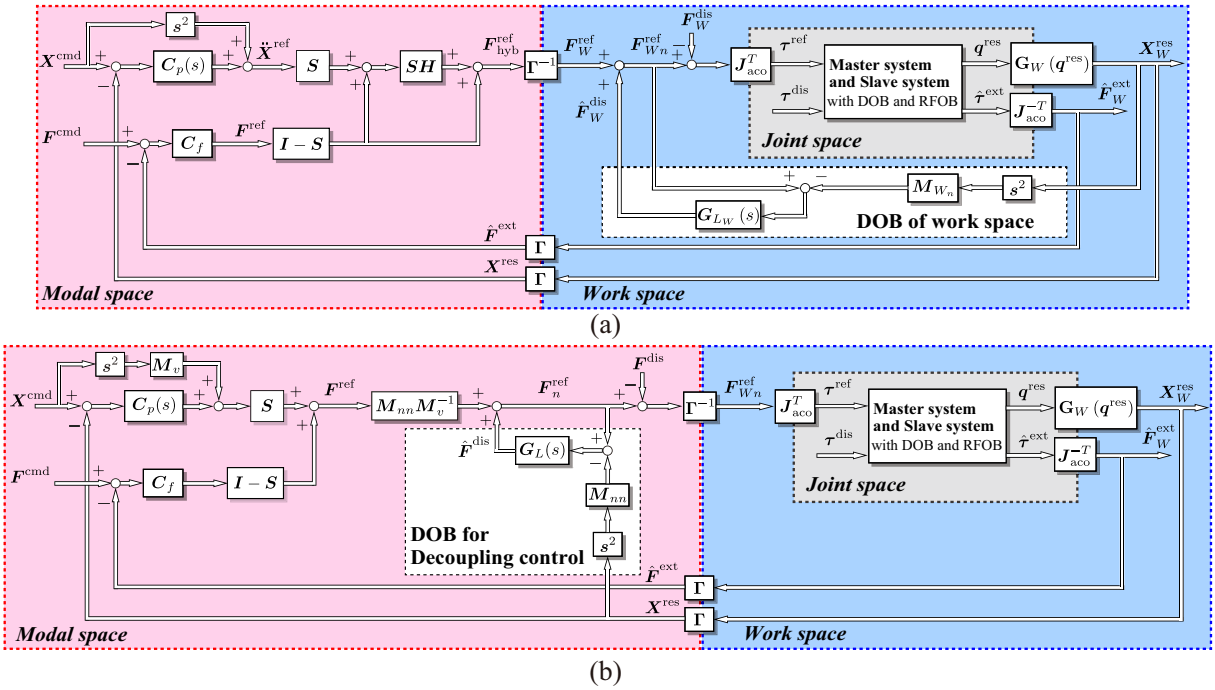

Fig. 4-1: Block diagram of force/position hybrid controller. (a) Hybrid matrix based method. (b) MDOB based decoupling controller.

The control goals shown in (4.1) and (4.2) are expressed in the first element of (4.19) and second element of (4.18). The first element of the modal space (direction of force control) is known as "common mode" and the second element is known as "differential mode" [46]. The common mode corresponds to a kind of barycentric position with respect to master and slave systems. The differential mode corresponds to a relative position of master and slave systems.

4.2.2 Dynamics of Bilateral Control Based on Force Controller

To achieve robust control, we utilize DOBs in the joint space as shown in Fig. 4-1. The motion equation for the joint space of the manipulators is expressed as follows:

$$\boldsymbol{J}_n\ddot{\boldsymbol{q}}^{\mathrm{res}} = \boldsymbol{\tau}^{\mathrm{ref}} - \boldsymbol{\tau}^{\mathrm{load}} - \boldsymbol{\tau}^{\mathrm{ext}} = \boldsymbol{\tau}^{\mathrm{ref}} - \boldsymbol{\tau}^{\mathrm{dis}} \tag{4.20}$$

$$\boldsymbol{\tau}^{\mathrm{load}} = \boldsymbol{\tau}^{\mathrm{fric}} + \boldsymbol{C}\left(\boldsymbol{q}^{\mathrm{res}}, \dot{\boldsymbol{q}}^{\mathrm{res}}\right) + \Delta\boldsymbol{J}\ddot{\boldsymbol{q}}^{\mathrm{res}} - \Delta\boldsymbol{K}_t\boldsymbol{I}^{\mathrm{ref}} \tag{4.21}$$

where $\boldsymbol{\tau}^{\mathrm{dis}}$ represents the disturbance term including external torque. $\boldsymbol{\tau}^{\mathrm{load}}$ represents the load torque excluding the external torque (a friction term $\boldsymbol{\tau}^{\mathrm{fric}}$, and the torque resulting from variations in the param-

eters $\Delta \boldsymbol{J}\ddot{\boldsymbol{q}}^{\mathrm{res}} - \Delta \boldsymbol{K}_t \boldsymbol{I}^{\mathrm{ref}}$). The disturbance torque is estimated by the DOB, as follows:

$$\hat{\boldsymbol{\tau}}^{\mathrm{dis}} = \boldsymbol{g}_l^{\mathrm{dis}}(s)\left(\boldsymbol{\tau}_n^{\mathrm{ref}} - \boldsymbol{J}_n s^2 \boldsymbol{q}^{\mathrm{res}}\right) = \boldsymbol{g}_l^{\mathrm{dis}}(s)\boldsymbol{\tau}^{\mathrm{dis}} \tag{4.22}$$

$$\boldsymbol{\tau}_n^{\mathrm{ref}} = \boldsymbol{\tau}^{\mathrm{ref}} + \hat{\boldsymbol{\tau}}^{\mathrm{dis}} \tag{4.23}$$

where $\hat{\boldsymbol{\tau}}^{\mathrm{dis}}$ and $\boldsymbol{g}_l^{\mathrm{dis}}(s)$ represent the estimated disturbance torque and a diagonal matrix with low-pass filters, respectively. $\boldsymbol{g}_l^{\mathrm{dis}}(s)$ is inserted to reduce the noise effect in the differentiation of the position response. For the force controllers, the torque reference for the joint space $\boldsymbol{\tau}^{\mathrm{ref}}$ is given by using a transpose of the Jacobian matrix, as shown in Fig. 4-1. The dynamics of the joint space with the DOB are obtained as

$$\boldsymbol{J}_n \ddot{\boldsymbol{q}}^{\mathrm{res}} = \boldsymbol{\tau}_n^{\mathrm{ref}} - \boldsymbol{\tau}^{\mathrm{dis}} = \boldsymbol{\tau}^{\mathrm{ref}} - \boldsymbol{g}_h^{\mathrm{dis}}(s)\boldsymbol{\tau}^{\mathrm{dis}} = \boldsymbol{\tau}^{\mathrm{ref}} - \boldsymbol{p}^{\mathrm{dis}} \tag{4.24}$$

where $\boldsymbol{g}_h^{\mathrm{dis}}(s)$ is a diagonal matrix with high-pass filters. The cutoff frequency of $\boldsymbol{g}_h^{\mathrm{dis}}(s)$ is set to a sufficiently large value, such that the effect of the remaining disturbance, $\boldsymbol{p}^{\mathrm{dis}}$, becomes negligibly small for the lower frequency components. The higher frequency components of $\boldsymbol{p}^{\mathrm{dis}}$ still remain. By transforming (4.24) using a Jacobian matrix, the dynamics of the workspace are given as

$$\boldsymbol{J}_n \boldsymbol{J}_{\mathrm{aco}}^{-1} \ddot{\boldsymbol{X}}_W^{\mathrm{res}} = \boldsymbol{\tau}^{\mathrm{ref}} + \boldsymbol{J}_n \boldsymbol{J}_{\mathrm{aco}}^{-1} \dot{\boldsymbol{J}}_{\mathrm{aco}} \dot{\boldsymbol{q}}^{\mathrm{res}} - \boldsymbol{p}^{\mathrm{dis}} \tag{4.25}$$

$$\boldsymbol{M}_W \ddot{\boldsymbol{X}}_W^{\mathrm{res}} = \boldsymbol{F}_W^{\mathrm{ref}} + \boldsymbol{M}_W \dot{\boldsymbol{J}}_{\mathrm{aco}} \dot{\boldsymbol{q}}^{\mathrm{res}} - \boldsymbol{J}_{\mathrm{aco}}^{-T} \boldsymbol{p}^{\mathrm{dis}} \tag{4.26}$$

$$\boldsymbol{M}_W = \boldsymbol{J}_{\mathrm{aco}}^{-T} \boldsymbol{J}_n \boldsymbol{J}_{\mathrm{aco}}^{-1}. \tag{4.27}$$

The non-diagonal elements in $\boldsymbol{M}_W$ cause interference in the workspace. In addition, the second term in (4.26) is a disturbance term caused by the coordinate transformation. The third term is the transformed remaining disturbance. These terms appear as workspace disturbances $\boldsymbol{F}_W^{\mathrm{dis}}$ as shown in Fig. 4-1. Here, the DOB in the workspace (WDOB) [21] is introduced to decouple the workspace responses. The disturbance in the workspace is defined as

$$\boldsymbol{F}_W^{\mathrm{dis}} = \boldsymbol{F}_W^{\mathrm{ref}} - \boldsymbol{M}_{Wn} \ddot{\boldsymbol{X}}_W^{\mathrm{res}} \tag{4.28}$$

$$= \boldsymbol{J}_{\mathrm{aco}}^{-T} \boldsymbol{p}^{\mathrm{dis}} + \boldsymbol{\Delta M}_W \ddot{\boldsymbol{X}}_W^{\mathrm{res}} - \boldsymbol{M}_W \dot{\boldsymbol{J}}_{\mathrm{aco}} \dot{\boldsymbol{q}}^{\mathrm{res}} \tag{4.29}$$

where $\boldsymbol{M}_{Wn}$ and $\boldsymbol{\Delta M}_W$ represent the nominal mass matrix and variation from the nominal mass matrix, respectively. The disturbance in the workspace is obtained by the WDOB through use of a low-pass filter that suppresses the noise effect $\boldsymbol{G}_{L_W}^{\mathrm{dis}}(s)$ and is included in the workspace force reference $\boldsymbol{F}_{Wn}^{\mathrm{ref}}$. The

motion equation for the workspace is given as

$$\begin{aligned} \boldsymbol{M}_{Wn}\ddot{\boldsymbol{X}}_W^{\mathrm{res}} &= \boldsymbol{F}_{Wn}^{\mathrm{ref}} - \boldsymbol{F}_W^{\mathrm{dis}} = \boldsymbol{F}_W^{\mathrm{ref}} + \boldsymbol{G}_{L_W}^{\mathrm{dis}}(s)\boldsymbol{F}_W^{\mathrm{dis}} - \boldsymbol{F}_W^{\mathrm{dis}} \\ &= \boldsymbol{F}_W^{\mathrm{ref}} - \boldsymbol{G}_{H_W}^{\mathrm{dis}}(s)\boldsymbol{F}_W^{\mathrm{dis}} \end{aligned} \tag{4.30}$$

where $\boldsymbol{G}_{H_W}^{\mathrm{dis}}(s)$ is the high-pass filter resulting from the compensation of the disturbance. From (4.30), it is found that decoupled control can be realized in the workspace provided $\boldsymbol{M}_{Wn}$ is set to a diagonal matrix. The motion equation in the modal space is derived from (4.30), as follows:

$$\boldsymbol{M}_n\ddot{\boldsymbol{X}}^{\mathrm{res}} = \boldsymbol{\Gamma}\boldsymbol{F}_W^{\mathrm{ref}} - \boldsymbol{\Gamma}\boldsymbol{G}_{H_W}^{\mathrm{dis}}(s)\boldsymbol{F}^{\mathrm{dis}} \tag{4.31}$$

$$= \boldsymbol{\Gamma}\boldsymbol{\Gamma}^{-1}\boldsymbol{F}^{\mathrm{ref}} - \boldsymbol{\Gamma}\boldsymbol{G}_{H_W}^{\mathrm{dis}}(s)\boldsymbol{F}^{\mathrm{dis}} = \boldsymbol{F}^{\mathrm{ref}} - \boldsymbol{\Gamma}\boldsymbol{G}_{H_W}^{\mathrm{dis}}(s)\boldsymbol{F}^{\mathrm{dis}} \tag{4.32}$$

$$\boldsymbol{M}_n = \boldsymbol{\Gamma}\boldsymbol{M}_{Wn}\boldsymbol{\Gamma}^{-1} = \begin{bmatrix} \boldsymbol{M}_{\mathrm{FF}n} & \boldsymbol{M}_{\mathrm{FX}n} \\ \boldsymbol{M}_{\mathrm{XF}n} & \boldsymbol{M}_{\mathrm{XX}n} \end{bmatrix} \tag{4.33}$$

where $\boldsymbol{M}_n$ represents an equivalent mass matrix in the modal space. The non-diagonal elements of $\boldsymbol{M}_n$ also cause interference in the modal space (i.e. interference between the force and position control).

4.3 Decoupling Strategies for Bilateral Control

4.3.1 Hybrid Matrix Based Method

This section explains a hybrid control system based on a hybrid matrix. The force and acceleration references for force and position control are given as

$$\boldsymbol{F}_F^{\mathrm{ref}} = \boldsymbol{C}_f\left(\boldsymbol{F}_F^{\mathrm{cmd}} - \hat{\boldsymbol{F}}_F^{\mathrm{ext}}\right) = -\boldsymbol{C}_f\hat{\boldsymbol{F}}_F^{\mathrm{ext}},\ \boldsymbol{F}_F^{\mathrm{cmd}} = \boldsymbol{0} \tag{4.34}$$

$$\ddot{\boldsymbol{X}}_X^{\mathrm{ref}} = \boldsymbol{C}_p(s)\left(\boldsymbol{X}_X^{\mathrm{cmd}} - \boldsymbol{X}_X^{\mathrm{res}}\right) + \ddot{\boldsymbol{X}}_X^{\mathrm{cmd}},\ \boldsymbol{X}_X^{\mathrm{cmd}} = \boldsymbol{0} \tag{4.35}$$

where $\boldsymbol{C}_f$ and $\boldsymbol{C}_p(s)$ represent diagonal matrices with force control gains and position controllers, respectively. Here, $\hat{}$ indicates an estimated value for the reaction force observer (RFOB) [6], used to obtain external force information in this chapter. The cutoff frequency of low-pass filter $\boldsymbol{g}_L(s)$ in the RFOB is set to a sufficiently large value. In the decoupling strategy based on the hybrid matrix, the following relationship between the force and acceleration control references is assumed:

$$\boldsymbol{M}_n\boldsymbol{X}^{\mathrm{ref}} = \boldsymbol{M}_n\left[\ddot{\boldsymbol{X}}_F^{\mathrm{ref}}\ \ddot{\boldsymbol{X}}_X^{\mathrm{ref}}\right]^T = \boldsymbol{F}^{\mathrm{ref}} = \left[\boldsymbol{F}_F^{\mathrm{ref}}\boldsymbol{F}_X^{\mathrm{ref}}\right]^T. \tag{4.36}$$

Unknown variables $\ddot{\boldsymbol{X}}_F^{\mathrm{ref}}$ and $\boldsymbol{F}_X^{\mathrm{ref}}$ are obtained as follows:

$$\begin{bmatrix} \boldsymbol{M}_{\mathrm{FF}n} & \boldsymbol{0} \\ \boldsymbol{M}_{\mathrm{XF}n} & -\boldsymbol{I} \end{bmatrix} \begin{bmatrix} \ddot{\boldsymbol{X}}_F^{\mathrm{ref}} \\ \boldsymbol{F}_X^{\mathrm{ref}} \end{bmatrix} = \begin{bmatrix} \boldsymbol{I} & -\boldsymbol{M}_{\mathrm{FX}n} \\ \boldsymbol{0} & -\boldsymbol{M}_{\mathrm{XX}n} \end{bmatrix} \begin{bmatrix} \boldsymbol{F}_F^{\mathrm{ref}} \\ \ddot{\boldsymbol{X}}_X^{\mathrm{ref}} \end{bmatrix} \tag{4.37}$$

$$\begin{bmatrix} \ddot{\boldsymbol{X}}_F^{\mathrm{ref}} \\ \boldsymbol{F}_X^{\mathrm{ref}} \end{bmatrix} = \boldsymbol{H} \begin{bmatrix} \boldsymbol{F}_F^{\mathrm{ref}} \\ \ddot{\boldsymbol{X}}_X^{\mathrm{ref}} \end{bmatrix} = \begin{bmatrix} \boldsymbol{H}_{11} & \boldsymbol{H}_{12} \\ \boldsymbol{H}_{21} & \boldsymbol{H}_{22} \end{bmatrix} \begin{bmatrix} \boldsymbol{F}_F^{\mathrm{ref}} \\ \ddot{\boldsymbol{X}}_X^{\mathrm{ref}} \end{bmatrix} \tag{4.38}$$

where $\boldsymbol{H}$ is a hybrid matrix [79, 80]

$$\boldsymbol{H} = \begin{bmatrix} \boldsymbol{M}_{\mathrm{FF}n}^{-1} & \boldsymbol{M}_{\mathrm{FF}n}^{-1}\boldsymbol{M}_{\mathrm{FX}n} \\ \boldsymbol{M}_{\mathrm{XF}n}\boldsymbol{M}_{\mathrm{FF}n}^{-1} & \boldsymbol{M}_{\mathrm{XX}n} - \boldsymbol{M}_{\mathrm{XF}n}\boldsymbol{M}_{\mathrm{FF}n}^{-1}\boldsymbol{M}_{\mathrm{FX}n} \end{bmatrix}. \tag{4.39}$$

The force references are refined as follows:

$$\boldsymbol{F}_{\mathrm{hyb}}^{\mathrm{ref}} = \begin{bmatrix} \boldsymbol{F}_F^{\mathrm{ref}} \\ \boldsymbol{F}_X^{\mathrm{ref}} \end{bmatrix} = (\boldsymbol{I} - \boldsymbol{S}) \begin{bmatrix} \boldsymbol{F}_F^{\mathrm{ref}} \\ \boldsymbol{0} \end{bmatrix} + \boldsymbol{S}\boldsymbol{H} \begin{bmatrix} \boldsymbol{F}_F^{\mathrm{ref}} \\ \ddot{\boldsymbol{X}}_X^{\mathrm{ref}} \end{bmatrix} \tag{4.40}$$

$$\boldsymbol{S}\boldsymbol{H} = \begin{bmatrix} \boldsymbol{0} & \boldsymbol{0} \\ \boldsymbol{0} & \boldsymbol{I} \end{bmatrix} \boldsymbol{H} = \begin{bmatrix} \boldsymbol{0} & \boldsymbol{0} \\ \boldsymbol{H}_{21} & \boldsymbol{H}_{22} \end{bmatrix} \tag{4.41}$$

where $\boldsymbol{S}$ is a selection matrix. From (4.32) and (4.40), the dynamics of the hybrid control system are described as

$$\boldsymbol{M}_{\mathrm{FF}n}\ddot{\boldsymbol{X}}_F^{\mathrm{res}} + \boldsymbol{M}_{\mathrm{FX}n}\ddot{\boldsymbol{X}}_X^{\mathrm{res}} = \boldsymbol{F}_F^{\mathrm{ref}} \tag{4.42}$$

$$\boldsymbol{M}_{\mathrm{XF}n}\ddot{\boldsymbol{X}}_F^{\mathrm{res}} + \boldsymbol{M}_{\mathrm{XX}n}\ddot{\boldsymbol{X}}_X^{\mathrm{res}} = \boldsymbol{F}_X^{\mathrm{ref}}. \tag{4.43}$$

Here, the remaining disturbances through the high-pass filters are neglected for simplicity. By substituting (4.42) for $\boldsymbol{F}_X^{\mathrm{ref}}$ in (4.40), the motion equation of the position control system (4.43) is rewritten as

$$\boldsymbol{F}_X^{\mathrm{ref}} = \boldsymbol{H}_{21}\boldsymbol{F}_F^{\mathrm{ref}} + \boldsymbol{H}_{22}\ddot{\boldsymbol{X}}_X^{\mathrm{ref}} \tag{4.44}$$

$$= \boldsymbol{M}_{\mathrm{XFn}}\ddot{\boldsymbol{X}}_F^{\mathrm{res}} + \boldsymbol{M}_{\mathrm{XFn}}\boldsymbol{M}_{\mathrm{FF}n}^{-1}\boldsymbol{M}_{\mathrm{FXn}}\ddot{\boldsymbol{X}}_X^{\mathrm{res}} + \boldsymbol{H}_{22}\ddot{\boldsymbol{X}}_X^{\mathrm{ref}} \tag{4.45}$$

$$= \boldsymbol{M}_{\mathrm{XFn}}\ddot{\boldsymbol{X}}_F^{\mathrm{res}} + \boldsymbol{M}_{\mathrm{XXn}}\ddot{\boldsymbol{X}}_X^{\mathrm{res}} \tag{4.46}$$

$$\boldsymbol{H}_{22}\ddot{\boldsymbol{X}}_X^{\mathrm{ref}} = \boldsymbol{H}_{22}\ddot{\boldsymbol{X}}_X^{\mathrm{res}}. \tag{4.47}$$

From (4.47), the realization of decoupling control in respect to the position control system can be confirmed, as follows:

$$\ddot{\boldsymbol{X}}_X^{\mathrm{res}} = \ddot{\boldsymbol{X}}_X^{\mathrm{ref}}. \tag{4.48}$$

The overall dynamics of the hybrid control system based on the hybrid matrix are obtained as

$$\boldsymbol{M}_{\mathrm{hyb}}\ddot{\boldsymbol{X}}^{\mathrm{res}} = \boldsymbol{M}_{\mathrm{hyb}}\left[\ddot{\boldsymbol{X}}_F^{\mathrm{res}}\ \ddot{\boldsymbol{X}}_X^{\mathrm{res}}\right]^T = \left[\boldsymbol{F}_F^{\mathrm{ref}}\ \ddot{\boldsymbol{X}}_X^{\mathrm{ref}}\right]^T \tag{4.49}$$

$$\boldsymbol{M}_{\mathrm{hyb}} = \begin{bmatrix} \boldsymbol{M}_{\mathrm{FF}n} & \boldsymbol{M}_{\mathrm{FX}n} \\ \boldsymbol{0} & \boldsymbol{I} \end{bmatrix} \tag{4.50}$$

where $\boldsymbol{M}_{\mathrm{hyb}}$ is the equivalent mass matrix of the hybrid control system based on the hybrid matrix. This matrix does not become a diagonal matrix. The appearance of a non-diagonal element can be attributed to the modification restricted to the position control system, as shown in (4.40). The force control system is affected by the position controller due to the presence of the non-diagonal element, as follows:

$$\begin{bmatrix} \ddot{\boldsymbol{X}}_F^{\mathrm{res}} \\ \ddot{\boldsymbol{X}}_X^{\mathrm{res}} \end{bmatrix} = \begin{bmatrix} \boldsymbol{M}_{\mathrm{FF}n}^{-1}\boldsymbol{F}_F^{\mathrm{ref}} - \boldsymbol{M}_{\mathrm{FF}n}^{-1}\boldsymbol{M}_{\mathrm{FX}n}\boldsymbol{C}_p(s)\boldsymbol{X}_X^{\mathrm{res}} \\ \ddot{\boldsymbol{X}}_X^{\mathrm{ref}} \end{bmatrix} \tag{4.51}$$

$$\boldsymbol{M}_{\mathrm{FF}n}^{-1}\boldsymbol{M}_{\mathrm{FX}n} = \left(\boldsymbol{M}_{mn} + \boldsymbol{M}_{sn}\right)^{-1}\left(\boldsymbol{M}_{sn} - \boldsymbol{M}_{mn}\right). \tag{4.52}$$

Eq. (4.51) means that interference in the force control direction is present as long as the non-diagonal elements of the equivalent mass matrix of the hybrid control system are not zeros. Additionally, as the difference in the masses of the master and slave systems increases, the effect of the interference term becomes more significant in the case of a bilateral control system. It is found that hybrid control based on the hybrid matrix is a combination of a force controller (in a force control system) and an acceleration controller (in a position control system).

4.3.2 Decoupling Control Based on MDOB [81]

To realize decoupling control in the modal space, the following disturbance is estimated by MDOB:

$$\boldsymbol{F}^{\mathrm{dis}} = \boldsymbol{F}_n^{\mathrm{ref}} - \boldsymbol{M}_{nn}s^2\boldsymbol{X}^{\mathrm{res}} \tag{4.53}$$

$$= \boldsymbol{\Delta}\boldsymbol{M}_n\ddot{\boldsymbol{X}}^{\mathrm{res}} + \boldsymbol{\Gamma}\boldsymbol{M}_W\dot{\boldsymbol{J}}_{\mathrm{aco}}\dot{\boldsymbol{q}}^{\mathrm{res}} - \boldsymbol{P}^{\mathrm{dis}} \tag{4.54}$$

$$\boldsymbol{P}^{\mathrm{dis}} = \boldsymbol{\Gamma}\boldsymbol{J}_{\mathrm{aco}}^{-T}\boldsymbol{p}^{\mathrm{dis}} \tag{4.55}$$

$$\boldsymbol{M}_{nn} = \begin{bmatrix} \boldsymbol{M}_{\mathrm{FF}nn} & \boldsymbol{0} \\ \boldsymbol{0} & \boldsymbol{M}_{\mathrm{XX}nn} \end{bmatrix}. \tag{4.56}$$

The first term in the right side of (4.54) is the inertia force caused by non-diagonal elements and variations from the nominal values of the equivalent mass matrix. This term gives rise to the interference. The second term on the right side of (4.54) is a disturbance term caused by the simplification of the inverse kinematics. The estimated disturbance term is added to the force reference in the modal space, as follows:

$$\boldsymbol{F}_n^{\mathrm{ref}} = \boldsymbol{F}^{\mathrm{ref}} + \hat{\boldsymbol{F}}^{\mathrm{dis}} = \boldsymbol{F}^{\mathrm{ref}} + \boldsymbol{G}_L^{\mathrm{dis}}(s)\boldsymbol{F}^{\mathrm{dis}} \tag{4.57}$$

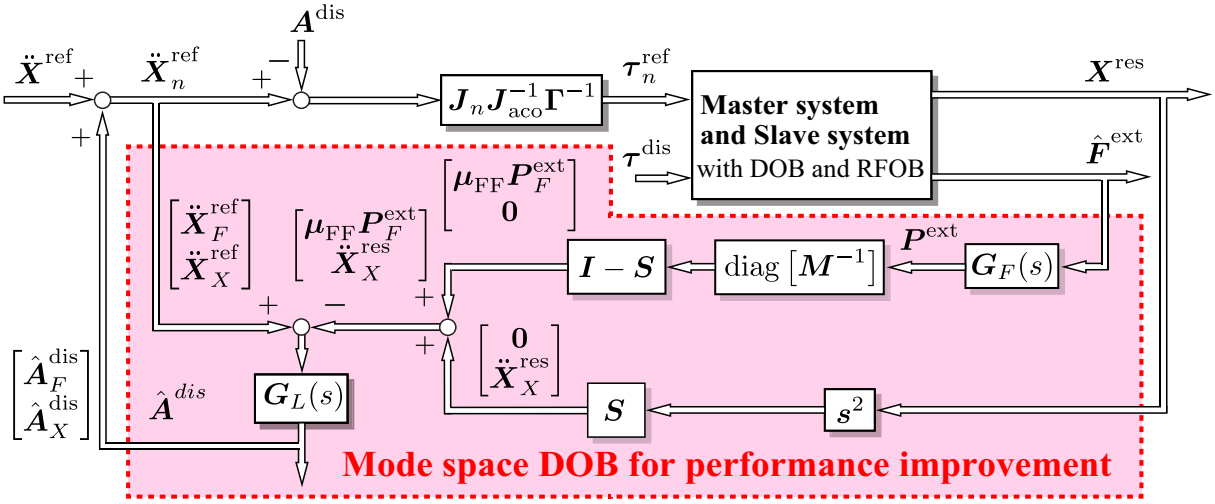

Fig. 4-2: Proposed mode space DOB in acceleration dimension.

where $\boldsymbol{G}_L^{\mathrm{dis}}(s)$ is a diagonal matrix with low-pass filters for suppressing noise effects in the MDOB. If the equivalent mass matrix is diagonalized (nominalized) and the cutoff frequency of $\boldsymbol{G}_L^{\mathrm{dis}}(s)$ is sufficiently high, force control and position control are decoupled as

$$\boldsymbol{M}_{nn}\ddot{\boldsymbol{X}}^{\mathrm{res}} = \boldsymbol{F}^{\mathrm{ref}} - \boldsymbol{G}_H^{\mathrm{dis}}(s)\boldsymbol{F}^{\mathrm{dis}} = \boldsymbol{F}^{\mathrm{ref}} - \boldsymbol{P}^{\mathrm{dis}\prime}. \tag{4.58}$$

In this case, all of the reference vectors are unified as force vectors. If the nominal mass matrix in the modal space $\boldsymbol{M}_{nn}$ is inserted in front of $\boldsymbol{F}^{\mathrm{ref}}$, the equivalent mass matrix is substituted for the arbitrary virtual mass matrix $\boldsymbol{M}_v$, as follows:

$$\boldsymbol{M}_{nn}\ddot{\boldsymbol{X}}^{\mathrm{res}} = \boldsymbol{M}_{nn}\boldsymbol{M}_v^{-1}\boldsymbol{F}^{\mathrm{ref}} - \boldsymbol{P}^{\mathrm{dis}\prime} \tag{4.59}$$

$$\boldsymbol{M}_v\ddot{\boldsymbol{X}}^{\mathrm{res}} = \boldsymbol{F}^{\mathrm{ref}} - \boldsymbol{M}_v\boldsymbol{M}_{nn}^{-1}\boldsymbol{P}^{\mathrm{dis}\prime}. \tag{4.60}$$

Decoupling control is realized when $\boldsymbol{M}_n$ and $\boldsymbol{M}_v$ are fixed to diagonal matrices. The efficacy of this method relative to the hybrid matrix based method is shown in [81]. However, it is known that the stability of the force controllers based on the workspace (modal space) observer depends on the configuration of the manipulators [21]. This fact implies that the system could become unstable when the system configuration experiences substantial fluctuations (as in bilateral control cases).

4.4 Proposed Hybrid Controller for Bilateral Control System

This section shows that the acceleration controller can be extended to the hybrid controller in the modal space and that the decoupling controller can be realized. Furthermore, a novel disturbance observer in the acceleration dimension for the performance improvement of the hybrid controller is proposed.

4.4.1 Acceleration controller in modal space

An acceleration controller based on a joint space DOB exhibits better performance than a force controller based on WDOB, except for a singular point [21]. Of course, an acceleration controller based on the joint space DOB can be extended to the modal space controller. The acceleration and torque (force) references in the joint space are given as

$$\ddot{\boldsymbol{q}}^{\mathrm{ref}} = \boldsymbol{J}_{\mathrm{aco}}^{-1}\boldsymbol{\Gamma}^{-1}\boldsymbol{M}_v^{-1}\boldsymbol{F}^{\mathrm{ref}} = \boldsymbol{J}_{\mathrm{aco}}^{-1}\boldsymbol{\Gamma}^{-1}\ddot{\boldsymbol{X}}^{\mathrm{ref}} \tag{4.61}$$

$$\boldsymbol{\tau}^{\mathrm{ref}} = \boldsymbol{J}_n\ddot{\boldsymbol{q}}^{\mathrm{ref}} \tag{4.62}$$

$$\boldsymbol{F}^{\mathrm{ref}} = \begin{bmatrix}\boldsymbol{F}_F^{\mathrm{ref}}\\ \boldsymbol{F}_X^{\mathrm{ref}}\end{bmatrix} = \begin{bmatrix}\boldsymbol{C}_f\left(\boldsymbol{F}_F^{\mathrm{cmd}} - \hat{\boldsymbol{F}}_F^{\mathrm{ext}}\right)\\ \boldsymbol{C}_p(s)\left(\boldsymbol{X}_X^{\mathrm{cmd}} - \boldsymbol{X}_X^{\mathrm{res}}\right) + \boldsymbol{M}_{vX}\ddot{\boldsymbol{X}}_X^{\mathrm{cmd}}\end{bmatrix}. \tag{4.63}$$

Unlike the force controllers described in Section III, the acceleration reference of the joint space is derived by using an inverse Jacobian matrix. The dynamics of the modal space are described as follows:

$$\boldsymbol{M}\ddot{\boldsymbol{X}}^{\mathrm{res}} = \boldsymbol{\Gamma}\boldsymbol{J}_{\mathrm{aco}}^{-T}\boldsymbol{\tau}^{\mathrm{ref}} + \boldsymbol{\Gamma}\boldsymbol{M}_W\dot{\boldsymbol{J}}_{\mathrm{aco}}\dot{\boldsymbol{q}}^{\mathrm{res}} - \boldsymbol{P}^{\mathrm{dis}} \tag{4.64}$$

$$= \boldsymbol{M}\boldsymbol{M}_v^{-1}\boldsymbol{F}^{\mathrm{ref}} + \boldsymbol{\Gamma}\boldsymbol{M}_W\dot{\boldsymbol{J}}_{\mathrm{aco}}\dot{\boldsymbol{q}}^{\mathrm{res}} - \boldsymbol{P}^{\mathrm{dis}} \tag{4.65}$$

$$\boldsymbol{M} = \boldsymbol{\Gamma}\boldsymbol{M}_W\boldsymbol{\Gamma}^{-1}. \tag{4.66}$$

Because the equivalent mass matrix of modal space $\boldsymbol{M}$ is inserted as a forward gain matrix in front of the acceleration reference, the effect of the non-diagonal elements is canceled. As a result, the equivalent matrix is replaced by a virtual mass matrix in modal space $\boldsymbol{M}_v$. Fundamentally, decoupling control is realized by setting $\boldsymbol{M}_v$ as a diagonal matrix, as follows:

$$\boldsymbol{M}_v\ddot{\boldsymbol{X}}^{\mathrm{res}} = \boldsymbol{F}^{\mathrm{ref}} + \boldsymbol{M}_v(\boldsymbol{\Gamma}\dot{\boldsymbol{J}}_{\mathrm{aco}}\dot{\boldsymbol{q}}^{\mathrm{res}} - \boldsymbol{M}^{-1}\boldsymbol{P}^{\mathrm{dis}}) \tag{4.67}$$

$$\begin{bmatrix}\boldsymbol{M}_{vF}\ddot{\boldsymbol{X}}_F^{\mathrm{res}}\\ \boldsymbol{M}_{vX}\ddot{\boldsymbol{X}}_X^{\mathrm{res}}\end{bmatrix} = \begin{bmatrix}\boldsymbol{C}_f\left(\boldsymbol{F}_F^{\mathrm{cmd}} - \hat{\boldsymbol{F}}_F^{\mathrm{ext}}\right)\\ \boldsymbol{C}_p(s)\left(\boldsymbol{X}_X^{\mathrm{cmd}} - \boldsymbol{X}_X^{\mathrm{res}}\right) + \boldsymbol{M}_{vX}\ddot{\boldsymbol{X}}_X^{\mathrm{cmd}}\end{bmatrix} + \begin{bmatrix}\boldsymbol{M}_{vF} & \boldsymbol{0}\\ \boldsymbol{0} & \boldsymbol{M}_{vX}\end{bmatrix}(\boldsymbol{\Gamma}\dot{\boldsymbol{J}}_{\mathrm{aco}}\dot{\boldsymbol{q}}^{\mathrm{res}} - \boldsymbol{M}^{-1}\boldsymbol{P}^{\mathrm{dis}}). \tag{4.68}$$

However, this does not eliminate the effects of the disturbance term caused by the simplification of the inverse kinematics, and the equivalent disturbance through the high-pass filter as shown in the second term on the right side of (4.68). Furthermore, if we focus on the response of the external force, a kind of inertial force $\boldsymbol{C}_f^{-1}\boldsymbol{M}_{vF}\ddot{\boldsymbol{X}}_F^{\mathrm{res}}$ affects the response as follows:

$$\hat{\boldsymbol{F}}_F^{\mathrm{ext}} = \boldsymbol{F}_F^{\mathrm{cmd}} - \boldsymbol{C}_f^{-1}\boldsymbol{M}_{vF}\ddot{\boldsymbol{X}}_F^{\mathrm{res}} + \boldsymbol{C}_f^{-1}\boldsymbol{M}_{vF}\begin{bmatrix}\boldsymbol{I} & \boldsymbol{0}\end{bmatrix}\left(\boldsymbol{\Gamma}\dot{\boldsymbol{J}}_{\mathrm{aco}}\dot{\boldsymbol{q}}^{\mathrm{res}} - \boldsymbol{M}^{-1}\boldsymbol{P}^{\mathrm{dis}}\right). \tag{4.69}$$

In the case of the bilateral control, the inertial force in particular behaves as the operational force. If the force is large, the operator feels heaviness when the manipulator is moved. As a result, the transparency of the bilateral control is degraded.

4.4.2 A Novel Disturbance Observer in Acceleration Dimension for Performance Improvement

To reduce the effects of the remaining disturbance terms, a novel disturbance observer in the acceleration controller is proposed for performance improvement. The following disturbance in the acceleration dimension can be considered:

$$\begin{aligned}
\boldsymbol{A}_F^{\mathrm{dis}} &= \ddot{\boldsymbol{X}}_F^{\mathrm{res}} - \begin{bmatrix}\boldsymbol{I} & \boldsymbol{0}\end{bmatrix}\left(\boldsymbol{\Gamma}\dot{\boldsymbol{J}}_{\mathrm{aco}}\dot{\boldsymbol{q}}^{\mathrm{res}} - \boldsymbol{M}^{-1}\begin{bmatrix}\boldsymbol{P}_F^{\mathrm{load}}\\ \boldsymbol{P}_X^{\mathrm{dis}}\end{bmatrix}\right) && (4.70)\\
&= \boldsymbol{M}_{vF}^{-1}\boldsymbol{F}_F^{\mathrm{ref}} - \boldsymbol{\mu}_{\mathrm{FF}}\boldsymbol{P}_F^{\mathrm{ext}} && (4.71)\\
\boldsymbol{A}_X^{\mathrm{dis}} &= -\begin{bmatrix}\boldsymbol{0} & \boldsymbol{I}\end{bmatrix}\left(\boldsymbol{\Gamma}\dot{\boldsymbol{J}}_{\mathrm{aco}}\dot{\boldsymbol{q}}^{\mathrm{res}} - \boldsymbol{M}^{-1}\boldsymbol{P}^{\mathrm{dis}}\right) && (4.72)\\
&= \boldsymbol{M}_{Xv}^{-1}\boldsymbol{F}_X^{\mathrm{ref}} - \ddot{\boldsymbol{X}}_X^{\mathrm{res}} && (4.73)
\end{aligned}$$

where $\boldsymbol{\mu}$ represents the elements of the inverse matrix of the equivalent mass matrix in modal space $\boldsymbol{M}^{-1}$. The disturbances correspond to the remaining disturbances and the inertial force term in (4.69). This disturbance is not considered by conventional MDOBs, which are not able to eliminate this term. Unlike the conventional force controller based on MDOB, the decoupling control is fundamentally realized by the acceleration controller; the non-diagonal elements are not included in the disturbance in the acceleration dimension. Total disturbance in the modal space of the force and position control systems are described as follows:

$$\begin{aligned}
\boldsymbol{A}^{\mathrm{dis}} &= \begin{bmatrix}\boldsymbol{A}_F^{\mathrm{dis}}\\ \boldsymbol{A}_X^{\mathrm{dis}}\end{bmatrix} && (4.74)\\
&= (\boldsymbol{I}-\boldsymbol{S})\ddot{\boldsymbol{X}}^{\mathrm{res}} - \boldsymbol{\Gamma}\dot{\boldsymbol{J}}_{\mathrm{aco}}\dot{\boldsymbol{q}}^{\mathrm{res}} + \left[\boldsymbol{M}^{-1} - (\boldsymbol{I}-\boldsymbol{S})\,\mathrm{diag}\left[\boldsymbol{M}^{-1}\right]\right]\boldsymbol{P}^{\mathrm{dis}}\\
&\quad + (\boldsymbol{I}-\boldsymbol{S})\,\mathrm{diag}\left[\boldsymbol{M}^{-1}\right]\boldsymbol{P}^{\mathrm{load}}. && (4.75)
\end{aligned}$$

Although it is difficult to obtain information regarding the equivalent external force through the HPF $\boldsymbol{P}^{\mathrm{ext}}$ directory, the term can be calculated as follows:

$$\boldsymbol{P}^{\mathrm{ext}} = \boldsymbol{G}_H^{\mathrm{dis}}(s)\boldsymbol{F}^{\mathrm{ext}} = \boldsymbol{G}_H^{\mathrm{dis}}(s)\left[\boldsymbol{G}_L^{\mathrm{dis}}(s)\right]^{-1}\hat{\boldsymbol{F}}^{\mathrm{ext}}. \tag{4.76}$$

By using (4.71), (4.73) and (4.76), the disturbance $\boldsymbol{A}^{\mathrm{dis}}$ is calculated as

$$\begin{aligned}
\boldsymbol{A}^{\mathrm{dis}} &= \boldsymbol{M}_v^{-1}\boldsymbol{F}_n^{\mathrm{ref}} - \boldsymbol{S}\ddot{\boldsymbol{X}}^{\mathrm{res}} - (\boldsymbol{I}-\boldsymbol{S})\,\mathrm{diag}\left[\boldsymbol{M}^{-1}\right]\boldsymbol{P}^{\mathrm{ext}} && (4.77)\\
&= \ddot{\boldsymbol{X}}_n^{\mathrm{ref}} - \boldsymbol{S}\ddot{\boldsymbol{X}}^{\mathrm{res}} - (\boldsymbol{I}-\boldsymbol{S})\,\mathrm{diag}\left[\boldsymbol{M}^{-1}\right]\boldsymbol{G}_F(s)\hat{\boldsymbol{F}}^{\mathrm{ext}} && (4.78)\\
\boldsymbol{G}_F(s) &= \left[\boldsymbol{I}-\boldsymbol{G}_L^{\mathrm{dis}}(s)\right]\left[\boldsymbol{G}_L^{\mathrm{dis}}(s)\right] = \boldsymbol{G}_H^{\mathrm{dis}}(s)\left[\boldsymbol{G}_L^{\mathrm{dis}}(s)\right]^{-1}. && (4.79)
\end{aligned}$$

Here, $\mathrm{diag}\left[\boldsymbol{M}^{-1}\right]$ represents the diagonal elements of the inverse matrix of the equivalent mass matrix in the modal space. As shown in the above equations, the disturbance can be estimated using the reference value, the position response, and the estimated external force. The disturbance is estimated through LPF $\boldsymbol{G}_L^{\mathrm{dis}}(s)$ to reduce the noise effect as follows:

$$\hat{\boldsymbol{A}}^{\mathrm{dis}} = \boldsymbol{G}_L^{\mathrm{dis}}(s)\boldsymbol{A}^{\mathrm{dis}}. \tag{4.80}$$

The block diagram of the proposed mode space DOB in the acceleration dimension is shown as Fig. 4-2. The estimated term is added to the acceleration reference, as follows:

$$\ddot{\boldsymbol{X}}_n^{\mathrm{ref}} = \boldsymbol{M}_v^{-1}\boldsymbol{F}_n^{\mathrm{ref}} = \boldsymbol{M}_v^{-1}\left(\boldsymbol{F}^{\mathrm{ref}} + \boldsymbol{M}_v\hat{\boldsymbol{A}}^{\mathrm{dis}}\right). \tag{4.81}$$

By adding $\hat{\boldsymbol{A}}^{\mathrm{dis}}$, the motion equation of the modal space (4.67) can be rewritten as follows:

$$\begin{aligned}
\boldsymbol{S}\ddot{\boldsymbol{X}}^{\mathrm{res}} &= \boldsymbol{X}^{\mathrm{ref}} - \boldsymbol{G}_H(s)\boldsymbol{A}^{\mathrm{dis}} - (\boldsymbol{I}-\boldsymbol{S})\,\mathrm{diag}[\boldsymbol{M}^{-1}]\boldsymbol{P}^{\mathrm{ext}} && (4.82)\\
\begin{bmatrix}\boldsymbol{F}_F^{\mathrm{ext}}\\ \boldsymbol{X}_X^{\mathrm{res}}\end{bmatrix} &= \boldsymbol{\mathcal{A}}\begin{bmatrix}\boldsymbol{F}_F^{\mathrm{cmd}}\\ \boldsymbol{X}_X^{\mathrm{cmd}}\end{bmatrix} - \boldsymbol{\mathcal{C}}^{-1}\boldsymbol{G}_H(s)\boldsymbol{A}^{\mathrm{dis}} && (4.83)\\
\boldsymbol{\mathcal{A}} &= (\boldsymbol{I}-\boldsymbol{S})\left(\boldsymbol{C}_f\boldsymbol{G}_L^{\mathrm{dis}\prime}(s) + \mathrm{diag}[\boldsymbol{M}^{-1}]\boldsymbol{G}_H^{\mathrm{dis}\prime}(s)\right)^{-1}\boldsymbol{C}_f + \boldsymbol{S}\boldsymbol{I} && (4.84)\\
\boldsymbol{\mathcal{C}} &= (\boldsymbol{I}-\boldsymbol{S})\left(\boldsymbol{C}_f\boldsymbol{G}_L^{\mathrm{dis}\prime}(s) + \mathrm{diag}[\boldsymbol{M}^{-1}]\boldsymbol{G}_H^{\mathrm{dis}\prime}(s)\right) + \boldsymbol{S}\left(s^2\boldsymbol{I} + \boldsymbol{C}_p(s)\right) && (4.85)\\
\boldsymbol{G}_L^{\mathrm{dis}\prime}(s) &= \boldsymbol{\Gamma}\boldsymbol{J}_{\mathrm{aco}}^{-T}\boldsymbol{g}_L(s)\boldsymbol{J}_{\mathrm{aco}}^{T}\boldsymbol{\Gamma}^{-1} && (4.86)\\
\boldsymbol{G}_H^{\mathrm{dis}\prime}(s) &= \boldsymbol{\Gamma}\boldsymbol{J}_{\mathrm{aco}}^{-T}\boldsymbol{g}_H(s)\boldsymbol{J}_{\mathrm{aco}}^{T}\boldsymbol{\Gamma}^{-1}. && (4.87)
\end{aligned}$$

As a result of the compensation, the high-pass filter matrix $\boldsymbol{G}_H\mathrm{dis}(s)$ is inserted in front of the disturbance term $\boldsymbol{A}^{\mathrm{dis}}$ and the performance is improved relative to (4.67).

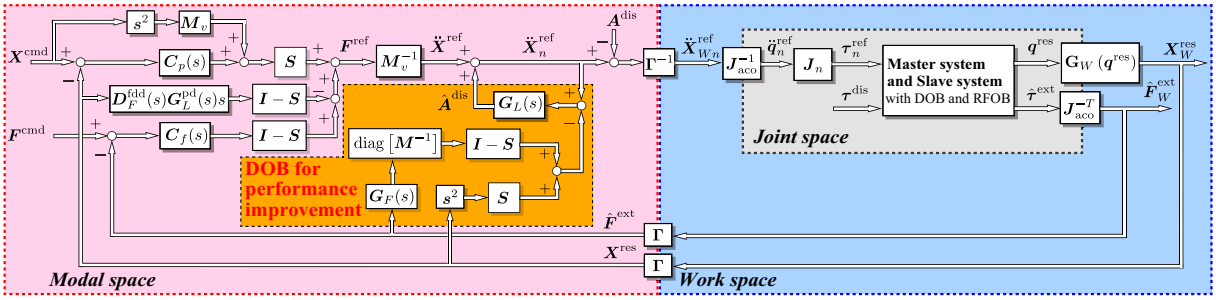

Fig. 4-3: Block diagram of the proposed method.

4.4.3 Modification of Force Control Reference

In order to enhance the stability of the force control system in the proposed method, the force control reference $\boldsymbol{F}_F^{\mathrm{ref}}$ in (4.63) is modified as follows:

$$\boldsymbol{F}_F^{\mathrm{ref}} = \boldsymbol{C}_f(s)\left(\boldsymbol{F}_F^{\mathrm{cmd}} - \hat{\boldsymbol{F}}_F^{\mathrm{ext}}\right) - \boldsymbol{D}_F^{\mathrm{fdd}}(s)\boldsymbol{G}_L^{\mathrm{pd}}(s)\dot{\boldsymbol{X}}_F^{\mathrm{res}} \tag{4.88}$$

$$\boldsymbol{C}_f(s) = \boldsymbol{C}_f\boldsymbol{G}^{\mathrm{phl}}(s) = \boldsymbol{K}_f\mathrm{diag}\left[\frac{\alpha s + g^{\mathrm{phl}}}{s + g^{\mathrm{phl}}}\right] \tag{4.89}$$

$$\boldsymbol{D}_F^{\mathrm{fdd}}(s) = \boldsymbol{d}_F\boldsymbol{G}_H^{\mathrm{fdd}}(s) = \boldsymbol{d}_F\mathrm{diag}\left[\frac{s}{s + g^{\mathrm{fdd}}}\right] \tag{4.90}$$

where $\boldsymbol{G}^{\mathrm{phl}}(s)$ is a phase lead compensator ($\alpha > 1$), and $\boldsymbol{D}_F^{\mathrm{fdd}}(s)$ and $\boldsymbol{d}_F$ represent a frequency domain damping (FDD) [27,28] and its damping coefficient, respectively. The FDD improves the stability of the force control system in the higher frequency domain. This is especially effective in contact motions. On the other hand, the damping effect has a small influence on the operationality [26] because the damping effect does not become active in the lower frequency domain.

Fig. 4-24 shows a block diagram of the proposed method.

4.5 Comparison Analysis

This section presents an analysis of the performance and stability of the proposed and conventional methods. The parameters used in the analysis are listed in Table 4.1. The parameters of the analysis are commonly used in the conventional methods and the proposed method.

Table 4.1: Parameters for analysis of bilateral control systems.

Parameters	Descriptions	Value
M_{mn}	mass of actuator	3.8 kg
M_{sn}	mass of actuator	0.228 kg
K_f	force control gain	0.6
K_p	position gain	1100
K_v	velocity gain	99.5
g	bandwidth of DOB and RFOB	300 rad/s
g_{M_d}	bandwidth of DOBs in mode space	64.2 rad/s
g^{phl}	pole of phase compensator	130rad/s
α	parameter of phase compensator	3
g^{fdd}	bandwidth of FDD	250 rad/s
d_F	damping coefficient of FDD	80
$Z_e(s)$	environmental impedance	3000+30s

4.5.1 Performance Comparison

Comparison based on operationality and reproducibility

The performance of the proposed method is compared to that of the conventional methods from the view point of the reproducibility and the operationality [26]. The relationship between the position and force on the master side is given by

$$F_m^{\mathrm{ext}} = P_o(s)X_m^{\mathrm{res}} + P_r(s)Z_e(s)X_m^{\mathrm{res}} \tag{4.91}$$

$$F_s^{\mathrm{ext}} = Z_e X_s^{\mathrm{res}}. \tag{4.92}$$

Reproducibility $P_r(s)$ represents the degree of reproduction of the environmental impedance on the master side. On the other hand, the operationality $P_o(s)$ represents the force required to operate the master device. The ideal $P_r(s)$ and $P_o(s)$ are equal to one and zero, respectively. Based on (4.51), (4.60), (4.67) and (4.82), $P_o(s)$, and $P_r(s)$ are derived. For simplicity, only one direction is considered and any nonlinear terms are neglected.

Fig 4-4 compares the gain diagrams for $P_r(s)$ and $P_o(s)$ with respect to the proposed method, and a variance in the cutoff frequency of the proposed DOB g_{M_d} of 6.4 to 64 rad/s, with the conventional methods with increased position and force control gains. In the case of the hybrid matrix based method, $P_r(s)$ with a variance in the position gain K_p of 1100 to 1800 is shown in Fig. 4-4 (a). On the other hand, $P_o(s)$ with a variance in the force gain K_f of 0.5 to 1.2 is shown in Fig. 4-4 (b). These figures confirm

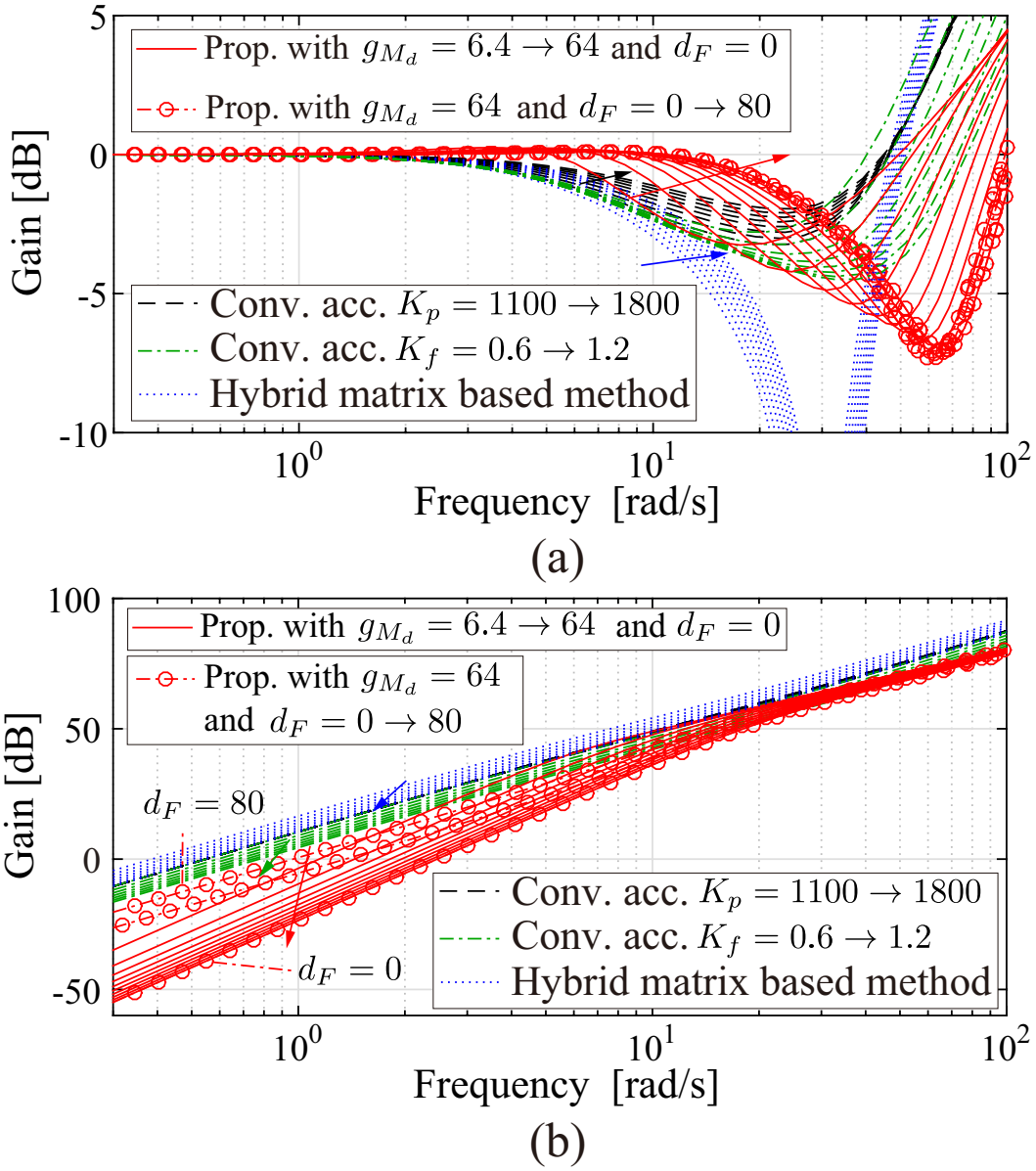

Fig. 4-4: Gain diagrams. (a) Reproducibility $P_r(s)$. (b) Operationality $P_o(s)$.

the performance improvement of the proposal relative to the increased position and force control gains in theses ranges. Additionally, the performance of the proposed method can be enhanced by increasing the value of g_{M_d}. As shown in 4-4 (a), it is found that the FDD has less influence on operationality. On the other hand, the larger d_F affects the operationality as shown in 4-4 (b). However, the proposed method shows better (smaller) operationality than conventional methods with the variation of d_f in this range. These results represent the fact that the proposal can improve the reproducibility and operationality while

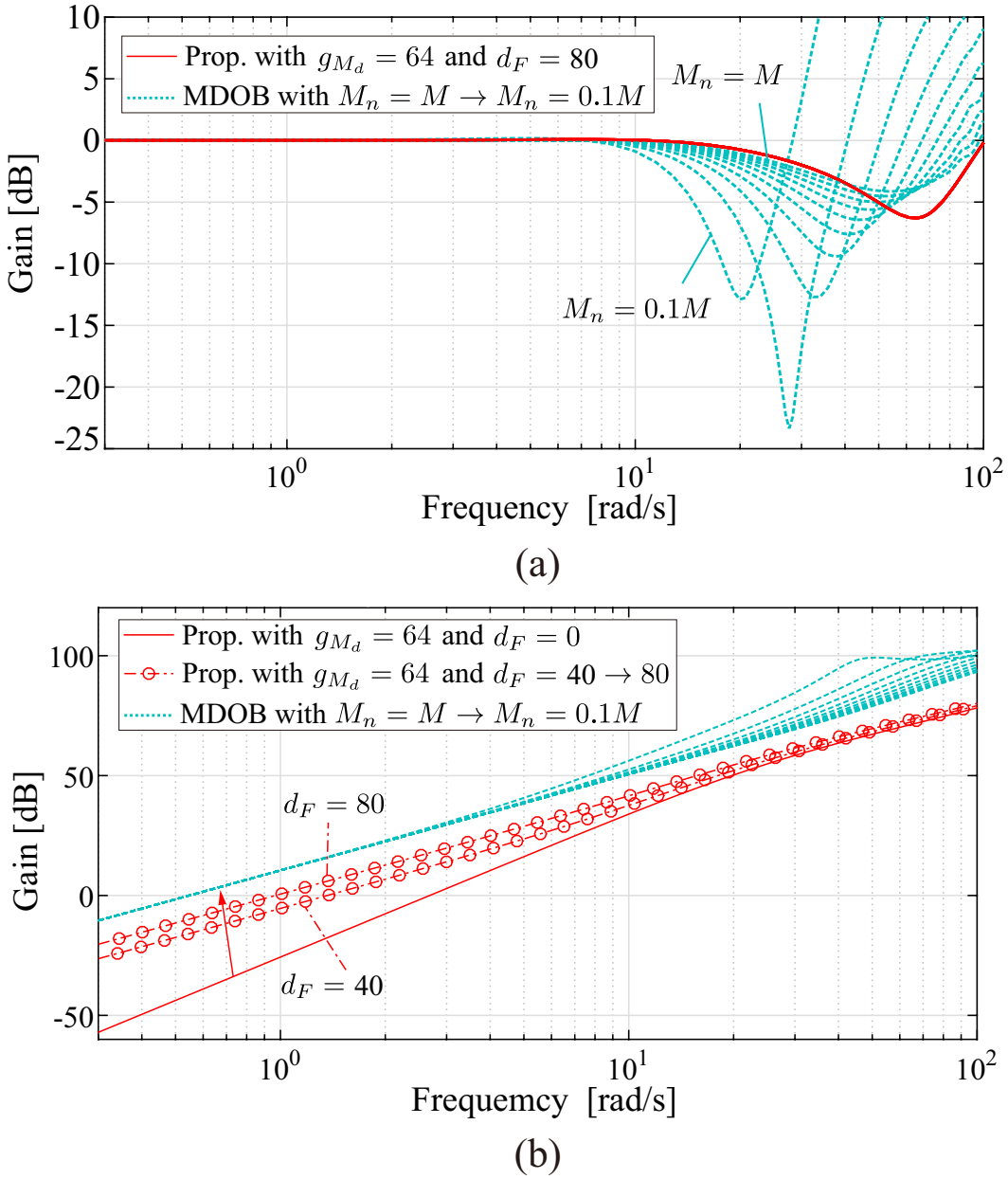

Fig. 4-5: Gain diagrams of the proposal and MDOB. (a) $P_r(s)$. (b) $P_o(s)$.

maintaining the stability by the FDD.

Fig. 4-5 compares the performance of the proposed method and the MDOB-based method. In this case, the nominal masses of the MDOB M_{Fn} and M_{Xn} are varied from 100 to 10% of the actual masses, M_F and M_X. This variance imitates the variation in the actual mass that depends on the manipulator configuration. With respect to $P_r(s)$, the performances of the MDOB-based method and the proposed

method are the same level if the nominal mass matrix is set to the actual value. However, the performance of the MDOB-based method is degraded in accordance with the variation in the nominal mass is the actual mass is large. On the other hand, $P_o(s)$ of the proposed method exhibits a higher level of performance than that of the MDOB-based method. This is mainly because the suppression of the inertial force in $\boldsymbol{A}^{dis}$.

Comparison with the Acceleration Observer [86]

Here, the proposed method is compared with the method based on the acceleration observer [86] because the method constructs the controller based on the joint space DOBs. The acceleration observer estimates the compensation value for the common modal space (force control) by using the estimated acceleration from master and slave sides, as follows:

$$\begin{aligned} \boldsymbol{A}_F^{\mathrm{cmp}} &= \boldsymbol{\Gamma}\boldsymbol{A}_W^{\mathrm{cmp}} = \boldsymbol{\Gamma}\begin{bmatrix}\boldsymbol{A}_m^{\mathrm{cmp}} & \boldsymbol{A}_s^{\mathrm{cmp}}\end{bmatrix}^T && (4.93)\\ &= \boldsymbol{G}_L(s)\left(\ddot{\boldsymbol{X}}_F^{\mathrm{ref}} - \boldsymbol{M}_{mn}^{-1}\boldsymbol{P}_m^{\mathrm{ext}} - \boldsymbol{M}_{sn}^{-1}\boldsymbol{P}_s^{\mathrm{ext}}\right) && (4.94)\\ &\neq \boldsymbol{G}_L(s)\left(\ddot{\boldsymbol{X}}_F^{\mathrm{ref}} - \boldsymbol{\mu}_{\mathrm{FF}}\boldsymbol{P}_F^{\mathrm{ext}}\right) = \hat{\boldsymbol{A}}_F^{\mathrm{dis}}. && (4.95)\end{aligned}$$

As shown in the above equations, the compensation value does not correspond to $\boldsymbol{A}^{\mathrm{dis}}$ as long as the mass matrices of the master and slave systems are different. The inappropriate compensation thus has the potential to affect the system performance.

4.5.2 Stability Analysis

The transfer function from the force to the position of the master side is obtained as

$$\frac{X_m^{\mathrm{res}}}{F_m^{\mathrm{ext}}} = \frac{1}{P_o(s) + P_r(s)Z_e(s)} = \frac{D(s)}{N_o(s) + N_r(s)Z_e(s)} \tag{4.96}$$

where $D(s)$, $N_r(s)$, and $N_o(s)$ represent the denominator and numerator of $P_r(s)$, as well as $P_o(s)$, respectively. Because $P_r(s)$ and $P_o(s)$ have the same part in denominator $D(s)$, the stability of the bilateral control is analyzed by using the characteristic equation $N_o(s) + N_r(s)Z_e(s) = 0$ [26]. Fig. 4-6 shows the displacements of the dominant poles of the proposed method and the conventional methods. Fig. 4-6 (a) shows the displacement with a variance in the mass M_{sn} of 3.8 to 0.1 kg. All of the poles related to the proposed method, conventional acceleration controller, and MDOB-based method exist in the left half plane. The hybrid control based on the hybrid matrix, however, has the potential to become

unstable if the difference in the mass between the master and slave systems is large, as indicated by the circles in the figure.

Fig. 4-6 (b) shows the pole displacements with a variance in the g_{M_d} from 6.4 to 64 rad/s with respect to the proposed and MDOB-based methods. Additionally, the pole displacements with a variance in the nominal mass of M_{Fn} and M_{Xn} relative to M_{Fn} of 100 to 10% of the actual masses M_F and M_X MDOB-based method. As indicated by the figure, the proposal will become unstable with increasing the g_{M_d} to obtain the better performance. It can be seen that there is a trade-off between the performance and stability improvement with respect to g_{M_d}. It is found that the inclusion of $G^{\mathrm{phl}}(s)$ shifts the poles in the stable direction compared with the proposed method excluding $G^{\mathrm{phl}}(s)$. If the variance in the actual mass from the nominal value is large, the MDOB-based method becomes unstable. Even if the bandwidth of the MDOB is set to a smaller value (16 rad/s), the system becomes unstable in accordance with the increase in the variance of the mass.

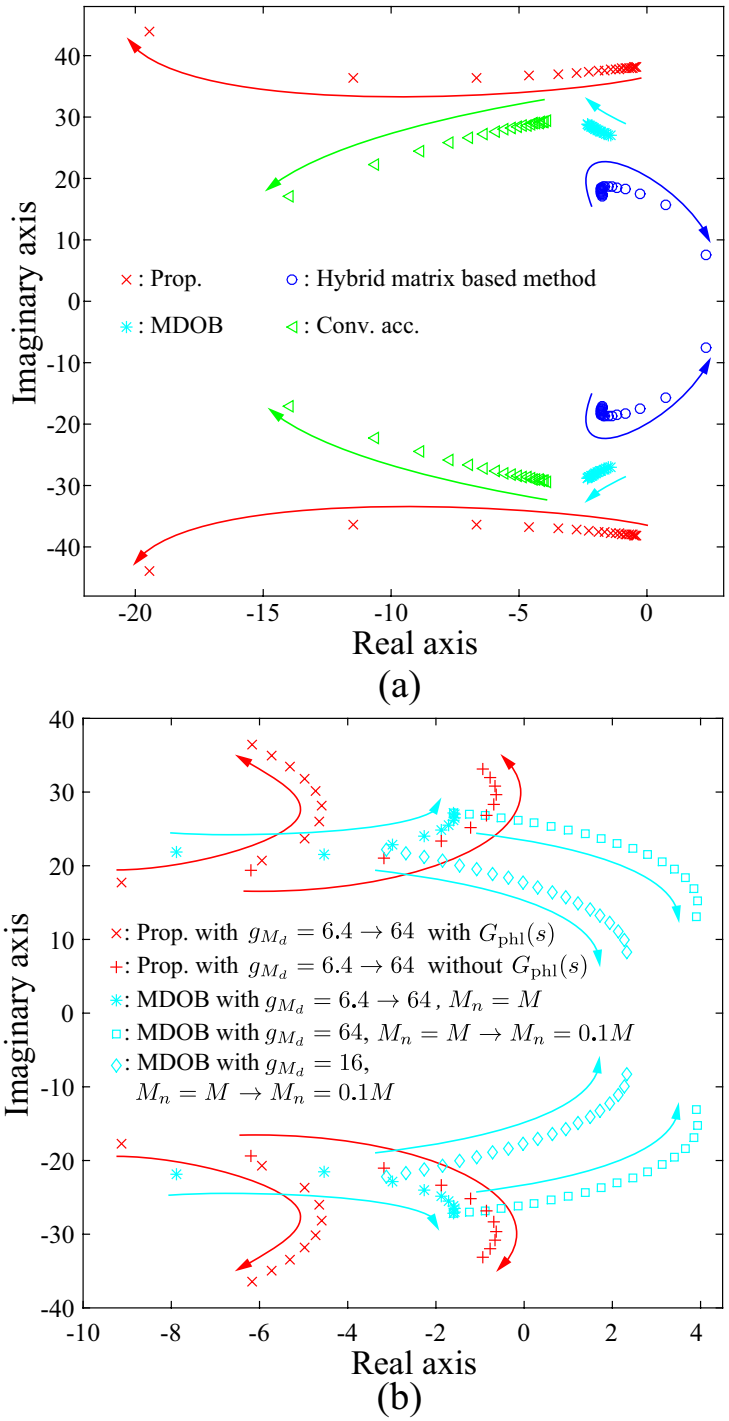

Fig. 4-6: Pole displacement. (a) Variation of mass. (b) Variation of g_{M_d} and nominal mass in MDOB based method.

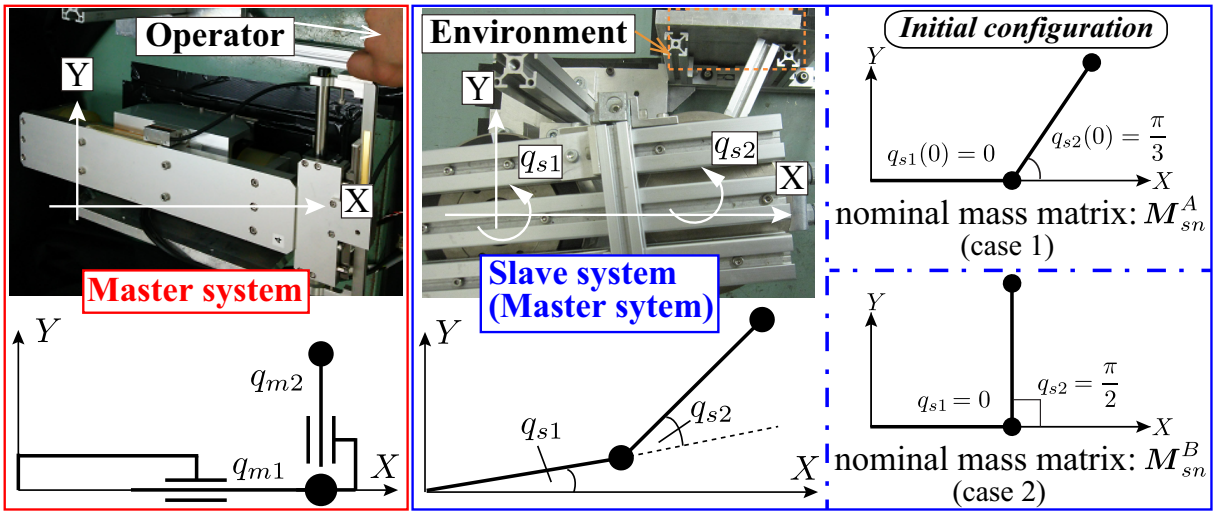

Fig. 4-7: Experimental system and models of MDOF manipulators.

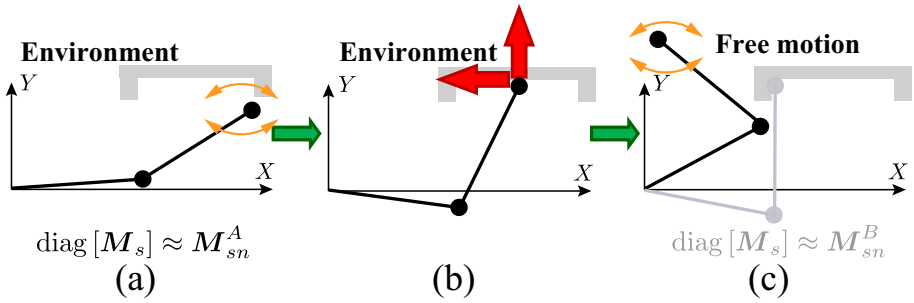

Fig. 4-8: Transition of experimental motions with identical structures. (a) Free motions around configuration A. (b) Contact motion. (c) Free motions far from configuration B.

4.6 Experiments of Bilateral Control with Identical Structure and Different Structure

4.6.1 Experimental Setup of MDOF Bilateral Control

To confirm the validity of the proposal, experiments using the bilateral control systems with identical structures and different structures were conducted. As a master system, a 2-DOF prismatic joint robot (X-Y plane) consisting of two linear motors was utilized. The slave system was a serial-link 2-DOF manipulator. Serial-link 2-DOF manipulators are used for the experiments of the bilateral control system with identical structures to confirm the influence of the variation of equivalent mass. As shown in Fig. 4-8, free motions around configuration A, contact motions, and free motions far from configuration B

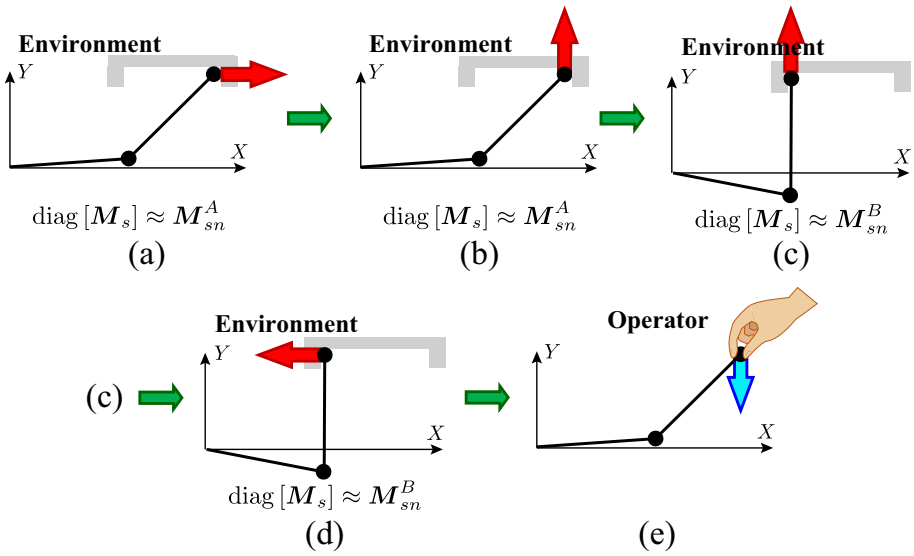

Fig. 4-9: Transition of experimental motions with different structures. (a) Contact in x direction around configuration A. (b) Contact in y direction around configuration A. (c) Contact in y direction around configuration B. (d) Contact in x direction around configuration B. (e) Contact to stator coil from slave side.

are performed. In the experiments with different structures, motions involving contact with an aluminum plate and frame were performed from the master side, and motions involving contact with a stator coil were performed from the slave side, were performed, as shown in Fig. 4-9. Additionally, experiments using a conventional acceleration controller, MDOB-based method and the proposed method were carried out, with only the free motions being performed. To confirm the effect of the value of the nominal mass, the diagonal elements of the nominal masses of the serial link 2-DOF manipulator were changed. We tested the following two cases, which relate to the configurations shown in Fig. 4-7, in the experiments relating to the hybrid matrix based method and the MDOB-based method.

1) Case 1: M_{xxn}^A = 2.23 kg, M_{yyn}^A = 3.40 kg (config. A)

2) Case 2: M_{xxn}^B = 0.41 kg, M_{yyn}^B = 3.11 kg (config. B).

To adjust the difference in the initial positions of the end effectors with different structure, a position control command is added as $\boldsymbol{X}_X^{\mathrm{cmd}} = -\boldsymbol{X}_{s0}$. Table 4.2 lists the experimental parameters for the identical structures. Table 4.3 lists the experimental parameters for the different structures. The other parameters used in the experiments with the different structures were the same as those used in the experiments for the identical structures, and are listed in Table 4.2. The parameters of the experiments are commonly used in the conventional methods and the proposed method. The other parameters were the same as those

Table 4.2: Experimental parameters with same structure

Parameter	Description	Value
T_s	sampling time	0.2 ms
$M^A_{\mathrm{xx}n}$	nominal mass of slave system in case 1	2.23 kg
$M^A_{\mathrm{yy}n}$	nominal mass of slave system in case 1	3.40 kg
$M^B_{\mathrm{xx}n}$	nominal mass of slave system in case 2	0.41 kg
$M^B_{\mathrm{yy}n}$	nominal mass of slave system in case 2	3.11 kg
J_n	inertia of rotary motor	2.88 gm^2
l	length of link	0.15 m
m_1	mass of link 1	2 kg
m_2	mass of link 2	0.1 kg
g_{M_d}	bandwidth of DOBs in mode space	19.3 rad/s
g^{phl}	pole of phase compensator	50rad/s
α	parameter of phase compensator	2
d_F	damping coefficient of FDD (x and y)	200
g^{fdd}	bandwidth of FDD (x and y)	50 rad/s
$q_1(0)$	initial angle of joint 1	0 rad
$q_2(0)$	initial angle of joint 2	π/3 rad

Table 4.3: Experimental parameters with different structure

Parameter	Description	Value
T_s	sampling time	0.2 ms
M_{mn1}	nominal mass of master system 1 (x)	3.8 kg
M_{mn2}	nominal mass of master system 2 (y)	0.3 kg
g_{Wx}	bandwidth of WDOB (x)	64 rad/s
g_{M_dx}	bandwidth of DOBs in mode space (x)	64 rad/s
g_{Wy}	bandwidth of WDOB (x)	32 rad/s
g_{M_dy}	bandwidth of DOBs in mode space (y)	32 rad/s
g_x^{phl}	pole of phase compensator (x)	130rad/s
g_y^{phl}	pole of phase compensator (y)	80rad/s
α_x, α_y	parameter of phase compensator (x and y)	3
d_{Fx} , d_{Fx}	damping coefficient of FDD (x and y)	80
g_x^{fdd}, g_y^{fdd}	bandwidth of FDD (x and y)	250 rad/s

used in the analysis, and are listed in Table 4.1.

4.6.2 Experimental Results for Identical Structures

Fig. 4-10 shows the experimental results of the bilateral control based on the MDOB with the identical structure. The position responses include an offset of 0.12 m. Fig. 4-10 (a) shows the position and force responses of the MDOB-based method in case 1. Here, the position control gain is reduced to $67s + 500$ because the higher gain ($99.5s + 1100$) is too oscillatory in nature to maintain the motions. As shown in the shaded area (A), where free motions are performed around configuration A, and shaded area (B), the system maintains stable motions. In shaded area (C) of Fig. 4-10 (a), however, unstable response results from variation of the equivalent mass because the configuration around the area is largely varied. As shown in Fig. 4-10 (b), the system oscillates and stable free/contact motion cannot be achieved in shaded areas (A) and (B), in which the configuration is far from configuration (B). Additionally, the oscillating responses are found in shaded area (C) of Fig. 4-10 (b) because of the variation in the mass from that of configuration (B). From these results, it is confirmed that the responses of the MDOB-based method become oscillatory and stable free/contact motions cannot be realized when the variation of the manipulator configuration is large (the variation of the mass from nominal value is large). On the other hand, the proposed method can achieve the free/contact motions with stability even if the variation of the manipulator configuration is large, as shown in Fig. 4-11.

The results indicate that the MDOB-based method is difficult to effectively apply for motions having wide working ranges. On the other hand, the proposed method can be applied to tasks for which the MDOB-based method cannot maintain stable motion.

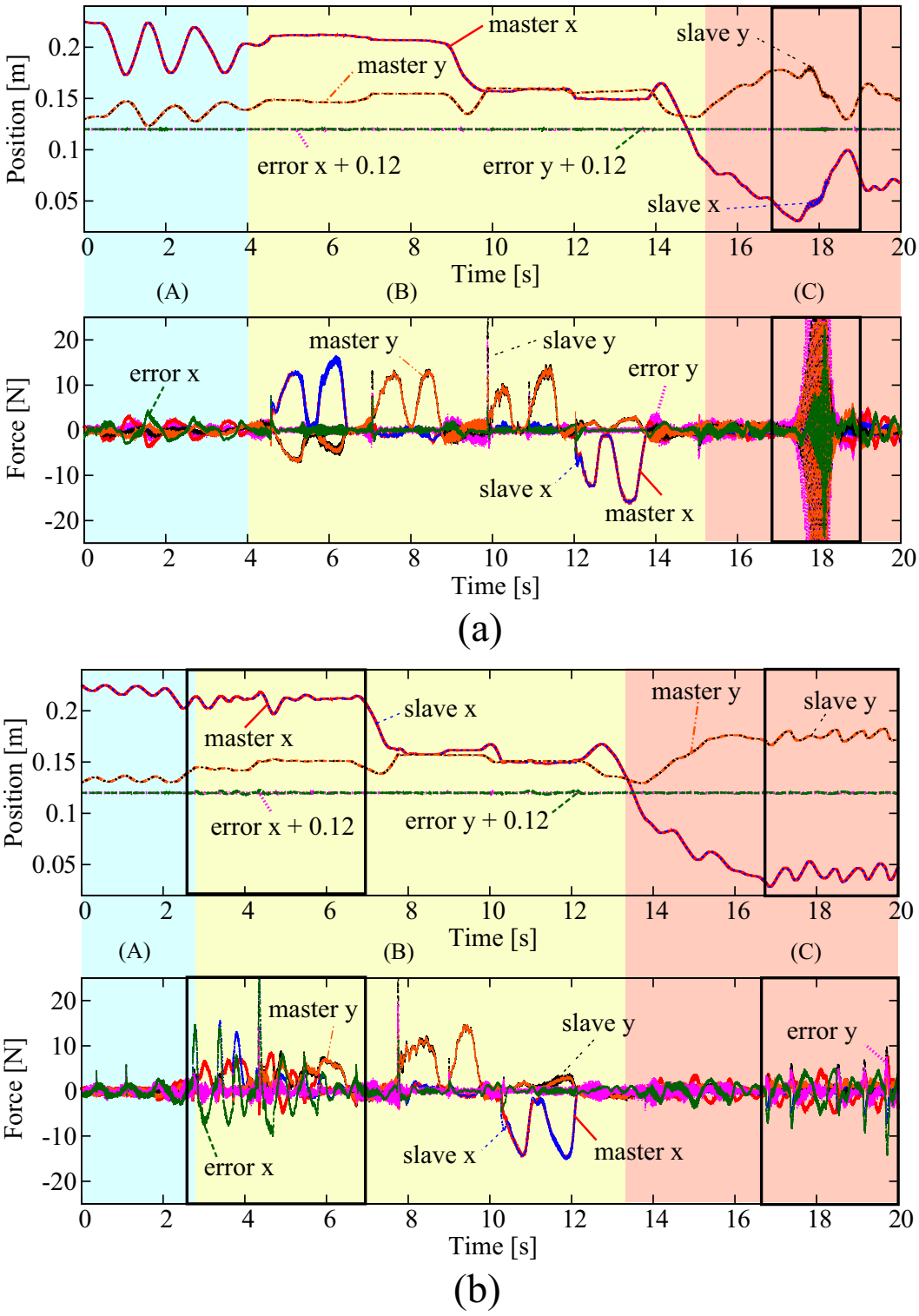

Fig. 4-10: Experimental results with identical structures. (a) MDOB in case 1. (b) MDOB in case 2.

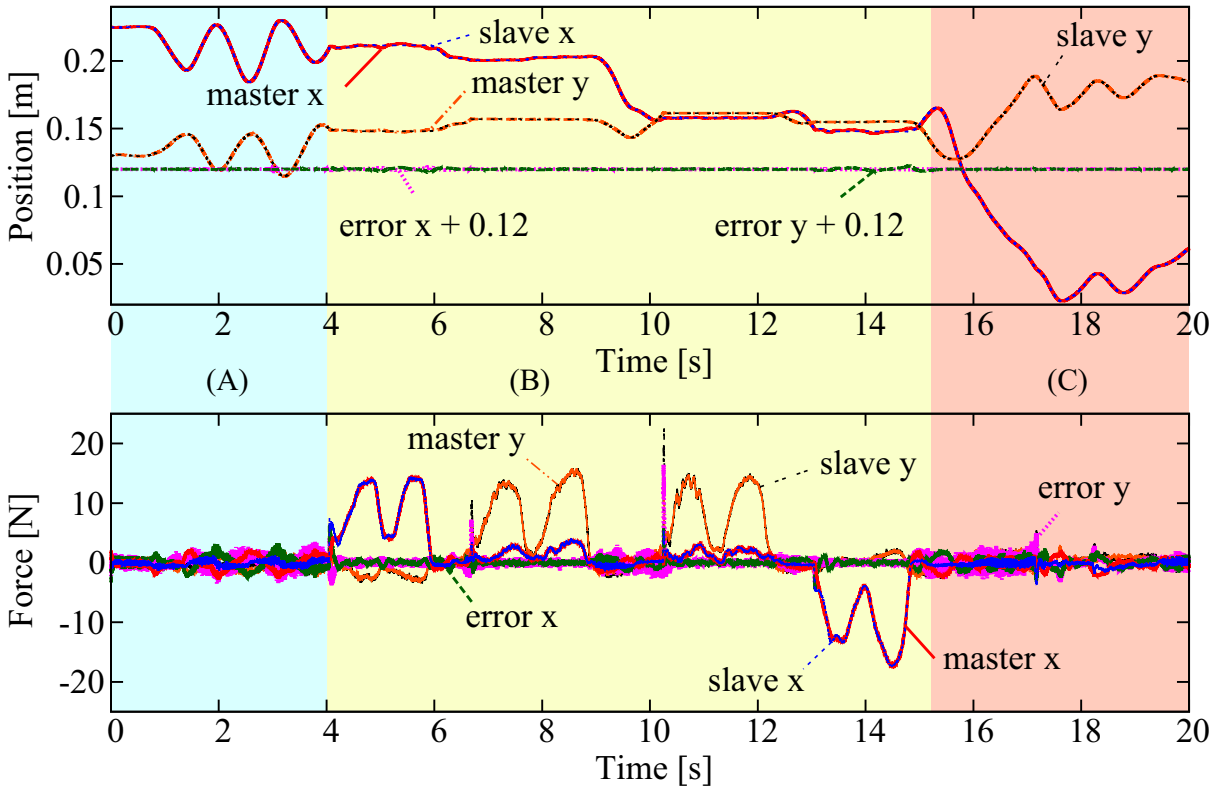

Fig. 4-11: Experimental results of the proposed method with identical structures.

4.6.3 Experimental Results for Different Structures

Force Controllers Based on the Hybrid Matrix and MDOB

Figs. 4-12 to 4-20 show the results of the bilateral control system experiments having different structures. The shaded areas (A), (B), (C), (D) and (E) correspond to the motions described in Figs. 4-9 (a), (b), (c), (d) and (e), respectively. The upper figures and lower figures correspond to the results of case 1 and the case 2, respectively. The responses of position include an offset of 0.12 m. Fig. 4-12 shows the results of the hybrid matrix-based method. The contact motions become oscillating because of the interference in the force control system as shown by (4.51). The contact motion in case 2 becomes more oscillatory as indicated by Fig. 4-12 (b) because the difference between the master and slave masses is larger than that of case 1 with regard to the x-axis as shown in Fig. 4-12 (a). This is because the interference term becomes larger with increasing difference in the masses. As a result, the interference in the contact motion given by (4.51) has a more profound effect. Additionally, the responses in (E) are more oscillatory than that of (B) and (C) with respect to the y-axis. This result indicates the bilateral control achieved using the hybrid matrix-based method does not have a symmetric property.

Figs. 4-13 and 4-14 show the results of the MDOB based-method with higher and lower position control gains, respectively. The responses in Fig. 4-13 are vibrating. As shown by the figures, the vibrational phenomena are reduced in Fig. 4-14 compared to Fig. 4-13, but still exist. With respect to case 1, the contact motions shown in (C) and (D) of Fig. 4-14 become more vibratory than (A) and (B) of Fig. 4-14 because the equivalent masses around (C) and (B) are varied from the nominal mass (configuration A). Similarly, the response (A) of Fig. 4-14 in case 2 is more vibratory than that of (D) in Fig. 4-14 because the nominal mass of around (D) is close to the equivalent mass. In all of these cases, stable contact motions are difficult to attain using the MDOB-based method.

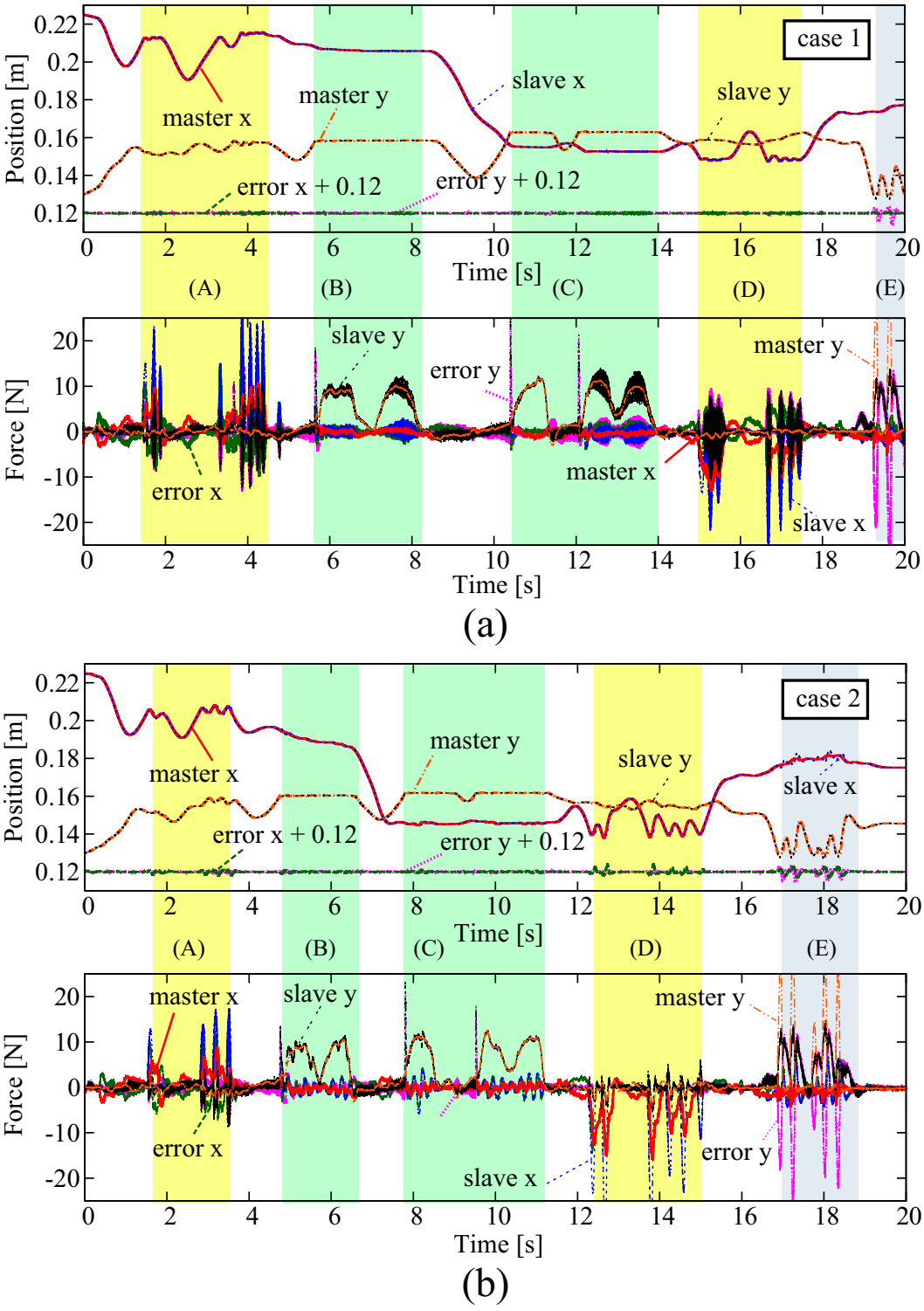

Fig. 4-12: Experimental results of the hybrid matrix based force controller. (a) Case 1. (b) Case 2.

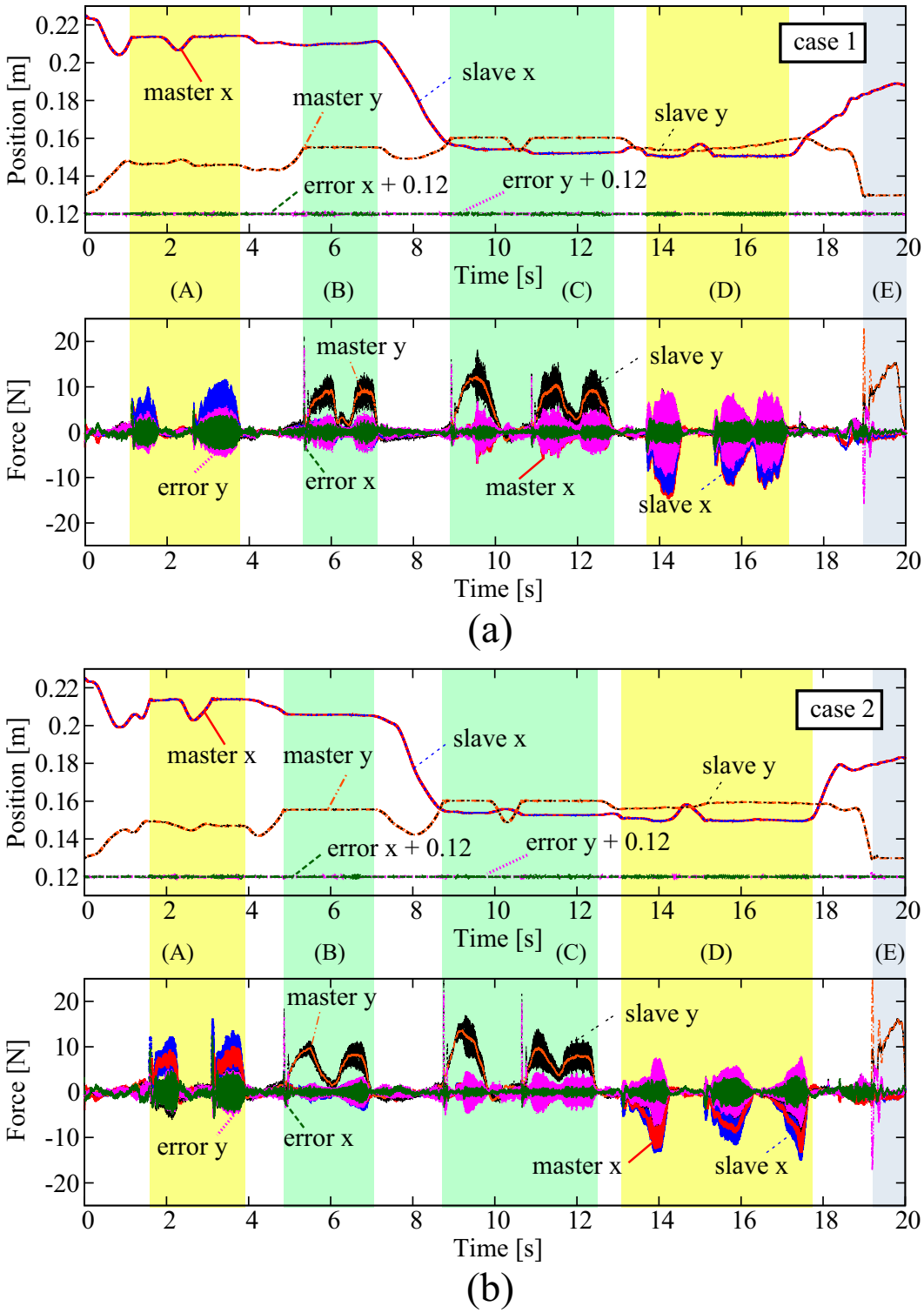

Fig. 4-13: Experimental results of MDOB based force controller with higher position control gain. (a) Case 1. (b) Case 2.

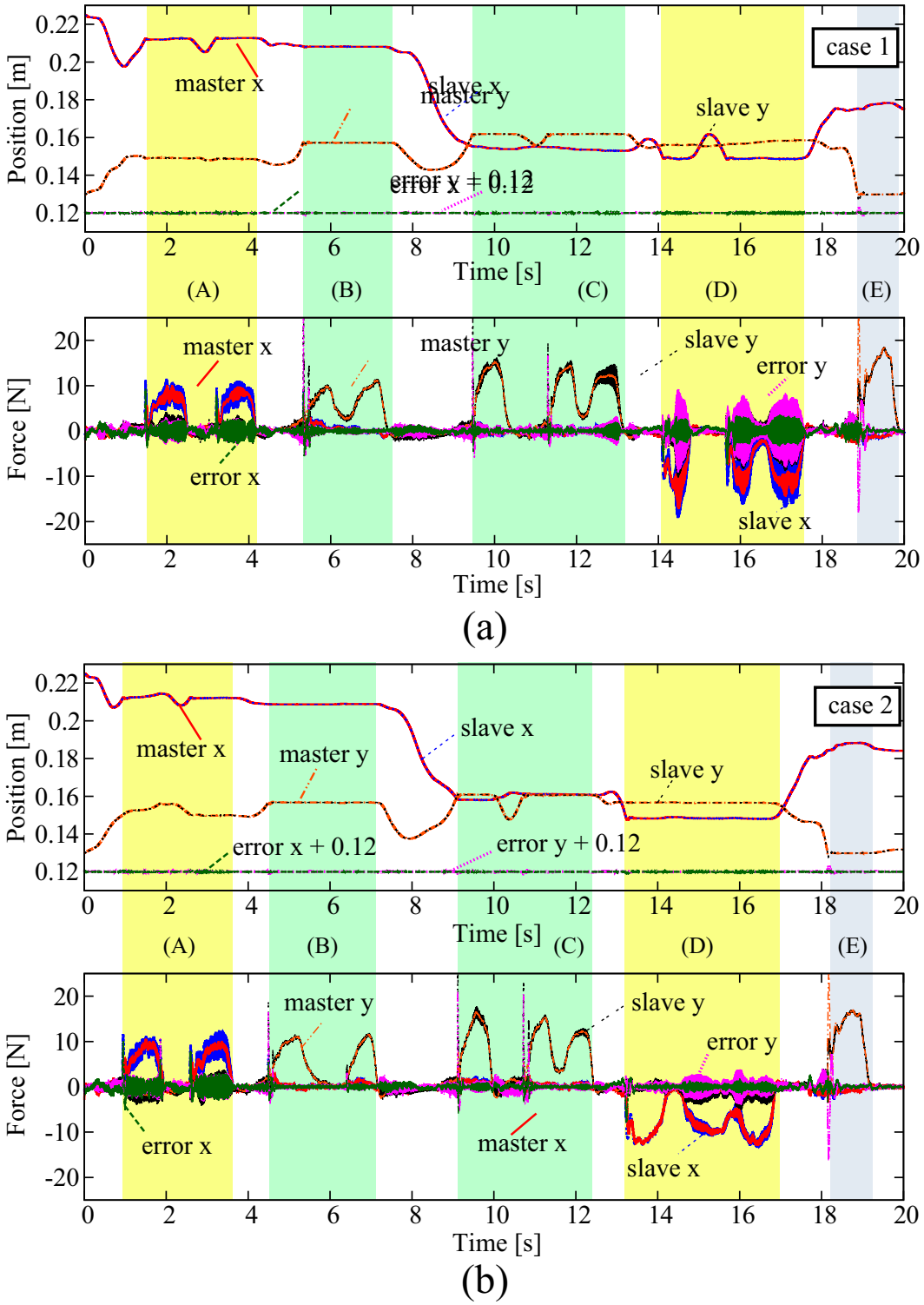

Fig. 4-14: Experimental results of MDOB based force controller with lower position control gain. (a) Case 1. (b) Case 2.

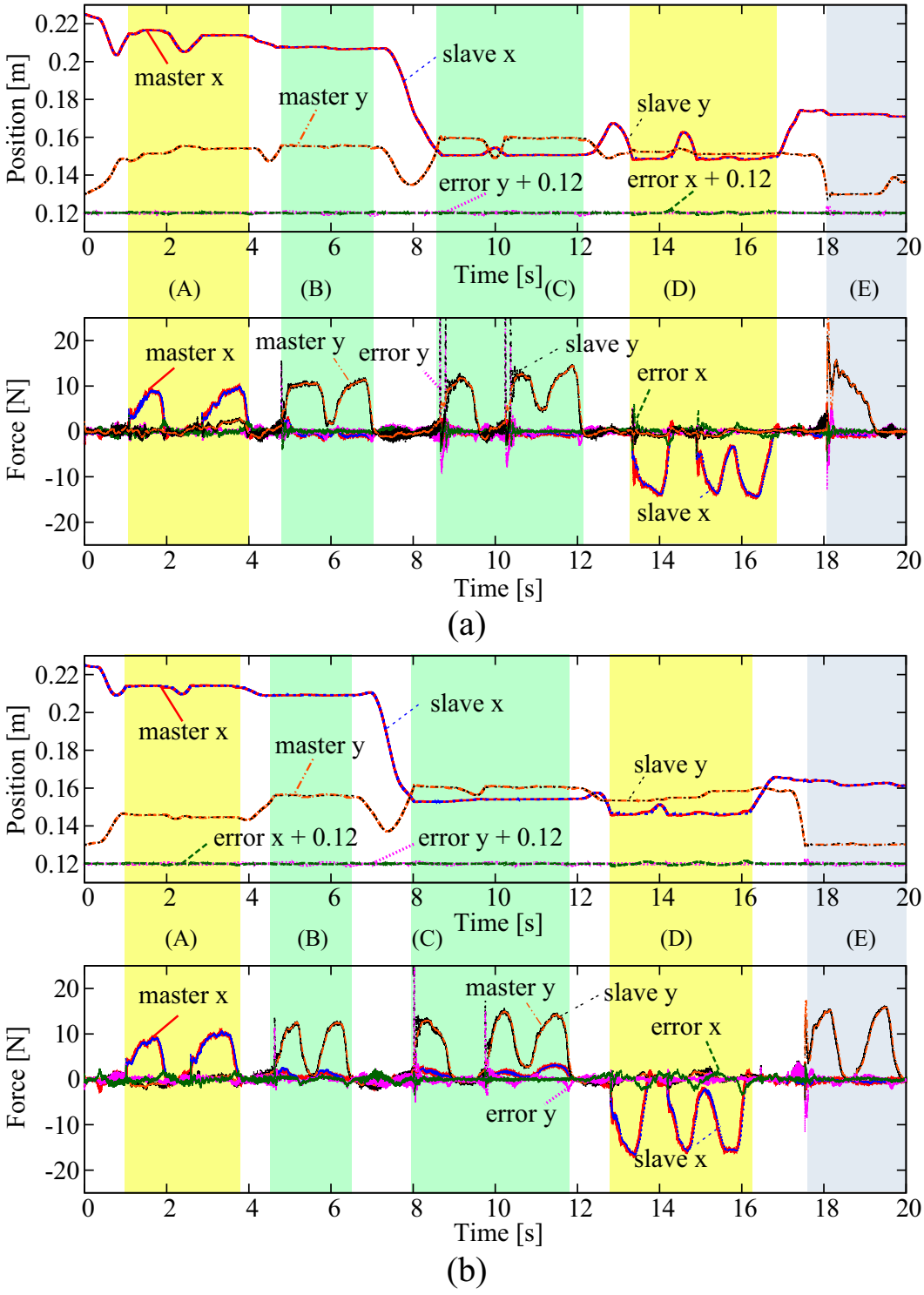

Fig. 4-15: Experimental results. (a) Acceleration observer. (b) Normal acceleration controller (conventional).

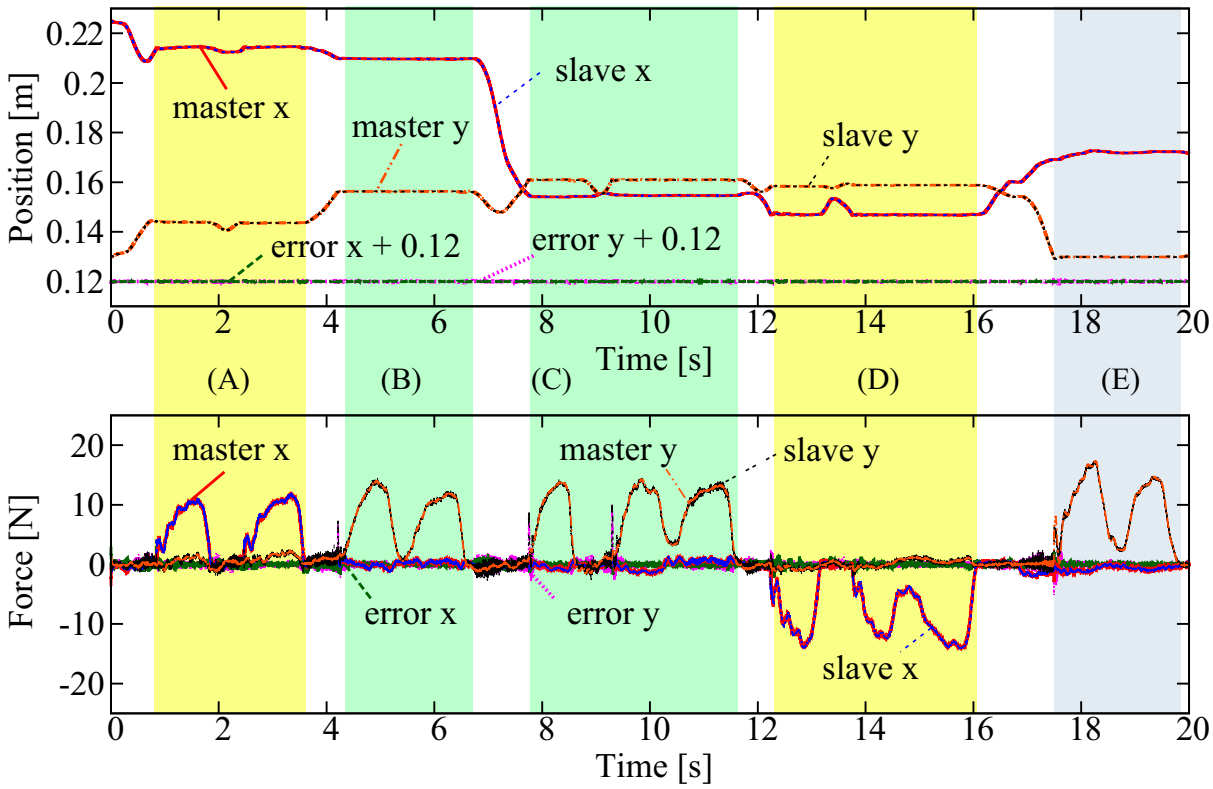

Fig. 4-16: Experimental result of the proposed method with the different structure.

Conventional Acceleration Controller and the Proposed Method

Figs. 4-15 (a) and (b) show the results of the experiments on the acceleration observer combining the FDD and normal acceleration controllers, respectively. Fig. 4-16 shows the results of the experiments using the proposed method. The oscillatory responses, which can be found in the results of hybrid matrix-based method, do not exist in the figures. These results confirm that the acceleration controller can also achieve decoupling control. Fig. 4-17 shows the force responses in the shaded areas (C) and (D). The left side of Fig. 4-17 shows the force responses of (D) with respect to the x-axis and the signs of the force responses are inverted. The right side of Fig. 4-17 shows the force responses of (C) with respect to the y-axis. If Figs. 4-15 (a) and (b) and (c) are compared, the response of the method based on the acceleration observer is relatively oscillatory in (C). The force response of the acceleration observer has an impulsive force in the beginning of the contact motion. This phenomenon is presumed to be the effect of neglect about modal space dynamics as shown in section 4.5.1. On the other hand, the proposed method can realize contact motions without such an impulsive force compared to the accelera-

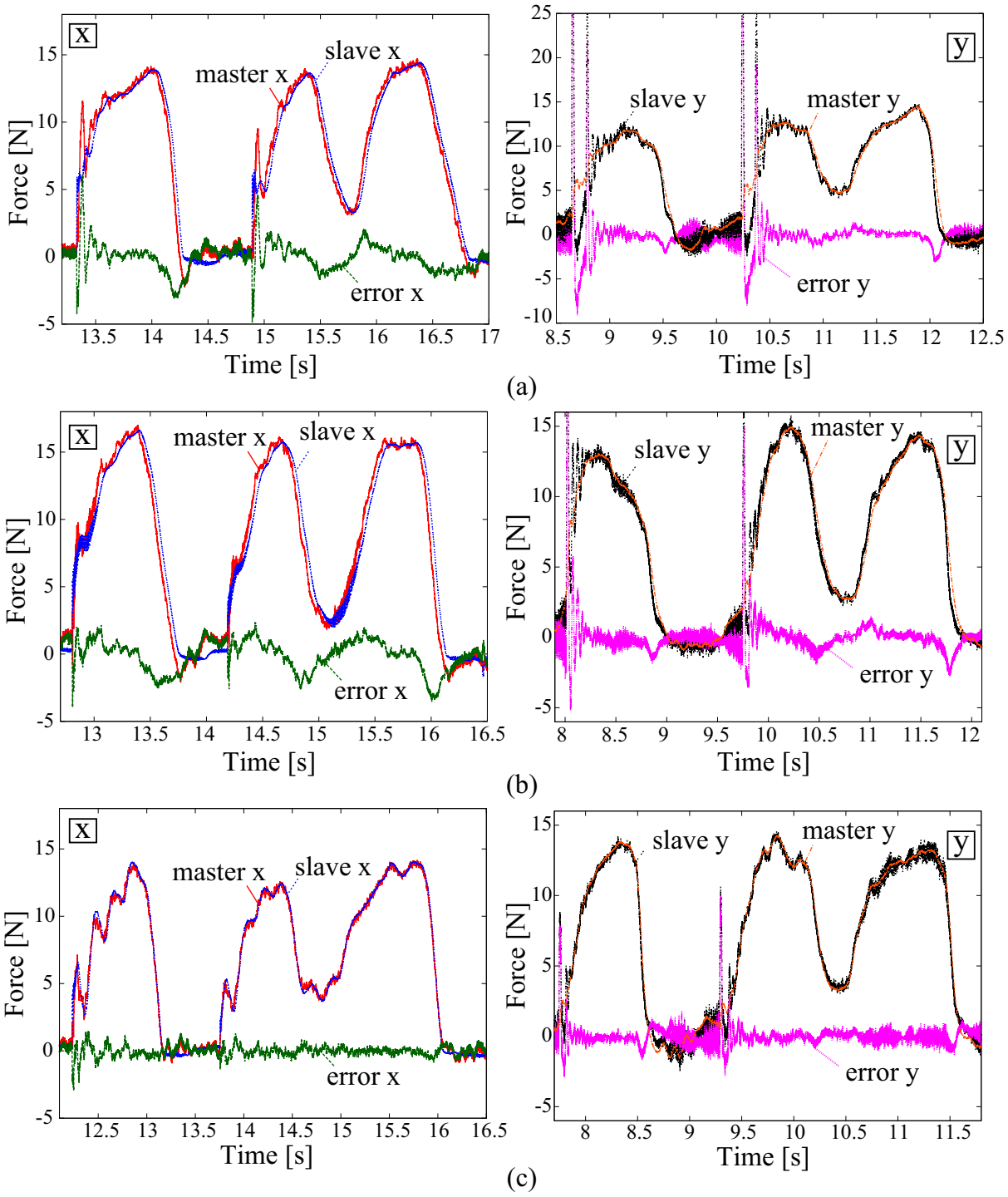

Fig. 4-17: Force responses in (C) and (D). (a) Acceleration observer. (b) Normal acceleration controller. (c) Proposed method.

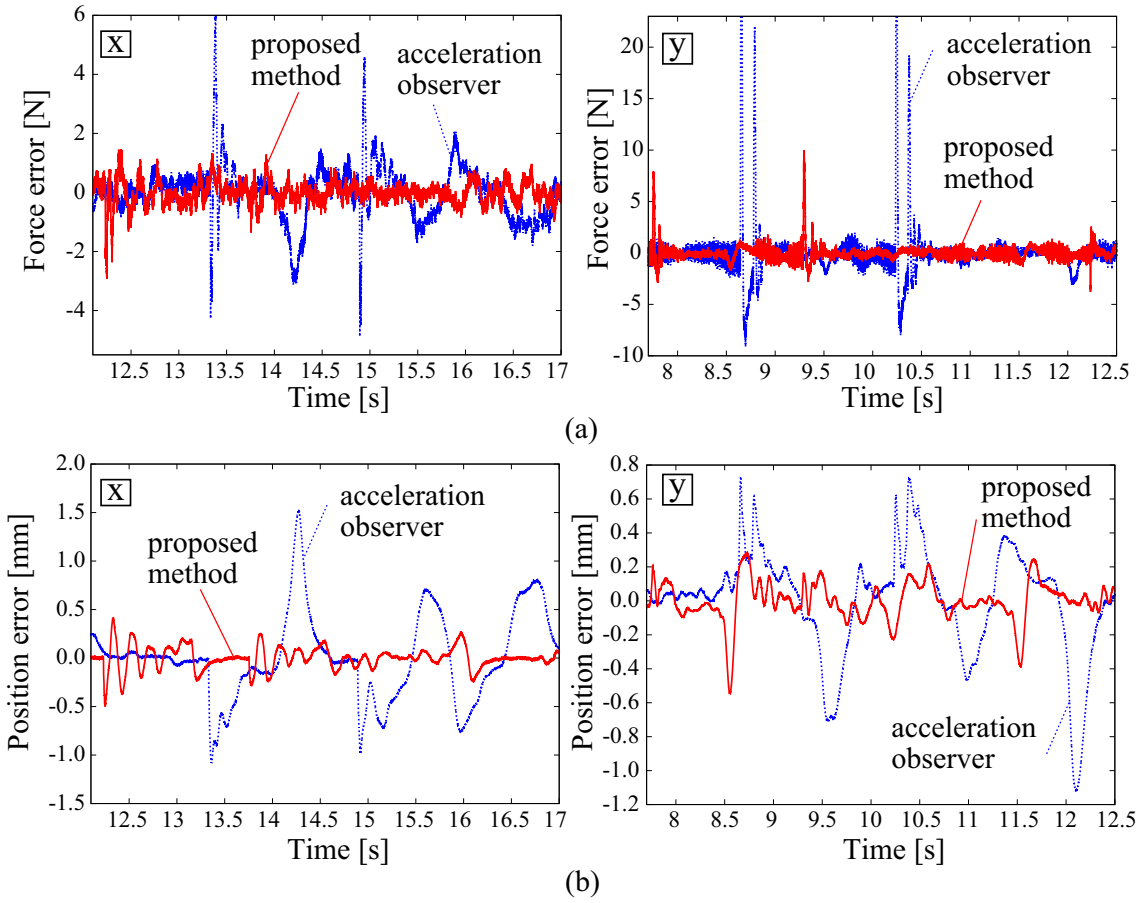

Fig. 4-18: Error comparison of acceleration observer (conventional) and the proposed method in (C) and (D). (a) Force error. (b) Position error.

tion observer-based method. Figs. 4-18 and 4-19 show the error comparison of the conventional methods (i.e. acceleration observer-based method and the normal acceleration observer) and the proposed method. The convergence of the force responses in the proposed method is better than those in the acceleration observer-based and the normal acceleration controller (conventional) methods, as shown in Figs. 4-18 (a) and 4-19 (a). Figs. 4-18 and 4-19 show that position tracking performance is also improved using the proposed method. Table 4.4 shows the root mean square error (RMSE) and maximum values of force and position tracking errors and their improvement ratios for the shaded areas (C) and (D). The table shows the proposed method improves the tracking performance over 60% in most cases. As a result, a higher reproducibility (transparency) of the bilateral control system is obtained by the proposed method.

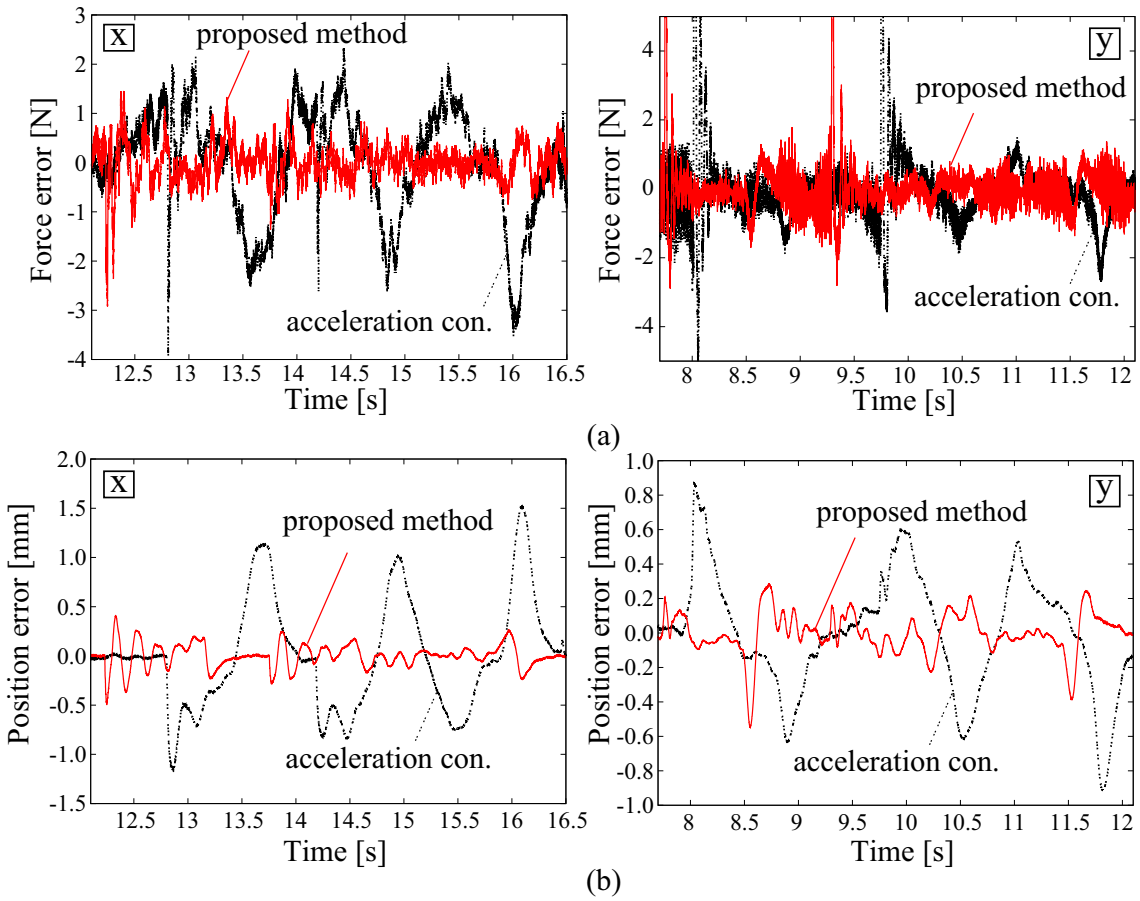

Fig. 4-19: Error comparison of normal acceleration controller (conventional) and the proposed method in (C) and (D). (a) Force error. (b) Position error.

Table 4.4: RMSE and maximum values of force and position errors in contact motions and improvement ratios

	Proposal	Acceleration observer	Normal acceleration controller
RMSE x (N)	0.391	0.954 (59.03%)	1.050 (62.74%)
MAX x (N)	1.456	6.103 (76.14%)	2.361 (38.30%)
RMSE y (N)	0.802	3.171 (74.71%)	1.661 (51.72%)
MAX y (N)	9.997	38.84 (74.26%)	24.75 (59.61%)
RMSE x (mm)	0.115	0.446 (74.29%)	0.530 (78.35%)
MAX x (mm)	0.406	1.517 (73.26%)	1.519 (73.29%)
RMSE y (mm)	0.117	0.315 (62.89%)	0.328 (64.39%)
MAX y (mm)	0.281	0.732 (61.55%)	0.869 (67.61%)

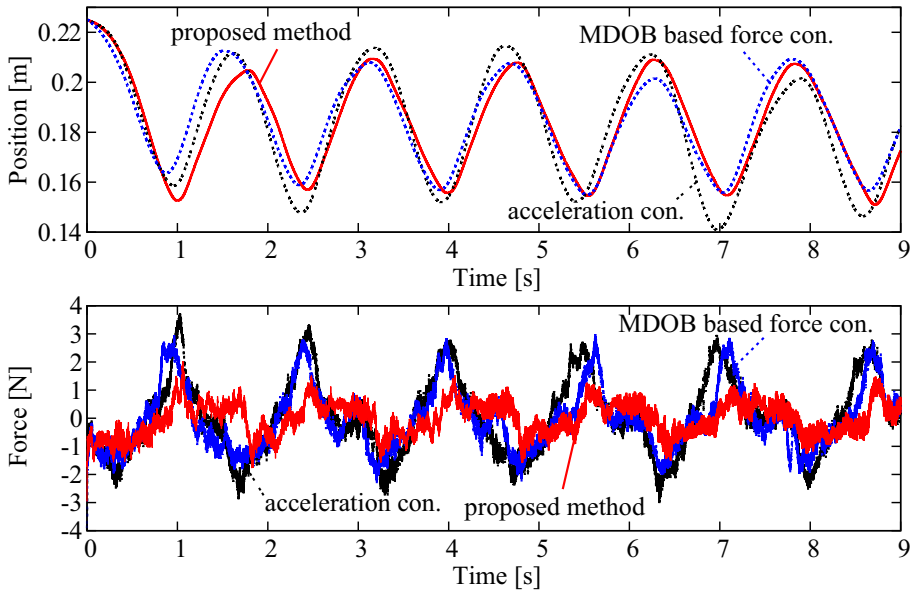

Fig. 4-20: Experimental results of free motion.

Table 4.5: RMSE and maximum values of operational force and position tracking error in free motions

	Proposal	MDOB	Normal acceleration controller
RMSE (N)	0.569	1.106 (48.52%)	1.340 (57.54%)
MAX (N)	1.775	2.750 (35.46%)	3.080 (42.37%)
RMSE (mm)	0.0172	0.0532(67.57%)	0.0344 (49.94%)
MAX (mm)	0.0853	0.153 (44.31%)	0.259 (67.09%)

Experimental Results of Free motion

Fig. 4-20 shows the additional experimental results related to the free motion of the normal acceleration controller, MDOB based-method, and the proposed method. In this experiment, the operator moves the master system quickly. As shown in the force response in Fig. 4-20, the proposed method achieves a reduction in the operational force, relative to the normal acceleration controller and MDOB-based method. This is the effect of the suppression of the inertial force shown in (4.70). Table 4.5 shows the RMSE and maximum values of the operational forces and position tracking errors. The table shows that the proposed method suppresses the operational force much more than the other method. The results indicate that the operationality of the bilateral control system is improved by the proposed method.

These results confirm the validity of the proposed method.

4.7 Extension to Redundant Systems and Combination with KFSOs

This part proposes a method for simultaneous implementation of performance improvement, decoupling of null space and suppression of the noise effect for a hybrid control system with a redundant degree of freedom (RDOF). Hybrid control systems with RDOF are necessary for motion control systems to achieve future applications for human support systems and robots in unknown and open environments. It is shown that the acceleration controller also performs decoupling of task (mode) spaces in the redundant system [97]. By extending the disturbance observer (DOB) for hybrid controllers to redundant systems, this study achieves the suppression of operating (inertia) force and interference from null space with the simplification of inverse kinematics [97]. Furthermore, the reconstruction of the DOB by combination with a Kalman filter is proposed in order to suppress the noise effect. Experiments of the scaled bilateral control, which is one of the hybrid control systems for the master and slave systems with RDOF, are conducted to validate the proposed method.

4.8 Kinematics and Dynamics of Hybrid Controller for Redundant System

4.8.1 Kinematics of Hybrid Controller for Redundant System

In general hybrid control systems, the tasks of hybrid control, including subtasks in modal space are described as follows:

$$\boldsymbol{F}_F^{\mathrm{ext}} = \boldsymbol{G}_F \left(\boldsymbol{F}_{W1}^{\mathrm{ext}} \ \cdots \ \boldsymbol{F}_{Wj}^{\mathrm{ext}} \right) = \boldsymbol{F}_F^{\mathrm{cmd}} \tag{4.97}$$

$$\boldsymbol{F}_{F\mathrm{sub}}^{\mathrm{ext}} = \boldsymbol{G}_{F\mathrm{sub}} \left(\boldsymbol{F}_{W1\mathrm{sub}}^{\mathrm{ext}} \ \cdots \ \boldsymbol{F}_{Wk\mathrm{sub}}^{\mathrm{ext}} \right) = \boldsymbol{F}_{F\mathrm{sub}}^{\mathrm{cmd}} \tag{4.98}$$

$$\boldsymbol{X}_X^{\mathrm{res}} = \boldsymbol{G}_X \left(\boldsymbol{X}_{W1}^{\mathrm{res}} \ \cdots \ \boldsymbol{X}_{Wj}^{\mathrm{res}} \right) = \boldsymbol{X}_X^{\mathrm{cmd}} \tag{4.99}$$

$$\boldsymbol{X}_{X\mathrm{sub}}^{\mathrm{res}} = \boldsymbol{G}_{X\mathrm{sub}} \left(\boldsymbol{X}_{W1\mathrm{sub}}^{\mathrm{res}} \ \cdots \ \boldsymbol{X}_{Wk\mathrm{sub}}^{\mathrm{res}} \right) = \boldsymbol{X}_{X\mathrm{sub}}^{\mathrm{cmd}}. \tag{4.100}$$

where the subscript sub represent a direction for subtasks. The kinematic relationships between work space and mode space are described as:

$$\boldsymbol{X}^{\mathrm{res}} = \begin{bmatrix} \boldsymbol{X}_F^{\mathrm{res}} \\ \boldsymbol{X}_{F\mathrm{sub}}^{\mathrm{res}} \\ \boldsymbol{X}_X^{\mathrm{res}} \\ \boldsymbol{X}_{X\mathrm{sub}}^{\mathrm{res}} \end{bmatrix} = \boldsymbol{G}\left(\boldsymbol{X}_W^{\mathrm{res}} \right) \tag{4.101}$$

$$= \boldsymbol{G}_X \left(\boldsymbol{X}_{W1}^{\mathrm{res}} \ \cdots \ \boldsymbol{X}_{Wj}^{\mathrm{res}} \ \boldsymbol{X}_{W1\mathrm{sub}}^{\mathrm{res}} \ \cdots \ \boldsymbol{X}_{Wk\mathrm{sub}}^{\mathrm{res}} \right). \tag{4.102}$$

If the relationship is linear, the coordinate transformation can be expressed by a transformation matrix as follows:

$$\boldsymbol{X}^{\mathrm{res}} = \begin{bmatrix} \boldsymbol{X}_F^{\mathrm{res}} \\ \boldsymbol{X}_{F\mathrm{sub}}^{\mathrm{res}} \\ \boldsymbol{X}_X^{\mathrm{res}} \\ \boldsymbol{X}_{X\mathrm{sub}}^{\mathrm{res}} \end{bmatrix} = \frac{\partial \boldsymbol{G}_X\left(\boldsymbol{X}_W^{\mathrm{res}}\right)}{\partial \boldsymbol{X}_W^{\mathrm{res}}} = \begin{bmatrix} \gamma_{F1} & \gamma_{F2} & \cdots & \gamma_{Fk} \\ \gamma_{F1\mathrm{sub}} & \gamma_{F2\mathrm{sub}} & \cdots & \gamma_{Fk\mathrm{sub}} \\ \gamma_{X1} & \gamma_{X2} & \cdots & \gamma_{Xk} \\ \gamma_{X1\mathrm{sub}} & \gamma_{X2\mathrm{sub}} & \cdots & \gamma_{Xk\mathrm{sub}} \end{bmatrix} \begin{bmatrix} \boldsymbol{X}_{W1}^{\mathrm{res}} \\ \vdots \\ \boldsymbol{X}_{Wj}^{\mathrm{res}} \\ \boldsymbol{X}_{W1\mathrm{sub}}^{\mathrm{res}} \\ \vdots \\ \boldsymbol{X}_{Wk\mathrm{sub}}^{\mathrm{res}} \end{bmatrix} \tag{4.103}$$

$$= \boldsymbol{\Gamma} \boldsymbol{X}_W^{\mathrm{res}} \tag{4.104}$$

where $\boldsymbol{\Gamma}$ corresponds to a Jacobian matrix of the hybrid control.

The relationship between the modal space velocity/acceleration and the joint space angular velocity/acceleration are described as follows:

$$\boldsymbol{X}^{\mathrm{res}} = \boldsymbol{\Gamma} \boldsymbol{G}_W\left(\boldsymbol{q}^{\mathrm{res}}\right) \tag{4.105}$$

$$\dot{\boldsymbol{X}}^{\mathrm{res}} = \boldsymbol{\Gamma} \boldsymbol{J}_{\mathrm{aco}} \dot{\boldsymbol{q}}^{\mathrm{res}} \tag{4.106}$$

$$\ddot{\boldsymbol{X}}^{\mathrm{res}} = \boldsymbol{\Gamma} \boldsymbol{J}_{\mathrm{aco}} \ddot{\boldsymbol{q}}^{\mathrm{res}} + \boldsymbol{\Gamma} \dot{\boldsymbol{J}}_{\mathrm{aco}} \dot{\boldsymbol{q}}^{\mathrm{res}}. \tag{4.107}$$

An inverse transformation of the acceleration from the modal space to the joint space is obtained as

$$\ddot{\boldsymbol{q}} = \boldsymbol{J}_{\mathrm{aco}}^{+} \boldsymbol{\Gamma}^{-1} \left[\ddot{\boldsymbol{X}} - \boldsymbol{\Gamma} \dot{\boldsymbol{J}}_{\mathrm{aco}} \dot{\boldsymbol{q}} \right] \tag{4.108}$$

where $\boldsymbol{J}_{\mathrm{aco}}^{+}$ is a pseudo inverse Jacobian matrix in the work space and is described as follows:

$$\boldsymbol{J}_{\mathrm{aco}}^{+} = \boldsymbol{J}_{\mathrm{aco}}^{T} \left(\boldsymbol{J}_{\mathrm{aco}} \boldsymbol{J}_{\mathrm{aco}}^{T} \right)^{-1}. \tag{4.109}$$

On the other hand, the transformation originates a joint torque to the modal space force, which is expressed as follows:

$$\boldsymbol{F} = \boldsymbol{\Gamma}_F \boldsymbol{F}_W = \boldsymbol{\Gamma} \boldsymbol{F}_W = \boldsymbol{\Gamma} \boldsymbol{J}_{\mathrm{aco}}^{+T} \boldsymbol{\tau}. \tag{4.110}$$

The position transformation matrix $\boldsymbol{\Gamma}_F$ can be determined by considering desired tasks arbitrarily. This dissertation utilizes the same transformation matrix as the position transformation. The control goals of bilateral control with different-degree-of-freedom are described in terms of the position and force

responses of the master and slave systems, as follows:

$$\boldsymbol{F}_F^{\mathrm{ext}} = \boldsymbol{F}_m^{\mathrm{ext}} + \boldsymbol{\alpha}\boldsymbol{F}_s^{\mathrm{ext}} = \boldsymbol{F}_F^{\mathrm{cmd}} = \boldsymbol{0} \tag{4.111}$$

$$\boldsymbol{F}_{F\mathrm{sub}}^{\mathrm{ext}} = \boldsymbol{F}_{F\mathrm{ssub}}^{\mathrm{ext}} = \boldsymbol{F}_{\mathrm{ssub}}^{\mathrm{cmd}} \tag{4.112}$$

$$\boldsymbol{X}_X^{\mathrm{res}} = \boldsymbol{X}_m^{\mathrm{res}} - \boldsymbol{\beta}\boldsymbol{X}_s^{\mathrm{res}} = \boldsymbol{X}_X^{\mathrm{cmd}} = \boldsymbol{0} \tag{4.113}$$

$$\boldsymbol{X}_{X\mathrm{sub}}^{\mathrm{res}} = \boldsymbol{X}_{X\mathrm{ssub}}^{\mathrm{res}} = \boldsymbol{X}_{\mathrm{ssub}}^{\mathrm{cmd}}. \tag{4.114}$$

Herein, the degrees of freedom in the slave side are assumed to be larger than those of master side. Eq. (4.111) represents the realization of haptic feedback (law of action and reaction) between the master and slave systems. On the other hand, (4.113) represents the position tracking of the master and slave systems. These control goals are achieved by the application of force control and position control. Therefore, a bilateral control system can be regarded as being a force-position hybrid control system [79–81]. In order to describe and realize hybrid control, the force and position information of the master and slave systems is transformed in the modal space. The direct kinematics (coordinate transformation) from the workspace to the modal space is represented as:

$$\boldsymbol{X}^{\mathrm{res}} = \begin{bmatrix} \boldsymbol{X}_F^{\mathrm{res}} \\ \boldsymbol{X}_X^{\mathrm{res}} \end{bmatrix} = \boldsymbol{G}\left(\boldsymbol{X}_W^{\mathrm{res}}\right) = \boldsymbol{\Gamma}\boldsymbol{X}_W^{\mathrm{res}} = \begin{bmatrix} \boldsymbol{I} & \boldsymbol{0} & \boldsymbol{\alpha}\boldsymbol{I} & \boldsymbol{0} \\ \boldsymbol{0} & \boldsymbol{I} & \boldsymbol{0} & \boldsymbol{0} \\ \boldsymbol{I} & \boldsymbol{0} & -\boldsymbol{\beta}\boldsymbol{I} & \boldsymbol{0} \\ \boldsymbol{0} & \boldsymbol{0} & \boldsymbol{0} & \boldsymbol{I} \end{bmatrix} \begin{bmatrix} \boldsymbol{X}_m^{\mathrm{res}} \\ \boldsymbol{X}_{F\mathrm{ssub}}^{\mathrm{res}} \\ \boldsymbol{X}_s^{\mathrm{res}} \\ \boldsymbol{X}_{X\mathrm{ssub}}^{\mathrm{res}} \end{bmatrix} \tag{4.115}$$

where $\boldsymbol{\Gamma}$ is the coordinate transformation matrix for bilateral control. The coordinate transformation of the force information is also defined by using the same matrix as below:

$$\boldsymbol{F}^{\mathrm{ext}} = \begin{bmatrix} \boldsymbol{F}_F^{\mathrm{ext}} \\ \boldsymbol{F}_X^{\mathrm{ext}} \end{bmatrix} = \boldsymbol{\Gamma}\boldsymbol{F}_W^{\mathrm{ext}} = \boldsymbol{\Gamma} \begin{bmatrix} \boldsymbol{F}_m^{\mathrm{ext}} \\ \boldsymbol{F}_s^{\mathrm{ext}} \end{bmatrix}. \tag{4.116}$$

4.8.2 Dynamics of Hybrid Controller

Motion equation with joint space DOBs are expressed as follows:

$$\boldsymbol{J}_n\ddot{\boldsymbol{q}}^{\mathrm{res}} = \boldsymbol{\tau}^{\mathrm{ref}} - \boldsymbol{g}_H^{\mathrm{dis}}(s)\boldsymbol{\tau}^{\mathrm{dis}} = \boldsymbol{p}^{\mathrm{dis}} \tag{4.117}$$

$$\boldsymbol{\tau}^{\mathrm{dis}} = \boldsymbol{\tau}^{\mathrm{ext}} + \boldsymbol{\tau}^{\mathrm{fric}} + \boldsymbol{C}\left(\boldsymbol{q},\, \dot{\boldsymbol{q}}\right) + \boldsymbol{\Delta}\boldsymbol{J}\ddot{\boldsymbol{q}}^{\mathrm{res}} - \boldsymbol{\Delta}\boldsymbol{K}_t\boldsymbol{I}^{\mathrm{ref}} \tag{4.118}$$

$$= \boldsymbol{\tau}^{\mathrm{ext}} + \boldsymbol{\tau}^{\mathrm{load}} \tag{4.119}$$

where $\boldsymbol{g}_H^{\mathrm{dis}}(s)$ is a diagonal matrix with high-pass filters. The cutoff frequency in $\boldsymbol{g}_h(s)$ is set to a sufficiently large value, such that the effect of the remaining disturbance $\boldsymbol{p}^{\mathrm{dis}}$ become negligible. By

using the Jacobian matrix, (4.117) is transformed and the dynamics in the workspace are given as:

$$\boldsymbol{J}_{\mathrm{aco}}^{+T}\boldsymbol{J}_n\boldsymbol{J}_{\mathrm{aco}}^{-1}\ddot{\boldsymbol{X}}_W^{\mathrm{res}} = \boldsymbol{J}_{\mathrm{aco}}^{+T}\boldsymbol{\tau}^{\mathrm{ref}} + \boldsymbol{M}_W\dot{\boldsymbol{J}}_{\mathrm{aco}}\dot{\boldsymbol{q}}^{\mathrm{res}} - \boldsymbol{J}_{\mathrm{aco}}^{+T}\boldsymbol{p}^{\mathrm{dis}} \tag{4.120}$$

$$\boldsymbol{M}_W\ddot{\boldsymbol{X}}_W^{\mathrm{res}} = \boldsymbol{F}_W^{\mathrm{ref}} + \boldsymbol{M}_W\dot{\boldsymbol{J}}_{\mathrm{aco}}\dot{\boldsymbol{q}}^{\mathrm{res}} - \boldsymbol{P}_W^{\mathrm{dis}} \tag{4.121}$$

$$\boldsymbol{M}_W = \left(\boldsymbol{J}_{\mathrm{aco}}\boldsymbol{J}_n^{-1}\boldsymbol{J}_{\mathrm{aco}}^{T}\right)^{-1}. \tag{4.122}$$

where $\boldsymbol{M}_W$ is an equivalent mass matrix in the workspace.

Furthermore, by using the transformation matrix $\boldsymbol{\Gamma}$, the dynamics of hybrid control in modal space are obtained as:

$$\boldsymbol{\Gamma}\boldsymbol{M}_W\boldsymbol{\Gamma}^{-1}\ddot{\boldsymbol{X}}^{\mathrm{res}} = \boldsymbol{\Gamma}\boldsymbol{F}_W^{\mathrm{ref}} + \boldsymbol{\Gamma}\boldsymbol{M}_W\dot{\boldsymbol{J}}_{\mathrm{aco}}\dot{\boldsymbol{q}}^{\mathrm{res}} - \boldsymbol{\Gamma}\boldsymbol{P}_W^{\mathrm{dis}} \tag{4.123}$$

$$\boldsymbol{M}\ddot{\boldsymbol{X}}^{\mathrm{res}} = \boldsymbol{F}^{\mathrm{ref}} + \boldsymbol{\Gamma}\boldsymbol{M}_W\dot{\boldsymbol{J}}_{\mathrm{aco}}\dot{\boldsymbol{q}}^{\mathrm{res}} - \boldsymbol{P}^{\mathrm{dis}} \tag{4.124}$$

$$\boldsymbol{M} = \boldsymbol{\Gamma}\boldsymbol{M}_W\boldsymbol{\Gamma}^{-1}. \tag{4.125}$$

If the joint space torque reference is given by the following equation, the modal space equivalent mass $\boldsymbol{M}$ is substituted by a virtual mass matrix $\boldsymbol{M}_v$.

$$\boldsymbol{\tau}^{\mathrm{ref}} = \boldsymbol{J}_n\ddot{\boldsymbol{q}}^{\mathrm{ref}} = \boldsymbol{J}_n\boldsymbol{J}_{\mathrm{aco}}^{+}\boldsymbol{\Gamma}^{-1}\boldsymbol{M}_v^{-1}\boldsymbol{F}^{\mathrm{ref}} = \boldsymbol{J}_n\boldsymbol{J}_{\mathrm{aco}}^{+}\boldsymbol{\Gamma}^{-1}\ddot{\boldsymbol{X}}^{\mathrm{ref}}. \tag{4.126}$$

The modal space dynamics are derived as follows:

$$\boldsymbol{M}\ddot{\boldsymbol{X}}^{\mathrm{res}} = \boldsymbol{\Gamma}\boldsymbol{J}_{\mathrm{aco}}^{+T}\boldsymbol{J}_n\boldsymbol{J}_{\mathrm{aco}}^{+}\boldsymbol{\Gamma}^{-1}\boldsymbol{M}_v^{-1}\boldsymbol{F}^{\mathrm{ref}} + \boldsymbol{\Gamma}\boldsymbol{M}_W\dot{\boldsymbol{J}}_{\mathrm{aco}}\dot{\boldsymbol{q}}^{\mathrm{res}} - \boldsymbol{\Gamma}\boldsymbol{J}_{\mathrm{aco}}^{+T}\boldsymbol{p}^{\mathrm{dis}} \tag{4.127}$$

$$\boldsymbol{M}\ddot{\boldsymbol{X}}^{\mathrm{res}} = \boldsymbol{M}\boldsymbol{F}^{\mathrm{ref}} + \boldsymbol{\Gamma}\boldsymbol{M}_W\dot{\boldsymbol{J}}_{\mathrm{aco}}\dot{\boldsymbol{q}}^{\mathrm{res}} - \boldsymbol{\Gamma}\boldsymbol{J}_{\mathrm{aco}}^{+T}\boldsymbol{p}^{\mathrm{dis}} \tag{4.128}$$

$$\boldsymbol{M}^{-1}\boldsymbol{M}\ddot{\boldsymbol{X}}^{\mathrm{res}} = \boldsymbol{M}^{-1}\boldsymbol{M}\boldsymbol{M}_v^{-1}\boldsymbol{F}^{\mathrm{ref}} + \boldsymbol{M}^{-1}\boldsymbol{\Gamma}\boldsymbol{M}_W\dot{\boldsymbol{J}}_{\mathrm{aco}}\dot{\boldsymbol{q}}^{\mathrm{res}} - \boldsymbol{M}^{-1}\boldsymbol{P}^{\mathrm{dis}} \tag{4.129}$$

$$\boldsymbol{M}_v\ddot{\boldsymbol{X}}^{\mathrm{res}} = \boldsymbol{F}^{\mathrm{ref}} + \boldsymbol{M}_v\boldsymbol{\Gamma}\dot{\boldsymbol{J}}_{\mathrm{aco}}\dot{\boldsymbol{q}}^{\mathrm{res}} - \boldsymbol{M}_v\boldsymbol{M}^{-1}\boldsymbol{P}^{\mathrm{dis}}. \tag{4.130}$$

If the virtual mass matrix is set to a diagonal matrix, the decoupling control in modal space is achieved. Additionally, if the virtual mass matrix is set to an identity matrix, the modal space controller becomes an acceleration controller:

$$\boldsymbol{F}^{\mathrm{ref}} = \begin{bmatrix}\boldsymbol{F}_F^{\mathrm{ref}}\\ \boldsymbol{F}_X^{\mathrm{ref}}\end{bmatrix} = \begin{bmatrix}\boldsymbol{M}_{vF}\boldsymbol{C}_f\left(\boldsymbol{F}_F^{\mathrm{cmd}} - \hat{\boldsymbol{F}}_F^{\mathrm{ext}}\right)\\ \boldsymbol{M}_{vX}\boldsymbol{C}_p(s)\left(\boldsymbol{X}_X^{\mathrm{cmd}} - \boldsymbol{X}_X^{\mathrm{res}}\right) + \boldsymbol{M}_v\ddot{\boldsymbol{X}}_X^{\mathrm{cmd}}\end{bmatrix}. \tag{4.131}$$

4.8.3 Effect of Null Space Motion

In order to determine tasks of null space motions, control references of the null space should be added to the joint space reference. If the null space acceleration reference $\ddot{\boldsymbol{q}}_{\rm null}^{\rm ref}$ is directly added to (4.126), the modal space dynamics is rewritten as follows:

$$\boldsymbol{M}\ddot{\boldsymbol{X}}^{\rm res} = \boldsymbol{\Gamma}\boldsymbol{J}_{\rm aco}^{+T}\boldsymbol{J}_n\left(\boldsymbol{J}_{\rm aco}^{+}\boldsymbol{\Gamma}^{-1}\boldsymbol{M}_v^{-1}\boldsymbol{F}^{\rm ref} + \ddot{\boldsymbol{q}}_{\rm null}^{\rm ref}\right) + \boldsymbol{\Gamma}\boldsymbol{M}_W\dot{\boldsymbol{J}}_{\rm aco}\dot{\boldsymbol{q}}^{\rm res} - \boldsymbol{\Gamma}\boldsymbol{J}_{\rm aco}^{+T}\boldsymbol{p}^{\rm dis} \quad (4.132)$$

$$\boldsymbol{M}_v\ddot{\boldsymbol{X}}^{\rm res} = \boldsymbol{F}^{\rm ref} + \boldsymbol{M}_v\boldsymbol{\Gamma}\boldsymbol{J}_{\rm aco}\ddot{\boldsymbol{q}}_{\rm null}^{\rm ref} + \boldsymbol{M}_v\boldsymbol{\Gamma}\dot{\boldsymbol{J}}_{\rm aco}\dot{\boldsymbol{q}}^{\rm res} - \boldsymbol{M}_v\boldsymbol{M}^{-1}\boldsymbol{P}^{\rm dis} \quad (4.133)$$

$$\ddot{\boldsymbol{q}}^{\rm ref} = \boldsymbol{J}_{\rm aco}^{+}\boldsymbol{\Gamma}^{-1}\boldsymbol{M}_v^{-1}\boldsymbol{F}^{\rm ref} + \ddot{\boldsymbol{q}}_{\rm null}^{\rm ref}. \quad (4.134)$$

The second term in (4.133) represents the interference term from null space in modal space. On the other hand, the third term in (4.133) is a disturbance term caused by coordinate transformation. Although the third term in (4.133) can be suppressed by setting the bandwidth of DOBs to be sufficiently high, the second and third terms cannot be suppressed .

4.8.4 Modal Space Observer for Simplification of Inverse Kinematics

In order to suppress the second and third terms in (4.133), the work space observer [84] in acceleration controller should be extended to the modal space control scheme, for simplification of the inverse kinematics. A disturbance of the redundant system in the modal space hybrid controller based on acceleration controller $\boldsymbol{F}^{\rm dis}$ is described as follows:

$$\boldsymbol{F}^{\rm dis} = \boldsymbol{F}^{\rm ref} - \boldsymbol{M}_v\ddot{\boldsymbol{X}}^{\rm res} \quad (4.135)$$

$$= -\boldsymbol{M}_v\left(\boldsymbol{\Gamma}\boldsymbol{J}_{\rm aco}\ddot{\boldsymbol{q}}_{\rm null}^{\rm ref} + \boldsymbol{\Gamma}\dot{\boldsymbol{J}}_{\rm aco}\dot{\boldsymbol{q}}^{\rm res}\right). \quad (4.136)$$

The disturbance in the acceleration dimension $\ddot{\boldsymbol{X}}^{\rm dis}$ is expressed as follows:

$$\ddot{\boldsymbol{X}}^{\rm dis} = \boldsymbol{M}_v^{-1}\boldsymbol{F}^{\rm ref} - \ddot{\boldsymbol{X}}^{\rm res} \quad (4.137)$$

$$= \ddot{\boldsymbol{X}}^{\rm ref} - \ddot{\boldsymbol{X}}^{\rm res} \quad (4.138)$$

$$= -\boldsymbol{\Gamma}\boldsymbol{J}_{\rm aco}\ddot{\boldsymbol{q}}_{\rm null}^{\rm ref} - \boldsymbol{\Gamma}\dot{\boldsymbol{J}}_{\rm aco}\dot{\boldsymbol{q}}^{\rm res}. \quad (4.139)$$

The disturbance is estimated by the disturbance observer in modal space as follows:

$$\hat{\ddot{\boldsymbol{X}}}^{\rm dis} = \boldsymbol{G}_L^{\rm dis}(s)\left[\ddot{\boldsymbol{X}}^{\rm ref} - \ddot{\boldsymbol{X}}^{\rm res}\right]. \quad (4.140)$$

A block diagram of the DOB in modal space is shown in Fig. 4-21. This is an extension of the WDOB [84] to the modal space. By feeding back the estimated disturbance, the disturbance in modal space is

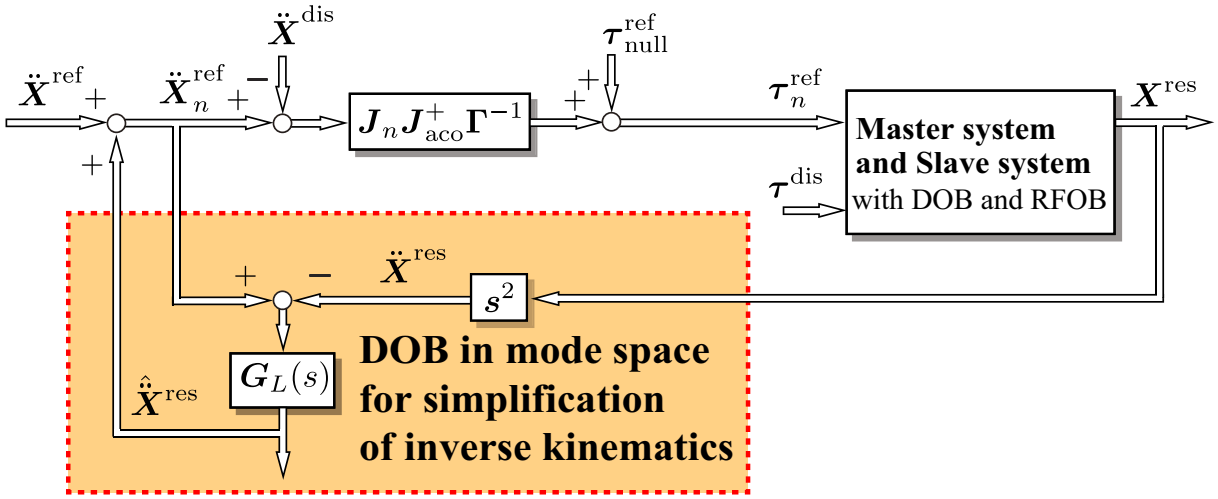

Fig. 4-21: Work space disturbance observer for simplification of inverse kinematics.

suppressed if the bandwidth of the $\boldsymbol{G}_L^{\mathrm{dis}}(s)$ is sufficiently high, as follows:

$$\begin{aligned} \boldsymbol{M}_v \ddot{\boldsymbol{X}}^{\mathrm{res}} &= \boldsymbol{F}_n^{\mathrm{ref}} + \boldsymbol{F}^{\mathrm{dis}} = \boldsymbol{F}^{\mathrm{ref}} + \boldsymbol{M}_v \hat{\ddot{\boldsymbol{X}}}^{\mathrm{dis}} - \boldsymbol{M}_v \ddot{\boldsymbol{X}}^{\mathrm{dis}} && (4.141) \\ &= \boldsymbol{F}^{\mathrm{ref}} + \boldsymbol{M}_v \boldsymbol{G}_H^{\mathrm{dis}}(s) \left(\boldsymbol{\Gamma} \boldsymbol{J}_{\mathrm{aco}} \ddot{\boldsymbol{q}}_{\mathrm{null}}^{\mathrm{ref}} + \boldsymbol{\Gamma} \dot{\boldsymbol{J}}_{\mathrm{aco}} \dot{\boldsymbol{q}}^{\mathrm{res}} \right) && (4.142) \\ &\approx \boldsymbol{F}^{\mathrm{ref}}. && (4.143) \end{aligned}$$

In this case, the acceleration reference in the joint space is expressed as below:

$$\begin{aligned} \ddot{\boldsymbol{q}}_n^{\mathrm{ref}} &= \boldsymbol{J}_{\mathrm{aco}}^{+} \boldsymbol{\Gamma}^{-1} \left(\ddot{\boldsymbol{X}}^{\mathrm{ref}} + \hat{\ddot{\boldsymbol{X}}}^{\mathrm{dis}} \right) + \ddot{\boldsymbol{q}}_{\mathrm{null}}^{\mathrm{ref}} && (4.144) \\ &= \boldsymbol{J}_{\mathrm{aco}}^{+} \boldsymbol{\Gamma}^{-1} \left(\ddot{\boldsymbol{X}}^{\mathrm{ref}} - \boldsymbol{\Gamma} \boldsymbol{J}_{\mathrm{aco}} \ddot{\boldsymbol{q}}_{\mathrm{null}}^{\mathrm{ref}} - \boldsymbol{\Gamma} \dot{\boldsymbol{J}}_{\mathrm{aco}} \dot{\boldsymbol{q}}^{\mathrm{res}} \right) + \ddot{\boldsymbol{q}}_{\mathrm{null}}^{\mathrm{ref}} && (4.145) \\ &= \boldsymbol{J}_{\mathrm{aco}}^{+} \boldsymbol{\Gamma}^{-1} \ddot{\boldsymbol{X}}^{\mathrm{ref}} - \dot{\boldsymbol{J}}_{\mathrm{aco}} \dot{\boldsymbol{q}}^{\mathrm{res}} + \ddot{\boldsymbol{q}}_{\mathrm{null}}^{\mathrm{ref}} - \boldsymbol{J}_{\mathrm{aco}}^{+} \boldsymbol{J}_{\mathrm{aco}} \ddot{\boldsymbol{q}}_{\mathrm{null}}^{\mathrm{ref}} && (4.146) \\ &= \boldsymbol{J}_{\mathrm{aco}}^{+} \boldsymbol{\Gamma}^{-1} \left(\ddot{\boldsymbol{X}}^{\mathrm{ref}} - \boldsymbol{\Gamma} \dot{\boldsymbol{J}}_{\mathrm{aco}} \dot{\boldsymbol{q}}^{\mathrm{res}} \right) + \left(\boldsymbol{I} - \boldsymbol{J}_{\mathrm{aco}}^{+} \boldsymbol{J}_{\mathrm{aco}} \right) \ddot{\boldsymbol{q}}_{\mathrm{null}}^{\mathrm{ref}}. && (4.147) \end{aligned}$$

Equation (4.147) represents that the simplification of the inverse kinematics and decoupling of the null space in modal space (calculation of the nonlinear term caused by coordinate transformation $\boldsymbol{\Gamma} \dot{\boldsymbol{J}}_{\mathrm{aco}} \dot{\boldsymbol{q}}^{\mathrm{res}}$ and null space projection matrix $\boldsymbol{I} - \boldsymbol{J}_{\mathrm{aco}}^{+} \boldsymbol{J}_{\mathrm{aco}}$ can be accomplished by the MDOB).

4.8.5 Effect of Inertia Force in Force Control System

The response of the force control system is expressed as below:

$$\begin{aligned}\hat{\boldsymbol{F}}_F^{\mathrm{ext}} &= \boldsymbol{F}_F^{\mathrm{cmd}} - \boldsymbol{C}_f^{-1}\boldsymbol{M}_{vF}\ddot{\boldsymbol{X}}_F^{\mathrm{res}} \\ &\quad + \boldsymbol{C}_f^{-1}\boldsymbol{M}_{vF}\begin{bmatrix}\boldsymbol{I}\\ \boldsymbol{0}\end{bmatrix}^T \boldsymbol{G}_H^{\mathrm{dis}}(s)\left(\boldsymbol{\Gamma}\boldsymbol{J}_{\mathrm{aco}}\ddot{\boldsymbol{q}}_{\mathrm{null}}^{\mathrm{ref}} + \boldsymbol{\Gamma}\dot{\boldsymbol{J}}_{\mathrm{aco}}\dot{\boldsymbol{q}}^{\mathrm{res}}\right). \end{aligned} \tag{4.148}$$

Although the disturbance terms are suppressed by DOBs, the effect of an inertia force remains as shown in the second term in the right side of (4.148).

4.9 Proposed DOB for Hybrid Controller in Redundant System

In order to obtain a simplification of inverse kinematics by decoupling the effect of the null space motion and suppressing the inertia force term, the mode space disturbance observer for hybrid controller in acceleration controller can also be applied on the redundant system.

4.9.1 Estimation and Compensation of Modal Space Disturbance in Hybrid Control System

The disturbance of the hybrid controller in the redundant system is expressed as follows:

$$\begin{aligned}\boldsymbol{A}^{\mathrm{dis}} &= (\boldsymbol{I}-\boldsymbol{S})\ddot{\boldsymbol{X}}^{\mathrm{res}} - \boldsymbol{\Gamma}\boldsymbol{J}_{\mathrm{aco}}\ddot{\boldsymbol{q}}_{\mathrm{null}}^{\mathrm{ref}} - \boldsymbol{\Gamma}\dot{\boldsymbol{J}}_{\mathrm{aco}}\dot{\boldsymbol{q}}^{\mathrm{res}} \\ &\quad + \left[\boldsymbol{M}^{-1} - (\boldsymbol{I}-\boldsymbol{S})\,\mathrm{diag}\left[\boldsymbol{M}^{-1}\right]\right]\boldsymbol{P}^{\mathrm{dis}} + (\boldsymbol{I}-\boldsymbol{S})\,\mathrm{diag}\left[\boldsymbol{M}^{-1}\right]\boldsymbol{P}^{\mathrm{load}}. \end{aligned} \tag{4.149}$$

In addition to the inertia force, the disturbance caused by simplification of inverse kinematics and the interference from the null space are included. The disturbance is estimated as follows:

$$\hat{\boldsymbol{A}}^{\mathrm{dis}} = \boldsymbol{G}_L^{\mathrm{dis}}(s)\left[\ddot{\boldsymbol{X}}_n^{\mathrm{ref}} - \boldsymbol{S}\ddot{\boldsymbol{X}}^{\mathrm{res}} - (\boldsymbol{I}-\boldsymbol{S})\,\mathrm{diag}\left[\boldsymbol{M}^{-1}\right]\boldsymbol{G}_F(s)\hat{\boldsymbol{F}}^{\mathrm{ext}}\right] \tag{4.150}$$

$$\boldsymbol{G}_F(s) = \boldsymbol{\Gamma}\boldsymbol{J}_{\mathrm{aco}}^{+T}\left[\boldsymbol{I} - \boldsymbol{g}_l^{\mathrm{ext}}(s)\right]\left[\boldsymbol{g}_l^{\mathrm{ext}}(s)\right]^{-1}\boldsymbol{J}_{\mathrm{aco}}^{T}\boldsymbol{\Gamma}^{-1} \tag{4.151}$$

$$= \boldsymbol{\Gamma}\boldsymbol{J}_{\mathrm{aco}}^{+T}\boldsymbol{g}_h^{\mathrm{ext}}(s)\left[\boldsymbol{g}_l^{\mathrm{ext}}(s)\right]^{-1}\boldsymbol{J}_{\mathrm{aco}}^{T}\boldsymbol{\Gamma}^{-1}. \tag{4.152}$$

Fig. 4-22 shows a block diagram of the proposed DOB for hybrid controller in redundant system. If the disturbance is compensated, the force and position responses are expressed as follows:

$$\boldsymbol{S}\ddot{\boldsymbol{X}}^{\mathrm{res}} = \boldsymbol{X}^{\mathrm{ref}} - \boldsymbol{G}_H^{\mathrm{dis}}(s)\boldsymbol{A}^{\mathrm{dis}} \tag{4.153}$$

$$\begin{bmatrix}\boldsymbol{F}_F^{\mathrm{ext}}\\ \boldsymbol{X}_X^{\mathrm{res}}\end{bmatrix} = \begin{bmatrix}\boldsymbol{F}_F^{\mathrm{cmd}}\\ \boldsymbol{X}_X^{\mathrm{cmd}}\end{bmatrix} - \begin{bmatrix}\boldsymbol{C}_f^{-1}\boldsymbol{M}_{vF}\boldsymbol{G}_H^{\mathrm{dis}}(s)\ddot{\boldsymbol{X}}_F^{\mathrm{res}}\\ \boldsymbol{0}\end{bmatrix} \approx \begin{bmatrix}\boldsymbol{F}_F^{\mathrm{cmd}}\\ \boldsymbol{X}_X^{\mathrm{cmd}}\end{bmatrix}. \tag{4.154}$$

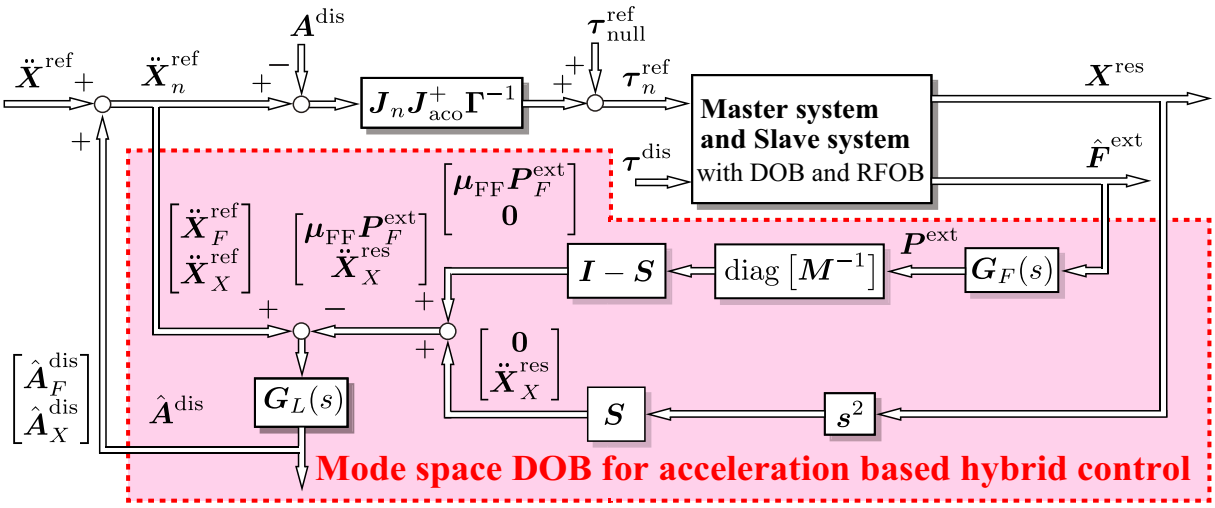

Fig. 4-22: Proposed DOB for Hybrid Controller in Redundant System.

As shown in (4.154), the nonlinear term, the interference from the null space and the inertia force are suppressed if the bandwidth of $\boldsymbol{G}_L^{\mathrm{dis}}(s)$ is set to be sufficiently high. The proposed observer can also perform the simplification of the inverse kinematics and decoupling of the null space in modal space as follows:

$$\ddot{\boldsymbol{q}}_n^{\mathrm{ref}} = \boldsymbol{J}_{\mathrm{aco}}^{+}\boldsymbol{\Gamma}^{-1}\left(\ddot{\boldsymbol{X}}^{\mathrm{ref}} + \hat{\boldsymbol{A}}^{\mathrm{dis}}\right) + \ddot{\boldsymbol{q}}_{\mathrm{null}}^{\mathrm{ref}} \tag{4.155}$$

$$= \boldsymbol{J}_{\mathrm{aco}}^{+}\boldsymbol{\Gamma}^{-1}\ddot{\boldsymbol{X}}^{\mathrm{ref}} - \dot{\boldsymbol{J}}_{\mathrm{aco}}\dot{\boldsymbol{q}}^{\mathrm{res}} - \boldsymbol{J}_{\mathrm{aco}}^{+}\boldsymbol{J}_{\mathrm{aco}}\ddot{\boldsymbol{q}}_{\mathrm{null}}^{\mathrm{ref}} + \ddot{\boldsymbol{q}}_{\mathrm{null}}^{\mathrm{ref}} \tag{4.156}$$

$$= \boldsymbol{J}_{\mathrm{aco}}^{+}\boldsymbol{\Gamma}^{-1}\left(\ddot{\boldsymbol{X}}^{\mathrm{ref}} - \boldsymbol{\Gamma}\dot{\boldsymbol{J}}_{\mathrm{aco}}\dot{\boldsymbol{q}}^{\mathrm{res}}\right) + \left(\boldsymbol{I} - \boldsymbol{J}_{\mathrm{aco}}^{+}\boldsymbol{J}_{\mathrm{aco}}\right)\ddot{\boldsymbol{q}}_{\mathrm{null}}^{\mathrm{ref}}. \tag{4.157}$$

By using the proposed DOB, we are not only suppressing the inertia force but also performing simplification of the inverse kinematics and the decoupling of the null space motion in the modal space, as well.

In order to improve the stability of the force control system, frequency domain damping (FDD) is used also in the redundant system. The controller in modal space is given by adding the frequency domain damping $\boldsymbol{D}_F^{\mathrm{fdd}}(s)$ [28] as follows:

$$\ddot{\boldsymbol{X}}_n^{\mathrm{ref}} = \ddot{\boldsymbol{X}}^{\mathrm{ref}} + \hat{\boldsymbol{A}}^{\mathrm{dis}} = \begin{bmatrix}\ddot{\boldsymbol{X}}_{Fn}^{\mathrm{ref}} \\ \ddot{\boldsymbol{X}}_{Xn}^{\mathrm{ref}}\end{bmatrix} \tag{4.158}$$

$$= \begin{bmatrix}\boldsymbol{C}_f\left(\boldsymbol{F}_F^{\mathrm{cmd}} - \hat{\boldsymbol{F}}_F^{\mathrm{ext}}\right) - \boldsymbol{D}_F^{\mathrm{fdd}}(s)\dot{\boldsymbol{X}}_F^{\mathrm{res}} \\ \boldsymbol{C}_p(s)\left(\boldsymbol{X}_X^{\mathrm{cmd}} - \boldsymbol{X}_X^{\mathrm{res}}\right) + \boldsymbol{M}_v\ddot{\boldsymbol{X}}_X^{\mathrm{cmd}}\end{bmatrix} + \begin{bmatrix}\hat{\boldsymbol{A}}_F^{\mathrm{dis}} \\ \hat{\boldsymbol{A}}_X^{\mathrm{dis}}\end{bmatrix} \tag{4.159}$$

$$\boldsymbol{D}_F^{\mathrm{fdd}}(s) = \boldsymbol{d}_F\boldsymbol{G}_H^{\mathrm{fdd}}(s). \tag{4.160}$$

In the lower frequency domain where FDD does not affect the force control system, (4.154) is established.

4.9.2 Comparison to Acceleration Observer [86]

As a method for suppressing the inertia force (operational force) in the bilateral control system, an acceleration observer based method [86] is proposed. The acceleration observer uses independently estimated accelerations in the master and slave systems. The estimated accelerations in the work space of the master and slave system are described as follows:

$$\hat{\ddot{\boldsymbol{X}}}_W^{\mathrm{res}} = \boldsymbol{G}_L^{\mathrm{acc}}(s)\left[\ddot{\boldsymbol{X}}_W^{\mathrm{ref}} - \mathrm{diag}\left[\boldsymbol{M}_W^{-1}\right]\boldsymbol{P}_W^{\mathrm{dis}}\right]. \tag{4.161}$$

The estimated acceleration is transformed to modal space as follows:

$$\begin{aligned}
\hat{\ddot{\boldsymbol{X}}}_F^{\mathrm{res}} &= \left[\boldsymbol{I}\ \ \boldsymbol{0}\right]\boldsymbol{\Gamma}\hat{\ddot{\boldsymbol{X}}}_W^{\mathrm{res}} && (4.162)\\
&= \ddot{\boldsymbol{X}}_{Wm}^{\mathrm{ref}} + \boldsymbol{\alpha}\ddot{\boldsymbol{X}}_{Ws}^{\mathrm{ref}} - \mathrm{diag}\left[\boldsymbol{M}_{Wm}^{-1}\right]\boldsymbol{P}_{Wm}^{\mathrm{dis}} - \boldsymbol{\alpha}\mathrm{diag}\left[\boldsymbol{M}_{Ws}^{-1}\right]\boldsymbol{P}_{Ws}^{\mathrm{dis}} && (4.163)\\
&\neq \hat{\boldsymbol{A}}^{\mathrm{dis}}. && (4.164)
\end{aligned}$$

As shown in the above equations, the estimated term $\hat{\ddot{\boldsymbol{X}}}_F^{\mathrm{res}}$ does not correspond to $\boldsymbol{A}^{\mathrm{dis}}$. This explains why it is difficult for the acceleration observer to compensate the inertia force and to realize simplification of inverse kinematics and decoupling null space motions in modal space.

4.9.3 Null Space Controller

For the null space controller, a term for maximizing the manipulability of a manipulator is added [101, 114, 115]. The control input is determined as follows:

$$\boldsymbol{K}_{o\mathrm{null}}\frac{\partial \boldsymbol{V}\left(\boldsymbol{q}^{\mathrm{res}}\right)}{\partial \boldsymbol{q}^{\mathrm{res}}} \tag{4.165}$$

where $\boldsymbol{K}_{o\mathrm{null}}$ is the proportional gain and $\boldsymbol{V}\left(\boldsymbol{q}^{\mathrm{res}}\right)$ is the manipulability which is expressed as:

$$\boldsymbol{V}\left(\boldsymbol{q}^{\mathrm{res}}\right) = \sqrt{\det\left(\boldsymbol{J}_{\mathrm{aco}}\boldsymbol{J}_{\mathrm{aco}}^T\right)}. \tag{4.166}$$

In addition to the term for manipulability, the position controller, velocity and external torque terms are added for the null space acceleration reference. The resulting acceleration reference of the null space is given as follows:

$$\ddot{\boldsymbol{q}}_{\mathrm{null}}^{\mathrm{ref}} = \boldsymbol{K}_{o\mathrm{null}}\frac{\partial \boldsymbol{V}\left(\boldsymbol{q}^{\mathrm{res}}\right)}{\partial \boldsymbol{q}^{\mathrm{res}}} + \boldsymbol{K}_{p\mathrm{null}}\left(\boldsymbol{q}_{\mathrm{null}}^{\mathrm{cmd}} - \boldsymbol{q}^{\mathrm{res}}\right) - \boldsymbol{K}_{v\mathrm{null}}\dot{\boldsymbol{q}}^{\mathrm{res}} - \boldsymbol{K}_{f\mathrm{null}}\boldsymbol{\tau}^{\mathrm{ext}}. \tag{4.167}$$

4.10 Proposed Hybrid Controller Based on KFSO.

In order to suppress noise effects, the Kalman filter based state observer (KFSO) [65] is introduced and a substitution of Kalman filters for conventional DOBs are considered in this part.

4.10.1 State Estimation Based on Kalman Filter

A discrete dynamics model of a joint actuator can be formulated in the state-space form as:

$$\begin{aligned} \boldsymbol{Z}(k+1) &= \mathbf{A}_d \boldsymbol{Z}(k) + \mathbf{B}_d u(k) + \boldsymbol{v}(k) && (4.168)\\ &= \left[q^{\mathrm{res}}(k) \;\; \dot{q}^{\mathrm{res}}(k) \;\; \tau^{\mathrm{dis}}(k) \right] && (4.169)\\ \boldsymbol{y}(k) &= \boldsymbol{c}\boldsymbol{Z}(k) + \boldsymbol{w}(k) && (4.170)\\ u(k) &= \tau^{\mathrm{ref}} && (4.171) \end{aligned}$$

where

$$\mathbf{A}_d = \begin{bmatrix} 1 & T_s & -\dfrac{T_s^2}{2J_n} \\ 0 & 1 & -\dfrac{T_s}{J_n} \\ 0 & 0 & 1 \end{bmatrix}, \; \mathbf{B}_d = \begin{bmatrix} \dfrac{T_s^2}{2J_n} \\ \dfrac{T_s}{J_n} \\ 0 \end{bmatrix}, \; \boldsymbol{c} = \begin{bmatrix} 1 \\ 0 \\ 0 \end{bmatrix}^T. \tag{4.172}$$

Based on (4.168), a Kalman filter is constructed. A Predicted (a priori) state estimate and predicted (a priori) estimate error covariance matrix are given as follows:

$$\begin{aligned} \hat{\boldsymbol{Z}}^{-}(k) &= \mathbf{A}_d \hat{\boldsymbol{Z}}(k-1) + \mathbf{B}_d u(k-1) && (4.173)\\ &= \left[\hat{q}_{\mathrm{kf}}^{-\mathrm{res}}(k) \;\; \hat{\dot{q}}_{\mathrm{kf}}^{-\mathrm{res}}(k) \;\; \hat{\tau}_{\mathrm{kf}}^{-\mathrm{dis}}(k) \right]^T && (4.174)\\ \mathbf{P}^{-}(k) &= \mathbf{A}_d \mathbf{P}(k-1)\mathbf{A}_d^T + \mathbf{Q}. && (4.175) \end{aligned}$$

The Kalman filter gain matrix $\boldsymbol{G}_{\mathrm{kf}}(\mathrm{k})$ is calculated as

$$\boldsymbol{G}_{\mathrm{kf}}(\mathrm{k}) = \mathbf{P}^{-}(k)\boldsymbol{c}^T(\boldsymbol{c}\mathbf{P}^{-}(k)\boldsymbol{c}^T + \mathbf{R})^{-1}. \tag{4.176}$$

The estimated (a posteriori) state vector and the (a posteriori) error matrix covariance matrix are updated by an actual measurement $\boldsymbol{y}(k)$ of motion sensors at every sampling instant as follows:

$$\begin{aligned} \hat{\boldsymbol{Z}}(k) &= \hat{\boldsymbol{Z}}^{-}(k) + \boldsymbol{G}_{\mathrm{kf}}(\mathrm{k}) \left(\boldsymbol{y}(\mathrm{k}) - \boldsymbol{c}\hat{\boldsymbol{Z}}^{-}(\mathrm{k}) \right) && (4.177)\\ &= \left[\hat{q}_{\mathrm{kf}}^{\mathrm{res}}(k) \;\; \hat{\dot{q}}_{\mathrm{kf}}^{\mathrm{res}}(k) \;\; \hat{\tau}_{\mathrm{kf}}^{\mathrm{dis}}(k) \right]^T && (4.178)\\ \mathbf{P}(k) &= (\boldsymbol{I} - \boldsymbol{G}_{\mathrm{kf}}(\mathrm{k})\boldsymbol{c})\, \mathbf{P}^{-}(k). && (4.179) \end{aligned}$$

The estimated (a posteriori) state variables are used for the hybrid control systems. The joint space angle vector, angular velocity vector and external/disturbance torque vectors are expressed by using the estimated variables as follows:

$$\hat{\boldsymbol{q}}_{\rm kf}^{\rm res} = \left[\hat{q}_{1\rm kf}^{\rm res}(k) \ \cdots \ \hat{q}_{i\rm kf}^{\rm res}(k)\right]^T \tag{4.180}$$

$$\hat{\dot{\boldsymbol{q}}}_{\rm kf}^{\rm res} = \left[\hat{\dot{q}}_{1\rm kf}^{\rm res}(k) \ \cdots \ \hat{\dot{q}}_{i\rm kf}^{\rm res}(k)\right]^T \tag{4.181}$$

$$\hat{\boldsymbol{\tau}}_{\rm kf}^{\rm ext} = \left[\hat{\tau}_{1\rm kf}^{\rm ext}(k) \ \cdots \ \hat{\tau}_{i\rm kf}^{\rm ext}(k)\right]^T \tag{4.182}$$

$$\hat{\boldsymbol{\tau}}_{\rm kf}^{\rm dis} = \left[\hat{\tau}_{1\rm kf}^{\rm dis}(k) \ \cdots \ \hat{\tau}_{i\rm kf}^{\rm dis}(k)\right]^T. \tag{4.183}$$

The vectors composed by the estimated variables are transformed by using transformation matrices $\boldsymbol{\Gamma}$ as follows:

$$\hat{\boldsymbol{X}}_{\rm kf}^{\rm res} = \boldsymbol{\Gamma}\mathbf{G}\left(\hat{\boldsymbol{q}}_{\rm kf}^{\rm res}\right) \tag{4.184}$$

$$\hat{\dot{\boldsymbol{X}}}_{\rm kf}^{\rm res} = \boldsymbol{\Gamma}\boldsymbol{J}_{\rm aco}\hat{\dot{\boldsymbol{q}}}_{\rm kf}^{\rm res} \tag{4.185}$$

$$\hat{\boldsymbol{F}}_{\rm kf}^{\rm ext} = \boldsymbol{\Gamma}_F\boldsymbol{F}_W^{\rm ext} = \boldsymbol{\Gamma}\boldsymbol{F}_W^{\rm ext} = \boldsymbol{\Gamma}\boldsymbol{J}_{\rm aco}^{+T}\hat{\boldsymbol{\tau}}_{\rm kf}^{\rm ext}. \tag{4.186}$$

The equivalent disturbance through the high pass filter is expressed as follows:

$$\hat{\mathbf{P}}_{\rm kf}^{\rm ext} = \boldsymbol{G}_{F\rm kf}(z)\hat{\boldsymbol{F}}_{\rm kf}^{\rm ext} \tag{4.187}$$

$$\boldsymbol{G}_{F\rm kf}(z) = \boldsymbol{\Gamma}\boldsymbol{J}_{\rm aco}^{+T}\left[\boldsymbol{I} - \boldsymbol{g}_{l\rm kf}^{\rm ext}(z)\right]\left[\boldsymbol{g}_{l\rm kf}^{\rm ext}(z)\right]^{-1}\boldsymbol{J}_{\rm aco}^{T}\boldsymbol{\Gamma}^{-1} \tag{4.188}$$

$$= \boldsymbol{\Gamma}\boldsymbol{J}_{\rm aco}^{+T}\boldsymbol{g}_{h\rm kf}^{\rm ext}(z)\left[\boldsymbol{g}_{l\rm kf}^{\rm ext}(z)\right]^{-1}\boldsymbol{J}_{\rm aco}^{T}\boldsymbol{\Gamma}^{-1} \tag{4.189}$$

$$= \boldsymbol{\Gamma}\boldsymbol{J}_{\rm aco}^{+T}\boldsymbol{g}_{F\rm kf}(z)\boldsymbol{J}_{\rm aco}^{T}\boldsymbol{\Gamma}^{-1}. \tag{4.190}$$

The information of the equivalent disturbance $\hat{\mathbf{P}}_{\rm kf}^{\rm ext}$ is necessary for constructing the proposed DOB for the hybrid controller. However, the actual information of $\boldsymbol{g}_{h\rm kf}^{\rm ext}(z)$ and $\boldsymbol{g}_{h\rm kf}^{\rm ext}(z)$ that is needed to calculate $\hat{\mathbf{P}}_{\rm kf}^{\rm ext}$ is difficult to obtain in the case of the Kalman filter.

4.10.2 Implementation of Proposed DOB in Mode Space with Joint Space KFSO

As shown in (4.189),LPF for joint space disturbance estimation and the resulting HPF for disturbance compensation are required for the proposed DOB in mode space. However, it is difficult to directly obtain the LPF and HPF from KFSO. Therefore, this dissertation uses the steady state Kalman filter as a substitute for the LPF and HPF of KFSO.

In order to obtain the steady state Kalman gain, the following Algebraic Riccati Equation (ARE) [105] should be solved:

$$\mathbf{P} = \mathbf{A}_d \left[\mathbf{P} - \mathbf{P}\boldsymbol{c}^T \left(\boldsymbol{c}\mathbf{P}\boldsymbol{c}^T + \mathbf{R} \right)^{-1} \boldsymbol{c}\mathbf{P} \right] \mathbf{A}_d^T + \mathbf{Q}. \tag{4.191}$$

By using the solution of ARE $\boldsymbol{\mathcal{P}}$, the steady state Kalman gain $\boldsymbol{\mathcal{G}}_{\rm skf}$ is obtained as follows:

$$\boldsymbol{\mathcal{G}}_{\rm skf} = \boldsymbol{\mathcal{P}}\boldsymbol{c}^T \left(\boldsymbol{c}\boldsymbol{\mathcal{P}}\boldsymbol{c}^T + \mathbf{R} \right). \tag{4.192}$$

By using $\boldsymbol{\mathcal{G}}_{\rm skf}$, the estimated state by the steady state Kalman filter is derived from (4.173) and (4.177) as follows:

$$\hat{\boldsymbol{Z}}_{\rm skf}(z) \;=\; \left[\boldsymbol{I} - (\boldsymbol{I} - \boldsymbol{\mathcal{G}}_{\rm skf}\boldsymbol{c})\, \mathbf{A}_d z^{-1} \right]^{-1} \left[\boldsymbol{\mathcal{G}}_{\rm skf}\boldsymbol{y}(z) + (\boldsymbol{I} - \boldsymbol{\mathcal{G}}_{\rm skf}\boldsymbol{c})\, \mathbf{A}_d z^{-1} u(z) \right]. \tag{4.193}$$

From (4.193), a steady state Kalman filter for disturbance estimation $g^{\rm ext}_{l{\rm skf}}(z)$ is derived as

$$\hat{\tau}^{\rm ext}_{\rm skf} \;=\; \frac{n^{\rm ext}_{l{\rm skf}}(z)}{d^{\rm ext}_{\rm skf}(z)} \tau^{\rm ext} = g^{\rm ext}_{l{\rm skf}}(z)\tau^{\rm ext} \tag{4.194}$$

where $n^{\rm ext}_{l{\rm skf}}(z)$ and $d^{\rm ext}_{\rm skf}(z)$ represent a numerator and denominator of the steady state Kalman filter, respectively. An equivalent high-pass filter of the disturbance suppression $g^{\rm ext}_{h{\rm skf}}(z)$is derived as follows:

$$g^{\rm ext}_{h{\rm skf}}(z) \;=\; \left[1 - g^{\rm ext}_{l{\rm skf}}(z) \right] = \left[\frac{d^{\rm ext}_{\rm skf}(z) - n^{\rm ext}_{l{\rm skf}}(z)}{D^{\rm ext}_{\rm skf}(z)} \right] = \frac{n^{\rm ext}_{h{\rm skf}}(z)}{d^{\rm ext}_{\rm skf}(z)} \tag{4.195}$$

where $N^{\rm dis}_{H{\rm skf}}(z)$ represents a numerator of the high-pass filter.

By using the low-pass filter and high-pass filter of the steady state Kalman filter, the approximated equivalent disturbance in the joint space $\hat{p}^{\rm ext}_{\rm skf}$ is obtained as follows:

$$\hat{p}^{\rm ext}_{\rm skf} = \frac{g^{\rm ext}_{h{\rm skf}}(z)}{g^{\rm ext}_{l{\rm skf}}(z)} \hat{\tau}^{\rm ext}_{\rm skf} = \frac{n^{\rm ext}_{h{\rm skf}}(z)}{n^{\rm ext}_{l{\rm skf}}(z)} \hat{\tau}^{\rm ext}_{\rm kf} = g_{F{\rm skf}}(z)\hat{\tau}^{\rm ext}_{\rm kf}. \tag{4.196}$$

By considering a bilinear transform, $\hat{p}^{\rm ext}_{\rm skf}$ can be also described as

$$\hat{p}^{\rm ext}_{\rm skf} = \frac{2}{T_s}\frac{z-1}{z+1} \frac{\tilde{n}^{\rm ext}_{h{\rm skf}}(z)}{\tilde{n}^{\rm ext}_{l{\rm skf}}(z)} \hat{\tau}^{\rm ext}_{\rm kf} = \frac{2}{T_s}\frac{z-1}{z+1} \tilde{g}_{F{\rm skf}}(z)\hat{\tau}^{\rm ext}_{\rm kf} \tag{4.197}$$

where $\tilde{\bullet}$ represent variables from which elements of the differentiation are removed. In order to construct the proposed DOB in force control system based on Kalman filter, a new variable λ is defined as

$$\hat{\dot{\lambda}}^{\rm ext}_{\rm skf} = \tilde{g}_{F{\rm skf}}(z)\hat{\tau}^{\rm ext}_{\rm kf}. \tag{4.198}$$

The vectors of the equivalent disturbance and the integrated variable in joint space are expressed as follows:

$$\hat{\boldsymbol{p}}^{\rm ext}_{\rm skf} = \frac{2}{T_s}\frac{z-1}{z+1}\boldsymbol{g}^{\rm ext}_{h\rm skf}(z)[\boldsymbol{g}^{\rm ext}_{l\rm skf}(z)]^{-1}\hat{\boldsymbol{\tau}}^{\rm ext}_{\rm kf} \tag{4.199}$$

$$= \boldsymbol{n}^{\rm ext}_{h\rm skf}(z)\left[\boldsymbol{n}^{\rm ext}_{l\rm skf}(z)\right]^{-1}\hat{\boldsymbol{\tau}}^{\rm ext}_{\rm kf} = \boldsymbol{g}_{F\rm skf}(z)\hat{\boldsymbol{\tau}}^{\rm ext}_{\rm kf} \tag{4.200}$$

$$\hat{\boldsymbol{\lambda}}^{\rm ext}_{\rm skf} = \tilde{\boldsymbol{n}}^{\rm ext}_{h\rm skf}(z)\left[\tilde{\boldsymbol{n}}^{\rm ext}_{l\rm skf}(z)\right]^{-1}\hat{\boldsymbol{\tau}}^{\rm ext}_{\rm kf} = \tilde{\boldsymbol{g}}_{F\rm skf}(z)\hat{\boldsymbol{\tau}}^{\rm ext}_{\rm kf}. \tag{4.201}$$

where $\boldsymbol{n}\mathrm{ext}_{\rm skf}$ is a diagonal elements with numerators of $\boldsymbol{g}_{l\rm skf}(z)$ and $\boldsymbol{g}_{h\rm skf}$. The vectors are transformed to the modal space as follows:

$$\hat{\mathbf{P}}^{\rm ext}_{\rm skf} = \frac{2}{T_s}\frac{z-1}{z+1}\boldsymbol{\Gamma}\boldsymbol{J}^{+T}_{\rm aco}\tilde{\boldsymbol{g}}_{F\rm skf}(z)\boldsymbol{J}^{T}_{\rm aco}\boldsymbol{\Gamma}^{-1}\hat{\boldsymbol{F}}^{\rm ext}_{\rm kf} \tag{4.202}$$

$$= \frac{2}{T_s}\frac{z-1}{z+1}\tilde{\boldsymbol{G}}_{F\rm skf}(z)\hat{\boldsymbol{F}}^{\rm ext}_{\rm kf} \tag{4.203}$$

$$\hat{\boldsymbol{\Lambda}}^{\rm ext}_{\rm skf} = \boldsymbol{\Gamma}\boldsymbol{J}^{+T}_{\rm aco}\tilde{\boldsymbol{g}}_{F\rm skf}(z)\boldsymbol{J}^{T}_{\rm aco}\boldsymbol{\Gamma}^{-1}\hat{\boldsymbol{F}}^{\rm ext}_{\rm kf} \tag{4.204}$$

$$= \tilde{\boldsymbol{G}}_{F\rm skf}(z)\hat{\boldsymbol{F}}^{\rm ext}_{\rm kf}. \tag{4.205}$$

By using $\hat{\boldsymbol{\Lambda}}^{\rm ext}_{\rm skf}$, the mode space observer based on Kalman filter for the force control can be constructed.

The state space equation in the force control system is expressed as follows:

$$\dot{\boldsymbol{Z}}_F(t) = \mathbf{A}_F\boldsymbol{Z}_F(t) + \mathbf{B}_F\boldsymbol{U}_F(t) + \boldsymbol{v}_F \tag{4.206}$$

$$\boldsymbol{Z}_F(t) = \left[\boldsymbol{\mu}_{\rm FF}\hat{\boldsymbol{\Lambda}}^{\rm ext}_{F\rm skf} \quad \boldsymbol{A}^{\rm dis}_F\right]^T \tag{4.207}$$

$$\dot{\boldsymbol{Z}}_F(t) = \left[\boldsymbol{\mu}_{\rm FF}\hat{\boldsymbol{P}}^{\rm ext}_{F\rm skf} \quad \dot{\boldsymbol{A}}^{\rm dis}_F\right]^T \tag{4.208}$$

$$\boldsymbol{U}_F(t) = \ddot{\boldsymbol{X}}^{\rm ref}_F \tag{4.209}$$

$$\boldsymbol{Y}_F(t) = \boldsymbol{c}_F\boldsymbol{Z}_F(t) + \boldsymbol{w}_F \tag{4.210}$$

where

$$\mathbf{A}_F = \begin{bmatrix}\mathbf{0} & -\boldsymbol{I}\\ \mathbf{0} & \mathbf{0}\end{bmatrix},\ \mathbf{B}_F = \begin{bmatrix}\boldsymbol{I}\\ \mathbf{0}\end{bmatrix},\ \boldsymbol{c}_F = \begin{bmatrix}\boldsymbol{I}\\ \mathbf{0}\end{bmatrix}^T. \tag{4.211}$$

In the above state space equation, the disturbance model is defined as

$$\dot{\boldsymbol{A}}^{\rm dis}_F = \boldsymbol{v}^{\rm dis}_{F\rm dif^0}. \tag{4.212}$$

Through the Kalman filtering process, the estimated value is obtained as:

$$\hat{\boldsymbol{Z}}_{F\rm kf}(k) = \left[\boldsymbol{\mu}_{\rm FF}\hat{\boldsymbol{\Lambda}}^{\rm ext}_{\rm kf}(k) \quad \hat{\boldsymbol{A}}^{\rm dis}_{F\rm kf}(k)\right]^T. \tag{4.213}$$

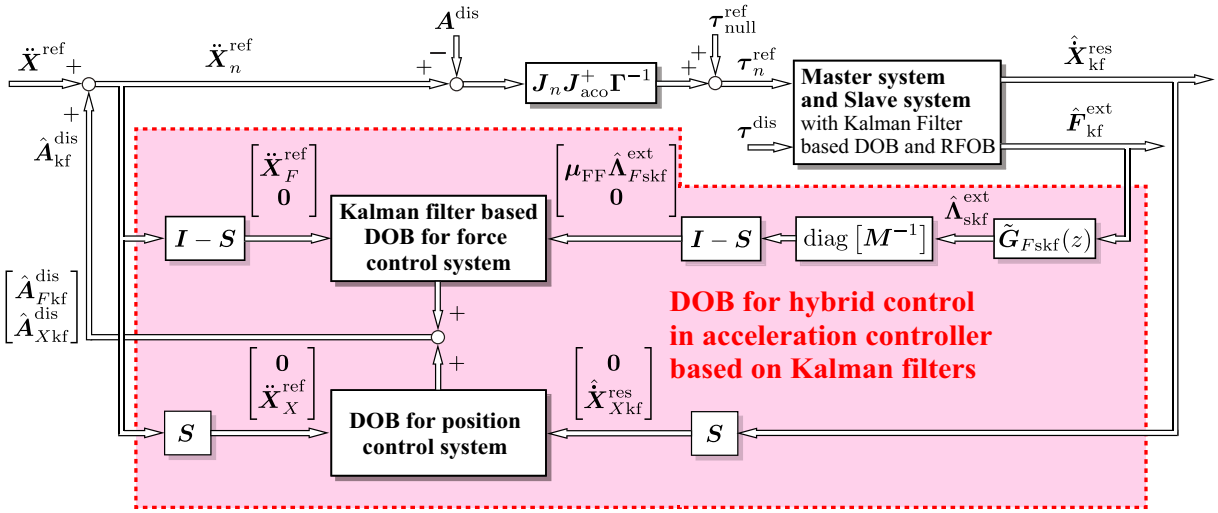

Fig. 4-23: Proposed DOB for Hybrid Controller in Redundant System.

The estimated variable $\hat{\boldsymbol{A}}^{\mathrm{dis}}_{F\mathrm{kf}}(k)$ is used for the compensation of the disturbance.

On the other hand, the disturbance in the position control system is obtained by using the estimated and transformed velocity by the Kalman filters as follows:

$$\hat{\boldsymbol{A}}^{\mathrm{dis}}_{X\mathrm{kf}} = \boldsymbol{G}^{\mathrm{dis}}_{L}(z)\left[\ddot{\boldsymbol{X}}^{\mathrm{ref}}_{X} - \frac{2}{T_s}\frac{1-z^{-1}}{1+z^{-1}}\dot{\hat{\boldsymbol{X}}}^{\mathrm{res}}_{X\mathrm{kf}}\right]. \tag{4.214}$$

Finally, the disturbance acceleration dimension is obtained by using the estimated variables of the KFSO as follows:

$$\hat{\boldsymbol{A}}^{\mathrm{dis}}_{\mathrm{kf}} = \boldsymbol{S}\hat{\boldsymbol{A}}^{\mathrm{dis}}_{X\mathrm{kf}} + (\boldsymbol{I}-\boldsymbol{S})\,\hat{\boldsymbol{A}}^{\mathrm{dis}}_{F\mathrm{kf}} = \begin{bmatrix}\hat{\boldsymbol{A}}^{\mathrm{dis}}_{F\mathrm{kf}} \\ \hat{\boldsymbol{A}}^{\mathrm{dis}}_{X\mathrm{kf}}\end{bmatrix} \tag{4.215}$$

Fig. 4-23 shows the block diagram of the Kalman filter based mode space disturbance observer for hybrid controller in redundant system. By using the proposed Kalman filter based DOB, the suppression of the inertia force, and simplification of the inverse kinematics and the decoupling of the null space in the modal space are all done without enhancing noise effect.

The estimated variables of Kalman filters are substituted with the parameters of the proposed hybrid controller, as follows:

$$\ddot{\boldsymbol{X}}^{\mathrm{ref}}_{n} = \ddot{\boldsymbol{X}}^{\mathrm{ref}} + \hat{\boldsymbol{A}}^{\mathrm{dis}}_{\mathrm{kf}} = \begin{bmatrix}\ddot{\boldsymbol{X}}^{\mathrm{ref}}_{Fn} \\ \ddot{\boldsymbol{X}}^{\mathrm{ref}}_{Xn}\end{bmatrix} \tag{4.216}$$

$$= \begin{bmatrix}\boldsymbol{C}_f\left(\boldsymbol{F}^{\mathrm{cmd}}_{F} - \hat{\boldsymbol{F}}^{\mathrm{ext}}_{F\mathrm{kf}}\right) - \boldsymbol{D}^{\mathrm{fdd}}_{F}(z)\dot{\hat{\boldsymbol{X}}}^{\mathrm{res}}_{F\mathrm{kf}} \\ \boldsymbol{C}_p(s)\left(\boldsymbol{X}^{\mathrm{cmd}}_{X} - \hat{\boldsymbol{X}}^{\mathrm{res}}_{X\mathrm{kf}}\right) + \boldsymbol{M}_v\ddot{\boldsymbol{X}}^{\mathrm{cmd}}_{X}\end{bmatrix} + \begin{bmatrix}\hat{\boldsymbol{A}}^{\mathrm{dis}}_{F\mathrm{kf}} \\ \hat{\boldsymbol{A}}^{\mathrm{dis}}_{X\mathrm{kf}}\end{bmatrix}. \tag{4.217}$$

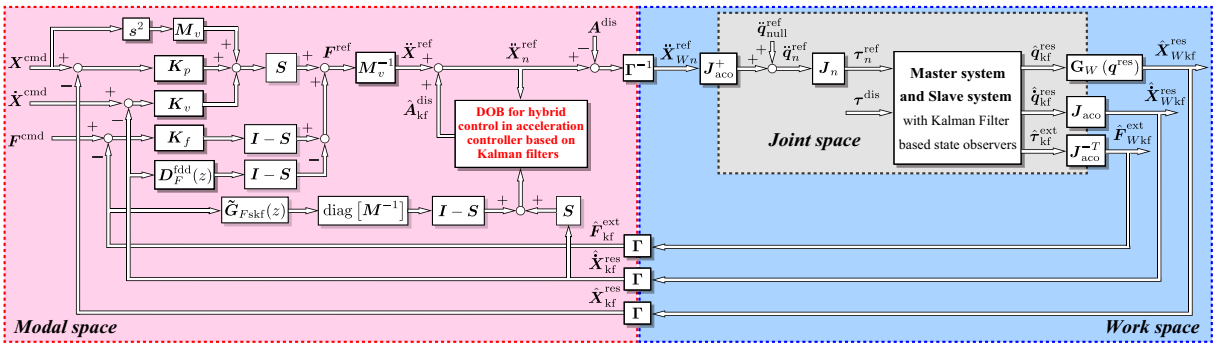

Fig. 4-24: Block diagram of the proposed hybrid controller based on DOB in mode space combined with Kalman Filters.

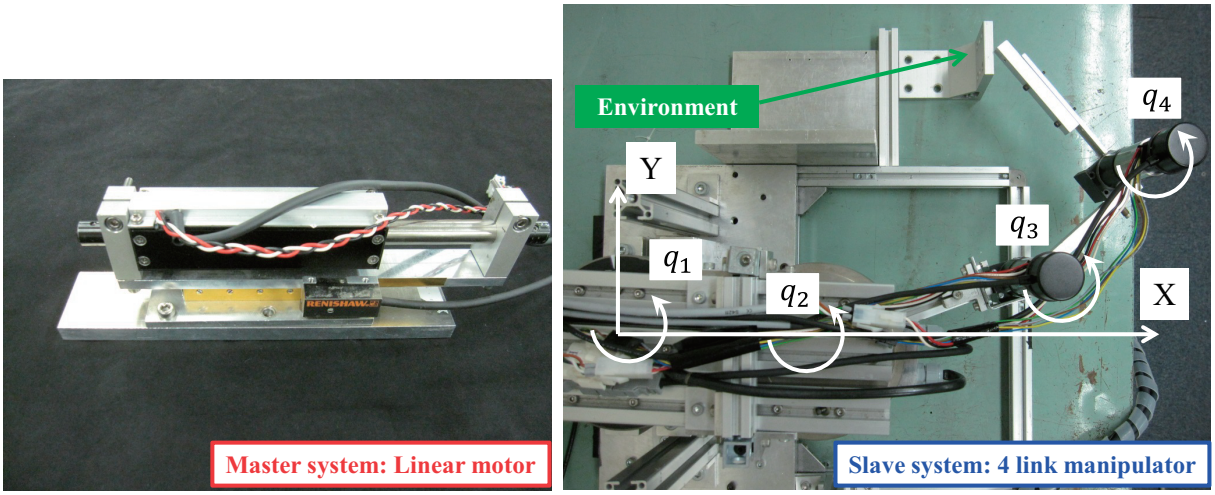

Fig. 4-25: Experimental system and models of MDOF manipulators.

Fig. 4-24 is a whole block diagram of the proposed hybrid controller. The proposed structure improves the hybrid control, including the bilateral control system, due to the effect of the proposed disturbance observer for hybrid controller. In addition, the proposed acceleration controller can reduce noise effects because of characteristic of the Kalman filters.

4.11 Experiments of Bilateral Control with Redundant System

4.11.1 Experimental Setup for Bilateral Control with Redundant System

In order to confirm the validity of the proposal, experiments regarding the bilateral control between different structure systems are conducted. A 1-DOF linear motor as a master system and a 4-DOF serial

Table 4.6: Experimental parameters for bilateral control within a redundant system.

Parameter	Description	Value
T_s	sampling time	0.2 ms
M_m	nominal mass of master system	0.3 kg
J_{1ns}	inertia of slave	0.0366 kgm^2
J_{2ns}	inertia of slave	0.0031 kgm^2
J_{3ns}	inertia of slave	0.0012 kgm^2
J_{4ns}	inertia of slave	7.0850$\times 10^{-5}$ kgm^2
K_f	force control gain	0.5
K_p	proportional gain	900
K_v	differential gain	180
d_F^{fdd}	damping of FDD	200
g^{fdd}	bandwidth of FDD	100
g_l	bandwidth of joint disturbance/external torque estimation	400 rad/s
g_{FL}^{dis}	bandwidth of mode disturbance estimation in force control	86 rad/s
g_{XL}^{dis}	bandwidth of mode disturbance estimation in position control	100 rad/s
g_v^{pd}	bandwidth of velocity estimation	890 rad/s
ΔX_m	resolution of msaster encoder	1.0 $\times$ 10 ^{6} pulses/rev
ΔX_s	resolution of slave encoder	1.0 $\times$ 10^4 pulses/rev
α	scaling factor of force	0.4 and 20
β	scaling factor of position	0.4 and 20

link redundant manipulator as a slave system are used for the experiments as shown in Fig. 4-25.

Bilateral control system is constructed between the linear motor and the X axis of the manipulator. In the bilateral control, free motions and contact motions to the aluminum block as an experimental environment are performed. On the other hand, position controls are implemented in Y axis of the redundant manipulator. Additionally, a step response is given in a null space (Joint 2).

The following control structures are tested.

1) An Acceleration controller without mode space observers (based on (4.134))

2) An Acceleration controller with acceleration observer with DOB in the position control system

3) An Acceleration controller without simplification of inverse kinematics (only the decoupling of null space in modal space is considered)

$$\ddot{\boldsymbol{q}}^{\mathrm{ref}} = \boldsymbol{J}_{\mathrm{aco}}^{+}\boldsymbol{\Gamma}^{-1}\ddot{\boldsymbol{X}}^{\mathrm{ref}} + \left(\boldsymbol{I} - \boldsymbol{J}_{\mathrm{aco}}^{+}\boldsymbol{J}_{\mathrm{aco}}\right)\ddot{\boldsymbol{q}}_{\mathrm{null}}^{\mathrm{ref}} \tag{4.218}$$

4) An Acceleration controller with a mode space observer

5) The proposed DOB for hybrid controller in acceleration controller

6) The proposed DOB for hybrid controller in acceleration controller based on Kalman filters

In the case of 1) and 3), the controller gains in modal space K_f, K_v and K_p are doubled compared with the cases of the observer based methods. Two experiments with different scaling factors ($\alpha = \beta = 0.4$ and $\alpha = \beta = 20$) are conducted. In the first case with $\alpha = \beta = 0.4$, the master side motions are enlarged at the slave side.

On the other hand, master side motions are reduced in the second case with $\alpha = \beta = 20$. This case is tested only on the proposed MDOB with and without Kalman filters. In other words, the slave side effect is enlarged at the master side (e. g. noise effects).

The position commands and null space control gains are given as follows:

$$\boldsymbol{X}^{\mathrm{cmd}} = \begin{bmatrix} \boldsymbol{X}_X^{\mathrm{cmd}} & \boldsymbol{X}_{X\mathrm{sub}}^{\mathrm{cmd}} \end{bmatrix} = \begin{bmatrix} \boldsymbol{X}_X^{\mathrm{cmd}} & \boldsymbol{Y}^{\mathrm{cmd}} \end{bmatrix} = \begin{bmatrix} -X_s(0) & 0 \end{bmatrix} \tag{4.219}$$

$$\boldsymbol{q}_{\mathrm{null}}^{\mathrm{cmd}} = \begin{cases} \begin{bmatrix} q_1(0) & q_2(0) + \frac{\pi}{48} & q_3(0) & q_4(0) \end{bmatrix} & 0.1 \leq t < 1.3 \\ \begin{bmatrix} q_1(0) & q_2(0) & q_3(0) & q_4(0) \end{bmatrix} & t \geq 1.3 \end{cases} \tag{4.220}$$

$$\boldsymbol{K}_{o\mathrm{null}} = \begin{bmatrix} 50 & 50 & 50 & 50 \end{bmatrix} \tag{4.221}$$

$$\boldsymbol{K}_{p\mathrm{null}} = \begin{bmatrix} 0 & 900 & 0 & 0 \end{bmatrix} \tag{4.222}$$

$$\boldsymbol{K}_{v\mathrm{null}} = \begin{bmatrix} 270 & 270 & 270 & 270 \end{bmatrix} \tag{4.223}$$

$$\boldsymbol{K}_{f\mathrm{null}} = \begin{bmatrix} 50 & 10 & 5 & 5 \end{bmatrix}. \tag{4.224}$$

Herein the null space step command is given only in the case of $\alpha = \beta = 0.4$.

Table 4.6 lists the experimental parameters.

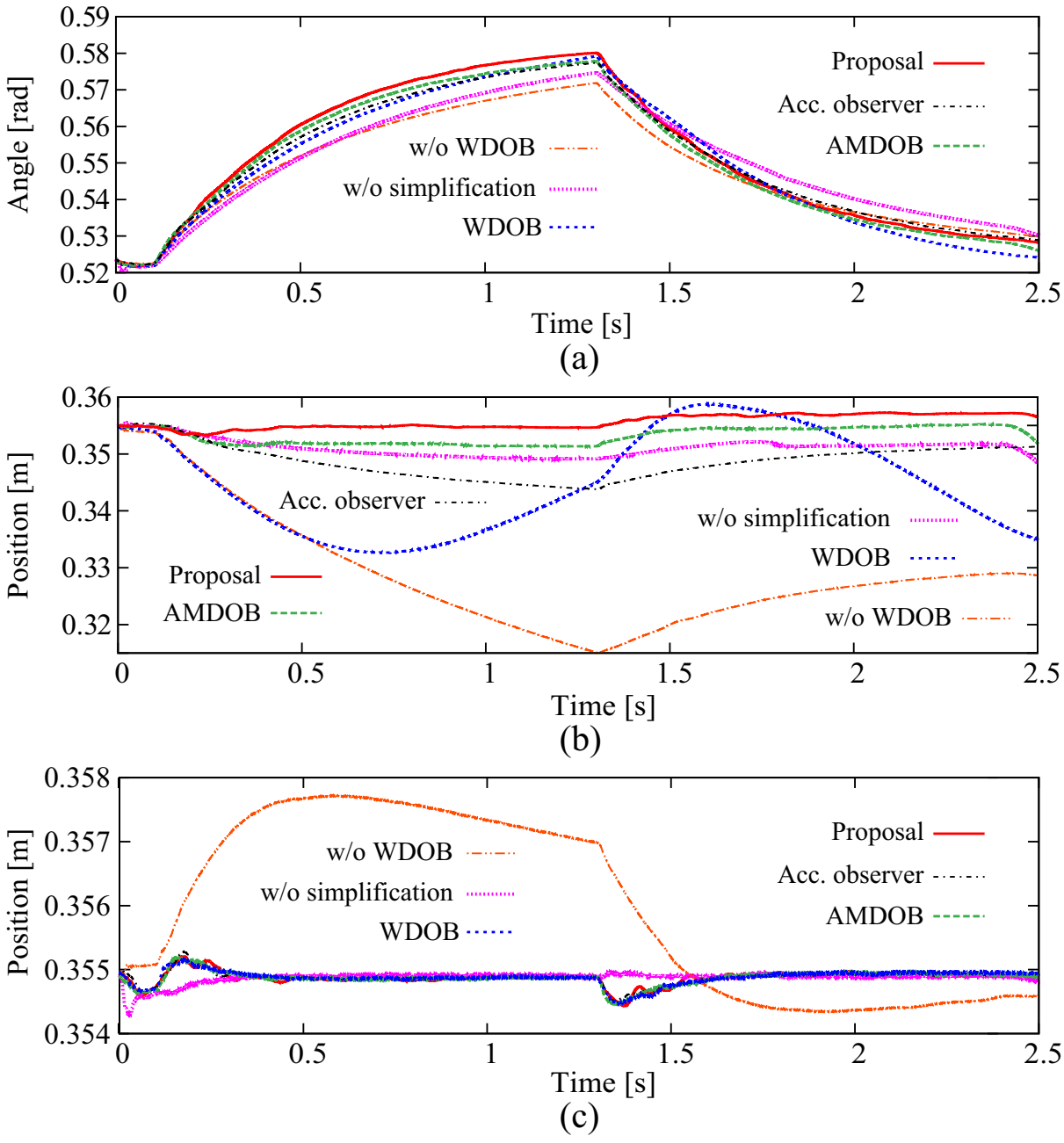

Fig. 4-26: Experimental results of null space motion. (a) null space responses (joint 2). (b) work space response (X axis). (c) work space response (Y axis).

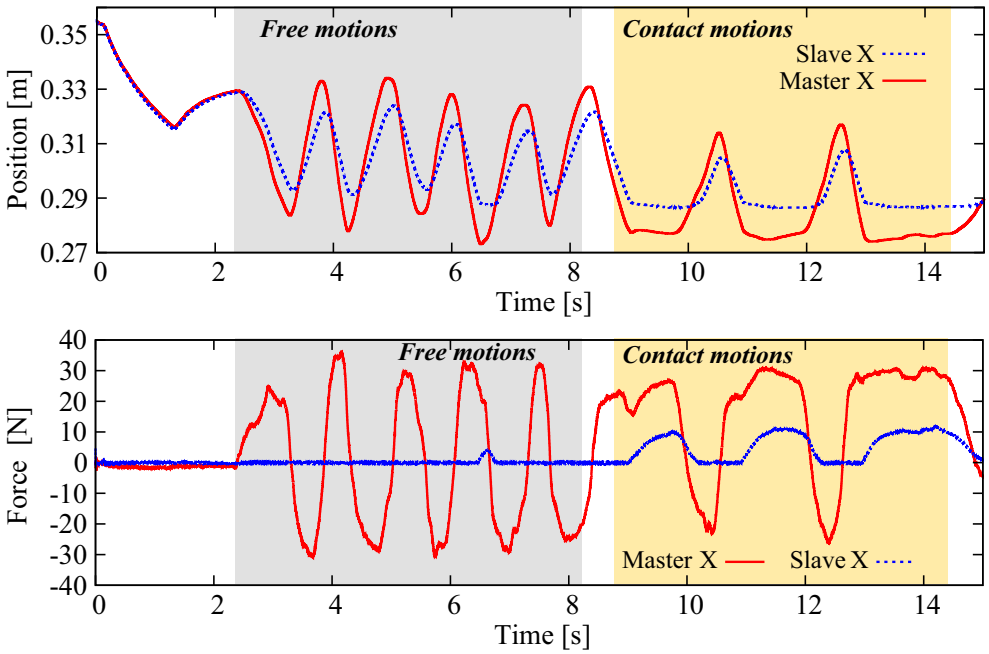

Fig. 4-27: Experimental results of the controller without MDOBs.

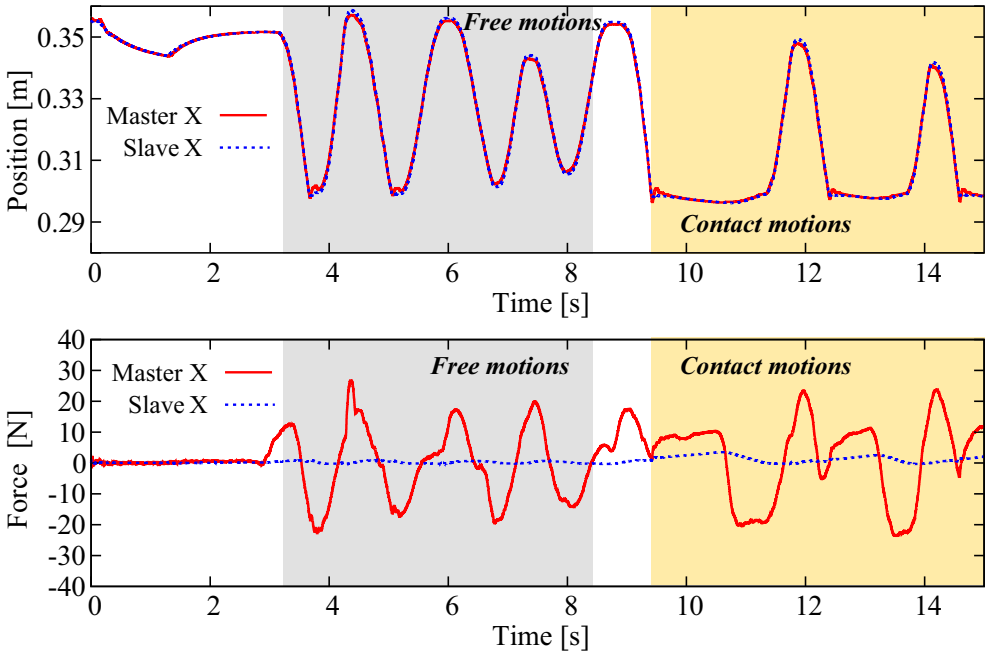

Fig. 4-28: Experimental results of the controller based on the acceleration observer with DOB in the position control system.

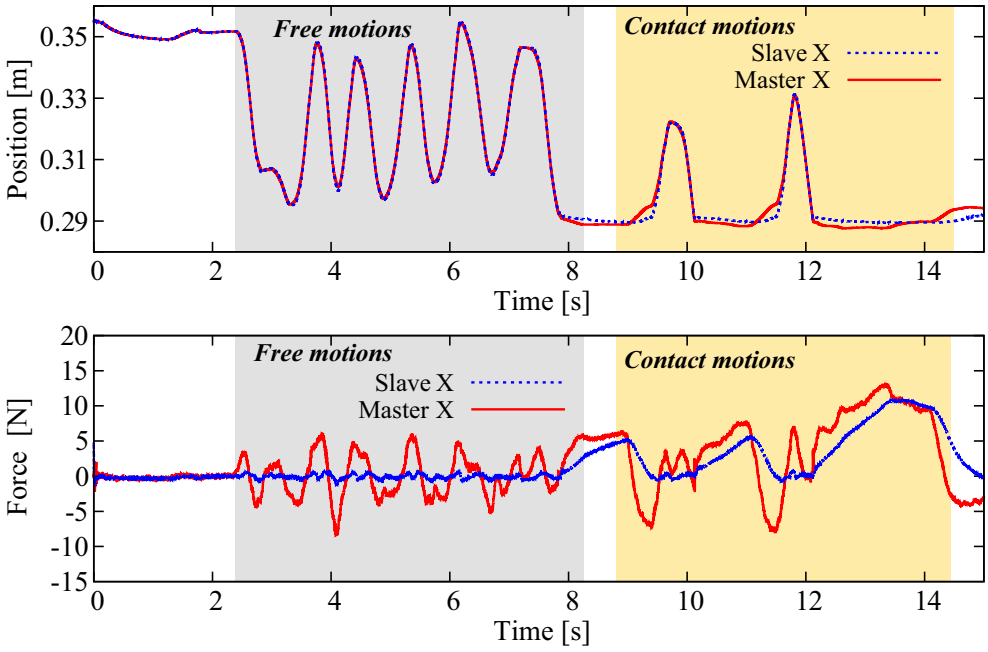

Fig. 4-29: Experimental results of the controller without simplification of the inverse kinematics.

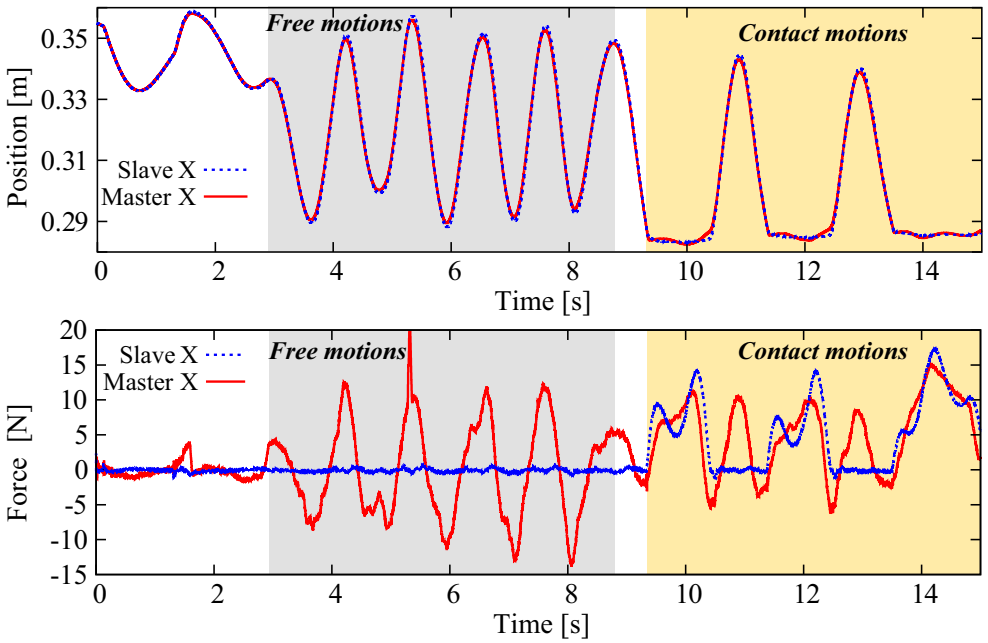

Fig. 4-30: Experimental results of the acceleration controller based on MDOB.

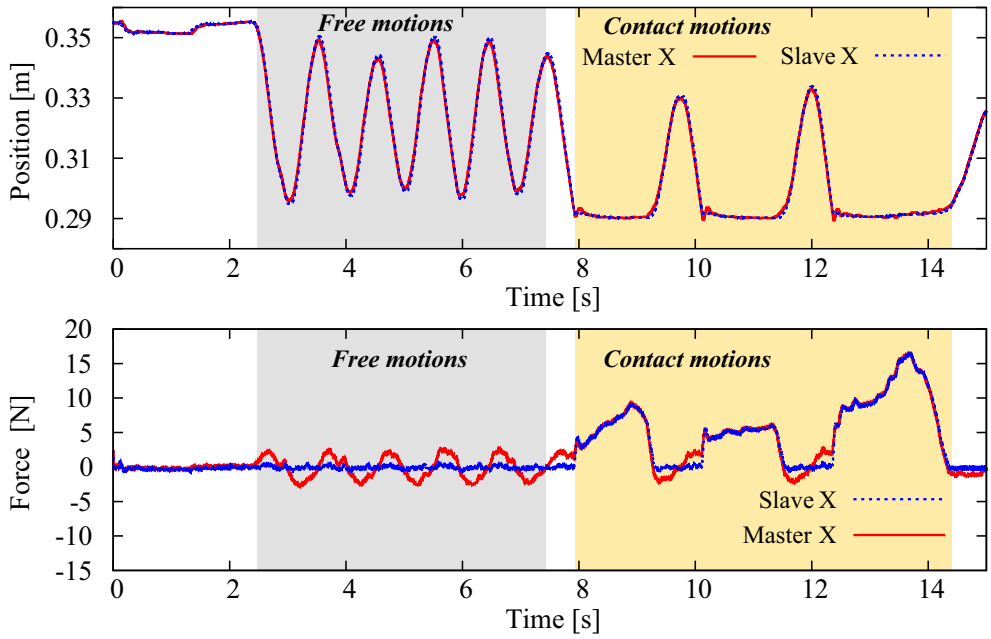

Fig. 4-31: Experimental results of the proposed MDOB for hybrid control in acceleration controller having a scaling factor 0.4.

4.11.2 Experimental Results of Bilateral Control with Scaling Factor $\alpha = \beta = 0.4$

Fig. 4-26 shows the experimental results with respect to null space motions and tip responses of the slave manipulator. Fig. 4-26 (a) represent angle responses of the joint 2. On the other hand, Figs. 4-26 (b) and (c) represents the tip motions. As shown in Fig. 4-26 (b) and (c), the tip responses of the method without MDOB are affected by the interference from the null space motions. Although the position responses of the other methods in X axis are different, they are all caused by the difference of the performance of the force control (bilateral control). Fig. 4-26 (b) and (c) represent the method with MDOBs and with the null space projection matrix well suppress the null space motions in the modal space compared to the method without MDOBs. From Fig. 4-27 to Fig. 4-32, the position and force responses of the bilateral control in the X axis are shown. As shown in Fig. 4-27, the method without MDOBs (based on eq. (4.134)) cannot achieve position and force tracking because of the disturbance caused by the coordinate transformation (simplification of the inverse kinematics) and interference from the null space. Furthermore, the method generates large operational force caused by the inertia force in addition to the above two terms.

Fig. 4-28 shows the experimental results of the method based on Kalman filters with acceleration

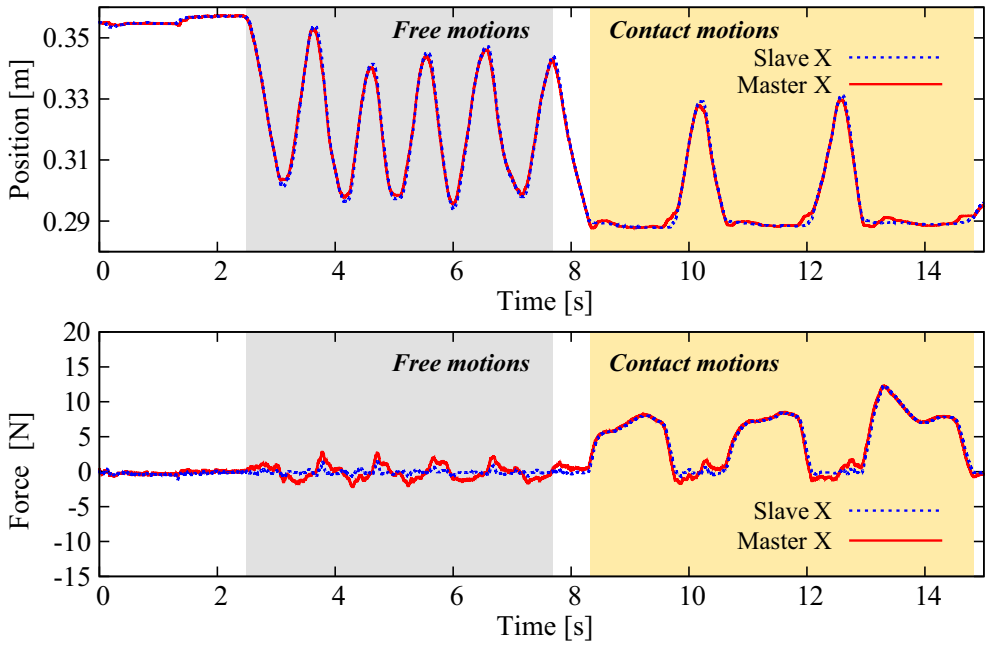

Fig. 4-32: Experimental results of the proposed method based on Kalman filters for hybrid control in acceleration controller having a scaling factor of 0.4.

observer. The difference between the proposed method and the method based on Kalman filters with acceleration observer is only the compensation value for the force control system. As shown in Fig. 4-28, the force control performance is deteriorated due to an inappropriate estimation of the compensation value by the acceleration observer, though the position control performance is better than Fig. 4-27 because of the implementation of the DOB in the position controller. Fig. 4-27 shows the experimental results of the method without simplification of the inverse kinematics. Despite the reducing of the operational force in the free motions compared to the above two methods, the position and force tracking control performance in contact motions are deteriorated due to the disturbance caused by the simplification of the inverse kinematics.

Fig. 4-30 shows the experimental results of the acceleration controller with MDOB. Compared to the three methods presented above, it is found that the position and force tracking performance is improved. However, the operational force caused by the inertia force is still large in the free motions.

On the other hand Figs. 4-31 and 4-32 show the experimental results of the proposed MDOB for hybrid control without and with Kalman filters, respectively. Compared to the other methods, the proposed methods achieve an improvement in the position and force tracking performance in contact motions and

suppressing operational force in the free motions.

4.11.3 Experimental Results of Bilateral Control with Scaling Factor $\alpha = \beta = 20$

Figs. 4-33 and 4-32 show the experimental result of macro-micro bilateral control with scaling factor $\alpha = \beta = 20$. Because the friction estimation errors in the RFOBs are enlarged and undesired responses arise, the friction compensation is omitted.

Fig. 4-33 shows the experimental result of the proposed method without Kalman filters. As shown by Fig. 4-33, the noise effect at the slave side is enlarged and transmitted to the master side. As a result, the force and position responses are fluctuated.

On the other hand, the proposed method based on the Kalman filter achieves suppressing noise effect, and the position and force responses show good tracking performances as shown in Fig. 4-33. From these results, the validity of the proposed methods are confirmed.

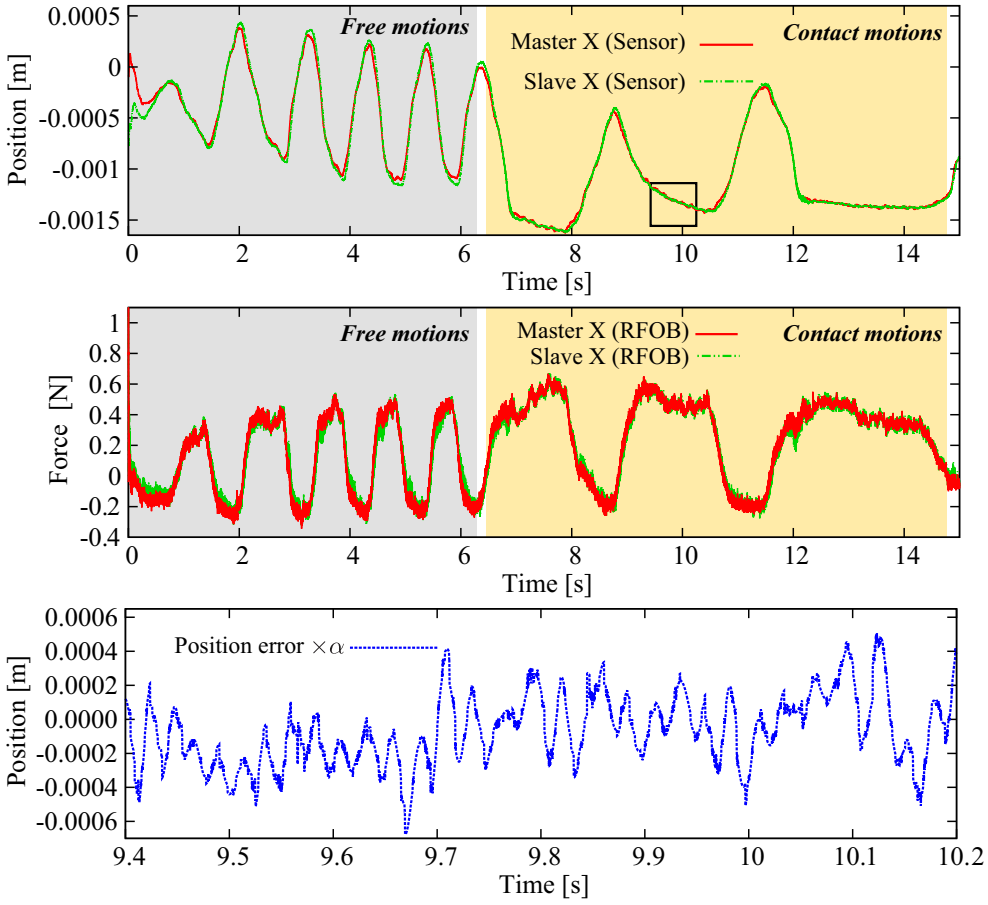

Fig. 4-33: Experimental results of the proposed MDOB for hybrid control in acceleration controller having a scaling factor of 0.4.

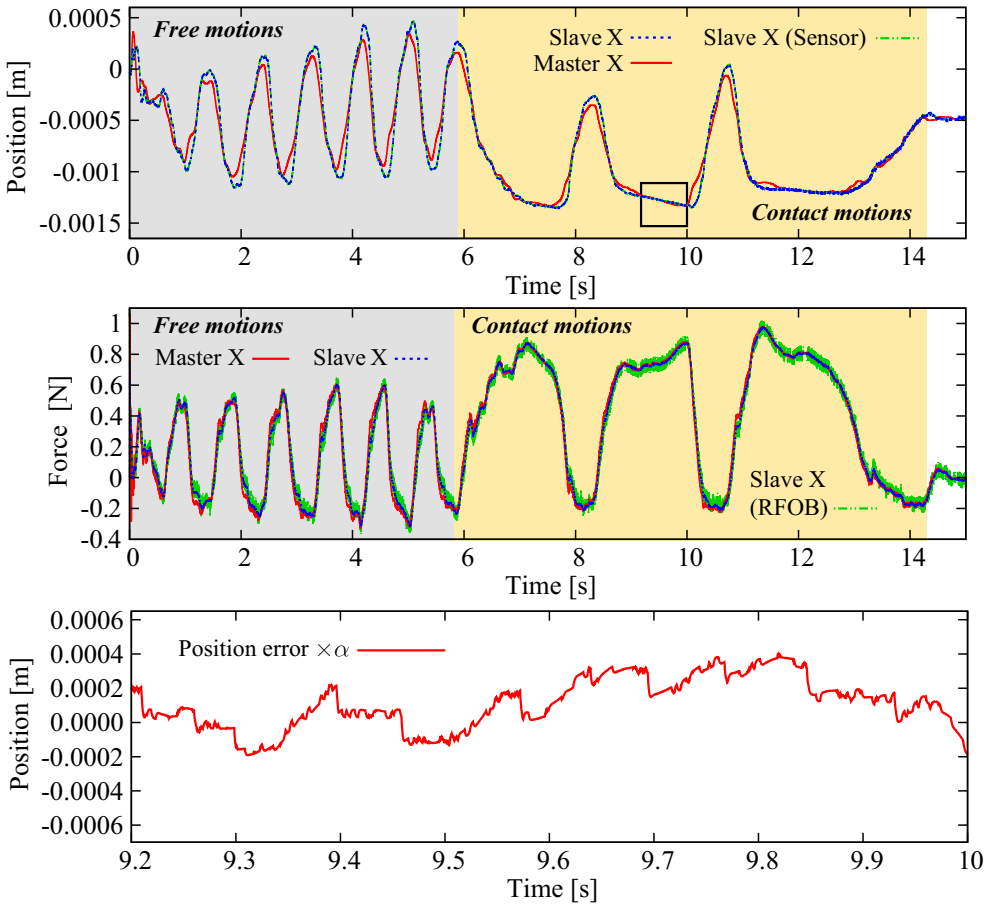

Fig. 4-34: Experimental results of the proposed method based on Kalman filters for hybrid control in acceleration controller having a scaling factor of 0.4.

4.12 Summary of Chapter 4

This chapter introduced a hybrid control system based on an acceleration controller in the modal space, which is capable of realizing decoupling control and performance improvement of the bilateral control system. This chapter showed how an acceleration controller can realize decoupling control in the modal space. Furthermore, a novel disturbance observer for enhancing the performance of an acceleration controller is proposed. Differently from the conventional hybrid controllers, the proposed controller does not affected by the variation of manipulator configurations except for neighborhood of a singular point because the structure of the proposed method is based on the acceleration controller.

This chapter also showed a method for the simultaneous realization of performance improvement, decoupling of null space and suppression of the noise effect for a hybrid control system with RDOF. Hybrid control systems with RDOF are necessary for future application on motion control systems for human support systems and robots in unknown and open environments. It was shown that the acceleration controller realizes decoupling of task (mode) spaces also in the redundant system. By extending the DOB for hybrid controllers to the redundant systems, this study realized the suppression of operating (inertia) force and the interference from null space with the simplification of inverse kinematics. Moreover, the reconstruction of the DOB by coupling with a Kalman filter was proposed for the suppression of the noise effect.

The validities of the proposal were confirmed by analyses and experiments.

Chapter 5

Environmental Disturbance Compensation for Motion Reproduction

5.1 Introduction of Chapter 5

Chapter 5 shows that an adaptation method for environmental variation between the motion extraction phase and motion reproduction phase. This chapter provides particular indices for the motion reproduction system and proposes a novel motion reproduction system based on a 2-DOF control structure to compensate for environmental variances [96].

In respect to reproduction of saved motions and the environmental variances, the loss or deterioration of the transparency corresponds to the use of one degree of freedom (1-DOF) control systems, which are unable to determine the response characteristics and disturbance suppression performance independently. Other methods for the motion reproduction systems [89, 90] also use 1-DOF control systems concerning the compensation of the environmental variances because the system structures are changed from the original motion reproduction system based on the bilateral control system using acceleration controller. Thus, general versatility cannot be obtained for the stored motions because the original motions of the human operators are degraded, even if there is no variance in the environment.

In contrast, 2-DOF control system [4] can be used to determine the response characteristics and disturbance suppression performance independently. In particular, disturbance rejection based on a disturbance observer (DOB) [5, 11, 12, 14] is known to be a simple and powerful technique. Therefore, a 2-DOF control structure that compensates for the environmental variance without degrading the response characteristics should be introduced in the motion reproduction phase.

First, a variance in the environment is regarded as an environmental disturbance (EnvD) that affects the motion reproduction system. In addition, the motion reproducibility (MR) and the EnvD suppression performance are defined as the particular characteristics of the motion reproduction system that correspond to the response characteristics and the disturbance suppression performance, respectively. The performances of the normal (standard) method [46] and conventional motion reproduction method (e.g. [88]) with regard to the MR and suppressing the EnvD were determined. The conventional motion reproduction method for adapting the environmental variation has a 1-DOF control structure against EnvD by sacrificing the MR. Because of the MR deterioration, the precise reproduction of the saved motion are not achieved by the conventional methods even though the EnvD is once reduced. Then, a novel reproduction method to compensate for the EnvD without causing the MR to deteriorate was designed. The proposal succeeds in simultaneous realization of both improvements of EnvD suppression and the precise motion reproduction. By canceling the EnvD in a kind of the feedforward structure, the proposal can achieve the robust force reproduction and robust position reproduction against EnvD.

Furthermore, storing the force information at the slave side to generate compensation values for EnvD is also the feature of the proposed method though the conventional methods extract only the master side information. This means the environmental information are able to be obtained as reaction forces. The bilateral control structure makes it possible to easily separate the action and reaction forces and to store the information, though conventional methods by programing by demonstrations are difficult to obtain the reaction force from the environments isolated from the operational force of the human operator. With the proposed method, the desired performance with regard to the EnvD suppression characteristics was realized in terms of the force and position reproduction, and the general versatility of the stored motions was markedly improved. The novelties and advantages of the proposed method are summarized as follows:

1) The characteristics peculiar to MCS are clarified by the introduction of EnvD and MR as novel indices for the motion reproduction, though the conventional methodologies maintain ambiguity [87–90]

2) In order to compensate the variation of the environment (EnvD), a novel-motion reproduction methodologies are derived for the both robust position and force reproduction, though the conventional methods addressed only force reproduction, but not both [87–90]

3) One of the advantages about the proposal compared with the conventional methods is simulta-

neous realization of precise reproduction about contact motion without the deterioration of MR and improvements about the EnvD suppression performance based on the 2-DOF control structure though the conventional reproduction methods are 1-DOF structure in respect to the EnvD and MR

4) Bilateral control structure makes it possible to easily separate the action and reaction forces and to store the reaction forces as the environmental information. This is one of the usefulness of the proposed method compared to the conventional methods by programing by demonstrations [43, 47–50].

In particular, the robust position reproduction and the compliant motion reproduction by the proposed methods will able to be applied to training systems and rehabilitation systems. Additionally, the proposed force reproduction compensator is expected to be applied especially to the industrial applications because the method is able to adopt the individual differences of manufactured articles. As a matter of course, the proposed methods are also expected to be useful under opposite circumstances. Furthermore, the position and force reproduction compensators are able to be combined according to the intended use.

Moreover, the EnvD compensation method for the motion reproduction is extended to the reproduction of MDOF cooperative motions. A novel coordinate transformation for extracting and to reproducing the MDOF cooperative motions is introduced. The proposed method was validated through analysis and experimental results.

The fundamental principle and design framework for the motion reproduction system is established in this chapter [96].

5.2 Motion Reproduction System with Environmental Disturbance

5.2.1 Definition of Environmental Disturbance

The control goals of the motion reproduction system are the same as those of bilateral control and are given by the following equations:

$$F_F^{R,\mathrm{ext}} = F_m^{S,\mathrm{ext}} + F_s^{R,\mathrm{ext}} = -F_s^{S,\mathrm{ext}} + F_s^{R,\mathrm{ext}} = 0 \tag{5.1}$$

$$X_X^{R,\mathrm{res}} = X_m^{S,\mathrm{res}} - X_s^{R,\mathrm{res}} = X_s^{S,\mathrm{res}} - X_s^{R,\mathrm{res}} = 0 \tag{5.2}$$

where superscripts S, R represent a saved variable and reproduced variable. However, the control goals are not achieved if the distance to the environment or environmental impedance is changed between the

saving and reproduction systems [46, 88]. In order to express the effect of the variance mathematically, elements of the external force are first formulated. The external force $F_s^{R,ext}$ that is added to the slave system in the motion reproduction phase is expressed by

$$F_s^{R,\mathrm{ext}} = Z_e^R(s)X_s^{R,\mathrm{res}} + F_{\mathrm{ad}}^{\mathrm{ext}} \tag{5.3}$$

where $Z_e^R(s)X_s^{R,\mathrm{res}}$ is a contact force generated by the environmental impedance and $F_{\mathrm{ad}}^{\mathrm{ext}}$ is an additional external force that does not exist in the motion saving phase. $Z_e^R(s)$ has a room of including variance of environmental impedance ΔZ_e compared to a impedance in the saving phase as $Z_e^S(s)$. In this expression, not only the variance in impedances but the variance in the size or location of the environment can also be included. If environmental locations are set at farther positions, e.g., $\Delta Z_e = -Z_e^S(s)$ ($F_s^{R,\mathrm{ext}} = 0$) slave systems cannot reproduce the saved motion. These terms caused by the environmental variances behave as disturbance forces on the motion reproduction. Therefore, they are defined as an environmental disturbance (EnvD) and are expressed as follows:

$$\begin{aligned} F_e^{\mathrm{dis}} &= -\Delta Z_e X_s^{R,\mathrm{res}} + F_{\mathrm{ad}}^{\mathrm{ext}} = Z_e^S(s)X_s^{R,\mathrm{res}} - F_s^{R,\mathrm{ext}} && (5.4)\\ &= F_e^{\mathrm{ref}} - F_s^{R,\mathrm{ext}}. && (5.5) \end{aligned}$$

5.2.2 Performance Characteristics of Motion Reproduction

In order to clarify the effect of the EnvD on motion reproduction, transfer functions for the performances are derived in following part. In this study, external force information is obtained by reaction force observer (RFOB) [7]. For simplicity, it is assumed that there are no disturbance forces except for the external force from the environment in this part. Fig. 5-1 shows an equivalent block diagram of the motion reproduction system. In the figure, $C_f(s)$ and $G_{in}^S(s)$ are expressed as

$$\begin{aligned} C_f(s) &= \frac{M_n C_f g + s}{M_n(s+g)} && (5.6)\\ G_{in}^S(s) &= g_l(s)C_f\left(H_o(s) + H_r(s)Z_e^S(s)\right) + C_p(s). && (5.7) \end{aligned}$$

In (5.7), $H_r(s)$ and $H_o(s)$ represent the reproducibility and operationality, respectively. $g_l(s)$ corresponds to the low-pass filter (LPF) of the DOB and RFOB. $H_r(s)$ and $H_o(s)$ are derived from the hybrid

matrix and the relationship $F_s^{S,\mathrm{ext}} = Z_e^S(s) X_s^{S,\mathrm{res}}$ as follows [26]:

$$\begin{bmatrix} F_m^{S,\mathrm{ext}} \\ X_m^{S,\mathrm{res}} \end{bmatrix} = \begin{bmatrix} H_{11}(s) & H_{12}(s) \\ H_{21}(s) & H_{22}(s) \end{bmatrix} \begin{bmatrix} X_s^{S,\mathrm{res}} \\ -F_s^{S,\mathrm{ext}} \end{bmatrix} \tag{5.8}$$

$$F_m^{S,\mathrm{ext}} = \left(H_o(s) + H_r(s) Z_e^S(s)\right) X_m^{S,\mathrm{res}} \tag{5.9}$$

$$H_o(s) = \frac{M_n s^2 (s+g)^2 (s^2 + C_p(s))}{D_{en}(s)} \tag{5.10}$$

$$H_r(s) = \frac{N_{um}(s)}{D_{en}(s)} \tag{5.11}$$

$$N_{\mathrm{um}}(s) = M_n g \frac{C_f}{2} (s^2 + C_p(s)) + s(s+g) \left(s^2 + \frac{C_p(s)}{2} \right) \tag{5.12}$$

$$D_{\mathrm{en}}(s) = (s+g) N_{\mathrm{um}}(s) + s \left(g C_f + \frac{s}{M_n} \right) Z_e^S(s) \tag{5.13}$$

where $H_o(s) X_m^{S,\mathrm{res}}$ corresponds to an operational force that is need to operate the master device and $H_r(s)$ is equal to 1 in the ideal case ($g = \infty$). Fig. 5-1 shows some similarities to a two-mass resonant system [24, 116, 117]. The EnvD, $C_p(s)/Z_e^S(s)$, $Z_e^S(s)$ and $1/C_f(s)$ correspond to the load-side disturbance, torsional force feedback gain, elastic coefficient and load mass, respectively [24]. The fact that the position control and force control goals are not achieved simultaneously in the presence of EnvD corresponds to the fact that load-side position and motor position tracking to a position command are also not achieved simultaneously. Additionally, even though the disturbances terms added to the system are compensated by implementing the DOBs, the EnvD are not eliminated and continue to affect the reproduced motions. This also corresponds to the fact that load side disturbance are not eliminated even though the DOBs are implemented for actuators in the case of load side position/force control of the two mass resonant system. From Fig. 5-1, the transfer functions of the motion reproduction are derived from (5.4) as follows:

$$F_s^{R,\mathrm{ext}} = G_r^f(s) Z_e^S(s) X_m^{S,\mathrm{res}} - G_d^f(s) F_e^{\mathrm{dis}} \tag{5.14}$$

$$X_s^{R,\mathrm{res}} = G_r^p(s) X_m^{S,\mathrm{res}} + G_d^p(s) \frac{F_e^{\mathrm{dis}}}{Z_e^S(s)} \tag{5.15}$$

where

$$G_d^f(s) = \frac{s^2 + C_p(s)}{s^2 + C_p(s) + C_f(s) Z_e^S(s)} \tag{5.16}$$

$$G_d^p(s) = \frac{C_f(s) Z_e^S(s)}{s^2 + C_p(s) + C_f(s) Z_e^S(s)}. \tag{5.17}$$

$G_d^f(s)$ and $G_d^p(s)$ represent the performance characteristics of the EnvD suppression for force and position reproduction, respectively. Because $Z_e^S(s) X_m^{S,\mathrm{res}}$ implies a force command generated by the opera-

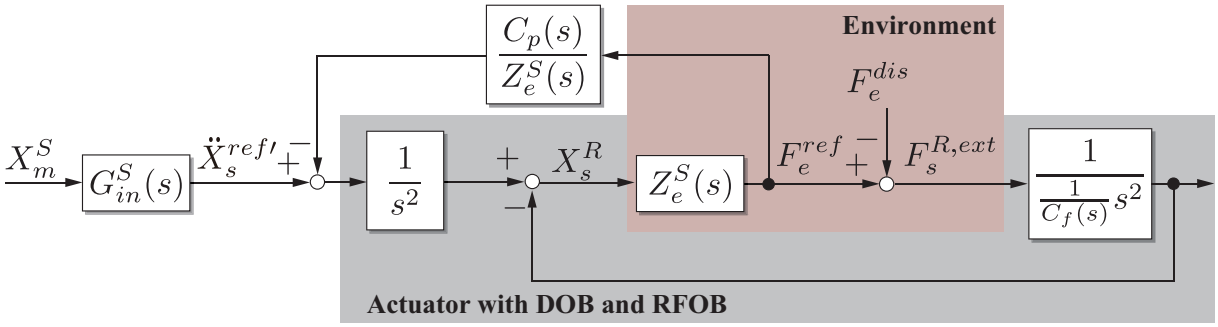

Fig. 5-1: Equivalent block diagram of motion reproduction with EnvD.

tor in the saving system, $G_r^f(s)$ can be regarded as the response characteristics for the force and position reproduction. Because the force and position reproduction system have the same response characteristics, the, motion reproducibility (MR) $P_r(s)$ is defined as an important characteristics of the motion reproduction as follows:

$$P_r(s) = G_r^f(s) = G_r^p(s) = \frac{G_{in}^S(s)}{s^2 + C_p(s) + C_f(s)Z_e^S(s)}. \tag{5.18}$$

The following relationship is also derived about EnvD suppression performances:

$$G_d^f(s) \ + \ G_d^p(s) = 1. \tag{5.19}$$

Equation (5.19) stands for the EnvD suppression for force and position reproduction cannot be achieved simultaneously in a normal motion loading system. These equations also show that the conventional method of using velocity information [88] is just a 1-DOF control system because $P_r(s)$ changes instead of the EnvD suppression performance $G_d^f(s)$ improving. Additionally, the velocity-based method is clearly a kind of force based compliance control [91] without the stiffness K_p. The conventional method cannot determine the characteristics independently. In order to improve the EnvD suppression performance without changing the reproduction performance, 2-DOF control structure that uses feedforward compensation should be introduced.

5.3 Design of Proposed Motion Reproduction System Based on EnvD Compensation

5.3.1 EnvD Rejection for Position Reproduction

In order to design the feedforward compensators for the motion reproduction, the cutoff frequency of the DOB and RFOB was assumed to be infinite as

$$\lim_{g\to\infty} \hat{F}^{\rm ext} = \lim_{g\to\infty} g_l(s)F^{\rm ext} = F^{\rm ext}. \tag{5.20}$$

where $\hat{}$ represents the estimated value of RFOBs. Thus, the following relationships are obtained from (5.6), (5.10) to (5.13) and (5.18):

$$\lim_{g\to\infty} C_f(s) = C_f \tag{5.21}$$

$$\lim_{g\to\infty} P_r(s) = 1 \tag{5.22}$$

$$\lim_{g\to\infty} P_r(s)Z_e^S(s)X_m^{S,\rm res} = F_s^{S,\rm ext}. \tag{5.23}$$

First, the EnvD suppression for position reproduction was considered. From Fig. 5-1, the transfer function from the common mode force that does not involve the operational force $F_F' = \hat{F}_s^{S,\rm ext} - \hat{F}_s^{R,\rm ext} = \tilde{F}_e^{\rm dis}$ to $X_s^{R,\rm res}$ is given by

$$X_s^{R,\rm res} = \frac{C_f}{s^2 + C_p(s)}\tilde{F}_e^{\rm dis}. \tag{5.24}$$

Considering (5.14) and (5.22) – (5.24), the following compensation value $X_{\rm cmp}^p$ is obtained to cancel the effect of $F_e^{\rm dis}$ on position reproduction:

$$X_{\rm cmp}^p = \frac{-C_f}{s^2 + C_p(s)}\tilde{F}_e^{\rm dis} = G_{\rm cmp}^p(s)\left(\hat{F}_s^{S,\rm ext} - \hat{F}_s^{R,\rm ext}\right) \tag{5.25}$$

$$= -\frac{C_f Z_e^S(s)}{s^2 + C_p(s) + C_f Z_e^S(s)}\frac{F_e^{\rm dis}}{Z_e^S(s)} = -G_d^p(s)\frac{F_e^{\rm dis}}{Z_e^S(s)}. \tag{5.26}$$

As shown in (5.26), the EnvD can be suppressed if the following output of $X_{\rm cmp}^p$ is achieved:

$$X_s^{R,\rm res} = X_m^{S,\rm res} + G_d^p(s)\frac{F_e^{\rm dis}}{Z_e^S(s)} + X_{\rm cmp}^p = X_m^{S,\rm res}. \tag{5.27}$$

In order to make the transfer function from $X_{\rm cmp}^p$ to $X_s^{R,\rm res}$ equal to 1, an acceleration feedforward term is calculated and added to the system as follows:

$$s^2 X_{\rm cmp}^p = \ddot{X}_{\rm cmp}^p = -K_f\left(F_F' - K_v\dot{X}_{\rm cmp}^p - K_p X_{\rm cmp}^p\right) \tag{5.28}$$

$$X_s^{R,\rm res} = \frac{C_p(s)}{s^2 + C_p(s)}X_{\rm cmp}^p + \frac{s^2 X_{\rm cmp}^p}{s^2 + C_p(s)} = X_{\rm cmp}^p. \tag{5.29}$$

Because the EnvD is perfunctorily rejected from the position reproduction system under ideal conditions ($g = \infty$), this method is defined as EnvD rejection in this chapter.

5.3.2 EnvD Compensation for Force Reproduction

In this part, an EnvD compensator for the force reproduction is described. The last part explains about the robust position reproduction. However, position control and force control have contradictory control goals. Setting an index that is known as control stiffness [7] is useful for representing these contradictions. The ideal control stiffness of a position control system is infinite (i.e. the system does not generate displacement by disturbances). On the other hand, the ideal control stiffness of the force controller is zero. This chapter extends the definition of the control stiffness to the EnvD suppression. A relationship between the EnvD and the position response is expressed as follows:

$$\frac{\partial F_e^{\rm dis}}{\partial X_s^{\rm res}} = \kappa_{\rm cmp}^{\rm dis} + K_e \tag{5.30}$$

where $\kappa_{\rm cmp}^{dis}$ represents the control stiffness against EnvD. Because the displacement should be zero in the case of the ideal robust position reproduction (EnvD rejection), $\kappa_{\rm cmp}^{\rm dis}$ becomes infinite. On the other hand, $\kappa_{\rm cmp}^{dis}$ of the ideal robust force reproduction system should be zero because the system generate arbitrary displacement against the EnvD except for the displacements constrained by the environmental stiffness K_e. Additionally, the system becomes compliant against EnvD if the $\kappa_{\rm cmp}^{dis}$ has a positive value. According to (5.4), EnvD rejection from the force response is possible if $Z_e^S(s)$ is known. However, obtaining the actual information of $Z_e^S(s)$ is difficult. As an alternative, the following compensation is introduced in the system for EnvD rejection:

$$X_{\rm cmp}^f = G_{\rm cmp}^f(s)\tilde{F}_e^{\rm dis} = G_{\rm cmp}^f(s)\left(\hat{F}_s^{S,\rm ext} - \hat{F}_s^{R,\rm ext}\right) \tag{5.31}$$

where

$$G_{\rm cmp}^f(s) = \frac{G_{\rm phl}^f(s)}{Z_{\rm cmp}^f(s)} = \frac{b^f}{a_2^f s^2 + a_1^f s + a_0^f}\frac{\alpha s + g}{s + g} \tag{5.32}$$

$$Z_{\rm cmp}^f(s) = \frac{a_2^f s^2 + a_1^f s + a_0^f}{b^f} \tag{5.33}$$

$$G_{\rm phl}^f(s) = \frac{\alpha s + g}{s + g}. \tag{5.34}$$

In (5.32), $G_{\rm phl}^f(s)$ represents a phase lead compensator to obtain stability in high-frequency areas. Because the displacement from the original position ΔX_s is fixed to $X_{\rm cmp}^f$, the error between the saved and

reproduced forces of the slave system can be equivalently expressed as

$$F_s^{S,\mathrm{ext}} - F_s^{R,\mathrm{ext}} \;=\; F_e^{\mathrm{dis}} - Z_e^S(s) X_{\mathrm{cmp}}^f. \tag{5.35}$$

Equation (5.35) means that $F_e^{\mathrm{dis}} - Z_e^S(s) X_{\mathrm{cmp}}^f$ is equivalently compensated by the compensator shown in (5.31). Here, b^f is a coefficient that is set to 1 or 0. If (5.35) is taken into account, $Z_{\mathrm{cmp}}^f(s)$ represents a impedance that determines the behavior of the reproduction system against F_e^{dis}. a_2^f , a_1^f and a_0^f correspond to a virtual mass (force control gain), a virtual viscosity (velocity feedback gain) and a virtual stiffness, respectively. These coefficients are design parameters that designers can determine. Just as in (5.28), the acceleration feedforward term is calculated as follows:

$$\ddot{X}_{\mathrm{cmp}}^f = b^f a_2^{f-1} \left(G_{\mathrm{phl}}^f(s) \tilde{F}_e^{\mathrm{dis}} - a_1^f \dot{X}_{\mathrm{cmp}}^f - a_0^f X_{\mathrm{cmp}}^f \right). \tag{5.36}$$

By substituting X_{cmp}^p, X_{cmp}^f and (5.22) into $X_m^{S,\mathrm{res}}$ of (5.15), the following equation is derived as

$$\begin{aligned} X_s^{R,\mathrm{res}} \;&=\; X_m^{S,\mathrm{res}} + X_{\mathrm{cmp}}^f + X_{\mathrm{cmp}}^p + G_d^p(s) \frac{F_e^{\mathrm{dis}}}{Z_e^S(s)} \\ &=\; X_m^{S,\mathrm{res}} + X_{\mathrm{cmp}}^f - G_d^p(s) \frac{F_e^{\mathrm{dis}}}{Z_e^S(s)} + G_d^p(s) \frac{F_e^{\mathrm{dis}}}{Z_e^S(s)} \\ &=\; X_m^{S,\mathrm{res}} + \frac{G_{\mathrm{phl}}^f(s)}{Z_{\mathrm{cmp}}^f(s)} \left(\hat{F}_s^{S,\mathrm{ext}} - \hat{F}_s^{R,\mathrm{ext}} \right). \end{aligned} \tag{5.37}$$

By considering (5.4), (5.20), (5.22) and (5.23), (5.37) is transformed as follows:

$$\begin{aligned} \frac{F_e^{\mathrm{dis}} + F_s^{R,\mathrm{ext}}}{Z_e^S(s)} \;&=\; X_m^{S,\mathrm{res}} + \frac{G_{\mathrm{phl}}^f(s)}{Z_{\mathrm{cmp}}^f(s)} \left(F_s^{S,\mathrm{ext}} - F_s^{R,\mathrm{ext}} \right) \\ F_e^{\mathrm{dis}} + F_s^{R,\mathrm{ext}} \;&=\; F_s^{S,\mathrm{ext}} \\ &\quad + \frac{G_{\mathrm{phl}}^f(s) Z_e^S(s)}{Z_{\mathrm{cmp}}^f(s)} \left(F_s^{S,\mathrm{ext}} - F_s^{R,\mathrm{ext}} \right). \end{aligned} \tag{5.38}$$

From (5.4) and (5.38), the force and position reproduction of the proposed method can be characterized as

$$F_s^{R,\mathrm{ext}} \;=\; F_s^{S,\mathrm{ext}} - \frac{Z_{\mathrm{cmp}}^f(s)}{G_{\mathrm{phl}}^f(s) Z_e^S(s) + Z_{\mathrm{cmp}}^f(s)} F_e^{\mathrm{dis}} \tag{5.39}$$

$$\;=\; \tilde{P}_r(s) Z_e^S(s) X_m^{S,\mathrm{res}} - \tilde{G}_d^f(s) F_e^{\mathrm{dis}} \tag{5.40}$$

$$X_s^{R,\mathrm{res}} \;=\; X_m^{S,\mathrm{res}} + \frac{G_{\mathrm{phl}}^f(s) Z_e^S(s)}{G_{\mathrm{phl}}^f(s) Z_e^S(s) + Z_{\mathrm{cmp}}^f(s)} \frac{F_e^{\mathrm{dis}}}{Z_e^S(s)} \tag{5.41}$$

$$\;=\; \tilde{P}_r(s) X_m^{S,\mathrm{res}} + \tilde{G}_d^p(s) \frac{F_e^{\mathrm{dis}}}{Z_e^S(s)} \tag{5.42}$$

where $\tilde{P}_r^f(s)$, $\tilde{G}_d^f(s)$ and $\tilde{G}_d^p(s)$ represent the MR and disturbance suppression performances, respectively, of the proposed method for force and position reproduction. In this structure, a_0^f/b^f corresponds to the control stiffness. If b^f is set to one, the force compensator is activated. From (5.39), the steady-state error $e^f = F_s^{S,\mathrm{ext}} - F_s^{R,\mathrm{ext}}$ converges depending on a_0^f as follows:

$$e^f = \lim_{s\to 0} s \frac{a_2^f s^2 + a_1^f s + a_0^f}{b^f G_{\mathrm{phl}}^f(s) Z_e^S(s) + a_2^f s^2 + a_1^f s + a_0^f} \frac{F_e^{\mathrm{dis}}}{s} \tag{5.43}$$

$$= \begin{cases} 0, & a_0^f = 0 \wedge b^f = 1 \\ \frac{a_0^f}{K_e + a_0^f} F_e^{\mathrm{dis}}, & a_0^f \neq 0 \wedge b^f = 1. \end{cases} \tag{5.44}$$

As the above equation shows, the system becomes force controller in respect to EnvD and e^f converges to zero in the case a_0^f is set to zero. From another perspective, this structure corresponds to a kind of reaction force controller based on position based compliance (admittance) control with a force controller a_2^f, a force command $F_s^{S,\mathrm{ext}}$ and the reaction force feedback of $F_s^{R,\mathrm{ext}}$. If a_1^f has a positive value, a_1^f behaves as a virtual damping. If a_0^f has a positive value, the system becomes compliance controller against EnvD as shown in (5.44). From (5.41), the steady state error of position responses $e^p = X_m^{S,\mathrm{res}} - X_s^{R,\mathrm{res}}$ is represented as follows:

$$e^p = \lim_{s\to 0} s \frac{-b^f G_{\mathrm{phl}}^f(s)}{b^f G_{\mathrm{phl}}^f(s) Z_e^S(s) + a_2^f s^2 + a_1^f s + a_0^f} \frac{F_e^{\mathrm{dis}}}{s} \tag{5.45}$$

$$= -\frac{1}{K_e + \frac{a_0^f}{b^f}} F_e^{\mathrm{dis}} \tag{5.46}$$

where $1/(K_e + \frac{a_0^f}{b^f})$ corresponds to the compliance value. On the other hand, if b^f is set to zero, the force compensator is deactivated. As a result, the control stiffness and total impedance in respect to EnvD (i.e. $Z_{\mathrm{cmp}}^f(s)$) become infinite as shown in (5.45) and the EnvD rejection is activated. As a result, the position error e^p converges to zero as follows:

$$e^p = -\frac{b^f G_{\mathrm{phl}}^f(s) Z_e^S(s)}{b^f G_{\mathrm{phl}}^f(s) Z_e^S(s) + a_2^f s^2 + a_1^f s + a_0^f} \frac{F_e^{\mathrm{dis}}}{Z_e^S(s)} = 0 \tag{5.47}$$

$$b^f = 0. \tag{5.48}$$

This case corresponds to the robust position control system. Though the force and position and force compensation are not achieved at the same time because of the constraint of (5.19), adaptation of environmental variation by robust force reproduction and robust position reproduction are easily realized in

a same direction only by switching or varying the coefficient b_f without deteriorating MR. This is one of the usefulness of the proposed structure. As described above, the behavior of the system against $F_e^{\rm dis}$ is arbitrarily determined by choosing $G_{\rm cmp}^f(s)$ for the sake of EnvD rejection. If the EnvD does not exist or is suppressed once, the compensators $X_{\rm cmd}^p$ and $X_{\rm cmd}^f$ are not activated. In these cases, $\tilde{P}_r(s)$ is equal to $P_r(s)$ that is the MR of the normal motion reproduction system.

Thus, the proposed compensation method can suppress the EnvD and the desired reproduction of stored motions is realized without deteriorating MR only by varying the coefficients of $G_{\rm cmp}^f(s)$ in the force compensator. This is one of the usefulness of the proposal. As a result, the proposed method is the novel motion reproduction method against the EnvD based on 2-DOF control system, though the conventional methods have 1-DOF control structure in respect to EnvD.

5.3.3 Implementation for MDOF Systems

This part presents how to implement the proposed method for an MDOF system. Here, a 2-DOF manipulator on a horizontal (X–Y) plane is considered.

Motion Extraction (Bilateral Control)

An acceleration-based four-channel bilateral control is utilized to extract human motions. Acceleration references for the master-slave system $\ddot{\boldsymbol{X}}^{\rm ref} = \begin{bmatrix} \ddot{\boldsymbol{X}}_m^{\rm ref} & \ddot{\boldsymbol{X}}_s^{\rm ref} \end{bmatrix}^T$ are calculated as follows:

$$\ddot{\boldsymbol{X}}^{\rm ref} = \boldsymbol{T}^{-1} \begin{bmatrix} \ddot{\boldsymbol{X}}_F^{\rm ref} \\ \ddot{\boldsymbol{X}}_X^{\rm ref} \end{bmatrix} = \frac{1}{2} \begin{bmatrix} \boldsymbol{I}_2 & \boldsymbol{I}_2 \\ \boldsymbol{I}_2 & -\boldsymbol{I}_2 \end{bmatrix} \begin{bmatrix} -\boldsymbol{C}_f \hat{\boldsymbol{F}}_F^{\rm ext} \\ -\boldsymbol{C}_p(s) \boldsymbol{X}_X^{\rm res} \end{bmatrix} \tag{5.49}$$

$$\hat{\boldsymbol{F}}_F^{\rm ext} = \hat{\boldsymbol{F}}_m^{\rm ext} + \hat{\boldsymbol{F}}_s^{\rm ext} = \boldsymbol{J}_{{\rm aco},m}^{-T} \hat{\boldsymbol{\tau}}_m^{\rm ext} + \boldsymbol{J}_{{\rm aco},s}^{-T} \hat{\boldsymbol{\tau}}_s^{\rm ext} \tag{5.50}$$

$$\boldsymbol{X}_X^{\rm res} = \boldsymbol{X}_m^{\rm res} - \boldsymbol{X}_s^{\rm res} = \boldsymbol{G}_{Wm}\left(\boldsymbol{q}_m^{\rm res}\right) - \boldsymbol{G}_{Ws}\left(\boldsymbol{q}_s^{\rm res}\right). \tag{5.51}$$

$\boldsymbol{C}_f$ and $\boldsymbol{C}_p(s)$ are diagonal matrices with force controllers and position controllers, respectively, in diagonal elements. The workspace dynamics is expressed by the following equation if the joint-space DOBs are implemented:

$$\ddot{\boldsymbol{X}}^{\rm res} = \boldsymbol{M}_{vn}^{-1} \boldsymbol{F}_n^{\rm ref} + \dot{\boldsymbol{J}}_{\rm aco} \dot{\boldsymbol{q}}^{\rm res} = \ddot{\boldsymbol{X}}_n^{\rm ref} + \dot{\boldsymbol{J}}_{\rm aco} \dot{\boldsymbol{q}}^{\rm res} \tag{5.52}$$

where $\boldsymbol{M}_{vn}$ represents a virtual mass matrix. If the matrices are set as identity matrices, the controller becomes a workspace acceleration controller [21]. In order to realize decoupling control in the workspace, the second term in (5.52) needs to be calculated. However, the calculation is sometimes cumbersome. As

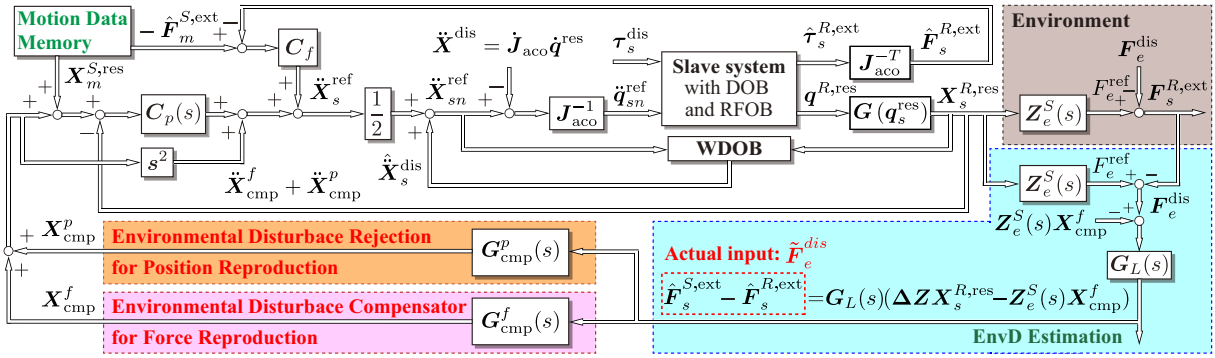

Fig. 5-2: The block diagram of the proposed motion reproduction system.

a substitution for the calculation, the term is defined as a disturbance term. The disturbance is estimated by a workspace observer (WDOB) [84] and added to the acceleration reference in order to cancel the term. The acceleration reference of the actuator space is obtained as

$$\ddot{\boldsymbol{q}}_n^{\mathrm{ref}} = \boldsymbol{J}_{\mathrm{aco}}^{-1}\boldsymbol{M}_{vn}^{-1}\boldsymbol{F}_n^{\mathrm{ref}} = \boldsymbol{J}_{\mathrm{aco}}^{-1}\left(\ddot{\boldsymbol{X}}^{\mathrm{ref}} + \hat{\ddot{\boldsymbol{X}}}^{\mathrm{dis}}\right) \tag{5.53}$$

where $\hat{\ddot{\boldsymbol{X}}}^{\mathrm{dis}}$ is the estimated disturbance. These processes are used to extract and save the human position and force information $\boldsymbol{X}_m^{\mathrm{res}}$ and $\boldsymbol{F}_m^{\mathrm{ext}}$.

Motion Reproduction

According to (5.25), (5.28), (5.31) and (5.36), the acceleration references of the slave-side manipulator for the motion reproduction are obtained as follows:

$$\begin{aligned}\ddot{\boldsymbol{X}}_s^{R,\mathrm{ref}} &= \frac{\boldsymbol{C}_f}{2}\left(-\hat{\boldsymbol{F}}_m^{S,\mathrm{ext}} - \hat{\boldsymbol{F}}_s^{R,\mathrm{ext}}\right) + \ddot{\boldsymbol{X}}_{\mathrm{cmp}}^{p} + \ddot{\boldsymbol{X}}_{\mathrm{cmp}}^{f} \\ &\quad + \frac{\boldsymbol{C}_p(s)}{2}\left(\boldsymbol{X}_m^{S,\mathrm{res}} + \boldsymbol{X}_{\mathrm{cmp}}^{p} + \boldsymbol{X}_{\mathrm{cmp}}^{f} - \boldsymbol{X}_s^{R,\mathrm{res}}\right)\end{aligned} \tag{5.54}$$

where $\boldsymbol{X}_{\mathrm{cmp}}^{p}$ and $\boldsymbol{X}_{\mathrm{cmp}}^{f}$ are compensation vectors comprising compensation values in each direction (X and Y). 1/2 in (44) corresponds to the determinant of the inverse matrix of $\boldsymbol{T}$. Fig. 5-2 shows a block diagram of the proposed method. If the coefficient of b^f is set to zero, only the EnvD rejection is activated in this direction. By tuning $\boldsymbol{G}_{\mathrm{cmp}}^{f}(s)$, the desired EnvD compensation for position/force reproduction is realized. Although the structure of the proposed system is similar to that of admittance control (position-based compliance control) [91], the method is a type of feedforward compensation with regard to the EnvD.

5.4 Analysis and Detailed Design

5.4.1 Performance Analysis

In order to analyze the system performance and stability, the characteristics of the proposed method were redefined except for the assumptions (5.20) to (5.23). For simplicity, only a direction (e.g. X) is discussed. The disturbance suppression performance of the EnvD rejection $G_d^{p\prime}(s)$ is derived as

$$G_d^{p\prime}(s) \;=\; g_h(s) g_d^p(s) \tag{5.55}$$

where $g_h(s)$ is a high-pass filter that is caused by the limited bandwidth of the RFOB in (5.25). By considering (5.4), (5.8), (5.14), (5.15) and section III, the MR and the EnvD suppression performances are also rewritten as

$$\tilde{P}_r(s) \;=\; \frac{Z_{\rm cmp}^f(s) P_r(s) + \frac{G_{\rm phl}^f(s) g_l(s) Z_e^S(s)}{H_{21}(s) - H_{22}(s) Z_e^S(s)}}{G_{\rm phl}^f(s) g_l(s) Z_e^S(s) + Z_{\rm cmp}^f(s)} \tag{5.56}$$

$$\tilde{G}_d^p(s) \;=\; \frac{G_{\rm phl}^f(s) g_l(s) Z_e^S(s) + Z_{\rm cmp}^f(s) G_d^{p\prime}(s)}{G_{\rm phl}^f(s) g_l(s) Z_e^S(s) + Z_{\rm cmp}^f(s)} \tag{5.57}$$

$$\tilde{G}_d^f(s) \;=\; \frac{Z_{\rm cmp}^f(s) \left(1 - G_d^{p\prime}(s)\right)}{G_{\rm phl}^f(s) g_l(s) Z_e^S(s) + Z_{\rm cmp}^f(s)}. \tag{5.58}$$

By applying the final value theorem, the following steady-state characteristics are obtained as:

$$\lim_{s\to 0} s G_d^{p\prime}(s) \frac{1}{s} \;=\; 0 \cdot \frac{K_f K_e^S}{K_p + K_f K_e^S} = 0 \tag{5.59}$$

$$\lim_{s\to 0} s \tilde{G}_d^f(s) \frac{1}{s} \;=\; \frac{a_0^f}{K_e^S + a_0^f} = 0 \; (a_0^f \to 0) \tag{5.60}$$

$$\lim_{s\to 0} s \tilde{P}_r(s) \frac{1}{s} \;=\; 1. \tag{5.61}$$

Equations (5.59) and (5.60) confirm that the proposed EnvD rejection and force reproduction compensator suppress the EnvD because $G_d^{p\prime}(s)$ and $\tilde{G}_d^f(s)$ converge to zero. According to (5.61) and [26], the slave system can reproduce contact forces

$$\begin{aligned} &\lim_{s\to 0} s \left(F_s^{R,\rm ext} - \tilde{P}_r(s) Z_e^S(s) X_m^{S,\rm ext} \right) \frac{1}{s} \\ &\quad = \lim_{s\to 0} s \left(F_s^{R,\rm ext} - F_s^{S,\rm ext} \right) \frac{1}{s} = 0. \end{aligned} \tag{5.62}$$

According to (5.16), the velocity-based method or a force controller can be used to suppress the steady-state error in the force reproduction by changing $C_p(s)$ to $C_v(s) = K_v s$ or getting rid of $C_p(s)$, respectively. The characteristics of EnvD suppression about the velocity-based method $G_{dv}^f(s)$ and the force

Table 5.1: Parameters of analysis for motion reproduction systems

Parameters	Descriptions	Value
M_n	mass of actuator	0.2560 kg
K_f	force control gain	1.0
K_p	position gain	6500
K_v	velocity gain	$2\sqrt{K_p}$
g	cutoff frequency of DOB and RFOB	500 rad/s
α	parameter of phase lead compensator	2

controller $G^f_{df}(s)$ are described as follows:

$$G^f_{dv}(s) = \frac{s^2 + K_v s}{s^2 + K_v s + C_f(s)Z^S_e(s)} \tag{5.63}$$

$$G^f_{df}(s) = \frac{s^2}{s^2 + C_f(s)Z^S_e(s)}. \tag{5.64}$$

On the other hand, a position controller can be used to suppress the steady-state error in the position reproduction by getting rid of C_f. The characteristics of EnvD suppression in the position reproduction $G^p_{dp}(s)$ is described as follows:

$$G^p_{dp}(s) = \frac{\frac{1}{M_n} g_h(s) Z^S_e(s)}{s^2 + C_p(s) + \frac{1}{M_n} g_h(s) Z^S_e(s)}. \tag{5.65}$$

However, such conversions affect the performances of the MRs as follows:

$$P_{rv}(s) = \frac{g_l(s)C_f\left(H_o(s) + H_r(s)Z^S_e(s)\right) + K_v s}{s^2 + K_v s + C_f(s)Z^S_e(s)} \tag{5.66}$$

$$P_{rf}(s) = \frac{g_l(s)C_f\left(H_o(s) + H_r(s)Z^S_e(s)\right)}{s^2 + C_f(s)Z^S_e(s)} \tag{5.67}$$

$$P_{rp}(s) = \frac{C_p(s)}{s^2 + C_p(s) + \frac{1}{M_n} g_h(s) Z^S_e(s)} \tag{5.68}$$

where $P_{rv}(s)$, $P_{rf}(s)$ and $P_{rp}(s)$ represent the MRs about velocity based method, force controller and position controller, respectively. On the contrary, the proposed method can enhance the EnvD suppression performance independently form the MR because EnvD suppression performances of the proposal $\tilde{G}^p_d(s)$ and $\tilde{G}^f_d(s)$ do not include C_f or $C_p(s)$. Because of these reasons, the proposal is necessary to realize the precise motion reproduction and improvement of the EnvD suppression simultaneously. The frequency characteristics of the motion reproduction system were analyzed. The position and velocity

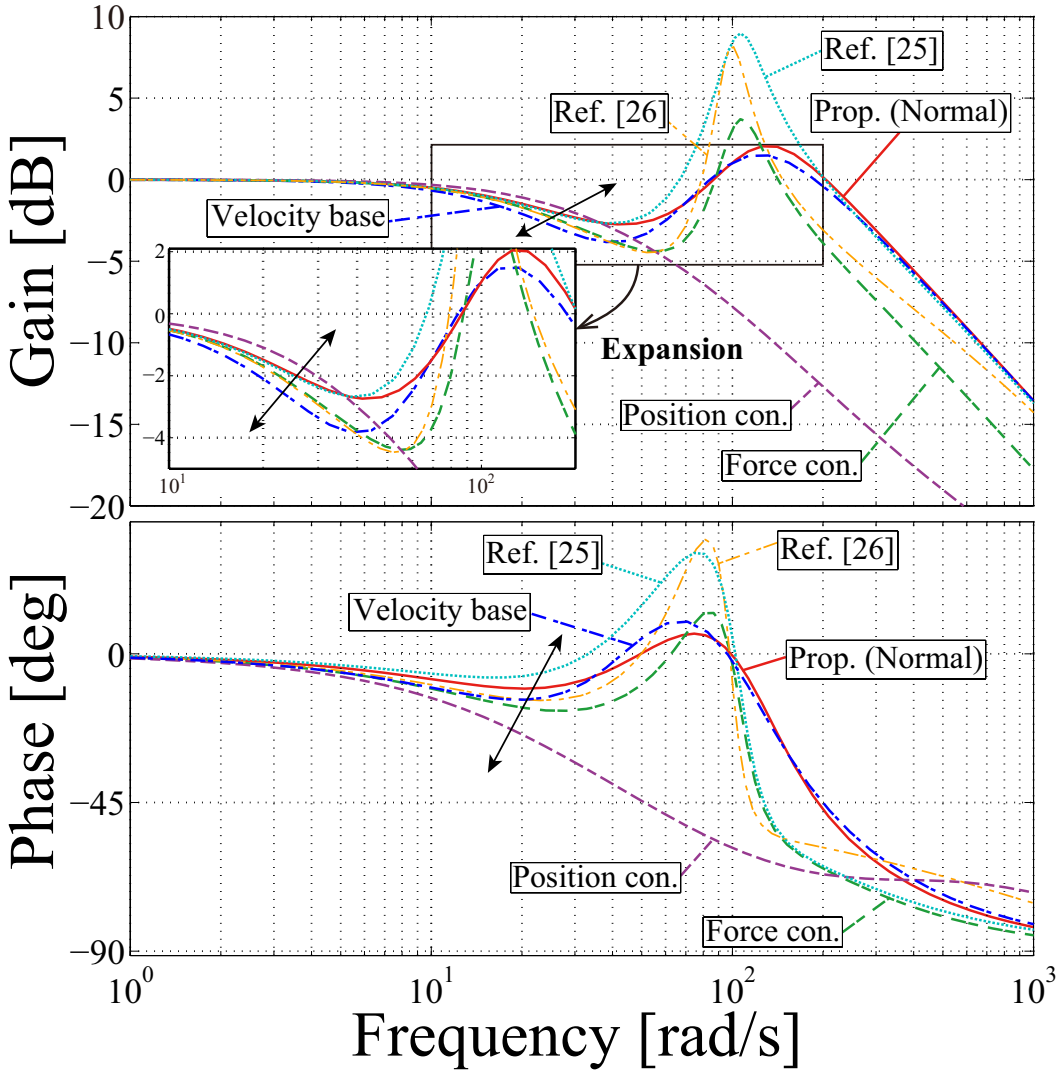

Fig. 5-3: Bode diagram of MRs ($Z_e(s) = 100s + 10000$).

gains were set to produce critical damping in the position control system [26]. Table. 5.1 lists the analysis parameters. Fig. 5-3 represents Bode diagrams of the MRs for the proposed method, velocity-based method, the conventional method (A) [89], the conventional method (B) [90], and force and position controller. MRs of the conventional method (A) $P_r^A(s)$ and the conventional method (B) $P_r^B(s)$ are described as follows:

$$P_r^A(s) = \frac{G_{in}^S(s) - \frac{C_p(s)}{H_{21}(s) - H_{22}(s)Z_e^S(s)}}{s^2 + C_f(s)Z_e^S(s)} \tag{5.69}$$

$$P_r^B(s) = \frac{G_{in}^S(s) + (G_h(s) - 1)C_p(s)}{s^2 + G_h(s)C_p(s) + C_f(s)Z_e^S(s)}. \tag{5.70}$$

In this comparison, the MR of the proposed method was set to the $P_r(s)$ in (5.18) in order to compare the performances without EnvD. As shown in Figs. 5-3 (a) and (b), the gain and phase characteristics of the velocity-based method, conventional methods [89] and [90], the force and position controllers were changed as a substitute for EnvD suppression. The results showed that the conventional methods degraded the transient responses of the reproduced motions. However, the proposed method was able to maintain the MR that was obtained by the acceleration-based bilateral control in the motion saving system because of the feedforward compensation. Fig. 5-4 shows the gain characteristics for the EnvD suppression performances of the conventional and proposed methods. For the proposed method, four types of force compensators (cases 1 – 4) and the EnvD rejection method were compared. The parameters of $Z^f_{\rm cmp}(s)$ were changed as follows: (case 1) s^2, (case 2) $s^2 + 40s$, (case 3) $s^2 + 40s + 2000$ and (case 4) $0.5s^2$. As shown by the black arrow in Fig. 5-4 (a), the EnvD suppression performance for position reproduction improved if the zero-order gain of $Z^f_{\rm cmp}(s)$ was set larger. The proposed EnvD rejection method showed the best performance compared to the other methods, including the position control, because of the feedforward structure with no change to the MR. As shown by the black arrow in Fig. 5-4 (b), the EnvD suppression performance for force reproduction is improved when the coefficients of the force compensator were set to smaller values. Even though the EnvD suppression performance of the case 1 is as well as the force controller, the peak magnitude about case 1 was smaller.

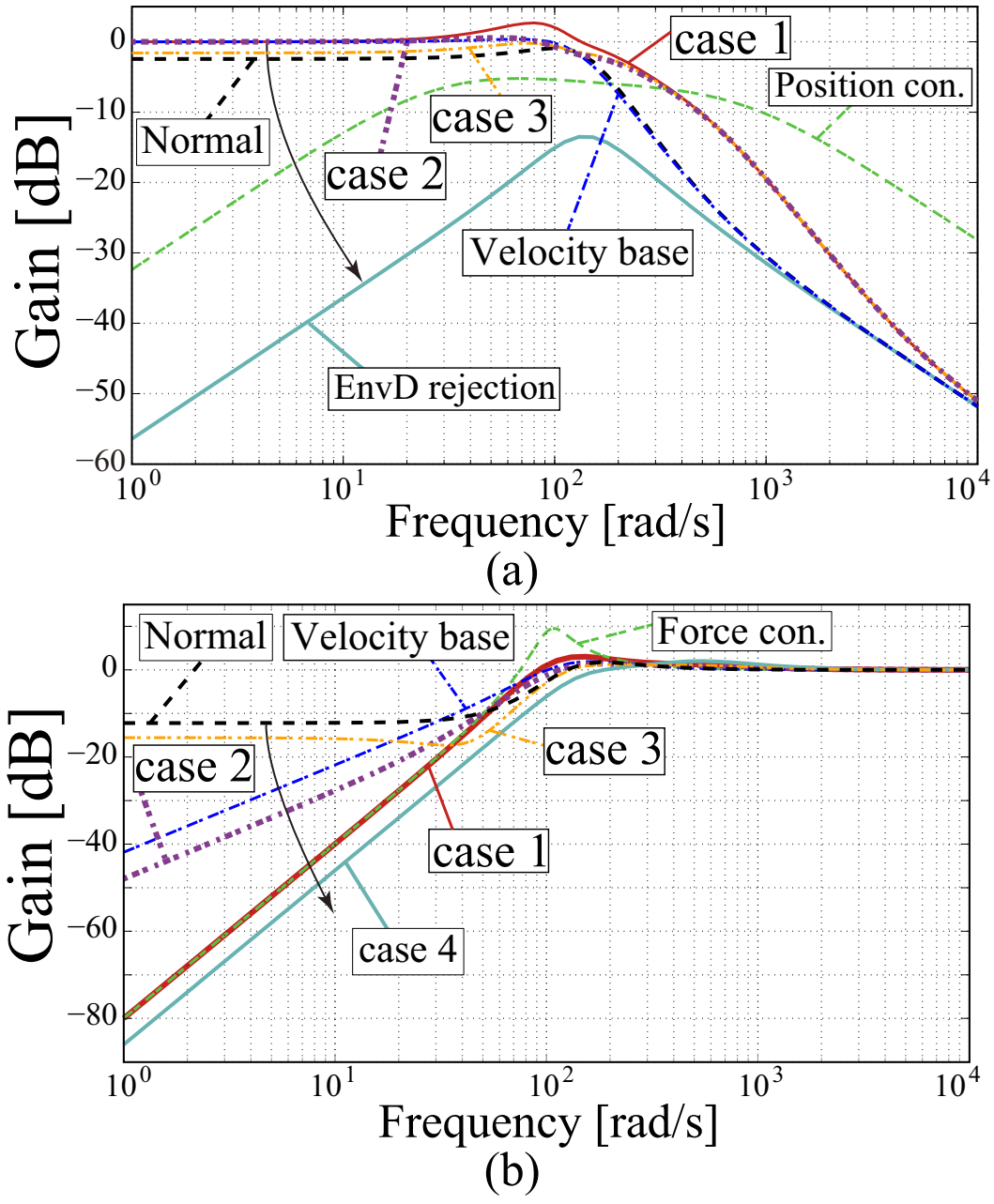

Fig. 5-4: Gain characteristics of EnvD suppression performance with the hard environment ($Z_e(s) = 100s + 10000$). (a) Position. (b) Force.

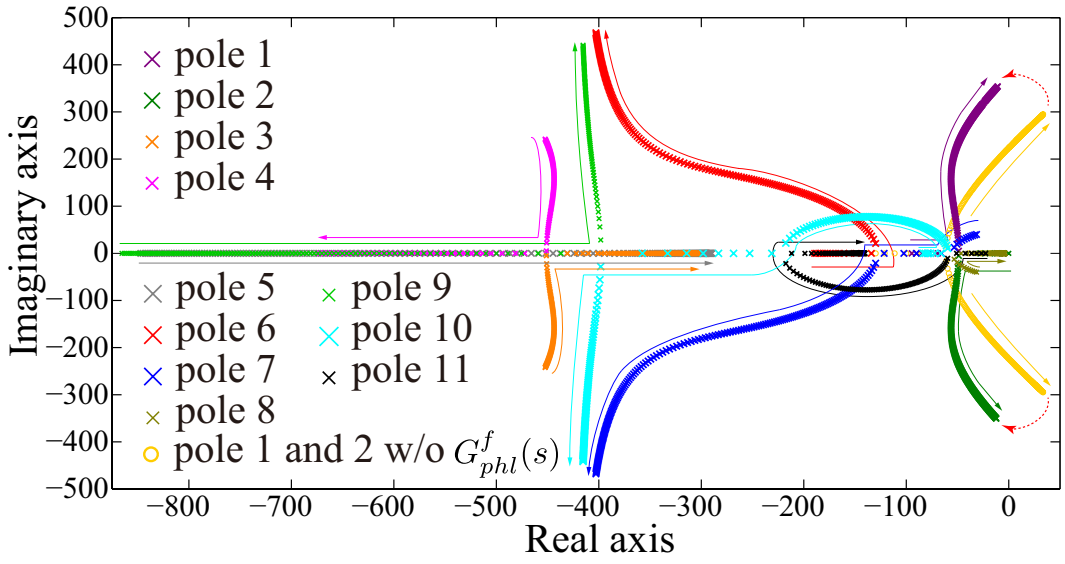

Fig. 5-5: Pole displacements with variance in environmental stiffness K_e of 0 – 10,0000 ($D_e = 100$).

5.4.2 Stability Analysis

In order to analyze the stability of the proposed system, pole displacements about $\tilde{P}_r(s)$ were evaluated according to changes in the parameters. Fig. 5-5 shows the pole displacements of $\tilde{P}_r(s)$ with a variance in the environmental stiffness K_e from 0 to 100000 with force compensator of case 1: $Z^f_{\rm cmp}(s) = s^2$. The viscosity of the environment was set to $D_e = 100$ Ns/m. In the figure, poles without $G^f_{\rm phl}(s)$ are shown with yellow circles for comparison. Dominant poles are removed, as shown by the read dotted arrows. The results confirmed the effect of $G^f_{\rm phl}(s)$. The system was stable with regard to the stiffness range because all poles existed on the left half of the plane. Fig. 5-6 shows the pole displacements of $\tilde{P}_r(s)$ with a variance in $Z^f_{\rm cmp}(s)$. The environmental impedance was fixed to $Z_e(s)$=100s+100000. The poles not related to $Z^f_{\rm cmp}(s)$ that coincide with the normal motion reproduction system are labeled by the black stars. Read x-marks show the pole displacements with a variance in a^f_2 of 0.5 – 2.5. As shown in the figure, the system may become unstable if a^f_2 is too small. The poles shown with the red arrows were not displaced by the compensator. Blue triangles show the pole displacements with a variance in a^f_1 of 0–200 in which a^f_2 and a^f_0 were set to 1 and zero, respectively. All poles existed on the left half of the plane, and some poles were stabilized when a^f_1 was increased. The poles of the standard motion reproduction system are labeled by the black stars. This means that the system may become unstable if the environmental stiffness or force gains are too high in the bilateral control system [26] for motion

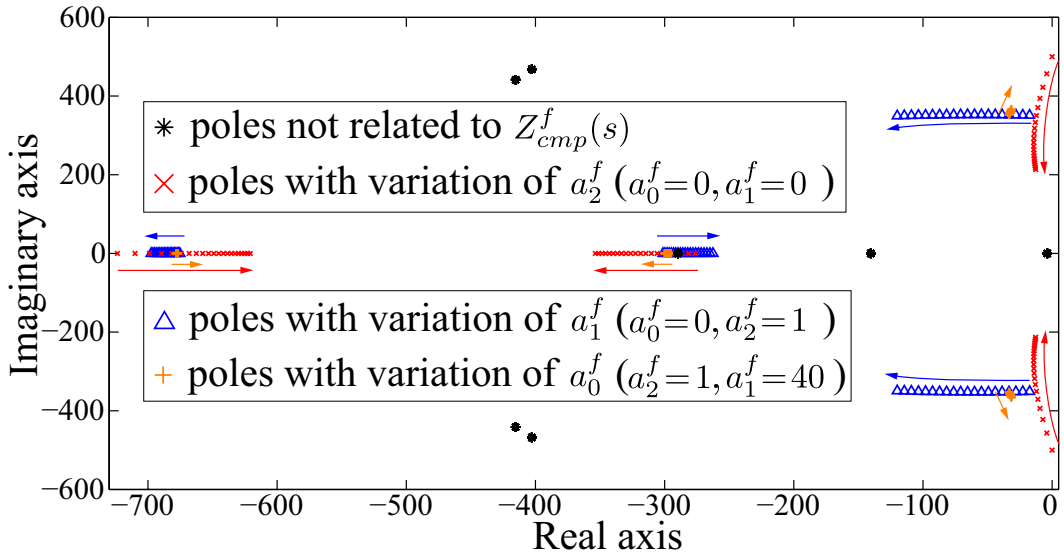

Fig. 5-6: Pole displacements with variance in parameters about force compensator $Z^f_{\rm cmp}(s)$ (a^f_2: $0.5 \rightarrow 2.5$, a^f_1: $0 \rightarrow 200$, a^f_0: $0 \rightarrow 10000$).

extraction. In such a case, the controller gains in the motion saving system should be modified. Orange crosses show the pole displacements with a variance in a^f_0 of 10 – 10000. All poles existed on the left half of the plane, and the displacements were relatively small compared to the other parameters. This indicates that the variance in a^f_0 had little effect on the system stability. From these results, it is found that the proposed system become more stable if the a^f_1 and a^f_2 are set to larger values, though the EnvD suppression performance in force reproduction is degraded as shown in section IV. A.

5.4.3 Simulations

In order to enhance the necessity and advantages of the proposed method, simulations that compare the proposed methods to position and force controllers combined with DOBs are conducted. In the cases of the proposed EnvD rejection for position reproduction and the position controller, an additional disturbance force (10 N) is added from 0 to 2 second. In the cases of the proposed force reproduction compensator and force controller, the distance from slave system to the environment is 10 mm farther than that of the saving system. The parameters of the proposed force compensator are same as that of case 2 in the analysis. Fig. 5-7 shows the simulation results of the motion reproduction systems. In the yellow shaded areas, contact motions are conducted. As shown by the figure, conventional methods seem to suppress the EnvDs in the steady states. As described in the Fig. 5-8, however, the transient responses

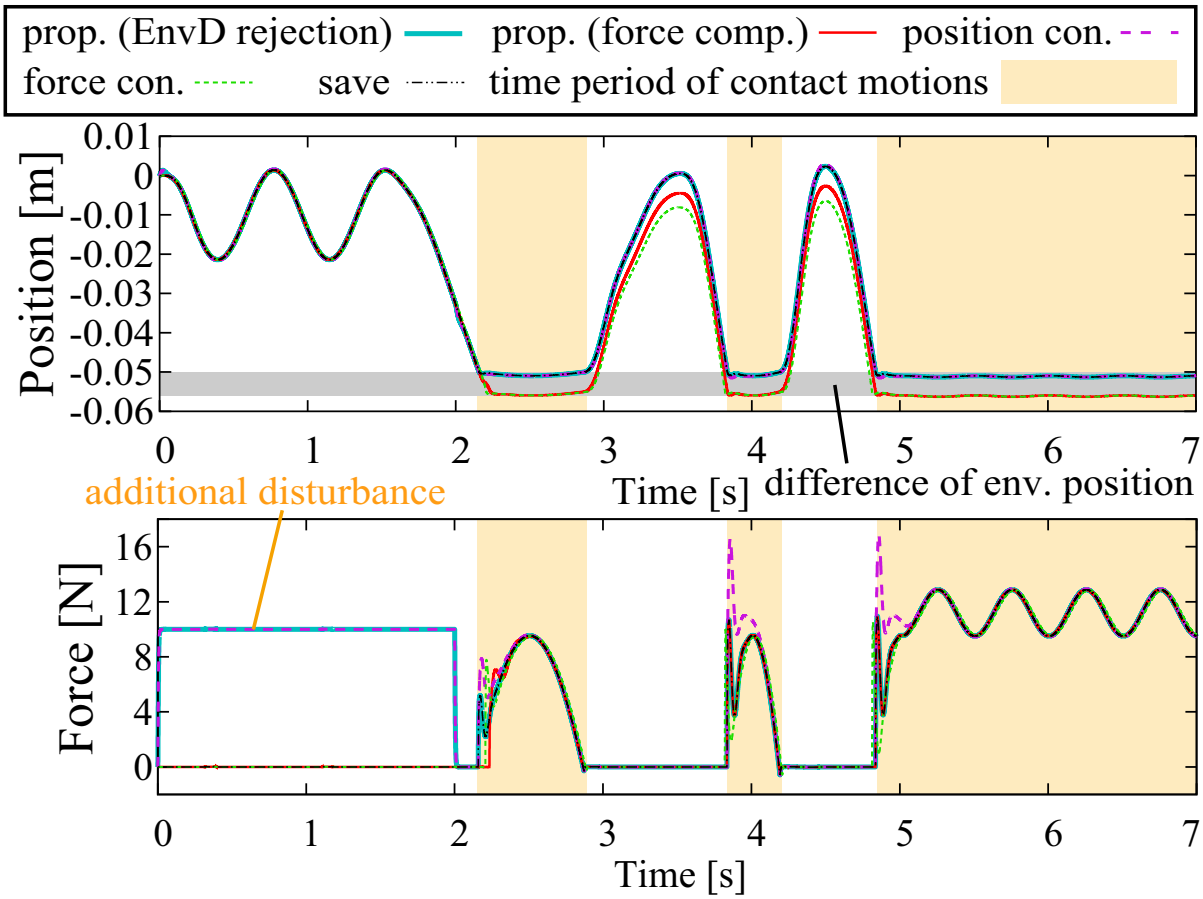

Fig. 5-7: Simulation results of position and external force responses.

of the conventional methods are degraded in both of the position and force responses. This is because the MRs of conventional methods are changed as represented in (5.67) and (5.68). Especially, the contact motions are not precisely reproduced even though the environment is not varied or the variances are once adopted. Here, if the second order differential of the position response at master side is added in the acceleration reference of the position control system, the reproduced responses have possibilities to be improved. However, the direct differentiation of the actual sensor signals has a risk for amplifying the noise. In addition, even though the term is included, $P_{rp}(s)$ and $P_r(s)$ are not coincident. On the other hand, the proposed methods can suppress the EnvDs (i.e. the additional disturbance and the difference of environmental position) quickly and the precise position and force reproduction are achieved. From these results, it is found that the proposed methods can realize the improvement in respect to the EnvD suppression and the precise motion reproduction, simultaneously though the conventional methods are

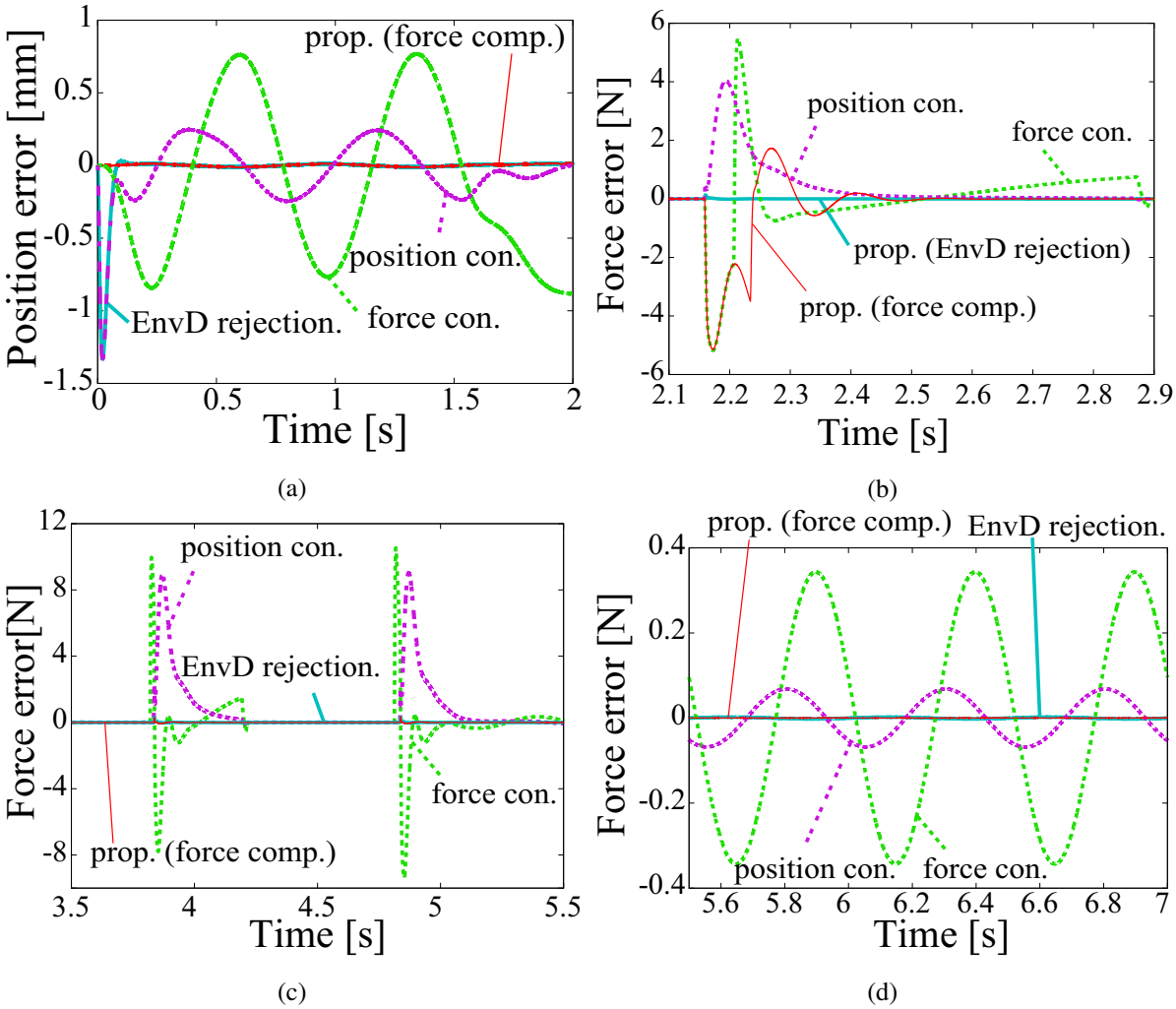

Fig. 5-8: Expanded views of error responses. (a) 0 to 2.0 sec. (b) 2.1 to 2.9 sec. (c)3.5 to 5.5 sec. (d) 5.5 to 7.0 sec.

not able to achieve. Then, the advantages and the necessity of the proposal are confirmed.

5.4.4 Detailed Design of Force Compensator

Based on the results, a_0^f, a_1^f and a_2^f should be set to smaller values to compensate for the force reproduction. On the other hand, a_0^f should have a positive value to reduce the steady-state error in the position response when turning back to the original saved position. However, these aims cannot be realized simultaneously according to the constraints of (5.19). For this reason, a_1^f and a_0^f should have

variable gains:

$$a_0^f = \kappa_0^f \exp\left[-\alpha_0^f G_L^f(s)\left(\left(F_s^{S,\mathrm{ext}}\right)^2 + \left(F_s^{R,\mathrm{ext}}\right)^2\right)\right] \tag{5.71}$$

$$a_1^f = \kappa_1^f \left\{1 - \exp\left[-\alpha_1^f G_L^f(s)\left(F_s^{R,\mathrm{ext}}\right)^2\right]\right\} \tag{5.72}$$

where α_0^f, α_1^f, κ_0^f and κ_1^f represent positive constants and $G_L^f(s)$ represents a LPF to suppress chattering. By setting a_0^f as given in (5.71), the steady-state errors in contact motions are eliminated according to (5.60) because a_0^f converges to zero in contact motions. On the other hand, by setting a_1^f as given in (5.71), a the stability of the contact motions is improved in the presence of an EnvD. In addition, the force error converges to zero more quickly according to Fig. 5-4 because a_1^f is smaller than κ_1^f if the slave system cannot contact with the environment in the motion reproduction phase.

Table 5.2: Parameters of experiments for motion-saving and motion-reproduction systems.

Parameters	Descriptions	Value
T_s	sampling time	0.1 ms
K_{tn}	torque coefficient	1.18 Nm/A
J_n	inertia of rotary motor	0.00288 kgm^2
K_v	velocity gain	600
g_W	cut-off frequency of WDOB	10 rad/s
g_l^f	cut-off frequency of $G_L^f(s)$	10 rad/s
κ_0^f	parameter of a_0^f	2000
κ_1^f	parameter of a_1^f	40
α_0^f, α_1^f	exponential part of a_0^f and a_1^f	1.0
a_2^f	parameter of force compensator	1.0

5.5 Experiments of Motion-saving System and Reproduction System

5.5.1 Experimental Setup for Motion-saving System and Reproduction System

Experimental tests were conducted in order to validate the proposed method. Fig. 5-9 shows the experimental setup, which used 2-DOF serial link manipulators and an aluminum board. Because direct drive motors are utilized for the manipulators, the frictions or backlashes are assumed to be negligibly small. In the experiment on the motion saving system, an operator conducted contact motions and free motions with the environment for 20 s, and the force and trajectory information was stored. For the comparison, both the proposed and conventional methods were tested in an experiment on the motion reproduction system. The proposed compensators were implemented in the X and Y directions. For the comparison, the velocity-based method was implemented in the Y direction, and a variable position gain was implemented in the X direction. The controller in the X direction was a kind of force-based variable compliance control [91]. The variable gain K_p^{con} was set as follows:

$$K_p^{\mathrm{con}} = K_p \exp\left[-\alpha_0^f G_L^f(s)\left(\left(F_s^{S,\mathrm{ext}}\right)^2 + \left(F_s^{R,\mathrm{ext}}\right)^2\right)\right]. \tag{5.73}$$

Two experiments were conducted on the motion reproduction system. In the first experiment, the distance from the manipulator to the environment was set to be the same as that for the motion saving system. In the second experiment, the distance was farther than that for the saving system. Furthermore, additional disturbance forces were added. In order to confirm the effectiveness of EnvD rejection for position reproduction, b^f in the X direction was set to become zero (the force compensator was deactivated)

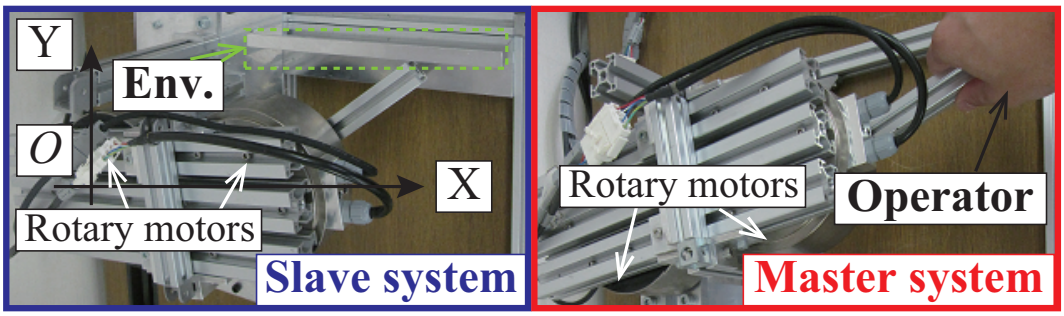

Fig. 5-9: Experimental setup for motion-saving and motion-reproduction systems.

after 16 s. K_p^{con} was set to become the constant value K_p after 16 s. Table 5.2 lists the experimental parameters. The other parameters were the same as those used in the analysis, which are given in Table 5.1.

5.5.2 Experimental Results for Motion-saving System and Reproduction System

Experimental Results with Same Distance to Environment

Figs. 5-10 and 5-11 show the experimental results when the motion saving and motion reproduction systems had the same distance. The green dashed and black solid lines show the position and force responses of the master and slave systems, respectively. The red dotted and blue dashed-dotted lines show the reproduced force and position responses of the proposed and conventional methods, respectively. The yellow shaded areas represent areas where contact motions with the environment were conducted. Figs. 5-10 (a) and (b) show that position tracking and the "law of action and reaction" were realized between the master and slave systems. Figs. 5-11 (a) and (b) show the errors of the position and force responses (saved data minus reproduced data) in the X and Y directions, respectively. Although the proposed method generated larger amplitudes for the position errors of the free motions than the conventional methods, this is because force reproduction was prioritized over trajectory reproduction, as shown in Fig. 5-10 (c). The trajectory was affected by differences of the neglected (uncertain) friction forces from the motion saving phase because a_0^f and a_1^f became small, and the EnvD suppression for position reproduction was low relative to that for force reproduction. However, the position errors were sufficiently small because the surrounding environment for the free motions was not affected by the manipulators. The position errors that appeared in the contact motions were caused by the difference in initial postures of the manipulators. As shown by the position responses in Fig. 5-11 (a), the conventional method had a

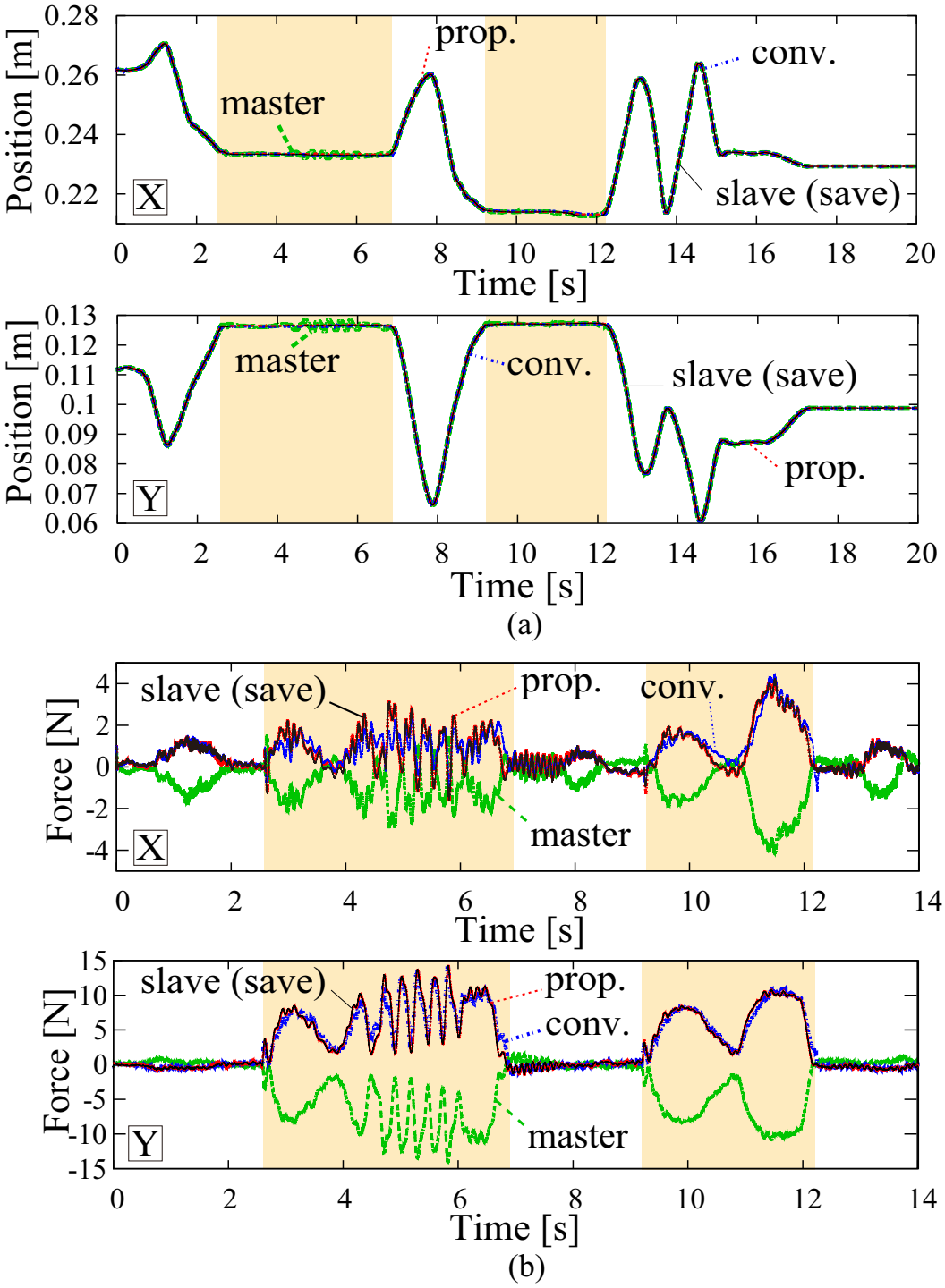

Fig. 5-10: Experimental results of motion extraction and reproduction with same environmental position. (a) Position. (b) External force.

steady-state error caused by the difference as indicated by the aqua blue-dashed and red solid circles. In addition, differences about the behavior of the uncertainties including nonlinear phenomena like friction forces also have possibilities to have affected the reproduced motions. On the other hand, the proposed method was able to return to the original trajectory because of the variable gains of a_0^f in the force reproduction compensator. The conventional methods showed the deterioration in the reproduced force responses, especially in the transient responses as shown in Fig. 5-11 (b). The deterioration was caused by the variable position gain and lack of the proportional position gain K_p because the MR in the X and Y directions changed and deteriorated even under the same environmental conditions, as discussed in the previous section. As a result, the contact forces to the environment were not reproduced properly. With the proposed method, there was almost no deterioration in the reproduced motions (especially in the contact motions), and the force and position were reproduced precisely because it can improve the EnvD suppression performance without degrading the MR. Based on the results, the conventional methods cannot reproduce original motions even under the same environmental conditions because of the deterioration in the MR. On the other hand, the proposed method can reproduce the saved motions precisely because it can improve the EnvD suppression performance without degrading the MR.

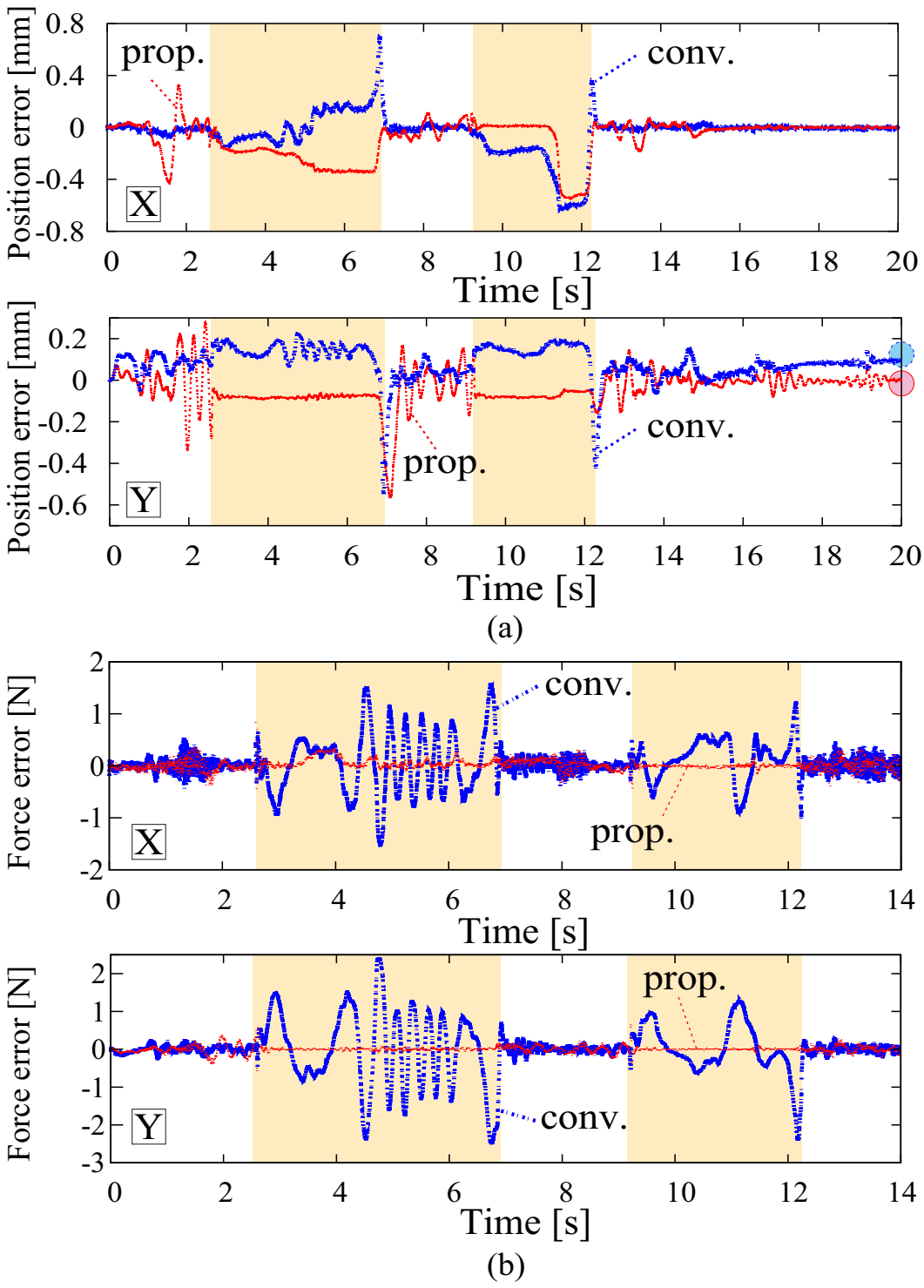

Fig. 5-11: Errors with same environmental position. (a) Position errors. (b) External force errors.

Experimental Results with Farther Distance to Environment

Figs. 5-12 and 5-13 show the experimental results with a farther distance between the manipulators and environment. The black solid, red dotted, and blue dashed-dotted arrows represent the time spans when contact motions were conducted in the saving system, the proposed system, and the conventional reproduction system, respectively. The brown-shaded areas represent the difference in the duration of contact between the saved motions and the proposed method. The gray-shaded areas represent the difference in the duration of contact between the proposed and conventional methods. The aqua blue shaded areas (A) represent the time span when the force compensator in the X direction was deactivated (b_f=0) and the position reproduction was prioritized. The green-shaded areas represent the difference in the distance to the environment between the saving and reproduction phases. Figs. 5-12 (a) and (b) show the reproduced position and force responses. Figs. 5-13 (a) and (b) show the errors of the position and force responses. The error for the proposed method in the first brown-shaded area of Fig. 5-13 (a) appears because the environment exists in the farther position and manipulator step forward. After contact with the environment, however, the manipulator tried to turn back to the original trajectory with the use of the variable gains. For both conventional methods, the error converged too slowly to reproduce the contact motions in the first gray shaded area. On the other hand, the proposed method was able to reach the environment immediately, and the EnvD was suppressed well based on the force responses as shown in Figs. 5-13 (a) and (b). After the first contact motions, an additional disturbance was added, as shown by the yellow solid circles. Again, the conventional methods converged the reproduced force with the saved force too slowly to reproduce the contact force properly. In this case, the conventional methods degraded the force reproduction for transient motions even after the manipulator contacted with the environment, as shown in the yellow-shaded areas. For the proposed method, because a_0 and a_1 became small with the contact motions, the displacement against the additional disturbance was large compared to that of the conventional method. However, the proposed method was able to quickly modify the trajectory and reproduce the contact force properly, even in the transient phases. As a result, the contact forces could be reproduced even after the disturbances were added. Another additional disturbance force was added in the aqua blue-shaded area (A). As shown by the position responses in Fig. 5-13 (a), the proposed method suppressed the disturbance well as an EnvD, even though it remained in the conventional (normal reproduction) method as a steady-state error. As shown by the aqua blue-dashed and red solid circles in Figs. 5-12(b) and 5-13 (a), the velocity-based method failed to return to the original end point, but

the proposed method was able to arrive at the end point because of the variable gains of the force reproduction compensator. As shown by these results, the proposed method was able to realize the desired characteristics for force and position reproduction without changing (degrading) the MR, in contrast to the conventional methods.

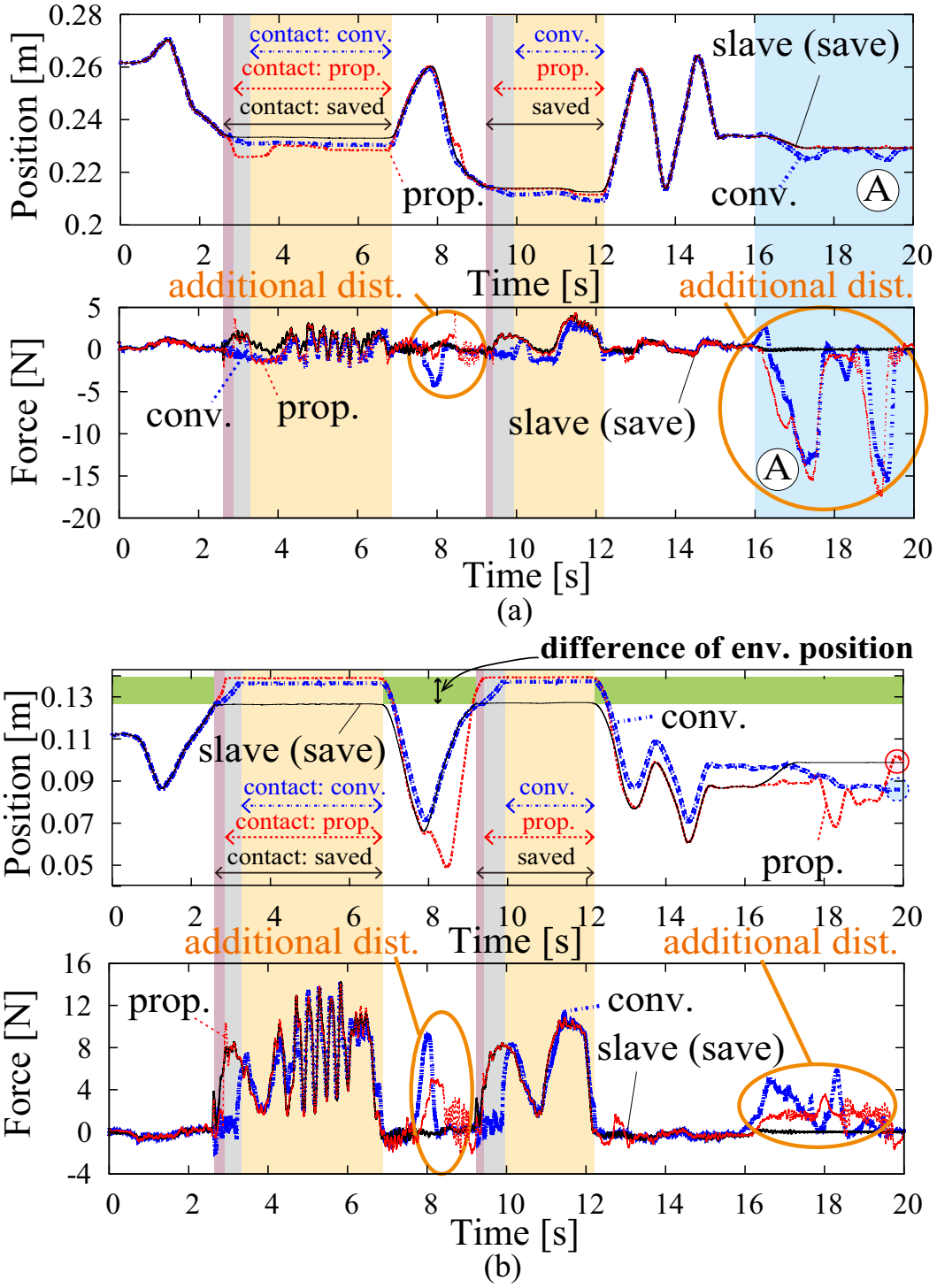

Fig. 5-12: Experimental results with farther environmental position (a) X direction. (b) Y direction.

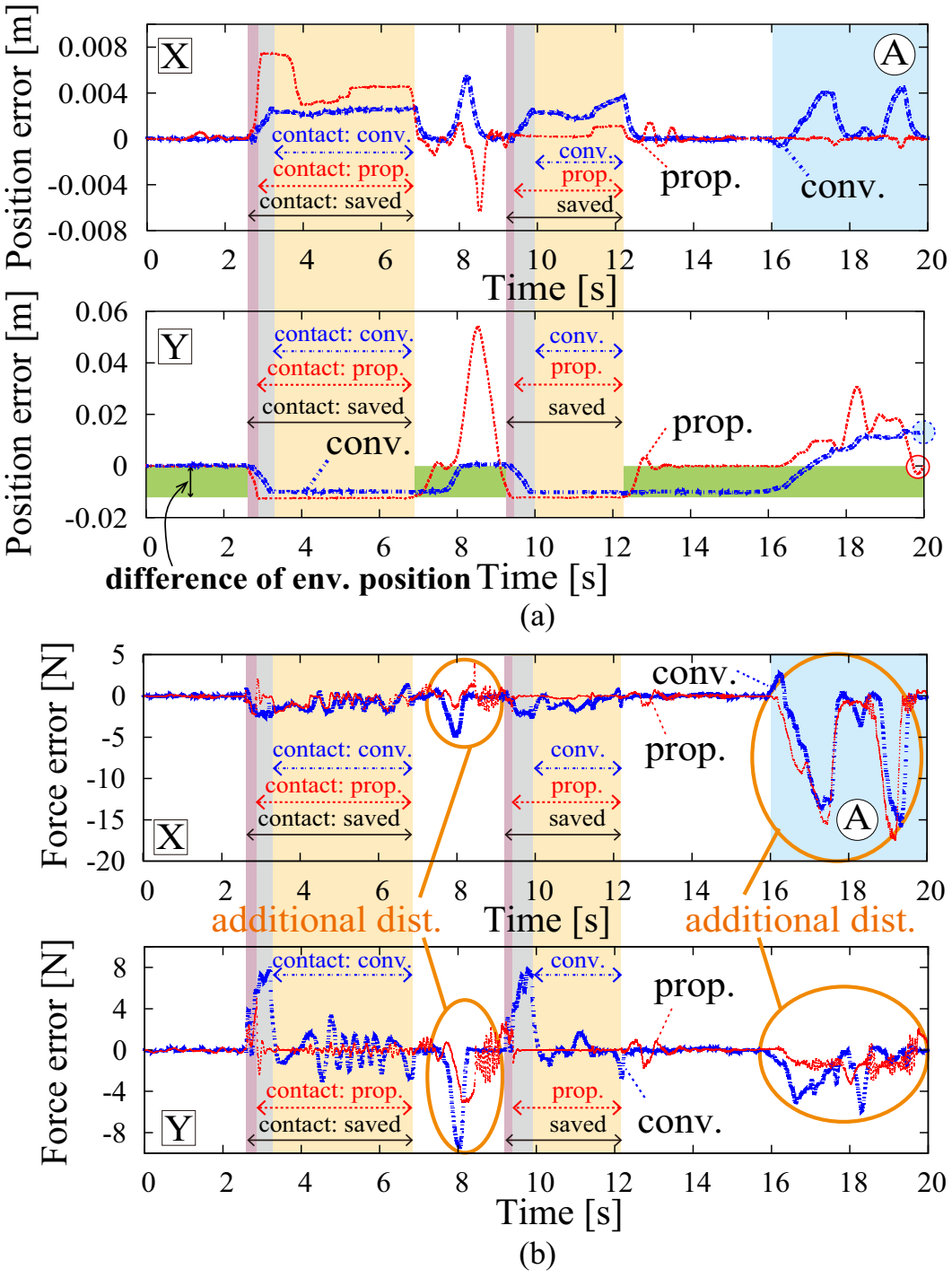

Fig. 5-13: Errors with farther environment. (a) Position errors. (b) External force errors.

5.6 Extension of EnvD Compensation to MDOF Cooperative Motion Reproduction

The last part clarifies the effect of difference about the environment between motion extraction and reproduction phase by defining the EnvD. In addition, analysis and design strategy of the motion reproduction are described about single DOF systems. It is possible to apply the compensation method of EnvD for a MDOF manipulator in 2 or 3-dimension cases.

Considering future practical realization, motion-copying system should be applied to human motions in which operators manipulate tools or objects and contact with other environments by grasping them in their hand. In order to realize such MDOF cooperative motions by robot manipulators, many researches have been developed [118–120]. Robust controller for the cooperative motions based on DOBs also have been developed [112, 113, 121, 122] Not only single robot cases but also multi robot cases like a bilateral control system have been developed for the grasping and manipulating tasks [123].

In the case of motion-copying system, the way of extraction and reproduction for the MDOF cooperative tasks should also be considered. In order to obtain the general versatility of saved human motions, slave systems should reproduce human motions even if the sizes of objects or distances to the target environments are different from motion extraction phase. However it is still unclear how extract and reproduce the MDOF cooperative tasks of operators and objects. This is because the difference about the size of object itself affects the systems as EnvD. In addition, kinematic and dynamics are changed compared to the extraction phase.

A conventional method which utilizes velocity information has been proposed for the cooperative task reproduction [124, 125]. However, the method is validated just in single DOF (one dimension) motions. The method also utilizes grasping manipulating modal transformation [123, 126–128], but the transformation cannot decouple rotational motions and tasks for generating internal force. On the other hand, a grasping matrix [109–111] can decouple the directions, but the method needs null space for expressing the direction of internal forced. This is difficult to use for task descriptions. In addition, velocity based method neglects to consider about the interaction of the grasped objects and the target environment. It is necessary for MDOF cooperative systems to take back objects or tools and to convert them in order to shift a task to the next one. The inherent property of velocity based method makes it impossible to achieve such simple and fundamental tasks. Saved motion data of cooperative tasks has a lack of versatility as a result.

In order to deal with these problems, this part proposes a method for realization of MDOF cooperative-task reproduction with EnvD. The modal transformation method and the grasping matrix based method are integrated and expanded to "extended object space". In addition, EnvD compensation is also extended to the MDOF cooperative tasks. As a result, the general versatility of saved human motions is able to be advanced.

5.7 Motion Extraction for MDOF Cooperative Task

The conventional extraction methods [123–128] for cooperative motions are suitable just for one DOF (one dimensional) motions. This is because decoupling of internal force direction and rotational direction are not considered. As a result, nonlinear tasks are not be able to be realized [129]. In order to extract a rotational and an internal force direction independently, a novel coordinate system for human motion extraction is proposed. In addition, an extraction method based on bilateral control is explained.

In this dissertation, following assumptions are made for the cooperative motions by MDOF manipulators.

- Three-fingered cooperative motions by MDOF manipulators are considered
- Effects of gravitational terms are negligibly small when planer motions are considered
- Point contact at end effectors is realized.
- Grasped object has a rigid body (without deformation)
- If the grasped object in motion reproduction is the same as that of motion saving system, the stability of grasp is guaranteed by motions of human operator in motion extraction phase.

5.7.1 Coordinate Transformation for Extraction of Human and Object Motions

This part, conventional modal transformations and grasping matrix are integrated and extended in order to decouple grasping and rotational tasks and to deal with the all tasks as main tasks.

Transformation to elemental motion components

A transformation of vectors form end-effectors to vectors for representing elements of cooperative motions are described as

$$\boldsymbol{X}_{Ei} = \sum_{j=1}^{3} e_{ij}\boldsymbol{X}_{Wj} \ \ (i = 1,\ 2,\ 3) \tag{5.74}$$

where

$$\boldsymbol{X}_{E1} = e_{11}\boldsymbol{X}_{W1} + e_{12}\boldsymbol{X}_{W2} + e_{13}\boldsymbol{X}_{W3} \tag{5.75}$$

$$\boldsymbol{X}_{E2} = e_{21}\boldsymbol{X}_{W1} + e_{22}\boldsymbol{X}_{W2} + e_{23}\boldsymbol{X}_{W3} \tag{5.76}$$

$$\boldsymbol{X}_{E3} = e_{31}\boldsymbol{X}_{W1} + e_{32}\boldsymbol{X}_{W2} + e_{33}\boldsymbol{X}_{W3}. \tag{5.77}$$

The elements of the cooperative motions can be described by using a transformation matrix $\boldsymbol{T}_E$ as follows:

$$\boldsymbol{X}_E = \boldsymbol{T}_E\boldsymbol{X}_W \tag{5.78}$$

where

$$\boldsymbol{T}_E = \begin{bmatrix} \frac{b}{a+b}\boldsymbol{I} & \frac{a}{a+b}\frac{q}{p+q}\boldsymbol{I} & \frac{a}{a+b}\frac{p}{p+q}\boldsymbol{I} \\ \frac{a}{a+b}\boldsymbol{I} & -\frac{a}{a+b}\frac{q}{p+q}\boldsymbol{I} & -\frac{a}{a+b}\frac{p}{p+q}\boldsymbol{I} \\ -\frac{ca}{a+b}\boldsymbol{I} & -A\boldsymbol{I} & B\boldsymbol{I} \end{bmatrix} \tag{5.79}$$

$$\begin{bmatrix} c & A & B \end{bmatrix} = \begin{bmatrix} \frac{q}{p+q}\frac{\boldsymbol{r}_{32}\cdot\boldsymbol{r}_{E_11}}{\|\boldsymbol{r}_{E_11}\|^2} & \frac{1}{p+q}\left(q - \frac{cqa}{a+b}\right) & \frac{1}{p+q}\left(q - \frac{cqa}{a+b}\right) \end{bmatrix}. \tag{5.80}$$

In and a, b, p and q are arbitrary constants. c is determined by norm of orthogonal projection vector $\boldsymbol{r}_23$. $\boldsymbol{X}_{E1}$ corresponds to the center of the (grasping) motion. $\boldsymbol{X}_{E2}$ corresponds to the vector from X_{E1} to $\boldsymbol{X}_{W1}$. $\boldsymbol{X}_{E3}$ corresponds to the vector from internally dividing point in $\boldsymbol{X}_{W2}\boldsymbol{X}_{W3}$ $(p : q)$ to $\boldsymbol{X}_{W2}$. A schematic figure of the transformation is shown in Fig. 5-14. By considering (5.78) and principle of virtual work, velocity, acceleration and force vectors in the elemental motion space are obtained as

$$\dot{\boldsymbol{X}}_E \approx \boldsymbol{T}_E\ddot{\boldsymbol{X}}_W \tag{5.81}$$

$$\ddot{\boldsymbol{X}}_E = \boldsymbol{T}_E\ddot{\boldsymbol{X}}_W \tag{5.82}$$

$$\boldsymbol{F}_E = \boldsymbol{T}_E^{-T}\boldsymbol{F}_W. \tag{5.83}$$

As shown in (5.79), $\boldsymbol{T}_E$ corresponds to a third order Quarry matrix $\boldsymbol{Q}_3$ [127, 128] when a, b p and q are 1 and c equal to zero. The conventional transformation based on modal transformation matrices

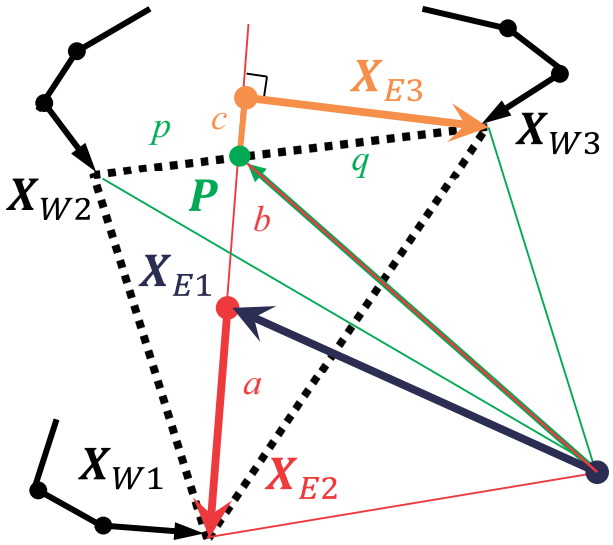

Fig. 5-14: A schematic figure of the transformation to elemental motion components.

considered to require the orthogonality of each modes [126–128] for decoupling the modes. As shown in chapter 4, however, this dissertation clarifies that the acceleration controller in modal space can realize decoupling control independently from the structure of the transformation matrices.

Kinematics of Cooperative Motions by Robots and Grasped Object

A coordinate transformation from element vectors to the extended object space which represents integrated motions of manipulators and grasped object is described as follows [129]:

$$\boldsymbol{Q}_O = \left[\boldsymbol{X}_O \;\; \boldsymbol{\Psi} \;\; \boldsymbol{\Lambda}\right]^T = \boldsymbol{G}_O\left(\boldsymbol{X}_{E1}\boldsymbol{X}_{E2}, \boldsymbol{X}_{E3}\right) \tag{5.84}$$

$$\left[\boldsymbol{X}_O \;\; \boldsymbol{\Lambda}\right]^T = \left[\boldsymbol{X}_O \;\; R \;\; L\right]^T = \left[\boldsymbol{X}_{E1} \;\; \|\boldsymbol{X}_{E2}\| \;\; \|\boldsymbol{X}_{E3}\|\right]^T \tag{5.85}$$

$$\boldsymbol{\Psi} = \left[\psi \;\; \vartheta \;\; \varphi \;\; \eta\right]^T = \begin{bmatrix} \tan^{-1}\left(\frac{Z_{E3}}{\sqrt{X_{E3}^2+Y_{E3}^2}}\right) \\ -\tan^{-1}\left(\frac{Z_{E2}}{\sqrt{X_{E2}^2+Y_{E2}^2}}\right) \\ \tan^{-1}\left(\frac{Y_{E2}}{X_{E2}}\right) \\ -\tan^{-1}\left(\frac{X_{E3}}{Y_{E3}}\right) \end{bmatrix} \tag{5.86}$$

$$\boldsymbol{\Theta}' = \left[\psi \;\; \vartheta \;\; \theta_z\right]^T = \left[\psi \;\; \vartheta \;\; \varphi+\eta\right]^T. \tag{5.87}$$

$\boldsymbol{X}_O$ represents the center of cooperative motions. $\boldsymbol{\Psi}$ corresponds to the rotational motion of the grasped object. $\boldsymbol{\Lambda}$ corresponds to tasks for grasping motions. The coordinate integrates directions with respect

to object motions and internal force direction. This means that both modal spaces and the object space extended in the coordinate. Then, this coordinate system is defined as extended object coordinate. Relationships of velocities and accelerations between the coordinate and grasping and manipulating modal spaces are expressed by

$$\dot{\boldsymbol{Q}}_O = \boldsymbol{\Xi}\, dot\boldsymbol{X}_E \tag{5.88}$$

$$\ddot{\boldsymbol{Q}}_O = \boldsymbol{\Xi}\ddot{\boldsymbol{X}}_E + \dot{\boldsymbol{\Xi}}\dot{\boldsymbol{X}}_E \tag{5.89}$$

where $\boldsymbol{\Xi}$ is a Jacobian matrix of the proposed coordinate. A relationship of force vector between the coordinate and grasping and manipulating modal spaces is also obtained as

$$\boldsymbol{N} = \boldsymbol{\Xi}^{-T}\boldsymbol{F}_E = \begin{bmatrix}\boldsymbol{F}_O & \boldsymbol{\tau}_\Psi & \boldsymbol{F}_\Lambda\end{bmatrix}^T = \boldsymbol{\Xi}^{-T}\boldsymbol{T}_X^{-T}\boldsymbol{F}_W. \tag{5.90}$$

Description by Grasping Matrix

The grasping matrix [109–111] (or conventional Jacobian matrix for the object motions [112,113,121, 122]) also can describe cooperative motions by manipulators and grasped object. The grasping matrix is described as below

$$\boldsymbol{G}_{\mathrm{ra}} = \begin{bmatrix}\boldsymbol{I} & \boldsymbol{I} & \boldsymbol{I} \\ \boldsymbol{R}_{O1} & \boldsymbol{R}_{O2} & \boldsymbol{R}_{O3}\end{bmatrix} \tag{5.91}$$

$$\boldsymbol{R}_{Oi} = \begin{bmatrix} 0 & -r_{zi} & r_{yi} \\ r_{zi} & 0 & -r_{zi} \\ -r_{yi} & r_{xi} & 0 \end{bmatrix} \ (i = 1,\ 2,\ 3) \tag{5.92}$$

where $\boldsymbol{G}_{\mathrm{ra}}$ is the grasping matrix. The transformation of force and torque vectors by the grasping matrix is expressed as follows:

$$\boldsymbol{F}_{O_b} = \boldsymbol{G}_{\mathrm{ra}}\boldsymbol{F}_W = \begin{bmatrix}\boldsymbol{F}_O & \boldsymbol{\tau}_O\end{bmatrix}^T \tag{5.93}$$

$$= \begin{bmatrix}F_{Ox} & F_{Oy} & F_{Oz} & \tau_{Ox} & \tau_{Oy} & \tau_{Oz}\end{bmatrix}^T. \tag{5.94}$$

Additionally, transformation of position vectors are described by direct kinematics with respect to a center of the motions as below

$$\boldsymbol{Q}_{O_b} = \boldsymbol{G}_{O_b}(\boldsymbol{X}_W) = \begin{bmatrix}\boldsymbol{X}_O & \boldsymbol{\Theta}_O\end{bmatrix}^T. \tag{5.95}$$

A schematic figure of the transformation by Grasping matrix is shown in Fig. 5-15. However elements for approaching and grasping motions gotten involved in null space of $\boldsymbol{G}_{\mathrm{ra}}$.

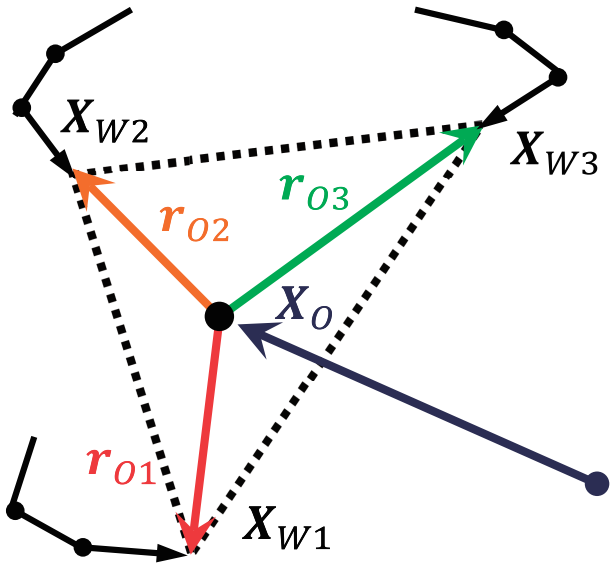

Fig. 5-15: A schematic figure of the transformation by Grasping matrix.

If the grasping tasks have to be determined, the control reference for the manipulator is given as

$$\boldsymbol{F}_W^{\mathrm{ref}} = \boldsymbol{G}_{\mathrm{ra}}^{+}\boldsymbol{F}_O^{\mathrm{ref}} + \left(\boldsymbol{I} - \boldsymbol{G}_{\mathrm{ra}}^{+}\boldsymbol{G}_{\mathrm{ra}}\right)\boldsymbol{F}_{\mathrm{null}}^{\mathrm{ref}}. \tag{5.96}$$

Therefore, if the grasping matrix is tried to be implemented for the motion reproduction, a part of obtained human motions are lost in null space of the matrix because $\boldsymbol{G}_{\mathrm{ra}}$ focuses on only object motion.

On the other hand, proposed coordinate include tasks for approaching grasping motions in $\boldsymbol{\Lambda}$. Therefor, all DOFs can be assigned and object and manipulator motions can be described

5.7.2 Dynamics of Proposed Coordinate System

By using (5.89) and (5.90), motion equation in element modal space is transformed and dynamics in extended object space is derived as

$$\boldsymbol{M}_{O_M}\ddot{\boldsymbol{Q}}_O^{\mathrm{res}} = \boldsymbol{N}_O^{\mathrm{ref}} - \boldsymbol{N}_{O_M}^{\mathrm{ext}} + \boldsymbol{H}_{O_M}\dot{\boldsymbol{Q}}_O^{\mathrm{res}} - \boldsymbol{\Xi}^{-T}\boldsymbol{T}_X^{-T}\boldsymbol{J}_{\mathrm{aco}}^{-T}\boldsymbol{h}(\boldsymbol{q}^{\mathrm{res}}, \dot{\boldsymbol{q}}^{\mathrm{res}}) \tag{5.97}$$

where

$$\boldsymbol{H}_{O_M} = \boldsymbol{M}_{O_M}\dot{\boldsymbol{\Xi}} + \boldsymbol{\Xi}^{-T}\boldsymbol{T}_X^{-T}\boldsymbol{M}_W\dot{\boldsymbol{J}}_{\mathrm{aco}}\boldsymbol{J}_{\mathrm{aco}}^{-1}\boldsymbol{T}_X^{-1}\boldsymbol{\Xi}^{-T}. \tag{5.98}$$

$\boldsymbol{M}_{O_M}$ is an equivalent mass matrix in extended mass matrix of manipulators.

$$\boldsymbol{M}_O = \boldsymbol{\Xi}^{-T}\boldsymbol{T}_X^{-T}\boldsymbol{J}_{\mathrm{aco}}^{-T}\boldsymbol{m}\boldsymbol{J}_{aco}^{-1}\boldsymbol{T}_X^{-1}\boldsymbol{\Xi}^{-1}. \tag{5.99}$$

If the manipulators grasp the object, on the other hand, motion equation of the grasped object can be expressed as follows:

$$\boldsymbol{M}_{O_b}\ddot{\boldsymbol{Q}}_{O_b}^{\mathrm{res}} = \boldsymbol{N}_{O_b}^{\mathrm{ext}} - \boldsymbol{H}_{O_b} \tag{5.100}$$

where

$$\boldsymbol{Q}_{O_b}^{\mathrm{res}} = \begin{bmatrix} \boldsymbol{X}_O & \boldsymbol{\Theta} & \boldsymbol{0} \end{bmatrix}^T \tag{5.101}$$

$$\boldsymbol{N}_{O_b}^{\mathrm{ext}} = \begin{bmatrix} \boldsymbol{F}_O & \boldsymbol{\tau} & \boldsymbol{0} \end{bmatrix}^T. \tag{5.102}$$

$\boldsymbol{M}_{O_b}$ and $\boldsymbol{H}_{O_b}$ represent a mass and inertia matrix and Coriolis of the grasped object, respectively. By adding (5.97) and (5.100), the dynamics of whole cooperative system including manipulators and the object is obtained by

$$\boldsymbol{M}_O\ddot{\boldsymbol{Q}}_O^{\mathrm{res}} = \boldsymbol{N}_O^{\mathrm{ref}} + \boldsymbol{H}_{O_M}\dot{\boldsymbol{Q}}_O^{\mathrm{res}} - \boldsymbol{N}_O^{\mathrm{ext}} - \boldsymbol{H}_O \tag{5.103}$$

where

$$\boldsymbol{M}_O = \boldsymbol{M}_{O_M} + \boldsymbol{M}_{O_b} \tag{5.104}$$

$$\boldsymbol{H}_O = \boldsymbol{H}_{O_b} + \boldsymbol{\Xi}^{-T}\boldsymbol{T}_X^{-T}\boldsymbol{J}_{\mathrm{aco}}^{-T}\boldsymbol{h}(\boldsymbol{q}^{\mathrm{res}}, \dot{\boldsymbol{q}}^{\mathrm{res}}) \tag{5.105}$$

$$\boldsymbol{N}_O^{\mathrm{ext}} = \boldsymbol{N}_{O_M}^{\mathrm{ext}} - \boldsymbol{N}_{O_b}^{\mathrm{ext}}. \tag{5.106}$$

If the joint space DOB is implemented, the dynamics of extended object space is rewritten as follows:

$$\begin{aligned} \boldsymbol{M}_{O_n}\ddot{\boldsymbol{Q}}_O^{\mathrm{res}} &= \boldsymbol{N}_O^{\mathrm{ref}} + \boldsymbol{H}_{O_M}\dot{\boldsymbol{Q}}_O^{\mathrm{res}} \\ &\quad -\boldsymbol{g}_h^{\mathrm{dis}}(s)\left(\boldsymbol{N}_O^{\mathrm{ext}} + \boldsymbol{H}_O\right) \approx \boldsymbol{N}_O^{\mathrm{ref}} + \boldsymbol{H}_{O_M}\dot{\boldsymbol{Q}}^{\mathrm{res}} \end{aligned} \tag{5.107}$$

$$\boldsymbol{M}_{O_n} = \boldsymbol{\Xi}^{-T}\boldsymbol{T}_X^{-T}\boldsymbol{J}_{\mathrm{aco}}^{-T}\boldsymbol{m}\boldsymbol{J}_{aco}^{-1}\boldsymbol{T}_X^{-1}\boldsymbol{\Xi}^{-1} \tag{5.108}$$

where $\boldsymbol{g}_h^{\mathrm{dis}}(s)$ is a matrix which has high-pass filters on diagonal elements resulting from the DOB. The second term in the right hand side of (5.107) is caused by coordinate transformations.

5.7.3 Motion Extraction by Using Bilateral Control

Motion saving system to extract information of cooperative motions is illustrated in this part. First, the position (angle) and force (torque) information are transformed into common and differential modes

as follows:

$$\boldsymbol{N}^{\mathrm{ext}} = \begin{bmatrix} \boldsymbol{N}_N^{\mathrm{ext}} & \boldsymbol{N}_Q^{\mathrm{ext}} \end{bmatrix}^T = \boldsymbol{\Gamma}\boldsymbol{N}_O^{\mathrm{ext}} = \boldsymbol{\Gamma}\begin{bmatrix} \hat{\boldsymbol{N}}_{Om}^{\mathrm{ext}} & \hat{\boldsymbol{N}}_{Os}^{\mathrm{ext}} \end{bmatrix}^T \tag{5.109}$$

$$\boldsymbol{Q}^{\mathrm{res}} = \begin{bmatrix} \boldsymbol{Q}_N^{\mathrm{res}} & \boldsymbol{Q}_Q^{\mathrm{res}} \end{bmatrix} = \boldsymbol{\Gamma}\boldsymbol{Q}_O^{\mathrm{res}} = \boldsymbol{\Gamma}\begin{bmatrix} \boldsymbol{Q}_{Om}^{\mathrm{res}} & \boldsymbol{Q}_{Os}^{\mathrm{res}} \end{bmatrix}^T \tag{5.110}$$

$$\boldsymbol{\Gamma} = \begin{bmatrix} \boldsymbol{I} & \boldsymbol{I} \\ \boldsymbol{I} & -\boldsymbol{I} \end{bmatrix}. \tag{5.111}$$

$\hat{\boldsymbol{N}}^{\mathrm{ext}}$ is estimated by RFOB. Control goals of motion extraction are same as that of bilateral control as follows:

$$\boldsymbol{N}_N^{\mathrm{ext}} = \hat{\boldsymbol{N}}_{Om}^{\mathrm{ext}} + \hat{\boldsymbol{N}}_{Os}^{\mathrm{ext}} = \boldsymbol{N}_N^{\mathrm{cmd}} = \boldsymbol{0} \tag{5.112}$$

$$\boldsymbol{Q}_Q^{\mathrm{res}} = \boldsymbol{Q}_{Om}^{\mathrm{res}} - \boldsymbol{Q}_{Os}^{\mathrm{res}} = \boldsymbol{Q}_Q^{\mathrm{cmd}} = \boldsymbol{0}. \tag{5.113}$$

In order to achieve these control goals, force controller and position controller are employed. Acceleration references of each direction to realize these control goals are obtained by

$$\boldsymbol{N}_N^{\mathrm{ref}} = \boldsymbol{C}_N\left(\boldsymbol{N}_N^{\mathrm{cmd}} - \boldsymbol{N}_N^{\mathrm{ext}}\right) = -\boldsymbol{C}_N\boldsymbol{N}_N^{\mathrm{ext}} \tag{5.114}$$

$$\boldsymbol{N}_Q^{\mathrm{ref}} = \boldsymbol{C}_Q(s)\left(\boldsymbol{Q}_Q^{\mathrm{cmd}} - \boldsymbol{Q}_Q^{\mathrm{res}}\right) = -\boldsymbol{C}_Q(s)\boldsymbol{Q}_Q^{\mathrm{res}} \tag{5.115}$$

where $\boldsymbol{C}_N$ and $\boldsymbol{C}_Q(s)$ represents a force (torque) servoing matrix and position (angle) regulator matrix, respectively. The dynamics of the hybrid control system is described as follows:

$$\boldsymbol{M}\ddot{\boldsymbol{Q}}^{\mathrm{res}} = \boldsymbol{N}^{\mathrm{ref}} + \boldsymbol{\Gamma}\boldsymbol{H}_{O_M}\dot{\boldsymbol{Q}}^{\mathrm{res}} \tag{5.116}$$

$$\boldsymbol{M} = \boldsymbol{\Gamma}\boldsymbol{M}_{O_n}\boldsymbol{\Gamma}^{-1} \tag{5.117}$$

$$\boldsymbol{N}^{\mathrm{ref}} = \boldsymbol{\Gamma}\boldsymbol{N}_O^{\mathrm{ref}} = \begin{bmatrix} \boldsymbol{N}_N^{\mathrm{ref}} & \boldsymbol{N}_Q^{\mathrm{ref}} \end{bmatrix}^T. \tag{5.118}$$

In order to realize an acceleration controller, the acceleration reference for the hybrid control and the reference torque for joint space are given as follows:

$$\ddot{\boldsymbol{Q}}_O^{\mathrm{ref}} = \boldsymbol{\Gamma}^{-1}\boldsymbol{M}_v^{-1}\boldsymbol{N}^{\mathrm{ref}} \tag{5.119}$$

$$\boldsymbol{f}^{\mathrm{ref}} = \boldsymbol{m}_n\boldsymbol{q}^{\mathrm{ref}} = \boldsymbol{m}_n\boldsymbol{J}_{\mathrm{aco}}^{-1}\boldsymbol{T}_X^{-1}\boldsymbol{\Xi}^{-1}\ddot{\boldsymbol{Q}}_O^{\mathrm{ref}}. \tag{5.120}$$

The process of constructing acceleration controller for the hybrid control is similar to the way shown in chapter 5. If $\boldsymbol{M}_v$ is set as an identity matrix, the decoupling control can be realized.

$$\boldsymbol{M}\ddot{\boldsymbol{Q}}^{\mathrm{res}} = \boldsymbol{M}\boldsymbol{M}_v^{-1}\boldsymbol{N}^{\mathrm{ref}} + \boldsymbol{\Gamma}\boldsymbol{H}_{O_M}\dot{\boldsymbol{Q}}_O^{\mathrm{res}} \tag{5.121}$$

$$\boldsymbol{M}_v\ddot{\boldsymbol{Q}}^{\mathrm{res}} = \boldsymbol{N}^{\mathrm{ref}} + \boldsymbol{M}_v\boldsymbol{\Gamma}\boldsymbol{M}_O^{-1}\boldsymbol{H}_{O_M}\dot{\boldsymbol{Q}}_O^{\mathrm{res}}. \tag{5.122}$$

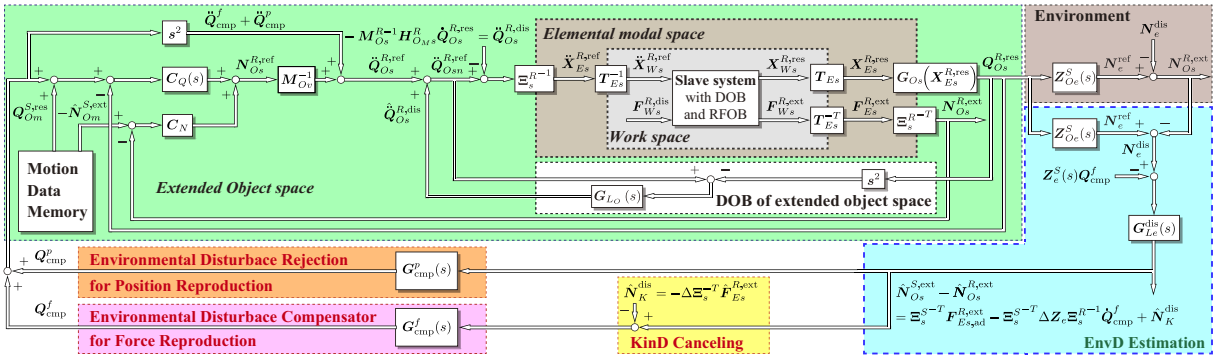

Fig. 5-16: Block diagram of proposed motion reproduction method for MDOF cooperative task

The second term in the right hand side of (5.122) should be eliminated. However, calculations of the term are complicated. In order to simplify the inverse kinematics of extended object space, the term is considered as a disturbance term and eliminated by a DOB [84, 97] as follows

$$\ddot{\boldsymbol{Q}}_O^{\rm dis} = -\boldsymbol{M}_O^{-1}\boldsymbol{H}_{O_M}\dot{\boldsymbol{Q}}_O^{\rm res} = \ddot{\boldsymbol{Q}}_{On}^{\rm ref} - \ddot{\boldsymbol{Q}}_O^{\rm res} \tag{5.123}$$

$$\ddot{\boldsymbol{Q}}_{On}^{\rm ref} = \ddot{\boldsymbol{Q}}_O^{\rm ref} + \hat{\ddot{\boldsymbol{Q}}}_O^{\rm dis} = \boldsymbol{G}_{LO}^{\rm dis}(s)\ddot{\boldsymbol{Q}}_O^{\rm dis} \tag{5.124}$$

where $\boldsymbol{G}_{LO}^{\rm dis}$ a matrix which has low-pass filters on diagonal elements. The decoupling control is achieved as follows:

$$\boldsymbol{M}_v\ddot{\boldsymbol{Q}}^{\rm res} = \boldsymbol{N}^{\rm ref} - \boldsymbol{M}_v\boldsymbol{\Gamma}\boldsymbol{G}_{HO}^{\rm dis}(s)\ddot{\boldsymbol{Q}}_O^{\rm dis} \approx \boldsymbol{N}^{\rm ref}. \tag{5.125}$$

By using the above processes, bilateral control about each direction is achieved independently. As a result, $\hat{\boldsymbol{N}}_m^{\rm ext}$ and $\boldsymbol{Q}_m^{\rm res}$ are stored in the motion data memory.

5.8 MDOF Cooperative Motion Reproduction with EnvD

Kinematic Disturbance

A Particular problem to MDOF cooperative systems is considered in the following part.

$\boldsymbol{N}_{Os}^{\rm ext}$ includes two force vectors. The one is a force vector $\boldsymbol{N}_M^{\rm ext}$ applied on the end effector of manipulators. The other one is a force vector $\boldsymbol{N}_{EN}^{\rm ext}$ applied on a grasped object from environment. The relationship is expressed as

$$\boldsymbol{N}_{Os}^{\rm ext} = \boldsymbol{N}_M^{\rm ext} + \boldsymbol{N}_{EN}^{\rm ext}. \tag{5.126}$$

On the other hand, if the size of grasped object is changed in the motion reproduction phase, the external force vector $\boldsymbol{N}_M^{R,\mathrm{ext}}$ is different from $\boldsymbol{N}_M^{S,\mathrm{ext}}$ as follows:

$$\boldsymbol{N}_M^{R,\mathrm{ext}} = \boldsymbol{N}_M^{S,\mathrm{ext}} + \boldsymbol{\Delta N} \tag{5.127}$$

where $\boldsymbol{\Delta N}$ is caused by difference about kinematics of a grasped object. The vector is described as

$$\boldsymbol{\Delta N} = \boldsymbol{\Delta \Xi}^{-T} \boldsymbol{F}_E^{\mathrm{ext}} = \begin{bmatrix} \boldsymbol{I} & \boldsymbol{0} \\ \boldsymbol{0} & \boldsymbol{\Delta \xi}^{-T} \end{bmatrix} \boldsymbol{F}_E = \begin{bmatrix} \boldsymbol{F}_O \\ \Delta \boldsymbol{\tau}_\Psi \\ \Delta \boldsymbol{F}_\Lambda \end{bmatrix} \tag{5.128}$$

where $\boldsymbol{\xi}$ represents a Jacobian matrix corresponds to $\boldsymbol{\Psi}$ and $\boldsymbol{\Lambda}$. This error force caused by difference of the kinematics is defined as Kinematic Disturbance (KinD) and obtained by

$$\begin{aligned} \boldsymbol{N}_K^{\mathrm{dis}} &= \boldsymbol{\Delta \Xi}^{-T} \boldsymbol{F}_E^{\mathrm{ext}} = \boldsymbol{\Xi}^{-T} \left(\boldsymbol{\Delta X}_E^{\mathrm{res}} \right) \boldsymbol{F}_E^{\mathrm{ext}} & (5.129) \\ &= \boldsymbol{\Xi}^{-T} \left(\boldsymbol{X}_E^{R,\mathrm{res}} - \boldsymbol{X}_E^{S,\mathrm{res}} \right) \boldsymbol{F}_E^{\mathrm{ext}} & (5.130) \end{aligned}$$

where $\boldsymbol{\Xi}^{-T}(\bullet)$ represent that $\boldsymbol{\Xi}^{-T}(\bullet)$ is a function of the parameters. Conventional methods which are discussed in the last part have deteriorations in rotational motion reproduction even if the grasped object does not contact with environments in the extraction phase. This is because KinD equivalently brings on additional EnvD in such a situation as follows:

$$\boldsymbol{N}_e^{\mathrm{dis}} = \boldsymbol{Z}_e^S(s) \boldsymbol{Q}_{Os}^{R,\mathrm{res}} - \boldsymbol{N}_{Os}^{R,\mathrm{ext}} = -\boldsymbol{\Delta Z} \boldsymbol{Q}_{Os}^{R,\mathrm{res}} + \boldsymbol{N}_{\mathrm{ad}}^{\mathrm{ext}} - \boldsymbol{N}_K^{\mathrm{dis}}. \tag{5.131}$$

Conventional methods tend to eliminate not only EnvD but also KinD because the methods cannot distinguish KinD and EnvD. The system changes the trajectory excessively in order to compensate the KinD in addition to EnvD.

This means that original information of object motions is reduced to two- thirds of original DOF in the two dimensional cases. In three dimensional cases, the situation will become serious because three rotational motions which is the half of original DOF. Because of this reason, conventional methods cannot deal with KinD and cannot realize appropriate reproduction for MDOF cooperative motions

5.8.1 Proposed Motion Reproduction for MDOF Cooperative Task

In order to reduce the deterioration of trajectory reproduction and to reproduce human interaction force through the grasped object even if the size of the object or initial positions of the environments are different, a novel motion reproduction method for MDOF cooperative systems is proposed in the following part. This method also takes KinD into account.

EnvD Rejection in MDOF Cooperative System

Differently from conventional approaches, proposed EnvD rejection methods can treat both EnvD and KinD without deteriorating response characteristics because proposed method has feed forward structures.

In order to cancel the effect of KinD, KinD is estimated based on (5.130) by using saved and reproduced information of $\boldsymbol{X}_G^{S,\mathrm{res}}$ and $\boldsymbol{X}_G^{R,\mathrm{res}}$ successively. EnvD which the estimated KinD is included is considered for compensations as follows:

$$\boldsymbol{N}_e^{\mathrm{dis}} + \boldsymbol{N}_K^{\mathrm{dis}} = \boldsymbol{Z}_e^S(s)\boldsymbol{Q}_{Os}^{R,\mathrm{res}} - \boldsymbol{N}_{Os}^{R,\mathrm{ext}} + \boldsymbol{N}_K^{\mathrm{dis}}. \tag{5.132}$$

Because KinD should be treated as EnvD concerning about the internal force direction, however, calculated KinD should not be added. Force and Position compensators derived in chapter 2 are expanded to the MDOF cooperative systems as follows:

$$\boldsymbol{Q}_{\mathrm{cmp}}^p = \boldsymbol{G}_{\mathrm{cmp}}^p(s)\tilde{\boldsymbol{N}}_e^{\mathrm{dis}} \tag{5.133}$$

$$\boldsymbol{Q}_{\mathrm{cmp}}^f = \boldsymbol{G}_{\mathrm{cmp}}^f(s)\tilde{\boldsymbol{N}}_e^{\mathrm{dis}\prime} \tag{5.134}$$

where

$$\tilde{\boldsymbol{N}}_e^{\mathrm{dis}\prime} = \boldsymbol{G}_L(s)\left(\boldsymbol{Z}_e^S(s)\boldsymbol{Q}_{Os}^{R,\mathrm{res}} - \boldsymbol{N}_{Os}^{R,\mathrm{ext}} - \boldsymbol{Z}_e^S(s)\boldsymbol{Q}_{\mathrm{cmp}}^f + \boldsymbol{N}_K^{\mathrm{dis}}\right) \tag{5.135}$$

$$= \hat{\boldsymbol{N}}_{Os}^{S,\mathrm{ext}} - \hat{\boldsymbol{N}}_{Os}^{R,\mathrm{ext}} + \hat{\boldsymbol{N}}_K^{\mathrm{dis}}. \tag{5.136}$$

$\boldsymbol{G}_{\mathrm{cmp}}^p(s)$ and $\boldsymbol{G}_{\mathrm{cmp}}^p(s)$ are matrices which have compensators in each directions on diagonal elements as follows: The acceleration reference vector in the motion reproduction phase is generated as follows:

$$\begin{aligned}\ddot{\boldsymbol{Q}}_{Osn}^{R,\mathrm{ref}} = {} & \frac{\boldsymbol{C}_N}{2}\left(-\hat{\boldsymbol{N}}_{Om}^{S,\mathrm{ext}} - \hat{\boldsymbol{N}}_{Os}^{R,\mathrm{ext}}\right) \\ & + \frac{\boldsymbol{C}_Q(s)}{2}\left(\boldsymbol{Q}_{Om}^{S,\mathrm{res}} + \boldsymbol{Q}_{\mathrm{cmp}}^p + \boldsymbol{Q}_{\mathrm{cmp}}^f - \boldsymbol{Q}_{Os}^{R,\mathrm{res}}\right) + \hat{\ddot{\boldsymbol{Q}}}_{Os}^{R,\mathrm{dis}}.\end{aligned} \tag{5.137}$$

Compensation values are included in position command as shown in the second term. DOB of the extended object space is implemented also in the reproduction phase. Once EnvD appears, the trajectory vector of the grasped object in the motion reproduction is modified as

$$\boldsymbol{Q}_{O_b}^{R,\mathrm{res}} = \boldsymbol{Q}_{O_b}^{S,\mathrm{res}} + \boldsymbol{Q}_{\mathrm{cmp}}^f. \tag{5.138}$$

As a result, the contact motion with environments trough the grasped object are reproduced. The Block diagram of the proposed motion reproduction method for MDOF cooperative systems is shown in Fig. 5-16.

Table 5.3: Experimental parameters for MDOF cooperative motion reproduction.

Parameter	Description	Value
T_s	sampling time	0.2 ms
K_{fn}	force coefficient	40.0 N/A
K_{tn}	torque coefficient	1.18 N/A
M_n	mass of linear motor	0.3 kg
J_n	inertia of DD motor	0.00288 kgm^2
K_f	force control gain	0.9
K_τ	torque control gain	70
K_p	proportional gain	3600
K_v	differential gain	120
g^{dis}, g^{ext}	cut-off frequency of DOB and RFOB	350 rad/s
g_O	cut-off frequency of extended object space DOB	15 rad/s

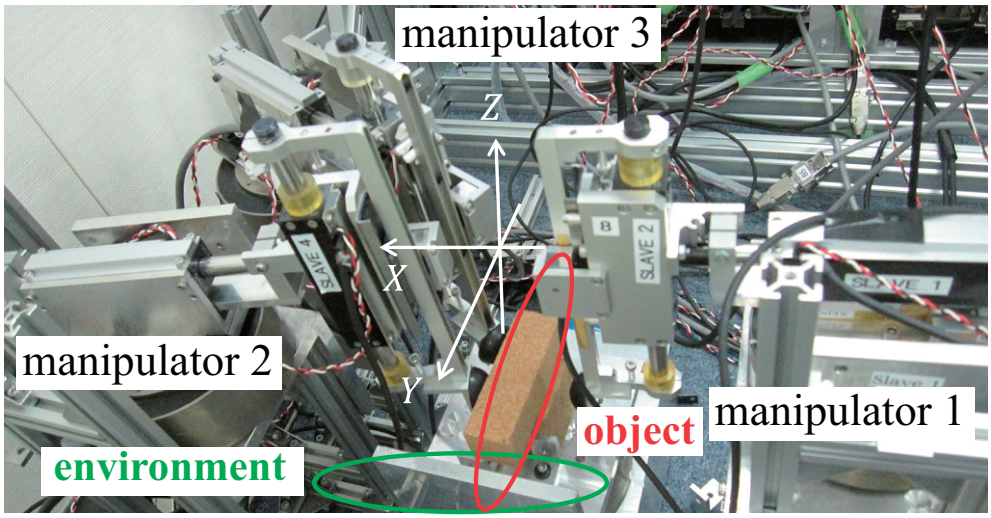

Fig. 5-17: Experimental set up for MDOF cooperative motion-extraction and reproduction.

5.9 Experiments of MDOF Cooperative Motion-Extraction and Reproduction

5.9.1 Experimental Setup for MDOF Cooperative Motion-Extraction and Reproduction

In order to confirm the validity of the proposed method, experiments of motion copying system by using two manipulators are executed. Experimental setup is shown in Fig. 5-17. The manipulators are composed by two linear motors and one rotational motor. As a grasped object, a cork block is used.

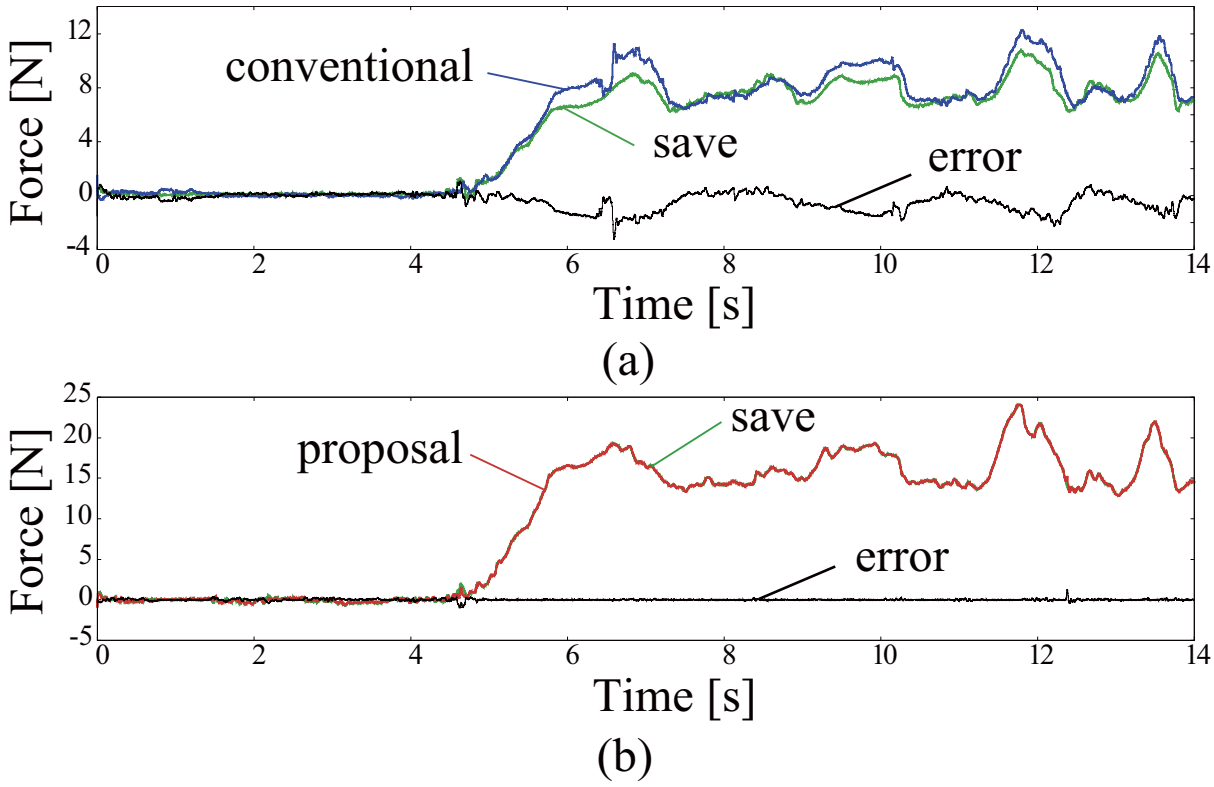

Fig. 5-18: Grasping force responses of motion-reproduction system. (a) Grasping matrix based method. (b) The proposed method.

Additionally, an aluminum plate is used for an external environment. Experiments for motion-extraction and motion-reproduction in a two dimension and a three dimension are tested. In the case of the two dimensional motion, responses of rotational motions (rotational angles) are measured by rotary encoder which is fixed to the grasped object.

Parameters used in experiments are shown in Table. 5.3.

5.9.2 Experimental Results of MDOF Cooperative Motion-Extraction and Reproduction

Experimental Results of Two Dimensional Cases

Fig. 5-18 shows the reproduced grasping force responses with respect to the grasping matrix and the proposed method. In the figure, the force response of the manipulator 1 in X axis is shown with respect to the case of the grasping matrix because grasping motions are difficult to express by using the grasping matrix. As shown in the figure, the grasping matrix based method deteriorates the force reproduction accuracy even though the object is same as that of motion-saving system. This means the conventional

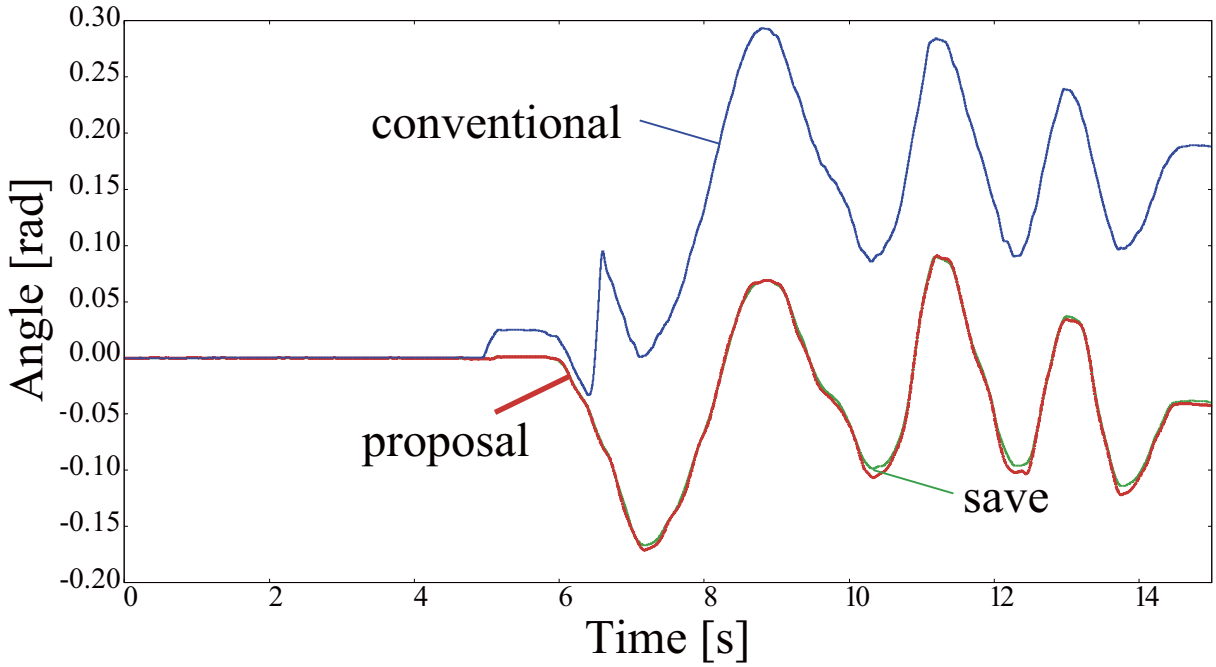

Fig. 5-19: Rotational motion responses of motion-reproduction system based on the grasping matrix and the proposed method.

method loses some motions obtained by bilateral control the null space. The deterioration of the force reproduction results in the deterioration of the rotational motion of the grasped object as shown in Fig. 5-19.

On the other hand, the proposed method achieves the appropriate reproduction of grasping force and rotational motions as shown in Figs. 5-18 and 5-19, respectively.

Fig. 5-20 shows the experimental result of the grasping motion with the smaller object with respect to the proposed method. As shown in the figure, the proposed method achieve to adapt the difference of the object size and to apply the adequate grasping force. Fig. 5-21 shows experimental results of rotational motion with the comparison between the conventional method based on the conventional modal transformation with the velocity based method and the proposed method. As shown in the figure, the conventional method cannot achieve reproduce the rotational motion because of the rotational motion and grasping motion are difficult to separate in MDOF cases. On the contrary, the proposed method can reproduce rotational motion more precisely than the conventional method even though the size of object is small.

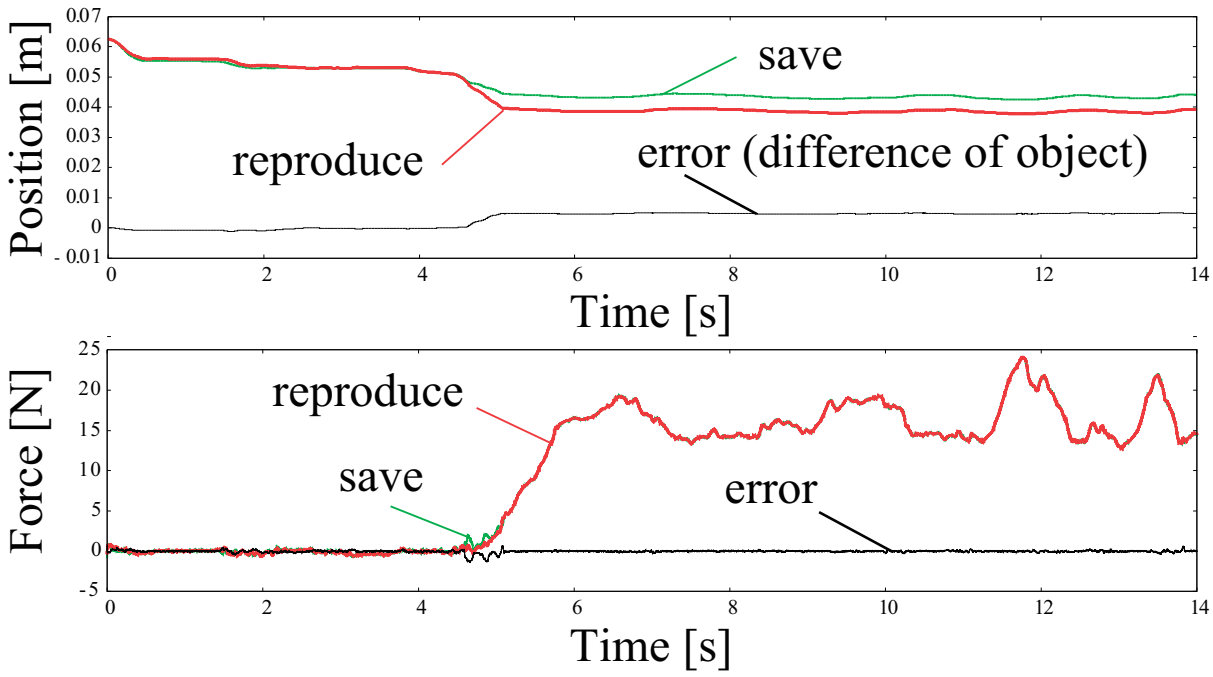

Fig. 5-20: Grasping force responses of motion-reproduction system based on the proposed method.

Experimental Results of Three Dimensional Cases

Figs. 5-22 and 5-23 show the experimental results by the proposed method for reproduction of the grasping motion and contact motions to the environment with the smaller size object in three dimensional, respectively. As shown in Fig. 5-22, grasping force is maintained even when contact motion to the environment is conducted. As a result, contact forces are reproduced even though the distance to the environment is different as shown in Fig. 5-23.

These results represent that saved human motions and object motions are appropriately reproduced by the proposal even if the size of object is different. The validities of the proposed method can be confirmed.

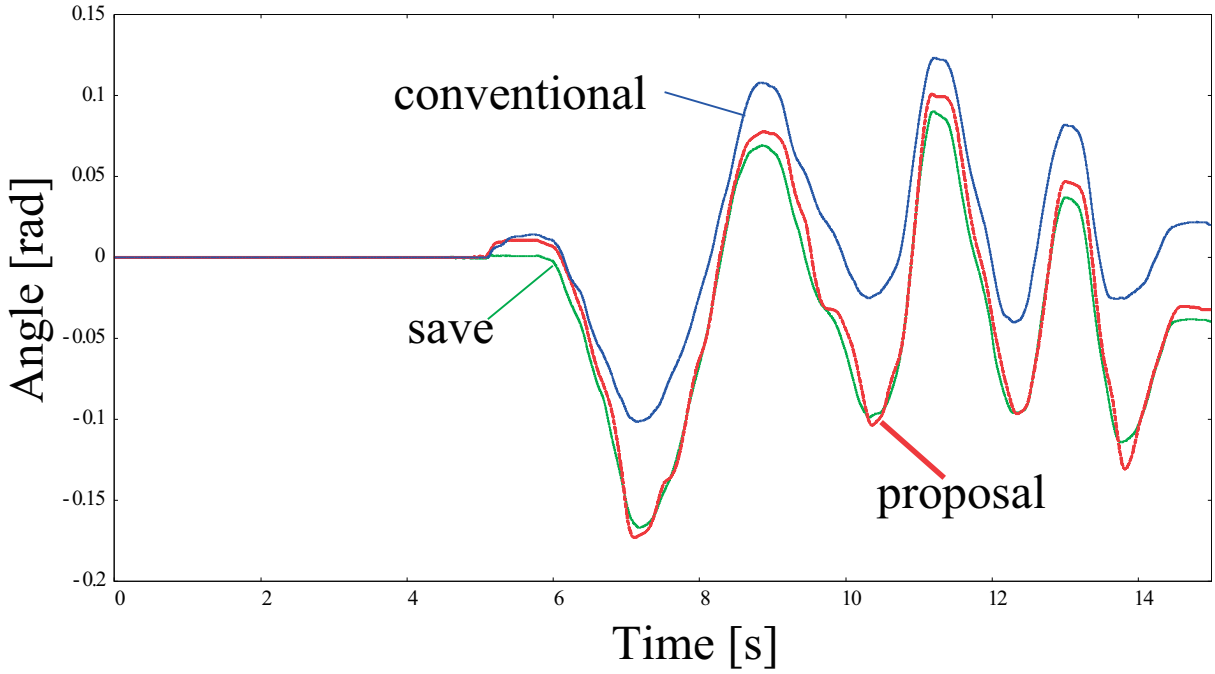

Fig. 5-21: Rotational motion responses in motion-reproduction system with the comparison between the conventional method and the proposed method.

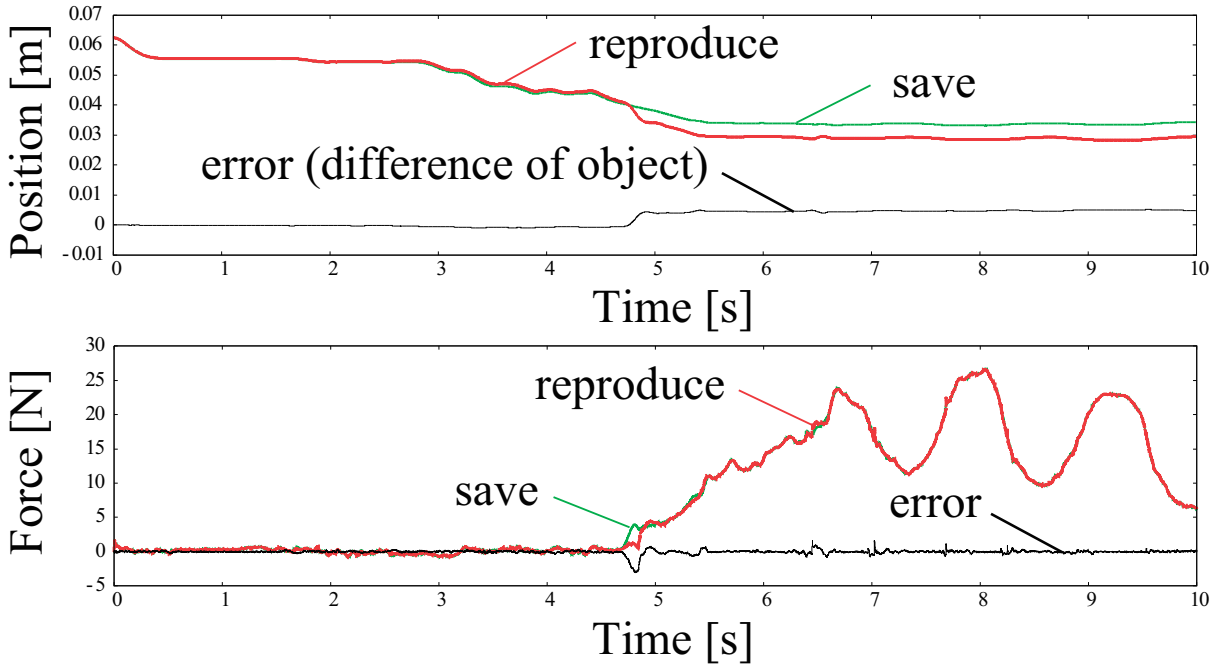

Fig. 5-22: Experimental result of grasping motion reproduction in 3 dimensional motions.

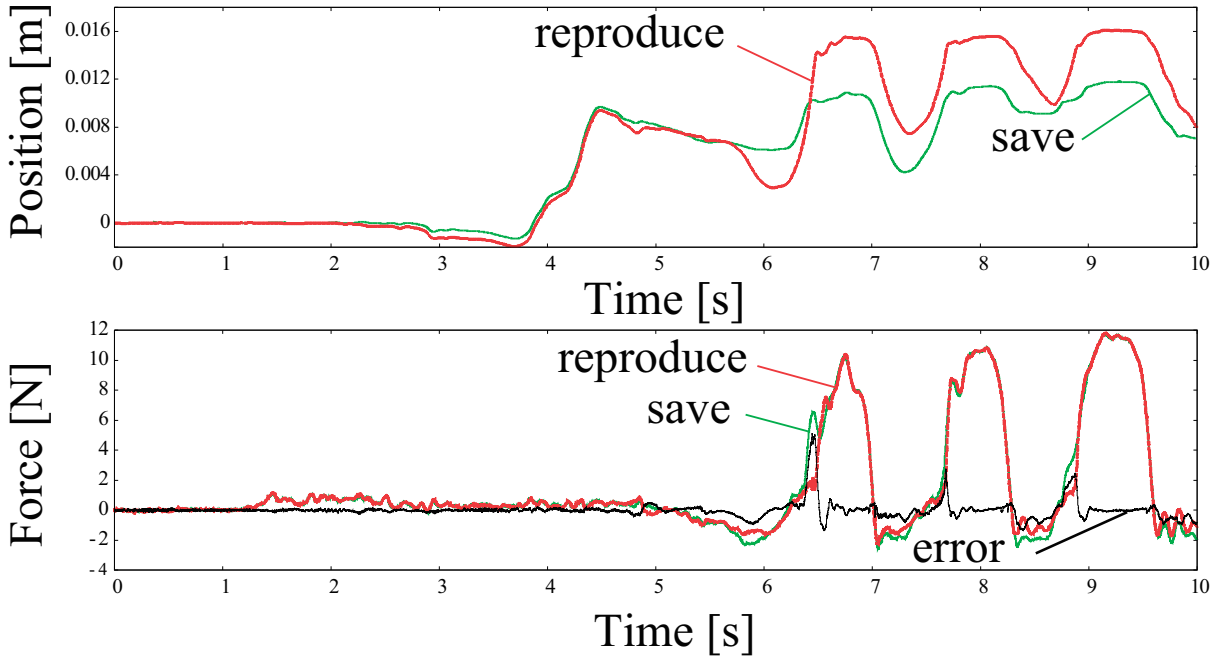

Fig. 5-23: Experimental result of grasping motion reproduction in 3 dimensional motions.

5.10 Summary of Chapter 5

This chapter showed the motion reproduction method based on EnvD compensation. Variances in the environment between the motion saving and reproduction phases are regarded as EnvDs. The motion reproduction and EnvD suppression performances were characterized. Compensation methods for both position and force reproduction are proposed. With the proposed method, the EnvD in the force or position reproduction can be summarily eliminated without the MR deteriorating because the proposed method is based on a 2-DOF control structure with respect to the EnvD. The system performances of the conventional and proposed methods were analyzed in terms of the MR and EnvD. It was found that the proposed method can realize the reproduction of contact motions (forces) much more precisely than the conventional methods with improving the EnvD suppression performance. Therefore, the proposal is useful and necessary for obtaining general versatility of motion reproduction systems.

Additionally, the EnvD compensation is extend to the reproduction for the MDOF cooperative motions. In order to describe the MDOF cooperative tasks, a coordinate transformation to an extended object space is introduced. The EnvD compensators are implemented in the proposed coordinate system. As a result, the general versatility of saved human motions is able to be advanced.

The experimental results showed the validity of the proposed method.

It is found that the fundamental principle and design framework for the motion reproduction system was established in this chapter.

Chapter 6

Expansion of Versatility of Stored Human Motions

6.1 Introduction of Chapter 6

This chapter proposes a method for extending the general versatility of information from recorded human-motions for precise and flexible human motion reproduction.

In considering future MCS applications for industries or general households, situations in which motion reproduction environments and devices differ from those of the motion saving phase must be taken into account. Depending upon the mechanical characteristics and performance of the sensing devices, undesired responses have a potential to occur. If control gains or bandwidths for estimation of disturbances are decreased, inappropriate responses may be suppressed. However, such a modification might cause the deterioration of motion reproducibility (MR) described in chapter 5. Thus, the conventional motion-reproduction system has a lack of versatility for the application of recorded human-motion resulting not only from environmental variations but also from the limitations of devices that reproduce the motions.

Therefore, by integrating the method described in former chapters, an integrative design method of the motion-reproduction system for obtaining precision and flexibility with respect to dissimilar (in other words, non-ideal) situations is required in order to extend the range of applications for stored human motions. The Kalman filter based hybrid controller described in chapter 4 is applied to both motion-saving and motion-reproduction systems in order to maintain the high transparency of the bilateral control by implementing a structure based on a hybrid controller using the proposed DOB. Additionally, the EnvD

compensators shown in chapter 5 are introduced for obtaining the flexibility to the variation of the environment from the motion extraction phase. Furthermore, integration of the disturbance/external force between the save and reproduction phases was described based on the concept of the position acceleration integrated disturbance observer (PAIDO) [55]. The PAIDO is a kind of sensor integration of the position and acceleration sensor for improving the estimation bandwidth of the force information. On the contrary, this research integrates the temporally distinct stored and reproduced force information. Information for the external force combines the higher frequency domain in the saving system and lower frequency domain in the reproduction phase. This is because the estimation accuracy of external force from the environment in the motion saving system is assumed better than that of the reproduction system. In order to adapt the unknown disturbances and environmental variations, the actual disturbance/external force is estimated as the highest domain possible using the Kalman filter-based approach described in chapter 2. The EnvD compensation enables the combination of stored and reproduced force information because an equivalent level of disturbance/external force is assured. Although the integration of saved and reproduced force can be found in [130], this approach does not consider the simultaneous adaptation to environmental variations and noise attenuations. The proposed method shown in this chapter is realized by the integration of the techniques shown in the former chapters.

By the proposed method shown in this chapter, flexible and robust motion reproduction is realized simultaneously against environmental variations and noise effects.

The validities of the proposal are confirmed by experiments.

6.2 Integration of saved and reproduced force information

This part explains the method for integrating the saved and reproduced disturbance/external force information. The saved force information is assumed to be appropriately estimated because the motion extraction has been accomplished successfully. Nevertheless, it is unclear whether the accuracy of the estimation is sufficient, because the motion reproduction devices have a potential to be changed from those of the saving phase.

Depending upon the characteristics of the device, a deterioration of the estimation is possible.

Therefore, this dissertation introduces a disturbance/external force estimation for the motion reproduction system in combination with the stored disturbance/external force information.

This method is based on the concept of the PAIDO [55]. The estimations of the disturbance and

external forces are expressed as follows:

$$\hat{F}^{R,\mathrm{dis}}_{\mathrm{Int}} = \frac{g^{S,\mathrm{dis}}_{\mathrm{skf}}}{s+g^{S,\mathrm{dis}}_{\mathrm{skf}}}\left[\hat{F}^{R,\mathrm{dis}}_{\mathrm{skf}} + \frac{s}{s+g^{R,\mathrm{dis}}_{\mathrm{skf}}}\hat{F}^{S,\mathrm{dis}}_{\mathrm{kf}}\right] \tag{6.1}$$

$$\hat{F}^{R,\mathrm{ext}}_{\mathrm{Int}} = \frac{g^{S,\mathrm{ext}}_{\mathrm{hskf}}}{s+g^{S,\mathrm{ext}}_{\mathrm{hskf}}}\left[\hat{F}^{R,\mathrm{ext}}_{\mathrm{hkf}} + \frac{s}{s+g^{R,\mathrm{ext}}_{\mathrm{hskf}}}\hat{F}^{S,\mathrm{ext}}_{\mathrm{hkf}}\right] \tag{6.2}$$

where F, X, s, g, superscripts dis, ext, S, R, subscripts Int, skf and hkf represent a force, a position, a Laplace operator, a cut-off frequency, a disturbance, an external force, saved information, reproduced information, integrated information, a steady state Kalman filter, and an estimated value by high-order Kalman filter, respectively. As shown in the above equations, this chapter utilizes the disturbance and higher-order external force estimated by KFSOs shown in chapter 3.

For the higher frequency domain, the estimated variables in the motion saving phase are utilized because they are assumed to include lower noise effects. Yet, the lower frequency domain in the motion reproduction phase is also utilized to adapt EnvDs and unknown disturbances. The bandwidth is combined by using low-pass filters and high-pass filters, which have same bandwidth as steady-state Kalman filters.

In accordance with the estimation of the higher-order external force, its time derivatives are also estimated as

$$\hat{\dot{F}}^{R,\mathrm{ext}}_{\mathrm{Int}} = \frac{g^{S,\mathrm{ext}}_{\mathrm{hskf}}}{s+g^{S,\mathrm{ext}}_{\mathrm{hskf}}}\left[\hat{\dot{F}}^{R,\mathrm{ext}}_{\mathrm{hkf}} + \frac{s}{s+g^{R,\mathrm{ext}}_{\mathrm{hskf}}}\hat{\dot{F}}^{S,\mathrm{ext}}_{\mathrm{hkf}}\right]. \tag{6.3}$$

where $\dot{\bullet}$ represents a time derivative.

Fig.6-1shows a block diagram for the integration. The motion reproduction system is constructed based on the integrated information.

6.3 Implementation in Motion Reproduction System

The proposed method in chapter 5 can be applied to the controller of a motion reproduction system. The saved master information and reproduced slave information are transformed to modal space as follows:

$$\boldsymbol{F}^{R,\mathrm{ext}}_{\mathrm{hkf}} = \left[\boldsymbol{F}^{R,\mathrm{ext}}_{F\mathrm{hkf}} \;\; \boldsymbol{F}^{R,\mathrm{ext}}_{X\mathrm{hkf}}\right]^T = \boldsymbol{\Gamma}\left[\boldsymbol{F}^{S,\mathrm{ext}}_{m\mathrm{hkf}} \;\; \boldsymbol{F}^{R,\mathrm{ext}}_{s\mathrm{Int}}\right]^T \tag{6.4}$$

$$\dot{\boldsymbol{F}}^{R,\mathrm{ext}}_{\mathrm{hkf}} = \left[\dot{\boldsymbol{F}}^{R,\mathrm{ext}}_{F\mathrm{hkf}} \;\; \dot{\boldsymbol{F}}^{R,\mathrm{ext}}_{X\mathrm{hkf}}\right]^T = \boldsymbol{\Gamma}\left[\dot{\boldsymbol{F}}^{S,\mathrm{ext}}_{m\mathrm{hkf}} \;\; \dot{\boldsymbol{F}}^{R,\mathrm{ext}}_{s\mathrm{Int}}\right]^T \tag{6.5}$$

$$\boldsymbol{X}^{R,\mathrm{res}}_{\mathrm{kf}} = \left[\boldsymbol{X}^{R,\mathrm{res}}_{F\mathrm{kf}} \;\; \boldsymbol{X}^{R,\mathrm{res}}_{X\mathrm{kf}}\right]^T = \boldsymbol{\Gamma}\left[\boldsymbol{X}^{S,\mathrm{res}}_{m\mathrm{kf}} \;\; \boldsymbol{X}^{R,\mathrm{res}}_{s\mathrm{Int}}\right]^T \tag{6.6}$$

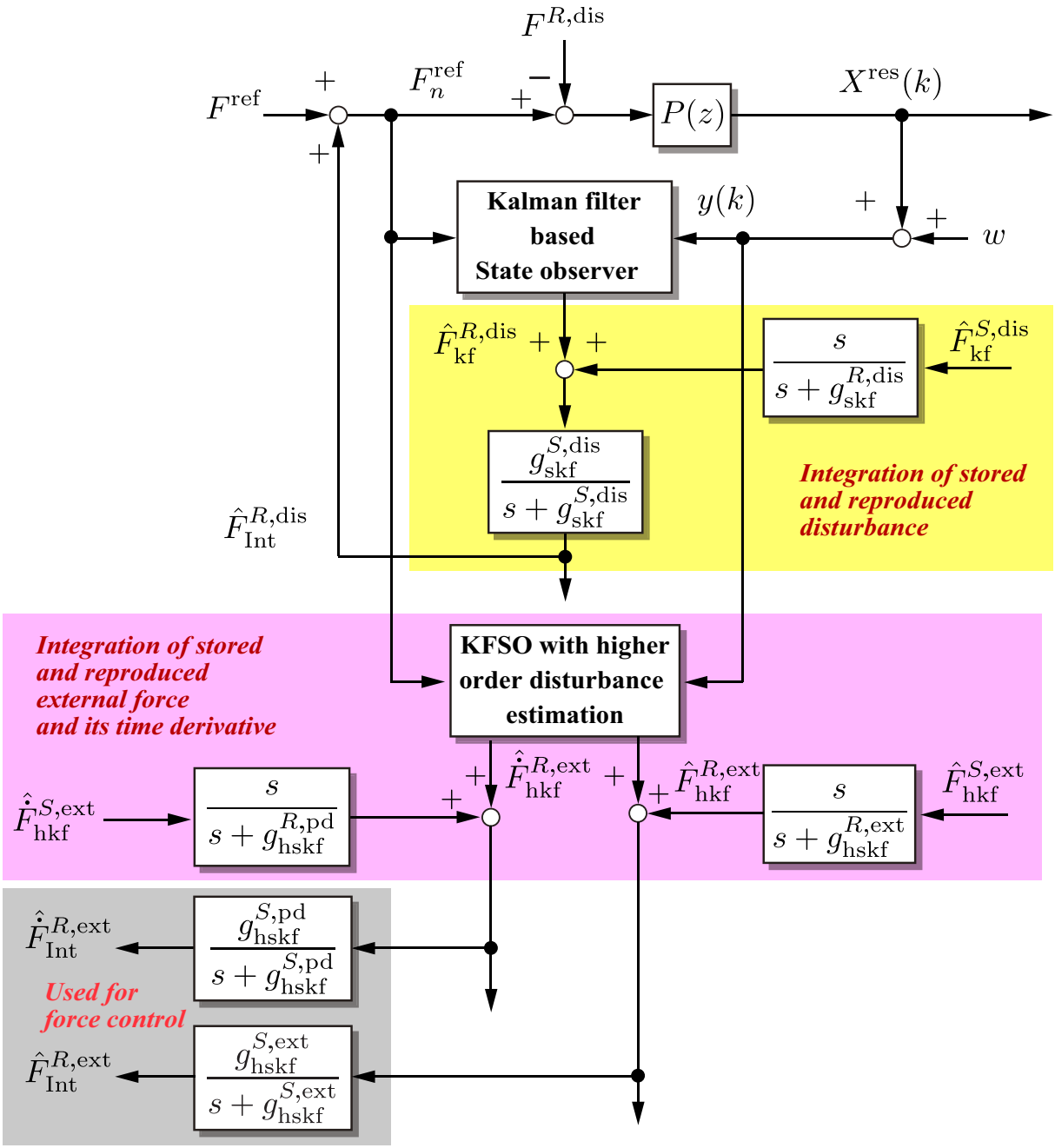

Fig. 6-1: Block diagram of the proposed method for integration of stored and reproduced external force and disturbance.

where bold types, a superscript res, subscripts kf, m, s, F and X represent a vector and/or matrix, a response value, an estimated value by Kalman filter, a master system, a slave system, a force control system and a position control system, respectively. In the same way as for a bilateral controller in a

motion-saving system, the slave-side acceleration reference is given by

$$\begin{aligned}\ddot{\boldsymbol{X}}_s^{R,\mathrm{ref}} &= \frac{1}{2}\Big[-\boldsymbol{K}_{fp}\hat{\boldsymbol{F}}_{F\mathrm{hkf}}^{R,\mathrm{ext}} - \boldsymbol{K}_{fd}\hat{\dot{\boldsymbol{F}}}_{F\mathrm{hkf}}^{R,\mathrm{ext}} - \boldsymbol{D}_F^{\mathrm{fdd}}(s)\hat{\dot{\boldsymbol{X}}}_{F\mathrm{kf}}^{R,\mathrm{res}} + \hat{\boldsymbol{A}}_{F\mathrm{hkf}}^{S,\mathrm{dis}} \\ &\quad + \boldsymbol{K}_p\left(\boldsymbol{X}_{X\mathrm{kf}}^{R,\mathrm{res}} + \boldsymbol{X}_{\mathrm{cmp}}^{f} + \boldsymbol{X}_{\mathrm{cmp}}^{p}\right) + \boldsymbol{K}_v\left(\dot{\boldsymbol{X}}_{X\mathrm{kf}}^{R,\mathrm{res}} + \dot{\boldsymbol{X}}_{\mathrm{cmp}}^{f} + \dot{\boldsymbol{X}}_{\mathrm{cmp}}^{p}\right) - \hat{\boldsymbol{A}}_X^{S,\mathrm{dis}}\Big] \\ &\quad + \ddot{\boldsymbol{X}}_{\mathrm{cmp}}^{f} + \ddot{\boldsymbol{X}}_{\mathrm{cmp}}^{p} \end{aligned} \tag{6.7}$$

where, $\ddot{\boldsymbol{X}}_s^{R,\mathrm{ref}}$, $\boldsymbol{K}_{fp}$, $\boldsymbol{K}_{fd}$, $\boldsymbol{K}_p$, $\boldsymbol{K}_v$, $\boldsymbol{A}^{\mathrm{dis}}$, $\boldsymbol{D}_F^{\mathrm{fdd}}(s)$, $\boldsymbol{X}_{\mathrm{cmp}}$, superscripts f and p represent an acceleration reference, a proportional force control gain matrix, a derivative force control gain matrix, a position control gain matrix, a velocity control gain matrix, an estimated disturbance in hybrid controller [97], a diagonal matrix with frequency domain damping [28], a compensation value of the EnvD compensator, force compensation and position compensation, respectively. In (6.7), 1/2 corresponds to the reciprocal of the determinant about $\boldsymbol{\Gamma}$. In (6.7), the novel disturbance observer for hybrid control based on Kalman filter in force control system is extended to higher-order disturbance estimation of $\hat{\boldsymbol{A}}_{F\mathrm{hkf}}^{S,\mathrm{dis}}$. The disturbance terms in hybrid controller is added as feed forward terms.

In the motion saving phase, the Kalman filter based DOB for force control systems are extended for the high-order disturbance estimation. The model of state space equation for the higher-order disturbance estimation is expressed as follows:

$$\dot{\boldsymbol{Z}}_F^h(t) = \mathbf{A}_F^h\boldsymbol{Z}_F^h(t) + \mathbf{B}_F^h\boldsymbol{U}_F^h(t) + \boldsymbol{v}_F^h(t) \tag{6.8}$$

$$\boldsymbol{Z}_F^h(t) = \left[\boldsymbol{\mu}_{\mathrm{FF}}\hat{\boldsymbol{\Lambda}}_{F\mathrm{skf}}^{\mathrm{ext}} \quad \boldsymbol{A}_F^{h\mathrm{dis}} \quad \dot{\boldsymbol{A}}_F^{h\mathrm{dis}}\right]^T \tag{6.9}$$

$$\dot{\boldsymbol{Z}}_F^h(t) = \left[\boldsymbol{\mu}_{\mathrm{FF}}\hat{\boldsymbol{P}}_{F\mathrm{skf}}^{\mathrm{ext}} \quad \dot{\boldsymbol{A}}_F^{h\mathrm{dis}} \quad \ddot{\boldsymbol{A}}_F^{h\mathrm{dis}}\right]^T \tag{6.10}$$

$$\boldsymbol{U}_F^h(t) = \ddot{\boldsymbol{X}}_F^{\mathrm{ref}} \tag{6.11}$$

$$\boldsymbol{Y}_F^h(t) = \boldsymbol{c}_F^h\boldsymbol{Z}_F^h(t) + \boldsymbol{w}_F^h \tag{6.12}$$

where

$$\mathbf{A}_F^h = \begin{bmatrix}\mathbf{0} & -\boldsymbol{I} & \mathbf{0}\\ \mathbf{0} & \mathbf{0} & \boldsymbol{I}\\ \mathbf{0} & \mathbf{0} & \mathbf{0}\end{bmatrix},\ \mathbf{B}_F^h = \begin{bmatrix}\boldsymbol{I}\\ \mathbf{0}\\ \mathbf{0}\end{bmatrix},\ \boldsymbol{c}_F^h = \begin{bmatrix}\boldsymbol{I}\\ \mathbf{0}\\ \mathbf{0}\end{bmatrix}^T. \tag{6.13}$$

In the above equations, t $\boldsymbol{Z}$, $\boldsymbol{U}$, $\boldsymbol{P}$, $\boldsymbol{\Lambda}$ $\boldsymbol{\mu}$, $\boldsymbol{v}$, $\boldsymbol{Y}$ w, a superscript h represent a time, a state vector, an input vector, an equivalent disturbance through high-pass filter [97], a value of integral for $\boldsymbol{P}$, an element of inverse matrix of an equivalent mass matrix [97], a system noise, an observation vector and an observation noise, respectively.

In addition to the hybrid control based structure, the EnvD compensation is also introduced. The compensation values for EnvD is also utilized the integrated information.

The saved force and position are reproduced using (6.7). The proposed structure realizes flexible and robust motion reproduction against the environmental variations and effects of noises.

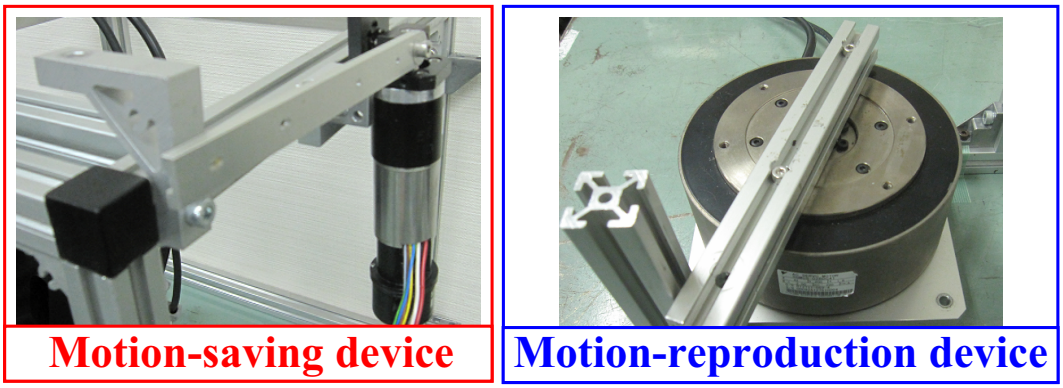

Fig. 6-2: Experimental set up for motion saving and reproduction systems

6.4 Experiments of Motion-Saving-System and Motion-Reproduction System with Different Device

6.4.1 Experimental Setup for Motion-Saving-System and Motion-Reproduction System with Different Device

Fig. 6-2 shows a single DOF manipulators for motion extraction and reproduction. Same type manipulator is utilized both in the master and slave systems for storing motions.

The other type of manipulator shown in right side of Fig. 6-2 is utilized for motion reproduction at slave side.

In addition to an experiment for motion-saving system, three cases of experiments for motion reproduction are tested as follows:

1) Motion reproduction system based on conventional DOB and RFOB based structure without EnvD compensators

2) Motion reproduction system based on the proposed hybrid control structure without integration of force information

3) Motion reproduction system based on the proposed method.

Parameters used in the motion saving and reproduction experiments are shown in Table 6.1. The bandwidth of the DOB and RFOB are set as the same value of KFSOs in motion-saving system.

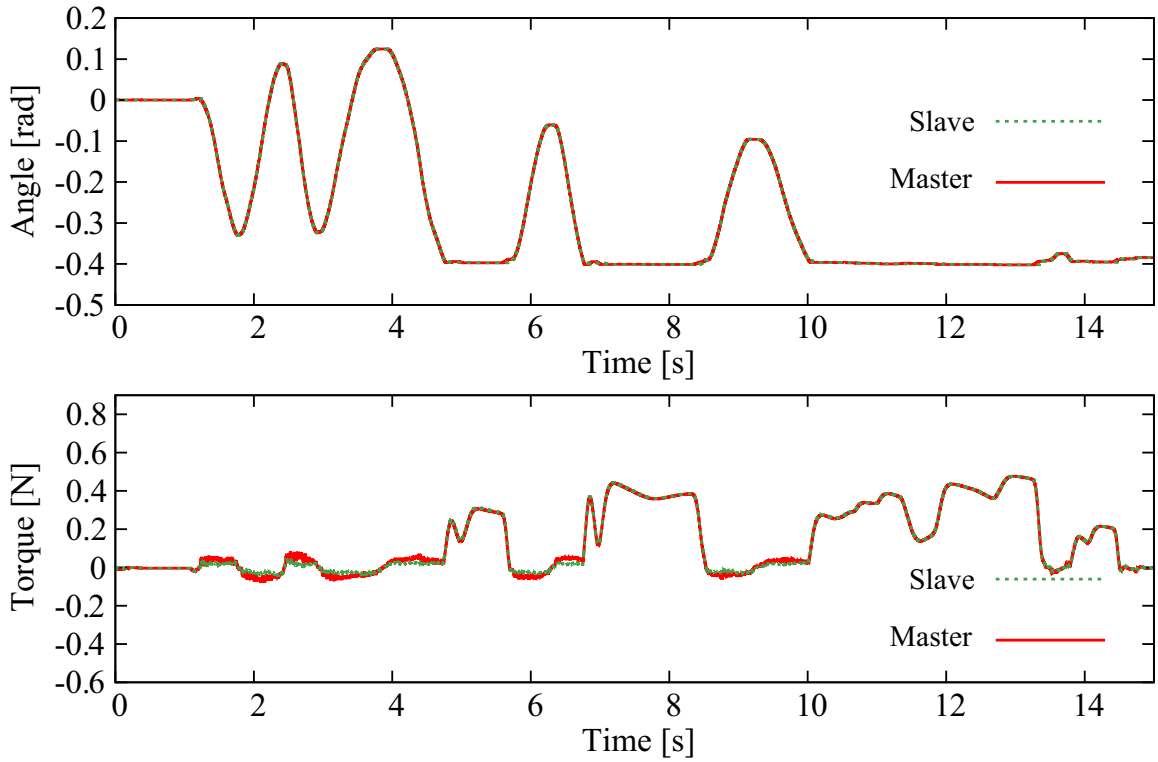

Fig. 6-3: Positron and force responses of the motion-saving system.

Table 6.1: Experimental parameters of motion-reproduction systems with different structure

Parameter	Description	Value
T_s	sampling time	0.2 ms
K_p	proportional gain of position control	10000
K_v	differential gain of position control	200
K_{fp}	proportional gain of force control	50
K_{fd}	differential gain of force control	0.05
$g_{\mathrm{hkf}}^{S,\mathrm{ext}}$	bandwidth of high-order RFOB in saving phase	765 rad/s
$g_{\mathrm{kf}}^{S,\mathrm{dis}}$	bandwidth of high-order DOB in saving phase	765 rad/s
$g_{\mathrm{hkf}}^{R,\mathrm{ext}}$	bandwidth of high-order RFOB for integration	400 rad/s
$g_{\mathrm{kf}}^{R,\mathrm{dis}}$	bandwidth of high-order DOB for integration	400 rad/s
g_F	bandwidth of DOB in force control	86 rad/s
g_X	bandwidth of DOB in position control	100 rad/s
d_F	damping coefficient of FDD	100
g^{fdd}	bandwidth of FDD	100 rad/s

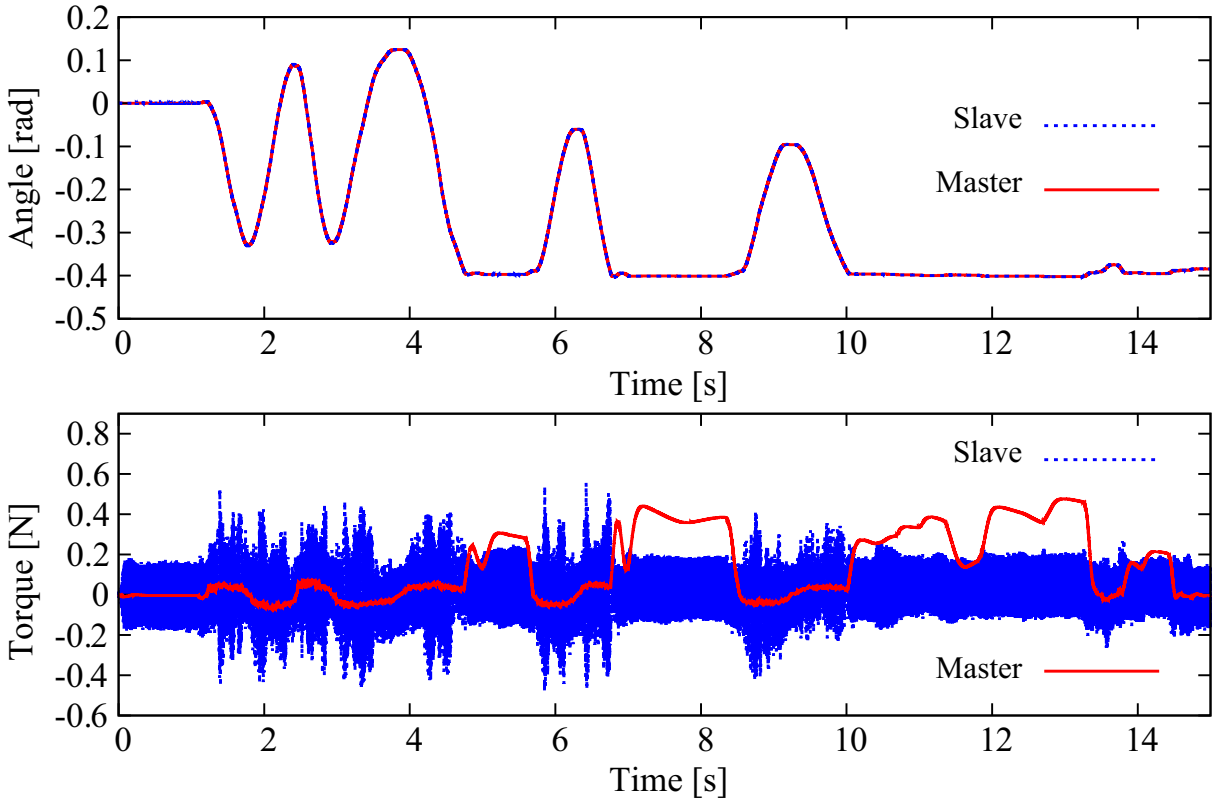

Fig. 6-4: Position and force responses of motion reproduction with conventional DOB based structures.

6.4.2 Experimental Results of Motion-Saving-System and Motion-Reproduction System with Different Device

Fig. 6-3 shows experimental results for the motion-saving system. As shown in the figure, the appropriate extraction of human motion can be confirmed. This figure also indicates that the higher order Kalman filter estimation can be applicable to the hybrid controllers. Fig. 6-4 shows the experimental results with the motion-reproduction system based on conventional DOB- and RFOB-based structure without EnvD compensators (case 1) As shown in the figure, the effect of noise is enlarged and an undesired response occurs. Additionally, the method cannot adapt to the variation of the environment.

Fig. 6-5 shows experimental results with the motion-reproduction system based on the proposed hybrid control structure without integration of force information (case 2). The method achieves adapting the difference of distance to an environment. However, the method still enlarges the noise effect even though the Kalman filters are used.

Fig. 6-6 shows the experimental results obtained with the motion-reproduction system based on the

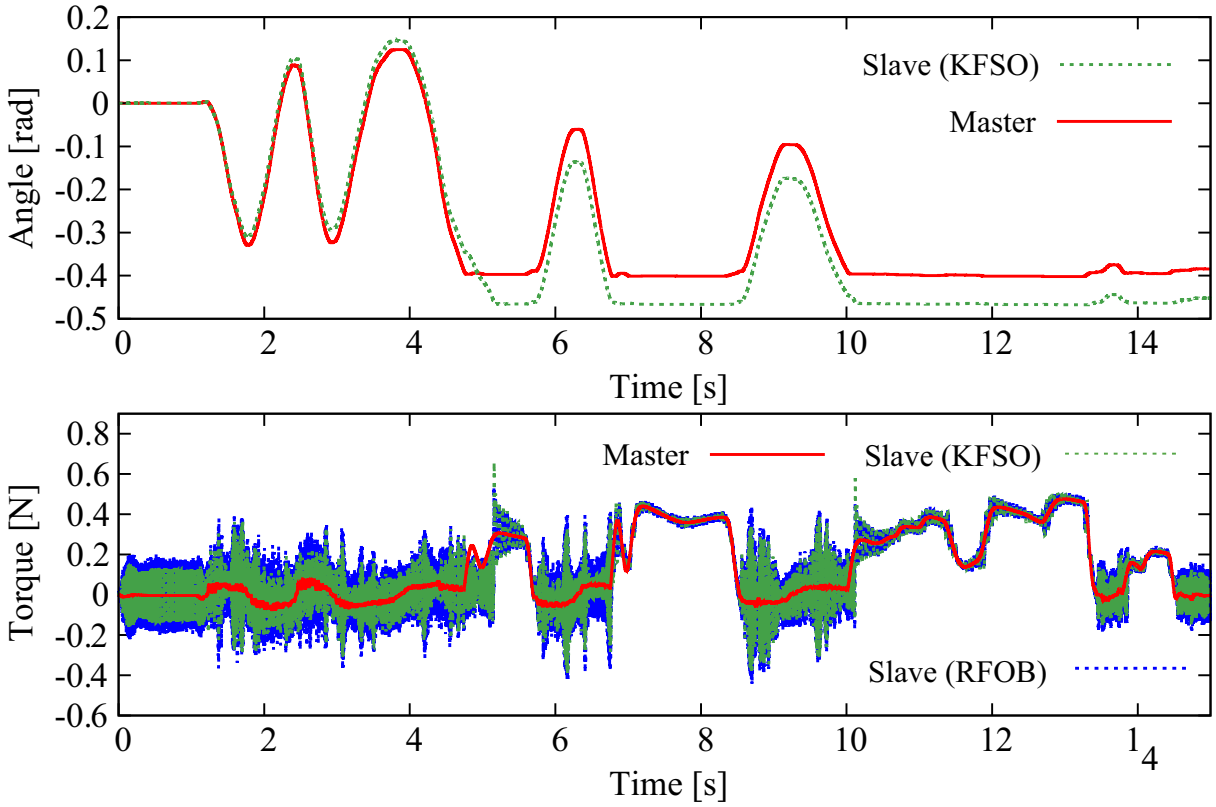

Fig. 6-5: Position and force responses of the motion reproduction without integration of force information.

proposed method using (6.7). It is found that the reproduced position and force responses closely follow the responses in the motion-saving system. As a result, the recorded human motions are reliably reproduced. It is confirmed that recorded human motions can be reproduced accurately while maintaining high transparency of the bilateral control obtained by the hybrid controller, based on the acceleration controller using the proposed DOB. Furthermore, the effect of the integration of the force information can be confirmed.

These results validate the proposed method.

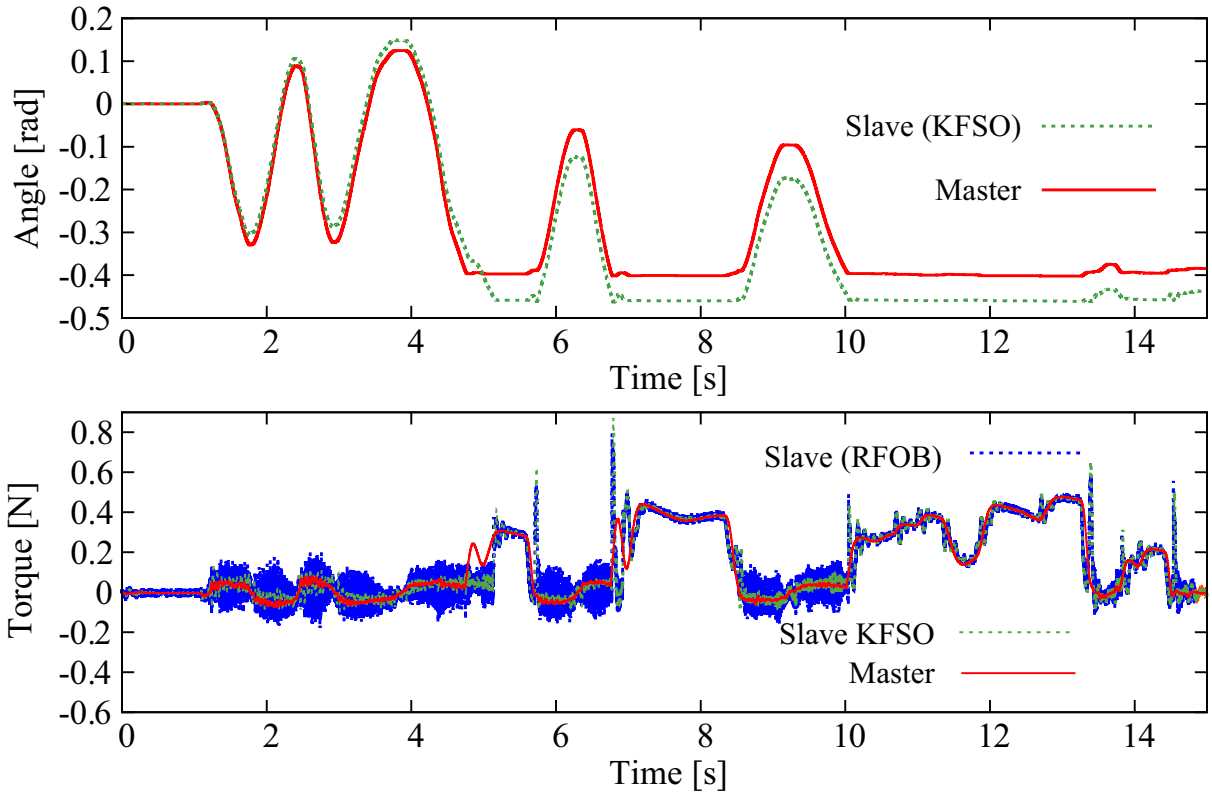

Fig. 6-6: Position and force responses of the motion reproduction with integration of the proposed method.

6.5 Summary of Chapter 6

This chapter described a proposed method for extending the general versatility of information from recorded human-motions by integrating the method described in former chapters. The Kalman filter based hybrid controller described in chapter 4 was applied to both motion-saving and motion-reproduction systems in order to maintain the high transparency of the bilateral control by implementing a structure based on a hybrid controller using the proposed DOB. Additionally, the EnvD compensators shown in chapter 5 were introduced for obtaining the flexibility to the variation of the environment from the motion extraction phase. Furthermore, integration of the disturbance/external force between the save and reproduction phases was described based on the concept of the position acceleration integrated disturbance observer (PAIDO) [55]. Information for the external force combines the higher frequency domain in the saving system and lower frequency domain in the reproduction phase. In order to adapt the unknown disturbances and the environmental variations, the actual disturbance/external force is estimated as the highest domain possible using the Kalman filter-based approach. The EnvD compensation enabled the combination of the stored and reproduced force information because an equivalent level of disturbance/external force is assured.

By integrating and applying the methods shown in the former chapters to a motion reproduction system, flexible and robust motion reproduction was realized against environmental variations and the effects of noise.

The validities of the proposal were confirmed by experiments.

The proposed integrated design for the motion-reproduction system will innovate the versatility of human motions.

Chapter 7

Conclusions

This dissertation proposed methods for estimation and compensation of high-order disturbance with noise attenuation to realize precise and flexible motion control systems including position/force hybrid control for the bilateral control systems and motion reproduction systems. Not only the disturbance suppression in an actuator, but also disturbances in multi-degree-of-freedom (MDOF) systems and environmental variations were included in category of aims in this dissertation. This dissertation focuses on the disturbance and noise attenuation to realize precise and flexible motion control systems including position/force hybrid control for the bilateral control systems and motion reproduction systems.

This dissertation addressed on higher-order disturbance estimation with considering stochastic behavior for noise suppression based on Kalman filters. Additionally, higher-order time derivatives of the disturbances were actively utilized for the performance improvement of the control systems.

A novel disturbance observer was introduced in this dissertation in order to improve performance of the position/force hybrid control systems including bilateral control. By using the proposed approach, the decoupling control, performance improvement of hybrid control and the simplification of controller design were achieved. Moreover, the novel disturbance observer was combined with a Kalman filters and extended for higher-order disturbance estimation.

This dissertation also realized flexible and stable force control system by focusing on the similarity between two mass resonant system and force control system. To construct the force control system, parameter variations of environment were defined as EnvD . The estimated higher-order disturbance and its time derivatives were utilized also for suppressing the EnvDs. Furthermore, the difference of environment between motion saving phase and reproduction phase were also regarded as a kind of EnvD.

The general framework for the motion reproduction based on compensation of EnvD was established in this dissertation.

Moreover, the proposed high-order disturbance estimation in actuators and environments was integrated for the motion reproduction system for flexible adapting the difference with respect to not only environment but also reproduction device itself.

In chapter 2, models of the high-order disturbances with considering stochastic behavior in actuators and environments were defined to clarify effects of noises in the estimation.

Chapter 2 also showed a fundamental approaches for designing KFSO based on the proposed modeling. A high-order disturbance observer based on a Kalman filter for realization of the precise force control was also shown.

By the proposed tuning structure, the numbers of parameters that have to be determined were reduced from nine to two parameters because the time derivative of system noise in torque dimension is taken into consideration in the disturbance model. Furthermore, the structure of Kalman filter-based external torque estimation without using nonlinear Kalman filter was proposed. In addition, the relationships between the two parameters were confirmed by utilizing the steady-state Kalman filter. It is observed that the Kalman filter is not able to estimate the disturbance/external torque appropriately if the tuning of the covariance matrix is failed by regarding the parameters in $\boldsymbol{Q}$ as just the gains of the Kalman filter. Experimental results validated the tuning method and analytical results.

Furthermore, this chapter also showed a method to improve the performance of a reaction torque control system by using a high-order disturbance/reaction torque estimation based on a Kalman filter. The proposed method can realize a reaction torque control system by using a proportional-derivative controller. It was confirmed that the proposed proportional derivative controller for the reaction torque can improve control system performance while suppressing the noise effect. This is because the estimated variables by the proposed Kalman-filter-based high-order disturbance/reaction torque observer are utilized in the PD controller. The observer can estimate the disturbance/external torque and its time derivative with lower noise levels than conventional DOBs or RTOBs.

Chapter 3 showed the method for stable contact motions for force tracking control based on the concept of resonance ratio control.

The similarity in the structure for admittance control for contact motions and two-mass resonance systems was derived. From the similarity, it was found that the concept of resonance ratio control is applicable to force tracking control. Based on the concept of resonance ratio control, an admittance con-

troller for contact motion with the EnvD compensation was proposed. By using the proposed method, vibration suppression during contact motion was realized even if the environment had no, or insufficient, viscosity. The response characteristics of contact motion for force tracking control can be determined arbitrarily by the proposed method. The proposed method enables to determine the parameters for obtaining stable contact motions and to maintain the fine control stiffness for the force control system. This part also considered utilizing the higher-order derivative terms in compensation for environmental disturbance. For the compensation of the environmental disturbance, only the zero order term inverse system was considered in order to avoid enlarging noise effect by implementing time derivatives of estimated environmental disturbance. The higher-order terms of timed derivatives were neglected also for the compensation of load disturbance in the two mass resonance system. In this chapter, the high-order EnvD was estimated by a Kalman filter including higher-order time derivatives of the EnvD. The estimated variable of the proposed Kalman filter based high-order environmental disturbance observer can be utilized for the compensation without enlarging noise effect in time derivatives.

Chapter 4 described a hybrid control system based on an acceleration controller in the modal space, which is capable of realizing decoupling control and performance improvement of the bilateral control system. This chapter showed how an acceleration controller can realize decoupling control in the modal space. Furthermore, a novel disturbance observer for enhancing the performance of an acceleration controller is proposed. Differently from the conventional hybrid controllers, the proposed controller does not affected by the variation of manipulator configurations except for neighborhood of a singular point because the structure of the proposed method is based on the acceleration controller.

Moreover, the proposed method was extended for the redundant systems and integration of the Kalman filter based disturbance estimation is also proposed. The proposed method can realize simplification of the inverse kinematics, decoupling of null space, enhancing performance and noise suppression in the hybrid controller simultaneously. The proposed method was applied to a scaled bilateral control system with a redundant manipulator.

Chapter 5 showed the motion reproduction method based on EnvD compensation. Variances in the environment between the motion saving and reproduction phases are regarded as EnvDs. The motion reproduction and EnvD suppression performances were characterized. Compensation methods for both position and force reproduction are proposed. With the proposed method, the EnvD in the force or position reproduction can be summarily eliminated without the MR deteriorating because the proposed method is based on a 2-DOF control structure with respect to the EnvD. The system performances of

the conventional and proposed methods were analyzed in terms of the MR and EnvD. It was found that the proposed method can realize the reproduction of contact motions (forces) much more precisely than the conventional methods with improving the EnvD suppression performance. Therefore, the proposal is useful and necessary for obtaining general versatility of motion reproduction systems.

Additionally, the EnvD compensation is extend to the reproduction for the MDOF cooperative motions. In order to describe the MDOF cooperative tasks, a coordinate transformation to an extended object space is introduced. The EnvD compensators are implemented in the proposed coordinate system. As a result, the general versatility of saved human motions is able to be advanced.

The experimental results showed the validity of the proposed method. It was found that the fundamental principle and design framework for the motion reproduction system was established in this chapter.

Chapter 6 described the method for expanding the versatility of the saved human-motions by integrating the method described in former chapters. The Kalman filter based hybrid controller described in chapter 4 was applied to both motion-saving and motion-reproduction systems in order to maintain the high transparency of the bilateral control by implementing a structure based on a hybrid controller using the proposed DOB. Additionally, the EnvD compensators shown in chapter 5 were introduced for obtaining the flexibility to the variation of the environment from the motion extraction phase. Furthermore, the integration of the disturbance/external force between the save and reproduction phases was described based on the concept of the position acceleration integrated disturbance observer (PAIDO) [55]. Information of the external of the higher frequency domain in saving system and lower frequency domain in the reproduction phase was combined. In order to adapt the unknown disturbances and the environmental variations, the actual disturbance/external force as higher domain as possible is estimated by Kalman filter based approach described in chapter 3. The EnvD compensation enables the combination because a same level of the disturbance/external force is guaranteed by the compensation.

The designed KFSOs for estimation of high-oder disturbance shown in chapters 2 and 3 including zero-th, first and second-order disturbance have -20 dB/dec gradient in higher frequency domain with respect to noise sensitivity, although the conventional method has almost zero gratitude. This means the Kalman filter based disturbance estimation based on the proposed strategies can achieve better noise suppression performance than the conventional methods. Therefore, the proposed method will contribute the extension of the application of the disturbance estimation because the proposed method will able to be applied for the sensing devices with low performance but low costs.

By integrating and applying the methods shown in the former chapters to a motion reproduction sys-

tem, the flexible and robust motion reproduction was realized against the environmental variations and effect of noises.

The framework derived in this dissertation for the estimation and compensation of high-order disturbance will play an important role for further improvement of performance of industrial applications. General versatility of the motion control systems in open environment will be enhanced by the concept and techniques which were proposed in this dissertation.

Although this dissertation assumes the observation noise and process noise to be the normal white noise, the extension of the proposed high-order disturbance estimation for the noises with the different characteristics should be considered. Additionally, the noises are also assumed not to have a correlation. Therefore, the noises with the correlation should also be dealt with by extending the proposed method.

With respect to the disturbance model, this dissertation assumes the disturbance to be modeled by a polynomial. The other type of the disturbance should also be addressed as a future subject.

AppendixA

Application of Environmental Disturbance Compensation for Motion Training System

A.1 Background of This Part

This part shows an application of EnvD compensation for training system based on recorded human motions [131].

Besides reproduction, the MCS is also anticipated to be applied to training [132] and power assist systems [52] to pass techniques down to younger generations and for rehabilitation with robots [53, 54]. However, the conventional motion reproduction system is composed by only a slave system [88, 89], so that human action force of the operator and reaction force from environments cannot decoupled. In addition, if environmental impedance or location of the environment is different, saved motions cannot be reproduced appropriately [46]. As a result, training with touching actuators is difficult because both appropriate trajectories and forces of trainer are not able to be presented for the trainee. This fact means that reproduced motion becomes different from motions of saved trainer if trainees perform the inadequate motion.

Furthermore, the trainee is subject to constraints from the time frame of the saved motions. The motion reproduction system will have finished reproducing saved motions of trainer even though the trainee does not perform appropriate motions because of the constraint. In order to deal with these problems, this part proposes a motion reproduction system for realization of the motion training system. The proposed method decouples the motion reproduction system to master and slave systems. A slave system is driven by motion data memory and act on actual environment. On the other hand, master side is manipulated by

trainee with kinesthetic feedback from slave side. By employing the dual motion reproduction structure, the proposed system partially resolves the constraint of motion reproduction shown in (5.19). For example, the slave system can reproduce contact motions even though the environmental condition is different from the saving phase, because the trainee interacts with not the slave side but the master side.

In addition, in order to correct inappropriate factor of trainee motions, compensators in position, force and time domains are introduced for a disturbance force caused by the trainee. The structures of the compensators are based on an admittance control (a position base impedance control). The admittance control attracts attention as applications for power assist control systems [52] and rehabilitations [53,54]. In this part, the concept of the admittance control is extended to the not only a spatial domain but a temporal domain. By using a compensation value generated by the temporal admittance controller, the trainee can train independently from the time frame of the saved motions.

A.2 Proposed Motion Training System Based on Dual Motion Reproduction System

A.2.1 Definition of Trainee Disturbance

If MCS is intended to be utilized for a motion training system, conventional reproduction system is inadequate because a trainee directory interact with the system and EnvD is generated invariably. In order to deal with effects of a trainee, trainee disturbance (TraD) F_t^{dis} is defined as follows:

$$F_t^{\mathrm{dis}} = \tilde{F}_t^{\mathrm{dis}} + Z_t^S(s) X_{\mathrm{cmp},m}^f \tag{A.1}$$

$$= F_m^{S,\mathrm{ext}} - F_m^{R,\mathrm{ext}} + Z_t^S(s) X_{\mathrm{cmp},m}^f. \tag{A.2}$$

Characteristics of this disturbance are same as EnvD. The emergence of TraD represents that the trainee does not perform appropriate motions which is different from saved motions of the trainer. Compensators for TraD are able to construct as the same structure of the EnvD compensators as follows:

$$X_{\mathrm{cmp},m}^p = -\frac{C_f}{s^2 + C_p(s)} G_{lt}(s) \tilde{F}_t^{\mathrm{dis}} = G_{\mathrm{cmp},m}^p(s) \hat{\tilde{F}}_t^{\mathrm{dis}} \tag{A.3}$$

$$X_{\mathrm{cmp},m}^f = \frac{b_m^f}{Z_{\mathrm{cmp},m}(s)} G_{lt}(s) \tilde{F}_t^{\mathrm{dis}} = G_{\mathrm{cmp},m}^f(s) \hat{\tilde{F}}_t^{\mathrm{dis}}. \tag{A.4}$$

A.2.2 Temporal Admittance

In an initial phase of the training, it is better for trainee to follow the saved motions of trainer iteratively. However, a trainee should not be subject to constraint of a time frame of the saved motions if the degree of proficiency is improved. In order to modulate the updating time of the saved motions, following acceleration of the command value for updating data time T^{cmd} is introduced as

$$\frac{d^2}{dt^2}T^{\mathrm{cmd}} = \begin{cases} 1 & (F_t^{\mathrm{dis}} = 0) \\ 0 & (F_t^{\mathrm{dis}} \neq 0) \end{cases} . \tag{A.5}$$

When the TraD is not generated, the acceleration arises and the time of saved motion is updated as shown in (A.5). However, (A.5) shows the ideal case. Frictions or other unknown forces perform as the TraD in actual case and the update of saved time is wrongly stopped. Because of this reason, the acceleration is approximated by using a sigmoid function as follows:

$$\frac{d^2T^{\mathrm{cmd}}}{dt^2} = \frac{1}{1+e^{\left[g_l^f(s)\tilde{F}_t^{\mathrm{dis}} - F_{\mathrm{lim}}\right]}} - \frac{1}{1+e^{\left[g_l^f(s)\tilde{F}_t^{\mathrm{dis}} + F_{\mathrm{lim}}\right]}} \tag{A.6}$$

where F_{lim} is a limitation of the forces and $g_l^f(s)$ represents the low-pass filter for preventing the chattering. In the discrete time space, the acceleration of time is integrated and the command value of time is derived as

$$\frac{d}{dt}T^{\mathrm{cmd}}(k) = \frac{d}{dt}T^{\mathrm{cmd}}(k-1) + \frac{d^2}{dt^2}T^{\mathrm{cmd}}T_s \tag{A.7}$$

$$T^{\mathrm{cmd}}(k) = T^{\mathrm{cmd}}(k-1) + \lfloor \frac{d}{dt}T^{\mathrm{cmd}}(k) \rfloor T_s \tag{A.8}$$

where $\lfloor \bullet \rfloor$ is a floor function. In addition, a compensation value for the time domain is also introduced to prevent the loss of saved motions when the TraD is generated. In order to generate the compensation value, temporal impedances are derived as

$$\hat{\tilde{F}}_t^{\mathrm{dis}} = M_T\frac{d^2}{dt^2}t_{\mathrm{cmp}} + D_T\frac{d}{dt}t_{\mathrm{cmp}} + K_T t_{\mathrm{cmp}} \tag{A.9}$$

where M_T, D_T and K_T represent a temporal mass, a temporal viscosity and temporal stiffness. By using (A.9), the compensation value of the time $T_{\mathrm{cmp}}(k)$ is derived as

$$t_{\mathrm{cmp}} = \iint \frac{d^2}{dt^2}t_{\mathrm{cmp}}dtdt = \frac{\hat{\tilde{F}}_t^{\mathrm{dis}}}{M_T s^2 + D_T s + K_T} \tag{A.10}$$

$$T_{\mathrm{cmp}}(k) = \lfloor b_m^t t_{\mathrm{cmp}} \rfloor = \lfloor b_m^t G_{m,\mathrm{cmp}}^t(s)\hat{\tilde{F}}_t^{\mathrm{dis}} \rfloor \tag{A.11}$$

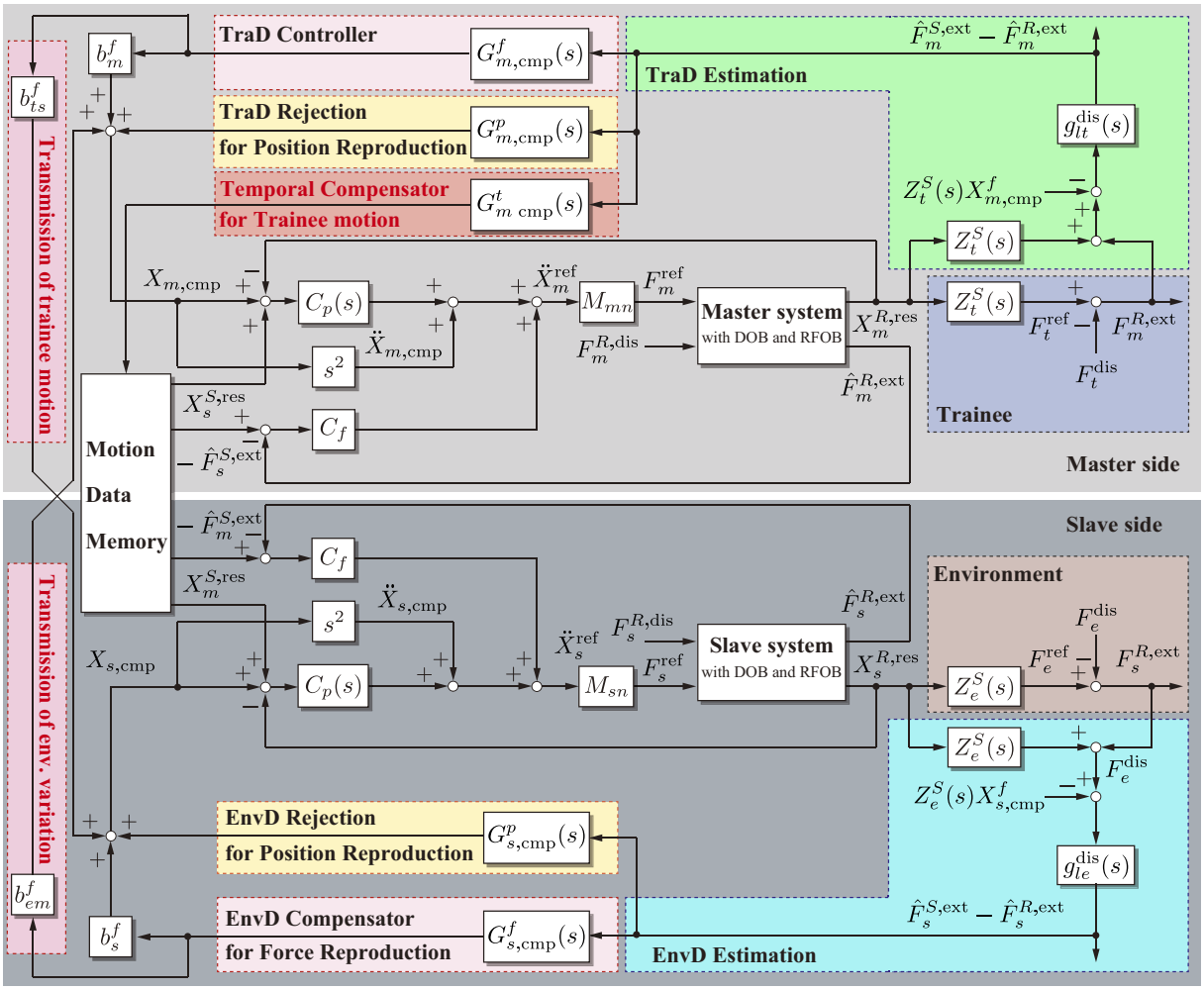

Fig. A-1: Whole block diagram of the proposed motion training system.

where b_m^t is the coefficient to change the sign of t_{cmp} and to inactivate the compensation while the T^{cmd} is activated as follows:

$$b_m^t = 1 - \frac{1}{1+e^{\left[g_l^f(s)\tilde{F}_t^{\mathrm{dis}} - F_{\mathrm{lim}}\right]}} - \frac{1}{1+e^{\left[g_l^f(s)\tilde{F}_t^{\mathrm{dis}} + F_{\mathrm{lim}}\right]}}. \tag{A.12}$$

An input value of time domain in the motion reproduction is given by using $T^{\mathrm{cmd}}(k)$ and $T_{\mathrm{cmp}}(k)$ as

$$T^R = T^{\mathrm{cmd}}(k) + T_{\mathrm{cmp}}(k). \tag{A.13}$$

By setting the input value of time as (A.13), the compensation of time domain is realized by $T_{\mathrm{cmp}}(k)$ that generated from temporal admittance controller.

A.2.3 Dual motion Reproduction System for Motion Training Based on Spatiotemporal Admittance Control

In order to apply MCS for the motion training, a dual motion reproduction system is proposed in this part. Control systems based on a motion reproduction system with the EnvD and TraD compensators and a temporal admittance controller are constructed not only in a slave system but also in a master system. The acceleration references of the master and slave systems are given as follows:

$$\begin{aligned}
\ddot{X}_m^{R,\mathrm{ref}} &= C_f\left(-\hat{F}_s^{S,\mathrm{ext}}(T^R) - \hat{F}_m^{R,\mathrm{ext}}\right) + \ddot{X}_{\mathrm{cmp},m} \\
&\quad + C_p(s)\left(X_{\mathrm{cmp},m} + X_s^{S,\mathrm{res}}(T^R) - X_m^{R,\mathrm{res}}\right) \qquad \text{(A.14)} \\
\ddot{X}_s^{R,\mathrm{ref}} &= C_f\left(-\hat{F}_m^{S,\mathrm{ext}}(T^R) - \hat{F}_s^{R,\mathrm{ext}}\right) + \ddot{X}_{\mathrm{cmp},s} \\
&\quad + C_p(s)\left(X_{\mathrm{cmp},s} + X_m^{S,\mathrm{res}}(T^R) - X_s^{R,\mathrm{res}}\right) \qquad \text{(A.15)} \\
X_{\mathrm{cmp},m} &= X_{\mathrm{cmp},m}^p + b_m^f X_{\mathrm{cmp},m}^f + b_{em}^f X_{\mathrm{cmp},s}^f \qquad \text{(A.16)} \\
X_{\mathrm{cmp},s} &= X_{\mathrm{cmp},s}^p + b_s^f X_{\mathrm{cmp},s}^f + b_{ts}^f X_{\mathrm{cmp},m}^f. \qquad \text{(A.17)}
\end{aligned}$$

The relationship of the position responses, saved data, EnvD and TraD are expressed as

$$\begin{aligned}
X_m^{R,\mathrm{res}} &= X_s^{S,\mathrm{res}}(T^R + G_{\mathrm{cmp},m}^f(s)\hat{\tilde{F}}_t^{\mathrm{dis}} + G_{\mathrm{cmp},em}^f(s)\hat{\tilde{F}}_e^{\mathrm{dis}} \qquad \text{(A.18)} \\
X_s^{R,\mathrm{res}} &= X_m^{S,\mathrm{res}}(T^R + G_{\mathrm{cmp},s}^f(s)\hat{\tilde{F}}_e^{\mathrm{dis}} + G_{\mathrm{cmp},ts}^f(s)\hat{\tilde{F}}_t^{\mathrm{dis}}. \qquad \text{(A.19)}
\end{aligned}$$

By adjusting the filters $G_{\mathrm{cmp}}^f(s)$, desired structures of the training system are realized. Additionally, the trainee can manipulate environment through the master and slave system.

Trajectory Training

Because it is difficult for trainee to apply adequate force in the initial phase of the training, master system should be robust against TraD if trajectory is tried to be taught. On the other hand, slave system should adapt environmental variation which is a difference of the distance to an environment, for example. Because of these reasons, following control goals and conditions of the coefficients b^f should be satisfied

$$\begin{aligned}
X_m^{S,\mathrm{res}}(T^{\mathrm{cmd}}) + X_{\mathrm{cmp},s}^f &= X_m^{R,\mathrm{res}} = X_s^{R,\mathrm{res}} \qquad \text{(A.20)} \\
F_m^{S,\mathrm{ext}}(T^{\mathrm{cmd}}) &= -F_s^{S,\mathrm{ext}}(T^{\mathrm{cmd}}) - F_s^{R,\mathrm{ext}} \qquad \text{(A.21)} \\
b_s^f = b_{em}^f = 1,\ b_m^f &= b_{ts}^f = b_m^t = 0. \qquad \text{(A.22)}
\end{aligned}$$

In this case, the EnvD suppression performances at slave the side are described as follows:

$$G^f_{d,s}(s) \;=\; 0 \tag{A.23}$$

$$G^p_{d,s}(s) \;=\; 1. \tag{A.24}$$

On the other hand, the TraD suppression performances at slave side are expressed as follows:

$$G^f_{d,m}(s) \;=\; 1 \tag{A.25}$$

$$G^p_{d,m}(s) \;=\; 0. \tag{A.26}$$

Force Training

In the force training phase, trainee should feel operating force which operator added to the master system in motion saving phase. The following control goals and conditions of the coefficients b^f should be satisfied

$$F^{S,\mathrm{ext}}_m(T^R) \;=\; F^{R,\mathrm{ext}}_m = -F^{S,\mathrm{ext}}_s(T^R) = -F^{R,\mathrm{ext}}_s \tag{A.27}$$

$$b^f_s \;=\; b^f_{em} = b^f_m = 1,\; b^f_{ts} = 0. \tag{A.28}$$

In this case, the EnvD suppression performances at slave the side are described as follows:

$$G^f_{d,s}(s) \;=\; 0 \tag{A.29}$$

$$G^p_{d,s}(s) \;=\; 1. \tag{A.30}$$

On the other hand, the TraD suppression performances at slave side are expressed as follows:

$$G^f_{d,m}(s) \;=\; 0 \tag{A.31}$$

$$G^p_{d,m}(s) \;=\; 1. \tag{A.32}$$

By implementing force compensator at the master side, force reproduction can be realized even though trainees operate master system inadequately. The trainee can learn motions of the saved trainer passively by using the trajectory and fore training system.

Active Training

After the initial phase of the training, trainee should train with activeness to the motions. In order to realize the active training, the control stiffness about $\tilde{F}^{\mathrm{dis}}_t$ should be changed according to the learning

level. By setting the coefficients $b^f = 1$, following control goal is realized.

$$\begin{aligned} X_m^{R,\mathrm{res}} &= X_m^{S,\mathrm{res}}(T^R) + X_{\mathrm{cmp},m}^f \\ &= X_s^{S,\mathrm{res}}(T^R) + X_{\mathrm{cmp},s}^f = X_s^{R,\mathrm{res}} \end{aligned} \tag{A.33}$$

As shown in (A.33), if the trainee generates inappropriate forces compared to the trainee, $X_{\mathrm{cmp},m}^f$ is activated and trainee can recognize the inaccuracy through impedance of $Z_{\mathrm{cmp},m}^f(s)$. However, trainees also have to feel the impedance of the environment. For this reason, stiffness and dampers of the admittance controller should have variable gains about the slave side force as follows:

$$K_{\mathrm{cmp},m}^f = K_{\mathrm{cmp},s}^f = k^f e^{-\alpha G_l^f(s)\left(F_s^{S,\mathrm{ext}\,2} + F_s^{R,\mathrm{ext}\,2}\right)} \tag{A.34}$$

$$D_{\mathrm{cmp},m}^f = D_{\mathrm{cmp},s}^f = d^f e^{-\alpha G_l^f(s)\left(F_s^{R,\mathrm{ext}\,2}\right)}. \tag{A.35}$$

where k^f and d^f and α are positive constants. By using these gains, control goals of the bilateral control as shown in (A.36) and (A.37) are established as follows:

$$X_X^{\mathrm{res}} = X_m^{\mathrm{res}} - X_s^{\mathrm{res}} = 0 \tag{A.36}$$

$$F_F^{\mathrm{ext}} = F_m^{\mathrm{ext}} + F_s^{\mathrm{ext}} = 0. \tag{A.37}$$

In this case, trainee can recognize impedance of the environment in the contact motions. If the values of the stiffness and dampers are gradually reduced and the stiffness and dampers are set to zero as in the final phase of the training, the training system becomes a bilateral control system as

$$X_m^{R,\mathrm{res}} - X_s^{R,\mathrm{res}} = 0 \tag{A.38}$$

$$F_m^{R,\mathrm{ext}} + F_s^{R,\mathrm{ext}} = 0. \tag{A.39}$$

In this case, M_{cmp}^f acts as a force control gain. The whole block diagram of proposed method is shown in Fig. A-1.

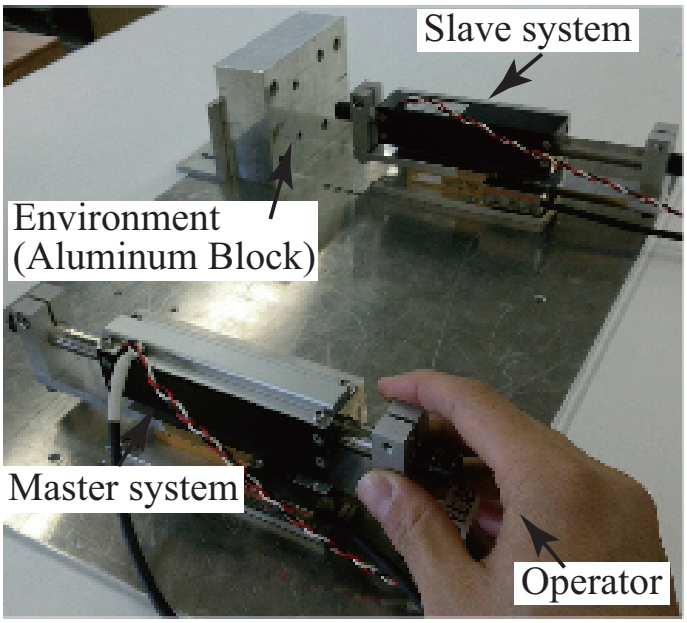

Fig. A-2: Experimental setup for motion training systems.

A.3 Experiments for Motion Training Systems

A.3.1 Experimental Setup for Motion Training Systems

In order to confirm the validities of the proposal, experiments about the motion-saving system and the training system are conducted. An experimental setup is shown in Fig. A-2. Master and slave system are composed by linear motors. Free motions and contact motion to an aluminum block is performed. The environmental position is set 10 mm farther than that of saving system in the experiment of motion training system. As a comparison, an experiment of the conventional motion training system based on multilateral control system [132] is applied. The acceleration references of the conventional method are given as

$$\ddot{X}_m^{R,\mathrm{ref}} = C_f\left(-0.5\hat{F}_m^{R,\mathrm{ext}} - \hat{F}_m^{S,\mathrm{ext}} - \hat{F}_s^{R,\mathrm{ext}}\right) + C_p(s)\left(X_s^{R,\mathrm{res}} - X_m^{R,\mathrm{res}}\right) \tag{A.40}$$

$$\ddot{X}_s^{R,\mathrm{ref}} = C_f\left(-0.5\hat{F}_m^{R,\mathrm{ext}} - \hat{F}_m^{S,\mathrm{ext}} - \hat{F}_s^{R,\mathrm{ext}}\right) + C_p(s)\left(X_m^{S,\mathrm{res}} - X_s^{R,\mathrm{res}}\right). \tag{A.41}$$

One of the master systems in the multilateral system is regarded as the trainer (saved data). Parameters of experiments are showing in Table A.1.

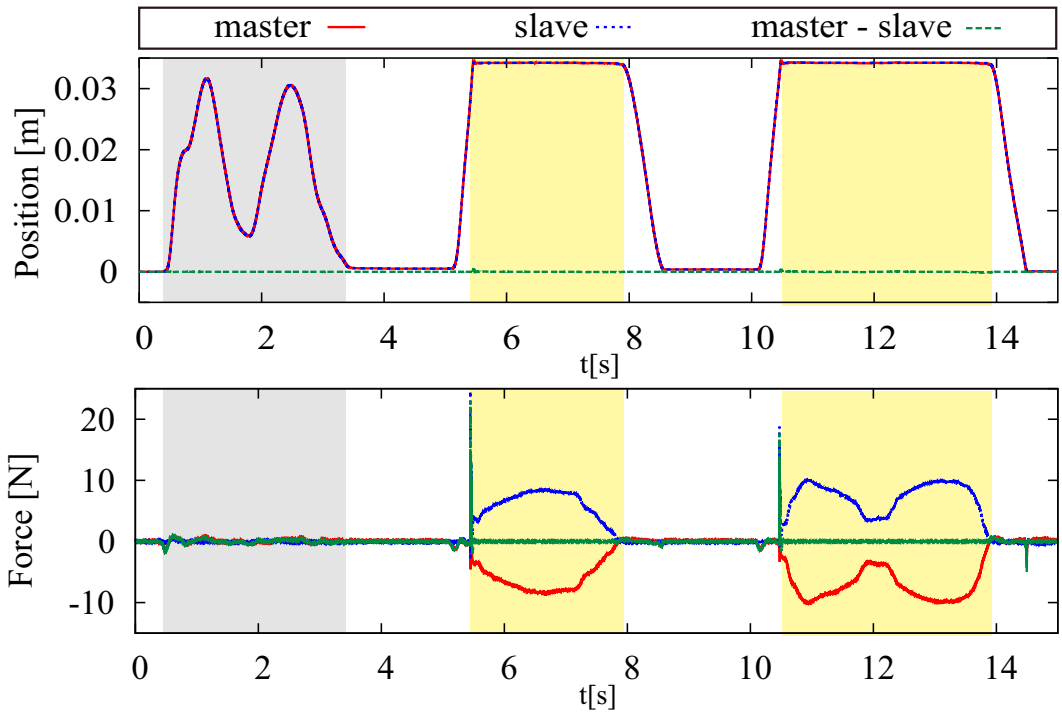

Fig. A-3: Experimental result of motion saving system for the extraction of trainer motions.

A.3.2 Experimental Results for Motion-Saving and Training Systems

Motion Saving System

The experimental result of motion saving system is shown in Fig. A-3.The gray shaded area represents the span where the free motion is conducted by the operator (trainer). On the other hand, contact motions to the environment are executed in the yellow shaded area. It is found that force and position responses show good tracking and the motions of the trainer are appropriately extracted.

Motion Training Systems

Fig. A-4 (a) shows the experimental result of the conventional method. As shown in the gray shaded area, the trajectory is different from both saved motions and slave motions if the trainee adds the inappropriate force compared to the saved trainer motions. As shown in the blue shaded areas, additionally, the slave system cannot adapt the difference of environmental position and contact motions are not reproduced. As a result, operator cannot train with checking the actual reproduced motions. From these results, conventional training system based on the multilateral control system is difficult to apply the

Table A.1: Experimental parameters of motion extraction and training systems.

Parameter	Description	Value
T_s	Sampling time	0.1 ms
K_{fn}	Force coefficient	40.0 N/A
M_n	Mass of linear motor	0.3 kg
K_f	Force control gain	1.0
K_p	Proportional gain	2500
K_v	Differential gain	$2\sqrt{K_p}$
g^{dis}	Cut-off frequency of DOB	1000 rad/s
g^{ext}	Cut-off frequency of RFOB	1000 rad/s
M^f_{cmp}	Mass of Compensator	0.5
d^f_{cmp}	Damper of Compensator	40
κ_s	Parameter of stiffness (slave side in trajectory training)	0
κ	Parameter of stiffness (otherwise)	1000
α	Parameter of stiffness	50
F_{lim}	EnD force limitation	0.8 N
M_T	Mass of temporal admittance	1×10^{-4}
D_T	Damper of temporal admittance	1
K_T	Stiffness of temporal admittance	10

training system with utilizing saved human motions. Conversely, the proposed method for trajectory training without temporal compensator can track the original trajectories and the slave system succeeds to adapt the difference as shown in the Fig. A-4 (b).

Fig. A-5 shows the experimental results of the proposed method with the space and time domain compensators. Fig. A-5 (a) shows the force and trajectory responses of the trajectory training phase. As shown in the figure, updating of the saved motions are activated only when the trainee adds the appropriate force to the master system. The trainee can learn the trajectory by applying the force as he can manipulate the system smoothly. Fig. A-5 (b) shows the experimental results of the force training. The force response of the trainee side shows the good tracking to the saved force of the trainee. The trainee can feel the force that trainer applied to the master system in the motion saving phase. Fig. A-6 shows the experimental results of the proposed spatiotemporal domain admittance control. As shown in the gray shaded area, trajectories of the master and slave systems show good tracking and trainee can recognize the admittance when inappropriate force are applied. In the yellow shaded areas, trainee can recognize the environmental impedance by grace of the variable gains because control goals of the

trajectory tracking and law of action and reaction are realized. Additionally, because the offset in the time domain is generated by the temporal admittance controller, trainee can train independently from the time span of the saved motions.

Fig. A-7 shows the experimental results of the active training based on the spatiotemporal domain admittance control without the stiffness and damper of the compensators. As a result, both trajectory tracking and realization of the law of action reaction are well achieved and the bilateral control is conducted. Figs. A-5 and A-7 show that the constraints from the system against the motions of the trainee are able to adjust according to the learning level by tuning the admittances. From these results, validities of the proposal are confirmed.

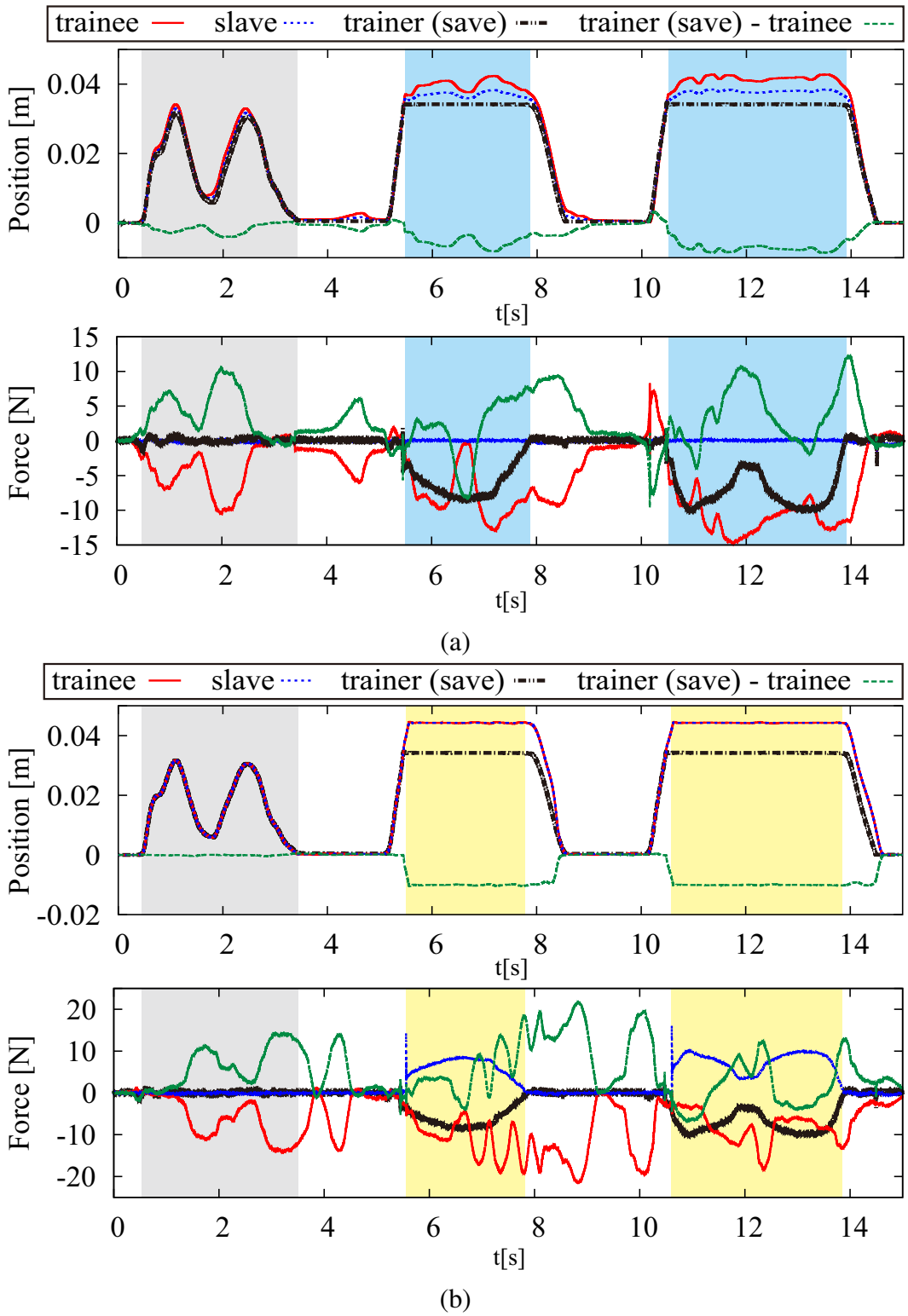

Fig. A-4: Experimental results of the motion training systems. (a) Conventional method. (b) Proposed method without temporal admittance control.

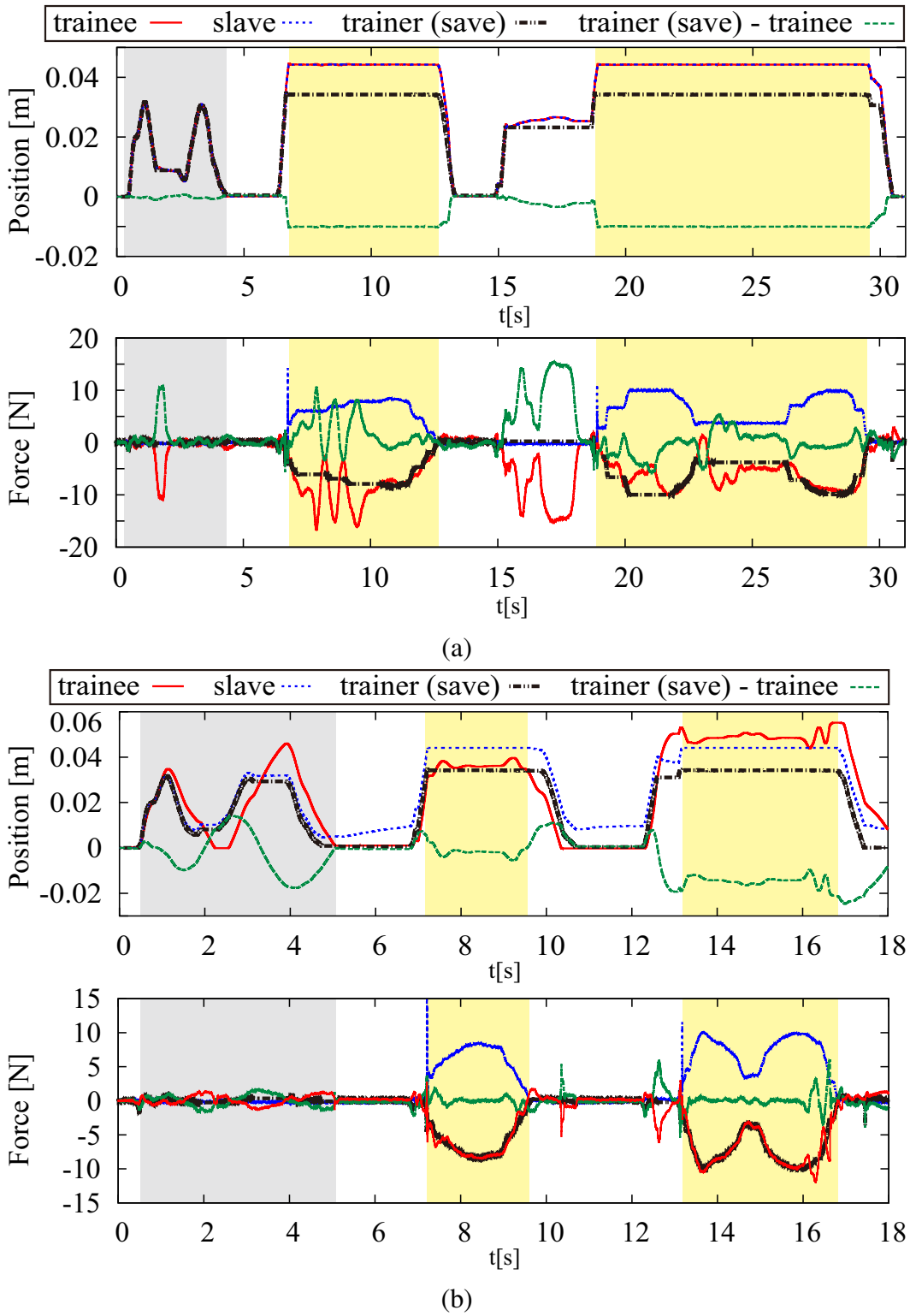

Fig. A-5: Experimental results of the proposal with space and time domain compensators. (a) Trajectory training. (b) Force training.

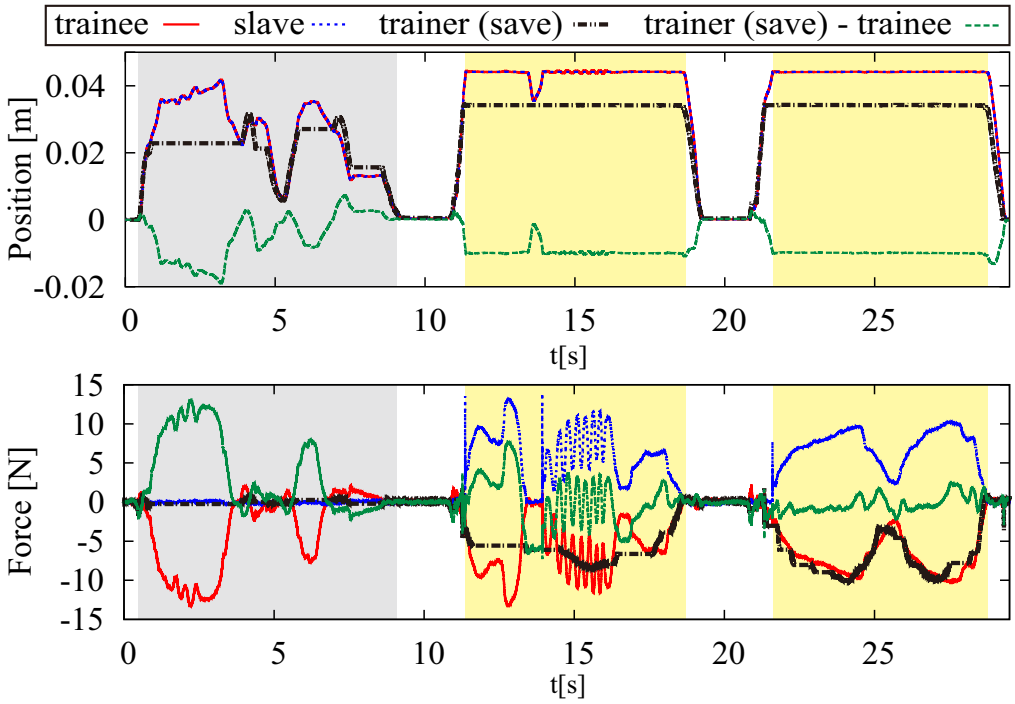

Fig. A-6: Experimental results of the proposed method for active training with variable gains.

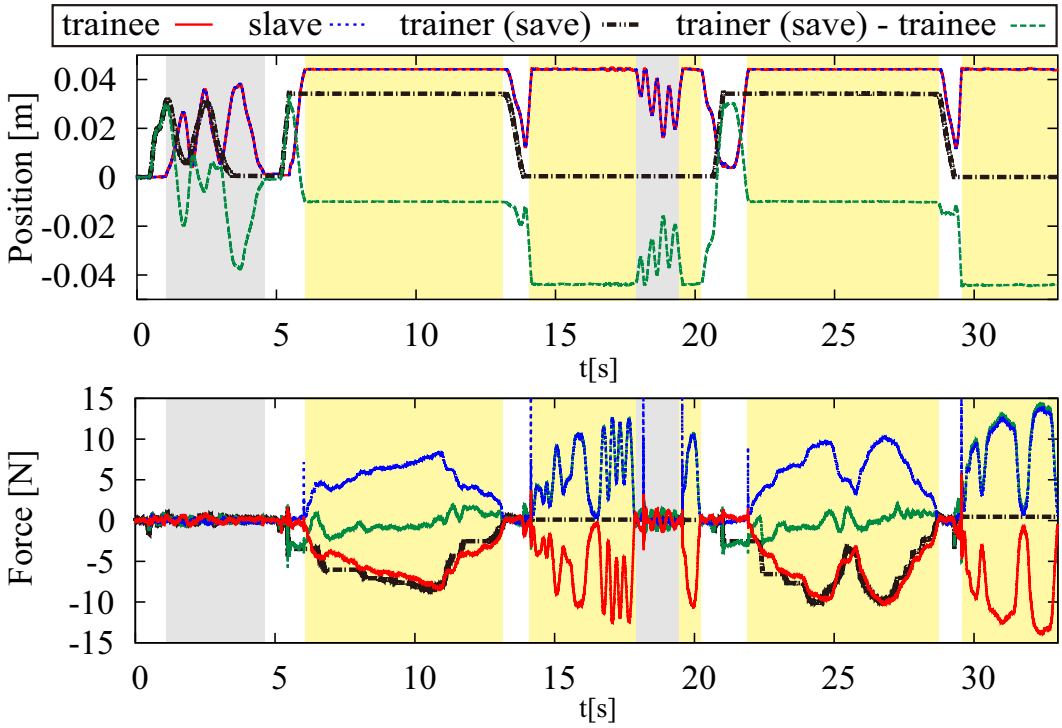

Fig. A-7: Experimental results of the proposal (bilateral controller).

A.4 Summary of This Part

This part proposed a dual motion reproduction system for realization of motion training system based on the spatiotemporal domain admittance control. In order to apply the MCS to motion training systems, the structure of dual motion reproduction system was introduced in which the structure based on a motion reproduction system was constructed not only at the slave system but also the master system. The slave system reproduced motions of trainer and acts on the actual environment with transmitting the difference of trainee's motions form the trainer by the spatial admittance control. As a result, the trainee was able to notice the difference of the motions from the trainer by the admittance. Simultaneously, a trainee was able to follow the saved motions of trainer and feel forces which trainer added to the system by using the space and time domain compensators based on the admittance control. In addition, the trainee was able to train independently from the time frame of the saved motions by grace of the time domain admittance control. Experimental results showed the validity of the proposed method. As future subjects, indexes for motion training by using the proposed method should be considered. Evaluation for the training system also should be conducted by executing actual training.

References

[1] "World Population Ageing: 1950-2050," http://www.un.org/esa/population/publications/worldageing19502050/.

[2] M. Vasic and A. Billard, "Safety issues in human-robot interactions," *2013 IEEE International Conference on Robotics and Automation, ICRA*, pp. 197–204, May, 2013.

[3] K. Yamazaki, R. Ueda, S. Nozawa, M. Kojima, K. Okada, K. Matsumoto, M. Ishikawa, I. Shimoyama, and M. Inaba, "Home-assistant robot for an aging society," *Proceedings of the IEEE*, vol. 100, no. 8, pp. 2429–2441, Aug., 2012.

[4] K. Seki, Y. Tsuchimoto, and M. Iwasaki, "Feedforward compensation by specified step settling with frequency shaping of position reference," *IEEE Transactions on Industrial Electronics*, vol. 61, no. 3, pp. 1552–1561, Mar., 2014.

[5] K. Ohishi, K. Ohnishi, and K. Miyachi, "Torque-speed regulation of DC motor based on load torque estimation method." *International Power Electronics Conference, IPEC*, pp. 1209–1218, Mar., 1983.

[6] T. Murakami, F. Yu, and K. Ohnishi, "Torque sensorless control in multidegree-of-freedom manipulator," *IEEE Transactions on Industrial Electronics*, vol. 40, no. 2, pp. 259–265, Apr., 1993.

[7] K. Ohnishi, M. Shibata, and T. Murakami, "Motion control for advanced mechatronics," *IEEE/ASME Transactions on Mechatronics*, vol. 1, no. 1, pp. 56–67, Mar., 1996.

[8] E. Sariyildiz and K. Ohnishi, "Stability and robustness of disturbance-observer-based motion control systems," *IEEE Transactions on Industrial Electronics*, vol. 62, no. 1, pp. 414–422, Jan., 2015.

[9] H. Liu, X. Tian, G. Wang, and T. Zhang, "Finite-time H_∞ control for high-precision tracking in robotic manipulators using backstepping control," *IEEE Transactions on Industrial Electronics*, vol. 63, no. 9, pp. 5501–5513, Sep., 2016.

[10] C. J. Fallaha, M. Saad, H. Y. Kanaan, and K. Al-Haddad, "Sliding-mode robot control with exponential reaching law," *IEEE Transactions on Industrial Electronics*, vol. 58, no. 2, pp. 600–610, Feb., 2011.

[11] Y. Maeda and M. Iwasaki, "Initial friction compensation using rheology-based rolling friction model in fast and precise positioning," *IEEE Transactions on Industrial Electronics*, vol. 60, no. 9, pp. 3865–3876, Sep., 2013.

[12] D. Grignion, X. Chen, N. Kar, and H. Qian, "Estimation of load disturbance torque for dc motor drive systems under robustness and sensitivity consideration," *IEEE Transactions on Industrial Electronics*, vol. 61, no. 2, pp. 930–942, Feb., 2014.

[13] M. Ruderman and M. Iwasaki, "Observer of nonlinear friction dynamics for motion control," *IEEE Transactions on Industrial Electronics*, vol. 62, no. 9, pp. 5941–5949, Sep., 2015.

[14] M. Ruderman, "Tracking control of motor drives using feedforward friction observer," *IEEE Transactions on Industrial Electronics*, vol. 61, no. 7, pp. 3727–3735, Jul., 2014.

[15] R. Antonello, K. Ito, and R. Oboe, "Acceleration measurement drift rejection in motion control systems by augmented-state kinematic kalman filter," *IEEE Transactions on Industrial Electronics*, vol. 63, no. 3, pp. 1953–1961, Mar., 2016.

[16] Q. Xu, "Robust impedance control of a compliant microgripper for high-speed position/force regulation," *IEEE Transactions on Industrial Electronics*, vol. 62, no. 2, pp. 1201–1209, Feb., 2015.

[17] B. Huard, M. Grossard, S. Moreau, and T. Poinot, "Sensorless force/position control of a single-acting actuator applied to compliant object interaction," *IEEE Transactions on Industrial Electronics*, vol. 62, no. 6, pp. 3651–3661, Jun., 2015.

[18] E. Sariyildiz and K. Ohnishi, "On the explicit robust force control via disturbance observer," *IEEE Transactions on Industrial Electronics*, vol. 62, no. 3, pp. 1581–1589, Mar., 2015.

[19] E. Sariyildiz and K. Ohnishi, "An adaptive reaction force observer design," *IEEE/ASME Transactions on Mechatronics*, vol. 20, no. 2, pp. 750–760, Apr., 2015.

[20] S. Katsura, Y. Matsumoto, and K. Ohnishi, "Modeling of force sensing and validation of disturbance observer for force control," *IEEE Transactions on Industrial Electronics*, vol. 54, no. 1, pp. 530–538, Feb., 2007.

[21] T. Murakami, N. Oda, Y. Miyasaka, and K. Ohnishi, "A motion control strategy based on equivalent mass matrix in multidegree-of-freedom manipulator," *IEEE Transactions on Industrial Electronics*, vol. 42, no. 2, pp. 123–130, Apr., 1995.

[22] K. Yuki, T. Murakami, and K. Ohnishi, "Vibration control of a 2 mass resonant system by the resonance ratio control," *IEEJ Transactions on Industry Applications*, vol. 113, no. 10, pp. 1162–1169, Oct., 1993.

[23] M. Matsuoka, T. Murakami, and K. Ohnishi, "Vibration suppression and disturbance rejection control of a flexible link arm," *Proceedings of the 1995 IEEE IECON 21st International Conference on Industrial Electronics, Control, and Instrumentation, 1995*, vol. 2, pp. 1260–1265, Nov., 1995.

[24] S. Katsura and K. Ohnishi, "Force servoing by flexible manipulator based on resonance ratio control," *IEEE Transactions on Industrial Electronics*, vol. 54, no. 1, pp. 539–547, Feb., 2007.

[25] K. Natori, T. Tsuji, K. Ohnishi, A. Hace, and K. Jezernik, "Time-delay compensation by communication disturbance observer for bilateral teleoperation under time-varying delay," *IEEE Transactions on Industrial Electronics*, vol. 57, no. 3, pp. 1050–1062, Mar., 2010.

[26] W. Iida and K. Ohnishi, "Reproducibility and operationality in bilateral teleoperation," *The 8th IEEE International Workshop on Advanced Motion Control, 2004. AMC '04.*, pp. 217–222, Mar., 2004.

[27] A. Suzuki and K. Ohnishi, "Frequency-domain damping design for time-delayed bilateral teleoperation system based on modal space analysis," *IEEE Transactions on Industrial Electronics*, vol. 60, no. 1, pp. 177–190, Jan., 2013.

[28] A. Suzuki and K. Ohnishi, "Novel four-channel bilateral control design for haptic communication under time delay based on modal space analysis," *IEEE Transactions on Control Systems Technology*, vol. 21, no. 3, pp. 882–890, May, 2013.

[29] D. A. Lawrence, "Stability and transparency in bilateral teleoperation," *IEEE Transactions on Robotics and Automation*, vol. 9, no. 5, pp. 624–637, Oct., 1993.

[30] L. Bate, C. D. Cook, and Z. Li, "Reducing wave-based teleoperator reflections for unknown environments," *IEEE Transactions on Industrial Electronics*, vol. 58, no. 2, pp. 392–397, Feb., 2011.

[31] A. F. Villaverde, A. B. Blas, J. Carrasco, and A. B. Torrico, "Reset control for passive bilateral teleoperation," *IEEE Transactions on Industrial Electronics*, vol. 58, no. 7, pp. 3037–3045, Jul., 2011.

[32] H. I. Son, J. H. Cho, T. Bhattacharjee, H. Jung, and D. Y. Lee, "Analytical and psychophysical comparison of bilateral teleoperators for enhanced perceptual performance," *IEEE Transactions on Industrial Electronics*, vol. 61, no. 11, pp. 6202–6212, Nov., 2014.

[33] I. G. Polushin, A. Takhmar, and R. V. Patel, "Projection-based force-reflection algorithms with frequency separation for bilateral teleoperation," *IEEE/ASME Transactions on Mechatronics*, vol. 20, no. 1, pp. 143–154, Feb., 2015.

[34] T. Kanno, E. B. V. Poorten, and Y. Yokokohji, "Variable-scale bilateral control for micro teleoperation," *Journal of the Robotics Society of Japan*, vol. 27, no. 2, pp. 239–248, Mar., 2009.

[35] S. Khan, A. Sabanovic, and A. O. Nergiz, "Scaled bilateral teleoperation using discrete-time sliding-mode controller," *IEEE Transactions on Industrial Electronics*, vol. 56, no. 9, pp. 3609–3618, Sep., 2009.

[36] W. Yamanouchi and S. Katsura, "Tele-operation of a mobile haptic system using dynamical modal transformation," *IEEJ Transactions on Industry Applications*, vol. 132, no. 3, pp. 315–321, Mar., 2012.

[37] S. Sakaino, T. Sato, and K. Ohnishi, "A novel motion equation for general task description and analysis of mobile-hapto," *IEEE Transactions on Industrial Electronics*, vol. 60, no. 7, pp. 2673–2680, July 2013.

[38] A. Hace and M. Franc, "FPGA implementation of sliding-mode-control algorithm for scaled bilateral teleoperation," *IEEE Transactions on Industrial Informatics*, vol. 9, no. 3, pp. 1291–1300, Aug., 2013.

[39] T. Mizoguchi, T. Nozaki, and K. Ohnishi, "Stiffness transmission of scaling bilateral control system by gyrator element integration," *IEEE Transactions on Industrial Electronics*, vol. 61, no. 2, pp. 1033–1043, Feb 2014.

[40] T. Nozaki, T. Mizoguchi, Y. Saito, D. Yashiro, and K. Ohnishi, "Recognition of grasping motion based on modal space haptic information using DP pattern-matching algorithm," *IEEE Transactions on Industrial Informatics*, vol. 9, no. 4, pp. 2043–2051, Nov., 2013.

[41] T. Nozaki, T. Mizoguchi, and K. Ohnishi, "Motion expression by elemental separation of haptic information," *IEEE Transactions on Industrial Electronics*, vol. 61, no. 11, pp. 6192–6201, Nov., 2014.

[42] C. M. N. Brigante, N. Abbate, A. Basile, A. C. Faulisi, and S. Sessa, "Towards miniaturization of a mems-based wearable motion capture system," *IEEE Transactions on Industrial Electronics*, vol. 58, no. 8, pp. 3234–3241, Aug., 2011.

[43] K. Ogawara, J. Takamatsu, H. Kimura, and K. Ikeuchi, "Extraction of essential interactions through multiple observations of human demonstrations," *IEEE Transactions on Industrial Electronics*, vol. 50, no. 4, pp. 667–675, Aug., 2003.

[44] M. Howard, D. J. Braun, and S. Vijayakumar, "Transferring human impedance behavior to heterogeneous variable impedance actuators," *IEEE Transactions on Robotics*, vol. 29, no. 4, pp. 847–862, Aug., 2013.

[45] G. Du, P. Zhang, and D. Li, "Human–manipulator interface based on multisensory process via kalman filters," *IEEE Transactions on Industrial Electronics*, vol. 61, no. 10, pp. 5411–5418, Oct., 2014.

[46] Y. Yokokura, S. Katsura, and K. Ohishi, "Stability analysis and experimental validation of a motion-copying system," *IEEE Transactions on Industrial Electronics*, vol. 56, no. 10, pp. 3906–3913, Oct., 2009.

[47] M. Skubic and R. A. Volz, "Acquiring robust, force-based assembly skills from human demonstration," *IEEE Transactions on Robotics and Automation*, vol. 16, no. 6, pp. 772–781, Dec., 2000.

[48] A. Vakanski, I. Mantegh, A. Irish, and F. Janabi-Sharifi, "Trajectory learning for robot programming by demonstration using hidden markov model and dynamic time warping," *IEEE Transactions on Systems, Man, and Cybernetics, Part B* (*Cybernetics*), vol. 42, no. 4, pp. 1039–1052, Aug., 2012.

[49] P. Slaets, T. Lefebvre, J. Rutgeerts, H. Bruyninckx, and J. D. Schutter, "Incremental building of a polyhedral feature model for programming by human demonstration of force-controlled tasks," *IEEE Transactions on Robotics*, vol. 23, no. 1, pp. 20–33, Feb., 2007.

[50] W. Meeussen, J. Rutgeerts, K. Gadeyne, H. Bruyninckx, and J. D. Schutter, "Contact-state segmentation using particle filters for programming by human demonstration in compliant-motion tasks," *IEEE Transactions on Robotics*, vol. 23, no. 2, pp. 218–231, Apr., 2007.

[51] S. M. M. Rahman, R. Ikeura, S. Hayakawa, and H. Sawai, "Design and control of a power assist system for lifting objects based on human operator's weight perception and load force characteristics," *IEEE Transactions on Industrial Electronics*, vol. 58, no. 8, pp. 3141–3150, Aug., 2011.

[52] S. Oh, K. Kong, and Y. Hori, "Design and analysis of force-sensor-less power-assist control," *IEEE Transactions on Industrial Electronics*, vol. 61, no. 2, pp. 985–993, Feb., 2014.

[53] M. Pietrusinski, I. Cajigas, G. Severini, P. Bonato, and C. Mavroidis, "Robotic gait rehabilitation trainer," *IEEE/ASME Transactions on Mechatronics*, vol. 19, no. 2, pp. 490–499, Apr., 2014.

[54] R. Lu, Z. Li, C. Y. Su, and A. Xue, "Development and learning control of a human limb with a rehabilitation exoskeleton," *IEEE Transactions on Industrial Electronics*, vol. 61, no. 7, pp. 3776–3785, July 2014.

[55] S. Katsura, K. Irie, and K. Ohishi, "Wideband force control by position-acceleration integrated disturbance observer," *IEEE Transactions on Industrial Electronics*, vol. 55, no. 4, pp. 1699–1706, Apr., 2008.

[56] B. Veselic, B. Perunicic-Drazenovic, and C. Milosavljevic, "Improved discrete-time sliding-mode position control using euler velocity estimation," *IEEE Transactions on Industrial Electronics*, vol. 57, no. 11, pp. 3840–3847, Nov., 2010.

[57] S. Chen, "Kalman filter for robot vision: A survey," *IEEE Transactions on Industrial Electronics*, vol. 59, no. 11, pp. 4409–4420, Nov., 2012.

[58] V. Lippiello, B. Siciliano, and L. Villani, "Position-based visual servoing in industrial multirobot cells using a hybrid camera configuration," *IEEE Transactions on Robotics*, vol. 23, no. 1, pp. 73–86, Feb., 2007.

[59] W. Zhang, J. Bae, and M. Tomizuka, "Modified preview control for a wireless tracking control system with packet loss," *IEEE/ASME Transactions on Mechatronics*, vol. 20, no. 1, pp. 299–307, Feb., 2015.

[60] M. Habibullah and D.-C. Lu, "A speed-sensorless fs-ptc of induction motors using extended Kalman filters," *IEEE Transactions on Industrial Electronics*, vol. 62, no. 11, pp. 6765–6778, Nov., 2015.

[61] F. Alonge, T. Cangemi, F. D'Ippolito, A. Fagiolini, and A. Sferlazza, "Convergence analysis of extended Kalman filter for sensorless control of induction motor," *IEEE Transactions on Industrial Electronics*, vol. 62, no. 4, pp. 2341–2352, Apr., 2015.

[62] G. Du and P. Zhang, "A markerless human -robot interface using particle filter and Kalman filter for dual robots," *IEEE Transactions on Industrial Electronics*, vol. 62, no. 4, pp. 2257–2264, Apr., 2015.

[63] L. Cantelli, G. Muscato, M. Nunnari, and D. Spina, "A joint-angle estimation method for industrial manipulators using inertial sensors," *IEEE/ASME Transactions on Mechatronics*, vol. 20, no. 5, pp. 2486–2495, Oct., 2015.

[64] A. Shimada and C. Yongyai, "Motion control of inverted pendulum robots using a Kalman filter based disturbance observer," *SICE Journal of Control, Measurement, and System Integration*, vol. 2, no. 1, pp. 50–55, Jan., 2009.

[65] C. Mitsantisuk, K. Ohishi, and S. Katsura, "Estimation of action/reaction forces for the bilateral control using Kalman filter," *IEEE Transactions on Industrial Electronics*, vol. 59, no. 11, pp. 4383–4393, Nov., 2012.

[66] K. Ito, R. Antonello, and R. Oboe, "Use of mems accelerometers for performance improvement of motion control systems with low resolution position sensors," *Industrial Electronics (ISIE), 2013 IEEE International Symposium on*, pp. 1–6, May, 2013.

[67] T. T. Phuong, K. Ohishi, Y. Yokokura, and C. Mitsantisuk, "FPGA-based high-performance force control system with friction-free and noise-free force observation," *IEEE Transactions on Industrial Electronics*, vol. 61, no. 2, pp. 994–1008, Feb., 2014.

[68] S. Bolognani, L. Tubiana, and M. Zigliotto, "Extended Kalman filter tuning in sensorless pmsm drives," *IEEE Transactions on Industry Applications*, vol. 39, no. 6, pp. 1741–1747, Nov., 2003.

[69] C. Mitsantisuk, K. Ohishi, S. Urushihara, and S. Katsura, "Kalman filter-based disturbance observer and its applications to sensorless force control," *Advanced Robotics*, vol. 25, no. 3-4, pp. 335–353, Nov., 2011.

[70] S. Katsura, Y. Matsumoto, and K. Ohnishi, "Analysis and experimental validation of force bandwidth for force control," *IEEE Transactions on Industrial Electronics*, vol. 53, no. 3, pp. 922–928, Jun., 2006.

[71] T. Miyagi and S. Katsura, "High-performance force control based on virtual bilateral control structure," *IEEJ Journal of Industry Applications*, vol. 4, no. 2, pp. 83–90, Mar., 2015.

[72] N. Motoi and R. Kubo, "Human-machine cooperative grasping/manipulating system using force-based compliance controller with force threshold," *IEEJ Journal of Industry Applications*, vol. 5, no. 2, pp. 39–46, Mar., 2016.

[73] S. Komada, K. Nomura, M. Ishida, and T. Hori, "Robust force control based on compensation for parameter variations of dynamic environment," *IEEE Transactions on Industrial Electronics*, vol. 40, no. 1, pp. 89–95, Feb., 1993.

[74] Y. Nagatsu and S. Katsura, "Realization of stable contact motion based on concept of resonance ratio control," *42nd Annual Conference of the IEEE Industrial Electronics Society, IECON 2016*, pp. 300–305, Oct., 2016.

[75] O. Khatib, "A unified approach for motion and force control of robot manipulators: The operational space formulation," *IEEE Journal on Robotics and Automation*, vol. 3, no. 1, pp. 43–53, Feb., 1987.

[76] C. Yang, Z. Qu, and J. Han, "Decoupled-space control and experimental evaluation of spatial electrohydraulic robotic manipulators using singular value decomposition algorithms," *IEEE Transactions on Industrial Electronics*, vol. 61, no. 7, pp. 3427–3438, Jul., 2014.

[77] Y. Jiang, Y. Zhu, K. Yang, C. Hu, and D. Yu, "A data-driven iterative decoupling feedforward control strategy with application to an ultraprecision motion stage," *IEEE Transactions on Industrial Electronics*, vol. 62, no. 1, pp. 620–627, Jan., 2015.

[78] T. Shimono, S. Katsura, S. Susa, T. Takei, and K. Ohnishi, "Transmission of force sensation by micro-macro bilateral control with respect to standardized modal space," *2007 IEEE International Conference on Mechatronics*, pp. 1–6, May, 2007.

[79] S. Sakaino, T. Sato, and K. Ohnishi, "Precise position/force hybrid control with modal mass decoupling and bilateral communication between different structures," *IEEE Transactions on Industrial Informatics*, vol. 7, no. 2, pp. 266–276, May, 2011.

[80] S. Sakaino, T. Sato, and K. Ohnishi, "Multi-DOF micro-macro bilateral controller using oblique coordinate control," *IEEE Transactions on Industrial Informatics*, vol. 7, no. 3, pp. 446–454, Aug., 2011.

[81] T. Nozaki, T. Mizoguchi, and K. Ohnishi, "Decoupling strategy for position and force control based on modal space disturbance observer," *IEEE Transactions on Industrial Electronics*, vol. 61, no. 2, pp. 1022–1032, Feb., 2014.

[82] T. Shibata and T. Murakami, "Null space motion control by PID control considering passivity in redundant manipulator," *IEEE Transactions on Industrial Informatics*, vol. 4, no. 4, pp. 261–270, Nov., 2008.

[83] N. ODA, H. OHTA, T. MURAKAMI, and K. OHNISHI, "A global compliant control of redundant manipulator by null space," *Journal of the Japan Society for Precision Engineering*, vol. 63, no. 10, pp. 1432–1438, Oct., 1997.

[84] T. Murakami, K. Kahlen, and R. W. A. A. D. Doncker, "Robust motion control based on projection plane in redundant manipulator," *IEEE Transactions on Industrial Electronics*, vol. 49, no. 1, pp. 248–255, Feb., 2002.

[85] S. Sakaino, T. Sato, and K. Ohnishi, "Force-based disturbance observer for dynamic force control and a position/force hybrid controller," *IEEJ Transactions on Electrical and Electronic Engineering*, vol. 8, no. 5, pp. 505–514, Jul., 2013.

[86] Y. Yokokura, K. Ohishi, and S. Katsura, "Fine force reproduction based on motion-copying system using acceleration observer," *IEEE Transactions on Industrial Electronics*, vol. 61, no. 11, pp. 6213–6221, Nov., 2014.

[87] N. Tsunashima and S. Katsura, "Reproduction of human motion using motion-copying system based on coordinate modification," *36th Annual Conference on IEEE Industrial Electronics Society, IECON 2010*, pp. 1609–1614, Nov., 2010.

[88] S. Yajima and S. Katsura, "Multi-dof motion reproduction using motion-copying system with velocity constraint," *IEEE Transactions on Industrial Electronics*, vol. 61, no. 7, pp. 3765–3775, Jul., 2014.

[89] A. Matsui and S. Katsura, "Motion-copying system using modal information for motion reproduction," *39th Annual Conference of the IEEE Industrial Electronics Society, IECON 2013*, pp. 6132–6137, Nov., 2013.

[90] T. Miyagi and S. Katsura, "Motion reproduction system considering control bandwidth in force transmission," *2014 IEEE 13th International Workshop on Advanced Motion Control AMC*, pp. 452–457, Mar., 2014.

[91] N. Motoi, T. Shimono, R. Kubo, and A. Kawamura, "Task realization by a force-based variable compliance controller for flexible motion control systems," *IEEE Transactions on Industrial Electronics*, vol. 61, no. 2, pp. 1009–1021, Feb., 2014.

[92] Y. Ohba, M. Sazawa, K. Ohishi, T. Asai, K. Majima, Y. Yoshizawa, and K. Kageyama, "Sensorless force control for injection molding machine using reaction torque observer considering torsion phenomenon," *IEEE Transactions on Industrial Electronics*, vol. 56, no. 8, pp. 2955–2960, Aug., 2009.

[93] S. Komada, T. Kimura, M. Ishida, and T. Hori, "Robust position control of manipulators based on disturbance observer and inertia identifier in task space," *1996 4th International Workshop on Advanced Motion Control, 1996. AMC '96-MIE. Proceedings*, vol. 1, pp. 225–230, Mar., 1996.

[94] K. Yamada, S. Komada, M. Ishida, and T. Hori, "Characteristics of servo system using high order disturbance observer," *Proceedings of the 35th IEEE Conference on Decision and Control, 1996*, vol. 3, pp. 3252–3257, Dec., 1996.

[95] K. Yamada, S. Komada, M. Ishida, and T. Hori, "Analysis and classical control design of servo system using high order disturbance observer," *23rd International Conference on Industrial Electronics, Control and Instrumentation, IECON 97*, vol. 1, pp. 4–9, Nov., 1997.

[96] Y. Nagatsu and S. Katsura, "Design strategies for motion reproduction based on environmental disturbance compensation," *IEEE Transactions on Industrial Electronics*, vol. 62, no. 9, pp. 5786–5798, Sep., 2015.

[97] Y. Nagatsu and S. Katsura, "Decoupling and performance enhancement of hybrid control for motion-copying system," *IEEE Transactions on Industrial Electronics*, vol. 64, no. 1, pp. 420–431, Jan., 2017.

[98] Y. Nagatsu and S. Katsura, "High-order disturbance estimation using kalman filter for precise reaction-torque control," *2016 IEEE 14th International Workshop on Advanced Motion Control, AMC*, pp. 79–84, Apr., 2016.

[99] Y. Nagatsu and S. Katsura, "A consideration on kalman filter based disturbance observer for hybrid control," *The IEEJ Papers of Technical Meeting on Mechatronics Control, MEC '16*, pp. 12–18, Sep., 2016.

[100] N. Kobayashi and T. Murakami, "Comparison of force control performance based on only acceleration sensor with KF/EKF," *IEEJ Journal of Industry Applications*, vol. 4, no. 5, pp. 559–567, May, 2015.

[101] R. Horie and T. Murakami, "Workspace based controller design and performance evaluation of mdof force sensorless bilateral system," *IEEJ Transactions on Industry Applications*, vol. 132, no. 7, pp. 755–763, Jul., 2012.

[102] S. Adachi and I. Maruta, "Fundamentals of Kalman filter," *Tokyo Denki University Press*, pp. 1–228, 2012.

[103] K. Natori, R. Kubo, T. Shimono, K. Ohnishi, K. Miura, H. Furukawa, and M. Takahata, "Time-delay compensation by communication disturbance observers of different orders in bilateral teleoperation systems," *IEEJ Transactions on Industry Applications*, vol. 129, no. 4, pp. 353–362, Feb., 2009.

[104] T. Shimoichi and S. Katsura, "Optimization method for disturbance compensation in bilateral control," *IEEJ Journal of Industry Applications*, vol. 2, no. 2, pp. 113–120, Mar., 2013.

[105] I. Arnold, W.F. and A. Laub, "Generalized eigenproblem algorithms and software for algebraic riccati equations," *Proceedings of the IEEE*, vol. 72, no. 12, pp. 1746–1754, Dec., 1984.

[106] A. Morbi and M. Ahmadi, "Safely rendering small impedances in admittance-controlled haptic devices," *IEEE/ASME Transactions on Mechatronics*, vol. 21, no. 3, pp. 1272–1280, Jun., 2016.

[107] S. Katsura, J. Suzuki, and K. Ohnishi, "Pushing operation by flexible manipulator taking environmental information into account," *IEEE Transactions on Industrial Electronics*, vol. 53, no. 5, pp. 1688–1697, Oct. 2006.

[108] T. Yoshioka, A. Yabuki, Y. Yokokura, K. Ohishi, T. Miyazaki, and T. T. Phuong, "Stable force control of industrial robot based on spring ratio and instantaneous state observer," *IEEJ Journal of Industry Applications*, vol. 5, no. 2, pp. 132–140, Mar., 2016.

[109] T. Yoshikawa, "Foundations of grasping and manipulation 1. passive closure and active closure," *Journal of the Robotics Society of Japan*, vol. 13, no. 7, pp. 950–957, Oct., 1995.

[110] T. Yoshikawa, "Foundations of grasping and manipulation 2. fingertip force," *Journal of the Robotics Society of Japan*, vol. 14, no. 1, pp. 48–54, Jan., 1996.

[111] T. Yoshikawa, "Foundations of grasping and manipulation 3. control," *Journal of the Robotics Society of Japan*, vol. 14, no. 4, pp. 505–511, May, 1996.

[112] E. Leksono, T. Murakami, and K. Ohnishi, "Cooperative motion control of multimanipulator based on workspace disturbance observer with variable compliance gain," *IEEJ Transactions on Industry Applications*, vol. 118, no. 1, pp. 16–23, Jan., 1998.

[113] E. Leksono, T. Murakami, and K. Ohnishi, "Observer based robust force control in cooperative motion systems," *Proceedings of the 24th Annual Conference of the IEEE Industrial Electronics Society, IECON '98*, vol. 3, pp. 1801–1806, Aug. 1998.

[114] T. Yoshikawa, "Analysis and control of robot manipulators with redundancy," *Robotics research: the first international symposium, MIT Press Cambridge, MA*, pp. 735–747, 1984.

[115] T. Yoshikawa, "Manipulability and redundancy control of robotic mechanisms," *Proceedings., 1985 IEEE International Conference on Robotics and Automation*, vol. 2, pp. 1004–1009, Mar., 1985.

[116] T. M. O'Sullivan, C. M. Bingham, and N. Schofield, "Observer-based tuning of two-inertia servo-drive systems with integrated saw torque transducers," *IEEE Transactions on Industrial Electronics*, vol. 54, no. 2, pp. 1080–1091, Apr., 2007.

[117] K. Erenturk, "Fractional-order $PI^{\lambda}D^{\mu}$ andd active disturbance rejection control of nonlinear two-mass drive system," *IEEE Transactions on Industrial Electronics*, vol. 60, no. 9, pp. 3806–3813, Sep., 2013.

[118] A. Cole, J. Hauser, and S. Sastry, "Kinematics and control of multifingered hands with rolling contact," *Proceedings of the 1988 IEEE International Conference on Robotics and Automation, 1988.*, pp. 228–233 vol.1, Apr., 1988.

[119] R. Ozawa, S. Arimoto, S. Nakamura, and J.-H. Bae, "Control of an object with parallel surfaces by a pair of finger robots without object sensing," *IEEE Transactions on Robotics*, vol. 21, no. 5, pp. 965–976, Oct., 2005.

[120] S. Arimoto, M. Yoshida, and J.-H. Bae, "Stable "blind grasping" of a 3-d object under non-holonomic constraints," *Proceedings of the 2006 IEEE International Conference on Robotics and Automation, ICRA 2006*, pp. 2124–2130, May, 2006.

[121] E. Leksono, T. Murakami, and K. Ohnishi, "On hybrid position/force cooperative control of multimanipulator based on workspace disturbance observer," *Proceedings of the 1996 IEEE IECON 22nd International Conference on Industrial Electronics, Control, and Instrumentation*, vol. 3, pp. 1873–1878, Aug. 1996.

[122] E. Leksono, T. Murakami, and K. Ohnishi, "Robust cooperative control systems for multiple manipulators in the presence of external force," *Journal of the Japan Society for Precision Engineering*, vol. 64, no. 5, pp. 690–694, May, 1998.

[123] R. Kubo, T. Shimono, and K. Ohnishi, "Flexible controller design of bilateral grasping systems based on a multilateral control scheme," *IEEE Transactions on Industrial Electronics*, vol. 56, no. 1, pp. 62–68, Jan., 2009.

[124] S. Yajima and S. Katsura, "Velocity based motion-copying system for grasping/manipulation motion reproduction," *2011 IEEE/SICE International Symposium on System Integration, SII*, pp. 515–520, Dec. 2011.

[125] S. Yajima, E. Saito, and S. Katsura, "Controller design for reproduction of grasping/manipulation motion of grasping objects with different diameters," *IEEJ Journal of Industry Applications*, vol. 2, no. 1, pp. 7–13, Jan., 2013.

[126] T. Tsuji, K. Ohnishi, and A. Sabanovic, "A controller design method based on functionality," *IEEE Transactions on Industrial Electronics*, vol. 54, no. 6, pp. 3335–3343, Dec., 2007.

[127] S. Katsura and K. Ohishi, "Modal system design of multirobot systems by interaction mode control," *IEEE Transactions on Industrial Electronics*, vol. 54, no. 3, pp. 1537–1546, Jun., 2007.

[128] S. Katsura and K. Ohishi, "Acquisition and analysis of finger motions by skill preservation system," *IEEE Transactions on Industrial Electronics*, vol. 54, no. 6, pp. 3353–3361, Dec., 2007.

[129] Y. Nagatsu and S. Katsura, "Motion reproducing system for pinching and rotational tasks with different size of objects by using a transformation to polar coordinates," *2013 IEEE International Conference on Mechatronics,* (*ICM*), pp. 546–551, Feb., 2013.

[130] E. Fujii, Y. Nagatsu, H. Onoyama, and S. Katsura, "Improvement of general versatility of motion reproduction by function observer," *The 32nd Annual Conference of the Robotics Society of Japan*, no. 1E2-02, Sep., 2014.

[131] Y. Nagatsu and S. Katsura, "A motion reproduction method for training system based on spatiotemporal admittance control," *2015 IEEE International Conference on Industrial Technology, ICIT*, pp. 46–51, Mar. 2015.

[132] T. Shimono, R. Kubo, K. Ohnishi, S. Katsura, and K. Ohishi, "Multilateral control with haptic transmission ratio," *IEEJ Transactions on Industry Applications*, vol. 127, no. 8, pp. 875–883, Aug. 2007.

List of Achievements

Journals (As a first author)

[1] Yuki Nagatsu and Seiichiro Katsura, "Design strategies for motion reproduction based on environmental disturbance compensation," *IEEE Transactions on Industrial Electronics*, Vol. 62, No. 9, pp. 5786–5798, Sep., 2015.

[2] Yuki Nagatsu and Seiichiro Katsura, "Decoupling and performance enhancement of hybrid control for motion-copying system," *IEEE Transactions on Industrial Electronics*, Vol. 64, No. 1, pp. 420–431, Jan., 2017.

International Conference (As a first author)

[1] Yuki Nagatsu and Seiichiro Katsura, "Bilateral control considering transition of subsystems based on ability to oppose the thumb," *The 38th Annual Conference on IEEE Industrial Electronics Society, IECON '12-MONTREAL*, pp. 4388–4393, Oct., 2012.

[2] Yuki Nagatsu and Seiichiro Katsura, "Motion reproducing system for pinching and rotational tasks with different size of objects by using a transformation to polar coordinates," *IEEE International Conference on Mechatronics, ICM '13-VICENZA*, pp. 546–551, Feb., 2013.

[3] Yuki Nagatsu and Seiichiro Katsura, "Scaled bilateral control using kalman filter based state estimation for reduction of noise effect," *The 22nd IEEE International Symposium on Industrial Electronics, ISIE '13-TAIPEI*, pp. 1–6, May, 2013.

[4] Yuki Nagatsu and Seiichiro Katsura, "macro–micro bilateral control using Kalman filter based state observer for noise reduction and decoupling of modal space," *The 39th Annual Conference of the IEEE Industrial Electronics Society, IECON '13-VIENNA*, pp. 4192–4197, Nov., 2013.

[5] Yuki Nagatsu and Seiichiro Katsura, "A motion reproduction method for training system based on spatiotemporal admittance control," *The 2015 IEEE International Conference on Industrial Technology, ICIT '16-SEVILLE*, pp. 46–51, Mar., 2015.

[6] Yuki Nagatsu and Seiichiro Katsura, "High-order disturbance estimation using Kalman filter for precise reaction-torque control," *The 14th International Workshop on Advanced Motion Control, AMC '16-AUKLAND*, pp. 79–84, Apr., 2016.

[7] Yuki Nagatsu and Seiichiro Katsura, "Realization of stable contact motion based on concept of resonance ratio control," *The 42nd Annual Conference of the IEEE Industrial Electronics Society, IECON '16-FIRENZE*, pp. 300–305, Oct., 2016.

Domestic Conference (As a first author)

[1] Yuki Nagatsu and Seiichiro Katsura, "An analysis of finger motion based on thumb opposability," *The IEEJ Papers of Technical Meeting on Industrial Instrumentation and Control, IIC '12*, pp.37–42, Mar., 2012.

[2] Yuki Nagatsu and Seiichiro Katsura, "Improvement of task reproducibility based on degeneracy and enlargement of finger motion," *The 2011 Annual Meeting of the Institute of Electrical Engineers of Japan*, pp. 372–373, Mar., 2012. (in Japanese)

[3] Yuki Nagatsu and Seiichiro Katsura, "A bilateral control system for environmental adaptation based on thumb opposability," *Mechanical Engineering Congress 2012, KANAZAWA '12*, No. G150024, pp. 1–5, Sep., 2012. (in Japanese)

[4] Yuki Nagatsu and Seiichiro Katsura, "Task assist for bilateral control with different structure considering rotational motion," *The 30th Annual Conference of the Robotics Society of Japan, SAPPORO '12*, No. 2E3-2, pp. 1–4, Sep., 2012. (in Japanese)

[5] Yuki Nagatsu and Seiichiro Katsura, "A control method for manipulators based on polar coordinate transformation," *The 55th Administration Committee of Japan Joint Automatic Control Conference, JACC12*, No. 2H401, pp. 1145–1450, Nov., 2012.

[6] Yuki Nagatsu and Seiichiro Katsura, "Reproduction of grasping motion based on compensation for spatiotemporal disturbance," *The IEEJ Papers of Technical Meeting on "Industrial Instrumentation and Control" and "Mechatronics Control," IIC '13 and MEC '13*, pp. 75–80, Mar., 2013.

[7] Yuki Nagatsu, Noboru Tsunashima, and Seiichiro Katsura, "Reproduction of pushing motion based on compensation for spatiotemporal disturbance," *The 2013 Annual Meeting of the Institute of Electrical Engineers of Japan*, pp. 304–305, Mar., 2013.

[8] Yuki Nagatsu and Seiichiro Katsura, "Reproduction of multi degrees-of-freedom cooperative motion based on spatiotemporal compliance control," *The 2013 IEE-Japan Industry Application Society Conference JIASC '13*, pp. 185–190, Aug., 2013.

[9] Yuki Nagatsu and Seiichiro Katsura, "A spatiotemporal compensation for motion-copying system considering duration of contact," *The IEEJ Papers of Technical Meeting on Mechatronics Control, MEC '13*, pp. 75–80, Nov., 2013.

[10] Yuki Nagatsu and Seiichiro Katsura, "A motion teaching method based on motion reproduction system by considering trainee disturbance," *The IEEJ Papers of Technical Meeting on "Industrial Instrumentation and Control" and "Mechatronics Control," IIC '14 and MEC '14*, pp. 115–120, Mar., 2014.

[11] Yuki Nagatsu and Seiichiro Katsura, "A motion teaching method based on motion copying system by using force and position compensaotrs," *The 2014 Annual Meeting of the Institute of Electrical Engineers of Japan*, pp. 285–286, Mar., 2014.

[12] Yuki Nagatsu and Seiichiro Katsura, "A consideration on Kalman filter based disturbance observer for hybrid control," *The IEEJ Papers of Technical Meeting on Mechatronics Control, MEC '16*, pp. 13–18, Sep., 2016.

Domestic Conference (As a co-author)

[1] E. Fujii, Y. Nagatsu, H. Onoyama, and S. Katsura, "Improvement of General Versatility of Motion Reproduction by Function Observer," *The 32nd Annual Conference of the Robotics Society of Japan, FUKUOKA '14*, No. 1E2-02, pp. 1–4, Sep., 2014. (in Japanese)

[2] S. Nishimura, Y. Osawa, H. Kurumatani, Y. Nagatsu, K. Miura, and S. Katsura, "Kinethetic and Thermal Sensation Presentation Using Multilateral Control under Time Delay," *The IEEJ Papers of Technical Meeting on Mechatronics Control, MEC '16*, pp. 55–60, Sep., 2016. (in Japanese)